

Color Appearance Models

Second Edition

Mark D. Fairchild

Munsell Color Science Laboratory
Rochester Institute of Technology, USA



John Wiley & Sons, Ltd

Color Appearance Models

Wiley-IS&T Series in Imaging Science and Technology

Series Editor:

Michael A. Kriss

Formerly of the Eastman Kodak Research Laboratories and the University of Rochester

The Reproduction of Colour (6th Edition)

R. W. G. Hunt

Color Appearance Models (2nd Edition)

Mark D. Fairchild

Published in Association with the Society for Imaging Science
and Technology



Color Appearance Models

Second Edition

Mark D. Fairchild

Munsell Color Science Laboratory
Rochester Institute of Technology, USA



John Wiley & Sons, Ltd

Copyright © 2005 John Wiley & Sons Ltd, The Atrium, Southern Gate, Chichester,
West Sussex PO19 8SQ, England

Telephone (+44) 1243 779777

This book was previously published by Pearson Education, Inc

Email (for orders and customer service enquiries): cs-books@wiley.co.uk
Visit our Home Page on www.wileyeurope.com or www.wiley.com

All Rights Reserved. No part of this publication may be reproduced, stored in a retrieval system or transmitted in any form or by any means, electronic, mechanical, photocopying, recording, scanning or otherwise, except under the terms of the Copyright, Designs and Patents Act 1988 or under the terms of a licence issued by the Copyright Licensing Agency Ltd, 90 Tottenham Court Road, London W1T 4LP, UK, without the permission in writing of the Publisher. Requests to the Publisher should be addressed to the Permissions Department, John Wiley & Sons Ltd, The Atrium, Southern Gate, Chichester, West Sussex PO19 8SQ, England, or emailed to permreq@wiley.co.uk, or faxed to (+44) 1243 770571.

This publication is designed to offer Authors the opportunity to publish accurate and authoritative information in regard to the subject matter covered. Neither the Publisher nor the Society for Imaging Science and Technology is engaged in rendering professional services. If professional advice or other expert assistance is required, the services of a competent professional should be sought.

Other Wiley Editorial Offices

John Wiley & Sons Inc., 111 River Street, Hoboken, NJ 07030, USA

Jossey-Bass, 989 Market Street, San Francisco, CA 94103-1741, USA

Wiley-VCH Verlag GmbH, Boschstr. 12, D-69469 Weinheim, Germany

John Wiley & Sons Australia Ltd, 33 Park Road, Milton, Queensland 4064, Australia

John Wiley & Sons (Asia) Pte Ltd, 2 Clementi Loop #02-01, Jin Xing Distripark, Singapore 129809

John Wiley & Sons Canada Ltd, 22 Worcester Road, Etobicoke, Ontario, Canada M9W 1L1

British Library Cataloguing in Publication Data

A catalogue record for this book is available from the British Library

ISBN 0-470-01216-1

Typeset in 10/12pt Bookman by Graphicraft Limited, Hong Kong

Printed and bound by Grafos S. A., Barcelona, Spain

This book is printed on acid-free paper responsibly manufactured from sustainable forestry in which at least two trees are planted for each one used for paper production.

To those that don't let me forget to be the ball,
Lisa, Acadia, Elizabeth, Sierra, and Cirrus



*How much of beauty — of color
as well as form — on which our eyes daily rest
goes unperceived by us?*

Henry David Thoreau

Contents

Series Preface	xiii
Preface	xv
Introduction	xix
1 Human Color Vision	1
1.1 Optics of the Eye	1
1.2 The Retina	6
1.3 Visual Signal Processing	12
1.4 Mechanisms of Color Vision	17
1.5 Spatial and Temporal Properties of Color Vision	26
1.6 Color Vision Deficiencies	30
1.7 Key Features for Color Appearance Modeling	34
2 Psychophysics	35
2.1 Psychophysics Defined	36
2.2 Historical Context	37
2.3 Hierarchy of Scales	40
2.4 Threshold Techniques	42
2.5 Matching Techniques	45
2.6 One-Dimensional Scaling	46
2.7 Multidimensional Scaling	49
2.8 Design of Psychophysical Experiments	50
2.9 Importance in Color Appearance Modeling	52
3 Colorimetry	53
3.1 Basic and Advanced Colorimetry	53
3.2 Why is Color?	54
3.3 Light Sources and Illuminants	55
3.4 Colored Materials	59
3.5 The Human Visual Response	66
3.6 Tristimulus Values and Color Matching Functions	70
3.7 Chromaticity Diagrams	77
3.8 CIE Color Spaces	78
3.9 Color Difference Specification	80
3.10 The Next Step	82

4 Color Appearance Terminology	83
4.1 Importance of Definitions	83
4.2 Color	84
4.3 Hue	85
4.4 Brightness and Lightness	86
4.5 Colorfulness and Chroma	87
4.6 Saturation	88
4.7 Unrelated and Related Colors	88
4.8 Definitions in Equations	90
4.9 Brightness–Colorfulness vs Lightness–Chroma	91
5 Color Order Systems	94
5.1 Overview and Requirements	94
5.2 The Munsell Book of Color	96
5.3 The Swedish Natural Color System (NCS)	99
5.4 The Colorcurve System	102
5.5 Other Color Order Systems	103
5.6 Uses of Color Order Systems	106
5.7 Color Naming Systems	109
6 Color Appearance Phenomena	111
6.1 What Are Color Appearance Phenomena?	111
6.2 Simultaneous Contrast, Crispening, and Spreading	113
6.3 Bezold–Brücke Hue Shift (Hue Changes with Luminance)	116
6.4 Abney Effect (Hue Changes with Colorimetric Purity)	117
6.5 Helmholtz–Kohlrausch Effect (Brightness Depends on Luminance and Chromaticity)	119
6.6 Hunt Effect (Colorfulness Increases with Luminance)	120
6.7 Stevens Effect (Contrast Increases with Luminance)	122
6.8 Helson–Judd Effect (Hue of Nonselective Samples)	123
6.9 Bartleson–Breneman Equations (Image Contrast Changes with Surround)	125
6.10 Discounting the Illuminant	127
6.11 Other Context and Structural Effects	127
6.12 Color Constancy?	132
7 Viewing Conditions	134
7.1 Configuration of the Viewing Field	134
7.2 Colorimetric Specification of the Viewing Field	138
7.3 Modes of Viewing	141
7.4 Unrelated and Related Colors Revisited	144
8 Chromatic Adaptation	146
8.1 Light, Dark, and Chromatic Adaptation	147
8.2 Physiology	149
8.3 Sensory and Cognitive Mechanisms	157

8.4 Corresponding-colors Data	159
8.5 Models	162
8.6 Computational Color Constancy	164
9 Chromatic Adaptation Models	166
9.1 von Kries Model	168
9.2 Retinex Theory	171
9.3 Nayatani <i>et al.</i> Model	172
9.4 Guth's Model	174
9.5 Fairchild's Model	177
9.6 Herding CATs	179
9.7 CAT02	181
10 Color Appearance Models	183
10.1 Definition of Color Appearance Models	183
10.2 Construction of Color Appearance Models	184
10.3 CIELAB	185
10.4 Why Not Use Just CIELAB?	193
10.5 What About CIELUV?	194
11 The Nayatani <i>et al.</i> Model	196
11.1 Objectives and Approach	196
11.2 Input Data	197
11.3 Adaptation Model	198
11.4 Opponent Color Dimensions	200
11.5 Brightness	201
11.6 Lightness	202
11.7 Hue	202
11.8 Saturation	203
11.9 Chroma	203
11.10 Colorfulness	204
11.11 Inverse Model	204
11.12 Phenomena Predicted	205
11.13 Why Not Use Just the Nayatani <i>et al.</i> Model?	205
12 The Hunt Model	208
12.1 Objectives and Approach	208
12.2 Input Data	209
12.3 Adaptation Model	211
12.4 Opponent Color Dimensions	215
12.5 Hue	216
12.6 Saturation	217
12.7 Brightness	218
12.8 Lightness	220
12.9 Chroma	220
12.10 Colorfulness	220

12.11	Inverse Model	221
12.12	Phenomena Predicted	222
12.13	Why Not Use Just the Hunt Model?	224
13	The RLAB Model	225
13.1	Objectives and Approach	225
13.2	Input Data	227
13.3	Adaptation Model	228
13.4	Opponent Color Dimensions	230
13.5	Lightness	232
13.6	Hue	232
13.7	Chroma	234
13.8	Saturation	234
13.9	Inverse Model	234
13.10	Phenomena Predicted	236
13.11	Why Not Use Just the RLAB Model?	236
14	Other Models	238
14.1	Overview	238
14.2	ATD Model	239
14.3	LLAB Model	245
15	The CIE Color Appearance Model (1997), CIECAM97s	252
15.1	Historical Development, Objectives, and Approach	252
15.2	Input Data	255
15.3	Adaptation Model	255
15.4	Appearance Correlates	257
15.5	Inverse Model	259
15.6	Phenomena Predicted	259
15.7	The ZLAB Color Appearance Model	260
15.8	Why Not Use Just CIECAM97s?	264
16	CIECAM02	265
16.1	Objectives and Approach	265
16.2	Input Data	266
16.3	Adaptation Model	267
16.4	Opponent Color Dimensions	271
16.5	Hue	271
16.6	Lightness	272
16.7	Brightness	272
16.8	Chroma	273
16.9	Colorfulness	273
16.10	Saturation	273
16.11	Cartesian Coordinates	273
16.12	Inverse Model	274
16.13	Implementation Guidelines	274

16.14 Phenomena Predicted	275
16.15 Why Not Use Just CIECAM02?	275
16.16 Outlook	277
17 Testing Color Appearance Models	278
17.1 Overview	278
17.2 Qualitative Tests	279
17.3 Corresponding Colors Data	283
17.4 Magnitude Estimation Experiments	285
17.5 Direct Model Tests	287
17.6 CIE Activities	291
17.7 A Pictorial Review of Color Appearance Models	295
18 Traditional Colorimetric Applications	299
18.1 Color Rendering	299
18.2 Color Differences	301
18.3 Indices of Metamerism	304
18.4 A General System of Colorimetry?	306
19 Device-independent Color Imaging	308
19.1 The Problem	309
19.2 Levels of Color Reproduction	310
19.3 A Revised Set of Objectives	312
19.4 General Solution	315
19.5 Device Calibration and Characterization	316
19.6 The Need for Color Appearance Models	321
19.7 Definition of Viewing Conditions	321
19.8 Viewing-conditions-independent Color Space	323
19.9 Gamut Mapping	324
19.10 Color Preferences	327
19.11 Inverse Process	328
19.12 Example System	328
19.13 ICC Implementation	330
20 Image Appearance Modeling and The Future	334
20.1 From Color Appearance to Image Appearance	335
20.2 The iCAM Framework	340
20.3 A Modular Image-difference Model	346
20.4 Image Appearance and Rendering Applications	350
20.5 Image Difference and Quality Applications	355
20.6 Future Directions	357
References	361
Index	378

Series Preface

There is more to colour than meets the eye! This may be taken as a shopworn comment for a serious text entitled **Color Appearance Models**, but nothing could be more to the point about colour. Since the *Commission Internationale de l'Eclairage* (CIE) established the basis for modern colorimetry, researchers have been developing theories and testing them experimentally in the hope of finding a unified model to explain how people 'see' colours (given spectral reflection curves under given illuminants within given viewing conditions). As with the unified field theory in physics, no final, all-inclusive colour appearance model has been established and tested, although considerable progress has been made over the last fifteen years. The second offering in the **Wiley-IS&T Series in Imaging Science and Technology** is the Second Edition of **Color Appearance Models** by Mark D. Fairchild. This outstanding text provides an expansive, detailed and clear exposition of the progress made since 1998 along with a thorough development of the fundamental aspects of colour science required to fully understand the current theories and results. **Color Appearance Models** is an absolute requirement for any colour science researcher or engineer, be they in industry or academia.

Consider the following 'real life' problems, which will find solutions in a fuller understanding of **Color Appearance Models**. Digital still cameras have well understood means of automatically balancing the red-green-blue exposures to compensate for an obvious shift in taking illuminant (for example, from daylight to tungsten). However, these 'global' shifts in exposure do not reflect the ability of the human visual system to adjust in a local manner to a complexly illuminated scene like a sunrise or sunset in the desert or mountains. Using the results of advanced colour appearance models it will be possible to construct digital image processing algorithms that automatically analyse the entire image, segment the image into areas of 'different' illuminants and apply local corrections that match the adjustments made by the human visual system at the time the image was recorded. A second practical problem is: how does an inkjet manufacturer develop the proper combination of inks and halftone algorithms, which will minimize the colour shifts in the hardcopy as it is viewed under a variety of illuminants (daylight, shaded daylight, tungsten, fluorescent, etc)? These are just two of the important, practical problems that will only be solved as progress is made toward a unified colour appearance model.

Mark Fairchild received his B.S. and M.S. degrees in Imaging Science from the *Rochester Institute of Technology* and his Ph.D. in Vision Science from

the *University of Rochester*. Upon receiving his doctorate Mark returned to the *Rochester Institute of Technology* where he has conducted research in colour science for over fourteen years in the *Munsell Color Science Laboratory*, which is part of the *Chester F. Carlson Center for Imaging Science*. Mark is currently the Director of the *Munsell Color Science Laboratory*. Mark is leader among a new breed of colour scientists who have expanded and extended the 'classical' colour research of J. von Kreis, W.D. Wright, D.L. MacAdam, G. Wyszecki, W.S. Stiles, R.W.G. Hunt, and many others who laid the foundations of colour science. This new breed, which also includes researchers like B.W. Wandell, B.V. Funt, G.D. Finlayson and D.R. Williams, are combining the results of vision research and basic colour measurements to form the genesis of a unified colour appearance theory. It is with great expectations that we start to follow and chronicle the results and applications of Mark's research and those of his colleagues.

MICHAEL A. KRISS

*Formerly of the Eastman Kodak Research Laboratories
and the University of Rochester*

Preface

The law of proportion according to which the several colors are formed, even if a man knew he would be foolish in telling, for he could not give any necessary reason, nor indeed any tolerable or probable explanation of them.

Plato

Despite Plato's warning, this book is about one of the major unresolved issues in the field of color science, the efforts that have been made toward its resolution, and the techniques that can be used to address current technological problems. The issue is the prediction of the color appearance experienced by an observer when viewing stimuli in natural, complex settings. Useful solutions to this problem have impacts in a number of industries such as lighting, materials, and imaging. In lighting, color appearance models can be used to predict the color rendering properties of various light sources, allowing specification of quality rather than just efficiency. In materials fields (coatings, plastics, textiles, etc.), color appearance models can be used to specify tolerances across a wider variety of viewing conditions than is currently possible and to more accurately evaluate metamerism. The imaging industries have produced the biggest demand for accurate and practical color appearance models. The rapid growth in color imaging technology, particularly the desktop publishing market, has led to the emergence of color management systems. It is widely acknowledged that such systems require color appearance models to allow images originating in one medium and viewed in a particular environment to be acceptably reproduced in a second medium and viewed under different conditions. While the need for color appearance models is recognized, their development has been at the forefront of color science and largely confined to the discourse of academic journals and conferences. This book brings the fundamental issues and current solutions in the area of color appearance modeling together in a single place for those needing to solve practical problems or looking for background for ongoing research projects.

Everyone knows what color is, but the accurate description and specification of colors is quite another story. In 1931, the Commission Internationale de l'Éclairage (CIE) recommended a system for color measurement establishing the basis for modern colorimetry. That system allows the specification of color matches through CIE XYZ tristimulus values. It was immediately recognized that more advanced techniques were required. The CIE recommended the CIELAB and CIELUV color spaces in 1976 to enable uniform

international practice for the measurement of color differences and establishment of color tolerances. While the CIE system of colorimetry has been applied successfully for nearly 70 years, it is limited to the comparison of stimuli that are identical in every spatial and temporal respect and viewed under matched viewing conditions. CIE XYZ values describe whether or not two stimuli match. CIELAB values can be used to describe the perceived differences between stimuli in a single set of viewing conditions. Color appearance models extend the current CIE systems to allow the description of what color stimuli look like under a variety of viewing conditions. The application of such models opens up a world of possibilities for the accurate specification, control, and reproduction of color.

Understanding color appearance phenomena and developing models to predict them have been the topics of a great deal of research — particularly in the last 15 to 20 years. Color appearance remains a topic of much active research that is often being driven by technological requirements. Despite the fact that the CIE is not yet able to recommend a single color appearance model as the best available for all applications, there are many who need to implement some form of a model to solve their research, development, and engineering needs. One such application is the development of color management systems based on the ICC Profile Format that is being developed by the International Color Consortium and incorporated into essentially all modern computer operating systems. Implementation of color management using ICC profiles requires the application of color appearance models with no specific instructions on how to do so. Unfortunately, the fundamental concepts, phenomena, and models of color appearance are not recorded in a single source. Generally, one interested in the field must search out the primary references across a century of scientific journals and conference proceedings. This is due to the large amount of active research in the area. While searching for and keeping track of primary references is fine for those doing research on color appearance models, it should not be necessary for every scientist, engineer, and software developer interested in the field. The aim of this book is to provide the relevant information for an overview of color appearance and details of many of the most widely used models in a single source. The general approach has been to first provide an overview of the fundamentals of color measurement and the phenomena that necessitate the development of color appearance models. This eases the transition into the formulation of the various models and their applications that appear later in the book. This approach has proven quite useful in various university courses, short courses, and seminars in which the full range of material must be presented in a limited time.

Chapters 1 through 3 provide a review of the fundamental concepts of human color vision, psychophysics, and the CIE system of colorimetry that are prerequisite to understanding the development and implementation of color appearance models. Chapters 4 through 7 present the fundamental definitions, descriptions, and phenomena of color appearance. These chapters

provide a review of the historical literature that has led to modern research and development of color appearance models. Chapters 8 and 9 concentrate on one of the most important component mechanisms of color appearance, chromatic adaptation. The models of chromatic adaptation described in Chapter 9 are the foundation of the color appearance models described in later chapters. Chapter 10 presents the definition of color appearance models and outlines their construction using the CIELAB color space as an example. Chapters 11 through 13 provide detailed descriptions of the Nayatani *et al.*, Hunt, and RLAB color appearance models along with the advantages and disadvantages of each. Chapter 14 reviews the ATD and LLAB appearance models that are of increasing interest for some applications. Chapter 15 presents the CIECAM97s model established as a recommendation by the CIE just as the first edition of this book went to press (and included as an appendix in that edition). Also included is a description of the ZLAB simplification of CIECAM97s. Chapter 16 describes the recently formulated CIECAM02 model that represents a significant improvement of CIECAM97s and is the best possible model based on current knowledge. Chapters 17 and 18 describe tests of the various models through a variety of visual experiments and colorimetric applications of the models. Chapter 19 presents an overview of device-independent color imaging, the application that has provided the greatest technological push for the development of color appearance models. Finally, Chapter 20 introduces the concept of image appearance modeling as a potential future direction for color appearance modeling research and provides an overview of iCAM as one example of an image appearance model.

While the field of color appearance modeling remains young and likely to continue developing in the near future, this book includes extensive material that will not change. Chapters 1 through 10 provide overviews of fundamental concepts, phenomena, and techniques that will change little, if at all, in the coming years. Thus, these chapters should serve as a steady reference. The models, tests, and applications described in the later chapters will continue to be subject to evolutionary changes as research progresses. However, these chapters do provide a useful snapshot of the current state of affairs and provide a basis from which it should be much easier to keep track of future developments. To assist readers in this task, a worldwide web page has been set up <www.cis.rit.edu/Fairchild/CAM.html> that lists important developments and publications related to the material in this book. A spreadsheet with example calculations can also be found there.

*'Yes,' I answered her last night;
'No,' this morning sir, I say,
Colours seen by candle-light
Will not look the same by day.*

Elizabeth Barrett Browning

ACKNOWLEDGEMENTS

A project like this book is never really completed by a single author. I particularly thank my family for the undying support that encouraged completion of this work. The research and learning that led to this book is directly attributable to my students. Much of the research would not have been completed without their tireless work and I would not have learned about color appearance models were it not for their keen desire to learn more and more about them from me. I am deeply indebted to all of my students and friends — those that have done research with me, those working at various times in the Munsell Color Science Laboratory, and those that have participated in my university and short courses at all levels. There is no way to list all of them without making an omission, so I will take the easy way out and thank them as a group. I am indebted to those that reviewed various chapters while the first edition of this book was being prepared and provided useful insights, suggestions, and criticisms. These reviewers include: Paula J. Alessi, Edwin Breneman, Ken Davidson, Ron Gentile, Robert W.G. Hunt, Lindsay MacDonald, Mike Pointer, Michael Stokes, Jeffrey Wang, Eric Zeise, and Valerie Zelenty. Thank you to Addison-Wesley for convincing me to write the first edition and then publishing it and to IS&T, the Society for Imaging Science and Technology, (particularly Calva Leonard) and John Wiley & Sons, Ltd for having the vision to publish this second edition. It has been a joy to work with all of the IS&T staff throughout my color imaging career. Thanks to all of the industrial and government sponsors of our research and education in the Munsell Color Science Laboratory at R.I.T., particularly Thor Olson of Management Graphics for the donation of the Opal image recorder and loan of the 120-camera back used to output the color images for the first edition. (It is a reflection of technological advancement in color imaging that no hard-copy versions of the images were required for the second edition!). Valerie Hemink has provided unwavering, excellent, and at times seemingly psychic, support of my activities in her role as the Munsell Color Science Laboratory administrative assistant. Last, but not least, I thank Colleen Desimone for her support, friendship, and excellent work as the MCSL outreach coordinator, particularly in her help with the second edition of this book. I couldn't possible function coherently without the outstanding support of Val and Colleen that makes going to the office so much easier. This edition would not have been possible without them.

M.D.F.
Honeoye Falls, N.Y.

*Ye'll come away from the links
with a new hold on life, that is certain
if ye play the game with all yer heart.*

Michael Murphy, *Golf in the Kingdom*

Introduction

Standing before it, it has no beginning; even when followed, it has no end. In the now, it exists; to the present apply it, follow it well, and reach its beginning.

Tao Te Ching, 300–600 BCE

Like beauty, color is in the eye of the beholder. For as long as human scientific inquiry has been recorded, the nature of color perception has been a topic of great interest. Despite tremendous evolution of technology, fundamental issues of color perception remain unanswered. Many scientific attempts to explain color rely purely on the physical nature of light and objects. However, without the human observer there is no color. It is often asked whether a tree falling in the forest makes a sound if no one is there to observe it. Perhaps equal philosophical energy should be spent wondering what color its leaves are.

WHAT IS A COLOR APPEARANCE MODEL?

It is common to say that certain wavelengths of light, or certain objects, are a given color. This is an attempt to relegate color to the purely physical domain. It is more correct to state that those stimuli are perceived to be of a certain color when viewed under specified conditions. Attempts to specify color as a purely physical phenomenon fall within the domain of spectrophotometry and spectroradiometry. When the lowest level sensory responses of an average human observer are factored in, the domain of colorimetry has been entered. When the many other variables that influence color perception are considered, in order to better describe our perceptions of stimuli, one is within the domain of color appearance modeling — the subject of this book.

Consider the following observations.

- The headlights of an oncoming automobile are nearly blinding at night, but barely noticeable during the day.
- As light grows dim, colors fade from view while objects remain readily apparent.
- Stars disappear from sight during the daytime.
- The walls of a freshly painted room appear significantly different from the color of the sample that was used to select the paint in a hardware store.

- Artwork displayed in different color mat board takes on a significantly different appearance.
- Printouts of images do not match the originals displayed on a computer monitor.
- Scenes appear more colorful and of higher contrast on a sunny day.
- Blue and green objects (e.g., *game pieces*) become indistinguishable under dim incandescent illumination.
- It is nearly impossible to select appropriate socks (e.g., *black, brown, or blue*) in the early morning light.
- There is no such thing as a gray, or brown, light bulb.
- There are no colors described as reddish-green, or yellowish-blue.

None of the above observations can be explained by physical measurements of materials and/or illumination alone. Rather, such physical measurements must be combined with other measurements of the prevailing viewing conditions and models of human visual perception in order to make reasonable predictions of these effects. This aggregate is precisely the task that color appearance models are designed to embrace. Each of the observations outlined above, and many more like them, can be explained by various color appearance phenomena and models. They cannot be explained by the established techniques of color measurement, sometimes referred to as *basic colorimetry*. This book details the differences between basic colorimetry and color appearance models, provides fundamental background on human visual perception and color appearance phenomena, and describes the application of color appearance models to current technological problems such as digital color reproduction. Upon completion of this book, a reader should be able to fairly easily explain each of the appearance phenomena listed above.

Basic colorimetry provides the fundamental color measurement techniques that are used to specify stimuli in terms of their sensory potential for an average human observer. These techniques are absolutely necessary as the foundation for color appearance models. However, on their own, the techniques of basic colorimetry can only be used to specify whether or not two stimuli, viewed under identical conditions, match in color for an average observer. Advanced colorimetry aims to extend the techniques of basic colorimetry to enable the specification of color difference perceptions and, ultimately, color appearance. There are several established techniques for color difference specification that have been formulated and refined over the past few decades. These techniques have also reached the point that a few, agreed upon, standards are used throughout the world. Color appearance models aim to go the final step. This would allow the mathematical description of the appearance of stimuli in a wide variety of viewing conditions. Such models have been the subject of much research over the past two decades and more recently become required for practical applications. There are a variety of models that have been proposed. These models are beginning to find their way into color imaging systems through the refinement of color

management techniques. This requires an ever-broadening array of scientists, engineers, programmers, imaging specialists, and others to understand the fundamental philosophy, construction, and capabilities of color appearance models as described in the ensuing chapters.

So as not to make the learning process too difficult, here are some clues to the explanation of the color appearance observations listed near the beginning of this introduction.

- The change of appearance of oncoming headlights can be largely explained by the processes of light adaptation and described by Weber's law.
- The fading of color in dim light while objects remain clearly visible is explained by the transition from trichromatic cone vision to monochromatic rod vision.
- The incremental illumination of a star on the daytime sky is not large enough to be detected, while the same physical increment on the darker nighttime sky is easily perceived, because the visual threshold to luminance increments has changed between the two viewing conditions.
- The paint chip doesn't match the wall due to changes in the size, surround, and illumination of the stimulus.
- Changes in the color of a surround or background profoundly influence the appearance of stimuli. This can be particularly striking for photographs and other artwork.
- Assuming the computer monitor and printer are accurately calibrated and characterized, differences in media, white point, luminance level, and surround can still force the printed image to look significantly different from the original.
- The Hunt effect and Stevens effect describe the apparent increase in colorfulness and contrast of scenes with increases in illumination level.
- Low levels of incandescent illumination do not provide the energy required by the short-wavelength sensitive mechanisms of the human visual system (the least sensitive of the color mechanisms) to distinguish green objects from blue objects.
- In the early morning light, the ability to distinguish dark colors is diminished.
- The perceptions of gray and brown only occur as related colors, thus they cannot be observed as light sources that are the brightest element of a scene.
- The hue perceptions red and green (or yellow and blue) are encoded in a bipolar fashion by our visual system and thus cannot exist together.

Given those clues, it is time to read on and further unlock the mysteries of color appearance.

Human Color Vision

Color appearance models aim to extend basic colorimetry to the level of specifying the perceived color of stimuli in a wide variety of viewing conditions. To fully appreciate the formulation, implementation, and application of color appearance models, several fundamental topics in color science must first be understood. These are the topics of the first few chapters of this book. Since color appearance represents several of the dimensions of our visual experience, any system designed to predict correlates to these experiences must be based, to some degree, on the form and function of the human visual system. All of the color appearance models described in this book are derived with human visual function in mind. It becomes much simpler to understand the formulations of the various models if the basic anatomy, physiology, and performance of the visual system is understood. Thus, this book begins with a treatment of the human visual system.

As necessitated by the limited scope available in a single chapter, this treatment of the visual system is an overview of the topics most important for an appreciation of color appearance modeling. The field of vision science is immense and fascinating. Readers are encouraged to explore the literature and the many useful texts on human vision in order to gain further insight and details. Of particular note are the review paper on the mechanisms of color vision by Lennie and D'Zmura (1988), the text on human color vision by Kaiser and Boynton (1996), the more general text on the foundations of vision by Wandell (1995), the comprehensive treatment by Palmer (1999), and edited collections on color vision by Backhaus *et al.* (1998) and Gegenfurtner and Sharpe (1999). Much of the material covered in this chapter is treated in more detail in those references.

1.1 OPTICS OF THE EYE

Our visual perceptions are initiated and strongly influenced by the anatomical structure of the eye. Figure 1.1 shows a schematic representation of

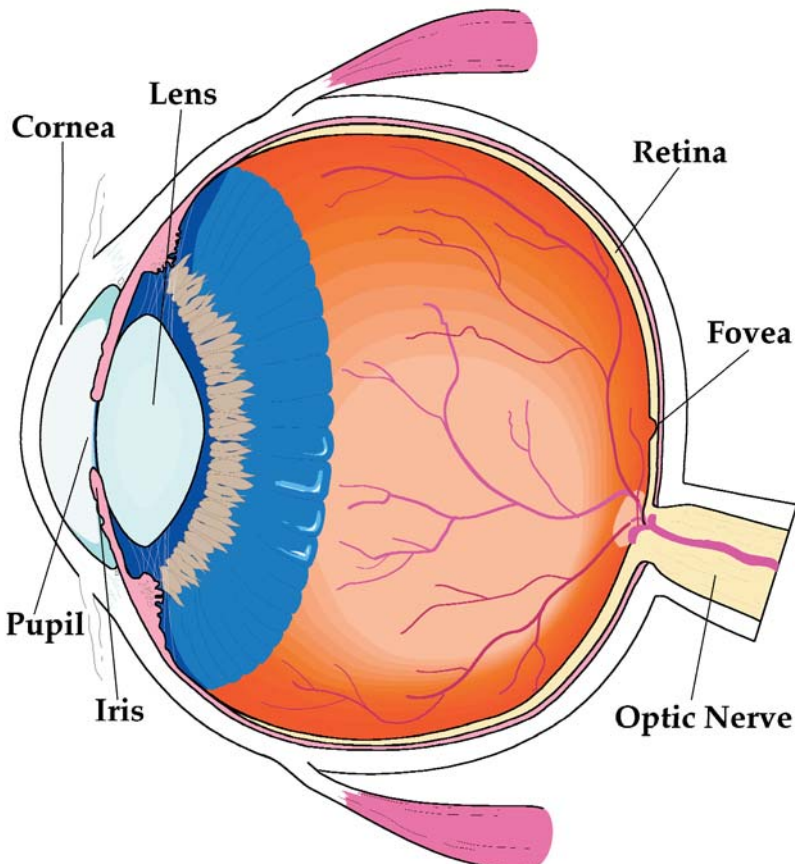


Figure 1.1 Schematic diagram of the human eye with some key structures labeled

the optical structure of the human eye with some key features labeled. The human eye acts like a camera. The cornea and lens act together like a camera lens to focus an image of the visual world on the retina at the back of the eye, which acts like the film or other image sensor of a camera. These and other structures have a significant impact on our perception of color.

The Cornea

The *cornea* is the transparent outer surface of the front of the eye through which light passes. It serves as the most significant image-forming element of the eye since its curved surface at the interface with air represents the largest change in index of refraction in the eye's optical system. The cornea is avascular, receiving its nutrients from marginal blood vessels and the fluids surrounding it. Refractive errors, such as nearsightedness (myopia),

farsightedness (hyperopia), or astigmatism, can be attributed to variations in the shape of the cornea and are sometimes corrected with laser surgery that reshapes the cornea.

The Lens

The *lens* serves the function of accommodation. It is a layered, flexible structure that varies in index of refraction. It is a naturally occurring gradient-index optical element with the index of refraction higher in the center of the lens than at the edges. This feature serves to reduce some of the aberrations that might normally be present in a simple optical system.

The shape of the lens is controlled by the ciliary muscles. When we gaze at a nearby object, the lens becomes 'fatter' and thus has increased optical power to allow us to focus on the near object. When we gaze at a distant object, the lens becomes 'flatter' resulting in the decreased optical power required to bring far away objects into sharp focus. As we age, the internal structure of the lens changes resulting in a loss of flexibility. Generally, when an age of about 50 years is reached the lens has completely lost its flexibility and observers can no longer focus on near objects (this is called presbyopia, or 'old eye'). It is at this point that most people need reading glasses or bifocals.

Concurrent with the hardening of the lens is an increase in its optical density. The lens absorbs and scatters short-wavelength (blue and violet) energy. As it hardens, the level of this absorption and scattering increases. In other words, the lens becomes more and more yellow with age. Various mechanisms of chromatic adaptation generally make us unaware of these gradual changes. However, we are all looking at the world through a yellow filter that not only changes with age, but is significantly different from observer to observer. The effects are most noticeable when performing critical color matching or comparing color matches with other observers. The effect is particularly apparent with purple objects. Since an older lens absorbs most of the blue energy reflected from a purple object, but does not affect the reflected red energy, older observers will tend to report that the object is significantly more red than reported by younger observers. Important issues regarding the characteristics of lens aging and its influence on visual performance are discussed by Pokorny *et al.* (1987), Werner and Schefrin (1993), and Schefrin and Werner (1993).

The Humors

The volume between the cornea and lens is filled with the *aqueous humor*, which is essentially water. The region between the lens and retina is filled with *vitreous humor*, which is also a fluid, but with a higher viscosity, similar to that of gelatin. Both humors exist in a state of slightly elevated pressure

(relative to air pressure) to assure that the flexible eyeball retains its shape and dimensions in order to avoid the deleterious effects of wavering retinal images. The flexibility of the entire eyeball serves to increase its resistance to injury. It is much more difficult to break a structure that gives way under impact than one of equal ‘strength’ that attempts to remain rigid. Since the indices of refraction of the humors are roughly equal to that of water, and those of the cornea and lens are only slightly higher, the rear surface of the cornea and the entire lens have relatively little optical power.

The Iris

The *iris* is the sphincter muscle that controls pupil size. The iris is pigmented, giving each of us our specific eye color. Eye color is determined by the concentration and distribution of melanin within the iris. The pupil, which is the hole in the middle of the iris through which light passes, defines the level of illumination on the retina. Pupil size is largely determined by the overall level of illumination, but it is important to note that it can also vary with non-visual phenomena such as arousal. (This effect can be observed by enticingly shaking a toy in front of a cat and paying attention to its pupils.) Thus it is difficult to accurately predict pupil size from the prevailing illumination. In practical situations, pupil diameter varies from about 3 mm to about 7 mm. This change in pupil diameter results in approximately a five-fold change in pupil area, and therefore retinal illuminance. The visual sensitivity change with pupil area is further limited by the fact that marginal rays are less effective at stimulating visual response in the cones than central rays (the Stiles–Crawford effect). The change in pupil diameter alone is not sufficient to explain excellent human visual function over prevailing illuminance levels that can vary over 10 orders of magnitude.

The Retina

The optical image formed by the eye is projected onto the retina. The retina is a thin layer of cells, approximately the thickness of tissue paper, located at the back of the eye and incorporating the visual system’s photosensitive cells and initial signal processing and transmission ‘circuitry.’ These cells are neurons, part of the central nervous system, and can appropriately be considered a part of the brain. The photoreceptors, *rods* and *cones*, serve to transduce the information present in the optical image into chemical and electrical signals that can be transmitted to the later stages of the visual system. These signals are then processed by a network of cells and transmitted to the brain through the optic nerve. More detail on the retina is presented in the next section.

Behind the retina is a layer known as the *pigmented epithelium*. This dark pigment layer serves to absorb any light that happens to pass through the

retina without being absorbed by the photoreceptors. The function of the pigmented epithelium is to prevent light from being scattered back through the retina, thus reducing the sharpness and contrast of the perceived image. Nocturnal animals give up this improved image quality in exchange for a highly reflective *tapetum* that reflects the light back in order to provide a second chance for the photoreceptors to absorb the energy. This is why the eyes of a deer, or other nocturnal animal, caught in the headlights of an oncoming automobile, appear to glow.

The Fovea

Perhaps the most important structural area on the retina is the fovea. The *fovea* is the area on the retina where we have the best spatial and color vision. When we look at, or fixate, an object in our visual field, we move our head and eyes such that the image of the object falls on the fovea. As you are reading this text, you are moving your eyes to make the various words fall on your fovea as you read them. To illustrate how drastically spatial acuity falls off as the stimulus moves away from the fovea, try to read preceding text in this paragraph while fixating on the period at the end of this sentence. It is probably difficult, if not impossible, to read text that is only a few lines away from the point of fixation. The fovea covers an area that subtends about two degrees of visual angle in the central field of vision. To visualize two degrees of visual angle, a general rule is that the width of your thumbnail, held at arm's length, is approximately one degree of visual angle.

The Macula

The fovea is also protected by a yellow filter known as the macula. The *macula* serves to protect this critical area of the retina from intense exposures to short-wavelength energy. It might also serve to reduce the effects of chromatic aberration that cause the short-wavelength image to be rather severely out of focus most of the time. Unlike the lens, the macula does not become more yellow with age. However, there are significant differences in the optical density of the macular pigment from observer to observer and in some cases between a single observer's left and right eyes. The yellow filters of the lens and macula, through which we all view the world, are the major source of variability in color vision between observers with normal color vision.

The Optic Nerve

A last key structure of the eye is the *optic nerve*. The optic nerve is made up of the *axons* (outputs) of the ganglion cells, the last level of neural processing in the retina. It is interesting to note that the optic nerve is made up of

approximately one million fibers, carrying information generated by approximately 130 million photoreceptors. Thus there is a clear compression of the visual signal prior to transmission to higher levels of the visual system. A one-to-one ‘pixel map’ of the visual stimulus is never available for processing by the brain’s higher visual mechanisms. This processing is explored in greater detail below. Since the optic nerve takes up all of the space that would normally be populated by photoreceptors, there is a small area in each eye in which no visual stimulation can occur. This area is known as the *blind spot*.

The structures described above have a clear impact in shaping and defining the information available to the visual system that ultimately results in the perception of color appearance. The action of the pupil serves to define retinal illuminance levels that, in turn, have a dramatic impact on color appearance. The yellow-filtering effects of the lens and macula modulate the spectral responsivity of our visual system and introduce significant inter-observer variability. The spatial structure of the retina serves to help define the extent and nature of various visual fields that are critical for defining color appearance. The neural networks in the retina reiterate that visual perception in general, and specifically color appearance, cannot be treated as simple point-wise image processing problems. Several of these important features are discussed in more detail in the following sections on the retina, visual physiology, and visual performance.

1.2 THE RETINA

Figure 1.2 illustrates a cross-sectional representation of the retina. The retina includes several layers of neural cells, beginning with the photoreceptors, the *rods* and *cones*. A vertical signal processing chain through the retina can be constructed by examining the connections of photoreceptors to bipolar cells, which are in turn connected to ganglion cells, which form the optic nerve. Even this simple pathway results in the signals from multiple photoreceptors being compared and combined. This is because multiple photoreceptors provide input to many of the bipolar cells and multiple bipolar cells provide input to many of the ganglion cells. More importantly, this simple concept of retinal signal processing ignores two other significant types of cells. These are the *horizontal cells*, that connect photoreceptors and bipolar cells laterally to one another, and the *amacrine cells*, that connect bipolar cells and ganglion cells laterally to one another. Figure 1.2 provides only a slight indication of the extent of these various interconnections.

The specific processing that occurs in each type of cell is not completely understood and is beyond the scope of this chapter. However, it is important to realize that the signals transmitted from the retina to the higher levels of the brain via the ganglion cells are not simple point-wise representations of the receptor signals, but rather consist of sophisticated combinations of the receptor signals. To envision the complexity of the retinal processing, keep in mind that each synapse between neural cells can effectively perform

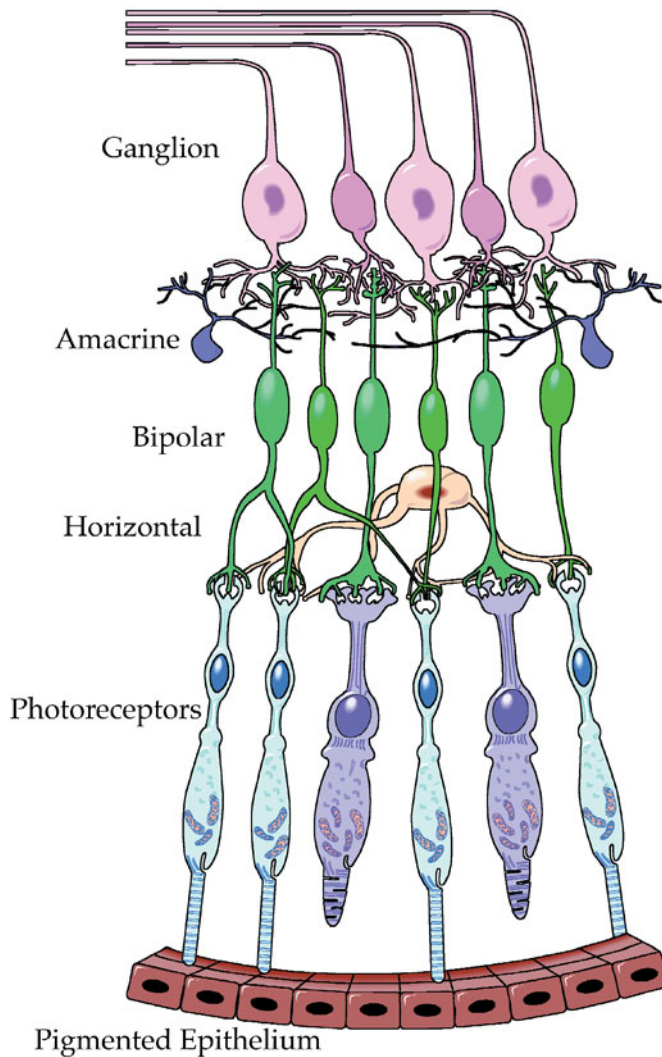


Figure 1.2 Schematic diagram of the ‘wiring’ of cells in the human retina

a mathematical operation (add, subtract, multiply, divide) in addition to the amplification, gain control, and nonlinearities that can occur within the neural cells. Thus the network of cells within the retina can serve as a sophisticated image computer. This is how the information from 130 million photoreceptors can be reduced to signals in approximately one million ganglion cells without loss of visually meaningful data.

It is interesting to note that light passes through all of the neural machinery of the retina prior to reaching the photoreceptors. This has little impact on visual performance since these cells are transparent and in fixed position, thus not perceived. It also allows the significant amounts of nutrients

required and waste produced by the photoreceptors to be processed through the back of the eye.

Rods and Cones

Figure 1.3 provides a representation of the two classes of retinal photoreceptors, rods and cones. Rods and cones derive their respective names from their prototypical shape. Rods tend to be long and slender while peripheral cones are conical. This distinction is misleading since foveal cones, which are tightly packed due to their high density in the fovea, are long and slender, resembling peripheral rods.

The more important distinction between rods and cones is in visual function. Rods serve vision at low luminance levels (e.g., less than 1 cd/m^2) while cones serve vision at higher luminance levels. Thus the transition from rod to cone vision is one mechanism that allows our visual system to function over a large range of luminance levels. At high luminance levels (e.g., greater than 100 cd/m^2) the rods are effectively saturated and only the cones function. In the intermediate luminance levels, both rods and cones function and contribute to vision. Vision when only rods are active is referred to as *scotopic vision*. Vision served only by cones is referred to as *photopic vision* and the term *mesopic vision* is used to refer to vision in which both rods and cones are active.

Rods and cones also differ substantially in their spectral sensitivities as illustrated in Figure 1.4(a). There is only one type of rod receptor with a peak spectral responsivity at approximately 510 nm. There are three types of cone receptors with peak spectral responsivities spaced through the visual spectrum.

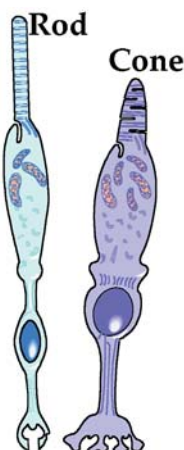


Figure 1.3 Illustrations of prototypical rod and cone photoreceptors

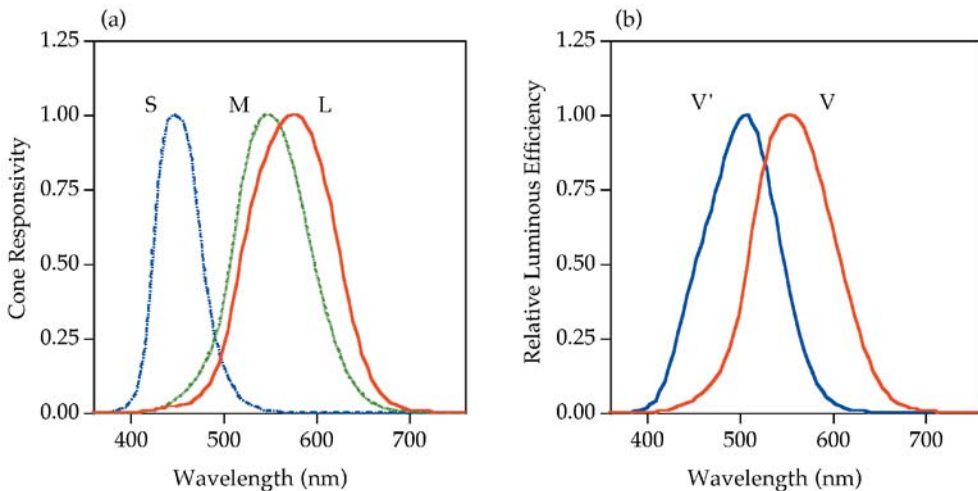


Figure 1.4 (a) Spectral responsivities of the L , M , and S cones; (b) the CIE spectral luminous efficiency functions for scotopic, $V'(\lambda)$, and photopic, $V(\lambda)$, vision

The three types of cones are most properly referred to as L , M , and S cones. These names refer to the long-wavelength, middle-wavelength, and short-wavelength sensitive cones, respectively. Sometimes the cones are denoted with other symbols such as RGB or $\rho\gamma\beta$ suggestive of red, green, and blue sensitivities. As can be seen in Figure 1.4(a) this concept is erroneous and the LMS names are more appropriately descriptive. Note that the spectral responsivities of the three cone types are broadly overlapping; a design that is significantly different from the ‘color separation’ responsivities that are often built into physical imaging systems. Such sensitivities, typically incorporated in imaging systems for practical reasons, are the fundamental reason that accurate color reproduction is often difficult, if not impossible to achieve.

The three types of cones clearly serve color vision. Since there is only one type of rod, the rod system is incapable of color vision. This can easily be observed by viewing a normally colorful scene at very low luminance levels. Figure 1.4(b) illustrates the two CIE spectral luminous efficiency functions, the $V'(\lambda)$ function for scotopic (rod) vision and the $V(\lambda)$ function for photopic (cone) vision. These functions represent the overall sensitivity of the two systems with respect to the perceived brightness of the various wavelengths. Since there is only one type of rod, the $V(\lambda)$ function is identical to the spectral responsivity of the rods and depends on the spectral absorption of *rhodopsin*, the photosensitive pigment in rods. The $V(\lambda)$ function, however, represents a combination of the three types of cone signals rather than the responsivity of any single cone type.

Note the difference in peak spectral sensitivity between scotopic and photopic vision. With scotopic vision we are more sensitive to shorter

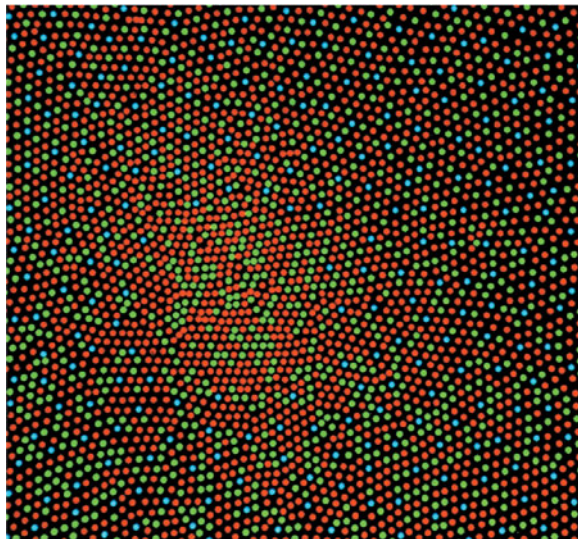


Figure 1.5 A representation of the retinal photoreceptor mosaic artificially colored to represent the relative proportions of *L* (colored red), *M* (green), and *S* (blue) cones in the human retina. Modeled after Williams *et al.* (1991)

wavelengths. This effect, known as the *Purkinje shift*, can be observed by finding two objects, one blue and the other red, that appear the same lightness when viewed in daylight. When the same two objects are viewed under very low luminance levels, the blue object will appear quite light while the red object will appear nearly black because of the scotopic spectral sensitivity function.

Another important feature about the three cone types is their relative distribution in the retina. It turns out that the *S* cones are relatively sparsely populated throughout the retina and completely absent in the most central area of the fovea. There are far more *L* and *M* cones than *S* cones and there are approximately twice as many *L* cones as *M* cones. The relative populations of the *L:M:S* cones are approximately 12:6:1 (with reasonable estimates as high as 40:20:1). These relative populations must be considered when combining the cone responses. (plotted with individual normalizations in Figure 1.4a) to predict higher level visual responses. Figure 1.5 provides a schematic representation of the foveal photoreceptor mosaic with false coloring to represent a hypothetical distribution with the *L* cones in red, *M* cones in green, and *S* cones in blue. Figure 1.5 is presented simply as a convenient visual representation of the cone populations and should not be taken literally.

As illustrated in Figure 1.5, there are no rods present in the fovea. This feature of the visual system can also be observed when trying to look directly at a small dimly illuminated object, such as a faint star at night. It disappears since its image falls on the foveal area where there are no rods to

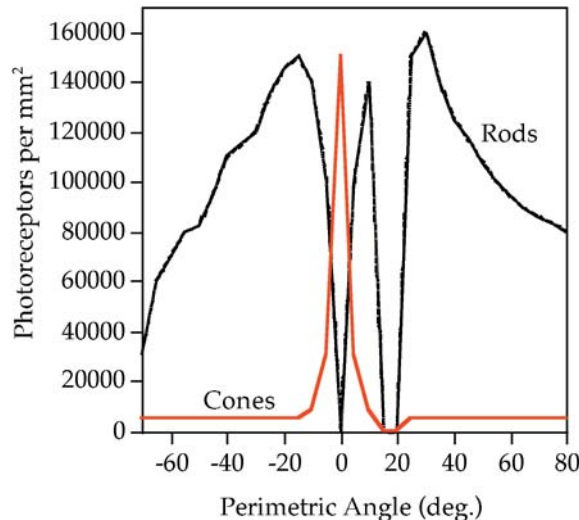


Figure 1.6 Density (receptors per square millimeter) of rod and cone photoreceptors as a function of location on the human retina

detect the dim stimulus. Figure 1.6 shows the distribution of rods and cones across the retina. Several important features of the retina can be observed in Figure 1.6. First, notice the extremely large numbers of photoreceptors. In some retinal regions there are about 150 000 photoreceptors per square millimeter of retina! Also notice that there are far more rods (around 120 million per retina) than cones (around 7 million per retina). This might seem somewhat counterintuitive since cones function at high luminance levels and produce high visual acuity while rods function at low luminance levels and produce significantly reduced visual acuity (analogous to low-speed fine-grain photographic film vs high-speed coarse-grain film). The solution to this apparent mystery lies in the fact that single cones feed into ganglion cell signals while rods pool their responses over hundreds of receptors (feeding into a single ganglion cell) in order to produce increased sensitivity at the expense of acuity. This also partially explains how the information from so many receptors can be transmitted through one million ganglion cells. Figure 1.6 also illustrates that cone receptors are highly concentrated in the fovea and more sparsely populated throughout the peripheral retina while there are no rods in the central fovea. The lack of rods in the central fovea allows for valuable space to be used to produce the highest possible spatial acuity with the cone system. A final feature to be noted in Figure 1.6 is the blind spot. This is the area, 12–15° from the fovea, where the optic nerve is formed and there is no room for photoreceptors.

Figure 1.7 provides some stimuli that can be used to demonstrate the existence of the *blind spot*. One reason the blind spot generally goes unnoticed is that it is located on opposite sides of the visual field in each of

(a)



(b)



Figure 1.7 Stimuli used to illustrate presence of the blind spot and ‘filling in’ phenomena. Close your left eye. Fixate the cross with your right eye and adjust the viewing distance until (a) the spot falls on your blind spot or (b) the gap in the line falls on your blind spot. Notice the perception in that area in each case

the two eyes. However, even when one eye is closed, the blind spot is not generally noticed. To observe your blind spot, close your left eye and fixate the cross in Figure 1.7(a) with your right eye. Then adjust the viewing distance of the book until the spot to the right of the cross disappears when it falls on the blind spot. Note that what you see when the spot disappears is not a black region, but rather it appears to be an area of blank paper. This is an example of a phenomenon known as *filling in*. Since your brain no longer has any signal indicating a change in the visual stimulus at that location, it simply fills in the most probable stimulus, in this case a uniform white piece of paper. The strength of this filling in can be illustrated by using Figure 1.7(b) to probe your blind spot. In this case, with your left eye closed, fixate the cross with your right eye and adjust the viewing distance until the gap in the line disappears when it falls on your blind spot. Amazingly the perception is that of a continuous line since that is now the most probable visual stimulus. If you prefer to perform these exercises using your left eye, simply turn the book upside down to find the blind spot on the other side of your visual field.

The filling in phenomenon goes a long way to explain the function of the visual system. The signals present in the ganglion cells represent only local changes in the visual stimulus. Effectively, only information about spatial or temporal transitions (i.e., edges) is transmitted to the brain. Perceptually this code is sorted out by examining the nature of the changes and filling in the appropriate uniform perception until a new transition is signaled. This coding provides tremendous savings in bandwidth to transmit the signal and can be thought of as somewhat similar to run-length encoding that is sometimes used in digital imaging.

1.3 VISUAL SIGNAL PROCESSING

The neural processing of visual information is quite complex within the retina and becomes significantly, if not infinitely, more complex at later

stages. This section provides a brief overview of the paths that some of this information takes. It is helpful to begin with a general map of the steps along the way. The optical image on the retina is first transduced into chemical and electrical signals in the photoreceptors. These signals are then processed through the network of retinal neurons (horizontal, bipolar, amacrine, and ganglion cells) described above. The ganglion cell axons gather to form the optic nerve, which projects to the lateral geniculate nucleus (LGN) in the thalamus. The LGN cells, after gathering input from the ganglion cells, project to visual area one (V1) in the occipital lobe of the cortex. At this point, the information processing begins to become amazingly complex. Approximately 30 visual areas have been defined in the cortex with names such as V2, V3, V4, MT, etc. Signals from these areas project to several other areas and vice versa. The cortical processing includes many instances of feed-forward, feed-back, and lateral processing. Somewhere in this network of information our ultimate perceptions are formed. A few more details of these processes are described in the following paragraphs.

Light incident on the retina is absorbed by photopigments in the various photoreceptors. In rods, the photopigment is *rhodopsin*. Upon absorbing a photon, rhodopsin changes in structure, setting off a chemical chain reaction that ultimately results in the closing of ion channels in its cell walls which produce an electrical signal based on the relative concentrations of various ions (e.g., sodium and potassium) inside and outside the cell wall. A similar process takes place in cones. Rhodopsin is made up of *opsin* and *retinal*. Cones have similar photopigment structures. However, in cones the ‘cone-opsins’ have slightly different molecular structures resulting in the various spectral responsivities observed in the cones. Each type of cone (*L*, *M*, or *S*) contains a different form of ‘cone-opsin.’ Figure 1.8 illustrates the relative responses of the photoreceptors as a function of retinal exposure.

It is interesting to note that these functions show characteristics similar to those found in all imaging systems. At the low end of the receptor responses there is a threshold, below which the receptors do not respond. There is then a fairly linear portion of the curves, followed by response saturation at the high end. Such curves are representations of the photocurrent at the receptors and represent the very first stage of visual processing. These signals are then processed through the retinal neurons and synapses until a transformed representation is generated in the ganglion cells for transmission through the optic nerve.

Receptive Fields

For various reasons, including noise suppression and transmission speed, the amplitude-modulated signals in the photoreceptors are converted into frequency-modulated representations at the ganglion-cell and higher levels. In these, and indeed most, neural cells the magnitude of the signal is represented in terms of the number of spikes of voltage per second fired by the

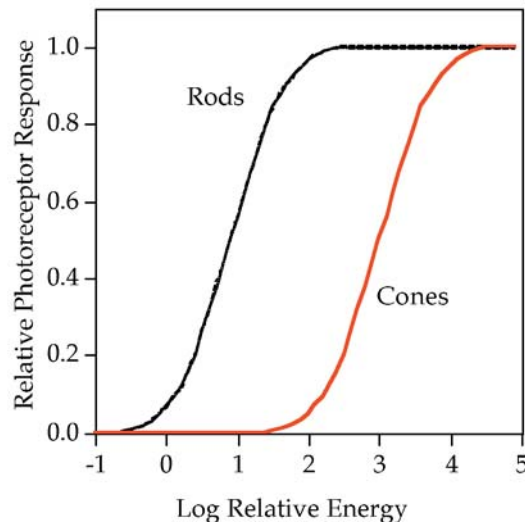


Figure 1.8 Relative energy responses for the rod and cone photoreceptors

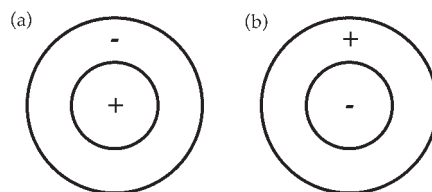


Figure 1.9 Typical center-surround antagonistic receptive fields: (a) on-center, (b) off-center

cell rather than by the voltage difference across the cell wall. To represent the physiological properties of these cells, the concept of receptive fields becomes useful.

A *receptive field* is a graphical representation of the area in the visual field to which a given cell responds. In addition, the nature of the response (e.g., positive, negative, spectral bias) is typically indicated for various regions in the receptive field. As a simple example, the receptive field of a photoreceptor is a small circular area representing the size and location of that particular receptor's sensitivity in the visual field. Figure 1.9 represents some prototypical receptive fields for ganglion cells. They illustrate center-surround antagonism, which is characteristic at this level of visual processing. The receptive field in Figure 1.9(a) illustrates a positive central response, typically generated by a positive input from a single cone, surrounded by a negative surround response, typically driven by negative inputs from several neighboring cones. Thus the response of this ganglion cell is made up of inputs from a number of cones with both positive and negative signs. The result is that

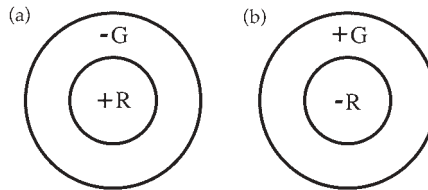


Figure 1.10 Examples of (a) red–green and (b) green–red spectrally and spatially antagonistic receptive fields

the ganglion cell does not simply respond to points of light, but serves as an edge detector (actually a ‘spot’ detector). Readers familiar with digital image processing can think of the ganglion cell responses as similar to the output of a convolution kernel designed for edge detection.

Figure 1.9(b) illustrates that a ganglion cell response of opposite polarity is equally likely. The response in Figure 1.9(a) is considered an *on-center ganglion cell* while that in Figure 1.9(b) is called an *off-center ganglion cell*. Often on-center and off-center cells will occur at the same spatial location, fed by the same photoreceptors, resulting in an enhancement of the system’s dynamic range.

Note that the ganglion cells represented in Figure 1.9 will have no response to uniform fields (given that the positive and negative areas are balanced). This illustrates one aspect of the image compression carried out in the retina. The brain is not bothered with redundant visual information; only information about changes in the visual world is transmitted. This spatial information processing in the visual system is the fundamental basis of the important impact of the background on color appearance. Figure 1.9 illustrates spatial opponency in ganglion cell responses. Figure 1.10 shows that in addition to spatial opponency, there is often spectral opponency in ganglion cell responses. Figure 1.10(a) shows a red–green opponent response with the center fed by positive input from an *L* cone and the surround fed by negative input from *M* cones. Figure 1.10(b) illustrates the off-center version of this cell. Thus, before the visual information has even left the retina, processing has occurred with a profound affect on color appearance.

Figures 1.9 and 1.10 illustrate typical ganglion cell receptive fields. There are other types and varieties of ganglion cell responses, but they all share these basic concepts. On their way to the primary visual cortex, visual signals pass through the LGN. While the ganglion cells do terminate at the LGN, making synapses with LGN cells, there appears to be a one-to-one correspondence between ganglion cells and LGN cells. Thus, the receptive fields of LGN cells are identical to those of ganglion cells. The LGN appears to act as a relay station for the signals. However, it probably serves some visual function since there are neural projections from the cortex back to the LGN that could serve as some type of switching or adaptation feedback mechanism. The axons of LGN cells project to visual area one (V1) in the visual cortex.

Processing in Area V1

In area V1 of the cortex, the encoding of visual information becomes significantly more complex. Much as the outputs of various photoreceptors are combined and compared to produce ganglion cell responses, the outputs of various LGN cells are compared and combined to produce cortical responses. As the signals move further up in the cortical processing chain, this process repeats itself with the level of complexity increasing very rapidly to the point that receptive fields begin to lose meaning. In V1, cells can be found that selectively respond to various types of stimuli, including

- Oriented edges or bars
- Input from one eye, the other, or both
- Various spatial frequencies
- Various temporal frequencies
- Particular spatial locations
- Various combinations of these features

In addition, cells can be found that seem to linearly combine inputs from LGN cells and others with nonlinear summation. All of these various responses are necessary to support visual capabilities such as the perceptions of size, shape, location, motion, depth, and color. Given the complexity of cortical responses in V1 cells, it is not difficult to imagine how complex visual responses can become in an interwoven network of approximately 30 visual areas.

Figure 1.11 schematically illustrates a small portion of the connectivity of the various cortical areas that have been identified. Bear in mind that Figure 1.11 is showing connections of areas, not cells. There are of the order of 10⁹ cortical neurons serving visual functions. At these stages it becomes

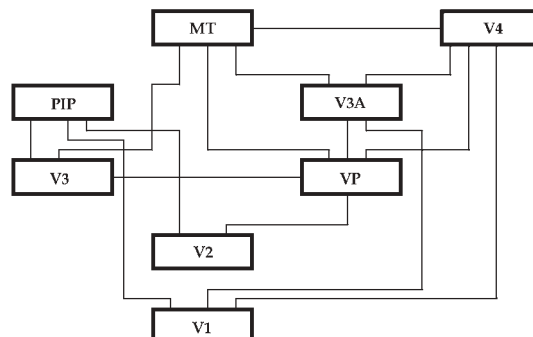


Figure 1.11 Partial flow diagram to illustrate the many streams of visual information processing in the visual cortex. Information can flow in both directions along each connection

exceedingly difficult to explain the function of single cortical cells in simple terms. In fact, the function of a single cell might not have meaning since the representation of various perceptions must be distributed across collections of cells throughout the cortex. Rather than attempting to explore the physiology further, the following sections will describe some of the overall perceptual and psychophysical properties of the visual system that help to specify its performance.

1.4 MECHANISMS OF COLOR VISION

Historically, there have been many theories that attempt to explain the function of color vision. A brief look at some of the more modern concepts provides useful insight into current concepts.

Trichromatic Theory

In the later half of the 19th century, the *trichromatic theory of color vision* was developed, based on the work of Maxwell, Young, and Helmholtz. They recognized that there must be three types of receptors, approximately sensitive to the red, green, and blue regions of the spectrum, respectively. The trichromatic theory simply assumed that three images of the world were formed by these three sets of receptors and then transmitted to the brain where the ratios of the signals in each of the images was compared in order to sort out color appearances. The trichromatic (three-receptor) nature of color vision was not in doubt, but the idea of three images being transmitted to the brain is both inefficient and fails to explain several visually observed phenomena.

Hering's Opponent-Colors Theory

At around the same time, Hering proposed an *opponent-colors theory of color vision* based on many subjective observations of color appearance. These observations included appearance of hues, simultaneous contrast, afterimages, and color vision deficiencies. Hering noted that certain hues were never perceived to occur together. For example, a color perception is never described as reddish-green or yellowish-blue, while combinations of red and yellow, red and blue, green and yellow, and green and blue are readily perceived. This suggested to Hering that there was something fundamental about the red-green and yellow-blue pairs causing them to oppose one another. Similar observations were made of simultaneous contrast in which objects placed on a red background appear greener, on a green background appear redder, on a yellow background appear bluer, and on a blue background appear yellower. Figure 1.12 demonstrates the opponent nature of visual afterimages. The afterimage of red is green, green is red, yellow



Figure 1.12 Stimulus for the demonstration of opponent afterimages. Fixate upon the black spot in the center of the four colored squares for about 30 seconds then move your gaze to fixate the black spot in the uniform white area. Note the colors of the afterimages relative to the colors of the original stimuli

is blue, and blue is yellow. (It is worth noting that afterimages can also be easily explained in terms of complementary colors due to adaptation in a trichromatic system. Hering only referred to light-dark afterimages in support of opponent theory, not chromatic afterimages.) Lastly, Hering observed that those with color vision deficiencies lose the ability to distinguish hues in red-green or yellow-blue pairs.

All of these observations provide clues regarding the processing of color information in the visual system. Hering proposed that there were three types of receptors, but Hering's receptors had bipolar responses to light-dark, red-green, and yellow-blue. At the time, this was thought to be physiologically implausible and Hering's opponent theory did not receive appropriate acceptance.

Modern Opponent-Colors Theory

In the middle of the 20th century, Hering's opponent theory enjoyed a revival of sorts when quantitative data supporting it began to appear. For example, Svaetichin (1956) found opponent signals in electrophysiological measurements of responses in the retinas of goldfish (which happen to be trichromatic!). DeValois *et al.* (1958), found similar opponent physiological responses in the LGN cells of the macaque monkey. Jameson and Hurvich (1955) also added quantitative psychophysical data through their hue-cancellation experiments with human observers that allowed measurement of the relative spectral sensitivities of opponent pathways. These data, combined with

the overwhelming support of much additional research since that time, have led to the development of the modern opponent theory of color vision (sometimes called a *stage theory*) as illustrated in Figure 1.13.

Figure 1.13 illustrates that the first stage of color vision, the receptors, is indeed trichromatic as hypothesized by Maxwell, Young, and Helmholtz. However, contrary to simple trichromatic theory, the three ‘color-separation’ images are not transmitted directly to the brain. Instead the neurons of the retina (and perhaps higher levels) encode the color into opponent signals. The outputs of all three cone types are summed ($L + M + S$) to produce an achromatic response that matches the CIE $V(\lambda)$ curve as long as the summation is taken in proportion to the relative populations of the three cone types. Differencing of the cone signals allows construction of red-green ($L - M + S$) and yellow-blue ($L + M - S$) opponent signals. The transformation from LMS signals to the opponent signals serves to decorrelate the color information carried in the three channels, thus allowing more efficient signal transmission and reducing difficulties with noise. The three opponent pathways also have distinct spatial and temporal characteristics that are important for predicting color appearance. They are discussed further in Section 1.5.

The importance of the transformation from trichromatic to opponent signals for color appearance is reflected in the prominent place that it finds within the formulation of all color appearance models. Figure 1.13 includes not only a schematic diagram of the neural ‘wiring’ that produces opponent responses, but also the relative spectral responsivities of these mechanisms both before and after opponent encoding.

Adaptation Mechanisms

However, it is not enough to consider the processing of color signals in the human visual system as a static ‘wiring diagram.’ The dynamic mechanisms of adaptation that serve to optimize the visual response to the particular viewing environment at hand must also be considered. Thus an overview of the various types of adaptation is in order. Of particular relevance to the study of color appearance are the mechanisms of dark, light, and chromatic adaptation.

Dark Adaptation

Dark adaptation refers to the change in visual sensitivity that occurs when the prevailing level of illumination is decreased, such as when walking into a darkened theater on a sunny afternoon. At first the entire theater appears completely dark, but after a few minutes one is able to clearly see objects in the theater such as the aisles, seats, and other people. This happens because the visual system is responding to the lack of illumination by becoming more sensitive and therefore capable of producing a meaningful visual response at the lower illumination level.

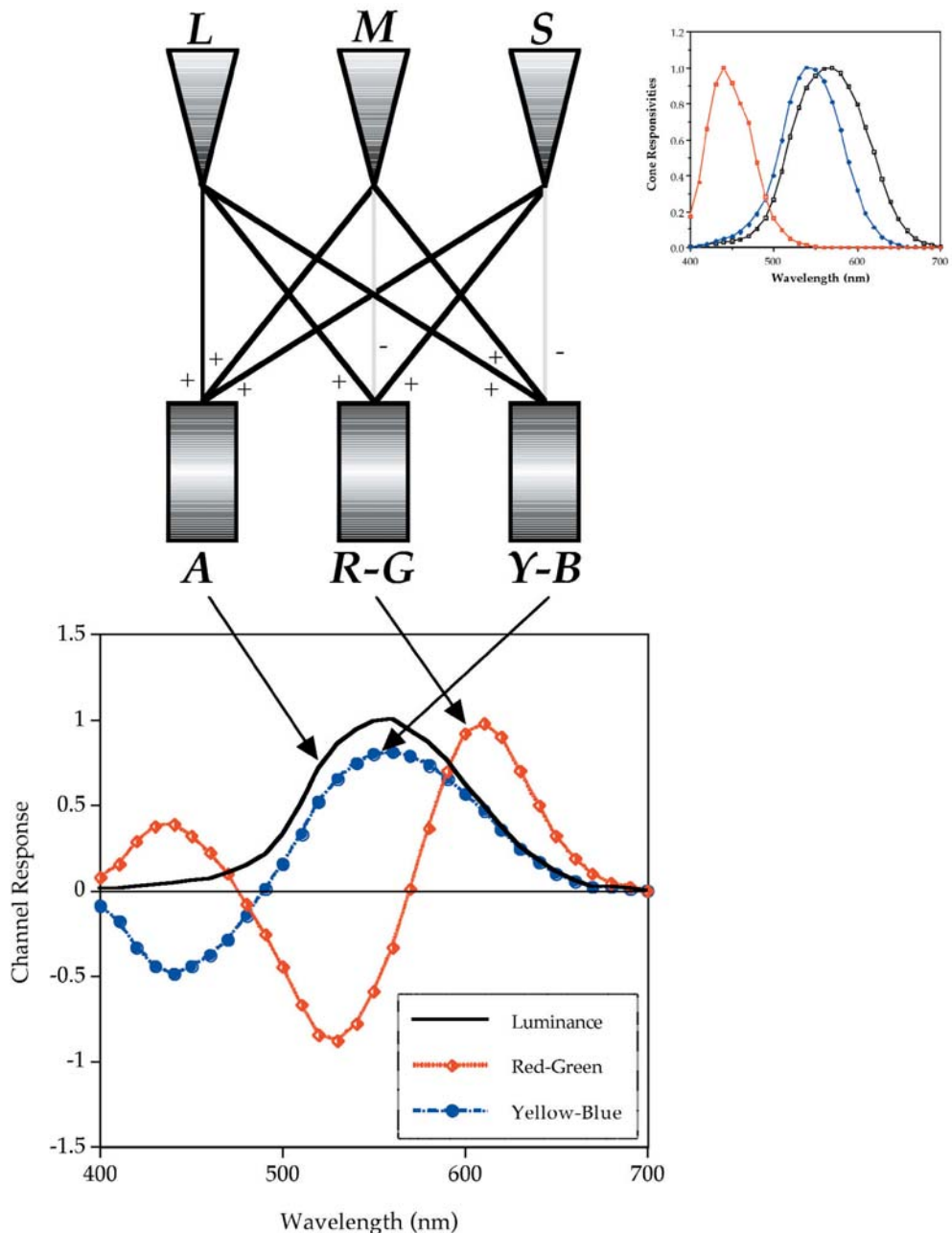


Figure 1.13 Schematic illustration of the encoding of cone signals into opponent-color signals in the human visual system

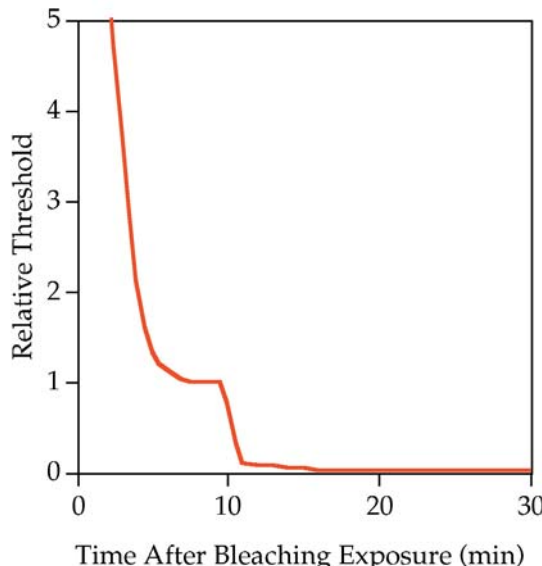


Figure 1.14 Dark-adaptation curve showing the recovery of threshold after a bleaching exposure. The break in the curve illustrates the point at which the rods become more sensitive than the cones

Figure 1.14 shows the recovery of visual sensitivity (decrease in threshold) after transition from an extremely high illumination level to complete darkness. At first, the cones gradually become more sensitive until the curve levels off after a couple of minutes. Then, until about 10 minutes have passed, visual sensitivity is roughly constant. At that point, the rod system, with a longer recovery time, has recovered enough sensitivity to outperform the cones and thus the rods begin controlling overall sensitivity. The rod sensitivity continues to improve until it becomes asymptotic after about 30 minutes.

Recall that the five-fold change in pupil diameter is not sufficient to serve vision over the large range of illumination levels typically encountered. Therefore, neural mechanisms must produce some adaptation. Mechanisms thought to be responsible for various types of adaptation include the following:

- Depletion and regeneration of photopigment
- The rod–cone transition
- Gain control in the receptors and other retinal cells
- Variation of pooling regions across photoreceptors
- Spatial and temporal opponency
- Gain control in opponent and other higher-level mechanisms
- Neural feedback
- Response compression
- Cognitive interpretation

Light Adaptation

Light adaptation is essentially the inverse process of dark adaptation. However, it is important to consider it separately since its visual properties differ. Light adaptation occurs when leaving the darkened theater and returning outdoors on a sunny afternoon. In this case, the visual system must become less sensitive in order to produce useful perceptions since there is significantly more visible energy available.

The same physiological mechanisms serve light adaptation, but there is an asymmetry in the forward and reverse kinetics resulting in the time course of light adaptation being on the order of 5 minutes rather than 30 minutes. Figure 1.15 illustrates the utility of light adaptation. The visual system has a limited output dynamic range, say 100:1, available for the signals that produce our perceptions. The world in which we function, however, includes illumination levels covering at least 10 orders of magnitude from a starlit night to a sunny afternoon. Fortunately, it is almost never important to view the entire range of illumination levels at the same time. If a single response function were used to map the large range of stimulus intensities into the visual system's output, then only a small range of the available output would be used for any given scene. Such a response is shown by the dashed line in Figure 1.15. Clearly, with such a response function, the

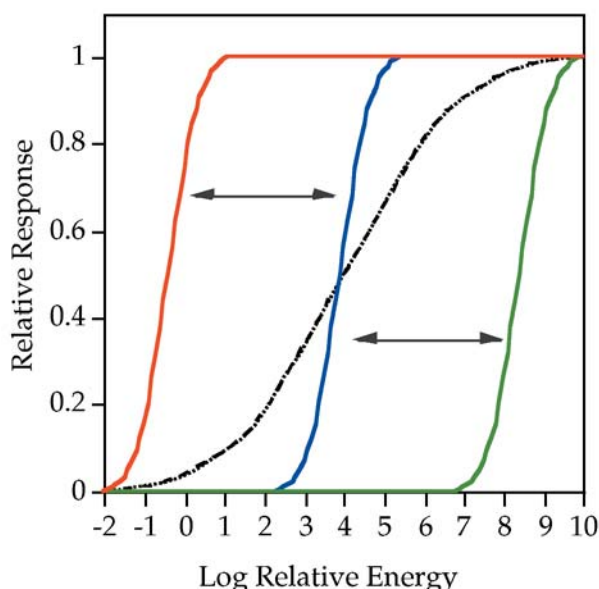


Figure 1.15 Illustration of the process of light adaptation whereby a very large range of stimulus intensity levels can be mapped into a relatively limited response dynamic range. Solid curves show a family of adapted responses. Dashed curve shows a hypothetical response with no adaptation

perceived contrast of any given scene would be limited and visual sensitivity to changes would be severely degraded due to signal-to-noise issues.

On the other hand, light adaptation serves to produce a family of visual response curves as illustrated by the solid lines in Figure 1.15. These curves map the useful illumination range in any given scene into the full dynamic range of the visual output, thus resulting in the best possible visual perception for each situation. Light adaptation can be thought of as the process of sliding the visual response curve along the illumination level axis in Figure 1.15 until the optimum level for the given viewing conditions is reached. Light and dark adaptation can be thought of as analogous to an automatic exposure control in a photographic system.

Chromatic Adaptation

The third type of adaptation, closely related to light and dark adaptation, is *chromatic adaptation*. Again, similar physiological mechanisms are thought to produce chromatic adaptation. Chromatic adaptation is the largely independent sensitivity control of the three mechanisms of color vision. This is illustrated schematically in Figure 1.16, which shows that the overall height of the three cone spectral responsivity curves can vary independently. While chromatic adaptation is often discussed and modeled as independent sensitivity control in the cones, there is no reason to believe that it does not occur in opponent and other color mechanisms as well.

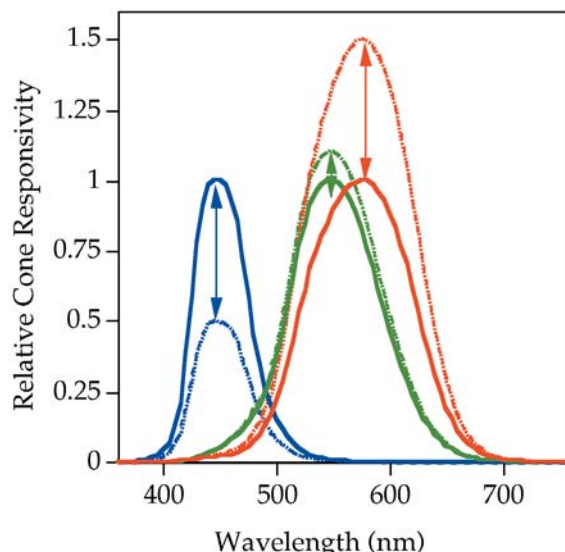


Figure 1.16 Conceptual illustration of the process of chromatic adaptation as the independent sensitivity regulation of the three cone responsivities

Chromatic adaptation can be observed by examining a white object, such as a piece of paper, under various types of illumination (e.g., daylight, fluorescent, and incandescent). Daylight contains relatively far more short-wavelength energy than fluorescent light, and incandescent illumination contains relatively far more long-wavelength energy than fluorescent light. However, the paper approximately retains its white appearance under all three light sources. This is because the S-cone system becomes relatively less sensitive under daylight to compensate for the additional short-wavelength energy and the L-cone system becomes relatively less sensitive under incandescent illumination to compensate for the additional long-wavelength energy.

Chromatic adaptation can be thought of as analogous to an automatic white-balance in video cameras. Figure 1.17 provides a visual demonstration of chromatic adaptation in which the two halves of the visual field are conditioned to produce disparate levels of chromatic adaptation. Given its fundamental importance in color appearance modeling, chromatic adaptation is covered in more detail in Chapter 8.

Visual Mechanisms Impacting Color Appearance

There are many important cognitive visual mechanisms that impact color appearance. These are described in further detail in Chapters 6–8. They include memory color, color constancy, discounting the illuminant, and object recognition.

- *Memory color* refers to the phenomenon that recognizable objects often have a prototypical color that is associated with them. For example, most people have a memory for the typical color of green grass and can produce a stimulus of this color if requested to do so in an experiment. Interestingly, the memory color often is not found in the actual objects. For example, green grass and blue sky are typically remembered as being more saturated than the actual stimuli.
- *Color constancy* refers to the everyday perception that the colors of objects remain unchanged across significant changes in illumination color and luminance level. Color constancy is served by the mechanisms of chromatic adaptation and memory color and can easily be shown to be very poor when careful observations are made.
- *Discounting the illuminant* refers to an observer's ability to automatically interpret the illumination conditions and perceive the colors of objects after discounting the influences of illumination color.
- *Object recognition* is generally driven by the spatial, temporal, and light-dark properties of the objects rather than by chromatic properties (Davidoff 1991).

Thus once the objects are recognized, the mechanisms of memory color and discounting the illuminant can fill in the appropriate color. Such mechanisms

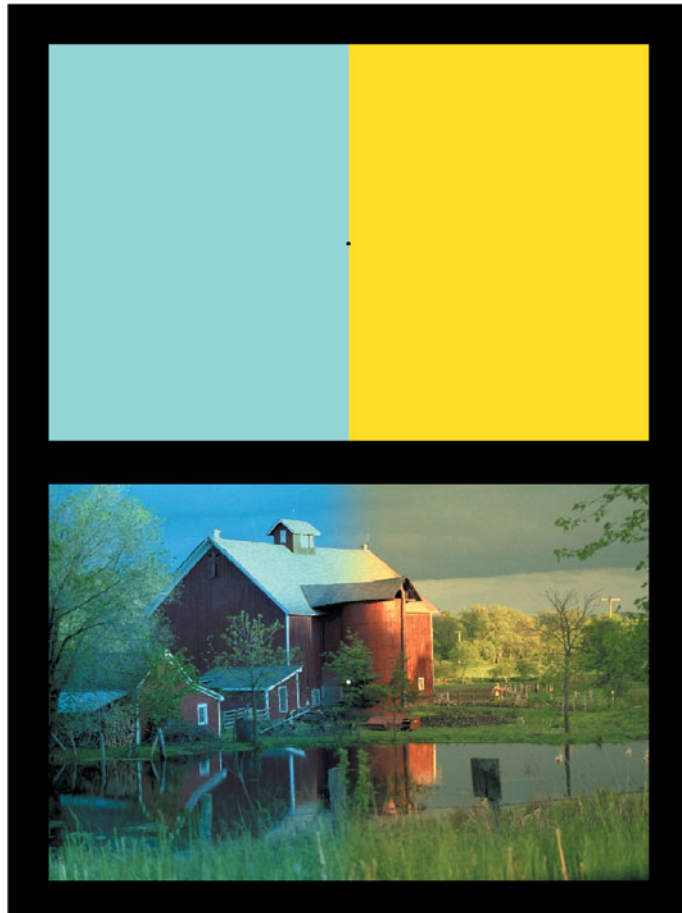


Figure 1.17 A demonstration of retinally localized chromatic adaptation. Fixate the black spot in between the uniform blue and yellow areas for about 30 seconds then shift your gaze to the white spot in the center of the barn image. Note that the barn image appears approximately uniform after this adaptation. Original barn image from Kodak Photo Sampler PhotoCD

have fascinating impacts on color appearance and become of critical importance when performing color comparisons across different media.

Clearly, visual information processing is extremely complex and not yet fully understood (perhaps it never will be). It is of interest to consider the increasing complexity of cortical visual responses as the signal moves through the visual system. Single-cell electrophysiological studies have found cortical cells with extremely complex driving stimuli. For example, cells in monkeys that respond only to images of monkey paws or faces have been occasionally found in physiological experiments. The existence of such cells raises the question of how complex a single-cell response can become.

Clearly it is not possible for every perception to have its own cortical cell. Thus, at some point in the visual system, the representation of perceptions must be distributed with combinations of various signals producing various perceptions. Such distributed representations open up the possibilities for numerous permutations on a given perception, such as color appearance. It is clear from the large number of stimulus variables that impact color appearance that our visual system is often experimenting with these permutations.

1.5 SPATIAL AND TEMPORAL PROPERTIES OF COLOR VISION

No dimension of visual experience can be considered in isolation. The color appearance of a stimulus is not independent of its spatial and temporal characteristics. For example, a black and white stimulus flickering at an appropriate temporal frequency can be perceived as quite colorful. The spatial and temporal characteristics of the human visual system are typically explored through measurement of *contrast sensitivity functions*. Contrast sensitivity functions (CSFs) in vision science are analogous to modulation transfer functions (MTFs) in imaging science. However, CSFs cannot legitimately be considered MTFs since the human visual system is highly nonlinear and CSFs represent threshold sensitivity and not suprathreshold modulation. A contrast sensitivity function is defined by the threshold response to contrast (sensitivity is the inverse of threshold) as a function of spatial or temporal frequency. *Contrast* is typically defined as the difference between maximum and minimum luminance in a stimulus divided by the sum of the maximum and minimum luminances, and CSFs are typically measured with stimuli that vary sinusoidally across space or time. Thus a uniform pattern has a contrast of zero and sinusoidal patterns with troughs that reach a luminance of zero have a contrast of 1.0, no matter what their mean luminance is.

Figure 1.18 conceptually illustrates typical spatial contrast sensitivity functions for luminance (black–white) and chromatic (red–green and yellow–blue at constant luminance) contrast. The luminance contrast sensitivity function is band-pass in nature, with peak sensitivity around 5 cycles per degree. This function approaches zero at zero cycles per degree, illustrating the tendency for the visual system to be insensitive to uniform fields. It also approaches zero at about 60 cycles per degree, the point at which detail can no longer be resolved by the optics of the eye or the photoreceptor mosaic. The band-pass contrast sensitivity function correlates with the concept of center-surround antagonistic receptive fields that would be most sensitive to an intermediate range of spatial frequency. The chromatic mechanisms are of a low-pass nature and have significantly lower cutoff frequencies. This indicates the reduced availability of chromatic information for fine details (high spatial frequencies) that is often taken advantage of in image coding and compression schemes (e.g., NTSC or JPEG).

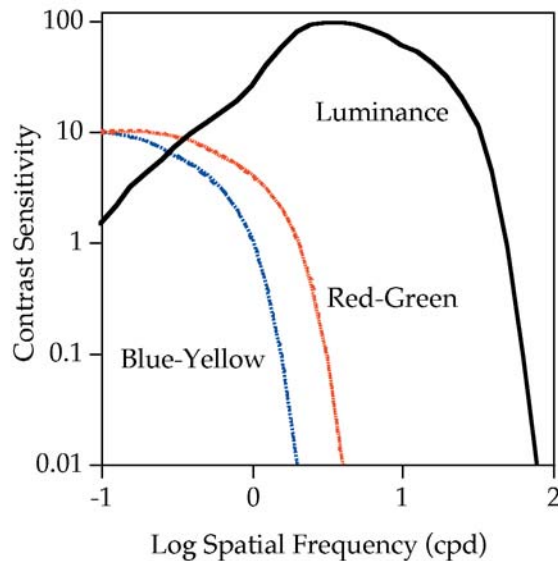


Figure 1.18 Spatial contrast sensitivity functions for luminance and chromatic contrast

The low-pass characteristics of the chromatic mechanisms also illustrate that edge detection/enhancement does not occur along these dimensions. The blue–yellow chromatic CSF has a lower cutoff frequency than the red–green chromatic CSF due to the scarcity of S cones in the retina. It is also of note that the luminance CSF is significantly higher than the chromatic CSFs, indicating that the visual system is more sensitive to small changes in luminance contrast compared with chromatic contrast. The spatial CSFs for luminance and chromatic contrast are generally not directly incorporated in color appearance models although there is significant interest in doing so. Zhang and Wandell (1996) presented an interesting technique for incorporating these types of responses into the CIELAB color space calculations. Johnson and Fairchild (2003b) provide a more recent implementation of the model.

Figure 1.19 illustrates the spatial properties of color vision with a spatial analysis of a typical image. Figure 1.19(a) shows the original image. The luminance information is presented alone in Figure 1.19(b) and the residual chromatic information is presented alone in Figure 1.19(c). It is clear that far more spatial detail can be visually obtained from the luminance image than from the chromatic residual image. This is further illustrated in Figure 1.19(d), in which the image has been reconstructed using the full-resolution luminance image combined with the chromatic image after subsampling by a factor of four. This form of image compression produces no noticeable degradation in perceived resolution or color.

Figure 1.20 conceptually illustrates typical temporal contrast sensitivity functions for luminance and chromatic contrast. They share many



Figure 1.19 Illustration of the spatial properties of color vision: (a) original image, (b) luminance information only, (c) chromatic information only, (d) reconstruction with full resolution luminance information combined with chromatic information subsampled by a factor of four. Original motorcycles image from Kodak Photo Sampler PhotoCD

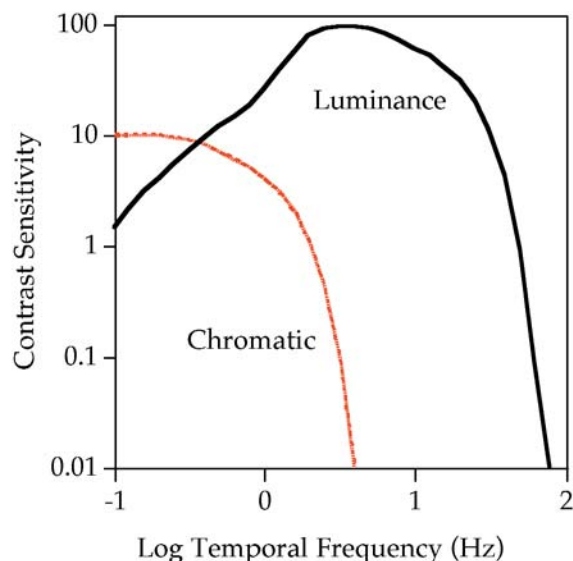


Figure 1.20 Temporal contrast sensitivity functions for luminance and chromatic contrast

characteristics with the spatial CSFs shown in Figure 1.18. Again, the luminance temporal CSF is higher in both sensitivity and cutoff frequency than the chromatic temporal CSFs, and it shows band-pass characteristics suggesting the enhancement of temporal transients in the human visual system. Again, temporal CSFs are not directly incorporated in color appearance models, but they might be of importance to consider when viewing time-varying images such as digital video clips that might be rendered at differing frame rates.

It is important to realize that the functions in Figures 1.18 and 1.20 are typical and not universal. As stated earlier, the dimensions of human visual perception cannot be examined independently. The spatial and temporal CSFs interact with one another. A spatial CSF measured at different temporal frequencies will vary tremendously and the same is true for a temporal CSF measured at various spatial frequencies. These functions also depend on other variables such as luminance level, stimulus size, retinal locus. See Kelly (1994) for a detailed treatment of these interactions.

The Oblique Effect

An interesting spatial vision phenomenon is the *oblique effect*. This refers to the fact that visual acuity is better for gratings oriented at 0° or 90° (relative to the line connecting the two eyes) than for gratings oriented at 45° . This phenomenon is considered in the design of rotated halftone screens that are set up such that the most visible pattern is oriented at 45° . The effect can be observed by taking a black-and-white halftone newspaper image and adjusting the viewing distance until the halftone dots are just barely imperceptible. If the image is kept at this viewing distance and then rotated 45° , the halftone dots will become clearly perceptible (since they will then be oriented at 0° or 90°).

CSFs and Eye Movements

The spatial and temporal CSFs are also closely linked to the study of eye movements. A static spatial pattern becomes a temporally varying pattern when observers move their eyes across the stimulus. Noting that both the spatial and temporal luminance CSFs approach zero as either form of frequency variation approaches zero, it follows that a completely static stimulus is invisible. This is indeed the case. If the retinal image can be fixed using a video feedback system attached to an eye tracker, the stimulus does disappear after a few seconds (Kelly 1994). (Sometimes this can be observed by carefully fixating an object and noting that the perceptions of objects in the periphery begin to fade away after a few seconds. The centrally fixated object does not fade away since the ability to hold the eye completely still has variance greater than the high spatial resolution in the fovea.)

To avoid this rather unpleasant phenomenon in typical viewing, our eyes are constantly moving. Large eye movements take place to allow viewing of different areas of the visual field with the high-resolution fovea. Also, there are small constant eye movements that serve to keep the visual world nicely visible. This also explains why the shadows of retinal cells and blood vessels are generally not visible since they do not move *on* the retina, but rather move *with* the retina. The history of eye movements has significant impact on adaptation and appearance through integrated exposure of various retinal areas and the need for movements to preserve apparent contrast. Recent technological advances have allowed psychophysical investigation of these effects (e.g., Babcock *et al.* 2003).

1.6 COLOR VISION DEFICIENCIES

There are various types of inherited and acquired color vision deficiencies. Kaiser and Boynton (1996) provide a current and comprehensive overview of the topic. This section concentrates on the most common inherited deficiencies.

Protanopia, Deutanopia, and Tritanopia

Some color vision deficiencies are caused by the lack of a particular type of cone photopigment. Since there are three types of cone photopigments, there are three general classes of these color vision deficiencies, namely protanopia, deutanopia, and tritanopia. An observer with protanopia, known as a protanope, is missing the *L*-cone photopigment and therefore is unable to discriminate reddish and greenish hues since the red-green opponent mechanism cannot be constructed. A deutanope is missing the *M*-cone photopigment and therefore also cannot distinguish reddish and greenish hues due to the lack of a viable red-green opponent mechanism. Protanopes and deutanopes can be distinguished by their relative luminous sensitivity since it is constructed from the summation of different cone types. The protanopic luminous sensitivity function is shifted toward shorter wavelengths. A tritanope is missing the *S*-cone photopigment and therefore cannot discriminate yellowish and bluish hues due to the lack of a yellow-blue opponent mechanism.

Anomalous Trichromacy

There are also anomalous trichromats who have trichromatic vision, but the ability to discriminate particular hues is reduced either due to shifts in the spectral sensitivities of the photopigments or contamination of photopigments (e.g., some *L*-cone photopigment in the *M*-cones). Among the anomalous trichromats are those with any of the following:

- Protanomaly (weak in *L*-cone photopigment or *L*-cone absorption shifted toward shorter wavelengths)
- Deuteranomaly (weak in *M*-cone photopigment or *M*-cone absorption shifted toward longer wavelengths)
- Tritanomaly (weak in *S*-cone photopigment or *S*-cone absorption shifted toward longer wavelengths).

There are also some cases of cone monochromatism (effectively only one cone type) and rod monochromatism (no cone responses).

While it is impossible for a person with normal color vision to experience what the visual world looks like to a person with a color vision deficiency, it is possible to illustrate the hues that become indistinguishable. Figure 1.21 provides such a demonstration. To produce Figure 1.21, the two color-normal images (Figure 1.21a) processed according to a simulation algorithm published by Brettel *et al.* (1997) as implemented at <www.vischeck.com> to generate the images. This allows an illustration of the various colors that would be confused by protanopes, deutanopes, and tritanopes. The study of color vision deficiencies is of more than academic interest in the field of color appearance modeling and color reproduction. This is illustrated in Table 1.1 showing the approximate percentages of the population with various types of color vision deficiencies.

It is clear from Table 1.1 that color deficiencies are not extremely rare, particularly in the male population (about 8%) and that it might be important to account for the possibility of color deficient observers in many applications.

Color Vision Deficiencies and Gender

Why the disparity between the occurrence of color vision deficiencies in males and females? This can be traced back to the genetic basis of color vision deficiencies. It turns out that the most common forms of color vision deficiencies are sex-linked genetic traits.

The genes for photopigments are present on the X chromosome. Females inherit one X chromosome from their mother and one from their father. Only one of these need have the genes for the normal photopigments in order to produce normal color vision. On the other hand, males inherit an X chromosome from their mother and a Y chromosome from their father. If the single X chromosome does not include the genes for the photopigments, the son will have a color vision deficiency. If a female is color deficient, it means she has two deficient X chromosomes and all male children are destined to have a color vision deficiency. It is clear that the genetic 'deck of cards' is stacked against males when it comes to inheriting deficient color vision.

Knowledge regarding the genetic basis of color vision has grown tremendously in recent years. John Dalton was an early investigator of deficient color vision. He studied his own vision, which was formerly thought to have been protanopic based on his observations, and came up with a theory as to



Figure 1.21 Images illustrating the color discrimination capabilities that are missing from observers with various color vision deficiencies: (a) original images, (b) protanope, (c) deutanope, (d) tritanope. Original birds image from Kodak Photo Sampler PhotoCD. Original girls image from the author. Images were processed at <www.vischeck.com>

the cause of his deficiencies. Dalton hypothesized that his color vision deficiency was caused by a coloration of his vitreous humor causing it to act like a filter. Upon his death, he donated his eyes to have them dissected to experimentally confirm his theory. Unfortunately Dalton's theory was incorrect. However, Dalton's eyes have been preserved to this day in a museum in Manchester, UK. D.M. Hunt *et al.* (1995) performed DNA tests on Dalton's preserved eyes and were able to show that Dalton was a deutanope rather than a protanope, but with an *L*-cone photopigment having a spectral responsivity shifted toward the shorter wavelengths. They were also able to

Table 1.1 Approximate percentage occurrences of various color vision deficiencies.
Based on data in Hunt (1991a)

Type	Male (%)	Female (%)
Protanopia	1.0	0.02
Deutanopia	1.1	0.01
Trianopia	0.002	0.001
Cone monochromatism	~0	~0
Rod monochromatism	0.003	0.002
Protanomaly	1.0	0.02
Deutanomaly	4.9	0.38
Tritanomaly	~0	~0
Total	8.0	0.4

complete a colorimetric analysis to show that their genetic results were consistent with the observations originally recorded by Dalton.

Screening Observers Who Make Color Judgements

Given the fairly high rate of occurrence of color vision deficiencies, it is necessary to screen observers prior to allowing them to make critical color appearance or color matching judgements. There are a variety of tests available, but two types, pseudoisochromatic plates and the Farnsworth–Munsell 100-Hue test, are of practical importance.

Pseudoisochromatic plates (e.g., Ishihara's Tests for Colour-Blindness) are color plates made up of dots of random lightness that include a pattern or number in the dots formed out of an appropriately contrasting hue. The random lightness of the dots is a design feature to avoid discrimination of the patterns based on lightness difference only. The plates are presented to observers under properly controlled illumination and they are asked to respond by either tracing the pattern or reporting the number observed. Various plates are designed with color combinations that would be difficult to discriminate for observers with the different types of color vision deficiencies. These tests are commonly administered as part of a normal ophthalmological examination and can be obtained from optical suppliers and general scientific suppliers. Screening with a set of pseudoisochromatic plates should be considered as a minimum evaluation for anyone carrying out critical color judgements.

The Farnsworth–Munsell 100-Hue test, available through the Munsell Color company, consists of four sets of chips that must be arranged in an orderly progression of hue. Observers with various types of color vision deficiencies will make errors in the arrangement of the chips at various locations around the hue circle. The test can be used to distinguish between the different types of deficiencies and also to evaluate the severity of color

discrimination problems. This test can also be used to identify observers with normal color vision, but poor color discrimination for all colors.

1.7 KEY FEATURES FOR COLOR APPEARANCE MODELING

This chapter provides a necessarily brief overview of the form and function of the human visual system, concentrating on the features that are important in the study, modeling, and prediction of color appearance phenomena. What follows is a short review of the key features.

Important features in the optics of the eye include the lens, macula, and cone photoreceptors. The lens and macula impact color matching through their action as yellow filters. They impact inter-observer variability since their optical density varies significantly from person to person. The cones serve as the first stage of color vision, transforming the spectral power distribution on the retina into a three-dimensional signal that defines what is available for processing at higher levels in the visual system. This is the basis of metamerism, the fundamental governing principle of colorimetry.

The numerical distribution of the cones ($L:M:S$ of about 12:6:1) is important in constructing the opponent signals present in the visual system. Proper modeling of these steps requires the ratios to be accounted for appropriately. The spatial distribution of rods and cones and their lateral interactions are critical in the specification of stimulus size and retinal locus. A color appearance model for stimuli viewed in the fovea would be different from one for peripheral stimuli. The spatial interaction in the retina, represented by horizontal and amacrine cells, is critical for mechanisms that produce color appearance effects due to changes in background, surround, and level of adaptation.

The encoding of color information through the opponent channels along with the adaptation mechanisms before, during, and after this stage are perhaps the most important feature of the human visual system that must be incorporated into color appearance models. Each such model incorporates a chromatic adaptation stage, an opponent processing stage, and nonlinear response functions. Some models also incorporate light and dark adaptation effects and interactions between the rod and cone systems.

Lastly, the cognitive mechanisms of vision such as memory color and discounting the illuminant have a profound impact on color appearance. These and other color appearance phenomena are described in greater detail in Chapters 6–8.

2

Psychophysics

Clearly, an understanding of the basic function of the human visual system is necessary for appreciation of the formulation, implementation, and application of color appearance models. The need for a basic understanding of the principles of psychophysics might not seem so clear. Psychophysical techniques have produced most of our knowledge of human color vision and color appearance phenomena. These are the underpinnings of colorimetry and its extension through color appearance models. Also, psychophysical techniques are used to test, compare, and generate data for improving color appearance models. Thus to fully understand the use and evaluation of color appearance models, a basic appreciation of the field of psychophysics is essential. As an added bonus, psychophysical techniques such as those described in this chapter can help to prove that the implementation of a color appearance model truly improves a system.

This chapter provides an overview of experimental design and data analysis techniques for visual experiments. Carefully conducted visual experiments allow accurate quantitative evaluation of perceptual phenomena that are often thought of as being completely subjective. Such results can be of immense value in a wide variety of fields, including color measurement and the evaluation of perceived image quality. Issues regarding the choice and design of viewing environments, an overview of various classes of visual experiments, and a review of experimental techniques for threshold, matching, and scaling experiments are also described. Data reduction and analysis procedures are also briefly discussed. The treatment of psychophysics presented in this chapter is based on the ASTM Standard Guide for Designing and Conducting Visual Experiments (ASTM 1996), which was based on materials from the RIT course work of this book's author. There are several excellent texts on psychophysics that provide additional details on the topics covered in this chapter. Of particular note are those of Gescheider (1985), Bartleson and Grum (1984), Torgerson (1958), and Thurstone (1959). Unfortunately, the last three references are out of print and can only be found in libraries. An interesting overview of the application of psychophysics

to image quality has been presented by Engeldrum (1995). The text by Engeldrum (2000) on psychometric scaling provides an excellent, modern review of psychophysical techniques and their application.

2.1 PSYCHOPHYSICS DEFINED

Psychophysics is the scientific study of the relationships between the physical measurements of stimuli and the sensations and perceptions that those stimuli evoke. Psychophysics can be considered a discipline of science similar to the more traditional disciplines such as physics, chemistry, and biology.

The tools of psychophysics are used to derive quantitative measures of perceptual phenomena that are often considered subjective. It is important to note that the results of properly designed psychophysical experiments are just as objective and quantitative as the measurement of length with a ruler (or any other physical measurement). One important difference is that the uncertainties associated with psychophysical measurements tend to be significantly larger than those of physical measurements. However, the results are equally useful and meaningful as long as those uncertainties are considered (as they always should be for physical measurements as well). Psychophysics is used to study all dimensions of human perception. Since the topic of this book is color appearance, visual psychophysics is specifically discussed.

Two Classes of Visual Experiments

Visual experiments tend to fall into two broad classes:

1. Threshold and matching experiments, designed to measure visual sensitivity to small changes in stimuli (or perceptual equality)
2. Scaling experiments, intended to generate a relationship between the physical and perceptual magnitudes of a stimulus

It is critical to first determine which class of experiment is appropriate for a given application. Threshold experiments are appropriate for measuring sensitivity to changes and the detectability of stimuli. For example, threshold experiments could be used to determine whether an image compression algorithm was truly visually lossless or if the performance of two color appearance models is perceptibly different in some practical application.

Scaling experiments are appropriate when it is necessary to specify the relationships between stimuli. For example, a scaling experiment might be used to develop a quantitative relationship between the perceived quality of a printed image and the spatial addressability of the printer. In color

appearance modeling, the results of scaling experiments are used to derive relationships between physically measurable colorimetric quantities (e.g., CIE XYZ tristimulus values) and perceptual attributes such as lightness, chroma, and hue.

2.2 HISTORICAL CONTEXT

As with any scientific discipline, a better appreciation of psychophysics can be obtained with a brief look at the historical development of the field. While scientists have been making and recording careful observations of their perceptions for centuries, the formal discipline of psychophysics is less than 150 years old. Important milestones in the history of psychophysics can be represented in the work of Weber, Fechner, and Stevens.

Weber's Work

In the early part of the 19th century, E.H. Weber investigated the perception of the heaviness of lifted weights. Weber asked observers to lift a given weight and then he added to the weight (with all of the necessary experimental controls) until the observers could just distinguish the new weight from the original. This is a measurement of the threshold for change in weight. Weber noted that as the initial weight increased, the change in weight required to reach a threshold increased proportionally. If the initial magnitude of the stimulus (weight in this case) is denoted I , and the change required to achieve a threshold is denoted ΔI , Weber's results can be expressed by stating that the ratio $\Delta I/I$ is constant. In fact, this general relationship holds approximately true for many perceptual stimuli and has come to be known as *Weber's law*.

Weber's result is quite intuitive. For example, imagine carrying a few sheets of paper and then adding a 20-page document to the load. Clearly the difference between the two weights would be perceived. Now imagine carrying a briefcase full of books and papers and then adding another 20-page document to the case. Most likely the added weight of 20 more pages would go unnoticed. That is because a greater change is required to reach a perceptual threshold when the initial stimulus intensity is higher. Weber's law can also be used to explain why stars cannot be seen during the daytime. At night, the stars represent a certain increment in intensity ΔI over the background illumination of the sky I , that exceeds the visual threshold and therefore they can be seen. During the day, the stars still produce the same increment in intensity ΔI over the background illumination. However, the background intensity of the daytime sky I is much larger than at night. Therefore the ratio $\Delta I/I$ is far lower during the day than at night. So low, in fact, that the stars cannot be perceived during the day.

Fechner's Work

The next milestone is the work of Fechner. Fechner built on the work of Weber to derive a mathematical relationship between stimulus intensity and perceived magnitude. While Fechner's motivation was to solve the mind-body problem by proving that functions of the mind could be physically measured, he inadvertently became known as the father of psychophysics through his publication of *Elements of Psychophysics* in 1860 (Fechner 1966).

Fechner started with two basic assumptions:

1. Weber's law was indeed valid.
2. A just-noticeable difference (JND) can be considered a unit of perception.

Weber's results showed that the JNDs measured on the physical scale were not equal as the stimulus intensity increased, but rather increased in proportion to the stimulus intensity. Fechner strived to derive a transformation of the physical stimulus intensity scale to a perceptual magnitude scale on which the JNDs were of equal size for all perceptual magnitudes. This problem essentially becomes one of solving the differential equation posed by Weber's law. Since JNDs followed a geometric series on the stimulus intensity scale, the solution is straightforward, that a logarithmic transformation will produce JNDs of equal incremental size on a perceptual scale. Thus the JNDs represented by equal ratios on the physical scale become transformed into equal increments on a perceptual scale according to what has come to be known as *Fechner's law*.

Simply put, Fechner's law states that the perceived magnitude of a stimulus is proportional to the logarithm of the physical stimulus intensity. This relationship is illustrated in Figure 2.1. Fechner's law results in a compressive nonlinear relationship between the physical measurement and perceived magnitude that illustrates a decreasing sensitivity (i.e., slope of the curve in Figure 2.1) with increasing stimulus intensity. If Fechner's law were strictly valid, then the relationship would follow the same nonlinear form for all perceptions. While the general trend of a compressive nonlinearity is valid for most perceptions, various perceptions take on relationships with differently shaped functions. This means that Fechner's law is not completely accurate. However, there are numerous examples in the vision science literature of instances in which Fechner's law (or at least Weber's law) is obeyed.

Stevens' Work

Addressing the lack of generality in Fechner's result, Stevens (1961) published an intriguing paper entitled 'To honor Fechner and repeal his law.' Stevens studied the relationship between physical stimulus intensity and perceptual magnitude for over 30 different types of perceptions using a mag-

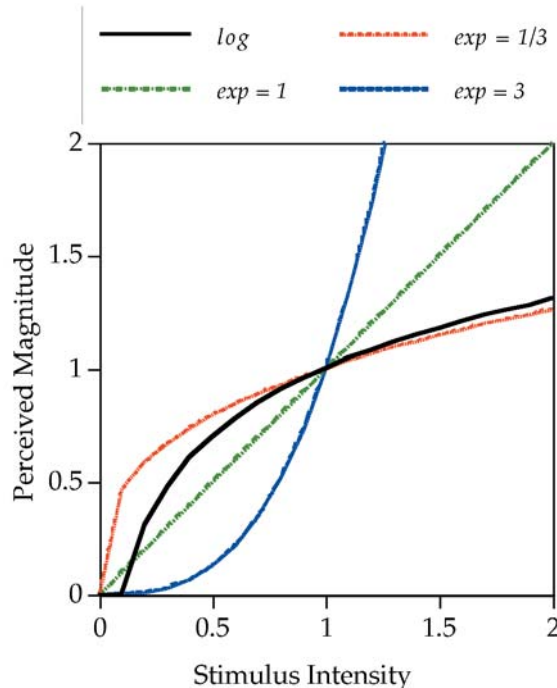


Figure 2.1 Various psychophysical response functions including the logarithmic function suggested by Fechner and power-law relationships with various exponents as suggested by Stevens

nitude estimation technique. Stevens found that his results produced straight lines when the logarithm of perceived magnitude was plotted as a function of the logarithm of stimulus intensity. However, the straight lines for various perceptions had different slopes. Straight lines on log–log coordinates are equivalent to power functions on linear coordinates with the slopes of the lines on the log–log coordinates equivalent to the exponents of the power functions on linear axes. Thus, Stevens hypothesized that the relationship between perceptual magnitude and stimulus intensity followed a power law with various exponents for different perceptions rather than Fechner’s logarithmic function. This result is often referred to as the *Stevens power law*.

Figure 2.1 illustrates three power law relationships with differing exponents. When the exponent is less than unity, a power law follows a compressive nonlinearity typical of most perceptions. When the exponent is equal to unity, the power law becomes a linear relationship. While there are few examples of perceptions that are linearly related to physical stimulus intensity, an important one is the relationship between perceived and physical length over short distances. A power law with an exponent greater than unity results in an expansive nonlinearity. Such perceptual relationships do exist in cases where the stimulus might be harmful and thus result in the

perception of pain. A compressive function for the pain perception could be quite dangerous since the observer would become less and less sensitive to the stimulus as it became more and more dangerous.

The Stevens power law can be used to model many perceptual phenomena, and can be found in fundamental aspects of color measurement such as the relationship between CIE XYZ tristimulus values and the predictors of lightness and chroma in the CIELAB color space that are based on a cube-root compressive power-law nonlinearity.

2.3 HIERARCHY OF SCALES

When deriving perceived magnitude scales, it is critical to understand the properties of the resulting scales. Often a psychophysical technique will produce a scale with only limited mathematical utility. In such cases it is critical that inappropriate mathematical manipulations are not applied to the scale. Four key types of scales have been defined. In order of increasing mathematical power and complexity, they are nominal, ordinal, interval, and ratio scales.

Nominal Scales

Nominal scales are relatively trivial in that they scale items simply by name; for color a nominal scale could consist of reds, yellows, greens, blues, and neutrals. Scaling in this case would simply require deciding which color belonged in which category. Only naming can be performed with nominal data.

Ordinal Scales

Ordinal scales are scales in which elements are sorted in ascending or descending order based on greater or lesser amount of a particular attribute. A set of color swatches could be sorted by hue and then in each hue range the colors could be sorted from the lightest to the darkest. Since the swatch colors are not evenly spaced, there might be three dark, one medium, and two light green swatches. If these were numbered from one to six in order of increasing lightness, an ordinal scale would be created. There is no information on such a scale as to how much lighter one of the green swatches is than another and it is clear that they are not evenly spaced. For an ordinal scale all that matters is that the samples be arranged in increasing or decreasing amounts of an attribute. The spacing between samples can be large or small and can change up and down the scale. Logical operations such as greater-than, less-than, or equal-to can be performed with ordinal scales.

Interval Scales

Interval scales have equal intervals. On an interval scale if a pair of samples was separated by two units and a second pair at some other point on the scale was also separated by two units, the differences between the pairs would be perceptually equal. However, there is no meaningful zero point on an interval scale. In addition to the mathematical operations listed for the above scales, addition and subtraction can be performed with interval data. The Celsius and Fahrenheit temperature scales are interval scales.

Ratio Scales

Ratio scales have all the properties of the above scales plus a meaningfully defined zero point. Thus it is possible to properly equate ratios of numbers on a ratio scale. Ratio scales in visual work are often difficult and sometimes impossible to obtain. This is sometimes the case since a meaningful zero point does not exist. For example, an interval scale of image quality is relatively easy to derive, but try to imagine an image with zero quality. Similarly it is relatively straightforward to derive interval scales of hue, but there is no physically meaningful zero hue. All of the mathematical operations that can be performed on an interval scale can also be performed on a ratio scale. In addition, multiplication and division can be performed.

Example of the Use of Scales

It is helpful to reinforce the concepts of the hierarchy of scales by example. Imagine that it is necessary to measure the heights of all the people in a room. If only a nominal scale were available, you could choose a first subject and assign a name to his or her height, say Joe. Then you could examine the height of each additional subject relative to the height of Joe. If another person had the same height as Joe (assuming some reasonable tolerance), their height would also be assigned the name Joe. If their height differed from Joe, they would be given a different name. This process could be completed by comparing the heights of everyone in the room until each unique height was assigned a unique name. Note that there is no information regarding who is taller or shorter than anyone else. The only information available is whether subjects share the same height (and therefore name) or not.

If, instead, an ordinal scale was used to measure height. Joe could arbitrarily be assigned a height of zero. If the next subject was taller than Joe, he or she would be assigned any number larger than Joe's, say 10. If a third subject was found to be taller than Joe, but shorter than the second subject, they would be assigned a number between zero and 10. This would continue until everyone in the room was assigned a number to represent their height. Since the magnitude of the numbers was assigned arbitrarily, nothing can

be said about how much shorter or taller one subject is than another. However they could be put in order from shortest to tallest.

If an interval scale was available for measurement of height, Joe could again be arbitrarily assigned a height of zero. However, other subjects could then be assigned heights relative to Joe's in terms of meaningful increments such as +3 cm (taller than Joe) or -2 cm (shorter than Joe). If subjects A and B had heights of +3 cm and -2 cm, respectively on this interval scale, it can be determined that subject A is 5 cm taller than subject B. Note however that there is still no information to indicate how tall either of the subjects is. The only information available with the interval scale are differences between subjects.

Finally, if a ratio scale is available to measure height (the normal situation), Joe might be measured and found to be 182 cm tall. Then subjects A and B would have heights of 185 cm and 180 cm, respectively. If another subject came along who was 91 cm tall, it could be concluded that Joe is twice as tall as this subject. Since zero cm tall is a physically meaningful zero point, a true ratio scale is available for the measurement of height and thus multiplications and divisions of scale values can be performed.

2.4 THRESHOLD TECHNIQUES

Threshold experiments are designed to determine the just-perceptible change in a stimulus, sometimes referred to as a just-noticeable difference (JND). Threshold techniques are used to measure the observers' sensitivity to changes in a given stimulus. Absolute thresholds are defined as the just-perceptible difference for a change from no stimulus, while difference thresholds represent the just-perceptible difference from a particular stimulus level greater than zero. Thresholds are reported in terms of the physical units used to measure the stimulus. For example, a brightness threshold might be measured in luminance units of cd/m^2 . Sensitivity is defined as the inverse of the threshold since a low threshold implies high sensitivity. Threshold techniques are useful for defining visual tolerances such as those for perceived color differences.

Types of Threshold Experiments

There are several basic types of threshold experiments presented below in order of increasing complexity of experimental design and utility of the data generated. Many modifications of these techniques have been developed for particular applications. Experimenters strive to design experiments that remove as much control of the results from the observers as possible, thus minimizing the influence of variable observer judgement criteria. Generally

this comes at the cost of implementing more complicated experimental procedures. Threshold techniques include the following:

- Method of adjustment
- Method of limits
- Method of constant stimuli

Method of Adjustment

The method of adjustment is the simplest and most straightforward technique for deriving threshold data. In it, the observer controls the stimulus magnitude and adjusts it to a point that is just perceptible (absolute threshold), or just perceptibly different (difference threshold) from a starting level. The threshold is taken to be the average setting across a number of trials by one or more observers. The method of adjustment has the advantage that it is quick and easy to implement. However, a major disadvantage is that the observer is in control of the stimulus. This can bias the results due to variability in observers' criteria and adaptation effects. If an observer approaches the threshold from above, adaptation might result in a higher threshold than if it were approached from below. Often the method of adjustment is used to obtain a first estimate of the threshold to be used in the design of more sophisticated experiments. The method of adjustment is also commonly used in matching experiments, including asymmetric matching experiments used in color appearance studies.

Method of Limits

The method of limits is only slightly more complex than the method of adjustment. In the method of limits, the experimenter presents the stimuli at predefined discrete intensity levels in either ascending or descending series. For an ascending series, the experimenter presents a stimulus, beginning with one that is certain to be imperceptible, and asks the observers to respond 'yes' if they perceive it and 'no' if they do not. If they respond 'no', the experimenter increases the stimulus intensity and presents another trial. This continues until the observer responds 'yes'. A descending series begins with a stimulus intensity that is clearly perceptible and continues until the observers respond 'no' — that is, they cannot perceive the stimulus. The threshold is taken to be the average stimulus intensity at which the transition from 'no' to 'yes' (or 'yes' to 'no') responses occurs for a number of ascending and descending series. Averaging over both types of series minimizes adaptation effects. However, the observers are still in control of their criteria since they can respond 'yes' or 'no' at their own discretion.

Method of Constant Stimuli

In the method of constant stimuli, the experimenter chooses several stimulus intensity levels (typically about 5 or 7) around the level of the threshold. Then each of these stimuli is presented multiple times in random order. Over the trials, the frequency with which each stimulus level is perceived is determined. From such data, a frequency-of-seeing curve, or psychometric function, can be derived that allows determination of the threshold and its uncertainty. The threshold is generally taken to be the intensity at which the stimulus is perceived on 50% of the trials. Psychometric functions can be derived either for a single observer (through multiple trials) or for a population of observers (one or more trials per observer). Two types of response can be obtained:

- Yes–no (or pass–fail)
- Forced choice

Yes–No Method

In a yes–no method of constant stimuli procedure, the observers are asked to respond ‘yes’ if they detect the stimulus (or stimulus change) and ‘no’ if they do not. The psychometric function is then simply the percentage of ‘yes’ responses as a function of stimulus intensity; 50% ‘yes’ responses would be taken as the threshold level. Alternatively, this procedure can be used to measure visual tolerances above threshold by providing a reference stimulus intensity (e.g., a color difference anchor pair) and asking observers to pass stimuli that fall below the intensity of the reference (e.g., a smaller color difference) and fail those that fall above it (e.g., a larger color difference). The psychometric function is then taken to be the percent of fail responses as a function of stimulus intensity and the 50% fail level is deemed to be the point of visual equality.

Forced Choice Procedures

A forced-choice procedure eliminates the influence of varying observer criteria on the results. This is accomplished by presenting the stimulus in one of two intervals defined by either a spatial or temporal separation. The observers are then asked to indicate in which of the two intervals the stimulus was presented. The observers are not allowed to respond that the stimulus was not present and are forced to guess one of the two intervals if they are unsure (hence the name forced choice). The psychometric function is then plotted as the percentage of correct responses as a function of stimulus intensity. The function ranges from 50% correct when the observers are simply guessing to 100% correct for stimulus intensities at which they can

always detect the stimulus. Thus the threshold is defined as the stimulus intensity at which the observers are correct 75% of the time and therefore detecting the stimulus 50% of the time. As long as the observers respond honestly, their criteria, whether liberal or conservative, cannot influence the results.

Staircase Procedures

Staircase procedures are a modification of the forced-choice procedure designed to measure only the threshold point on the psychometric function. Staircase procedures are particularly applicable to situations in which the stimulus presentations can be fully automated. A stimulus is presented and the observer is asked to respond. If the response is correct, the same stimulus intensity is presented again. If the response is incorrect, the stimulus intensity is increased for the next trial. Generally, if the observer responds correctly on three consecutive trials, the stimulus intensity is decreased. The stimulus intensity steps are decreased until some desired precision in the threshold is reached. The sequence of three correct or one incorrect response prior to changing the stimulus intensity will result in a convergence to a stimulus intensity that is correctly identified on 79% of the trials ($0.793 = 0.5$), very close to the nominal threshold level of 75%. Often several independent staircase procedures are run simultaneously to further randomize the experiment. A staircase procedure could also be run with yes-no responses.

Probit Analysis of Threshold Data

Threshold data that generate a psychometric function can be most usefully analyzed using Probit analysis. Probit analysis is used to fit a cumulative normal distribution to the data (psychometric function). The threshold point and its uncertainty can then be easily determined from the fitted distribution. There are also several significance tests that can be performed to verify the suitability of the analyses. Finney (1971) provides details on the theory and application of Probit analysis. Several commercially available statistical software packages can be used to perform Probit analyses.

2.5 MATCHING TECHNIQUES

Matching techniques are similar to threshold techniques except that the goal is to determine when two stimuli are not perceptibly different. Measures of the variability in matching are sometimes used to estimate thresholds. Matching experiments provided the basis for CIE colorimetry through the metameristic matches used to derive color matching functions. For example, if

a given color is perceptually matched by an additive mixture of red, green, and blue primary lights that do not mix to produce a spectral energy distribution that is identical to the test color, then the match is considered metamer. The physical properties of such matches can be used to derive the fundamental responsivities of the human visual system and ultimately be used to derive a system of tristimulus colorimetry as outlined in Chapter 3.

Asymmetric Matching

Matching experiments are often used in the study of chromatic adaptation and color appearance as well. In such cases, asymmetric matches are made. An asymmetric match is a color match made across some change in viewing conditions. For example, a stimulus viewed in daylight illumination might be matched to another stimulus viewed under incandescent illumination to derive a pair of corresponding colors for this change in viewing conditions. Such data can then be used to formulate and test color appearance models designed to account for such changes in viewing condition. One special case of an asymmetric matching experiment is the haploscopic experiment in which one eye views a test stimulus in one set of viewing conditions and the other eye simultaneously views a matching stimulus in a different set of viewing conditions. The observer simultaneously views both stimuli and produces a match.

Memory Matching

Another type of matching experiment that is sometimes used in the study of color appearance is called memory matching. In such experiments observers produce a match to a previously memorized color. Typically such matches are asymmetric to study viewing conditions dependencies. Occasionally memory matches are made to mental stimuli such as an ideal achromatic (gray) color or a unique hue (e.g., a unique red with no blue or yellow content).

2.6 ONE-DIMENSIONAL SCALING

Scaling experiments are intended to derive relationships between perceptual magnitudes and physical measures of stimulus intensity. Depending on the type and dimensionality of the scale required, several approaches are possible. Normally the type of scale required and the scaling method to be used are decided upon before any visual data are collected. One-dimensional scaling requires the assumption that both the attribute to be scaled and the physical variation of the stimulus are one dimensional. Observers are asked to make their judgements on a single perceptual attribute (e.g., how light is

one sample compared with another, what is the quality of the difference between a pair of images). A variety of scaling techniques have been devised for the measurement of one-dimensional psychophysical scales, which are described in the following paragraphs:

- Rank order
- Graphical rating
- Category scaling
- Paired comparisons
- Partition scaling
- Magnitude estimation or production
- Ratio estimation or production

In a rank order experiment, the observer is asked to arrange a given set of samples according to increasing or decreasing magnitudes of a particular perceptual attribute. With a large number of observers the data may be averaged and reranked to obtain an ordinal scale. To obtain an interval scale, certain assumptions about the data need to be made and additional analyses need to be performed. In general it is somewhat dubious to attempt to derive interval scales from rank order data. One of the more reasonable assumptions is to treat the data as if each pair of stimuli were compared, thereby deriving paired comparison data from the rank results.

Graphical rating allows direct determination of an interval scale. Observers are presented stimuli and asked to indicate the magnitude of their perception on a one-dimensional scale with defined endpoints. For example, in a lightness scaling experiment a line might be drawn with one end labeled white and the other end labeled black. When the observers are presented with a medium gray that is perceptually halfway between white and black, they would make a mark on the line at the midpoint. If the sample was closer to white than black, they would make a mark at the appropriate physical location along the line, closer to the end labeled white. The interval scale is taken to be the mean location on the graphical scale for each stimulus. This technique relies on the well-established fact that the perception of length over short distances is linear with respect to physically measured length.

Category scaling is a popular technique for deriving ordinal or interval scales for large numbers of stimuli. An observer is asked to separate a large number of samples into various categories. With several observers, the number of times each particular sample is placed in a category is recorded. For this to be an effective scaling method the samples need to be similar enough that they are not always placed in the distinct categories by different observers or by the same observer on different occasions. Interval scales may be obtained by this method by assuming that the perceptual magnitudes are normally distributed and by making use of the standard normal distribution according to the law of categorical judgements (Torgerson 1954).

When the number of different stimuli is smaller, a paired comparison experiment can be performed. In this method, all samples are presented to the observer in all the possible pairwise combinations, usually one pair at a time (sometimes with a third stimulus as a reference). The proportion of times a particular sample is judged greater in some attribute than each other sample is calculated and recorded. Interval scales can be obtained from such data by applying the law of comparative judgements (Thurstone, 1927). Thurstone's law of comparative judgements and its extensions can be usefully applied to ordinal data (such as paired comparisons and category scaling) to derive meaningful interval scales. The perceptual magnitudes of the stimuli are normally distributed on the resulting scales. Thus, if it is safe to assume that the perceptual magnitudes are normally distributed on the true perceptual scale; these analyses derive the desired scale. They also allow useful evaluation of the statistical significance of differences between stimuli since the power of the normal distribution can be utilized. Torgerson (1958), Bartleson and Grum (1984), and Engeldrum (2000) describe these and other related analyses in detail. ASTM (1996) describes a simple method for deriving confidence limits on Thurstonian interval scales. That technique, while conservative, might be less than optimal and is difficult to derive with statistical rigor. Montag *et al.* (2004) describe a Monte Carlo simulation of the problem and recommends a more appropriate method for deriving confidence intervals. Handley (2001) also describes some related techniques.

A rather direct method for deriving interval scales is through partition scaling. A common method is by equating intervals through bisection. The observer is given two different samples (*A* and *B*) and asked to select a third such that the difference between it and *A* appears equal to the difference between it and *B*. A full interval scale may be obtained by successive bisections.

Ratio scales can be directly obtained through the methods of magnitude estimation or production. In such experiments, the observer is asked to assign numbers to the stimuli according to the magnitude of the perception. Alternatively, observers are given a number and asked to produce a stimulus with that perceptual magnitude. This is one of the few techniques that can be used to generate a ratio scale. It can also be used to generate data for multidimensional scaling by asking observers to scale the differences between pairs of stimuli.

A slightly more complicated technique involves ratio estimation or production. The observer is asked for judgements in one of two ways: (1) select or produce a sample that bears some prescribed ratio to a standard; or (2) given two or more samples, to state the apparent ratios among them. A typical experiment is to give the observers a sample and ask them to find, select, or produce a test sample that is one-half or twice the standard in some attribute. For most practical visual work this method is too difficult to use, either because of the sample preparation or the judgement by the observers. However, it can be also used to generate a ratio scale.

2.7 MULTIDIMENSIONAL SCALING

Multidimensional scaling (MDS) is a method similar to one-dimensional scaling, but it does not require the assumption that the attribute to be scaled is one-dimensional. The dimensionality is found as part of the analysis. In multidimensional scaling, the data are interval or ordinal scales of the similarities or dissimilarities between each of the stimuli, and the resulting output is a multidimensional geometric configuration of the perceptual relationships between the stimuli, as on a map.

The dissimilarity data required for MDS can conveniently be obtained using paired comparison and triadic combination experiments. In a paired comparison experiment, all samples in all possible pairs are presented and the observer is asked to make a magnitude estimation of the perceived difference between each pair. The resulting estimates for each pairwise combination can then be subjected to MDS analyses. In the method of triadic combinations, observers are presented with each possible combination of the stimuli taken three at a time. They are then asked to judge which two of the stimuli in each triad are most similar to one another and which two are most different. The data can then be converted into frequencies of times each pair is judged most similar or most different. These frequency data can then be combined into either a similarity or dissimilarity matrix for use in MDS analyses.

MDS analysis techniques take such similarity or dissimilarity data as input and produce a multidimensional configuration of points representing the relationships and dimensionality of the data. It is necessary to use such techniques when either the perception in question is multidimensional (such as color — hue, lightness, and chroma) or the physical variation in the stimuli is multidimensional. Kruskal and Wish (1978) provide details of these techniques. There are several issues with respect to MDS analyses. There are two classes of MDS: metric, which requires interval data, and non-metric, which only requires ordinal data. Both classes of MDS techniques result in interval-scale output. Various MDS software packages process input data according to specific assumptions regarding the input data, treatment of individual cases, goodness-of-fit metrics (stress), distance metrics (e.g., Euclidean or cityblock), etc. Several commercial statistical software packages provide MDS capabilities.

A classic example of MDS analysis is the construction of a map from data representing the distances between cities (Kruskal and Wish 1978). In this example, a map of the USA is constructed from the dissimilarity matrix of distances between eight cities gathered from a road atlas, as illustrated in Table 2.1.

The dissimilarity data are then analyzed via MDS. Stress (RMS error) is used as a measure of goodness-of-fit in order to determine the dimensionality of the data. In this example, the stress of a one-dimensional fit is about 0.12, while the stress in two or more dimensions is essentially zero. This indicates that a two-dimensional fit, as expected, is appropriate. The results

Table 2.1 Dissimilarity matrix consisting of distances between cities in the USA

	ATL	BOS	CHI	DAL	DEN	LA	SEA	NYC
ATL								
BOS	1037							
CHI	674	963						
DAL	795	1748	917					
DEN	1398	1949	996	781				
LA	2182	2979	2054	1387	1059			
SEA	2618	2976	2013	2078	1307	1131		
NYC	841	206	802	1552	1771	2786	2815	

Table 2.2 Output two-dimensional coordinates for each city in the USA. MDS example

City	Dimension 1	Dimension 2
Atlanta	-0.63	0.40
Boston	-1.19	-0.31
Chicago	-0.36	-0.15
Dallas	0.07	0.55
Denver	0.48	0.00
Los Angeles	1.30	0.36
Seattle	1.37	-0.66
New York City	-1.04	-0.21

output include the coordinates in each of the two dimensions for each of the cities as listed in Table 2.2.

Plotting the coordinates of each city in the two output dimensions will result in a familiar map of the USA, as shown in Figure 2.2. However, it should be noted that dimension 1 goes from east to west and dimension 2 goes from north to south, resulting in a map that has the axes reversed from a traditional map. This illustrates a feature of MDS, namely that the definition of the output dimensions requires *post hoc* analysis by the experimenter. MDS experiments can be used to explore the dimensionality and structure of color appearance spaces (e.g., Indow 1988).

2.8 DESIGN OF PSYCHOPHYSICAL EXPERIMENTS

The previous sections provide an overview of some of the techniques used to derive psychophysical thresholds and scales. However there are many more issues that arise in the design of psychophysical experiments that have a significant impact on the experimental results, particularly when color appearance is concerned. Many of these experimental factors are the key

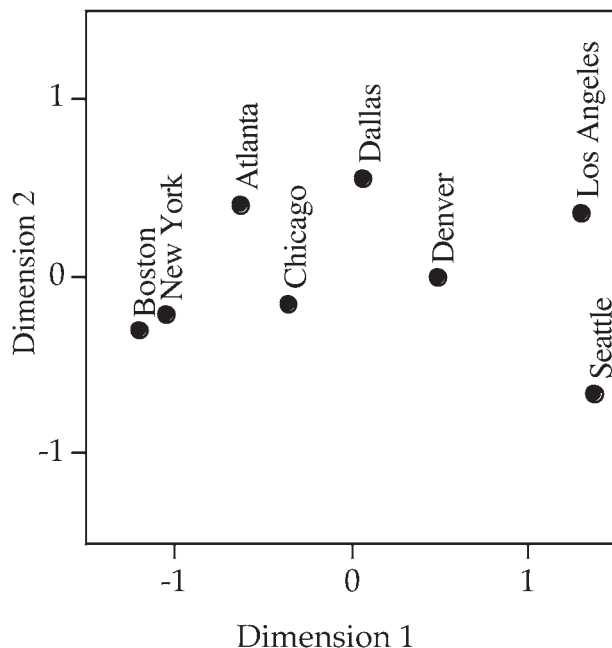


Figure 2.2 The output of a multidimensional scaling (MDS) program used to generate a map of the USA from input data on the proximities of cities

variables that have illustrated the need to extend basic colorimetry with the development of color appearance models. A complete description of all of the variables involved in visual experiments could easily fill several books and many of the critical issues for color appearance phenomena are described in more detail in later chapters. At this point a simple listing of some of the issues that require consideration should be sufficient to bring these issues to light. Important factors in visual experiments include (in no particular order):

Observer age	Control and history of eye movements
Observer experience	Adaptation state
Number of observers	Complexity of observer task
Screening for color vision deficiencies	Controls
Observer acuity	Repetition rate
Instructions	Range effects
Context	Regression effects
Feedback	Image content
Rewards	Number of images
Illumination level	Duration of observation sessions
Illumination color	Number of observation sessions
Illumination geometry	Observer motivation
Background conditions	Cognitive factors
Surround conditions	Statistical significance of results

All these items, and probably many more, can have a profound effect on psychophysical results and should be carefully specified and/or controlled. Such issues need to be addressed both by those performing experiments and by those trying to interpret and utilize the results for various applications.

2.9 IMPORTANCE IN COLOR APPEARANCE MODELING

A fundamental understanding of the processes involved in psychophysical experiments provides useful insight for understanding the need for and development and evaluation of color appearance models. Psychophysical experiments provided much of the information reviewed in Chapter 1 on the human visual system. Psychophysics is the basis of colorimetry presented in Chapter 3. The results of psychophysical experiments are also presented in Chapters 6, 8, and 17 on color appearance phenomena, chromatic adaptation, and testing color appearance models. Simply put, without extensive psychophysical experimentation, none of the information required to create and use color appearance models would exist.

3

Colorimetry

Colorimetry serves as the fundamental underpinning of color appearance specification. This chapter reviews the well-established practice of colorimetry according to the CIE (International Commission on Illumination) system first established in 1931. This system allows the specification of color matches for an average observer and has amazingly withstood an onslaught of technological pressures and remained a useful international standard for over 65 years (Wright 1981b, Fairchild 1993b). However, CIE colorimetry provides only the starting point. Color appearance models enhance this system in an effort to predict the actual appearances of stimuli in various viewing conditions rather than simply whether or not two stimuli will match. This chapter provides a general review of the concepts of colorimetry to set the stage for development of various color appearance models. It is not intended to be a complete reference on colorimetry since there are a number of excellent texts on the subject available. For introductions to colorimetry, readers are referred to the texts of Berns (2000), Hunt (1991a), Berger-Schunn (1994), and Hunter and Harold (1987). The precise definition of colorimetry can be found in the primary reference, *CIE Publication 15.2* (CIE 1986), which is currently being updated to *Publication 15.3*. For complete details in an encyclopedic reference volume, the classic book by Wyszecki and Stiles (1982), *Color Science*, should be consulted. Fundamental insight into the mathematics and theory of visual color matching can be found in the work of Cohen (2001).

3.1 BASIC AND ADVANCED COLORIMETRY

Colorimetry refers to the measurement of color. Wyszecki (1973) described an important distinction between basic and advanced colorimetry (see also Wyszecki 1986). This distinction is the basis of this book and warrants attention. It is perhaps most enlightening to quote Wyszecki's exact words in

making the distinction. Wyszecki's (1973) description of basic colorimetry is as follows.

Colorimetry, in its strict sense, is a tool used to make a prediction on whether two lights (visual stimuli) of different spectral power distributions will match in colour for certain given conditions of observation. The prediction is made by determining the tristimulus values of the two visual stimuli. If the tristimulus values of a stimulus are identical to those of the other stimulus, a colour match will be observed by an average observer with normal colour vision.

Wyszecki (1973) went on to describe the realm of advanced colorimetry.

Colorimetry in its broader sense includes methods of assessing the appearance of colour stimuli presented to the observer in complicated surroundings as they may occur in everyday life. This is considered the ultimate goal of colorimetry, but because of its enormous complexity, this goal is far from being reached. On the other hand, certain more restricted aspects of the overall problem of predicting colour appearance of stimuli seem somewhat less elusive. The outstanding examples are the measurement of colour differences, whiteness, and chromatic adaptation. Though these problems are still essentially unresolved, the developments in these areas are of considerable interest and practical importance.

This chapter describes the well-established techniques of basic colorimetry that form the foundation for color appearance modeling. It also describes some of the widely used methods for color difference measurement, one of the first objectives of advanced colorimetry. Wyszecki's distinction between basic and advanced colorimetry serves to highlight the purpose of this book, an account of the research and modeling aimed at the extension of basic colorimetry toward the ultimate goals of advanced colorimetry.

3.2 WHY IS COLOR?

To begin a discussion of the measurement of color, one must first consider the nature of color. Figure 3.1 illustrates the answer to the question — ‘why is color?’ ‘Why’ is a more appropriate question than the more typical ‘what’ since color is not a simple thing that can be easily described to someone who has never experienced it. Color cannot even be defined without resort to examples (see Chapter 4). Color is an attribute of visual sensation and the color appearance of objects depends on the three components making up the triangle in Figure 3.1. The first requirement is a source of visible electromagnetic energy necessary to initiate the sensory process of vision. This energy is then modulated by the physical and chemical properties of an object. The modulated energy is then imaged by the eye, detected by photoreceptors,

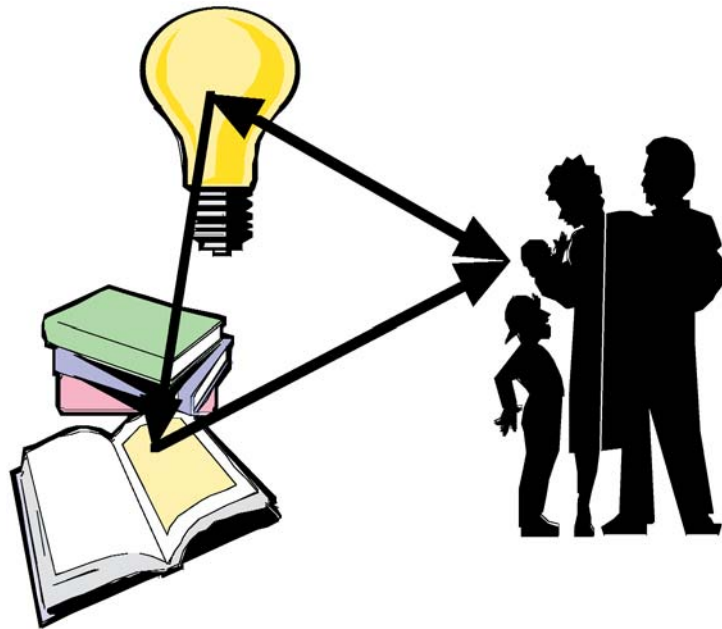


Figure 3.1 The triangle of color. Color exists due to the interaction of light sources, objects, and the human visual system

and processed by the neural mechanisms of the human visual system to produce our perceptions of color. Note that the light source and visual system are also linked in Figure 3.1 to indicate the influence that the light source itself has on color appearance through chromatic adaptation, etc.

Since all three aspects of the triangle in Figure 3.1 are required to produce color, they must also be quantified in order to produce a reliable system of physical colorimetry. Light sources are quantified through their spectral power distribution and standardized as illuminants. Material objects are specified by the geometric and spectral distribution of the energy they reflect or transmit. The human visual system is quantified through its color matching properties that represent the first stage response (cone absorption) in the system. Thus colorimetry, as a combination of all these areas, draws upon techniques and results from the fields of physics, chemistry, psychophysics, physiology, and psychology.

3.3 LIGHT SOURCES AND ILLUMINANTS

The first component of the triangle of color in Figure 3.1 is the light source. Light sources provide the electromagnetic energy required to initiate visual responses. The specification of the color properties of light sources is performed in two ways for basic colorimetry, through measurement and through

standardization. The distinction between these two techniques is clarified in the definition of light sources and illuminants. *Light sources* are actual physical emitters of visible energy. Incandescent light bulbs, the sky at any given moment, and fluorescent tubes represent examples of light sources. *Illuminants*, on the other hand, are simply standardized tables of values that represent a spectral power distribution typical of some particular light source. CIE illuminants A, D65, and F2 are standardized representations of typical incandescent, daylight, and fluorescent sources. Some illuminants have corresponding sources that are physical embodiments of the standardized spectral power distributions. For example, CIE source A is a particular type of tungsten source that produces the relative spectral power distribution of CIE illuminant A. Other illuminants do not have corresponding sources. For example, CIE illuminant D65 is a statistical representation of an average daylight with a correlated color temperature of approximately 6500 K and thus there is no CIE source D65 capable of producing the illuminant D65 spectral power distribution. The importance of distinguishing between light sources and illuminants in color appearance specification is discussed in Chapter 7 (see Table 7.1). Since there are likely to be significant differences between the spectral power distributions of a CIE illuminant and a light source designed to simulate it, the actual spectral power distribution of the light source must be used in colorimetric calculations of stimuli used in color appearance specification.

Spectroradiometry

The measurement of the spectral power distributions of light sources is the realm of spectroradiometry. *Spectroradiometry* is the measurement of radiometric quantities as a function of wavelength. In color measurement, the wavelength region of interest encompasses electromagnetic energy of wavelengths from approximately 400 nm (violet) to 700 nm (red). There are a variety of radiometric quantities that can be used to specify the properties of a light source. Of particular interest in color appearance measurement are irradiance and radiance. Both are measurements of the power of light sources with basic units of watts.

Irradiance is the radiant power per unit area incident onto a surface and has units of watts per square meter (W/m^2). Spectral irradiance adds the wavelength dependency and has units of $\text{W}/\text{m}^2 \text{ nm}$, sometimes expressed as W/m^3 . *Radiance* differs from irradiance in that it is a measure of the power emitted from a source (or surface), rather than incident upon a surface, per unit area per unit solid angle with units of watts per square meter per steradian ($\text{W}/\text{m}^2 \text{ sr}$). Spectral radiance includes the wavelength dependency having units of $\text{W}/\text{m}^2 \text{ sr nm}$ or $\text{W}/\text{m}^3 \text{ sr}$.

Radiance has the interesting properties that it is preserved through optical systems (neglecting absorption) and is independent of distance. Thus, the human visual system responds commensurably to radiance, making it a key

measurement in color appearance specification. The retina itself responds commensurably to the irradiance incident upon it, but in combination with the optics of the eyeball, retinal irradiance is proportional to the radiance of a surface. This can be demonstrated by viewing an illuminated surface from various distances and observing that the perceived brightness does not change (consistent with the radiance of the surface). The irradiance at the eye from a given surface falls off with the square of distance from the surface. Radiance does not fall off in this fashion since the decrease in power incident on the pupil is directly canceled by a proportional decrease in the solid angle subtended by the pupil with respect to the surface in question. The spectral radiance $L(\lambda)$ of a surface with a spectral reflectance factor of $R(\lambda)$ can be calculated from the spectral irradiance $E(\lambda)$ falling upon the surface by using Equation 3.1 with the assumption that the surface is a Lambertian diffuser (i.e., equal radiance in all directions).

$$L(\lambda) = \frac{R(\lambda)E(\lambda)}{\pi} \quad (3.1)$$

A *spectral power distribution* (see Figure 3.2) is simply a plot, or table, of a radiometric quantity as a function of wavelength. Since the overall power levels of light sources can vary over many orders of magnitude, spectral power distributions are often normalized to facilitate comparisons of color properties. The traditional approach is to normalize a spectral power distribution such that it has a value of 100 (or sometimes 1.0) at a wavelength of 560 nm (arbitrarily chosen as near the center of the visible spectrum). Such

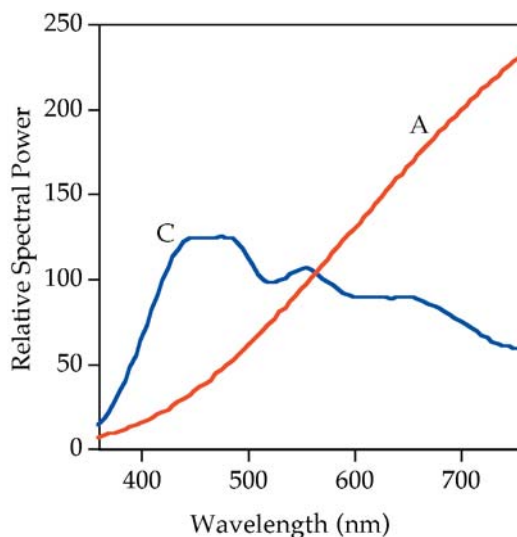


Figure 3.2 Relative spectral power distributions of CIE illuminants A and C

normalized spectral power distributions are referred to as *relative spectral power distributions* and are dimensionless.

Black-body Radiators

Another important radiometric quantity is the color temperature of a light source. A special type of theoretical light source, known as a *black-body radiator*, or *Planckian radiator*, emits energy due only to thermal excitation and is a perfect emitter of energy. The energy emitted by a black body increases in quantity and shifts toward shorter wavelengths as the temperature of the black body increases. The spectral power distribution of a black-body radiator can be specified using Planck's equation as a function of a single variable, absolute temperature (in Kelvin). Thus, if the absolute temperature of a black body is known, so is its spectral power distribution. The temperature of a black body is referred to as its color temperature since it uniquely specifies the color of the source. Since black-body radiators seldom exist outside specialized laboratories, color temperature is not a generally useful quantity. A second quantity, correlated color temperature, is more generally useful. A light source need not be a black-body radiator in order to be assigned a correlated color temperature. The correlated color temperature (CCT) of a light source is simply the color temperature of a black-body radiator that has most nearly the same color as the source in question. As examples, an incandescent source might have a CCT of 2800 K, a typical fluorescent tube 4000 K, an average daylight 6500 K, and the white-point of a computer graphics display 9300 K. As the correlated color temperature of a source increases, it becomes more blue, or less red.

CIE Illuminants

The CIE has established a number of spectral power distributions as CIE illuminants for colorimetry. These include CIE illuminants A, C, D65, D50, F2, F8, and F11:

- CIE illuminant A represents a Planckian radiator with a color temperature of 2856 K and is used for colorimetric calculations when incandescent illumination is of interest.
- CIE illuminant C is the spectral power distribution of illuminant A as modified by particular liquid filters defined by the CIE and represents a daylight simulator with a CCT of 6774 K.
- CIE Illuminants D65 and D50 are part of the CIE D-series of illuminants that have been statistically defined based upon a large number of measurements of real daylight. Illuminant D65 represents an average daylight with a CCT of 6504 K and D50 represents an average daylight with a CCT of 5003 K. D65 is commonly used in colorimetric applications, while D50

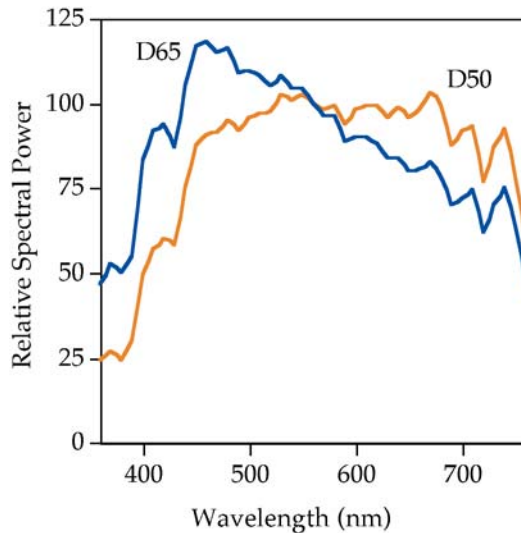


Figure 3.3 Relative spectral power distributions of CIE illuminants D50 and D65

is often used in graphic arts applications. CIE D illuminants with other correlated color temperatures can be easily obtained.

- CIE F illuminants (12 in all) represent typical spectral power distributions for various types of fluorescent sources. CIE illuminant F2 represents a cool-white fluorescent with a CCT of 4230 K, F8 represents a fluorescent D50 simulator with a CCT of 5000 K, and F11 represents a triband fluorescent source with a CCT of 4000 K. Triband fluorescent sources are popular because of their efficiency, efficacy, and pleasing color-rendering properties.
- The equal-energy illuminant (sometimes called illuminant E) is often of mathematical utility. It is defined with a relative spectral power of 100.0 at all wavelengths.

Table 3.1 includes the spectral power distributions and useful colorimetric data for the CIE illuminants described above. The relative spectral power distributions of these illuminants are plotted in Figures 3.2–3.4.

3.4 COLORED MATERIALS

Once the light source or illuminant is specified, the next step in the colorimetry of material objects is the characterization of their interaction with visible radiant energy as illustrated in the second corner of the triangle in Figure 3.1. The interaction of radiant energy with materials obeys the law of conservation of energy. There are only three fates that can befall radiant energy incident on an object—absorption, reflection, and transmission. Thus

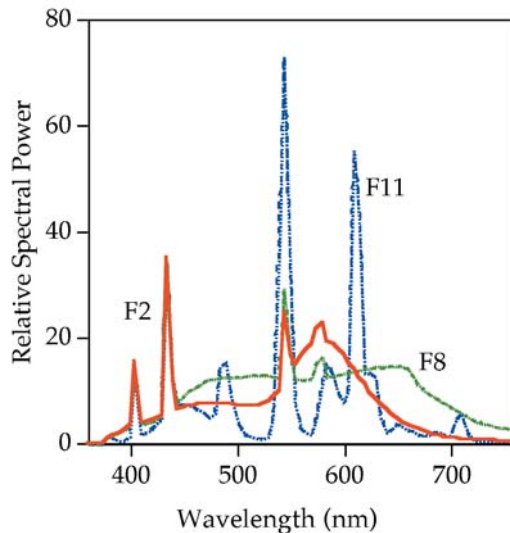


Figure 3.4 Relative spectral power distributions of CIE illuminants F2, F8, and F11

the sum of the absorbed, reflected, and transmitted radiant power must sum to the incident radiant energy at each wavelength as illustrated in Equation 3.2 where $\Phi(\lambda)$ is used as a generic term for incident radiant flux, $R(\lambda)$ is the reflected flux, $T(\lambda)$ is the transmitted flux, and $A(\lambda)$ is the absorbed flux.

$$\Phi(\lambda) = R(\lambda) + T(\lambda) + A(\lambda) \quad (3.2)$$

Reflection, transmission, and absorption are the phenomena that take place when light interacts with matter, and reflectance, transmittance, and absorptance are the quantities measured to describe these phenomena. Since these quantities always must sum to the incident flux, they are typically measured in relative terms as percentages of the incident flux rather than as absolute radiometric quantities. Thus *reflectance* can be defined as the ratio of the reflected energy to the incident energy, *transmittance* as the ratio of transmitted energy to incident energy, and *absorptance* as the ratio of absorbed energy to incident energy. Note that all of these quantities are ratio measurements, the subject of *spectrophotometry*, which is defined as the measurement of ratios of radiometric quantities. Spectrophotometric quantities are expressed as either percentages (0–100%) or as factors (0.0–1.0). Figure 3.5 illustrates the spectral reflectance, transmittance, and absorptance of a red translucent object. Note that since the three quantities sum to 100%, it is typically unnecessary to measure all three. Generally either reflectance or transmittance is of particular interest in a given application.

Table 3.1 Relative spectral power distributions and colorimetric data for some example CIE illuminants. Colorimetric data are for the CIE 1931 standard colorimetric observer (2°)

Wavelength (nm)	A	C	D65	D50	F2	F8	F11
360	6.14	12.90	46.64	23.94	0.00	0.00	0.00
365	6.95	17.20	49.36	25.45	0.00	0.00	0.00
370	7.82	21.40	52.09	26.96	0.00	0.00	0.00
375	8.77	27.50	51.03	25.72	0.00	0.00	0.00
380	6.14	12.90	46.64	23.94	0.00	0.00	0.00
385	6.95	17.20	49.36	25.45	0.00	0.00	0.00
390	7.82	21.40	52.09	26.96	0.00	0.00	0.00
395	8.77	27.50	51.03	25.72	0.00	0.00	0.00
380	9.80	33.00	49.98	24.49	1.18	1.21	0.91
385	10.90	39.92	52.31	27.18	1.48	1.50	0.63
390	12.09	47.40	54.65	29.87	1.84	1.81	0.46
395	13.35	55.17	68.70	39.59	2.15	2.13	0.37
400	14.71	63.30	82.75	49.31	3.44	3.17	1.29
405	16.15	71.81	87.12	52.91	15.69	13.08	12.68
410	17.68	80.60	91.49	56.51	3.85	3.83	1.59
415	19.29	89.53	92.46	58.27	3.74	3.45	1.79
420	21.00	98.10	93.43	60.03	4.19	3.86	2.46
425	22.79	105.80	90.06	58.93	4.62	4.42	3.33
430	24.67	112.40	86.68	57.82	5.06	5.09	4.49
435	26.64	117.75	95.77	66.32	34.98	34.10	33.94
440	28.70	121.50	104.87	74.82	11.81	12.42	12.13
445	30.85	123.45	110.94	81.04	6.27	7.68	6.95
450	33.09	124.00	117.01	87.25	6.63	8.60	7.19
455	35.41	123.60	117.41	88.93	6.93	9.46	7.12
460	37.81	123.10	117.81	90.61	7.19	10.24	6.72
465	40.30	123.30	116.34	90.99	7.40	10.84	6.13
470	42.87	123.80	114.86	91.37	7.54	11.33	5.46
475	45.52	124.09	115.39	93.24	7.62	11.71	4.79
480	48.24	123.90	115.92	95.11	7.65	11.98	5.66
485	51.04	122.92	112.37	93.54	7.62	12.17	14.29
490	53.91	120.70	108.81	91.96	7.62	12.28	14.96
495	56.85	116.90	109.08	93.84	7.45	12.32	8.97
500	59.86	112.10	109.35	95.72	7.28	12.35	4.72
505	62.93	106.98	108.58	96.17	7.15	12.44	2.33
510	66.06	102.30	107.80	96.61	7.05	12.55	1.47
515	69.25	98.81	106.30	96.87	7.04	12.68	1.10
520	72.50	96.90	104.79	97.13	7.16	12.77	0.89
525	75.79	96.78	106.24	99.61	7.47	12.72	0.83
530	79.13	98.00	107.69	102.10	8.04	12.60	1.18
535	82.52	99.94	106.05	101.43	8.88	12.43	4.90
540	85.95	102.10	104.41	100.75	10.01	12.22	39.59
545	89.41	103.95	104.23	101.54	24.88	28.96	72.84
550	92.91	105.20	104.05	102.32	16.64	16.51	32.61
555	96.44	105.67	102.02	101.16	14.59	11.79	7.52
560	100.00	104.11	100.00	100.00	16.16	11.76	2.83

Table 3.1 (continued)

Wavelength (nm)	A	C	D65	D50	F2	F8	F11
565	103.58	102.30	98.17	98.87	17.56	11.77	1.96
570	107.18	100.15	96.33	97.74	18.62	11.84	1.67
575	110.80	97.80	96.06	98.33	21.47	14.61	4.43
580	114.44	95.43	95.79	98.92	22.79	16.11	11.28
585	118.08	93.20	92.24	96.21	19.29	12.34	14.76
590	121.73	91.22	88.69	93.50	18.66	12.53	12.73
595	125.39	89.70	89.35	95.59	17.73	12.72	9.74
600	129.04	88.83	90.01	97.69	16.54	12.92	7.33
605	132.70	88.40	89.80	98.48	15.21	13.12	9.72
610	136.35	88.19	89.60	99.27	13.80	13.34	55.27
615	139.99	88.10	88.65	99.16	12.36	13.61	42.58
620	143.62	88.06	87.70	99.04	10.95	13.87	13.18
625	147.24	88.00	85.49	97.38	9.65	14.07	13.16
630	150.84	87.86	83.29	95.72	8.40	14.20	12.26
635	154.42	87.80	83.49	97.29	7.32	14.16	5.11
640	157.98	87.99	83.70	98.86	6.31	14.13	2.07
645	161.52	88.20	81.86	97.26	5.43	14.34	2.34
650	165.03	88.20	80.03	95.67	4.68	14.50	3.58
655	168.51	87.90	80.12	96.93	4.02	14.46	3.01
660	171.96	87.22	80.21	98.19	3.45	14.00	2.48
665	175.38	86.30	81.25	100.60	2.96	12.58	2.14
670	178.77	85.30	82.28	103.00	2.55	10.99	1.54
675	182.12	84.00	80.28	101.70	2.19	9.98	1.33
680	185.43	82.21	78.28	99.13	1.89	9.22	1.46
685	188.70	80.20	74.00	93.26	1.64	8.62	1.94
690	191.93	78.24	69.72	87.38	1.53	8.07	2.00
695	195.12	76.30	70.67	89.49	1.27	7.39	1.20
700	198.26	74.36	71.61	91.60	1.10	6.71	1.35
705	201.36	72.40	72.98	92.25	0.99	6.16	4.10
710	204.41	70.40	74.35	92.89	0.88	5.63	5.58
715	207.41	68.30	67.98	84.87	0.76	5.03	2.51
720	210.37	66.30	61.60	76.85	0.68	4.46	0.57
725	213.27	64.40	65.74	81.68	0.61	4.02	0.27
730	216.12	62.80	69.89	86.51	0.56	3.66	0.23
735	218.92	61.50	72.49	89.55	0.54	3.36	0.21
740	221.67	60.20	75.09	92.58	0.51	3.09	0.24
745	224.36	59.20	69.34	85.40	0.47	2.85	0.24
750	227.00	58.50	63.59	78.23	0.47	2.65	0.20
755	229.59	58.10	55.01	67.96	0.43	2.51	0.24
760	232.12	58.00	46.42	57.69	0.46	2.37	0.32
X	109.85	98.07	95.05	96.42	99.20	96.43	100.96
Y	100.0	100.0	100.0	100.0	100.0	100.0	100.0
Z	35.58	118.23	108.88	82.49	67.40	82.46	64.37
x	0.4476	0.3101	0.3127	0.3457	0.3721	0.3458	0.3805
y	0.4074	0.3162	0.3290	0.3585	0.3751	0.3586	0.3769
CCT	2856 K	6800 K	6504 K	5003 K	4230 K	5000 K	4000 K

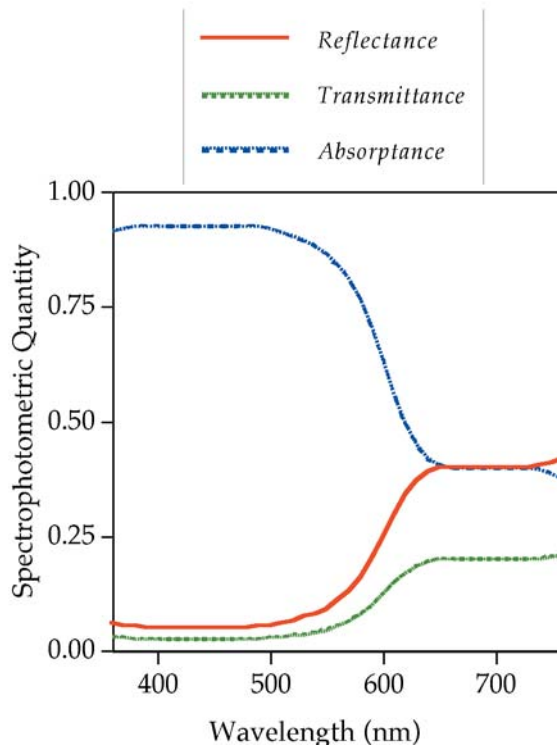


Figure 3.5 Spectral absorptance, reflectance, and transmittance of a red translucent plastic material

Unfortunately (for colorimetrists), the interaction of radiant energy with objects is not just a simple spectral phenomenon. The reflectance or transmittance of an object is not just a function of wavelength, but also a function of the illumination and viewing geometry. Such differences can be illustrated by the phenomenon of gloss. Imagine matte, semigloss, and glossy photographic paper or paint. The various gloss characteristics of these materials can be ascribed to the geometric distribution of the specular reflectance from the surface of the object. This is just one geometric appearance effect. Many others exist such as interesting changes in the color of automotive finishes with illumination and viewing geometry (e.g., metallic, pearlescent, and other ‘effect’ coatings). To fully quantify such effects, complete bidirectional reflectance (or transmittance) distribution functions, BRDFs, must be obtained for each possible combination of illumination angle, viewing angle, and wavelength. Measurement of such functions is prohibitively difficult and expensive, and produces massive quantities of data that are difficult to meaningfully utilize. To avoid this explosion of colorimetric data, a small number of standard illumination and viewing geometries have been established for colorimetry.

CIE Illumination and Viewing Geometries

The CIE has historically defined four standard illumination and viewing geometries for spectrophotometric reflectance measurements. (More detailed designations and specifications will be part of the forthcoming CIE *Publication 15.3* on colorimetry.) These come as two pairs of optically reversible geometries:

1. Diffuse/normal (d/0) and normal/diffuse (0/d)
2. 45/normal (45/0) and normal/45 (0/45)

The designations indicate first the illumination geometry and then the viewing geometry following the slash (/).

Diffuse/Normal and Normal/Diffuse

In the diffuse/normal geometry, the sample is illuminated from all angles using an integrating sphere and viewed at an angle near the normal to the surface. In the normal/diffuse geometry, the sample is illuminated from an angle near to its normal and the reflected energy is collected from all angles using an integrating sphere. These two geometries are optical reverses of one another and therefore produce the same measurement results (assuming all other instrumental variables are constant). The measurements made are of total reflectance. In many instruments, an area of the integrating sphere, corresponding to the angle of specular (regular) reflection of the illumination in a 0/d geometry or the angle from which specular reflection would be detected in a d/0 geometry, can be replaced with a black trap such that the specular component of reflection is excluded and only diffuse reflectance is measured. Such measurements are referred to as 'specular component excluded' measurements as opposed to 'specular component included' measurements made when the entire sphere is intact.

45/Normal and Normal/45

The second pair of geometries is the 45/normal (45/0) and normal/45 (0/45) measurement configurations. In a 45/0 geometry, the sample is illuminated with one or more beams of light incident at an angle of 45° from the normal and measurements are made along the normal. In the 0/45 geometry, the sample is illuminated normal to its surface and measurements are made using one or more beams at a 45° angle to the normal. Again, these two geometries are optical reverses of one another and produce identical results given equality of all other instrumental variables. Use of the 45/0 and 0/45 measurement geometries ensures that all components of gloss are excluded from the measurements. Thus these geometries are typically used in

applications where it is necessary to compare the colors of materials having various levels of gloss (e.g., graphic arts and photography). It is critical to note the instrumental geometry used whenever reporting colorimetric data for materials.

The definition of reflectance as the ratio of reflected energy to incident energy is perfectly appropriate for measurements of total reflectance ($d/0$ or $0/d$). However, for bidirectional reflectance measurements ($45/0$ and $0/45$), the ratio of reflected energy to incident energy is exceedingly small since only a small range of angles of the distribution of reflected energy is detected. Thus, to produce more practically useful values for any type of measurement geometry, reflectance factor measurements are made relative to a perfect reflecting diffuser. A *perfect reflecting diffuser* (PRD) is a theoretical material that is both a perfect reflector (100% reflectance) and perfectly Lambertian (radiance equal in all directions). Thus, measurements of reflectance factor are defined as the ratio of the energy reflected by the sample to the energy that would be reflected by a PRD illuminated and viewed in the identical geometry. For the integrating sphere geometries, measuring total reflectance, this definition of reflectance factor is identical to the definition of reflectance. For the bidirectional geometries, measurement of reflectance factor relative to the PRD results in a zero-to-one scale similar to that obtained for total reflectance measurements. Since PRDs are not physically available, reference standards that are calibrated relative to the theoretical aim are provided by national standardizing laboratories (such as NIST, the National Institute for Standards and Technology, in the USA) and instrument manufacturers.

Fluorescence

One last topic of importance in the colorimetric analysis of materials is fluorescence. Fluorescent materials absorb energy in a region of wavelengths and then emit this energy in a region of longer wavelengths. For example, a fluorescent orange material might absorb blue energy and emit it as orange energy. Fluorescent materials obey the law of conservation of energy as stated in Equation 3.2. However, their behavior is different in that some of the absorbed energy is emitted at (normally) longer wavelengths. A full treatment of the color measurement of fluorescent materials is complex and beyond the scope of this book. In general; a fluorescent material is characterized by its total radiance factor, which is the sum of the reflected and emitted energy at each wavelength relative to the energy that would be reflected by a PRD. This definition allows total radiance factors greater than 1.0, which is often the case. It is important to note that the total radiance factor will depend on the light source used in the measuring instrument since the amount of emitted energy is directly proportional to the amount of absorbed energy in the excitation wavelengths. Spectrophotometric measurements of reflectance or transmittance of nonfluorescent materials are

insensitive to the light source in the instrument since its characteristics are normalized in the ratio calculations. This important difference highlights the major difficulty in measuring fluorescent materials. Unfortunately, many artificial materials (such as paper and inks) are fluorescent and thus significantly more difficult to measure accurately.

3.5 THE HUMAN VISUAL RESPONSE

Measurement or standardization of light sources and materials provides the necessary physical information for colorimetry. What remains is a quantitative technique to predict the response of the human visual system as illustrated by the third corner of the triangle in Figure 3.1. Following Wyszecki's (1973) definition of basic colorimetry, quantification of the human visual response focuses on the earliest level of vision, absorption of energy in the cone photoreceptors, through the psychophysics of color matching. The ability to predict when two stimuli match for an average observer, the basis of colorimetry, provides great utility in a variety of applications. While such a system does not specify color appearance, it provides the basis of color appearance specification and allows the prediction of matches for various applications and the tools required to set up tolerances on matches necessary for industry. The properties of human color matching are defined by the spectral responsivities of the three cone types. This is because, once the energy is absorbed by the three cone types, the spectral origin of the signals is lost and, if the signals from the three cone types are equal for two stimuli, they must match in color when seen in the same conditions since there is no further information introduced within the visual system to distinguish them.

Thus, if the spectral responsivities of the three cone types are known, two stimuli, denoted by their spectral power distributions $\Phi_1(\lambda)$ and $\Phi_2(\lambda)$, will match in color if the product of their spectral power distributions and each of the three cone responsivities, $L(\lambda)$, $M(\lambda)$, and $S(\lambda)$, integrated over wavelength, are equal. This equality for a visual match is illustrated in Equations 3.3–3.5. Two stimuli match if all three of the equalities in Equations 3.3–3.5 hold true.

$$\int_{\lambda} \Phi_1(\lambda)L(\lambda)d\lambda = \int_{\lambda} \Phi_2(\lambda)L(\lambda)d\lambda \quad (3.3)$$

$$\int_{\lambda} \Phi_1(\lambda)M(\lambda)d\lambda = \int_{\lambda} \Phi_2(\lambda)M(\lambda)d\lambda \quad (3.4)$$

$$\int_{\lambda} \Phi_1(\lambda)S(\lambda)d\lambda = \int_{\lambda} \Phi_2(\lambda)S(\lambda)d\lambda \quad (3.5)$$

Equations 3.3–3.5 illustrate the definition of metamerism. Since only the three integrals need be equal for a color match, it is not necessary for the spectral power distributions of the two stimuli to be equal for every wavelength. The cone spectral responsivities are quite well known today, as described in Chapter 1. With such knowledge, a system of basic colorimetry becomes nearly as simple to define as Equations 3.3–3.5. However, reasonably accurate knowledge of the cone spectral responsivities is a rather recent scientific development. The need for colorimetry predates this knowledge by several decades. Thus the CIE, in establishing the 1931 system of colorimetry, needed to take a less direct approach.

The System of Photometry

To illustrate the indirect nature of the CIE system of colorimetry, it is useful to first explore the system of photometry, which was established in 1924. The aim for a system of photometry was the development of a spectral weighting function that could be used to describe the perception of brightness matches. (More correctly, the system describes the results of flicker photometry experiments rather than heterochromatic brightness matches as described further in Chapter 6.) In 1924, the CIE spectral luminous efficiency function $V(\lambda)$ was established for photopic vision. This function, plotted in Figure 3.6 and enumerated in Table 3.2, indicates that the visual system is more sensitive (with respect to the perception of brightness) to wavelengths in the middle of the spectrum and becomes less and less sensitive to wavelengths near the extremes of the visual spectrum. The $V(\lambda)$ function is used as a spectral weighting function to convert radiometric quantities into photometric quantities via spectral integration, as shown in Equation 3.6.

$$\Phi_V = \int_{\lambda} \Phi(\lambda)V(\lambda)d\lambda \quad (3.6)$$

The term Φ_V in Equation 3.6 refers to the appropriate photometric quantity defined by the radiometric quantity, $\Phi(\lambda)$, used in the calculation. For example, the radiometric quantities of irradiance, radiance, and reflectance factor are used to derive the photometric quantities of illuminance (lumen/ m^2 or lux), luminance (cd/m^2), or luminance factor (dimensionless). All of the optical properties and relationships for irradiance and radiance are preserved for illuminance and luminance. To convert irradiance or radiance to illuminance or luminance, a normalization constant of 683 lumen/W is required to preserve the appropriate units. For the calculation of luminance factor, a different type of normalization, described in the next section, is required.

The $V(\lambda)$ function is clearly not one of the cone responsivities. In fact, according to the opponent theory of color vision, such a result would not be

Table 3.2 CIE photopic luminous efficiency function, $V(\lambda)$ and scotopic luminous efficiency function, $V'(\lambda)$

Wavelength (nm)	$V(\lambda)$	$V'(\lambda)$	Wavelength (nm)	$V(\lambda)$	$V'(\lambda)$
360	0.0000	0.0000	560	0.9950	0.3288
365	0.0000	0.0000	565	0.9786	0.2682
370	0.0000	0.0000	570	0.9520	0.2076
375	0.0000	0.0000	575	0.9154	0.1644
380	0.0000	0.0006	580	0.8700	0.1212
385	0.0001	0.0014	585	0.8163	0.0934
390	0.0001	0.0022	590	0.7570	0.0655
395	0.0002	0.0058	595	0.6949	0.0494
400	0.0004	0.0093	600	0.6310	0.0332
405	0.0006	0.0221	605	0.5668	0.0246
410	0.0012	0.0348	610	0.5030	0.0159
415	0.0022	0.0657	615	0.4412	0.0117
420	0.0040	0.0966	620	0.3810	0.0074
425	0.0073	0.1482	625	0.3210	0.0054
430	0.0116	0.1998	630	0.2650	0.0033
435	0.0168	0.2640	635	0.2170	0.0024
440	0.0230	0.3281	640	0.1750	0.0015
445	0.0298	0.3916	645	0.1382	0.0011
450	0.0380	0.4550	650	0.1070	0.0007
455	0.0480	0.5110	655	0.0816	0.0005
460	0.0600	0.5670	660	0.0610	0.0003
465	0.0739	0.6215	665	0.0446	0.0002
470	0.0910	0.6760	670	0.0320	0.0001
475	0.1126	0.7345	675	0.0232	0.0001
480	0.1390	0.7930	680	0.0170	0.0001
485	0.1693	0.8485	685	0.0119	0.0000
490	0.2080	0.9040	690	0.0082	0.0000
495	0.2586	0.9430	695	0.0057	0.0000
500	0.3230	0.9820	700	0.0041	0.0000
505	0.4073	0.9895	705	0.0029	0.0000
510	0.5030	0.9970	710	0.0021	0.0000
515	0.6082	0.9660	715	0.0015	0.0000
520	0.7100	0.9350	720	0.0010	0.0000
525	0.7932	0.8730	725	0.0007	0.0000
530	0.8620	0.8110	730	0.0005	0.0000
535	0.9149	0.7305	735	0.0004	0.0000
540	0.9540	0.6500	740	0.0002	0.0000
545	0.9803	0.5655	745	0.0002	0.0000
550	0.9950	0.4810	750	0.0001	0.0000
555	1.0000	0.4049	755	0.0001	0.0000
			760	0.0001	0.0000

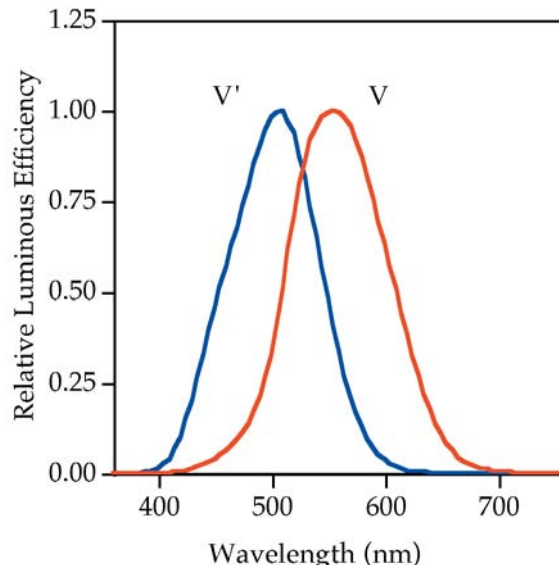


Figure 3.6 CIE scotopic, $V'(\lambda)$, and photopic, $V(\lambda)$, luminous efficiency functions

expected. Instead, as suggested by the opponent theory of color vision, the $V(\lambda)$ function corresponds to a weighted sum of the three cone responsivity functions. When the cone functions are weighted according to their relative population in the retina and summed, the overall responsivity matches the CIE 1924 $V(\lambda)$ function. Thus the photopic luminous response represents a combination of cone signals. This sort of combination is present in the entire system of colorimetry. The use of a spectral weighting function to predict luminance matches is the first step toward a system of colorimetry.

There is also a luminous efficiency function for scotopic vision (rods) known as the $V'(\lambda)$ function. This function, used for photometry at very low luminance levels is plotted in Figure 3.6 and presented in Table 3.2 along with the $V(\lambda)$ function. Since there is only one type of rod photoreceptor, the $V'(\lambda)$ function corresponds exactly to the spectral responsivity of the rods after transmission through the ocular media. Figure 3.6 illustrates the shift in peak spectral sensitivity toward shorter wavelengths during the transition from photopic to scotopic vision. This shift, known as the *Purkinje shift*, explains why blue objects tend to look lighter than red objects at very low luminance levels. The $V'(\lambda)$ function is used in a way similar to the $V(\lambda)$ function.

It has long been recognized in vision research that the $V(\lambda)$ function might underpredict observed responsivity in the short-wavelength region of the spectrum. To address this issue and standard practice in the vision community, an additional function, the CIE 1988 spectral luminous efficiency function, $V_M(\lambda)$, was established (CIE 1990).

3.6 TRISTIMULUS VALUES AND COLOR MATCHING FUNCTIONS

Following the establishment of the CIE 1924 luminous efficiency function $V(\lambda)$, attention was turned to development of a system of colorimetry that could be used to specify when two metameristic stimuli match in color for an average observer. Since the cone responsivities were unavailable at that time, a system of colorimetry was constructed based on the principles of trichromacy and Grassmann's laws of additive color mixture. The concept of this system is that color matches can be specified in terms of the amounts of three additive primaries required to visually match a stimulus. This is illustrated in the equivalence statement of Equation 3.7.

$$C \equiv R(\mathcal{R}) + G(\mathcal{G}) + B(\mathcal{B}) \quad (3.7)$$

The way Equation 3.7 reads is that a color C is matched by R units of the \mathcal{R} primary, G units of the \mathcal{G} primary, and B units of the \mathcal{B} primary. The terms, RGB , define the particular set of primaries and indicate that for different primary sets, different amounts of the primaries will be required to make a match. The terms RGB indicate the amounts of the primaries required to match the color and are known as tristimulus values. Since any color can be matched by certain amounts of three primaries, those amounts (tristimulus values), along with a definition of the primary set, allow the specification of a color. If two stimuli can be matched using the same amounts of the primaries, (i.e., they have equal tristimulus values) then they will also match each other when viewed in the same conditions.

Tristimulus Values for Any Stimulus

The next step in the derivation of colorimetry is the extension of tristimulus values such that they can be obtained for any given stimulus, defined by a spectral power distribution. To accomplish this, two steps are required. The first is to obtain tristimulus values for matches to spectral colors. The second is to take advantage of Grassmann's laws of additivity and proportionality to sum tristimulus values for each spectral component of a stimulus spectral power distribution in order to obtain the integrated tristimulus values for the stimulus. Conceptually, the tristimulus values of the spectrum (i.e., spectral tristimulus values) are obtained by matching a unit amount of power at each wavelength with an additive mixture of three primaries. Figure 3.7 illustrates a set of spectral tristimulus values for monochromatic primaries at 435.6 nm (\mathcal{B}), 546.1 nm (\mathcal{G}), and 700.0 nm (\mathcal{R}). Spectral tristimulus values for the complete spectrum are also known as *color matching functions*, or sometimes *color mixture functions*. Notice that some of the spectral tristimulus values plotted in Figure 3.7 are negative. This implies the addition of a negative amount of power into the match. For example, a negative amount of the \mathcal{R} primary is required to match a monochromatic 500 nm

stimulus. This is because that wavelength is too saturated to be matched by the particular primaries (i.e., it is out of gamut). Clearly, a negative amount of light can not be added to a match. Negative tristimulus values are obtained by adding the primary to the monochromatic light to desaturate it and bring it within the gamut of the primaries. Thus, a 500 nm stimulus mixed with a given amount of the R primary is matched by an additive mixture of appropriate amounts of the G and B primaries.

The color matching functions illustrated in Figure 3.7 indicate the amounts of the primaries required to match unit amounts of power at each wavelength. By considering any given stimulus spectral power as an additive mixture of various amounts of monochromatic stimuli, the tristimulus values for a stimulus can be obtained by multiplying the color matching functions by the amount of energy in the stimulus at each wavelength (Grassmann's proportionality) and integrating across the spectrum (Grassmann's additivity). Thus, the generalized equations for calculating the tristimulus values of a stimulus with spectral power distribution $\Phi(\lambda)$ are given by Equations 3.8–3.10 where $\bar{r}(\lambda)$, $\bar{g}(\lambda)$, $\bar{b}(\lambda)$ and are the color matching functions.

$$R = \int_{\lambda} \Phi(\lambda) \bar{r}(\lambda) d\lambda \quad (3.8)$$

$$G = \int_{\lambda} \Phi(\lambda) \bar{g}(\lambda) d\lambda \quad (3.9)$$

$$B = \int_{\lambda} \Phi(\lambda) \bar{b}(\lambda) d\lambda \quad (3.10)$$

With the utility of tristimulus values and color matching functions established, it remains to derive a set of color matching functions that are representative of the population of observers with normal color vision. Color matching functions for individual observers, all with normal color vision, can be significantly different due to variations in lens transmittance; macula transmittance; and cone density, population, and spectral responsivities. Thus to establish a standardized system of colorimetry it is necessary to obtain a reliable estimate of the average color matching functions of the population of observers with normal color vision.

Estimating Average Color Matching Functions

In the late 1920s two sets of experiments were completed to estimate average color matching functions. These experiments were completed by Wright (1928–29) using monochromatic primaries and Guild (1931) using

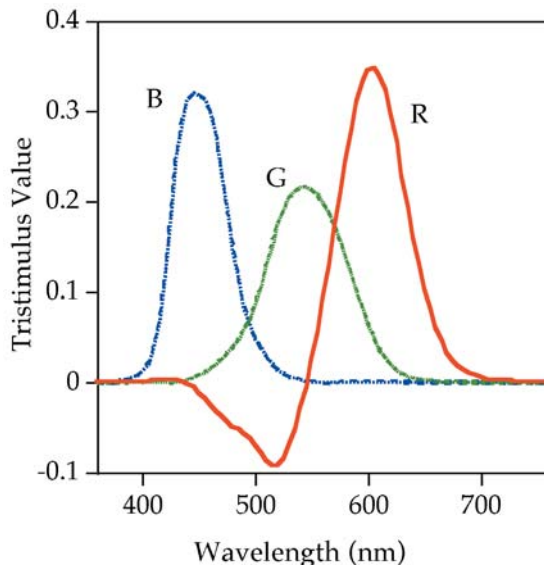


Figure 3.7 Spectral tristimulus values for the CIE RGB system of colorimetry with monochromatic primaries at 435.8, 546.1, and 700.0 nm

broadband primaries. Since the primaries from one experiment can be specified in terms of tristimulus values to match them using the other system, it is possible to derive a linear transform (3×3 matrix transformation) to convert tristimulus values from one set of primaries to another. This transformation also applies to the color matching functions since they are themselves tristimulus values. Thus, a transformation was derived to place the data from Wright's and Guild's experiments into a common set of primaries. When this was done, the agreement between the two experiments was extremely good, verifying the underlying theoretical assumptions in the derivation and use of color matching functions. Given this agreement, the CIE decided to establish a standard set of color matching functions based on the mean results of the Wright and Guild experiments. These mean functions were transformed to **RGB** primaries of 700.0, 546.1 and 435.8 nm, respectively, and are illustrated in Figure 3.7.

In addition, the CIE decided to transform to yet another set of primaries, the **xyz** primaries. The main objectives in performing this transformation were to eliminate the negative values in the color matching functions and to force one of the color matching functions to equal the CIE 1924 photopic luminous efficiency function $V(\lambda)$. The negative values were removed by selecting primaries that could be used to match all physically realizable color stimuli. This can only be accomplished with imaginary primaries that are more saturated than monochromatic lights. This is a straightforward mathematical construct and it should be noted that, although the primaries are imaginary, the color matching functions derived for those primaries are

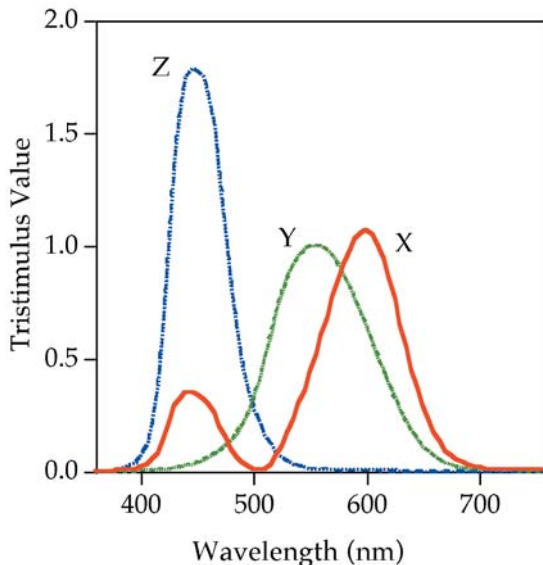


Figure 3.8 Spectral tristimulus values of the CIE 1931 standard colorimetric observer

based on very real color matching results and the validity of Grassmann's laws. Forcing one of the color matching functions to equal the $V(\lambda)$ function serves the purpose of incorporating the CIE system of photometry (established in 1924) into the CIE system of colorimetry (established in 1931). This is accomplished by choosing two of the imaginary primaries, χ and ζ , such that they produce no luminance response, leaving all of the luminance response in the third primary, γ . The color matching functions for the $\chi\gamma\zeta$ primaries, $\bar{x}(\lambda)$, $\bar{y}(\lambda)$, and $\bar{z}(\lambda)$, respectively, known as the color matching functions of the CIE 1931 standard colorimetric observer, are listed in Table 3.3 and plotted in Figure 3.8 for the practical wavelength range of 360–760 nm in 5 nm increments. (The CIE defines color matching functions from 360–830 nm in 1 nm increments and with more digits after the decimal point.)

XYZ tristimulus values for colored stimuli are calculated in the same fashion as the RGB tristimulus values described above. The general equations are given in Equations 3.11–3.13 where $\Phi(\lambda)$ is the spectral power distribution of the stimulus $\bar{x}(\lambda)$, $\bar{y}(\lambda)$, and $\bar{z}(\lambda)$ are the color matching functions, and k is a normalizing constant.

$$X = k \int_{\lambda} \Phi(\lambda) \bar{x}(\lambda) d\lambda \quad (3.11)$$

$$Y = k \int_{\lambda} \Phi(\lambda) \bar{y}(\lambda) d\lambda \quad (3.12)$$

Table 3.3 Color matching functions for the CIE 1931 standard colorimetric observer (2°)

Wavelength (nm)	\bar{x}	\bar{y}	\bar{z}	\bar{x}	\bar{y}	\bar{z}	
360	0.0000	0.0000	0.0000	560	0.5945	0.9950	0.0039
365	0.0000	0.0000	0.0000	565	0.6784	0.9786	0.0027
370	0.0000	0.0000	0.0000	570	0.7621	0.9520	0.0021
375	0.0000	0.0000	0.0000	575	0.8425	0.9154	0.0018
380	0.0014	0.0000	0.0065	580	0.9163	0.8700	0.0017
385	0.0022	0.0001	0.0105	585	0.9786	0.8163	0.0014
390	0.0042	0.0001	0.0201	590	1.0263	0.7570	0.0011
395	0.0077	0.0002	0.0362	595	1.0567	0.6949	0.0010
400	0.0143	0.0004	0.0679	600	1.0622	0.6310	0.0008
405	0.0232	0.0006	0.1102	605	1.0456	0.5668	0.0006
410	0.0435	0.0012	0.2074	610	1.0026	0.5030	0.0003
415	0.0776	0.0022	0.3713	615	0.9384	0.4412	0.0002
420	0.1344	0.0040	0.6456	620	0.8544	0.3810	0.0002
425	0.2148	0.0073	1.0391	625	0.7514	0.3210	0.0001
430	0.2839	0.0116	1.3856	630	0.6424	0.2650	0.0000
435	0.3285	0.0168	1.6230	635	0.5419	0.2170	0.0000
440	0.3483	0.0230	1.7471	640	0.4479	0.1750	0.0000
445	0.3481	0.0298	1.7826	645	0.3608	0.1382	0.0000
450	0.3362	0.0380	1.7721	650	0.2835	0.1070	0.0000
455	0.3187	0.0480	1.7441	655	0.2187	0.0816	0.0000
460	0.2908	0.0600	1.6692	660	0.1649	0.0610	0.0000
465	0.2511	0.0739	1.5281	665	0.1212	0.0446	0.0000
470	0.1954	0.0910	1.2876	670	0.0874	0.0320	0.0000
475	0.1421	0.1126	1.0419	675	0.0636	0.0232	0.0000
480	0.0956	0.1390	0.8130	680	0.0468	0.0170	0.0000
485	0.0580	0.1693	0.6162	685	0.0329	0.0119	0.0000
490	0.0320	0.2080	0.4652	690	0.0227	0.0082	0.0000
495	0.0147	0.2586	0.3533	695	0.0158	0.0057	0.0000
500	0.0049	0.3230	0.2720	700	0.0114	0.0041	0.0000
505	0.0024	0.4073	0.2123	705	0.0081	0.0029	0.0000
510	0.0093	0.5030	0.1582	710	0.0058	0.0021	0.0000
515	0.0291	0.6082	0.1117	715	0.0041	0.0015	0.0000
520	0.0633	0.7100	0.0782	720	0.0029	0.0010	0.0000
525	0.1096	0.7932	0.0573	725	0.0020	0.0007	0.0000
530	0.1655	0.8620	0.0422	730	0.0014	0.0005	0.0000
535	0.2257	0.9149	0.0298	735	0.0010	0.0004	0.0000
540	0.2904	0.9540	0.0203	740	0.0007	0.0002	0.0000
545	0.3597	0.9803	0.0134	745	0.0005	0.0002	0.0000
550	0.4334	0.9950	0.0087	750	0.0003	0.0001	0.0000
555	0.5121	1.0000	0.0057	755	0.0002	0.0001	0.0000
				760	0.0002	0.0001	0.0000

$$Z = k \int_{\lambda} \Phi(\lambda) \bar{z}(\lambda) d\lambda \quad (3.13)$$

The spectral power distribution of the stimulus is defined in different ways for various types of stimuli. For self-luminous stimuli (e.g., light sources and CRT displays), $\Phi(\lambda)$ is typically spectral radiance or a relative spectral power distribution. For reflective materials, $\Phi(\lambda)$ is defined as the product of the spectral reflectance factor of the material, $R(\lambda)$, and the relative spectral power distribution of the light source or illuminant of interest, $S(\lambda)$, that is $R(\lambda)S(\lambda)$. For transmitting materials, $\Phi(\lambda)$ is defined as the product of the spectral transmittance of the material, $T(\lambda)$, and the relative spectral power distribution of the light source or illuminant of interest, $S(\lambda)$, that is $T(\lambda)S(\lambda)$.

The normalization constant k in Equations 3.11–3.13, is defined differently for relative and absolute colorimetry. In absolute colorimetry, k is set equal to 683 lumen/W, making the system of colorimetry compatible with the system of photometry. For relative colorimetry, k is defined by Equation 3.14.

$$k = \frac{100}{\int_{\lambda} S(\lambda) \bar{y}(\lambda) d\lambda} \quad (3.14)$$

The normalization for relative colorimetry in Equation 3.14 results in tristimulus values that are scaled from zero to approximately 100 for various materials. It is useful to note that if relative colorimetry is used to calculate the tristimulus values of a light source, the Y tristimulus value is always equal to 100.

There is another, completely inappropriate, use of the term *relative colorimetry* in the graphic arts and other color reproduction industries. In some cases tristimulus values are normalized to the paper white rather than a perfect reflecting diffuser. This results in a Y tristimulus value for the paper of 100 rather than its more typical value of about 85. The advantage of this is that it allows transformation between different paper types, preserving the paper white as the lightest color in an image, without having to keep track of the paper color. Such a practice might be useful, but it is actually a gamut mapping issue rather than a color measurement issue. A more appropriate terminology for this practice might be normalized colorimetry to avoid confusion with the long-established practice of relative colorimetry. It is also worth noting that the practice of *normalized colorimetry* is not always consistent. In some cases, reflectance measurements are made relative to the paper white. This ensures that the Y tristimulus value is normalized between zero for a perfect black and 1.0 (or 100.0) for the paper white, however, the X and Z tristimulus values might still range above 1.0 (or 100.0) depending on the particular illuminant used in the colorimetric calculations.

Another approach is to normalize the tristimulus values for each stimulus color XYZ by the tristimulus values of the paper $X_p Y_p Z_p$ individually (X/X_p , Y/Y_p , and Z/Z_p). This is analogous to the white point normalization in CIELAB and is often used to adjust for white point changes and limited dynamic range in imaging systems. It is important to know which type of normalized colorimetry one is dealing with in various applications.

The relationship between CIE XYZ tristimulus values and cone responses (sometimes referred to as *fundamental tristimulus values*) is of great importance and interest in color appearance modeling. Like the $V(\lambda)$ function, the CIE XYZ color matching functions each represent a linear combination of cone responsivities. Thus the relationship between the two is defined by a 3×3 linear matrix transformation as described more fully in Chapter 9 (see Figure 9.1). Cone spectral responsivities can be thought of as the color matching functions for a set of primaries that are constructed such that each primary stimulates only one cone type. It is possible to produce a real primary that stimulates only the S cones. However, no real primaries can be produced that stimulate only the M or L cones since their spectral responsivities overlap across the visible spectrum. Thus, the required primaries are also imaginary and produce all-positive color matching functions, but do not incorporate the $V(\lambda)$ function as a color matching function (since that requires a primary that stimulates all three cone types). The historical development of and recent progress in the development of colorimetric systems based on physiological cone responsivities has been reviewed by Boynton (1996).

Two Sets of Color Matching Functions

It is important to be aware that there are two sets of color matching functions that have been established by the CIE. The CIE 1931 standard colorimetric observer was determined from experiments using a visual field that subtended 2° . Thus the matching stimuli were imaged onto the retina completely within the fovea. These color matching functions are used, almost exclusively, in color appearance modeling. Often they are referred to as the 2° *color matching functions* or the 2° *observer*. It is of historical interest to note that the 1931 standard colorimetric observer is based on data collected from fewer than 20 observers. In the 1950s, experiments were completed (Stiles and Burch 1959) to collect 2° color matching functions for more observers using more precise and accurate instrumentation. The results showed slight systematic discrepancies, but not of sufficient magnitude to warrant a change in the standard colorimetric observer. At the same time, experiments were completed (Stiles and Burch 1959) to collect color matching function data for large visual fields. This was prompted by discrepancies between colorimetric and visual determination of the whiteness of paper. These experiments were completed using a 10° visual field that excluded the central fovea. Thus the color matching functions include no influence of the

macular absorption. The results for large fields were deemed significantly different from the 2° standard to warrant the establishment of the CIE 1964 supplementary standard colorimetric observer, sometimes called the 10° observer. The difference between the two standard observers is significant, so care should be taken to report which observer is used with any colorimetric data. The differences are computationally significant, but certainly within the variability of color matching functions found for either 2° or 10° visual fields. Thus the two standard colorimetric observers can be thought of as representing the color matching functions of two individuals.

3.7 CHROMATICITY DIAGRAMS

The color of a stimulus can be specified by a triplet of tristimulus values. To provide a convenient two-dimensional representation of colors, chromaticity diagrams were developed. The transformation from tristimulus values to chromaticity coordinates is accomplished through a normalization that removes luminance information. This transformation is a one-point perspective projection of data points in the three-dimensional tristimulus space onto the unit plane of that space (with a center of projection at the origin) as defined by Equations 3.15–3.17.

$$x = \frac{X}{X + Y + Z} \quad (3.15)$$

$$y = \frac{Y}{X + Y + Z} \quad (3.16)$$

$$z = \frac{Z}{X + Y + Z} \quad (3.17)$$

Since there are only two-dimensions of information in chromaticity coordinates, the third chromaticity coordinate can always be obtained from the other two by noting that the three always sum to unity. Thus z can be calculated from x and y using Equation 3.18.

$$z = 1.0 - x - y \quad (3.18)$$

Chromaticity coordinates should be used with great care since they attempt to represent a three-dimensional phenomenon with just two variables. To fully specify a colored stimulus, one of the tristimulus values must be reported in addition to two (or three) chromaticity coordinates. Usually the Y tristimulus value is reported since it represents the luminance information. The equations for obtaining the other two tristimulus values from chromaticity coordinates and the Y tristimulus value are often useful and therefore given in Equations 3.19 and 3.20.

$$X = \frac{xY}{y} \quad (3.19)$$

$$Z = \frac{(1.0 - x - y)Y}{y} \quad (3.20)$$

Chromaticity coordinates, alone, provide no information about the color appearance of stimuli since they include no luminance (or therefore lightness) information and do not account for chromatic adaptation. As an observer's state of adaptation changes, the color corresponding to a given set of chromaticity coordinates can change in appearance dramatically (e.g., a change from yellow to blue could occur with a change from daylight to incandescent light adaptation).

Much effort has been expended in attempts to make chromaticity diagrams more perceptually uniform. While this is an intrinsically doomed effort (i.e., an attempt to convert a nominal scale into an interval scale), it is worth mentioning one of the results, which is actually the chromaticity diagram currently recommended by the CIE for general use. It is the CIE 1976 Uniform Chromaticity Scales (UCS) diagram defined by Equations 3.21 and 3.22.

$$u' = \frac{4X}{X + 15Y + 3Z} \quad (3.21)$$

$$v' = \frac{9Y}{X + 15Y + 3Z} \quad (3.22)$$

The use of chromaticity diagrams should be avoided in most circumstances, particularly when the phenomena being investigated are highly dependent on the three-dimensional nature of color. For example, the display and comparison of the color gamuts of imaging devices in chromaticity diagrams is misleading to the point of being almost completely erroneous.

3.8 CIE COLOR SPACES

The general use of chromaticity diagrams has been made largely obsolete by the advent of the CIE color spaces, CIELAB and CIELUV. These spaces extend tristimulus colorimetry to three-dimensional spaces with dimensions that approximately correlate with the perceived lightness, chroma, and hue of a stimulus. This is accomplished by incorporating features to account for chromatic adaptation and nonlinear visual responses. The main aim in the development of these spaces was to provide uniform practices for the measurement of color differences, something that cannot be done reliably in tristimulus or chromaticity spaces. In 1976, two spaces were recommended

for use since there was no clear evidence to support one over the other at that time. The CIELAB and CIELUV color spaces are described in more detail in Chapter 10. Their equations are briefly summarized in this section. Wyszecki (1986) provides an overview of the development of the CIE color spaces.

CIELAB

The CIE 1976 (L^* a^* b^*) color space, abbreviated CIELAB, is defined by Equations 3.23–3.27 for tristimulus values normalized to the white that are greater than 0.008856.

$$L^* = 116(Y/Y_n)^{1/3} - 16 \quad (3.23)$$

$$a^* = 500[(X/X_n)^{1/3} - (Y/Y_n)^{1/3}] \quad (3.24)$$

$$b^* = 200[(Y/Y_n)^{1/3} - (Z/Z_n)^{1/3}] \quad (3.25)$$

$$C_{ab}^* = \sqrt{(a^{*2} + b^{*2})} \quad (3.26)$$

$$h_{ab} = \tan^{-1}(b^*/a^*) \quad (3.27)$$

In these equations X , Y , and Z are the tristimulus values of the stimulus and X_n , Y_n , and Z_n are the tristimulus values of the reference white. L^* represents lightness, a^* approximate redness–greenness, b^* approximate yellowness–blueness, C_{ab}^* chroma, and h_{ab} hue. The L^* , a^* , and b^* coordinates are used to construct a Cartesian color space as illustrated in Figure 3.9. The L^* , C_{ab}^* , and h_{ab} coordinates are the cylindrical representation of the same space. The CIELAB space, including the full set of equations for dark colors, is described in greater detail in Chapter 10.

CIELUV

The CIE 1976 (L^* u^* v^*) color space, abbreviated CIELUV, is defined by Equations 3.28–3.32. Equation 3.28 is also restricted to tristimulus values normalized to the white that are greater than 0.008856.

$$L^* = 116(Y/Y_n)^{1/3} - 16 \quad (3.28)$$

$$u^* = 13L^*(u' - u'_n) \quad (3.29)$$

$$v^* = 13L^*(v' - v'_n) \quad (3.30)$$

$$C_{uv}^* = \sqrt{(u^{*2} + v^{*2})} \quad (3.31)$$

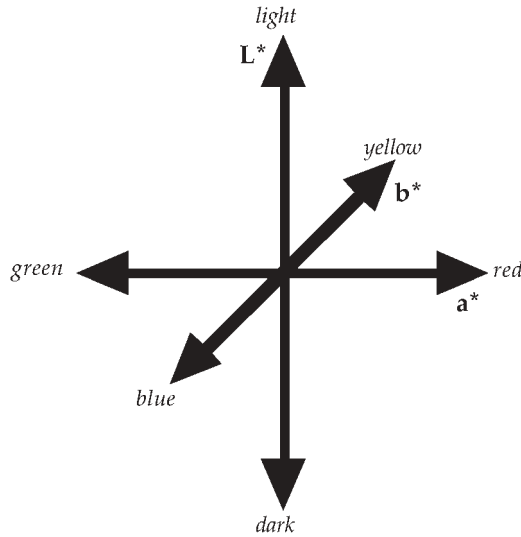


Figure 3.9 Three-dimensional representation of the CIELAB L^* , a^* , and b^* coordinates

$$h_{uv} = \tan^{-1}(v^*/u^*) \quad (3.32)$$

In these equations u' and v' are the chromaticity coordinates of the stimulus and u'_n and v'_n are the chromaticity coordinates of the reference white. L^* represents lightness, u^* redness–greenness, v^* yellowness–blueness, C_{uv}^* chroma, and h_{uv} hue. As in CIELAB, the L^* , u^* , and v^* coordinates are used to construct a Cartesian color space and the L^* , C_{uv}^* , and h_{uv} coordinates are the cylindrical representation of the same space.

The CIELAB and CIELUV spaces were both recommended as interim solutions to the problem of color difference specification of reflecting samples in 1976. Since that time, CIELAB has become almost universally used for color specification and particularly color difference measurement. At this time there appears to be no reason to use CIELUV over CIELAB.

3.9 COLOR DIFFERENCE SPECIFICATION

Color differences are measured in the CIELAB space as the Euclidean distance between the coordinates for the two stimuli. This is expressed in terms of a CIELAB ΔE_{ab}^* , which can be calculated using Equation 3.33. It can also be expressed in terms of lightness, chroma, and hue differences as illustrated in Equation 3.34 by using the combination of Equations 3.33 and 3.35.

$$\Delta E_{ab}^* = [\Delta L^{*2} + \Delta a^{*2} + \Delta b^{*2}]^{1/2} \quad (3.33)$$

$$\Delta E_{ab}^* = [\Delta L^{*2} + \Delta C_{ab}^{*2} + \Delta H_{ab}^{*2}]^{1/2} \quad (3.34)$$

$$\Delta H_{ab}^* = [\Delta E_{ab}^{*2} - \Delta L^{*2} - \Delta C_{ab}^{*2}]^{1/2} \quad (3.35)$$

While the CIELAB color space was designed with the goal of having color differences be perceptually uniform throughout the space (i.e., a ΔE_{ab}^* of 1.0 for a pair of red stimuli is perceived to be equal in magnitude to a ΔE_{ab}^* of 1.0 for a pair of gray stimuli), this goal was not strictly achieved.

To improve the uniformity of color difference measurements, modifications to the CIELAB ΔE_{ab}^* equation have been made based upon various empirical data. One of the most widely used modifications is the CMC color difference equation (Clarke *et al.* 1984), which is based on a visual experiment on color difference perception in textiles. The CIE (1995b) has recently evaluated such equations, and the available visual data, recommending a new color difference equation for industrial use. This system for color difference measurement is called the CIE 1994 ($\Delta L^* \Delta C_{ab}^* \Delta H_{ab}^*$) color difference model with the symbol ΔE_{94}^* and abbreviation CIE94. Use of the CIE94 equation is preferred over a simple CIELAB ΔE_{ab}^* . CIE94 color differences are calculated using Equations 3.36–3.39.

$$\Delta E_{94}^* = \left[\left(\frac{\Delta L^*}{k_L S_L} \right)^2 + \left(\frac{\Delta C_{ab}^*}{k_C S_C} \right)^2 + \left(\frac{\Delta H_{ab}^*}{k_H S_H} \right)^2 \right]^{1/2} \quad (3.36)$$

$$S_L = 1 \quad (3.37)$$

$$S_C = 1 + 0.045 C_{ab}^* \quad (3.38)$$

$$S_H = 1 + 0.015 C_{ab}^* \quad (3.39)$$

The parametric factors, k_L , k_C , and k_H are used to adjust the relative weighting of the lightness, chroma, and hue components, respectively, of color difference for various viewing conditions and applications that depart from the CIE94 reference conditions. It is also worth noting that, when averaged across the color space, CIE94 color differences are significantly smaller in magnitude than CIELAB color differences for the same stimuli pairs. Thus, use of CIE94 color differences to report overall performance in applications such as the colorimetric characterization of imaging devices results in the appearance of significantly improved performance if the numbers are mistakenly considered equivalent to CIELAB color differences. The same is true for CMC color differences.

The CIE (1995) established a set of reference conditions for use of the CIE94 color difference equations. These are:

- *Illumination:* CIE illuminant D65 simulator
- *Illuminance:* 1000 lux
- *Observer:* normal color vision
- *Background:* uniform, achromatic, $L^* = 50$

- *Viewing mode:* object
- *Sample size:* greater than 4° visual angle
- *Sample Separation:* direct edge contact
- *Sample Color-Difference Magnitude:* 0–5 CIELAB units
- *Sample Structure:* no visually apparent pattern or nonuniformity

The tight specification of reference conditions for the CIE94 equations highlights the vast amount of research that remains to be performed in order to generate a universally useful process for color difference specification. These issues are some of the same problems that must be tackled in the development of color appearance models. It should also be noted that for sample sizes greater than 4°, use of the CIE 1964 supplementary standard colorimetric observer is recommended.

More recently, the CIE has established the CIE DE2000 color difference equation (see Johnson and Fairchild 2003b, CIE 2001) that extends the concept of CIE94 with further complexity. While the DE2000 equation certainly performs better than CIE94 for some data sets, its added complexity is probably not justified for most practical applications.

3.10 THE NEXT STEP

This chapter has reviewed the fundamentals of basic colorimetry (and begun to touch on advanced colorimetry) as illustrated conceptually in Figure 3.1. While these techniques are well established and have been successfully used for decades, much more information needs to be added to the triangle of color in Figure 3.1 in order to extend basic colorimetry toward the specification of the color appearance of stimuli under a wide variety of viewing conditions. Some of the additional information that must be considered includes:

- chromatic adaptation,
- light adaptation,
- luminance level,
- background color,
- surround color,
- etc.

These issues are explored further along the road to the development and use of color appearance models presented in the remaining chapters of this book.

4

Color Appearance Terminology

In any scientific field a large portion of the knowledge is contained in the definitions of terms used by its practitioners. Newcomers to a field often realize that they understand the fundamental scientific concepts, but must first learn the language in order to communicate accurately, precisely, and effectively in the new discipline. Nowhere is this more true, or more important, than in the study of color appearance. Hunt (1978) showed concern that color scientists and technologists might be taking an attitude like Humpty Dumpty from *Alice Through the Looking Glass* who is quoted as saying 'When I use a word it means just what I choose it to mean — neither more nor less.' We all know what happened to Humpty Dumpty. The careful definition of color appearance terms presented in this chapter is intended to put everyone on a level playing field and help ensure that the concepts, data, and models discussed in this book are presented and interpreted in a consistent manner. As can be seen throughout this book, consistent use of terminology has not been the historical norm and continues to be one of the challenges of color appearance research and application.

4.1 IMPORTANCE OF DEFINITIONS

Why should it be particularly difficult to agree upon consistent terminology in the field of color appearance? Perhaps the answer lies in the very nature of the subject. Almost everyone *knows* what color is. After all, they have had first-hand experience of it since shortly after birth. However, very few can precisely describe their color experiences or even precisely define color. This innate knowledge, along with the imprecise use of color terms (e.g., warmer, cooler, brighter, cleaner, fresher), leads to a subject that everyone knows about, but few can discuss precisely. Clearly, if color appearance is to be

described in a systematic, mathematical way, definitions of the phenomena being described need to be precise and universally agreed upon.

Since color appearance modeling remains an area of active research, the required definitions have not been set in stone for decades. The definitions presented in this chapter have been culled from three sources. The first, and authoritative, source is the *International Lighting Vocabulary* published by the Commission International de l'Éclairage, CIE (CIE 1987). The *International Lighting Vocabulary* includes the definitions of approximately 950 terms and quantities related to light and color 'to promote international standardization in the use of quantities, units, symbols, and terminology.' The other two sources, articles by Hunt (1977, 1978), provide descriptions of some of the work that led to the latest revision of the *International Lighting Vocabulary*. It should be noted that the *International Lighting Vocabulary* is currently under revision and that there is also a relevant ASTM standard on appearance terminology (ASTM 1995).

Keep in mind that the definitions given below are of perceptual terms. These terms define our perceptions of colored stimuli. These are not definitions of specific colorimetric quantities. In the construction and use of color appearance models, the objective is to develop and use physically measurable quantities that correlate with the perceptual attributes of color appearance defined below.

4.2 COLOR

The definition of the word color itself provides some interesting challenges and difficulties. While most of us know what color is, it is an interesting challenge to try to write a definition of the word that does not contain an example. As can be seen below even the brightest and most dedicated color scientists who set out to write the *International Lighting Vocabulary*, could not meet this challenge.

Color

Attribute of visual perception consisting of any combination of chromatic and achromatic content. This attribute can be described by chromatic color names such as yellow, orange, brown, red, pink, green, blue, purple, etc., or by achromatic color names such as white, gray, black, etc., and qualified by bright, dim, light, dark, etc., or by combinations of such names.

The authors of this definition were also well aware that the perception of color was not a simple matter and added a note that captures the essence of why color appearance models are needed.

Note

Perceived color depends on the spectral distribution of the color stimulus, on the size, shape, structure, and surround of the stimulus area, on the state of

adaptation of the observer's visual system, and on the observer's experience of the prevailing and similar situations of observations.

The above note opens the door for the vast array of physical, physiological, psychological, and cognitive variables that influence color appearance — many of which are discussed in this book.

While the above definition might not be very satisfying due to its circularity, any definitions that avoid the circularity seem to be equally dissatisfying. One such example would be to define color as those attributes of a visual stimulus that are independent of spatial and temporal variations. Even this definition is flawed since in the absence of all temporal and spatial variation, even the perception of color vanishes. Despite the difficulty in defining color, the various attributes of color can be defined much more precisely and those are the terms that are of utmost importance in color appearance modeling.

4.3 HUE

Hue

Attribute of a visual sensation according to which an area appears to be similar to one of the perceived colors: red, yellow, green, and blue, or to a combination of two of them.

Achromatic Color

Perceived color devoid of hue.

Chromatic Color

Perceived color possessing a hue.

Once again, it is difficult, if not impossible to define hue without using examples. This is due, in part, to the nature of the hue perception. It is a natural interval scale as illustrated by the traditional description of a 'hue circle.' There is no natural 'zero' hue. Color without hue can be described, but there is no perception that corresponds to a meaningful hue of zero units. Thus the color appearance models described in later chapters never aspire to describe hue with more than an interval scale.

The 'circular' nature of hue can be observed in Figure 5.2, which illustrates the hue dimension in the *Munsell Book of Color*. The hue circle in Figure 5.2 also illustrates how all of the hues can be described using the terms red, yellow, green, blue, or combinations thereof as predicted by Hering's opponent theory of color vision. Other examples of hue include the variation of color witnessed in a projected visible spectrum or a rainbow. Three of the rendered cubes in Figure 4.1 are of three different hues: red, green, and blue. The fourth is white and thus achromatic, possessing no hue.



Figure 4.1 A computer graphics rendering of four solid blocks illuminated by two light sources of differing intensities and angle of illumination to be used for demonstration of various color appearance attributes

4.4 BRIGHTNESS AND LIGHTNESS

Brightness

Attribute of a visual sensation according to which an area appears to emit more or less light.

Lightness

The brightness of an area judged relative to the brightness of a similarly illuminated area that appears to be white or highly transmitting.

Note

Only related colors [see Section 4.7] exhibit lightness.

The definitions of brightness and lightness are straightforward and rather intuitive. The important distinction is that brightness refers to the absolute level of the perception while lightness can be thought of as relative brightness — normalized for changes in the illumination and viewing conditions.

A classic example is to think about a piece of paper, such as this book page. If this page was viewed in a typical office environment, the paper would have some brightness and a fairly high lightness (perhaps it is the lightest stimulus in the field of vision and therefore white). If the book was viewed outside on a sunny summer day, there would be significantly more energy reflected from the page and the paper would appear brighter. However, the page would still likely be the lightest stimulus in the field of vision and retain

its high lightness, approximately the same lightness it exhibited in office illumination. In other words, the paper still appears white, even though it is brighter outdoors. This is an example of approximate lightness constancy.

Figure 4.1 illustrates four rendered cubes that are illuminated by two light sources of different intensities, but the same color. Imagine that you are actually viewing the cubes in their illuminated environment. In this case, it would be clear that the different sides of the cubes are illuminated differently and exhibit different brightnesses. However, if you were asked to judge the lightness of the cubes, you could give one answer for all of the visible sides since you would interpret lightness as their brightness relative to the brightness of a similarly illuminated white object.

4.5 COLORFULNESS AND CHROMA

Colorfulness

Attribute of a visual sensation according to which the perceived color of an area appears to be more or less chromatic.

Note

For a color stimulus of a given chromaticity and, in the case of related colors, of a given luminance factor, this attribute usually increases as the luminance is raised, except when the brightness is very high.

Chroma

Colorfulness of an area judged as a proportion of the brightness of a similarly illuminated area that appears white or highly transmitting.

Note

For given viewing conditions and at luminance levels within the range of photopic vision, a color stimulus perceived as a related color, of a given chromaticity, and from a surface having a given luminance factor, exhibits approximately constant chroma for all levels of luminance except when the brightness is very high. In the same circumstances, at a given level of illuminance, if the luminance factor increases, the chroma usually increases.

As was discussed in Chapters 1 and 3, color perception is generally thought of as being three-dimensional. Two of those dimensions (hue and brightness/lightness) have already been defined. Colorfulness and chroma define the remaining dimension of color. Colorfulness is to chroma as brightness is to lightness. It is appropriate to think of chroma as relative colorfulness just as lightness can be thought of as relative brightness. Colorfulness describes the intensity of the hue in a given color stimulus. Thus, achromatic colors exhibit zero colorfulness and chroma, and as the amount of color content increases (with constant brightness/lightness and hue), colorfulness and chroma increase.

Like lightness, chroma is approximately constant across changes in luminance level. Note, however, that chroma is likely to change if the color of

the illumination is varied. Colorfulness, on the other hand, increases for a given object as the luminance level increases since it is an absolute perceptual quantity. Figure 4.1 illustrates the difference between colorfulness and chroma. Again, imagine you are in the illuminated environment with the cubes in Figure 4.1. Since different sides of each cube are illuminated with differing amounts of the same color energy, they vary in colorfulness. On the other hand, if you were to judge the chroma of the cubes, you could provide one answer for each of the cubes. This is because you would be judging each side relative to a similarly illuminated white object. The sides of the cubes with greater illumination exhibit greater colorfulness, but the chroma is roughly constant within each cube.

4.6 SATURATION

Saturation

Colorfulness of an area judged in proportion to its brightness.

Note

For given viewing conditions and at luminance levels within the range of photopic vision, a color stimulus of a given chromaticity exhibits approximately constant saturation for all luminance levels, except when brightness is very high.

Saturation is a unique perceptual experience separate from chroma. Like chroma, saturation can be thought of as relative colorfulness. However, saturation is the colorfulness of a stimulus relative to its own brightness, while chroma is colorfulness relative to the brightness of a similarly illuminated area that appears white. In order for a stimulus to have chroma, it must be judged in relation to other colors, while a stimulus seen completely in isolation can have saturation. An example of a stimulus that exhibits saturation, but not chroma, is a traffic signal light viewed in isolation on a dark night. The lights, typically red, yellow, or green, are quite saturated and can be compared with the color appearance of oncoming headlights whose saturation is very nearly zero (since they typically appear white).

Saturation is sometimes described as a shadow series. This refers to the range of colors observed when a single object has a shadow cast upon it. As the object falls into deeper shadow, it becomes darker, but saturation remains constant. This can be observed in Figure 4.1 by assuming that the rendered environment is illuminated by a single light source. The various sides of the cubes will all be of approximately constant saturation.

4.7 UNRELATED AND RELATED COLORS

Unrelated Color

Color perceived to belong to an area or object seen in isolation from other colors.

Related Color

Color perceived to belong to an area or object seen in relation to other colors.

The distinction between related and unrelated colors is critical for a firm understanding of color appearance. The definitions are simple enough; related colors are viewed in relation to other color stimuli, while unrelated colors are viewed completely in isolation. Almost every color appearance application of interest deals with the perception of related colors and they are the main focus of this book. However, it is important to keep in mind that many of the visual experiments that provide the foundations for understanding color vision and color appearance were performed with isolated stimuli — unrelated colors. It is important to keep the distinction in mind and not try to predict phenomena that only occur with related colors using models defined for unrelated colors and vice versa.

At times, related colors are thought of as object colors and unrelated colors are thought of as self-luminous colors. There is no correlation between the two concepts. An object color can be seen in isolation and thus be unrelated. Also, self-luminous stimuli (such as those presented on CRT displays) can be seen in relation to one another and thus be related colors.

There are various phenomena, discussed throughout this book, that only occur for related or unrelated colors. One interesting example is the perception of colors described by certain color names such as gray and brown. It is not possible to see unrelated colors that appear either gray or brown. Gray is an achromatic color with a lightness significantly lower than white. Brown is an orange color with low lightness. Both of these color name definitions require specific lightness levels. Since lightness and chroma require judgements relative to other stimuli that are similarly illuminated, they cannot possibly be perceived as unrelated stimuli. To convince yourself, search for a light that can be viewed in isolation (i.e., completely dark environment) and that appears either gray or brown. A nice demonstration of these related colors can be made by taking a spot of light that appears either white or orange and surrounding it with increasingly higher luminances of white light. As the luminance of the background light increases, the original stimuli will change in appearance from white and orange to gray and brown. If the background luminance is increased far enough, the original stimuli can be made to appear black. For interesting discussions on the color brown, see Bartleson (1976), Fuld *et al.* (1983), and Mausfeld and Niederée (1993).

The perceptual color terms defined previously are applied differently to related and unrelated colors. Unrelated colors only exhibit the perceptual attributes of hue, brightness, colorfulness, and saturation. The attributes that require judgement relative to a similarly illuminated white object cannot be perceived with unrelated colors. On the other hand, related colors exhibit all of the perceptual attributes of hue, brightness, lightness, colorfulness, chroma, and saturation.

4.8 DEFINITIONS IN EQUATIONS

The various terms used to carefully describe color appearance can be confusing at times. To keep the definitions straight, it is often helpful to think of them in terms of simple equations. These equations, while not strictly true in a mathematical sense, provide a first-order description of the relationships between the various color percepts. In fact, an understanding of the definitions in terms of the following equations provides the first building block toward understanding the construction of the various color appearance models.

Chroma can be thought of as colorfulness relative to the brightness of a similarly illuminated white as shown in Equation 4.1.

$$\text{Chroma} = \frac{\text{Colorfulness}}{\text{Brightness(White)}} \quad (4.1)$$

Saturation can be described as the colorfulness of a stimulus relative to its own brightness as illustrated in Equation 4.2.

$$\text{Saturation} = \frac{\text{Colorfulness}}{\text{Brightness}} \quad (4.2)$$

Finally, lightness can be expressed as the ratio of the brightness of a stimulus to the brightness of a similarly illuminated white stimulus as given in Equation 4.3.

$$\text{Lightness} = \frac{\text{Brightness}}{\text{Brightness(White)}} \quad (4.3)$$

The utility of these simple definitions in terms of equations is illustrated by a derivation of the fact that an alternative definition of saturation (used in some appearance models) is given by the ratio of chroma and lightness in Equation 4.4.

$$\text{Saturation} = \frac{\text{Chroma}}{\text{Lightness}} \quad (4.4)$$

This can be proven by first substituting the definitions of chroma and lightness from Equations 4.1 and 4.3 into Equation 4.4, arriving at Equation 4.5.

$$\text{Saturation} = \frac{\text{Colorfulness}}{\text{Brightness(White)}} \cdot \frac{\text{Brightness(White)}}{\text{Brightness}} \quad (4.5)$$

Completing the algebraic exercise by canceling out the brightness of the white terms in Equation 4.5 results in saturation being expressed as the

ratio of colorfulness to brightness as shown in Equation 4.6, which is identical to the original definition in Equation 4.2.

$$\text{Saturation} = \frac{\text{Colorfulness}}{\text{Brightness}} \quad (4.6)$$

4.9 BRIGHTNESS–COLORFULNESS VS LIGHTNESS–CHROMA

While color is typically thought of as three-dimensional and color matches can be specified by just three numbers, it turns out that three dimensions are not enough to completely specify color appearance. In fact, five perceptual dimensions are required for a complete specification of color appearance:

- Brightness
- Lightness
- Colorfulness
- Chroma
- Hue

Saturation is redundant since it is known if the five attributes above are known. However, in many practical color appearance applications it is not necessary to know all five attributes. Typically, related colors are of most interest and only the relative appearance attributes are of significant importance. Thus it is often sufficient to be concerned with only the relative appearance attributes of lightness, chroma, and hue.

There might seem to be some redundancy in using all five appearance attributes to describe a color appearance. However, this is not the case, as was elegantly described by Nayatani *et al.* (1990a). In that article, Nayatani *et al.* illustrated both theoretically and experimentally the distinction between brightness–colorfulness appearance matches and lightness–chroma appearance matches and showed that in most viewing conditions the two types of matches are distinct. Imagine viewing a yellow school bus outside on a sunny day. The yellow bus will exhibit its typical appearance attributes of hue (yellow), brightness (high), lightness (high), colorfulness (high), and chroma (high). Now imagine viewing a printed photographic reproduction of the school bus in the relatively subdued lighting of an office or home. The image of the bus could be a perfect match to the original object in hue (yellow), lightness (high), and chroma (high). However, the brightness and colorfulness of the print viewed in subdued lighting could never equal that of the original school bus viewed in bright sunlight. This is simply because of the lack of energy reflecting off the print relative to the original object. If that same print were carried outside into the bright sunlight that the original bus was viewed under, it is then possible that the reproduction could match the original object in all five appearance attributes.

So which is more important, the matching (i.e., reproduction) of brightness and colorfulness or the matching of lightness and chroma? (Note that

hue is defined the same way in either circumstance.) The answer depends on the application, but it is safe to say that much more often it is lightness and chroma that are of greater importance. As illustrated by the above example, in color reproduction applications it is typically possible and desirable to aspire to lightness–chroma matching. Imagine trying to make reproductions with a brightness–colorfulness matching objective. To reproduce the sunlight-illuminated school bus in office lighting, one would have to make a print that was literally glowing in order to reproduce brightness and colorfulness. This is not physically possible. Going in the other direction (subdued lighting to bright lighting) is possible, but is it desirable? Imagine taking a photograph of a person at a candlelight dinner and making a reproduction to be viewed under bright sunlight. It would be easy to reproduce the brightness and colorfulness of the original scene, but the print would be extremely dark (essentially black everywhere) and it would be considered a very poor print. Customers of such color reproductions expect lightness–chroma reproduction. Attempts to make such reproductions using a color appearance model across changes in luminance are given in Figures 4.2 and 4.3.

Reproduction at Higher Luminance

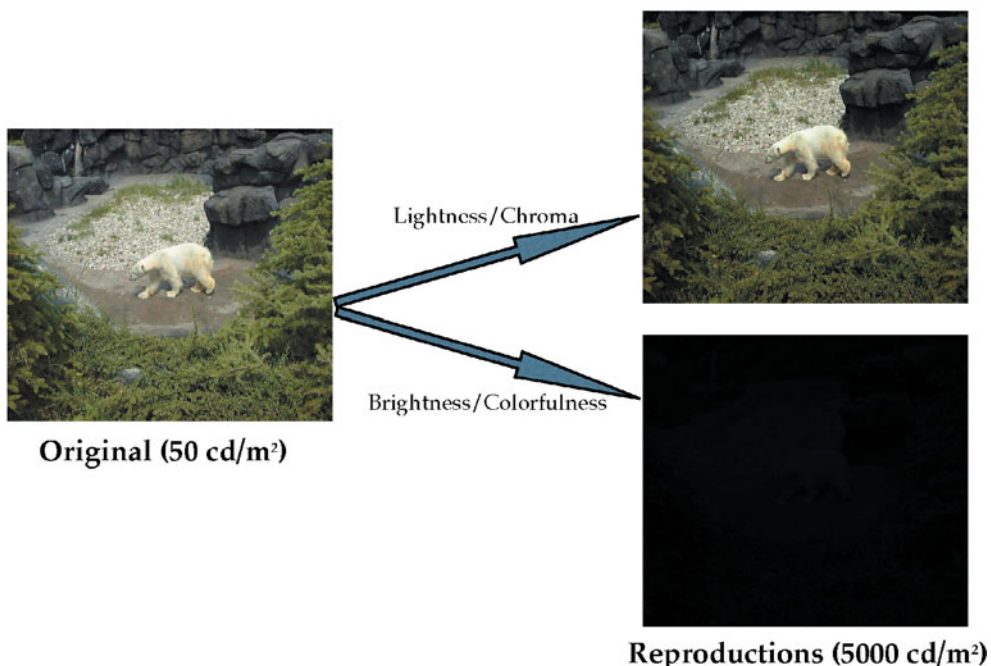


Figure 4.2 Comparison of lightness–chroma reproduction with brightness–colorfulness reproduction when the original is at a lower luminance than the reproduction. Brightness–chroma reproduction results in an image that is very dark to compensate for the increased level of illumination. Lightness–chroma reproduction represents more complete adaptation since they are relative appearance attributes

Reproduction at Lower Luminance

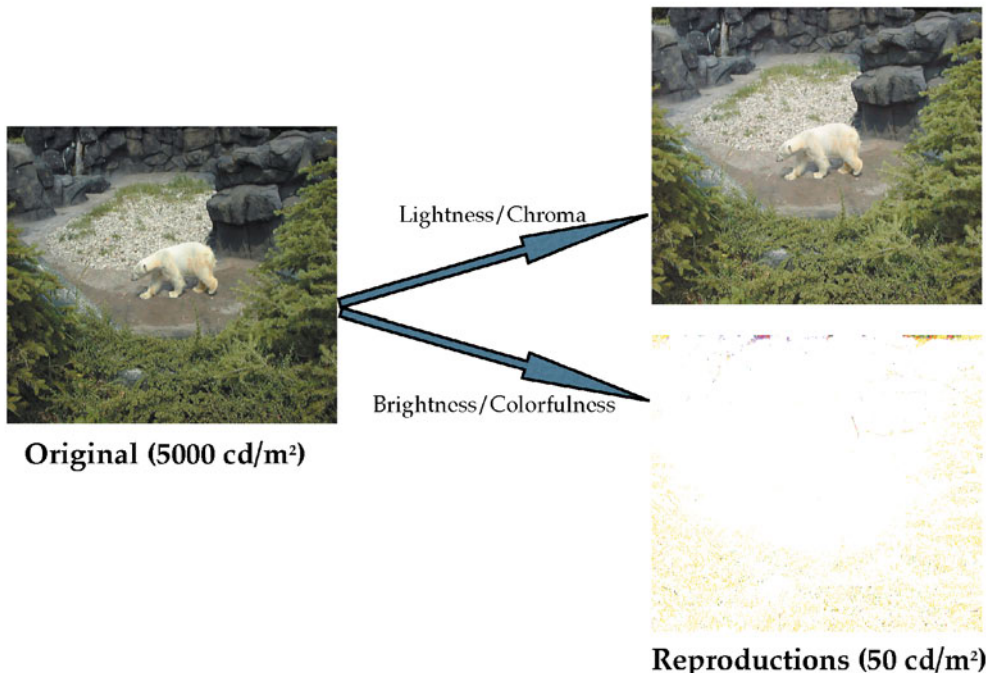


Figure 4.3 Comparison of lightness–chroma reproduction with brightness–colorfulness reproduction when the original is at a higher luminance than the reproduction. Brightness–chroma reproduction results in an image that is very bright to compensate for the decreased level of illumination. Lightness–chroma reproduction represents more complete adaptation since they are relative appearance attributes

There are a few situations in which brightness and colorfulness might be more important than lightness and chroma. Nayatani *et al.* (1990a) suggest a few such situations. One of those is in the specification of the color rendering properties of light sources. In such an application it might be more important to know how bright and colorful objects appear under a given light source, rather than just lightness and chroma. Another situation might be in the judgement of image quality for certain types of reproductions. For example, in comparing the quality of projected transparencies in a darkened (or not so darkened) room, observers might be more interested in the brightness and colorfulness of an image than in the lightness and chroma. In fact, the lightness and chroma of image elements might remain nearly constant as the luminance of the projector is decreased, while it is fairly intuitive that the perceived image quality would be decreasing. It is very rare for observers to comment that they wish the image from a slide or overhead projector was not so bright unless a bright overhead projector image is displayed adjacent to a dim 35 mm projector image!

Color Order Systems

Since color appearance is a basic perception, the most direct method to measure it is through psychophysical techniques designed to elucidate perceptually uniform scales of the various color appearance attributes defined in Chapter 4. When such experiments are performed, it is possible to specify stimuli using basic colorimetry that embody the perceptual color appearance attributes. A collection of such stimuli, appropriately specified and denoted, forms a color order system. Such a color order system does allow a fairly unambiguous specification of color appearance. However, there is no reason to expect that the specified appearances will generalize to other viewing conditions or be mathematically related to physical measurements in any straightforward way. Thus, color order systems provide data and a technique for specifying color appearance, but do not provide a mathematical framework to allow extension of that data to novel viewing conditions. Therefore color order systems are of significant interest in the development and testing of color appearance models, but cannot serve as a replacement for them.

This chapter provides an overview of some color order systems that are of particular interest in color appearance modeling and device-independent color imaging. Their importance and application will become self-evident in this and later chapters. Additional details on color order systems can be found in Berns' colorimetry text (Berns 2000), Hunt's text on color measurement (Hunt 1991a, 1998), Wyszecki and Stiles' reference volume on color science (Wyszecki and Stiles 1982), Wyszecki's review chapter on color appearance (Wyszecki 1986), Derefeldt's review on color appearance systems (Derefeldt 1991), and Kuehni's detailed historical review of color spaces (Kuehni 2003).

5.1 OVERVIEW AND REQUIREMENTS

Many definitions of color order systems have been suggested and it is probably most useful to adopt some combination of them. Wyszecki (1986) points out that color order systems fall into three broad groups:

- One based on the principles of additive mixtures of color stimuli. A well-known example of is the Ostwald system.
- One consisting of systems based on the principles of colorant mixtures. The Lovibond tintometer provides an example of a color specification system based on the subtractive mixture of colorants.
- One consisting of those based on the principles of color perception or color appearance.

In fact Derefeldt (1991) suggests that color appearance systems are the only systems appropriate for general use. She goes on to state that color appearance systems are defined by perceptual color coordinates or scales, and uniform or equal visual spacing of colors according to these scales.

This chapter focuses on color appearance systems such as the Natural Color System (NCS) and the Munsell system. Hunt (1991a) adds a useful constraint onto the definition of color order systems by stating that it must be possible to interpolate between samples in the system in an unambiguous way. Finally, a practical restriction on color order systems is that they be physically embodied with stable samples that are produced to tight tolerances. To summarize, color order systems are constrained in that they must:

- Be an orderly (and continuous) arrangement of colors.
- Include a logical system of denotation.
- Incorporate perceptually meaningful dimensions.
- Be embodied with stable, accurate, and precise samples.

A further objective for a generally useful color order system is that the perceptual scales represent perceived magnitudes uniformly or that differences on the scales be of equal perceived magnitude.

The above definition excludes some color systems that have been found useful in practical applications. For example, the Pantone Color Formula Guide is a useful color specification system for inks, but it is not a color order system since it does not include continuous scales or an appropriate embodiment. It is more appropriately considered a color naming system. Swatches used to specify paint colors also fall into this category.

There are a variety of applications of color order systems in the study of color appearance. They provide independent data on the perceptual scaling of various appearance attributes such as lightness, hue, and chroma that can be used to evaluate mathematical models. Their embodiments provide reliable sample stimuli that can be used unambiguously in psychophysical experiments on color appearance. Their nomenclature provides a useful system for the specification and communication of color appearances. They also provide a useful educational tool for the explanation of various color appearance attributes and phenomena. The uses of color order systems in color appearance modeling are discussed in more detail in Section 5.6.

5.2 THE MUNSELL BOOK OF COLOR

One of the most widely used color order systems, particularly in the United States, is the Munsell system, embodied in the Munsell Book of Color. The history of the Munsell system has been reviewed by Nickerson (1940, 1976a,b,c), and interesting insight can be obtained by reviewing the visual experiments leading to the renotation of the Munsell colors in the 1940s (Newhall 1940). The system was developed by an artist, Albert H. Munsell, in the early part of the 20th century. Munsell was particularly interested in developing a system that would aid in the education of children. The basic premise of the system is to specify color appearance according to three attributes:

- Hue (H)
- Value (V)
- Chroma (C)

The definitions of the three Munsell dimensions match the current definitions of the corresponding appearance attributes, with Munsell Value referring to lightness. Munsell's objective was to specify colors (both psychophysically and physically) with equal visual increments along each of the three perceptual dimensions.

Munsell Value

The Munsell value scale is the anchor of the system. There are ten main steps in the Munsell value scale with white given a notation of 10, black denoted zero, and intermediate grays given notations ranging between zero and 10. The design of the Munsell value scale is such that an intermediate gray with a Munsell value of 5 (denoted N5 for a neutral sample with value 5) is perceptually halfway between an ideal white (N10) and an ideal black (N0). Also, the perceived lightness difference between N3 and N4 samples is equivalent to the lightness difference between N6 and N7 samples, or any other samples varying by one step in Munsell value. Lightness perceptions falling in between two Munsell value steps are denoted with decimals. For example, Munsell value 4.5 falls perceptually halfway between Munsell value 4 and 5. It is important to note that the relationship between Munsell value V and relative luminance Y is nonlinear. In fact, it is specified by the fifth-order polynomial given in Equation 5.1 and plotted in Figure 5.1.

$$Y = 1.2219V - 0.23111V^2 + 0.23951V^3 - 0.021009V^4 + 0.0008404V^5 \quad (5.1)$$

As can be seen in Figure 5.1, a sample that is perceived to be a middle gray (N5) has a relative luminance (or luminous reflectance factor) of about 20%.

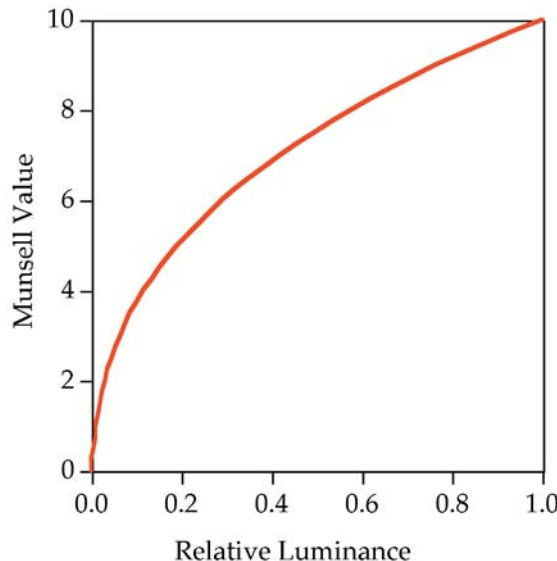


Figure 5.1 Munsell value as a function of relative luminance

The Munsell value of any color (independent of hue or chroma) is defined by the same univariate relationship with relative luminance. Thus, if the Munsell value of a sample is known, so is its relative luminance, CIE Y, and vice versa. Unfortunately, the fifth-order polynomial in Equation 5.1 cannot be analytically inverted for practical application. Since the CIE lightness scale L^* was designed to model the Munsell system, it provides a very good computational approximation to Munsell value. As a very useful and accurate general rule, the Munsell value of a stimulus can be obtained from its CIE L^* (Ill. C, 2° Obs.) by simply dividing by 10.

Munsell Hue

The next dimension of the Munsell system is hue. The hue circle in the Munsell system is divided into five principle hues (purple, blue, green, yellow, and red, denoted 5P, 5B, 5G, 5Y, and 5R, respectively) and is designed to divide the complete hue circle into equal perceptual intervals. Five intermediate hues are also designated in the Munsell system as 5PB, 5BG, 5GY, 5YR, and 5RP for a total of 10 hue names. For each of the ten hues there are ten integral hues with notations as illustrated by the range between 5PB and 5P, which is 6PB, 7PB, 8PB, 9PB, 10PB, 1P, 2P, 3P, and 4P. This type of sequence continues around the entire hue circle, resulting in 100 integer hue designations that are intended to be equal perceived hue intervals. Hues intermediate to the integer designations are denoted with decimal values (e.g., 7.5PB).

Munsell Chroma

The third dimension of the Munsell system is chroma. The chroma scale is designed to have equal visual increments from a chroma of zero for neutral samples to increasing chromas for samples with stronger hue content. There is no set maximum for the chroma scale. The highest chromas achieved depend on the hue and value of the samples and the colorants used to produce them. For example, there are no high chroma samples with a yellow hue and low value, or a purple hue and high value. Such stimuli cannot be physically produced due to the nature of the human visual response. Figure 5.2 illustrates the three-dimensional arrangement of the Munsell system in terms of a constant value plane (Figure 5.2a) and a constant hue plane (Figure 5.2b). Figure 5.3 illustrates similar planes and a three-dimensional perspective of the Munsell system generated using a computer graphics model of the system. The Munsell system is used to denote a specific colored stimulus using its Munsell hue, value, and chroma designations in a triplet arranged with the hue designation followed by the value, a forward slash (/), and then the chroma. For example, a red stimulus of medium lightness and fairly high chroma would be designated 7.5R5/10 (hue value/chroma).

Munsell Book of Color

The Munsell system is embodied in the *Munsell Book of Color*. The *Munsell Book of Color* consists of about 1500 samples arranged on 40 pages of constant hue. Each hue page is arranged in order of increasing lightness (bottom to top) and chroma (center of book to edge). The samples consist of painted paper and are available in both glossy and matte surfaces. Larger sized Munsell samples can also be purchased for special applications such as visual experiments or construction of test targets for imaging systems. Munsell samples are produced to colorimetric aim points that were specified by the experiments leading up to the Munsell renotation (Newhall, 1940). The chromaticity coordinates and luminance factors for each Munsell sample (including many that cannot be easily produced) can be found in Wyszecki and Stiles (1982). The colorimetric specifications utilize CIE illuminant C and the CIE 1931 Standard Colorimetric Observer (2°). These specifications should be kept in mind when viewing any embodiment of the Munsell system. The perceptual uniformity of the system is only valid under source C, on a uniform middle gray (N5) background, with a sufficiently high illuminance level (e.g., greater than 500 lux). Viewing the samples in the *Munsell Book of Color* under any other viewing conditions does not represent an embodiment of the Munsell system.

It is worth noting that the Munsell system was scaled as three one-dimensional scales of color appearance and the relationship between Munsell step size and perceived color difference is not constant across the three dimensions. It is generally accepted, see discussion of Nickerson Index

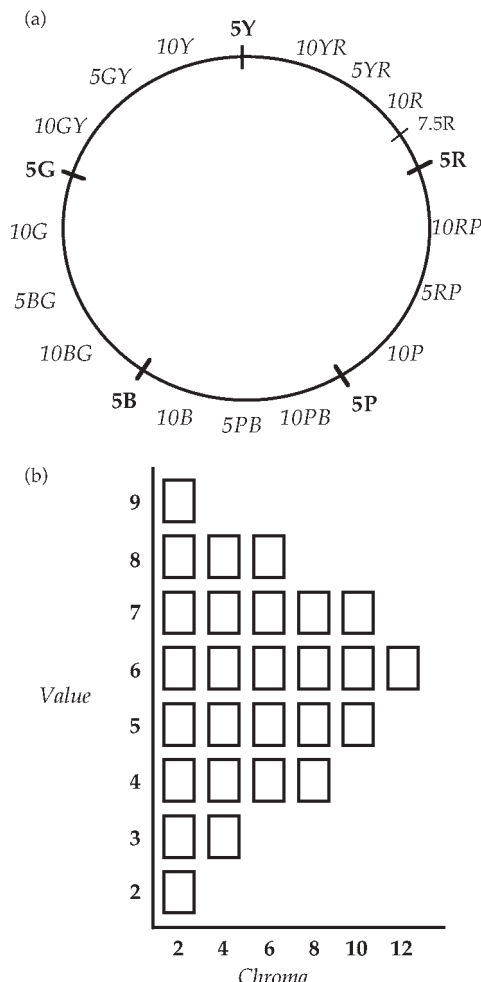


Figure 5.2 A graphical representation of (a) the hue circle and (b) a value/chroma plane of constant hue in the Munsell system

of Fading in Berns (2000) or discussion of Munsell system in Hunt (1998), that an increment of two Munsell chroma steps is perceptually equal the color change of one step in Munsell value. Step size in Munsell hue is dependent on the chroma of the samples in question.

5.3 THE SWEDISH NATURAL COLOR SYSTEM (NCS)

More recently, the Natural Color System, or NCS, has been developed in Sweden (Hard and Sivik, 1981) and adopted as a national standard in Sweden (SS 01 91 02 and SS 01 91 03) and a few other European countries.

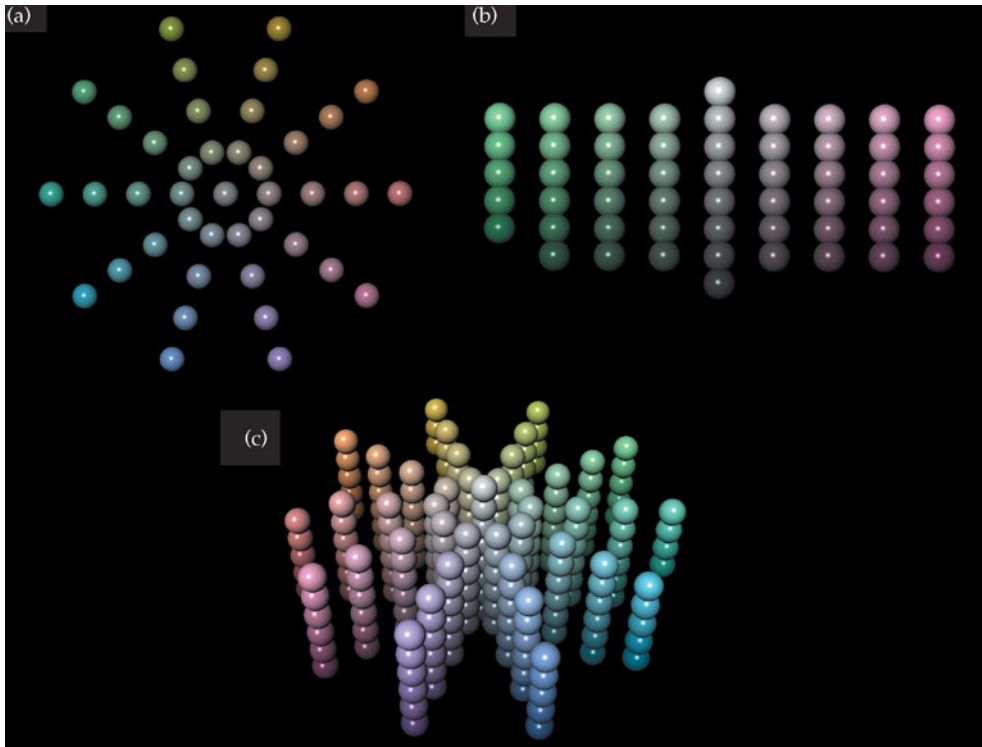


Figure 5.3 A color rendering of samples from the Munsell system in (a) a constant value plane, (b) a pair of constant hue planes, and (c) a three-dimensional perspective

The NCS is based on the opponent colors theory of Hering. The hue circle is broken up into four quadrants defined by the unique hues red, yellow, green, and blue as illustrated in Figure 5.4(a). The four unique hues are arranged orthogonally with equal numbers of steps between them. Thus, while the NCS hues are spaced with equal perceived intervals between each hue, the intervals are of different magnitude within each of the four quadrants. This is because there are more visually distinct hues between unique red and unique blue than between unique yellow and unique green, for example. Perceived hues that fall between the unique hues are given notations representing the relative perceptual composition of the two neighboring unique hues. For example, an orange hue that is perceived to be midway between unique red and unique yellow would be given the notation Y50R.

Once the NCS hue notation is established, the remaining two dimensions of relative color appearance are specified on trilinear axes as illustrated in Figure 5.4(b). The three corners of the triangle represent colors of maximal blackness (S), whiteness (W), and chromaticness (C). For any stimulus, the whiteness, blackness and chromaticness must sum to 100. Thus the sample of maximum blackness is denoted as $s = 100$, $w = 0$, and $c = 0$. The sample

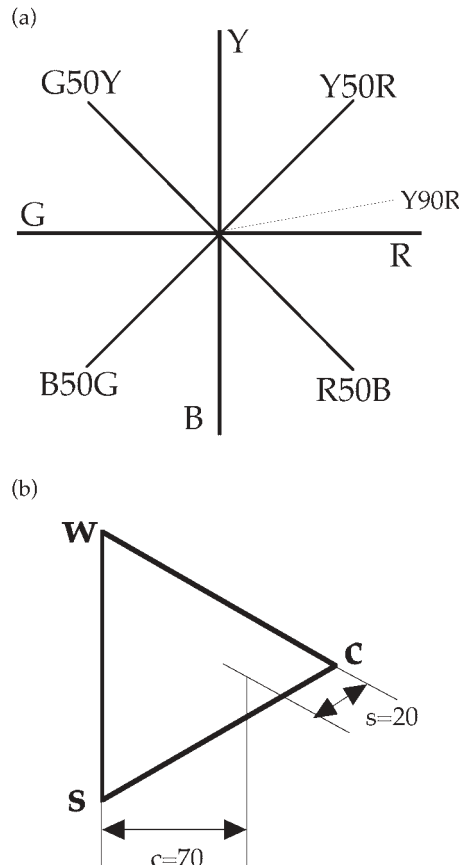


Figure 5.4 A graphical representation of (a) the hue circle and (b) a blackness/chromaticness plane of constant hue in the NCS system

of maximum whiteness is denoted as $s = 0$, $w = 100$, and $c = 0$. The sample of maximum chromaticness is denoted $s = 0$, $w = 0$, and $c = 100$. Since the three numbers must sum to 100, only two are required for a complete specification (along with the hue notation). Typically, blackness and chromaticness are used. For example an intermediate sample might be denoted $s = 20$ and $c = 70$, implying a whiteness, $w = 10$. The maximum chromaticness for each hue is defined using a mental anchor of the maximally chromatic sample that could be perceived for that hue. Thus there is no direct relationship between Munsell chroma and NCS chromaticness. Likewise, there is no simple relationship between Munsell value and NCS blackness. It is also important to note that the samples of maximum chromaticness are of different relative luminance and lightness for the various hues. The Munsell and NCS systems represent two different ways to specify perceptual color appearance. It is not possible to say that one is better than the other, it can

only be stated that the two are different. This was recently reaffirmed in the report of CIE TC1-31 (CIE, 1996a), which was requested by ISO to recommend a single color order system as an international standard along with techniques to convert from one to another. This international committee of experts concluded that such a task is impossible.

A color is denoted in the NCS by its blackness s , chromaticness c , and hue. For example, the stimulus described in the previous section with a Munsell designation of 7.5YR 5/10 has an NCS designation of 20, 70, Y90R. This suggests that the sample is nearly a unique red, with only 10% yellow content. It is further described as being highly chromatic (70%) with only a small amount of blackness (20%). Note that even though this sample is of medium Munsell value, it is of substantially lower blackness (or higher whiteness) in the NCS. This illustrates the fundamental difference between the Munsell value scale and the NCS whiteness–blackness–chromaticness scale.

Like the Munsell system, the NCS is embodied in an atlas and specified by CIE tristimulus values based on extensive visual observations. The NCS atlas includes 40 different hues and samples in steps of 10 along the blackness and chromaticness scales. Since it is not possible to produce all of the possible samples, due to limitations in pigments, there are approximately 1500 samples in the atlas. The NCS atlas should also be viewed under daylight illumination with appropriate luminance levels and background. NCS samples are also available in various sizes for different specialized applications. As a Swedish national standard, the NCS is taught at a young age and used widely in color communication in Sweden, providing an enviable level of precision in everyday color communication.

5.4 THE COLORCURVE SYSTEM

A recently developed color order system is the Colorcurve system (Stanziola 1992), designed as a color communication system representing a combination of a color appearance system and a color mixture system. The system is designed such that colors can be specified within the system and then spectral reflectance data for each sample can be used to formulate matching samples in various materials or media. Thus each sample in the system is specified not only by its colorimetric coordinates, but also by its spectral reflectance properties.

The Colorcurve system uses the CIELAB color space as a starting point. Eighteen different L^* levels were chosen at which to construct constant lightness planes in the system. The L^* levels range from 30 to 95 in steps of five units with a few extra levels incorporated at the higher lightness levels that are particularly important in design (e.g., light colors are popular for wall paint). At each lightness level, nine starting points were selected. These consisted of one gray ($a^* = 0$, $b^* = 0$) and eight chromatic colors with chroma C^* of 60. The chromatic starting points were red (60,0), orange (42.5, 42.5), yellow (0,60), yellow/green (-42.5, 42.5), green (-60,0), blue/green (-42.5,

–42.5), blue (0,–60), and purple (42.5,–42.5). Thus the starting points were defined using principles of a color appearance space.

The remainder of the system was constructed using additive color mixing. Each quadrant of the CIELAB a^*b^* plane was filled with a rectangular sampling of additive mixtures of the gray and three chromatic starting points in that quadrant. Equal steps in the Colorcurve designations represent equal additive mixtures between the four starting points. These principles were used to define all of the aim points for the Colorcurve system. The samples were then formulated with real pigments such that the system could be embodied along with the desired spectral reflectance curve specifications. The system is embodied in two atlases made up of samples of nitrocellulose lacquer coated on paper. The *Master Atlas* is made up of about 1200 samples at the 18 different lightness levels. There is also a *Gray and Pastel Atlas* made up of 956 additional samples that more finely sample the regions of color space that are near grays or pastels. Since the Colorcurve system is specified by the spectral reflectance characteristics of the samples, the viewing illumination is not critical as long as a spectral match is made to the color curve sample. If a spectral match is made, the sample produced will match the Colorcurve sample under all light sources. This is not possible with other color order systems. Like the other color order systems, Colorcurve samples can be obtained in a variety of forms and sizes for different applications.

One unique attribute of the Colorcurve system is of particular interest. The samples in the atlases are circular rather than square as found in most systems. The circular samples avoid two difficulties with color atlases. The first is the contrast illusion of dark spots that appear at the corners between square samples (the Hermann grid illusion). The second is that it is impossible to mount a circular sample crooked!

5.5 OTHER COLOR ORDER SYSTEMS

The Munsell and NCS systems described above are the most important color order systems in the study of color appearance models. The Colorcurve system provides an interesting combination of color appearance and color mixture systems that could provide a useful source of samples for color appearance and reproduction research. However, there are many other color order systems that have been created for a variety of purposes. Derefeldt (1991) and Wyszecki and Stiles (1982) provide more details, but there are a few systems that warrant mention here. These include the OSA Uniform Color Scales, the DIN system, and the Ostwald system.

OSA Uniform Color Scales

The Optical Society of America (OSA) set up a committee on Uniform Color Scales in 1947. The ultimate results of this committee's work were described

by MacAdam (1974, 1978) as the OSA Uniform Color Scales system, or OSA UCS. The OSA system is a color appearance system, but it is significantly different in nature from either the Munsell or NCS systems. The OSA system is designed such that a given sample is equal in perceptual color difference from each of its neighbors in three-dimensional color space (not simply one dimension at a time as in the Munsell system). The OSA space is designed in a three-dimensional Euclidean geometry with L , j , and g axes representing lightness, yellowness–blueness, and redness–greenness, respectively. In order to make each sample equally spaced from each of its neighbors, a regular rhombohedral sampling of the three-dimensional space is required in which each sample has 12 nearest neighbors, all at an equal distance. If the 12 points of the nearest neighbors to a sample are connected, they form a polyhedron known as a cubo-octohedron. Such sampling allows rectangularly sampled planes of the color space to be viewed from a variety of directions. Figure 5.5(a) shows a computer graphics representation of two adjacent constant lightness planes in the OSA system illustrating the sampling scheme. Figure 5.5(b) illustrates a three-dimensional representation of the OSA system. It is clear that the objective of equal color differences in all directions results in a very different type of color order system. Perhaps due to its complex geometry (and the lack of a useful embodiment), the OSA system is not very popular. It does provide another set of data that could be used in the evaluation of color appearance and color difference models. The OSA space was also specified in terms of equations to transform from CIE coordinates to the OSA system's L , j , and g coordinates. Unfortunately the equations are not invertible, limiting their practical utility. The equations and sample point specifications for the OSA system can be found in Wyszecki and Stiles (1982).

DIN System

The DIN (Deutsches Institut für Normung) system was developed in Germany with the perceptual variables of hue, saturation, and darkness. An historical overview of the DIN system was presented by Richter and Witt (1986). The specification of colors in the DIN system is closely related to colorimetric specification on a chromaticity diagram. Colors of equal hue in the DIN system fall on lines of constant dominant (or complementary) wavelength on the chromaticity diagram (i.e., straight lines radiating from the white point). Colors of constant DIN saturation represent constant chromaticities. The sampling of DIN hue and saturation is designed to be perceptually uniform. DIN darkness is related to the luminous reflectance of the sample relative to an ideal sample (a sample that either reflects all, or none, of the incident energy at each wavelength) of the same chromaticity resulting in a darkness scale that is similar to NCS blackness rather than Munsell value. The DIN system is embodied in the DIN Color Chart that includes constant hue pages with a rectangular sampling of darkness and saturation. Thus columns on a

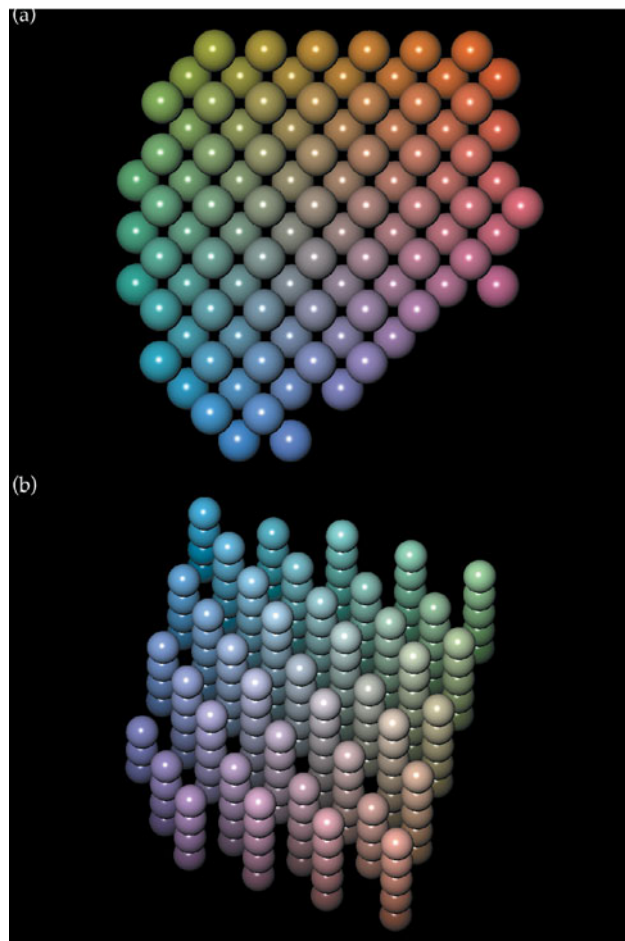


Figure 5.5 A color rendering of samples from the OSA UCS system in (a) a pair of adjacent constant lightness planes and (b) a three-dimensional projection

DIN page represent constant chromaticity (DIN saturation) and appear as a shadow series (a single object illuminated at various levels of the same illuminant). The DIN charts also illustrate that chromaticity differences become less distinguishable as darkness increases. The bottom row of any given DIN page appears uniformly black.

Ostwald System

The Ostwald system has been widely used in art and design and is therefore of substantial historical interest (Derefeldt 1991). Like the NCS system, the

Ostwald system is based on Hering's opponent colors theory. However, the Ostwald system, much like the Colorcurve system, represents a combination of a color appearance system and a color mixture system. Ostwald used Hering's four unique hues to set up a hue circle, but rather than placing the perceptually opponent hues opposite one another, he used colorimetric complements (chromaticities connected by a straight line through the white point on a chromaticity diagram) in the opposite positions on the hue circle. The Ostwald system also includes a trilinear representation of white content, black content, and full-color content on each constant hue plane. In the NCS system, these planes are defined according to perceptual color scales. However, in the Ostwald system, these planes were defined by additive color mixtures of the three maxima located at the corners of the triangles. Thus the Ostwald system was set up with color appearance in mind, but the samples were filled in using additive color mixing. (This is exactly analogous to the much more recent formulation of the Colorcurve system based on CIELAB.)

5.6 USES OF COLOR ORDER SYSTEMS

Color order systems have a variety of applications in the study of color appearance and related areas. These include use as samples in experiments, color design, communication, education, model testing, test targets, and other applications where physical samples are helpful.

Color Order Systems in Visual Experiments

Often in visual experiments aimed at studying color appearance it is necessary to view and/or match a variety of colored stimuli under different viewing conditions. Color order systems provide a useful source of samples for such experiments. For example, an experimenter might select a collection of Munsell, NCS, or Colorcurve samples to scale in a color appearance experiment. These samples will have well-known characteristics and in publishing the notations of the samples used, the researchers provide a useful definition of the stimuli that can be used by others to replicate the experiments. Note that actually using samples from the color order systems, and not just their designations on arbitrary samples, has the advantage that the reflectance characteristics of the samples are also defined. A related use of color order systems in appearance experiments involves teaching the system to observers and then asking them to assign designations (Munsell and NCS are particularly useful in this type of experiment) to samples viewed under a variety of conditions. This allows a specification of the change in appearance caused by various changes in viewing conditions which can be used, together with the colorimetric specifications of each sample in each viewing condition, to formulate and test color appearance models.

Color Order Systems in Art and Design

Color order systems are often used in art and design. Their very nature as an orderly arrangement of colors allows designers to easily select samples with various color relationships. For example, with the Munsell system it is simple to select a range of colors of constant lightness or hue, or to select hues that complement one another in various ways. Color mixing systems provide this utility in addition to providing some insight for artists to help them actually produce the colors in various media. The color order systems not only provide a design tool, but also incorporate a communication tool in their designations, allowing the chosen colors to be communicated to those producing the materials to be incorporated into a design.

Color Order Systems in Communication

Clearly, precise communication of color appearance is an application for color order systems. This is effective as long as those on both ends of the communication link are viewing the systems in properly controlled environments. While colorimetric coordinates have the potential to provide much more precise, accurate, and useful specifications of colors, the perceptual meaning is not so readily apparent to various users. A color order system can provide a more readily accessible communication tool. It can also be used to describe a color appearance to someone familiar with the system, but not necessarily in possession of an atlas. An interesting example of this type of communication can be found in the ANSI specifications for viewing of color images (ANSI 1989) in which the backgrounds are specified in terms of Munsell value when a reflectance factor alone is sufficient and potentially more precise.

Color Order Systems in Education

Color order systems are immensely useful in education regarding color appearance (as well as many other aspects of color). For example, examination of the Munsell system allows a visual definition of the color appearance attributes of lightness, chroma, and hue. Moving pages from the *Munsell Book of Color* from a low luminance level to a high luminance level allows for a nice demonstration of how brightness and colorfulness increase substantially while lightness and chroma remain nearly constant. The DIN system is useful to illustrate the difference between chroma and saturation and how saturation is related to a shadow series (a single object illuminated by decreasing illuminance levels of the same spectral power distribution). Color order systems can also be educational in their limitations. For example, in the Munsell system, constant value is defined as constant relative luminance. However, it is well known (Helmholtz–Kohlrausch effect described in

Chapter 6) that as samples increase in chroma at constant relative luminance they appear lighter. One need only examine a series of Munsell samples of constant value and varying chroma to see that indeed there is a large and systematic variation in lightness. Lastly, systems like the NCS systems can be a great aid in education regarding the opponent theory of color vision, particularly in their hue designations which closely follow the physiological encoding of color.

Color Order Systems to Evaluate Mathematical Color Appearance Models

Since color order systems such as Munsell and NCS are based on perceptual scaling of color appearance, they provide readily available data that can be used to evaluate mathematical color appearance models. For example, the Munsell system includes planes of constant lightness and hue, and cylindrical surfaces of constant chroma. The tristimulus specifications of the Munsell system can be converted into the appropriate color appearance predictors for a given color appearance model in order to see how well it predicts the constant hue, lightness, and chroma contours. Such an evaluation provides a useful, widely understood technique for the intercomparison of various color appearance models. Intercomparison of the predictions of Munsell and NCS contours in various models also allows further study to understand the fundamental differences between the two systems.

Color Order Systems and Imaging Systems

Color order systems can also be used as sources for test targets for imaging systems or other measurement devices. For example, the Macbeth Color Checker Chart (McCamy *et al.* 1976) is a commonly used test target for imaging systems that is partially based on samples from the Munsell system. Despite its common use, the Macbeth Color Checker Chart incorporates only a small sample of colors (24) and an incomplete sampling of color space. Targets of greater practical utility could fairly easily be constructed. Samples from various color order systems can be used to develop custom test targets that can be reliably specified and replicated elsewhere.

Limitations of Color Order Systems

While color order systems have a variety of useful applications in color appearance, they are not a substitute for a color appearance model. In general they suffer from two significant limitations in this regard. First, they are not specified mathematically in relationship to physically measurable values. While both the Munsell and NCS systems have colorimetric specifications for each sample in the system, there are no equations to relate the

colorimetric coordinates to the perceptual coordinates of the color order systems. Approximate equations have been derived by statistical fitting and neural network modeling, but the only reliable technique for transformation from CIE colorimetry to color order system coordinates remains look-up table interpolation. Clearly, the lack of mathematical definitions in the forward direction precludes the possibility of the analytical inverse models for the required reverse direction. Second, these color order systems have been established as perceptual scales of color appearance for a single viewing condition. They provide no data with respect to the changes in color appearance induced by changes in viewing conditions.

5.7 COLOR NAMING SYSTEMS

There are a variety of color specification systems available that do not meet the requirements for consideration as true color order systems, but are useful for some practical applications. Generally such systems, more properly considered color naming systems, are not arranged in a perceptually ordered manner (although some are arranged in order according to some imaging process), and are not presented or specified for controlled viewing conditions. In addition, the physical embodiments of these systems are not controlled with the colorimetric accuracy required for precise color communication. Examples of such systems include the Pantone, Toyo, Focoltone, and Trumatch systems.

The Pantone System

The main component of the Pantone system is the *Pantone Color Formula Guide*. This guide is a swatch book containing 1012 Pantone spot color ink mixtures on coated and uncoated stock. Each swatch has a numerical identifier that can be used to communicate the desired color to a printer. The printer will then mix the spot color ink using the prescribed Pantone formula and the resulting printed color should be a reasonable approximation to the color in the swatch book. This system is the prevalent tool for the specification of spot color in the USA.

The *Pantone Process Color Imaging Guide* includes 942 color swatches illustrating the Pantone spot colors that can be reasonably well simulated with a four-color (CMYK) printing process. The swatch book includes a patch of the Pantone spot color adjacent to the process-color simulation to indicate the variance that can be expected.

The Trumatch System

The *Trumatch Colorfinder* is a swatch book including over 2000 process color samples. These samples are arranged in an order that is slightly more

perceptually based than the Pantone system. Such a system allows computer users to select CMYK color specifications according to the appearance of printed swatches rather than relying on the approximate color represented on a CRT display for a given CMYK specification. The user finds the desired color in the swatch book, sets the particular area in an image to those CMYK values, and then proceeds to ignore the often inappropriate appearance of the computer display, with confidence that the final printed color will be a fairly close approximation to the color selected in the swatch book.

Other Systems

In addition to the Pantone and Trumatch process color guides that can be used as shortcuts to specification of colors that are ultimately to be printed, there is the *PostScript Process Color Guide* published by Agfa that includes over 16 000 examples of process colors representing a complete sampling of CMY combinations from 0% to 100% (dot coverage) in 5% increments with additional samples incorporating four different levels of black ink coverage. The samples are presented on both coated and uncoated stock.

Given the variability in printing inks, papers, and processes, these systems can only be considered as approximate guides. They are known to not be very stable and it is often recommended that swatch books be replaced every six months or so. However, their performance is far superior than working with no guides and uncalibrated/uncharacterized imaging systems. However, a system in which all of the imaging devices have been carefully calibrated and characterized, and in which viewing conditions are carefully controlled, will be capable of easily producing superior color accuracy and precision for within-gamut colors. For out-of-gamut colors (such as metallic inks which cannot be simulated on a two-dimensional computer graphics display) a swatch-book system might still prove invaluable.

6

Color Appearance Phenomena

Chapter 3 describes the fundamental concepts of basic colorimetry. While the CIE system of colorimetry has proven to be extremely useful, it is important to remember that it has limitations. Most of its limitations are inherent in the design of a system of tristimulus values based on color matching. Such a system can accurately predict color matches for an average observer, but it incorporates none of the information necessary for specifying the color appearance of those matching stimuli. Such is the realm of color appearance models. Tristimulus values can be considered as a nominal (or at best ordinal) scale of color. They can be used to state whether two stimuli match or not. The specification of color differences requires interval scales and the description of color appearance requires interval scales (for hue) and ratio scales (for brightness, lightness, colorfulness, and chroma). Additional information is needed, in conjunction with tristimulus values, to derive these more sophisticated scales.

Where is this additional information found? Why is it necessary? What causes tristimulus colorimetry to ‘fail’? These questions can be answered through examination of various color appearance phenomena, several of which are described in this chapter. These phenomena represent instances in which one of the necessary requirements for the success of tristimulus colorimetry is violated. Understanding what causes these violations and the nature of the discrepancies is what allows the construction of color appearance models.

6.1 WHAT ARE COLOR APPEARANCE PHENOMENA?

Given two stimuli with identical CIE XYZ tristimulus values, they will match in color for an average observer as long as certain constraints are followed.

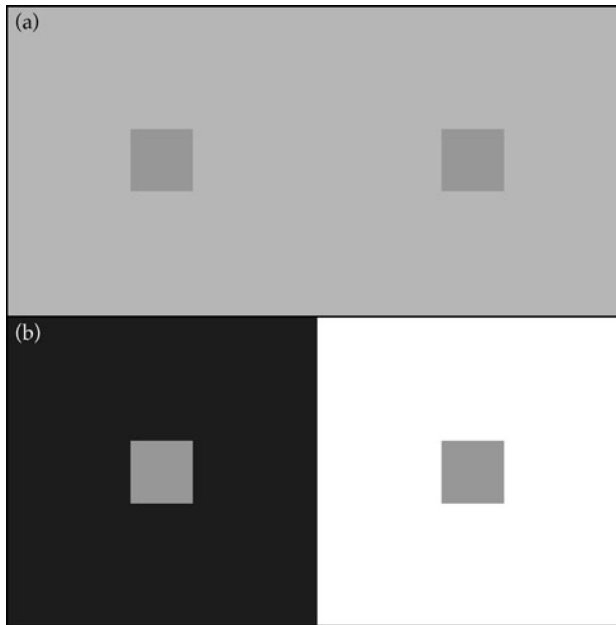


Figure 6.1 An example of simultaneous contrast. The gray patches on the gray background (a) are physically identical to those on the white and black backgrounds (b)

These constraints include factors such as the retinal locus of stimulation, the angular subtense, and the luminance level. In addition, the two stimuli must be viewed with identical surrounds, backgrounds, size, shape, surface characteristics, illumination geometry, etc. If any of the above constraints are violated, it is likely that the color match will no longer hold. However, in many practical applications, the constraints necessary for successful color-match prediction using simple tristimulus colorimetry cannot be met. It is these applications that require colorimetry to be enhanced to include the influences of these variables. Such enhancements are color appearance models. The various phenomena that ‘break’ the simple XYZ tristimulus system are the topics of the following sections of this chapter.

Figure 6.1 illustrates a simple example of one color appearance phenomenon: *simultaneous contrast*, or *induction*. In Figure 6.1(a), the two gray patches with identical XYZ tristimulus values match in color since they are viewed under identical conditions (both on the same gray background). If one of the gray patches is placed on a white background and the other on a black background as in Figure 6.1(b), the two patches no longer match in appearance, but their tristimulus values remain equal. Since the constraint that the stimuli are viewed in identical conditions is violated in Figure 6.1(b), tristimulus colorimetry can no longer predict a match. Instead, a model that includes the effect of background luminance factor on the appearance of the patches would be required.

Simultaneous contrast is just one of the many color appearance phenomena described in this chapter. Discussion of other phenomena will address the effects of changes in surround, luminance level, illumination color, cognitive interpretation, and other viewing parameters. These phenomena justify the need to develop color appearance models and define the required input data and output predictions.

6.2 SIMULTANEOUS CONTRAST, CRISPENING, AND SPREADING

Simultaneous contrast, crispening, and spreading are three color appearance phenomena that are directly related to the spatial structure of the stimuli.

Simultaneous Contrast

Figure 6.1 illustrates simultaneous contrast. The two identical gray patches presented on different backgrounds appear distinct. The black background causes the gray patch to appear lighter, while the white background causes the gray patch to appear darker. *Simultaneous contrast* causes stimuli to shift in color appearance when the color of their background is changed. These apparent color shifts follow the opponent theory of color vision in a contrasting sense along the opponent dimensions. In other words, a light background induces a stimulus to appear darker, a dark background induces a lighter appearance, red induces green, green induces red, yellow induces blue, and blue induces yellow. Josef Albers (1963), in his classic study, *Interaction of Color*, explores various aspects of simultaneous contrast and teaches artists and designers how to avoid the pitfalls and take advantage of the effects. More complete explorations of the effect are available in classic color vision texts such as Hurvich (1981), Boynton (1979), and Evans (1948). Cornelissen and Brenner (1991) explore the relationship between adaptation and chromatic induction based on the concept that induction can be at least partially explained by localized chromatic adaptation. Blackwell and Buchsbaum (1988a) describe some of the spatial and chromatic factors that influence the degree of induction.

Robertson (1996) has presented an interesting example, reproduced in Figure 6.2, of chromatic induction that highlights the complex spatial nature of this phenomenon. The red squares in Figure 6.2(a), or the cyan squares in Figure 6.2(b), are all surrounded by the same chromatic edges (two yellow edges and two blue edges for each square). If chromatic induction were strictly determined by the colors at the edges, then all of the red squares and all of the cyan squares should appear similar. However, it is clear in Figure 6.2 that the squares that appear to be falling on the yellow stripes are subject to induction from the yellow and thus appear darker and bluer. On the other hand, the squares falling on the blue stripes appear lighter and

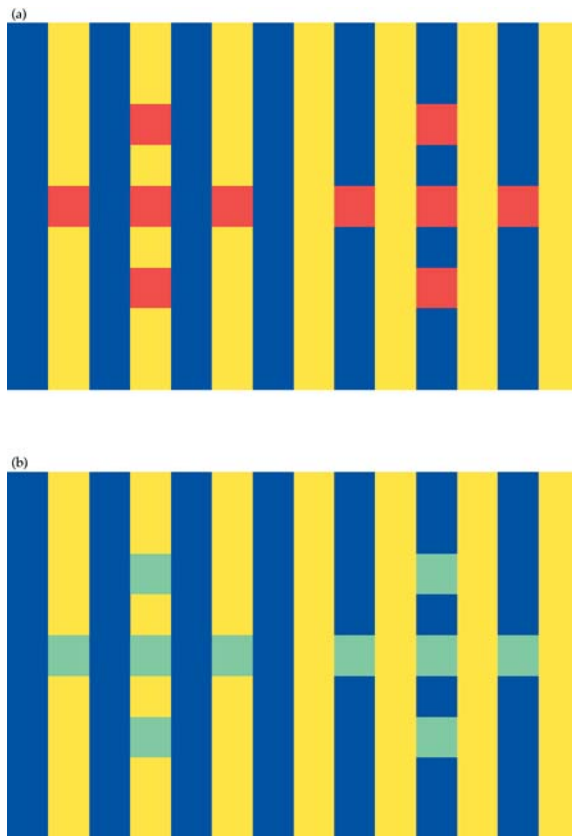


Figure 6.2 Stimuli patterns that illustrate the complexity of simultaneous contrast. The local contrasts for the left and right sets of squares are identical. However, simultaneous contrast is apparently driven by the stripes on which the square patches appear to rest. Tilt the page to one side and view the figure at a grazing angle to see an even larger effect

yellower. Clearly, the simultaneous contrast for these stimuli is dependent on more of the spatial structure than simply the local edges. This phenomenon, known as the *chromatic white effect*, has been the subject of various cognitive and computational explanations. Blakeslee and McCourt (1999) provide an interesting example of a computational vision model that can predict the effect.

Crispening

A related phenomenon is crispening. *Crispening* is the increase in perceived magnitude of color differences when the background on which the two

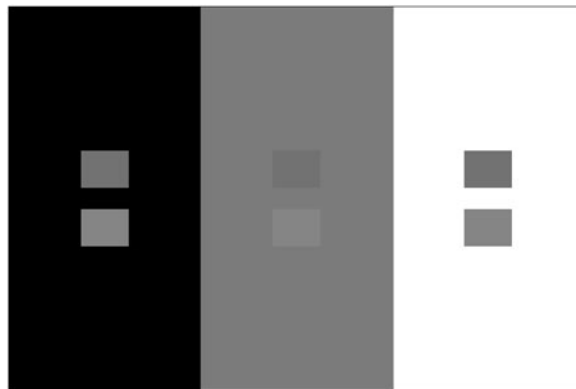


Figure 6.3 An example of crispening. The pairs of gray patches are physically identical on all three backgrounds

stimuli are compared is similar in color to the stimuli themselves. Figure 6.3 illustrates crispening for a pair of gray samples. The two gray stimuli appear to be of greater lightness difference on the gray background than on either the white or black backgrounds. Similar effects occur for color differences. Semmelroth (1970) published a comprehensive study on the crispening effect along with a model for its prediction.

Spreading

When the stimuli increase in spatial frequency, or become smaller, the simultaneous contrast effect disappears and is replaced with a spreading effect. *Spreading* refers to the apparent mixture of a color stimulus with its surround. This effect is complete at the point of spatial fusion when the stimuli are no longer viewed as discrete, but fuse into a single stimulus (such as when a halftone image is viewed at a sufficient distance such that the individual dots cannot be resolved). Spreading, however, occurs at spatial frequencies below those at which fusion occurs. Thus, the stimuli are still observed as distinct from the background, but their colors begin to blend.

Classic studies by Chevreul (1839) explored the importance of spreading and contrast in the design of tapestries where it was often desired to preserve the color appearance of design elements despite changes in spatial configuration and background color. Thus the tapestry designers were required to physically change the colors used throughout the tapestry in order to preserve color appearance. A related, although more complex, phenomenon known as neon spreading is discussed by Bressan (1993). Neon spreading is an interesting combination of perceptions of spreading and transparency.

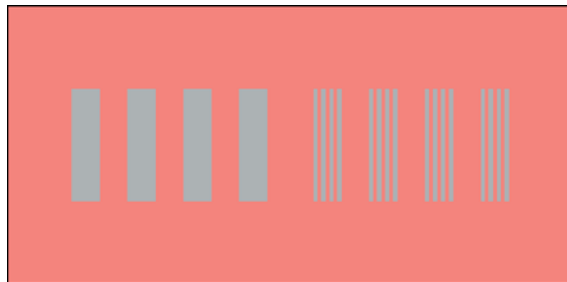


Figure 6.4 A demonstration of the difference between simultaneous contrast and spreading. The gray areas are physically identical, but appear different depending on their spatial scale with respect to the red background

Figure 6.4 illustrates both simultaneous contrast and spreading along a color dimension. Colorimetrically achromatic stimuli patches of various spatial frequency are presented on a red background. For the low-frequency (large) patches, simultaneous contrast takes place and the patches appear slightly greenish. However, at higher spatial frequencies (small patches), spreading occurs and the patches appear pinkish. The dependency on spatial frequency can be explored by examining Figure 6.4 from various viewing distances. Simultaneous contrast and spreading point to lateral interactions and adaptation effects in the human visual system.

6.3 BEZOLD–BRÜCKE HUE SHIFT (HUE CHANGES WITH LUMINANCE)

It is often assumed that hue can be specified by the wavelength of a monochromatic light. Unfortunately, this is not the case as illustrated by phenomena such as the Bezold–Brücke hue shift. This hue shift occurs when one observes the hue of a monochromatic stimulus while changing its luminance. The hue will not remain constant.

Some typical experimental results on the Bezold–Brücke hue shift have been reported by Purdy (1931). Figure 6.5 represents some of the results from the Purdy (1931) research. The data in Figure 6.5 indicate the change in wavelength required to preserve a constant hue appearance across a reduction in luminance by a factor of 10. For example, to match the hue of 650 nm light at a given luminance would require a light of 620 nm at one-tenth the luminance level (~30 nm shift). Recall that a given monochromatic light will have the same relative tristimulus values no matter what the luminance level (since absolute luminance level is usually not considered in tristimulus colorimetry). Thus, tristimulus values alone would predict that the color of a monochromatic light should remain constant at all luminance levels. Purdy's results clearly disprove that hypothesis and point to the

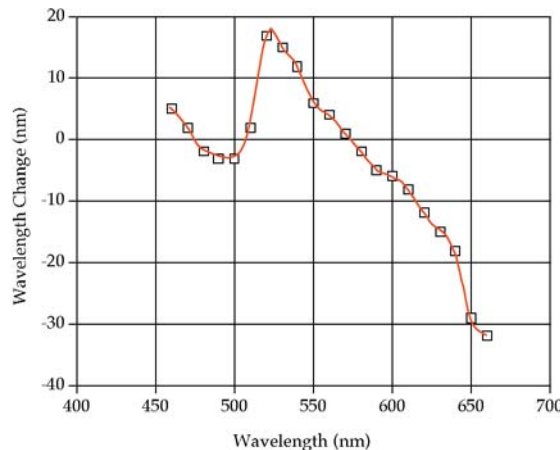


Figure 6.5 Example data illustrating the Bezold–Brücke hue shift. Plot shows the wavelength shift required to maintain constant hue across a 10× reduction in luminance

need to consider the absolute luminance level in order to predict color appearance.

The Bezold–Brücke hue shift suggests that there are nonlinear processes in the visual system after the point of energy absorption in the cones, but prior to the point that judgments of hue are made. Hunt (1989) has shown that the Bezold–Brücke hue shift does not occur for related colors.

6.4 ABNEY EFFECT (HUE CHANGES WITH COLORIMETRIC PURITY)

If one were to additively mix white light with a monochromatic light of a given wavelength, the mixture would vary in colorimetric purity while retaining a constant dominant wavelength. Perhaps it is reasonable that a collection of such mixtures, falling on a straight line between the white point and the monochromatic stimulus on a chromaticity diagram, would be of constant perceived hue. However, as the Bezold–Brücke hue shift illustrated, the wavelength of a monochromatic stimulus is not a good physical descriptor of perceived hue. Mixing a monochromatic light with white light also does not preserve constant hue. This phenomenon is known as the *Abney effect*.

The Abney effect can be illustrated by plotting lines of constant perceived hue for mixtures of monochromatic and white stimuli. Such results, from a study by Robertson (1970), are illustrated in Figure 6.6. Figure 6.6 shows several lines of constant perceived hue based on psychophysical results from three observers. The curvature of lines of constant perceived hue in chromaticity diagrams holds up for other types of stimuli as well. This can be illustrated for object-color stimuli (related stimuli) by examining lines of

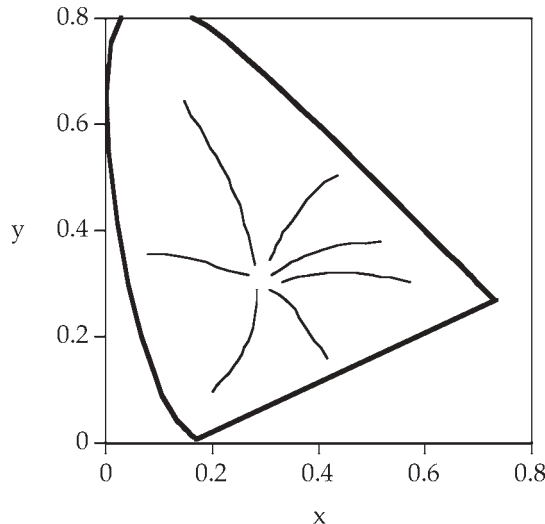


Figure 6.6 Contours of constant hue in the CIE 1931 chromaticity diagram illustrating the Abney effect

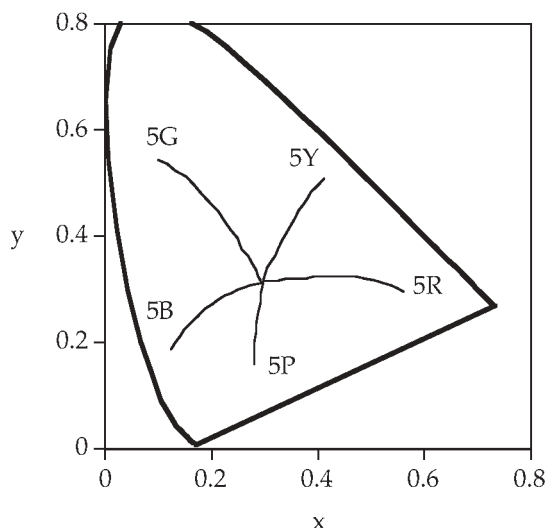


Figure 6.7 Contours of constant Munsell hue at value 5 plotted in the CIE 1931 chromaticity diagram

constant Munsell hue from the Munsell renotation studies published by Newhall (1940), an example of which is illustrated in Figure 6.7.

To summarize, the Abney effect points out that straight lines radiating from the white point in a chromaticity diagram are not lines of constant hue. Like the Bezold–Brücke effect, the Abney effect suggests nonlinearities in the

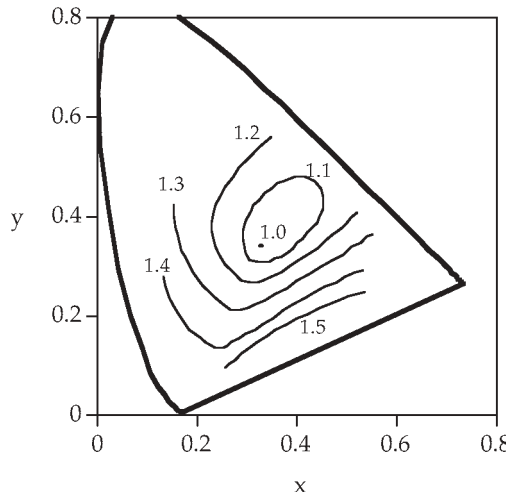


Figure 6.8 Contours of constant brightness-to-luminance ratio illustrating the Helmholtz–Kohlrausch effect

visual system between the stages of cone excitation and hue perception and was discussed by Purdy (1931). Experimental data on the Bezold–Brücke hue shift and Abney effect have been published by Ayama *et al.* (1987).

6.5 HELMHOLTZ–KOHLRAUSCH EFFECT (BRIGHTNESS DEPENDS ON LUMINANCE AND CHROMATICITY)

In the CIE system of colorimetry, the Y tristimulus value defines the luminance, or luminance factor, of a stimulus. Since luminance is intended to represent the effectiveness of the various stimulus wavelengths in evoking the perception of brightness, it is often erroneously assumed that the Y tristimulus value produces a direct estimate of perceived brightness.

One phenomenon that confirms this error is known as the Helmholtz–Kohlrausch effect. This effect is best illustrated by examining contours of constant brightness-to-luminance ratio as shown in Figure 6.8 adapted from Wyszecki and Stiles (1982). The contours represent chromaticity loci of constant perceived brightness at a constant luminance. The labels on the contours represent the brightness of those chromaticities relative to the white point, again with constant luminance. These contours illustrate that, at constant luminance, perceived brightness increases with increasing saturation. They also illustrate that the effect depends upon hue.

Various approaches have been taken to model the Helmholtz–Kohlrausch effect. One such approach involves using the Ware and Cowan Equations (Hunt 1991a). These equations rely on the calculation of a correction factor that depends on chromaticity as shown in Equation 6.1.

$$F = 0.256 - 0.184y - 2.527xy + 4.656x^3y + 4.657xy^4 \quad (6.1)$$

Correction factors are calculated for all of the stimuli in question and two stimuli are deemed to be equally bright if the equality in Equation 6.2 holds.

$$\log(L_1) + F_1 = \log(L_2) + F_2 \quad (6.2)$$

In Equation 6.2, L is luminance and F is the correction factor given by Equation 6.1.

The Ware and Cowan equations were derived for unrelated colors. Similar experiments have shown that the Helmholtz–Kohlrausch effect also holds for related colors. A review of some of this research and a derivation of a simple predictive equation was published by Fairchild and Pirrotta (1991). In this work, a correction to the CIELAB lightness predictor L^* was derived as a function of CIELAB chroma C_{ab}^* and hue angle h_{ab} . The predictor of chromatic lightness L^{**} had the form of Equation 6.3.

$$L^{**} = L^* + f_2(L^*)f_1(h_{ab})C_{ab}^* \quad (6.3)$$

Equation 6.3 describes the Helmholtz–Kohlrausch effect by adjusting the luminance-based predictor of lightness L^* with an additive factor of the chroma C_{ab}^* that is dependent upon the lightness and hue of the stimulus. Details of this predictor of lightness can be found in Fairchild and Pirrotta (1991).

An example of the Helmholtz–Kohlrausch effect can be witnessed by examining the samples of the *Munsell Book of Color*. Samples of constant Munsell value have been defined to also have constant luminance factor. Thus as one examines Munsell chips of a given hue and value, the luminance factor is constant while chroma is changing. Examining such sets of chips illustrates that the higher chroma chips do appear brighter and that the magnitude of the effect depends on the particular hue and value being examined.

The Helmholtz–Kohlrausch effect illustrates that perceived brightness (and thus lightness) cannot be strictly considered a one-dimensional function of stimulus luminance (or relative luminance). As a stimulus becomes more chromatic, at constant luminance, it appears brighter. The differences between spectral luminous efficiency measured by flicker photometry (as in the $V(\lambda)$ curve) and heterochromatic brightness matching (as described by the Helmholtz–Kohlrausch effect) as a function of observer age have been examined by Kraft and Werner (1994).

6.6 HUNT EFFECT (COLORFULNESS INCREASES WITH LUMINANCE)

Careful observation of the visual world shows that the color appearances of objects change significantly when the overall luminance level changes. Objects appear vivid and contrasty on a bright summer afternoon and more

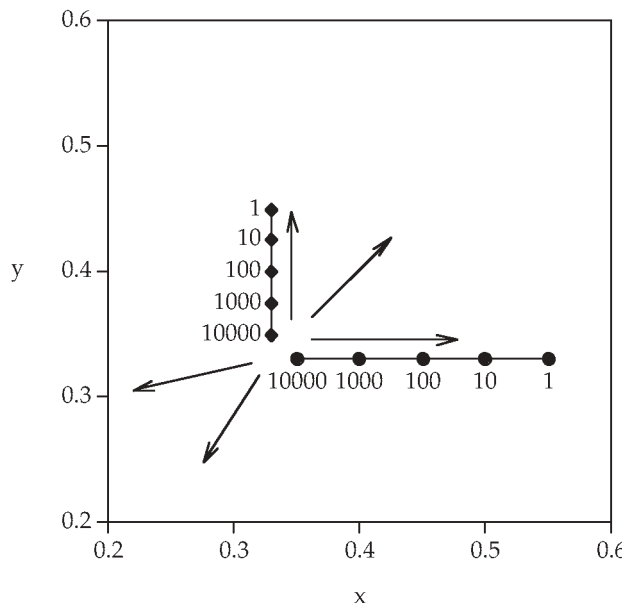


Figure 6.9 A schematic representation of corresponding chromaticities across changes in luminance showing the Hunt effect. Points are labeled with luminance levels

subdued at dusk. The Hunt effect and Stevens effect (Section 6.7) describe these attributes of appearance.

The Hunt effect obtains its name from a study on the effects of light and dark adaptation on color perception published by Hunt (1952). In that study, Hunt collected corresponding color data via haploscopic matching, in which each eye was adapted to different viewing conditions and matches were made between stimuli presented in each eye. Figure 6.9 shows a schematic representation of Hunt's results. The data points represent corresponding colors for various levels of adaptation. What these results show is that a stimulus of low colorimetric purity viewed at $10\,000\text{ cd/m}^2$ is required to match a stimulus of high colorimetric purity viewed at 1 cd/m^2 . Stated more directly, as the luminance of a given color stimulus is increased, its perceived colorfulness also increases.

The Hunt effect can be illustrated by viewing Figure 4.1 and imagining you are in the illuminated environment along with the rendered cubes. Notice that the sides of the cubes with more illumination falling on them appear more colorful. The Hunt effect can also be witnessed by taking a color image, such as Figure 4.1, and changing the level of illumination under which it is viewed. When the image is viewed under a low level of illumination the colorfulness of the various image elements will be quite low. If the image is then moved to a significantly brighter viewing environment (e.g., a viewing booth or bright sunlight), the image elements will appear significantly more colorful.

The Hunt effect can be summarized by the statement that the colorfulness of a given stimulus increases with luminance level. This effect highlights the

importance of considering the absolute luminance level in color appearance models — something that traditional colorimetry does not do.

6.7 STEVENS EFFECT (CONTRAST INCREASES WITH LUMINANCE)

The Stevens effect is a close relative of the Hunt effect. While the Hunt effect refers to an increase in chromatic contrast (colorfulness) with luminance, the Stevens effect refers to an increase in brightness (or lightness) contrast with increasing luminance. For the purposes of understanding these effects, contrast should be thought of as the rate of change of perceived brightness (or lightness) with respect to luminance. For a more complete discussion on contrast, refer to Fairchild (1995b).

Like the Hunt effect, the Stevens effect draws its name from a classic psychophysical study (Stevens and Stevens 1963). In this study, observers were asked to perform magnitude estimations on the brightness of stimuli across various adapting conditions. The results illustrated that the relationship between perceived brightness and measured luminance tended to follow a power function. This power function is sometimes referred to as Stevens power law in psychophysics. A relationship that follows a power function when plotted on linear coordinates becomes a straight line (with slope equal to the exponent of the power function) on log-log coordinates. Typical results from the experiments of Stevens and Stevens (1963) are plotted on logarithmic axes in Figure 6.10, which shows average relative brightness magnitude estimations as a function of relative luminance for four different adaptation levels. Figure 6.10 shows that the slope of this relationship (and thus the exponent of the power function) increases with increasing adapting luminance.

The Stevens effect indicates that, as the luminance level increases, dark colors will appear darker and light colors will appear lighter. While this prediction might seem somewhat counterintuitive, it is indeed the case. The Stevens effect can be demonstrated by viewing an image at high and low luminance levels. A black-and-white image is particularly effective for this demonstration. At a low luminance level, the image will appear of rather low contrast. White areas will not appear very bright and, perhaps surprisingly, dark areas will not appear very dark. If the image is then moved to a significantly higher level of illumination, white areas appear substantially brighter and dark areas darker — the perceived contrast has increased.

6.8 HELSON–JUDD EFFECT (HUE OF NONSELECTIVE SAMPLES)

The Helson–Judd effect is elusive and perhaps cannot even be observed in normal viewing conditions. It is probably unimportant in practical situations.

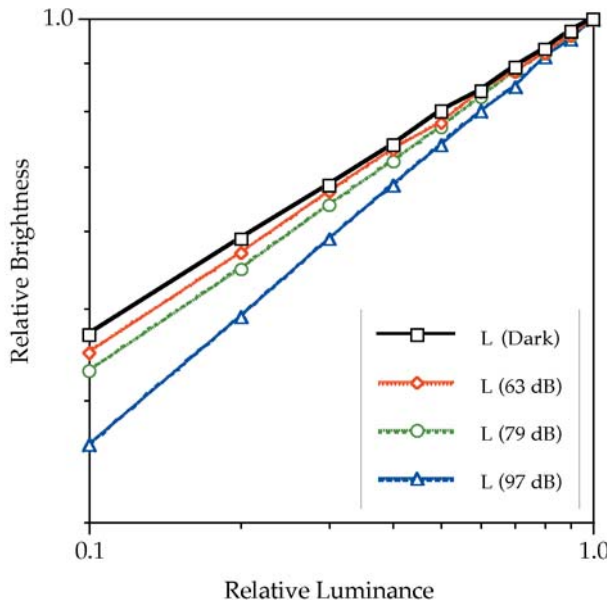


Figure 6.10 Changes in lightness contrast as a function of adapting luminance according to the Stevens effect

However, its description is included here since two color appearance models (Hunt and Nayatani *et al.*) make rather strong predictions of this effect. Thus it is important to understand its definition and consider its importance when implementing those models. The experimental data first describing the Helson–Judd effect were presented by Helson (1938).

In Helson's experiment, observers were placed in a light booth (effectively a closet) that was illuminated with nearly monochromatic light. They were then asked to assign Munsell designations (after a training period) to various nonselective (neutral Munsell patches) samples. Typical results are illustrated in Figure 6.11 for a background of Munsell value 5/. Similar trends were observed on black-and-white backgrounds. Figure 6.11 shows the perceived chroma (in Munsell units) for nonselective samples of various Munsell values. The results indicate that these nonselective samples did not appear neutral under strongly chromatic illumination. Samples lighter than the background exhibited chroma of the same hue as the source while samples darker than the background exhibited chroma of the hue of the source's complement. It is important to note that this effect only occurred for nearly monochromatic illumination. Helson (1938) stated that the effect completely disappeared if as little as 5% white light was added to the monochromatic light. Thus, the effect is of little practical importance since colored stimuli should never be evaluated under monochromatic illumination.

However, the effect is predicted by some color appearance models and has been observed in one recent experiment (Mori *et al.* 1991). The Mori *et al.*

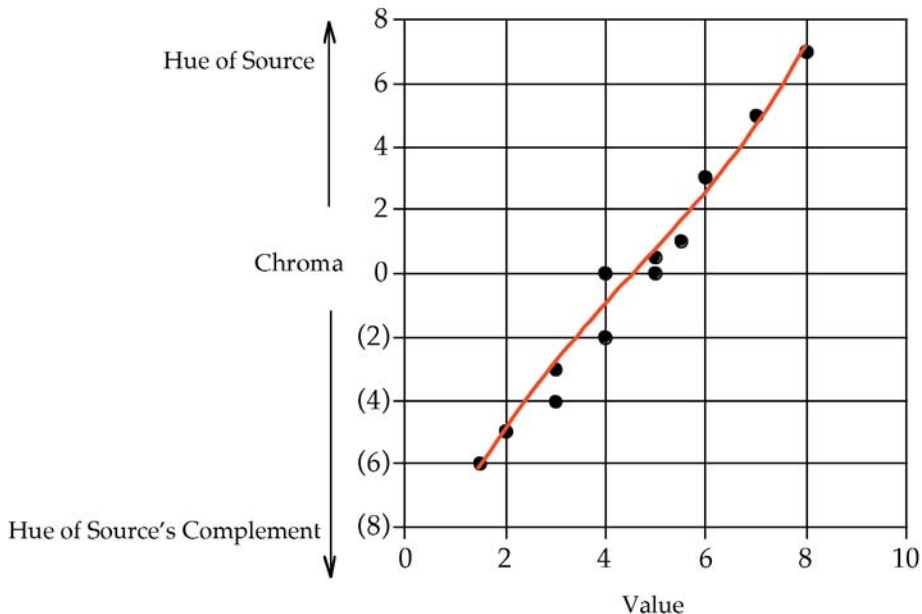


Figure 6.11 A representation of some of the original Helson (1938) results illustrating the Helson–Judd effect. Munsell hue and chroma scaling of nonselective samples under a green source on a gray background

experiment was performed with haploscopic viewing (each eye adapted differently), which might increase the chance of observing the Helson–Judd effect. However, it is not possible to observe or demonstrate the Helson–Judd effect under normal viewing conditions. This raises an interesting question with respect to the original Helson (1938) study. Why was the effect so large? While this question cannot be directly answered, perhaps the effect was caused by incomplete chromatic adaptation (explaining the hue of the light samples) and chromatic induction (explaining the hue of the dark samples). In normal viewing situations, cognitive mechanisms are thought to ‘discount the illuminant’ and thus result in the preservation of achromatic appearance of nonselective samples. Perhaps Helson’s monochromatic chamber and more recent haploscopic viewing experiments did not allow these cognitive mechanisms to fully function. Another difficulty with the Helson results is that observers scaled chroma as high as 6–8 Munsell units for samples with values less than 2. Such perceptions are not possible in the object mode since value 2 is nearly black and an object cannot appear both that dark and highly chromatic at the same time. It seems that observers see a highly chromatic ‘glowing light’ superimposed on the dark objects under these viewing conditions. This is consistent with an explanation through simultaneous contrast and incomplete adaptation.

Recent attempts to demonstrate the Helson–Judd effect in the Munsell Color Science Laboratory have verified the unique nature of the percept. The effect cannot be observed with complex stimuli. It is only observed when individual nonselective patches are viewed on a uniform background. (Even a step tablet of nonselective stimuli of various reflectances is too complex to produce the effect.) Also, nearly monochromatic light is required, as originally reported by Helson (1938). Under these conditions, observers do report a ‘glowing light’ of the hue complementary to the light source superimposed on the samples darker than the background. Interestingly, only about 50% of observers report seeing any effect at all.

While the practical importance of the Helson–Judd effect might be questionable, it does raise some interesting questions and warrants consideration since it influences the predictions of some color appearance models. To review, the Helson–Judd effect suggests that nonselective samples, viewed under highly chromatic illumination, take on the hue of the light source if they are lighter than the background and take on the complementary hue if they are darker than the background.

6.9 BARTLESON–BRENEMAN EQUATIONS (IMAGE CONTRAST CHANGES WITH SURROUND)

While Stevens and Stevens (1963) showed that perceived contrast increased with increasing luminance level, Bartleson and Breneman (1967) were interested in the perceived contrast of elements in complex stimuli (images) and how it varied with luminance level and surround. They observed results similar to those described by the Stevens effect with respect to luminance changes, but they also observed some interesting results with respect to changes in the relative luminance of an image’s surround.

Their experimental results, obtained through matching and scaling experiments, showed that the perceived contrast of images increased when the image surround was changed from dark to dim to light. This effect occurs because the dark surround of an image causes dark areas to appear lighter while having little effect on light areas (white areas still appear white despite changes in surround). Thus since there is more of a perceived change in the dark areas of an image than in the light areas, there is a resultant change in perceived contrast.

These results are consistent with the historical requirements for optimum image tone reproduction. Photographic prints viewed in an average surround are reproduced with a one-to-one relationship between relative luminances in the original scene and the print. Photographic transparencies intended for projection in a dark surround are reproduced with a system transfer function that is a power function with an exponent of approximately 1.5 (roughly that is a photographic gamma of 1.5 for the complete system). This is one reason transparencies are produced with a physically higher contrast in order to counteract the reduction in perceived contrast caused by the

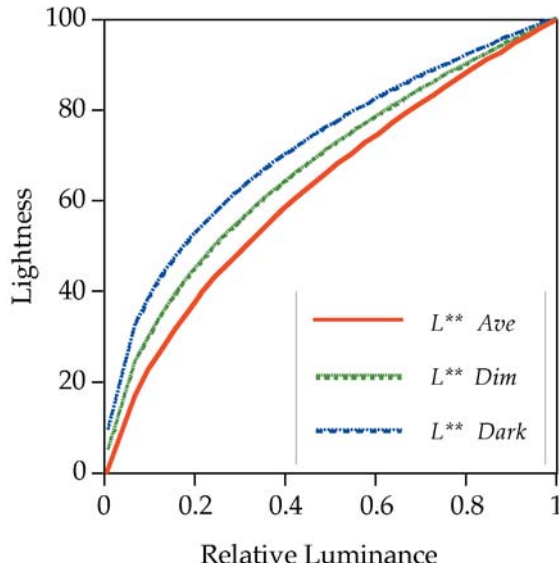


Figure 6.12 Changes in lightness contrast as a function of surround relative luminance according to the results of Bartleson and Breneman (Bartleson 1975)

dark surround. Similarly, television images, typically viewed in a dim surround, are reproduced using a power function with an exponent of about 1.25 (roughly the gamma for the complete television system). More details regarding the history and importance of surround compensation in image reproduction can be found in Hunt (1995) and Fairchild (1995a).

Bartleson and Breneman (1967) published equations that predict their experimental results quite well. Bartleson (1975), in a paper on optimum image tone reproduction, published a simplified set of equations that are of more practical value. Figure 6.12 illustrates predictions of perceived lightness as a function of relative luminance for various surround conditions according to results of the type described by Bartleson and Breneman. This plot is virtually identical to the results of Stevens and Stevens given in Figure 6.10 on logarithmic axes. The straight lines of various slopes on logarithmic axes transform into power functions with various exponents on linear axes such as those in Figure 6.12. Color appearance models such as Hunt's, RLAB, and the CIE models include predictions of the surround effects on perceived contrast of images.

Often, when working at a computer workstation, users turn off the room lights in order to make the CRT display appear of higher contrast. This produces a darker surround that should perceptually lower the contrast of the display. The predictions of Bartleson and Breneman are counter to everyday experience in this situation. The reason for this is that the room lights are usually introducing a significant amount of reflection off the face of the monitor and thus reducing the physical contrast of the displayed images. If the surround of the display can be illuminated without introducing reflection off

the face of the display (e.g., by placing a light source behind the monitor that illuminates the surrounding area), the perceived contrast of the display will actually be higher than when it is viewed in a completely darkened room.

6.10 DISCOUNTING THE ILLUMINANT

Mechanisms of chromatic adaptation can be classified as sensory or cognitive. It is well established (Hunt and Winter 1975, Fairchild 1992b, 1993a) that sensory mechanisms are not capable of complete chromatic adaptation. However, under most typical viewing conditions, observers perceive colored objects as if adaptation to the color of the illumination were complete (i.e., a white object appears white under tungsten light, fluorescent light, or daylight). Since the sensory mechanisms are incapable of mediating such perceptions, it can be shown that cognitive mechanisms (based on knowledge about objects, illumination, and the viewing environment) take over to complete the job. Further details of these different mechanisms of adaptation are presented in Chapter 8.

'Discounting the illuminant' refers to the cognitive ability of observers to interpret the colors of objects based on the illuminated environment in which they are viewed. This allows observers to perceive the colors of objects more independent of changes in the illumination and is consistent with the typical notion that color somehow 'belongs' to an object. Discounting the illuminant is important to understand and has been allowed for in some color appearance models (e.g., Hunt and RLAB). It is of importance in imaging applications where comparisons are made across various media. For example, when viewing prints, observers will be able to discount the illumination color. However, when viewing a computer display, there are no illuminated objects and discounting the illuminant does not occur. Thus in some situations it might be necessary to model this change in viewing mode.

There is a significant amount of recent research that addresses issues related to changes in color appearance induced by complex stimulus structure and observer interpretation. Examples of relevant references include Gilchrist (1980), Arend and Reeves (1986), Arend and Goldstein (1987, 1990), Schirillo *et al.* (1990), Arend *et al.* (1991), Arend (1993), Schirillo and Shevell (1993, 1996), Schirillo and Arend (1995), and Cornelissen and Brenner (1995). Work by Craven and Foster (1992) and Speigle and Brainard (1996) addresses the ability of observers to detect changes in illumination separate from changes in object colors. Lotto and Purves (2002) and Purves *et al.* (2002) have brought these concepts together nicely in an empirical theory of color perception.

6.11 OTHER CONTEXT AND STRUCTURAL EFFECTS

There are a wide variety of color appearance effects that depend on the structure and/or context of the stimuli. Some of them fall into the category of

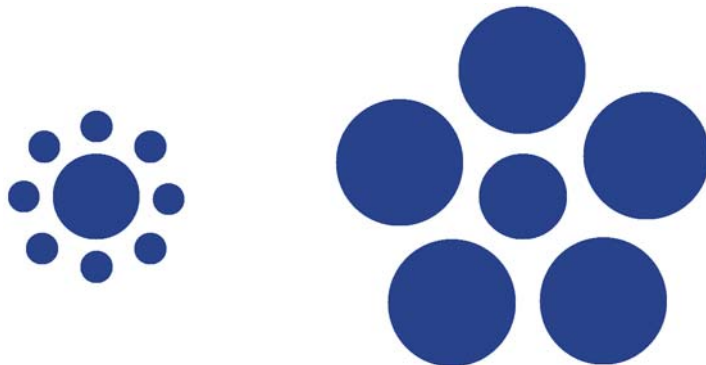


Figure 6.13 An example of simultaneous contrast in shape. The central circles in the two patterns are identical in size

optical illusions and others present interesting challenges to traditional colorimetry and, at times, color appearance modeling.

There are many interesting optical illusions and almost every good text on color or vision includes a number of interesting illusions (e.g., Wandell 1995, Barlow and Mollon 1982, Hurvich 1981). Thus, they will not be repeated here. However, a few examples do help to illustrate the importance of context and structural effects on color appearance. Figure 6.13 shows a structural illusion that has little to do with color, but does illustrate the importance of surround. The two central circles in Figure 6.13 are of physically identical diameter. However the one surrounded by larger circles appears smaller than the other. While this effect does not specifically address color issues, it does show how spatial variables can influence appearance and there is certainly an interaction between spatial and chromatic perceptions.

Various transparency effects help to illustrate the interaction of spatial and chromatic perceptions. One such demonstration has been constructed by Adelson (1993). Figure 6.14(a) shows two rows of identical gray diamonds. In Figure 6.14(b), tips of two different gray levels have been added to the diamonds with little or no effect on the appearance of the diamonds themselves. In Figure 6.14(c), the same diamonds have been partially placed on two different backgrounds. Since parts of the diamonds overlap the two backgrounds, the change in the appearance of the two rows is again minimal. However, in Figure 6.14(d), a more complete picture has been put together in which both the backgrounds and the tips have been added to the diamonds. Now there is a significant perceptual difference between the two rows of diamonds since the difference between them can be cognitively interpreted as either a transparency or shadow effect. The same demonstration can be completed in color by using, for example, yellow and blue backgrounds and tips. This demonstration illustrates that it is not just the spatial configuration of the stimuli, but their perceptual interpretation that influences appearance. Additional recent psychophysical data related to stimulus structure and appearance can be found in the work of Logvinenko and Menshikova (1994)

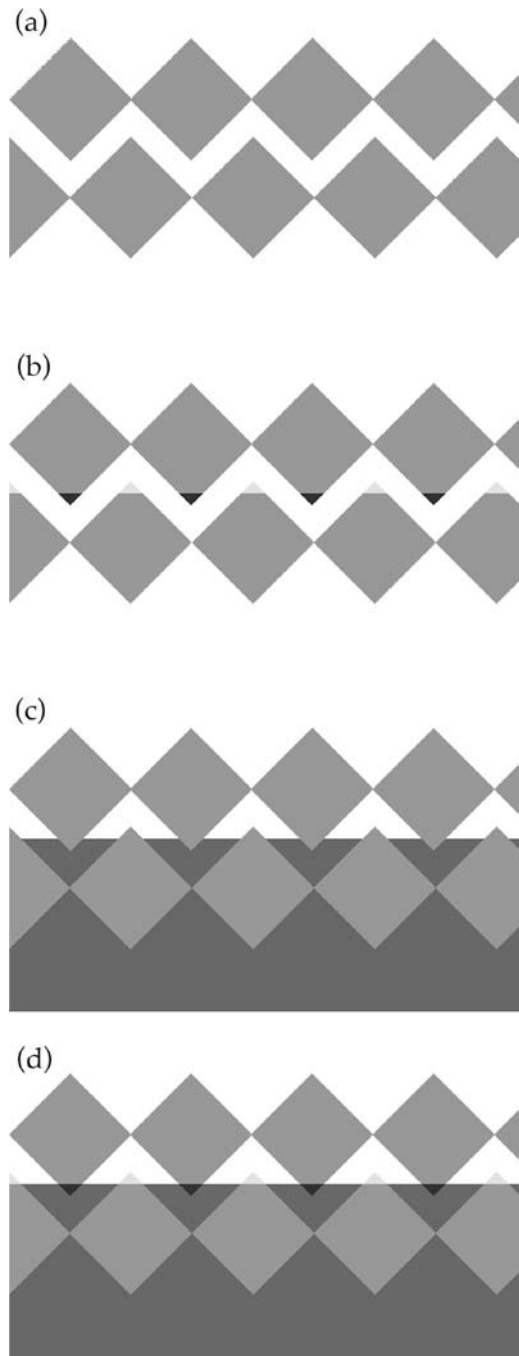


Figure 6.14 An apparent contrast effect that depends on interpretation of spatial structure. (a) Two rows of identical gray diamonds, (b) The same diamonds with tips added that have little influence on their appearance, (c) The same diamonds on two backgrounds that have little influence on appearance since the diamonds overlap both backgrounds, (d) The combination of the tips and backgrounds on the same diamonds. In (d) there is a striking appearance change since the lower row of diamonds can be interpreted as light objects that are partially in a shadow or behind a filter

and Taya *et al.* (1995). Not completely unrelated are the various perceptual phenomena of ‘filling in,’ which are discussed in recent work by De Weerd *et al.* (1998).

Other evidence of important structural effects on color appearance has been reported by Shevell (1993). In these experiments, simple spatial structures were added to the surrounds of colored stimuli with profound effects that could not be explained by the usual theories of simultaneous contrast and adaptation. Such results highlight the importance of considering spatial and color variables in conjunction with one another, not as separate entities. While various color appearance models do include spatial variables in a simple way, more complex approaches along the lines of those suggested by Poirson and Wandell (1993) need to be explored further.

Other interesting color demonstrations and effects rely to some degree on cognitive interpretation of the structure and context of the stimuli. Classic experiments on memory color that are often described in sensation and perception textbooks fall into this category. Memory color refers to the idea that observers remember prototypical colors for familiar objects. In image reproduction, objects such as sky, skin, and foliage are often mentioned (Hunt 1995, Bartleson 1960, Hunt *et al.* 1974). Other examples include simple experiments (which are quite repeatable!) in which, for example, cutouts in the shape of a tomato and a banana are made from orange construction paper and observers are asked to scale the color appearance of the two objects. The orange cutout in the shape of the banana will typically be perceived as slightly more yellow than an arbitrary shape cut out of the same paper and the cutout in the shape of a tomato will be perceived as more red. These effects are small, but consistent, and reiterate the importance of observers’ interpretations of stimuli. Additional experimental results on the characteristics of color memory have been published by Nilsson and Nelson (1981) and Jin and Shevell (1996).

Two-Color Projections

Partially related to memory color are the somewhat famous two-color projections that were demonstrated by Land (1959) and apparently included a full range of color appearances despite not having the three primaries required by conventional colorimetric theory. Figure 6.15 illustrates the process of the two-color projection. The original color image (Figure 6.15a) is separated into three black-and-white positive transparencies (Figure 6.15b), representing the red, green, and blue information, as done in Maxwell’s (1858–62) original color photographic process. Normally, the three transparencies would be projected through red, green, and blue filters and superimposed to produce an accurate reproduction of the original (as in Figure 6.15a). In the Land two-color projection, however, the red separation is projected through a red filter, the green separation is projected with white light, and the blue separation is not projected at all (Figure 6.15c). While one might expect such

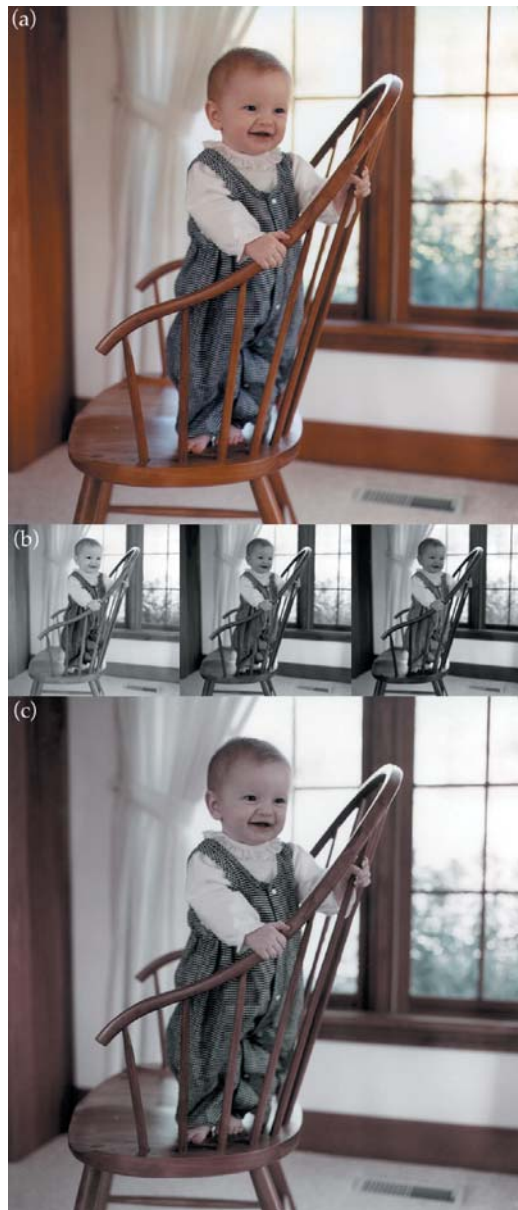


Figure 6.15 Example of a two-color image reproduction. (a) Original full-color image, (b) red, green, and blue separations of the image, (c) combination of the red separation ‘projected’ through a red filter and the green separation ‘projected’ with white light

a projection could only produce a pinkish image, the result does indeed appear to be fairly colorful (although not nearly as colorful as a three-color projection to which Land apparently never made a direct comparison!). The quality of the two-color projection depends on the subject matter since the effect is strengthened if memory color can be applied. The remainder of the colors appearing in the two-color projection can be quite easily explained by simultaneous contrast and chromatic adaptation (Judd 1960, Valberg and Lange-Malecki 1990).

Cognitive aspects of color appearance and recognition are of significant interest, but largely outside the scope of this book. An interesting monograph on the subject has been published by Davidoff (1991). It is noteworthy that the cognitive model proposed by Davidoff is consistent with the various interpretations of color appearance necessary to explain the phenomena and models described in this book. The topic of cognitive aspects of color appearance cannot be fully considered without reference to the classic work of Katz (1935) that provides fascinating insight into the topic.

6.12 COLOR CONSTANCY?

Color constancy is another phenomenon that is often discussed. Typically color constancy is defined as the apparent invariance in the color appearance of objects upon changes in illumination. This definition is somewhat misleading. The main reason for this is because color constancy does not exist in humans! The data presented in the previous sections of this chapter and the discussion of chromatic adaptation in Chapter 8 should make this point abundantly clear.

An interesting thought experiment also points out the difficulty with the term *color constancy*. If the colors of objects were indeed constant, then one would not have to include the light source in colormetric calculations in order to predict color matches. In fact, color appearance models would not be necessary as CIE XYZ colorimetry would define color appearance for all viewing conditions. Clearly, this is not the case as demonstrated, sometimes painfully, by metamerically object color matches. Such objects match in color under one light source, but mismatch under others. Clearly both objects in a metamerically pair cannot be color constant.

Then why does the term color constancy exist? Perhaps a quote from Evans (1943) answers that question best; ‘. . . in everyday life we are accustomed to thinking of most colors as not changing at all. This is due to the tendency to remember colors rather than to look at them closely.’ When colors are closely examined, the lack of color constancy becomes extremely clear. The study of color appearance and the derivation of color appearance models are, in fact, aiming to quantify and predict the failure of color constancy. Examples of more recent data are presented in the research of Blackwell and Buchsbaum (1988b), Foster and Nascimento (1994), Kuriki and Uchikawa (1996), and Bäuml (1999).

There still remains a great deal of interest in the concept of color constancy. At first this might seem strange, since it is known not to exist in human observers. However, the study of color constancy can potentially lead to theories describing how the human visual system might strive for approximate color constancy and the fundamental limitations preventing color constancy in the real world. Such studies take place in the arena of computational color constancy with applications in machine vision (e.g., Maloney and Wandell 1986, Drew and Finlayson 1994, Finlayson *et al.* 1994a,b).

Jameson and Hurvich (1989) discussed some interesting concepts in regard to color constancy, the lack thereof in humans, and the utility in not being color constant that are suitable to end this chapter. They pointed out the value of having multiple mechanisms of chromatic adaptation, thus producing imperfect color constancy and retaining information about the illumination, to provide important information about changes, such as weather, light, and time of day, and the constant physical properties of objects in the scene.

Viewing Conditions

Some of the various color appearance phenomena that produce the need for extensions to basic colorimetry were presented in Chapter 6. It is clear from these phenomena that various aspects of the visual field impact the color appearance of a stimulus. In this chapter, practical definitions and descriptions of the components of the viewing field that allow the development of reasonable color appearance models are given along with the required colorimetric measurements for these components. Accurate use of color appearance models requires accurate definition and measurement of the various components of the viewing field.

Different configurations of the viewing field will result in different cognitive interpretations of a stimulus and, in turn, different color perceptions. The last part of this chapter includes explanations of some of these phenomena and definitions of the various modes of viewing that can be observed for colored stimuli. Understanding these modes of viewing can help explain why seemingly physically identical stimuli can appear significantly different in color.

Related to the specification of viewing fields for color appearance models are the various definitions of standard viewing conditions used in different industries. These attempt to minimize difficulties with color appearance by defining appropriate viewing field configurations. One example of such a standard is the ANSI (1989) standard defining viewing conditions for prints and transparencies.

7.1 CONFIGURATION OF THE VIEWING FIELD

The color appearance of a stimulus depends on the stimulus itself as well as other stimuli that are nearby in either space or time. Temporal effects, while important, are generally not encountered in typical color appearance applications. They are dealt with by ensuring that observers have had adequate time to adapt to the viewing environment and presenting stimuli that do not

vary in time. (Of course, there are several recent applications, such as digital video, that will push color appearance studies toward the domain of temporal variation.) The spatial configuration of the viewing field is always of critical importance. (Since the eyes are constantly in motion it is impossible, in practical situations, to separate spatial and temporal effects.) The ideal spatial representation of the visual field would be to have a fully specified image of the scene. Such an image would have to have a spatial resolution greater than the visual acuity of the fovea and each pixel would be represented by a complete spectral power distribution. With such a representation of the entire visual field, one would have almost all of the information necessary to specify the color appearance of any element of the scene; however, cognitive experience of the observer and temporal information would still be missing. Some interesting data on the impact of the spatial configuration of stimulus and surround were published by Abramov *et al.* (1992).

Such a specification of the viewing field is not practical for several reasons. First, the extensive data required are difficult to obtain accurately, even in a laboratory setting. It is not plausible to require such data in practical applications. Second, even if the data could be obtained, the sheer volume would make its use quite difficult. Third, assuming these technical issues were overcome, one would then require a color appearance model capable of utilizing all of that data. Such a model does not exist and is not likely to be developed in the foreseeable future. When the inter-observer variability in color appearance judgements is considered, such a detailed model would certainly be unnecessarily complex.

Given all the above limitations, the situation is simplified by defining a minimum number of important components of the viewing field. The various color appearance models use different subsets of these viewing field components. The most extensive set is the one presented by Hunt (1991b, 1995) for use with his color appearance model. Since Hunt's definition of the viewing field includes a superset of the components required by all other models, his definitions are presented below. The viewing field is divided into four components:

1. Stimulus
2. Proximal field
3. Background
4. Surround.

Figure 7.1 schematically represents these components of the visual field.

Stimulus

The *stimulus* is defined as the color element for which a measure of color appearance is desired. Typically the stimulus is taken to be a uniform patch of about 2° angular subtense. Figure 7.1 illustrates a 2° stimulus when

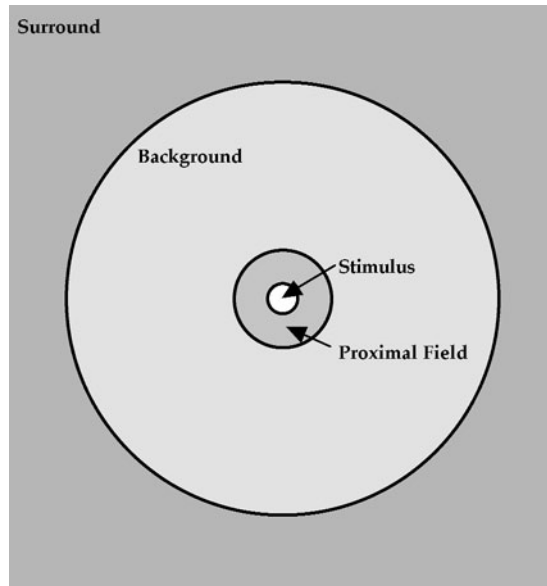


Figure 7.1 Specification of components of the viewing field. When viewed from a distance of 13 cm, the angular subtenses are correct (i.e., the 2° stimulus area will actually subtend a visual angle of 2°)

viewed from 13 cm. A stimulus of approximately 2° subtense is assumed to correspond to the visual field appropriate for use of the CIE 1931 standard colorimetric observer. The 1931 observer is considered valid for stimuli ranging from 1° to 4° in angular subtense (CIE 1986). Trichromatic vision breaks down for substantially smaller stimuli and the CIE 1964 supplementary standard colorimetric observer should be considered for use with larger stimuli (10° or greater angular subtense).

The inhomogeneity of the retina with respect to color responsivity is a fundamental theoretical limitation to this definition of the stimulus. However, it is a practical necessity that has served basic colorimetry well since 1931. A more practical limitation, especially in imaging applications, is that the angular subtense of image elements is often substantially smaller than 2° and rarely as large as 10°. Fortunately such limitations are often nulled, since in color reproduction, the objective is to reproduce a nearly identical spatial configuration of colors (i.e., the image). Thus any assumptions that are not completely valid are equally violated for both the original and the reproduction. Care should be taken, however, when reproducing images with significant size changes or when trying to reproduce a color from one scene in a completely different visual context (e.g., spot color or sampling color from an image).

When viewing real scenes, observers often consider an entire object as a 'uniform' stimulus. For example, one might ask what color is that car? Even

though different areas of the car will produce widely different color appearances, most observers would reply with a single answer. Thus, the stimulus is not a 2° field, but the entire object. This occurs to a limited extent in images, but it is more conceivable for observers to break an image apart into smaller image elements.

Proximal Field

The proximal field is defined as the immediate environment of the stimulus, extending for about 2° from the edge of the stimulus in all, or most, directions. Definition of the proximal field is useful for modeling local contrast effects such as lightness or chromatic induction, crispening, or spreading. Of current models, only that of Hunt (1991b) distinguishes the proximal field from the background.

While knowledge of the proximal field is necessary for detailed appearance modeling, it is often impractical to specify it precisely. For example, in an image, the proximal field for any given element would be defined by its surrounding pixels. While these data are available (at least in digital imaging applications), utilizing them should require the parameters of the color appearance model to be recalculated for each spatial location within the image. Often, such computations are prohibitive, and probably of little practical value. In cases where the proximal field is not known, it is normally specified to be equal to the background.

Background

The background is defined as the environment of the stimulus, extending for about 10° from the edge of the stimulus (or proximal field, if defined) in all, or most, directions. Specification of the background is absolutely necessary for modeling simultaneous contrast. If the proximal field is different, its specification can be used for more complex modeling.

Like the proximal field, it becomes difficult to define the background in imaging applications. When considering a given image element, the background is usually made up of the surrounding image areas, the exact specification of which will change with image content and from location to location in the image. Thus, precise specification of the background in images would require point-wise recalculation of appearance model parameters. Since this is impractical in any typical applications, it is usually assumed that the background is constant and of some medium chromaticity and luminance factor (e.g., a neutral gray with 20% luminance factor). Alternatively, the background can be defined as the area immediately adjacent to the image. However, such a definition tends to attribute more importance to this area than is warranted. The difficulty of such definitions of background and the impact on image reproduction are discussed by Braun

and Fairchild (1995, 1997). Fortunately, the need for precise definition of the background is minimized in most imaging applications since the same spatial configuration of colors can be found in the original and in the reproduction. However, careful consideration of the background is critical for spot color applications, in which it is desired to reproduce the same color appearance in various spatial configurations (e.g., application of the Pantone system).

Surround

The surround is defined as the field outside the background. In practical situations, the surround can be considered to be the entire room, or the environment in which the image (or other stimuli) is viewed. For example, printed images are usually viewed in an illuminated (average) surround, projected slides in a dark surround, and video displays in a dim surround. Thus, even in imaging applications, it is easy to specify the surround. It is the area outside the image display filling the rest of the visual field.

Specification of the surround is important for modeling long-range induction, flare (stimulus and within the eye), and overall image contrast effects (e.g., Bartleson and Breneman 1967, Fairchild 1995b). Practical difficulties arise in specifying the surround precisely when typical situations are encountered, particularly those involving a wide range of surround relative luminances and inhomogeneous spatial configurations.

7.2 COLORIMETRIC SPECIFICATION OF THE VIEWING FIELD

Various color appearance models utilize more or less colorimetric information on each component of the visual field. Essentially, it is necessary to know absolute (luminance or illuminance units) tristimulus values for each component of the field of view. However, some models require or utilize more or less data. In addition to the above components of the visual field, a specification of the ‘adapting stimulus’ is often required to implement color appearance models. The adapting stimulus is sometimes considered to be the background and at other times (or in other models) it is considered to be a measure of the light source itself. Thus it becomes necessary to specify absolute tristimulus values for the illumination or a white object under the given illumination.

When measuring the absolute tristimulus values for each of the visual fields, it is important to consider the standard observer used (usually the CIE 1931 2° standard colorimetric observer) and the geometry of measurement and viewing. It is ideal to make colorimetric measurements using the precise geometry under which the images will be viewed. Often this is not possible, and a compromise must be made. It is important to remember that this compromise, if necessary, has been made and can influence the correlation between model predictions and visual evaluation.

Table 7.1 CIELAB coordinates and ΔE_{ab}^* values for photographic samples evaluated using CIE Illuminants D50 and F8

Sample	D50			F8			ΔE_{ab}^*
	L*	a*	b*	L*	a*	b*	
Gray	53.7	-2.6	-9.7	53.6	-3.2	-9.8	0.6
Red	39.1	41.0	20.4	39.4	41.5	21.0	0.8
Green	43.2	-41.4	22.8	42.9	-40.6	22.0	1.2
Blue	26.5	11.2	-28.8	26.4	9.2	-28.5	2.0
Cyan	64.2	-38.7	-29.4	63.7	-40.8	-30.6	2.5
Magenta	54.7	57.3	-24.8	55.0	56.3	-23.6	1.6
Yellow	85.3	0.5	63.2	85.5	2.2	63.0	1.7
Average							1.49

When dealing with self-luminous displays (such as CRT and LCD monitors), the determination of absolute tristimulus values can be accomplished in a straightforward manner by measuring the display with a colorimeter or spectroradiometer. However, when dealing with reflective or transmissive media, the situation becomes more complex. Normally, such materials are characterized by their spectral reflectance, or transmittance, distributions as measured with a spectrophotometer. Colorimetric coordinates (such as CIE tristimulus values) are then calculated using a standard colorimetric observer and, normally, one of the defined illuminants (e.g., CIE illuminant D65, D50, A, F2). Such measurements and calculations are usually adequate in basic colorimetric applications. However, it is an extremely rare case in which images, or other colored objects, are actually viewed under light sources that closely approximate one of the CIE illuminants (Hunt 1992). The difference in color between that calculated using a CIE illuminant and that observed under a real source intended to simulate such an illuminant can be quite significant. A conservative example of the differences encountered is given in Table 7.1. The spectral reflectances for seven different colors produced on a digital photographic printer were measured and used to calculate CIELAB coordinates using CIE illuminants D50 and F8. Illuminant F8 is specified as a typical fluorescent illuminant with a correlated color temperature of 5000 K and can be thought of as an extremely high-quality illuminant D50 simulator. A real fluorescent lamp, intended to simulate illuminant D50 as found in typical viewing booths, would most likely have a spectral power distribution that deviates more from illuminant D50 than F8. The spectral power distributions of illuminants D50 and F8 are illustrated (for 10 nm increments) in Figure 7.2.

The color differences in Table 7.1 are as large as 2.5, a magnitude that would be perceptible in an image and easily perceptible in simple patches. While perceptible, the differences in this example are probably small enough

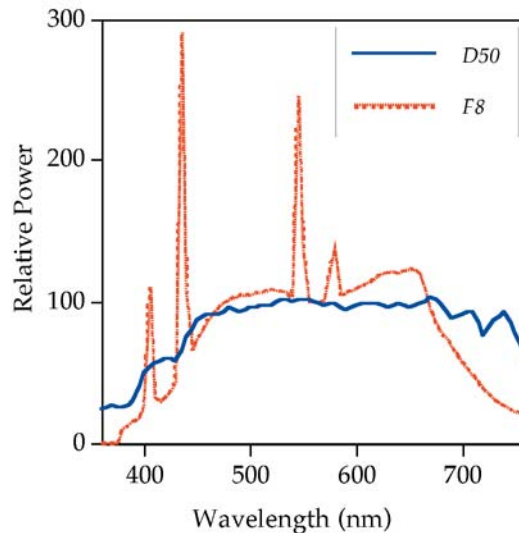


Figure 7.2 The relative spectral power distributions of CIE Illuminants D50 and F8 (each normalized to 100.0 at 560 nm)

to not be of significant concern. However, more typical light sources will produce substantially larger errors.

A common example is encountered when colorimetric values (e.g., CIELAB coordinates) are used to color balance an imaging system. When the colorimetric coordinates indicate that printed samples should be neutral (i.e., $a^* = b^* = 0.0$), significant chromatic content is often observed. This result can be traced to two causes. The first cause is differences between the standard illuminant used in the calculation and the light source used for observation, and the second cause is differences between the CIE standard observer and the particular human observer making the evaluation. Differences between individual observers can be significant. For color reproduction stimuli, the average CIELAB DE_{ab}^* between colors deemed to be matches by an individual observer is approximately 2.5 with maxima ranging up to 20 units (Fairchild and Alfvén 1995, Alfvén and Fairchild 1997). The former cause can be corrected by using the actual spectral power distribution of the observing condition in the colorimetric calculation. The latter is a fundamental limitation of colorimetry (indeed a limitation of any mean value) that cannot be corrected, but can only be understood.

To summarize, it is critical to use the actual spectral power distribution of illuminating sources, rather than CIE standard illuminants, when precise estimates of color appearance are required. When this is not feasible, viewing booths with light sources that are close approximations of the CIE illuminants should be used.

While it would be ideal to have absolute spectral power distributions (and thus absolute tristimulus values) for each component of the viewing field, it

is not necessary to have such detailed information for each model. The minimum data required for each subfield are described below. Some models require even less data as they do not consider each of the components of the visual field. The adapting field must be specified by at least its absolute tristimulus values (an alternative and equivalent specification is to have relative tristimulus values and the absolute luminance or illuminance). The stimulus must also be specified by absolute tristimulus values (preferably calculated with the actual light source). Similar data are also required for the proximal field and the background, although often the background is assumed to be achromatic and can then be specified using only its luminance factor.

The color of the surround is not considered in any appearance model; it is sufficient to know the relative luminance of the surround with respect to the image (or stimulus) areas. Often, this is even more detail on the surround than is necessary and the surround can be specified sufficiently with an adjective such as dark, dim, and average. As a practical definition of surround relative luminance, dark can be taken to be 0%, dim between 0% and 20%, and average between 20% and 100% of the luminance of the scene, or image, white.

7.3 MODES OF VIEWING

While it is often hard to accept, especially by those with an affinity for physical sciences and engineering, it has been clearly shown that the mode of appearance, and thus apparent color, depends upon the stimulus configuration and cognitive interpretation. This is most clearly illustrated by example and most clearly understood (and believed!) upon personal experience.

One example has been observed by the author (and others) when viewing a familiar house that was painted a light yellow color and had a front door of the same yellow color. On one occasion in the late evening it appeared that the door of this yellow house had been painted blue. A blue door on a yellow house is a noteworthy perception! However, upon closer examination, it was determined that the door was still its normal yellow color. The illumination was such that the house was illuminated directly by the sunlight from the setting sun (quite yellow), while a small brick wall (at first unnoticed) cast a shadow that just covered the door. Thus the door was illuminated only by skylight (and no direct sunlight) and therefore appeared substantially more blue than the rest of the house. On first sight, the scene was interpreted as a yellow house and blue door under uniform illumination. However, once it was understood that the illumination was not uniform (and the door was actually illuminated with blue light), the door actually changed in appearance from blue to yellow. The change in color appearance of the door was based completely on cognitive information about the illumination and could not be reversed once the illumination was known. A simulation of this effect is illustrated in Figure 7.3, which is an ambiguous figure that can be

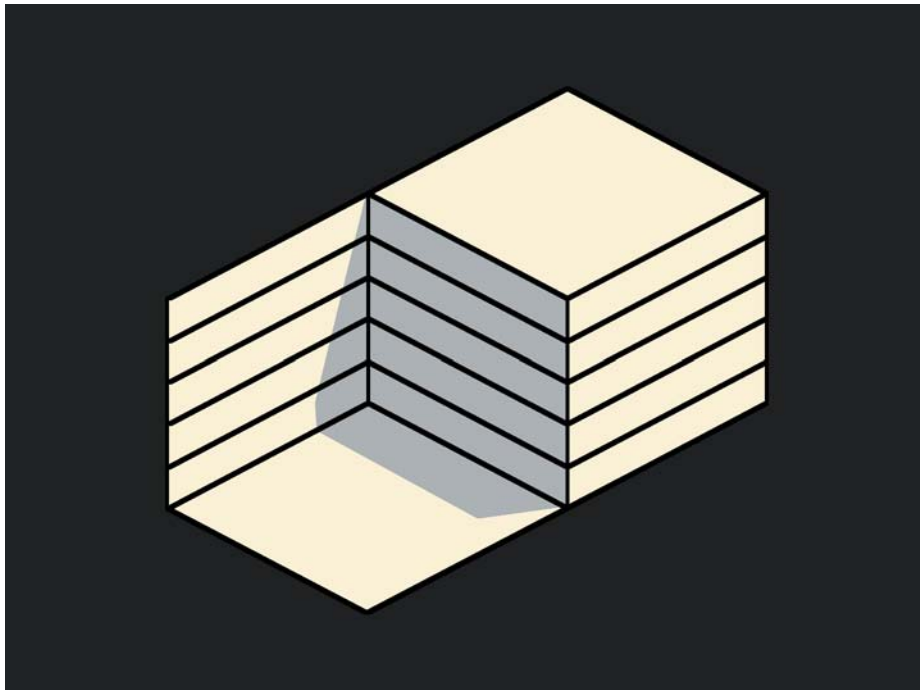


Figure 7.3 An ambiguous figure illustrating the concept of discounting the illuminant. In one spatial interpretation the gray area looks like a shadow, while in the other it appears to be paint on the object

geometrically interpreted in two ways. In one interpretation, the darker area looks like a shadow and the entire object seems to be of one yellowish color. In the other geometric interpretation, the darker area cannot be a shadow and is interpreted as a piece of the object ‘painted’ a different color. Turning the figure upside down can sometimes enhance the effect. This effect is similar to the transparency effect observed in Figure 6.14.

Another experience was related to the author in which a young child was watching black-and-white photographic prints being developed in a dark-room under an amber safelight. Of course, the prints were completely achromatic and the illumination was of a single, highly chromatic color. However, the child insisted she could recognize the colors of familiar objects in a print as it was being developed. Only when the parent took the black-and-white print out into an illuminated room did the child believe that the ‘known’ colors of the familiar objects were not present on the print. This is another example where knowledge of the object produced a color perception. This phenomenon is completely compatible with the cognitive model of color recognition proposed by Davidoff (1991). An interesting discussion of the apparent brightness of snow, in the context of viewing modes, was presented by Koenderink and Richards (1992).

Table 7.2 Color appearance attributes most commonly associated with the various modes of appearance. Those in parentheses are possible, although less likely

Attribute	Illuminant (glow)	Illumination (fills space)	Surface (object)	Volume (object)	Film (aperture)
Brightness	***	***			***
Lightness			***	***	(***)
Colorfulness	***	***			***
Chroma			***	***	(***)
Hue	***	***	***	***	***

Other similar phenomena and a systematic description of the modes of viewing that produce them have been described nicely in Chapter 5 of the OSA (1963) publication, *The Science of Color*. Following are the five modes of viewing defined in the OSA chapter:

1. Illuminant
2. Illumination
3. Surface
4. Volume
5. Film

These are defined and described in the following sections. Table 7.2 summarizes the color appearance attributes (see also Chapter 4) that are most commonly associated with each mode of viewing.

In addition to the normal color appearance attributes, other attributes such as duration, size, shape, location, texture, gloss, transparency, fluctuation, insistence, and pronouncedness (as defined by OSA 1963) can be considered. The modes of viewing described with respect to the interpretation of color appearance are strikingly similar to the types of ‘objects’ that efforts are made to produce realistic renderings of in the field of computer graphics (Chapter 16 of Foley *et al.* 1990). This similarity points to a fundamental link between the perception and interpretation of stimuli and their synthesis.

Illuminant

The *illuminant* mode of appearance is defined as color perceived as belonging to a source of light. Illuminant color perceptions are likely to involve the brightest perceived colors in the field of view. Thus objects much lighter than the surroundings can sometimes give rise to the illuminant mode perception. The illuminant mode of perception is an ‘object mode’ (i.e., the color belongs to an object) and can be typified as ‘glow’.

Illumination

The *illumination* mode of appearance is defined as color attributed to properties of the prevailing illumination rather than to objects. The ‘blue door’ example described earlier is an example of a mode change between illuminant and surface. OSA (1963) gave an example of a perception of irregular splotches of highly chromatic yellow paint (surface mode) on the dark shadowed side of a railroad coach. When the observer came closer, noticed the angle of the setting sun, and could see penumbral gradations, he realized that the yellow patches were due to sunlight masked off by obstructions (illumination mode). The illumination mode of perception is a ‘non-object’ mode and is mediated by the presence of illuminated objects that reflect light and cast shadows (sometimes particles in the atmosphere).

Surface

The *surface* mode of appearance is defined as color perceived as belonging to a surface. Any recognizable, illuminated object provides an example of the surface mode. This mode requires the presence of a physical surface and light being reflected from the surface. It is an ‘object mode.’

Volume

The *volume* mode of appearance is defined as color perceived as belonging to the bulk of a more or less uniform and transparent substance. For example, as the number of air bubbles in a block of ice increases, the lightness of the block increases toward white, while the transparency decreases toward zero. Thus a volume color transforms into a surface color. The volume mode of perception is an ‘object mode’ and requires transparency and a three-dimensional structure.

Film

The *film* mode of appearance (also referred to as aperture mode) is defined as color perceived in an aperture with no connection to an object. For example, failure to focus on a surface can cause a mode shift from surface to film. An aperture screen accomplishes this since the observer tends to focus on the plane of the aperture. The film mode of perception is a ‘non-object’ mode. All other modes of appearance can be reduced to film mode.

7.4 UNRELATED AND RELATED COLORS REVISITED

Unrelated and related colors were defined in Chapter 4. However, their fundamental importance in color appearance specification, their simplifying and unifying theme with respect to modes of appearance, and their

important relation to the specification of brightness-colorfulness or lightness-chroma appearance matches warrant a revisit. The distinction between related and unrelated colors is the single most important viewing-mode concept to understand.

Unrelated Color

Color perceived to belong to an area or object seen in isolation from other colors.

Related Color

Color perceived to belong to an area or object seen in relation to other colors.

Unrelated colors only exhibit the perceptual attributes of hue, brightness, colorfulness, and saturation. The attributes that require judgement relative to a similarly illuminated white object cannot be perceived with unrelated colors. On the other hand, related colors exhibit all of the perceptual attributes of hue, brightness, lightness, colorfulness, chroma, and saturation.

Recall that five perceptual dimensions are required for a complete specification of the color appearance of related colors. These are brightness, lightness, colorfulness, chroma, and hue. However, in most practical color appearance applications it is not necessary to know all five of these attributes. Typically, for related colors, only the three relative appearance attributes are of significant importance. Thus it is often sufficient to be concerned with only the relative appearance attributes of lightness, chroma, and hue. See Chapter 4 for a discussion of the distinction between brightness-colorfulness matching and lightness-chroma matching and their relative importance.

8

Chromatic Adaptation

Various color appearance phenomena were discussed in Chapter 6. These phenomena illustrated cases in which simple tristimulus colorimetry was not capable of adequately describing appearance. Many of those phenomena could be considered second-order effects. The topic of this chapter, chromatic adaptation, is clearly the most important first-order color appearance phenomenon. Tristimulus colorimetry tells us when two stimuli match for an average observer when viewed under identical conditions. Interestingly enough, such visual matches persist when the stimuli are viewed (as a pair) under an extremely wide range of viewing conditions. While the match persists, the color appearance of the two stimuli might be changing drastically. Changes in chromatic adaptation are one instance in which matches persist, but appearance changes. It is this change in appearance that must be understood to construct a color appearance model.

The term chromatic adaptation refers to the human visual system's capability to adjust to widely varying colors of illumination in order to approximately preserve the appearance of object colors. Perhaps it is best illustrated by considering a system that does not have the capacity for chromatic adaptation — photographic transparency film. Most transparency film is designed for exposure under daylight sources. If such film is used to make photographs of objects under incandescent illumination, the resulting transparencies have an unacceptable yellow-orange cast. This is because the film cannot adjust the relative responsivities of its red, green, and blue imaging layers in the way the human visual system adjusts the responsivities of its color mechanisms. Humans perceive relatively little change in the colors of objects when the illumination is changed from daylight to incandescent.

This chapter reviews some of the basic concepts of chromatic adaptation. Issues related to chromatic adaptation have been studied for much of modern history. The topic is even discussed by Aristotle (Wandell 1995).

In woven and embroidered stuffs the appearance of colors is profoundly affected by their juxtaposition with one another (purple, for instance, appears different on white than on black wool), and also by differences of illumination. Thus embroiderers say that they often make mistakes in their colors when they work by lamplight, and use the wrong ones.

There are many excellent discussions of chromatic adaptation available in books (e.g., Barlow and Mollon 1982, Wyszecki and Stiles 1982, Spillman and Werner 1990, Wandell 1995) and journals (e.g., Terstiege 1972, Hunt 1976, Bartleson 1978, Wright 1981a, Lennie and D'Zmura 1988). The interested reader is encouraged to explore this extensive and fascinating literature.

8.1 LIGHT, DARK, AND CHROMATIC ADAPTATION

Adaptation is the ability of an organism to change its sensitivity to a stimulus in response to changes in the conditions of stimulation. The general concept of adaptation applies to all domains of perception. The various mechanisms of adaptation can act over extremely short durations (of the order of milliseconds) or very long durations (weeks, months, or years!). In general, the mechanisms of adaptation serve to make the observer less sensitive to a stimulus when the physical intensity of the stimulus is greater. For example, one might be keenly aware of the ticking of a clock in the middle of a quiet night, but completely unable to perceive the same ticking during a busy cocktail party. In the realm of vision, three types of adaptation become important — light, dark, and chromatic.

Light Adaptation

Light adaptation is the decrease in visual sensitivity upon increases in the overall level of illumination. For example, it is easy to see millions of stars on a clear night. An equivalent number and variety of stars are present in the sky on a clear day; however, we are unable to perceive them. This is because the overall luminance level of the sky is several orders of magnitude higher in the daytime than at night. This causes visual sensitivity to changes in luminance to be reduced in the daytime relative to night. Thus the luminance change that served to produce the perception of millions of stars at night is inadequate to allow their perception during the day.

As another example, imagine waking up in the middle of the night and switching on a bright room light. At first your visual system is dazzled, you are unable to see much of anything, and you might even feel a little pain. Then, after tens of seconds, you begin to be able to view objects normally in the illuminated room. What has happened is that the mechanisms of vision were at their most sensitive in the dark room. When the light was first switched on, they were overloaded due to their high sensitivity. After a short

period, they light adapted, thus decreasing their sensitivity and allowing normal vision.

Dark Adaptation

Dark adaptation is similar to light adaptation, with the exception that dark adaptation refers to changes in the opposite direction. Thus dark adaptation is the increase in visual sensitivity experienced upon decreases in luminance level. While the phenomena associated with light and dark adaptation are similar, it is useful to distinguish the two since they are mediated by different mechanisms and exhibit different visual performance.

For example, light adaptation takes place much more quickly than dark adaptation. One can experience dark adaptation when entering a dark movie theater after being outdoors in bright sunlight. At first the theater will seem completely dark. Often people stop walking immediately upon entering a darkened room because they cannot see anything. However, after a short period objects in the room (theater seats, other people, etc.) begin to become visible. After several minutes, objects will become quite visible and there is little difficulty identifying other people, finding better seats, etc. All of this happens because the mechanisms of dark adaptation are gradually increasing the overall sensitivity of the visual system. Light and dark adaptation in the visual system can be thought of as analogous to automatic exposure controls in cameras.

Chromatic Adaptation

The processes of light and dark adaptation do have profound impacts on the color appearance of stimuli. Thus they will be considered in various color appearance models. However, a third type of visual adaptation, chromatic adaptation, is far more important and must be included in all color appearance models. *Chromatic adaptation* is the largely independent sensitivity regulation of the mechanisms of color vision. Often it is considered to be only the independent changes in responsivity of the three types of cone photoreceptors (while light and dark adaptation refer to overall responsivity changes in all of the receptors). However, it is important to keep in mind that there are other mechanisms of color vision (e.g., at the opponent level and even at the object recognition level) that are capable of changes in sensitivity that can be considered mechanisms of chromatic adaptation.

As an example of chromatic adaptation, consider a piece of white paper illuminated by daylight. When such a piece of paper is moved to a room with incandescent light, it still appears white despite the fact that the energy reflected from the paper has changed from predominantly blue to predominantly yellow (this is the change in illumination that the transparency film discussed in the introduction to this chapter couldn't adjust to). Figure 8.1

illustrates such a change in illumination. Figure 8.1(a) illustrates a typical scene under daylight illumination. Figure 8.1(b) shows what the scene would look like under incandescent illumination when viewed by a visual system that is incapable of chromatic adaptation. Figure 8.1(c) illustrates the same scene viewed under incandescent illumination by a visual system capable of adaptation similar to that observed in the human visual system.

Afterimages provide a second illustrative example of chromatic adaptation. These can be observed by viewing Figure 8.2. Stare at the black dot in the center of Figure 8.2 and memorize the positions of the various colors. After approximately 30 seconds, move your gaze to an illuminated white area such as a wall or blank piece of paper. Notice the various colors and their locations. These afterimages are the result of independent sensitivity changes of the color mechanisms. For example, the retinal areas exposed to the red area in Figure 8.2 became less sensitive to red energy during the adapting exposure, resulting in the cyan appearance of the afterimage when viewing a white area. This is caused by the lack of red response in this area that would normally be expected when viewing a white stimulus. Similar explanations hold for the other colors observed in the afterimage. While light adaptation can be thought of as analogous to an automatic exposure control, chromatic adaptation can be thought of as analogous to an automatic white-balance feature on a video camera or digital still camera.

8.2 PHYSIOLOGY

While the various phenomena of adaptation are interesting in their own right, it becomes necessary to understand something of the physiological mechanisms of adaptation in order to model them properly. There are a variety of mechanisms of adaptation ranging from strictly sensory, reflex-like responses, to purely cognitive. While all of these mechanisms are not fully understood, it is instructive to examine their variety in order to later understand how they are incorporated into various models. The mechanisms discussed here are the following:

- Pupil dilation/constriction
- Rod-cone transition
- Receptor gain control
- Subtractive mechanisms
- High-level adaptation

Pupil Dilation/Constriction

The most apparent mechanism of light and dark adaptation is dilation and constriction of the pupil. In ordinary viewing situations, the pupil diameter can range from about 3 to 7 mm. This represents a change in pupil area of



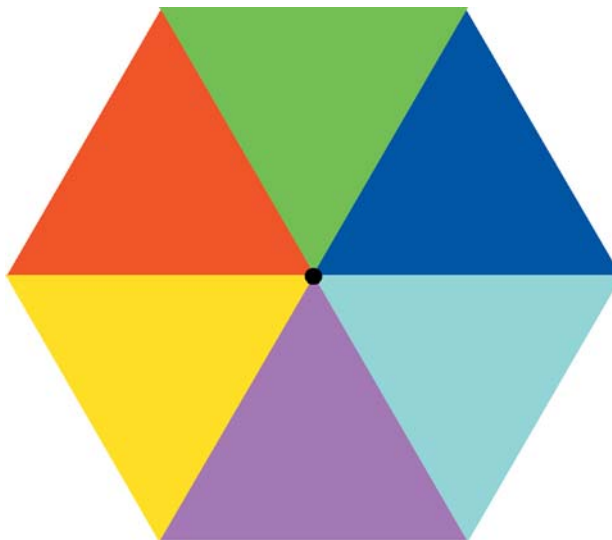


Figure 8.2 An example of afterimages produced by local retinal adaptation. Fixate the black spot in the colored pattern for about 30 seconds and then move your gaze to a uniform white area. Note the colors of the afterimages with respect to the original colors of the pattern

approximately a factor of 5. Thus, the change in pupil size could explain light and dark adaptation over a $5\times$ range of luminances. While this might seem significant, the range of luminance levels over which the human visual system can comfortably operate spans about 10 orders of magnitude. Clearly, while the pupil provides one mechanism of adaptation, it is insufficient to explain observed visual capabilities. Thus there must be additional adaptational mechanisms embedded in the physiological mechanisms of the retina and beyond.

Role of the Rods and Cones

There are two classes of photoreceptors in the human retina, rods and cones. The cones are less sensitive and respond to higher levels of illumination while the rods are more sensitive, responding to lower levels of illumination. Thus the transition from cone vision to rod vision (which occurs at

Figure 8.1 (opposite) Illustration of: (a) a scene illuminated by daylight; (b) the same scene illuminated by tungsten light as perceived by a visual system incapable of chromatic adaptation and (c), the scene illuminated by tungsten light as perceived by a visual system with typical von Kries-type chromatic adaptation (similar to the human visual system). Original lighthouse image from Kodak Photo Sampler PhotoCD

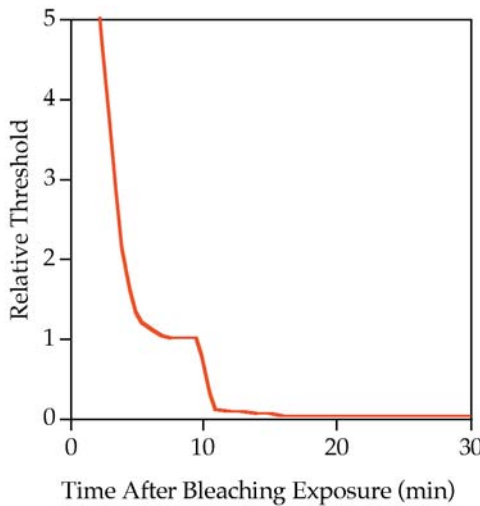


Figure 8.3 A typical dark adaptation curve showing the recovery of threshold after a strong exposure

luminances of the order of $0.1\text{--}1.0\text{ cd/m}^2$) provides an additional mechanism for light and dark adaptation.

The decrease in responsivity of the cones upon exposure to increased luminance levels (light adaptation) takes place fairly rapidly, requiring a few minutes at most, the increase in sensitivity of the rods upon exposure to decreased luminance levels requires more time. This can be illustrated with a classic dark adaptation curve showing the recovery of threshold after exposure to an extremely bright adapting stimulus as illustrated in Figure 8.3. The first phase of the curve shows the recovery of sensitivity of the cones, which levels off after a couple of minutes. Then, after about 10 minutes, the rods have recovered enough sensitivity to become more sensitive than the cones and the curve takes another drop. After about 20 minutes, the rods have reached their maximal sensitivity and the dark adaptation curve levels off. This curve explains the perceptions observed over time after entering a darkened movie theater.

In addition to providing a mechanism for light and dark adaptation, the rod-cone transition has a profound impact on color appearance. Recall that there are three types of cones to serve the requirements of color vision, but only one type of rod. Thus when luminance is reduced to levels at which only the rods are active, humans become effectively color blind, seeing the world only in shades of gray. Thus the rod-cone transition is of limited interest in color appearance and chromatic adaptation models, and other mechanisms must be considered. (Note: the influence of rods on color appearance can be important at low luminance levels and it is incorporated in Hunt's color appearance model.)

Receptor Gain Control

Perhaps the most important mechanism of chromatic adaptation is independent sensitivity changes in the photoreceptors, sometimes referred to as *receptor gain control*. It is possible imagine a gain control that varies the relationship between the number of photons incident on a photoreceptor and the electrochemical signal it produces in response to those photons. Chromatic adaptation would be served by turning down the gain when there are many photons (high levels of excitation for the particular cone type) and turning up the gain when photons are less readily available. The key to chromatic adaptation is that these gain controls are independent in each of the three cone types. (Gain control is certainly a mechanism of light adaptation as well, but light adaptation could be served by a single gain control for all three cone types. It is overly well served by independent mechanisms of chromatic adaptation.)

Physiologically, changes in photoreceptor gain can be explained by pigment depletion at higher luminance levels. Light breaks down molecules of visual pigment (part of the process of phototransduction) and thus decreases the number of molecules available to produce further visual response. Therefore, at higher stimulus intensities there is less photopigment available and the photoreceptors exhibit a decreased responsivity. While pigment depletion provides a nice explanation, there is evidence that the visual system adapts in a similar way at luminance levels for which there is insignificant pigment depletion. This adaptation is thought to be caused by gain-control mechanisms at the level of the horizontal, bipolar, and ganglion cells in the retina. Gain control in retinal cells beyond the photoreceptors helps to explain some of the spatially low-pass characteristics of chromatic adaptation. Delahunt and Brainard (2000) also discuss the interaction of various cone types in the control of chromatic adaptation.

Subtractive Mechanisms

There is also psychophysical evidence for subtractive mechanisms of chromatic adaptation in addition to gain control mechanisms (e.g., Walraven 1976, Shevell 1978). Physiological mechanisms for such subtractive adaptation can be found by examining the temporal impulse response of the cone photoreceptors, which is biphasic and thus enhances transients and suppresses steady signals. Similar processes are found in lateral inhibitory mechanisms in the retina that produce its spatially antagonistic impulse response that enhances spatial transients and suppresses spatially uniform stimuli. Physiological models of adaptation that require both multiplicative (gain) and subtractive mechanisms (e.g., Hayhoe *et al.* 1987, Hayhoe and Smith 1989) can be made completely compatible with models typically proposed in the field of color appearance (see Chapter 9) that include only gain controls by assuming that the subtractive mechanism takes place after a

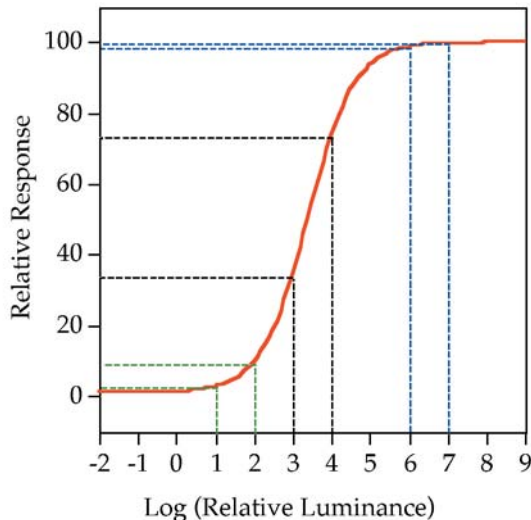


Figure 8.4 A prototypical response function for the human visual system illustrating response compression at low and high levels of the input signal

compressive nonlinearity. If the nonlinearity is taken to be logarithmic, then a subtractive change after a logarithmic transformation is identical to a multiplicative change before the nonlinearity. This bit of mathematical manipulation serves to provide consistency between the results of threshold psychophysics, physiology, and color appearance. It also highlights the importance of compressive nonlinearities as mechanisms of adaptation.

Figure 8.4 illustrates a nonlinear response function typical of the human visual system (or any imaging system). The function exhibits a threshold level below which the response is constant and a saturation level above which the response is also constant. The three sets of inputs with 100:1 ratios at different adapting levels are illustrated. It can be seen in Figure 8.4 that a 100:1 range of input stimuli produces a small output range at low and high adapting luminance levels and a large output range at intermediate levels. The decrease in response at low levels has to do with the fundamental limitation of the mechanism's sensitivity, while the response compression at high levels can be considered a form of adaptation (decreased responsivity with increased input signal). Nonlinear response functions such as the one illustrated in Figure 8.4 are required in color appearance models to predict phenomena such as the Stevens and Hunt effects described in Chapter 6.

High-level Adaptation Mechanisms

Thus far, the mechanisms discussed have been at the front end of the visual system. These are low-level mechanisms that respond and adapt to very

simple stimulus configurations. Webster and Mollon (1994) present interesting results that illustrate the relationship between spatial contrast, color appearance, and higher-level visual mechanisms. There are also numerous examples of visual adaptation that must take place at higher levels in the system (i.e., in the visual cortex). Examples of such cortical adaptation include

- The McCollough effect
- Spatial frequency adaptation
- Motion adaptation.

It is useful to consider these examples as illustrations of the potential for other types of high-level adaptation not yet considered.

A nice example of the McCollough effect can be found in Barlow and Mollon (1982). To experience the McCollough effect, one must intermittently view a pattern of red and black strips in one orientation, say horizontal, and another pattern of green and black strips of a second orientation, say vertical. By viewing each pattern for several seconds and then switching to the other, it is ensured that no simple afterimages are formed. After continuing this adaptation process for about four minutes, the observers can then turn their attention to patterns of black and white strips of spatial frequency similar to the adapting patterns. What will be observed is that black and white patterns of a vertical orientation will appear black and pink and black and white patterns in a horizontal pattern will appear black and pale green. The effect is contingent upon the color and orientation of the adapting stimuli and cannot be explained as a simple afterimage. It suggests adaptation at a cortical level in the visual system, where neurons that respond to particular orientations and spatial frequencies are first observed. The effect is also very persistent, sometimes lasting for several days or longer!

Spatial frequency adaptation can be observed by examining Figure 8.5. Adapt to Figure 8.5(a) by gazing at the black bar in the center for one to two minutes. In order to avoid producing simple afterimages, do not fixate a single point, but rather let your gaze move back and forth along the black bar. After the adaptation period, fixate on the black dot in the middle of Figure 8.5(b). The pattern on the left in Figure 8.5(b) should look as if it is of a higher spatial frequency than the pattern on the right. The two patterns in Figure 8.5(b) are identical. The difference in appearance after adaptation to Figure 8.5(a) is caused by the adaptation of mechanisms sensitive to various spatial frequencies. When adapting to a high spatial frequency, other patterns appear to be of lower spatial frequency and vice versa. Once again, this adaptation is attributed to cortical cells that selectively respond to various spatial frequencies.

Motion adaptation provides similar evidence in the temporal domain. An example of motion adaptation can be observed when viewing the credits at the end of a motion picture (or text scrolling up a computer terminal). If the credits are scrolling up the screen (and being observed) for several minutes,

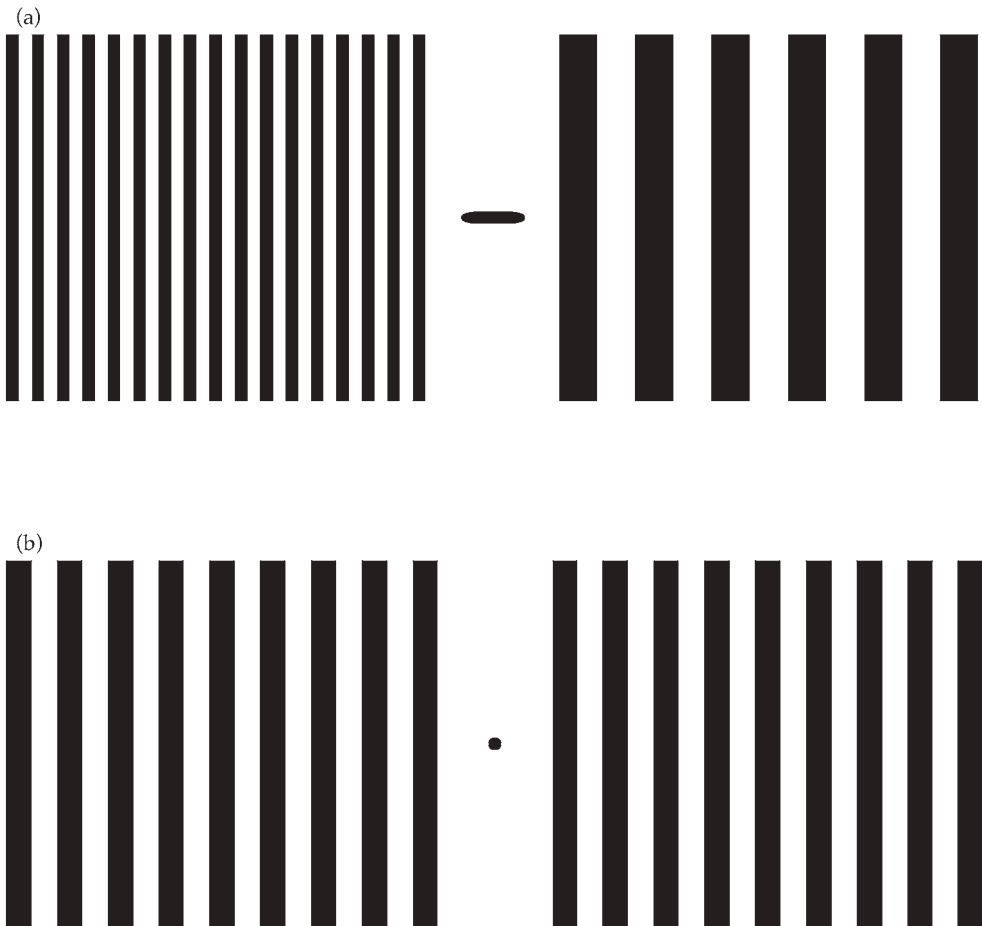


Figure 8.5 A stimulus configuration to illustrate spatial frequency adaptation. Gaze at the black bar in the middle of (a) for about 60 seconds and then fixate on the black point in the middle of (b). Note the perceived relative spatial frequencies of the two patterns in (b) after this adaptation period

it can be noticed that when the final credit is stationary on the screen it appears to be moving downward (and going nowhere at the same time!). This occurs because the cortical mechanisms selective for upward motion have become adapted while viewing the moving credits. Once the motion stops, the response of the upward and downward selective mechanisms should be nulled out, but the adapted (i.e., fatigued) upward mechanisms are not responding as strongly as they should and the stationary text appears to be moving downward. Motion adaptation can also be observed sometimes after driving a car on a highway for long periods of time. The visual system adapts to the motion toward the observer and then when the car is stopped, it can sometimes appear as if the outside world is moving away from the observer even though there is no real motion.

The examples of cortical adaptation discussed above lead to the next logical step. If there are adaptive mechanisms at such a high level in the visual system, is it possible that there are also cognitive mechanisms of adaptation? This issue is discussed in the following section.

8.3 SENSORY AND COGNITIVE MECHANISMS

It is tempting to assume that chromatic adaptation can be considered a sensory mechanism that is some sort of automatic response to changes in the stimulus configuration. However, there is clear evidence for mechanisms of chromatic adaptation that depend on knowledge of the objects and their illuminated environment (Fairchild 1992a,b, 1993a). These are cognitive mechanisms of adaptation.

Chromatic adaptation mechanisms can be classified into two groups:

- Sensory — those that respond automatically to the stimulus energy
- Cognitive — those that respond based upon observers' knowledge of scene content

Sensory Mechanisms

Sensory chromatic adaptation mechanisms are well known and have been widely discussed in the vision and color science literature. The physiological locus of such mechanisms is generally believed to be sensitivity control in the photoreceptors and neurons in the first few stages of the visual system, as discussed previously. Most modern theories and models of sensory chromatic adaptation trace their roots to the work of von Kries (1902) who wrote:

. . . the individual components present in the organ of vision are completely independent of one another and each is fatigued or adapted exclusively according to its own function.

These words of von Kries are known to be not precisely correct today, but the concept is accurate and provides useful insight. To this day, the idea that chromatic adaptation takes place through normalization of cone signals is known as the *von Kries coefficient law* and serves as the basis of all modern models of chromatic adaptation and color appearance.

Cognitive Mechanisms

Cognitive mechanisms have also been long recognized in the literature. However, perhaps because of the difficulty of quantifying cognitive effects, they are usually discussed briefly and are not as widely recognized or understood. To help understand the idea of cognitive chromatic adaptation mechanisms

it might be best to quote some of those that have mentioned them in the past two centuries. Helmholtz (1866) in his treatise on physiological optics discussed object color appearance:

We learn to judge how such an object would look in white light, and since our interest lies entirely in the object color, we become unconscious of the sensations on which the judgement rests. [Translation Woodworth 1938]

Hering (1920), who is known for hypothesizing the opponent-colors theory of color vision, discussed the concept of memory color:

All objects that are already known to us from experience, or that we regard as familiar by their color, we see through the spectacles of memory color. [Translation Hurvich and Jameson 1964]

Judd (1940) who made innumerable contributions to the field of color science referred to two types of chromatic adaptation mechanisms:

The processes by means of which the observer adapts to the illuminant or discounts most of the effect of a nondaylight illuminant are complicated; they are known to be partly retinal and partly cortical.

Lastly, Evans (1943) who wrote and lectured on many aspects of color photography and color perception discussed reasons why the colors in photographs look acceptable:

... in everyday life we are accustomed to thinking of most colors as not changing at all. This is in large part due to the tendency to remember colors rather than to look at them closely.

Jameson and Hurvich (1989) discussed the value of having multiple mechanisms of chromatic adaptation to provide important information both about changes such as weather, light, and time of day and constant physical properties of objects in the scene. Finally, Davidoff (1991) published a monograph on the cognitive aspects of color and object recognition.

Hard-copy Versus Soft-copy Output

While it is clear that chromatic adaptation is complicated and relies on both sensory and cognitive mechanisms, it is less clear how important it is to distinguish between the two types of mechanisms when viewing image displays. If an image is being reproduced in the same medium as the original and is viewed under similar conditions, it is safe to assume that the same chromatic adaptation mechanisms are active when viewing both the original and the reproduction. But, what happens when the original is presented in

one medium, such as a soft-copy display, and the reproduction is viewed in a second medium, such as a hard-copy output? A series of experiments have been described (Fairchild 1992b, 1993a) that quantify some of the characteristics of chromatic-adaptation mechanisms and indicate that the same mechanisms are not active when soft-copy displays are viewed as are active when hard-copy displays or original scenes are viewed.

When hard-copy images are being viewed, an image is perceived as an object that is illuminated by the prevailing illumination. Thus both sensory mechanisms, that respond to the spectral energy distribution of the stimulus, and cognitive mechanisms, that discount the 'known' color of the light source, are active. When a soft-copy display is being viewed, it cannot easily be interpreted as an illuminated object. Therefore there is no 'known' illuminant color and only sensory mechanisms are active. This can be demonstrated by viewing a white piece of paper under incandescent illumination and comparing the appearance to that of a CRT (or LCD) display of a uniform field with exactly the same chromaticity and luminance viewed in a darkened room. The paper will appear white or just slightly yellowish. The display will appear relatively high-chroma yellow. In fact, a white piece of paper illuminated by that display will appear white while the display itself retains a yellow appearance! Color appearance models such as RLAB, the Hunt model, and CIECAM02 include provisions for various degrees of cognitive 'discounting-the-illuminant.'

The Time-course of Adaptation

Another important feature of chromatic adaptation mechanisms is their time-course. The time-course of chromatic adaptation for color appearance judgements has been explored in detail (Fairchild and Lennie 1992, Fairchild and Reniff 1995). The results of these studies suggest that the sensory mechanisms of chromatic adaptation are about 90% complete after 60 seconds for changes in adapting chromaticity at constant luminance. Sixty seconds can be considered a good general rule for the minimum duration observers should adapt to a given viewing environment prior to making critical judgments. Adaptation is slightly slower when significant luminance changes are also involved (Hunt 1950). Cognitive mechanisms of adaptation rely on knowledge and interpretation of the stimulus configuration. Thus they can be thought of as effectively instantaneous once such knowledge is obtained. However, in some unusual viewing situations, the time required to interpret the scene can be quite lengthy, if not indefinite.

8.4 CORRESPONDING-COLORS DATA

The most extensively available visual data on chromatic adaptation are corresponding-colors data. *Corresponding colors* are defined as two stimuli,

viewed under differing viewing conditions, that match in color appearance. For example, a stimulus specified by the tristimulus values, XYZ_1 , viewed in one set of viewing conditions, might appear the same as a second stimulus specified by the tristimulus values, XYZ_2 , viewed in a second set of viewing conditions. XYZ_1 and XYZ_2 , together with specifications of their respective viewing conditions, represent a pair of corresponding colors. It is important to note, however, that XYZ_1 and XYZ_2 are rarely numerically identical.

Corresponding-colors data have been obtained through a wide variety of experimental techniques. Wright (1981a) provides an historical review of how and why chromatic adaptation has been studied. Some of the techniques, along with studies that have used them, are briefly described here.

Asymmetric Matching

Since the collection of corresponding-colors data requires a visual match to be determined across a change in viewing conditions, the experiments are sometimes referred to as *asymmetric matching experiments*. Ideally color matches are made by direct, side-by-side comparison of the two stimuli. This is technically impossible to accomplish with two sets of viewing conditions unless some simplifying assumptions are made. Perhaps the most fascinating example is an experiment reported by MacAdam (1961) in which differential retinal conditioning was used. In this experiment, two different areas of the retina (left and right halves) were exposed to different adapting stimuli and then test and matching stimuli were presented in the two halves of the visual field for color matching. This technique requires the assumption that differential adaptation of the two halves of the retina is similar to adaptation in normal viewing. This assumption is likely false and the differential retinal conditioning technique is only of historical interest.

Haploscopic Matching

The next type of experiment is *haploscopic matching* in which one eye is adapted to one viewing condition and the other eye is adapted to a second viewing condition. Then a test stimulus presented in one eye is compared and matched with a stimulus presented to the other eye. Haploscopic experiments require the assumption that adaptation takes place independently in the two eyes. This assumption might be valid for sensory mechanisms, but it is certainly not valid for cognitive mechanisms. Some of the advantages and disadvantages of haploscopic experiments in color-appearance research have been described by Fairchild *et al.* (1994). Hunt (1952) provides an example of a classic study using haploscopic viewing. Breneman (1987) described a clever device for haploscopic matching. An extensive study completed by the Color Science Association of Japan (Mori *et al.* 1991) used haploscopic viewing with object-color stimuli.

Memory Matching

To avoid the assumptions of differential retinal conditioning or haploscopic viewing, one must give up the precision of direct color matches in exchange for more realistic viewing conditions. One technique that allows more natural viewing is *memory matching*. In memory matching, observers generate a match in one viewing condition to the remembered color of a stimulus in a different viewing condition. Nelson, Judd, and Warren (1952) used a variation of memory matching in which observers assigned Munsell coordinates to various color stimuli. In effect, the observers were matching the stimuli to remembered Munsell samples under standard viewing conditions. Wright (1981a) suggested that achromatic memory matching (matching a gray appearance) would be an extremely useful technique for studying chromatic adaptation. Such a technique has been used to derive a variety of corresponding-colors data (Fairchild 1990, 1991b, 1992b, 1993a).

Magnitude Estimation

Another technique that allows natural viewing is magnitude estimation. In *magnitude estimation*, observers assign scale values to various attributes of appearance such as lightness, chroma, and hue, or brightness, colorfulness, and hue. Such experiments can provide color appearance data as well as corresponding-colors data. An extensive series of magnitude estimation experiments has been reported by Luo *et al.* (1991a,b) and summarized by Hunt and Luo (1994).

Cross-media Comparisons

Braun *et al.* (1996) published an extensive series of experiments aimed at comparing various viewing techniques for cross-media image comparisons. They concluded that a short-term memory matching technique produced the most reliable results. It is also worthwhile to note that the Braun *et al.* (1996) study showed that the common practice of comparing CRT displays and reflection prints side-by-side produces unpredictable color appearances (or, alternatively, predicted matching images that are unacceptable when viewed individually).

Given all of these experimental techniques for deriving corresponding-colors data, what can be learned from the results? Figure 8.6 illustrates corresponding-colors data from the study of Breneman (1987). The circles represent chromaticities under illuminant D65 adaptation that match the corresponding chromaticities under illuminant A adaptation plotted using triangles. Given these data, it can safely be assumed that the pairs of corresponding colors represent lightness–chroma matches in color appearance across the change in viewing conditions. This is the case since lightness and

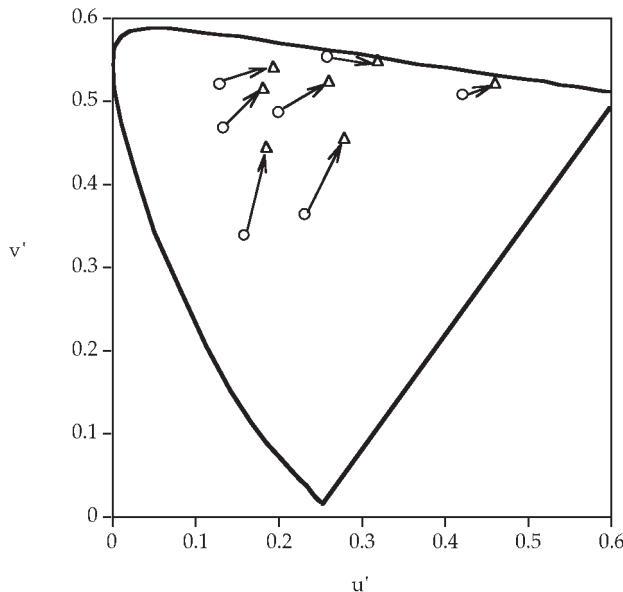


Figure 8.6 An example of corresponding-colors data for a change in chromatic adaptation from the chromaticity of illuminant D65 to that of illuminant A plotted in the $u'v'$ chromaticity diagram

chroma are the appearance parameters most intuitively judged for related colors. With this assumption, the corresponding-colors data can be used to test a color appearance model by taking the set of values for the first viewing condition, using the model to predict lightness–chroma matches for the second viewing condition, and comparing the predictions with the visual results.

This same sort of test can be completed with a simpler form of model, known as a *chromatic adaptation transform* (or chromatic adaptation model). A chromatic adaptation model does not include correlates of appearance attributes such as lightness, chroma, and hue. Instead, a chromatic adaptation model simply provides a transformation from tristimulus values in one viewing condition to matching tristimulus values in a second set of viewing conditions.

8.5 MODELS

As described in the previous section, a chromatic adaptation model allows prediction of corresponding-colors data. A general form of a chromatic adaptation model can be expressed as shown in Equations 8.1–8.3.

$$L_a = f(L, L_{\text{white}}, \dots) \quad (8.1)$$

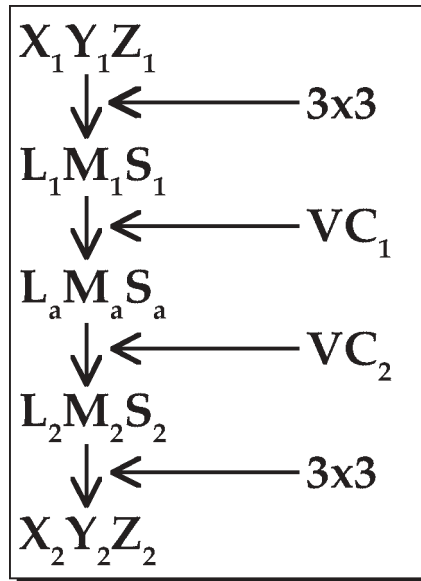


Figure 8.7 A flow chart of the application of a chromatic adaptation model to the calculation of corresponding colors

$$M_a = f(M, M_{\text{white}}, \dots) \quad (8.2)$$

$$S_a = f(S, S_{\text{white}}, \dots) \quad (8.3)$$

This generic chromatic adaptation model is designed to predict three cone signals, L_a , M_a , and S_a , after all of the effects of adaptation have acted upon the initial cone signals, L , M , and S . Such a model requires, as a minimum, the cone excitations for the adapting stimulus, L_{white} , M_{white} , and S_{white} . It is quite likely that an accurate model would require additional information as well (represented by the ellipses). A chromatic adaptation model can be converted into a chromatic adaptation transform by combining the forward model for one set of viewing conditions with the inverse model for a second set. Often such a transform is expressed in terms of CIE tristimulus values as shown in Equation 8.4.

$$XYZ_2 = f(XYZ_1, XYZ_{\text{white}1}, XYZ_{\text{white}2}, \dots) \quad (8.4)$$

In order to accurately model the physiological mechanisms of chromatic adaptation, it is necessary to express stimuli in terms of cone excitations LMS rather than CIE tristimulus values, XYZ . Fortunately, cone excitations can be reasonably approximated by a linear transformation (3×3 matrix) of CIE tristimulus values. Thus a generic chromatic adaptation transform can be described as shown in the flow chart in Figure 8.7. The complete process is as follows:

1. Begin with CIE tristimulus values ($X_1 Y_1 Z_1$) for the first viewing condition.
2. Transform them to cone excitations ($L_1 M_1 S_1$).
3. Incorporate information about the first set of viewing conditions (VC_1) using the chromatic adaptation model to predict adapted cone signals ($L_a M_a S_a$).
4. Reverse the process for the second set of viewing conditions (VC_2) to determine the corresponding color in terms of cone excitations ($L_2 M_2 S_2$) and ultimately CIE tristimulus values ($X_2 Y_2 Z_2$).

Examples of specific chromatic adaptation models are given in Chapter 9. The CIE (2003) has recently published a technical report reviewing the current status of chromatic adaptation transforms. Further details on derivation of modern measures of the LMS cone responsivities and their relationship with CIE tristimulus values can be found in the work of D.M. Hunt *et al.* (1998), Logvinenko (1998), and Stockman *et al.* (1999, 2000).

Chromatic adaptation models provide predictions of corresponding colors and thus can be used to predict required color reproductions for changes in viewing conditions. If this is the only requirement for a given application, then a chromatic adaptation model might provide a simpler alternative to a complete color appearance model. Chromatic adaptation models are also the basic building blocks of all color appearance models. However, they do have some disadvantages. A chromatic adaptation model does not provide any predictors of appearance attributes such as lightness, chroma, and hue. These attributes might be necessary for some applications, such as image editing and gamut mapping. In these circumstances, a more complete color appearance model is required.

8.6 COMPUTATIONAL COLOR CONSTANCY

There is another field of study that produces mathematical models that are, at times, closely related to chromatic adaptation models. This is the field of *computational color constancy*. The objective in this approach is to take limited color information available in a typically trichromatic representation of a scene and produce color-constant estimates of the objects. Essentially this reduces to an attempt to estimate signals that depend only on the spectral reflectances of objects and not on the illumination. On the other hand, chromatic adaptation models aim to predict the failure of color constancy actually observed in humans.

It is simple to prove that precise color constancy is not possible, or desirable, for the human visual system. The examples of metamerically colored object pairs that cannot both be color constant and the need to include illuminants in practical colorimetry suffice to make this point. All this means is that striving for the most color-constant model is not necessarily a good way to model the human visual system. There are, however, applications in

machine vision that could benefit greatly from having the most color-constant sensors possible.

The results in the field of computational color constancy provide some interesting constraints and techniques that could help in modeling human performance. For example, the results of Maloney and Wandell (1986) illustrate limits to the accuracy with which a trichromatic system could possibly estimate surface reflectances in a natural scene. D'Zmura and Lennie (1986) show how a trichromatic visual system can provide color-constant responses for one dimension of color appearance, hue, while sacrificing constancy for the other dimensions. The work of Finlayson *et al.* (1994a, b) illustrates how optimum sensory spectral responsivities can be derived to utilize the von Kries coefficient rule to obtain near color constancy.

These studies, and many more in the field, provide interesting insights into what the visual system could possibly do at the limits. Such insights can help in the construction, implementation, and testing of color appearance models. The techniques also provide definitive answers to questions pertaining to requirements for the collection of color images (digital still cameras, computer vision systems, and other image scanners), the synthesis of realistic images (computer graphics), and the design of colorimetric instrumentation (imaging colorimeters). Brill and West (1986) provide a useful review of the similarities and differences in the studies of chromatic adaptation and color constancy.

Chromatic Adaptation Models

Chromatic adaptation is the single most important property of the human visual system with respect to understanding and modeling color appearance. Given this importance in vision science, there is significant literature available on various aspects of the topic. Chapter 8 reviewed some of the important properties of adaptation phenomena and mechanisms. It also provided the generic outline of a chromatic adaptation model for predicting corresponding colors. This chapter builds upon that information by including more detailed descriptions of a few specific chromatic adaptation transformations. It is impossible to cover all of the models that have been published. An attempt has been made to cover a variety of models and show their fundamental relationships to each other. Readers interested in more detail on the models or historical developments should delve into the available literature.

There are several good places to start, including the review papers cited in Chapter 8 (Bartleson 1978, Terstiege 1972, Wright 1981a, Lennie and D'Zmura 1988). Further details on the early history of chromatic adaptation models can be found in an interesting overview in a study by Helson, Judd, and Warren (1952). Another excellent review of the entire field of color appearance with significant treatment of chromatic adaptation was written by Wyszecki (1986). Many of the classic papers in the field can be found in the collection edited by MacAdam (1993).

The models described in this chapter do allow the computation of corresponding colors, but they are not color appearance models. They include no predictors of appearance attributes such as lightness, chroma, and hue. They are, however, quite useful in predicting color matches across changes in viewing conditions. This is a significant extension of tristimulus colorimetry, all that is necessary in some applications, and the fundamental basis upon which all color appearance models are constructed.

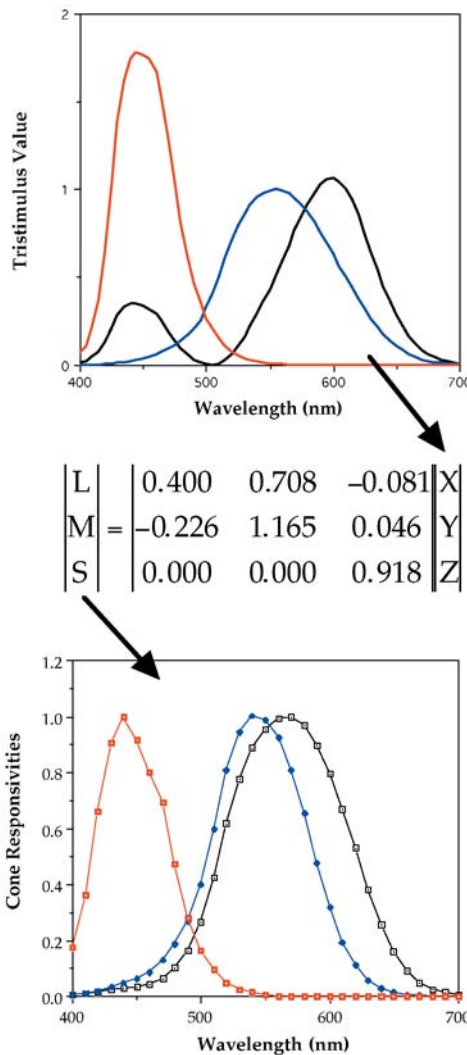


Figure 9.1 The process of transformation from XYZ tristimulus values to LMS cone responsivities using an example linear matrix multiplication

Any physiologically plausible model of chromatic adaptation must act on signals representing the cone responses (or at least relative cone responses). Thus, in applications for which the use of CIE colorimetry is important, it is necessary to first transform from CIE tristimulus values (XYZ) to cone responsivities (denoted LMS, RGB, or rgb, depending on the model). Fortunately, cone responsivities can be accurately represented using a linear transformation of CIE tristimulus values. An example of such a transformation is graphically illustrated in Figure 9.1. This transformation, or a similar one, is common to all chromatic adaptation and color appearance models that are

compatible with CIE colorimetry. Thus it will not be explicitly included in every case in this book. Where the particular transformation is of importance to a particular model, it will be explicitly included in this and following chapters.

9.1 VON KRIES MODEL

All viable modern chromatic adaptation models can trace their roots, both conceptually and mathematically, to the hypotheses of Johannes von Kries (1902). von Kries laid down some ideas about chromatic adaptation that, to this day, are being 'rediscovered.' His idea was to propose a simple model of chromatic adaptation that would serve as a 'straw man' for future research. He had fairly low expectations of his ideas as can be illustrated by the following quote from MacAdam's translation of the 1902 paper:

If some day it becomes possible to distinguish in an objective way the various effects of light by direct observation of the retina, people will perhaps recall with pitying smiles the efforts of previous decades which undertook to seek an understanding of the same phenomena by such lengthy detours.

Over nine decades later, there is no one looking back at von Kries' work with a 'pitying smile.' Rather, many are looking back at his work with astonishment at how well it has withstood the test of time.

von Kries (1902) did not outline a specific set of equations as representative of what is today referred to as the von Kries model, the von Kries proportionality law, the von Kries coefficient law, and other similar names. He simply outlined his hypothesis in words and described the potential impact of his ideas. In MacAdam's translation of von Kries' words:

This can be conceived in the sense that the individual components present in the organ of vision are completely independent of one another and each is fatigued or adapted exclusively according to its own function.

The ideas that von Kries outlined were considered by him to be an extension of Grassmann's laws of additive color mixture to two viewing conditions.

The modern interpretation of the von Kries hypothesis in terms of a chromatic adaptation model is expressed in Equations 9.1–9.3.

$$L_a = k_L L \quad (9.1)$$

$$M_a = k_M M \quad (9.2)$$

$$S_a = k_S S \quad (9.3)$$

L , M , and S represent the initial cone responses; k_L , k_M , and k_S are the coefficients used to scale the initial cone signals (i.e., gain control); and L_a ,

M_a , and S_a are the post-adaptation cone signals. Equations 9.1–9.3 represent a simple gain-control model of chromatic adaptation in which each of the three cone types has a separate gain coefficient. A key aspect of any model is how the particular values of k_L , k_M , and k_S are obtained. In most modern instantiations of the von Kries model, the coefficients are taken to be the inverse of the L , M , and S cone responses for the scene white or maximum stimulus as illustrated in Equations 9.4–9.6.

$$k_L = 1/L_{\max} \quad \text{or} \quad k_L = 1/L_{\text{white}} \quad (9.4)$$

$$k_M = 1/M_{\max} \quad \text{or} \quad k_M = 1/M_{\text{white}} \quad (9.5)$$

$$k_S = 1/S_{\max} \quad \text{or} \quad k_S = 1/S_{\text{white}} \quad (9.6)$$

Equations 9.4–9.6 are a mathematical representation of von Kries' statement that 'each is fatigued or adapted exclusively according to its own function.' Given the above interpretations of the gain coefficients, the von Kries model can be used to calculate corresponding colors between two viewing conditions by calculating the post-adaptation signals for the first condition, setting them equal to the post-adaptation signals for the second condition, and then reversing the model for the second condition. Performing these steps and completing the algebra results in the transformations given in Equations 9.7–9.9 that can be used to calculate corresponding colors.

$$L_2 = (L_1/L_{\max 1})L_{\max 2} \quad (9.7)$$

$$M_2 = (M_1/M_{\max 1})M_{\max 2} \quad (9.8)$$

$$S_2 = (S_1/S_{\max 1})S_{\max 2} \quad (9.9)$$

In some cases it becomes more convenient to express chromatic adaptation models in terms of matrix transformations. The interpretation of the von Kries model as described above is expressed in matrix notation in Equation 9.10.

$$\begin{vmatrix} L_a \\ M_a \\ S_a \end{vmatrix} = \begin{vmatrix} 1/L_{\max} & 0.0 & 0.0 \\ 0.0 & 1/M_{\max} & 0.0 \\ 0.0 & 0.0 & 1/S_{\max} \end{vmatrix} \begin{vmatrix} L \\ M \\ S \end{vmatrix} \quad (9.10)$$

The matrix notation can be extended to the calculation of corresponding colors across two viewing conditions and to explicitly include the transformation (matrix \mathbf{M}) from CIE tristimulus values (XYZ) to relative cone responses (LMS). This is illustrated in Equation 9.11.

$$\begin{vmatrix} X_2 \\ Y_2 \\ Z_2 \end{vmatrix} = \mathbf{M}^{-1} \begin{vmatrix} L_{\max 2} & 0.0 & 0.0 \\ 0.0 & M_{\max 2} & 0.0 \\ 0.0 & 0.0 & S_{\max 2} \end{vmatrix} \begin{vmatrix} 1/L_{\max 1} & 0.0 & 0.0 \\ 0.0 & 1/M_{\max 1} & 0.0 \\ 0.0 & 0.0 & 1/S_{\max 1} \end{vmatrix} \mathbf{M} \begin{vmatrix} X_1 \\ Y_1 \\ Z_1 \end{vmatrix} \quad (9.11)$$

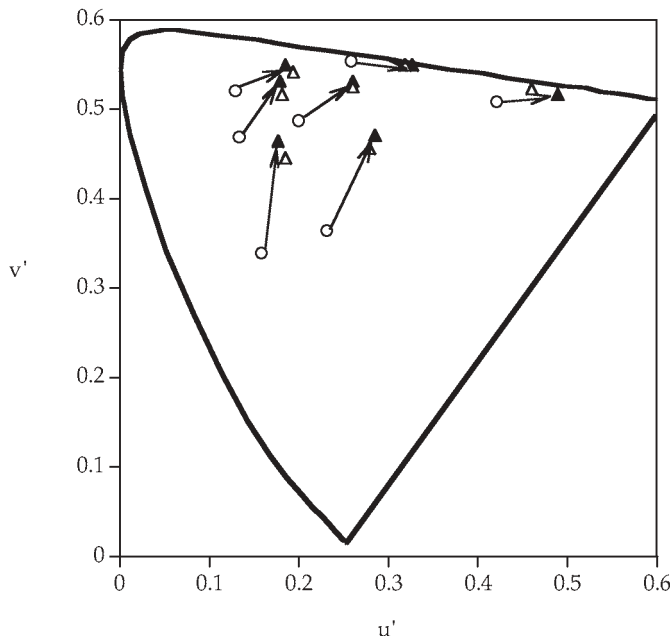


Figure 9.2 Prediction of some example corresponding colors data using the von Kries model. Open triangles represent visual data and filled triangles represent model predictions

The von Kries transformation was used to predict the visual data of Breneman (1987) that were described in Chapter 8. The results are illustrated in a $u'v'$ chromaticity diagram in Figure 9.2. The open symbols represent Breneman's corresponding colors data and the filled symbols represent the predictions using a von Kries model. Perfect model predictions would result in the filled triangles completely coinciding with the open triangles. In this calculation, the chromaticities under daylight adaptation (open circles in Figure 9.2) were used to predict the corresponding chromaticities under incandescent adaptation (triangles in Figure 9.2). It is clear in Figure 9.2 that the von Kries hypothesis was indeed a good one and that the modern interpretation as a chromatic adaptation transformation predicts the data surprisingly well.

Helson, Judd, and Warren (1952) presented an early study in which corresponding colors were derived by memory matching and the von Kries hypothesis was tested and performed quite well. Examples of recent experimental data and analyses that address the utility and limitations of the von Kries hypothesis can be found in the work of Brainard and Wandell (1992) and Chichilnisky and Wandell (1995). There are some discrepancies between these, and other, visual data and the predictions of the von Kries model. Such discrepancies have led investigators down many paths that are described in the remaining sections of this chapter and throughout this

book. Perhaps it shouldn't be too surprising to realize that von Kries (1902) himself foresaw this. The next line after his description of what is now referred to as the von Kries model reads:

But if the real physiological equipment is considered, on which the processes are based, it is permissible to doubt whether things are so simple.

Indeed things are not so simple, but it is amazing how close such a simple hypothesis comes to explaining the majority of the chromatic adaptation phenomenon.

9.2 RETINEX THEORY

An often discussed account of the mechanisms of chromatic adaptation under the rubric of color constancy is the retinex theory developed by Edwin Land and his colleagues (e.g., Land and McCann 1971, Land 1977, 1986). The retinex theory can be considered an enhanced version of the von Kries model. Various enhancements have been proposed, but the key feature is that the retinex algorithm explicitly treats the spatial distribution of colors in a scene in order to better model the visual perceptions that can be observed in complex scenes.

Land's theory was formulated to explain demonstrations of the independence of color appearance on the spectral distribution of reflected light (tristimulus values). Land suggested that color appearance is controlled by surface reflectances rather than the distribution of reflected light. The retinex algorithm, in its most recent form (Land 1986), is quite simple. Land proposed three color mechanisms with the spectral responsivities of the cone photoreceptors. He called these mechanisms retinexes since they are thought to be some combination of retinal and cortical mechanisms. Land hypothesized a three-dimensional color appearance space with the output of the long-, middle-, and short-wavelength-sensitive retinexes as the dimensions. The output of a retinex is determined by taking the ratio of the signal at any given point in the scene and normalizing it with an average of the signals in that retinex throughout the scene. The most interesting feature of this algorithm is that it acknowledges variations in color due to changes in the background of the stimulus. The influence of the background can be varied by changing the spatial distribution of the retinex signals that are used to normalize a given point in the scene. If one takes the normalizing signal to be the scene average for a given retinex, then the retinex algorithm reduces to a typical instantiation of a von Kries-type transformation. There are some flaws in the physiological implementation of the retinex model (Brainard and Wandell 1986; Lennie and D'Zmura 1988), but if one is more interested in the algorithm output than having a strict physiological model of the visual system (which is also the case for most color appearance models), then the concepts in the retinex theory might prove useful. For example, the

retinex algorithm has recently been applied in the development of a digital image processing algorithm for dynamic range compression and color correction (Jobson *et al.* 1997). Other applications, challenges, and successes for such a theory have been reviewed by McCann (1993).

The need to consider spatial as well as spectral dimensions in high-level color appearance models is undeniable. Concepts embedded in the retinex theory provide some insight on how this might be accomplished. Other approaches are also under development (e.g., Poirson and Wandell 1993, Zhang and Wandell 1996). The retinex theory sets the stage for other developments in chromatic adaptation models. The general theme is that the von Kries model provides a good foundation, but needs enhancement to address certain adaptation phenomena. Spatial models of chromatic adaptation and image appearance are discussed more fully in Chapter 20.

9.3 NAYATANI *et al.* MODEL

One important enhancement to the von Kries hypothesis is the nonlinear chromatic adaptation model developed by Nayatani and coworkers. This nonlinear model was developed from a colorimetric background (enhancement to CIE tristimulus colorimetry) within the field of illumination engineering. The early roots of this model can be traced to the work of MacAdam (1961).

MacAdam's Model

MacAdam (1961) described a nonlinear model of chromatic adaptation in which the output of the cones was expressed as a constant plus a multiplicative factor of the cone excitation raised to some power. This nonlinear model represented an empirical fit to MacAdam's (1956) earlier chromatic adaptation data. Interestingly enough, MacAdam required a visual system with five types of cones in order to explain his data with a linear model! (This is probably because MacAdam used a rather unusual experimental technique in which two halves of the same retina were differentially adapted.) MacAdam's nonlinear model provided a good fit to the data and was the precursor of later nonlinear models.

Nayatani's Model

The nonlinear model of Nayatani *et al.* (1980, 1981) begins with a gain adjustment followed by a power function with a variable exponent. In this model, the von Kries coefficients are proportional to the maximum long-, middle-, and short-wavelength cone responses and the exponents of the power functions depend on the luminance of the adapting field. The power

function nonlinearity was suggested in the classic brightness study by Stevens and Stevens (1963). Another interesting and important feature of the nonlinear model is that noise terms are added to the cone responses. This helps to model threshold behavior. Equations 9.12–9.14 are generalized expressions of the nonlinear model.

$$L_a = a_L \left(\frac{L + L_n}{L_0 + L_n} \right)^{\beta_L} \quad (9.12)$$

$$M_a = a_M \left(\frac{M + M_n}{M_0 + M_n} \right)^{\beta_M} \quad (9.13)$$

$$S_a = a_S \left(\frac{S + S_n}{S_0 + S_n} \right)^{\beta_S} \quad (9.14)$$

L_a , M_a , and S_a are the cone signals after adaptation; L , M , and S are the cone excitations; L_n , M_n , and S_n are the noise terms; L_0 , M_0 , and S_0 are the cone excitations for the adapting field; β_L , β_M , and β_S are the exponents and are monotonically increasing functions of the respective cone excitations for the adapting field; and a_L , a_M , and a_S are coefficients determined by the principle that exact color constancy holds for a nonselective sample of the same luminance factor as the adapting background.

The formulations for the exponents can be found in Nayatani *et al.* (1982). Takahama *et al.* (1984) extended the model to predict corresponding colors for backgrounds of various luminance factors. A version of the model (Nayatani *et al.*, 1987) was accepted for field trial by the CIE. This meant that the CIE, through its technical committee activities, wanted to collect additional data to test the model, possibly improve it, and determine whether it or some other model should be recommended for general use. The results of the field trials were inconclusive, so the CIE did not make a recommendation on this model. Refinements of the model were made during the course of field trials and these have been summarized in a CIE technical report (CIE 1994), which provides full details of the current formulation of the model.

The nonlinear model was used to predict Breneman's (1987) corresponding colors. The results, analogous to those presented in Figure 9.2 for the von Kries model, are illustrated in Figure 9.3. The predictions are quite good, but not as good as those of the simple von Kries model (for these particular data). One reason for this is that Breneman's data were collected under viewing conditions for which discounting-the-illuminant could not occur and thus chromatic adaptation was less complete. This is illustrated by the predictions of the Nayatani model, which are all shifted toward the yellow side of the visual data. This indicates that the incandescent adapting field in Breneman's experiment retained some yellowish appearance. Recent

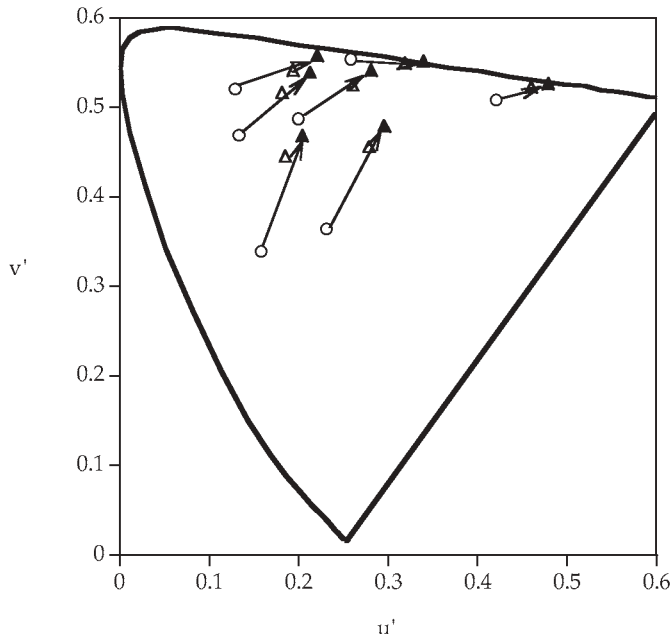


Figure 9.3 Prediction of some example corresponding colors data using the nonlinear model of Nayatani *et al.* Open triangles represent visual data and filled triangles represent model predictions

enhancements (Nayatani 1997) have provided techniques to estimate and account for the degree of chromatic adaptation in various experiments.

This nonlinear model is capable of predicting the Hunt (1952) effect (increase in colorfulness with adapting luminance), the Stevens effect (increase in lightness contrast with luminance), and the Helson–Judd effect (hue of nonselective samples under chromatic illumination). It is worth noting that the von Kries adaptation transform is luminance independent and therefore cannot be used to predict appearance phenomena that are functions of luminance. Also, the linear nature of the simple von Kries transform precludes it from predicting the Helson–Judd effect.

Nayatani's nonlinear model is important for several reasons. It provides a relatively simple extension of the von Kries hypothesis that is capable of predicting several additional effects, it has had a significant historical impact on the CIE work in chromatic adaptation and color appearance modeling, and it provides the basis for one of just two comprehensive color appearance models. The full Nayatani color appearance model is described in Chapter 11.

9.4 GUTH'S MODEL

There are many variations of the von Kries hypothesis. One significant variation that is in some ways similar to the Nayatani model, from the field of

vision science (rather than colorimetry), is the model described by Guth (1991, 1995). Guth's model is not directly related to CIE tristimulus colorimetry since the cone responsivities used are not linear transformations of the CIE color matching functions. This produces some practical difficulties in implementing the model, but for practical situations it is advisable and certainly not harmful to the predictions to use a set of cone responsivities that can be derived directly from CIE tristimulus values, along with the remainder of Guth's formulation. This model, part of the ATD vision model described in Chapter 14, has been developed over many years to predict the results of various vision experiments. Most of these experiments involve classical threshold psychophysics rather than scaling of the various dimensions of color appearance as defined in Chapter 4.

The general form of Guth's chromatic adaptation model is given in Equations 9.15–9.20.

$$L_a = L_r [1 - (L_{r0}/(\sigma + L_{r0}))] \quad (9.15)$$

$$L_r = 0.66L^{0.7} + 0.002 \quad (9.16)$$

$$M_a = M_r [1 - (M_{r0}/(\sigma + M_{r0}))] \quad (9.17)$$

$$M_r = 1.0M^{0.7} + 0.003 \quad (9.18)$$

$$S_a = S_r [1 - (S_{r0}/(\sigma + S_{r0}))] \quad (9.19)$$

$$S_r = 0.45S^{0.7} + 0.00135 \quad (9.20)$$

L_a , M_a , and S_a are the cone signals after adaptation; L , M , and S , are the cone excitations; L_{r0} , M_{r0} , and S_{r0} are the cone excitations for the adapting field after the nonlinear function; and σ is a constant (nominally 300) that can be thought of as representing a noise term. It is also important to note that the cone responses in this model must be expressed in absolute units since the luminance level does not enter the model elsewhere.

Some algebraic manipulation of the adaptation model as expressed above helps to illustrate its relationship with the von Kries model. Ignoring the initial nonlinearity, a von Kries-type gain control coefficient for the Guth model can be pulled out of Equation 9.15 as shown in Equation 9.21.

$$k_L = 1 - (L_{r0}/(\sigma + L_{r0})) \quad (9.21)$$

Using the algebraic substitutions illustrated in Equations 9.22–9.24, the relationship to the traditional von Kries coefficient becomes clear. The difference lies in the s term, which can be thought of as a noise factor that is more important at low stimulus intensities than at high intensities. Thus, as luminance level increases, the Guth model becomes more and more similar to the nominal von Kries model.

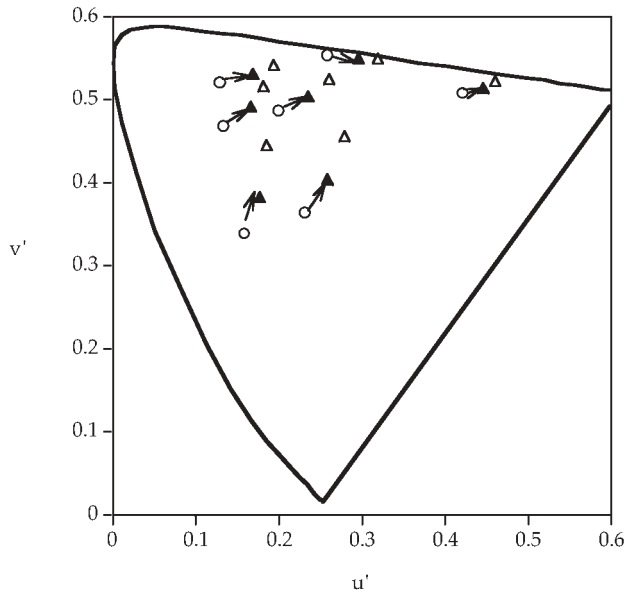


Figure 9.4 Prediction of some example corresponding-colors data using the Guth model. Open triangles represent visual data and filled triangles represent model predictions

$$k_L = ((\sigma + L_{r0}) / (\sigma + L_{r0})) - (L_{r0} / (\sigma + L_{r0})) \quad (9.22)$$

$$k_L = (\sigma + L_{r0} - L_r) / (\sigma + L_{r0}) \quad (9.23)$$

$$k_L = \sigma / (\sigma + L_{r0}) \quad (9.24)$$

Figure 9.4 shows the Guth model prediction of Breneman's (1987) corresponding-colors data. The calculations were carried out using the nominal, published form of the Guth model. It is clear that there is a systematic deviation between the observed and predicted results. This discrepancy can be traced to the σ parameter. The Breneman data are fairly well predicted using a simple von Kries model. Thus if the σ parameter were made smaller, the prediction of the Guth model would improve. This highlights a feature (or a drawback) of the Guth model. As a framework for a vision model, it is capable of making impressive predictions of available data. However, the model often requires a small amount of adjustment in its parameters for any given viewing condition or experiment. This is acceptable when trying to predict various observed phenomena, but is not practical in many applications such as cross-media color reproduction where the viewing conditions are often not known until it is time to calculate a predicted image and there is no chance for iterations. Thus to apply the Guth adaptation model (and the full ATD model described in Chapter 14) to such situations, some interpretation of how to implement the model is necessary.

9.5 FAIRCHILD'S MODEL

The Breneman (1987) results showing incomplete chromatic adaptation inspired a series of experiments (Fairchild 1990) aimed at measuring the degree of chromatic adaptation to various forms of adapting stimuli. This work led to the development of yet another modification of the von Kries hypothesis that included the ability to predict the degree of adaptation based on the adapting stimulus itself (Fairchild 1991a,b). This model, like Nayatani's model, is designed to be fully compatible with CIE colorimetry; however, it is more rooted in the field of imaging science than in illumination engineering. It was designed to be a relatively simple model and to include discounting-the-illuminant and the Hunt effect, in addition to incomplete chromatic adaptation.

The model is most clearly formulated as a series of matrix multiplications. The first step is a transformation from CIE tristimulus values XYZ to fundamental tristimulus values LMS for the first viewing condition as shown in Equations 9.25 and 9.26. The Hunt–Pointer–Estevez transformation with illuminant D65 normalization is used.

$$\begin{vmatrix} L_1 \\ M_1 \\ S_1 \end{vmatrix} = \mathbf{M} \begin{vmatrix} X_1 \\ Y_1 \\ Z_1 \end{vmatrix} \quad (9.25)$$

$$\mathbf{M} = \begin{vmatrix} 0.4002 & 0.7076 & -0.0808 \\ -0.2263 & 1.1653 & 0.0457 \\ 0.0 & 0.0 & 0.9182 \end{vmatrix} \quad (9.26)$$

The next step is to apply a modified form of the von Kries chromatic adaptation transform that takes incomplete chromatic adaptation into account as illustrated in Equations 9.27–9.31.

$$\begin{vmatrix} L'_1 \\ M'_1 \\ S'_1 \end{vmatrix} = \mathbf{A}_1 \begin{vmatrix} L_1 \\ M_1 \\ S_1 \end{vmatrix} \quad (9.27)$$

$$\mathbf{A} = \begin{vmatrix} a_L & 0.0 & 0.0 \\ 0.0 & a_M & 0.0 \\ 0.0 & 0.0 & a_S \end{vmatrix} \quad (9.28)$$

$$a_M = \frac{p_M}{M_n} \quad (9.29)$$

$$p_M = \frac{(1 + Y_n^v + m_E)}{(1 + Y_n^v + 1/m_E)} \quad (9.30)$$

$$m_E = \frac{3(M_n/M_E)}{L_n/L_E + M_n/M_E + S_n/S_E} \quad (9.31)$$

The p and a terms for the short- (S) and long-wavelength (L)-sensitive cones are derived in a similar fashion. Y_n is the luminance of the adapting stimulus in cd/m^2 , and terms with n subscripts refer to the adapting stimulus while terms with E subscripts refer to the equal-energy illuminant. The exponent v is set equal to 1/3. The form of these equations for incomplete adaptation is based on those used in the Hunt (1991b) color appearance model, which is described in more detail in Chapter 12. (A separate chromatic adaptation transformation was never published by Hunt; thus Hunt's model is treated in full in Chapter 12.) When cognitive discounting-the-illuminant occurs, the p_L , p_M , and p_S terms are all set equal to 1.0. The a terms are modified von Kries coefficients. The p terms represent the proportion of complete von Kries adaptation. They depart from 1.0 as adaptation becomes incomplete. The p values depend on the adapting luminance and color. As the luminance increases, the level of adaptation becomes more complete. As the adapting chromaticity moves farther and farther from a normalizing point (the equal-energy illuminant), adaptation becomes less complete. Equations 9.30 and 9.31 serve to ensure this behavior in the model. These predictions are consistent with the available experimental data (Hunt and Winter 1975, Breneman 1987, Fairchild 1992b).

The final step in the calculation of post-adaptation signals is a transformation that allows luminance-dependent interaction between the three cone types as shown in Equations 9.32–9.34.

$$\begin{vmatrix} L_a \\ M_a \\ S_a \end{vmatrix} = \mathbf{C}_1 \begin{vmatrix} L'_1 \\ M'_1 \\ S'_1 \end{vmatrix} \quad (9.32)$$

$$\mathbf{C} = \begin{vmatrix} 1.0 & c & c \\ c & 1.0 & c \\ c & c & 1.0 \end{vmatrix} \quad (9.33)$$

$$c = 0.219 - 0.0784 \log_{10}(Y_n) \quad (9.34)$$

The c term was derived from the work of Takahama *et al.* (1977) known as the linkage model. In that model, which the authors later gave up, citing a preference for the nonlinear model (Nayatani *et al.* 1981), the interaction terms were introduced to predict luminance-dependent effects. This is the same reason the \mathbf{C} matrix was included in this model.

To determine corresponding chromaticities for a second adapting condition, the \mathbf{A} and \mathbf{C} matrices must be derived for that condition, inverted, and applied as shown in Equations 9.35–9.37.

$$\begin{vmatrix} L'_2 \\ M'_2 \\ S'_2 \end{vmatrix} = \mathbf{C}_2^{-1} \begin{vmatrix} L_a \\ M_a \\ S_a \end{vmatrix} \quad (9.35)$$

$$\begin{vmatrix} L_2 \\ M_2 \\ S_2 \end{vmatrix} = \mathbf{A}_2^{-1} \begin{vmatrix} L'_2 \\ M'_2 \\ S'_2 \end{vmatrix} \quad (9.36)$$

$$\begin{vmatrix} X_2 \\ Y_2 \\ Z_2 \end{vmatrix} = \mathbf{M}^{-1} \begin{vmatrix} L_2 \\ M_2 \\ S_2 \end{vmatrix} \quad (9.37)$$

The entire model can be expressed as the single matrix Equation 9.38.

$$\begin{vmatrix} X_2 \\ Y_2 \\ Z_2 \end{vmatrix} = \mathbf{M}^{-1} \mathbf{A}_2^{-1} \mathbf{C}_2^{-1} \mathbf{C}_1 \mathbf{A}_1 \mathbf{M} \begin{vmatrix} X_1 \\ Y_1 \\ Z_1 \end{vmatrix} \quad (9.38)$$

Subsequent experiments (e.g., Pirrotta and Fairchild 1995) showed that the **C** matrix introduced an unwanted luminance dependency that resulted in an overall shift in lightness with luminance level. This shift did not impact the quality of image reproductions since the whole image shifted. However, it did introduce significant systematic error in predictions for simple object colors. Thus the model was revised (Fairchild 1994b) by eliminating the **C** matrix. This improved the predictions for simple colors, while having no impact on the results for images. It did remove the model's capability to predict the Hunt effect. However, in imaging applications, this turns out to be unimportant since any predictions of the Hunt effect would be counteracted by the process of gamut mapping. These changes, along with some further simplifications in the equations (different normalizations) were compiled and used as the basis for the latest version of the RLAB (Fairchild 1996) color appearance model presented in Chapter 13.

Figure 9.5 shows predictions of the Breneman (1987) corresponding-colors data using the Fairchild chromatic adaptation transformation. The predictions are identical for either version (original or simplified) of the model described above. The predictions are as good as, or better than, each of the models presented thus far. Quantitative analyses of all of Breneman's (1987) data confirms this result (Fairchild 1991a,b).

9.6 HERDING CATS

The CIE (1998) established the CIECAM97s color appearance model as described in Chapter 15. That model used a modified form of a chromatic

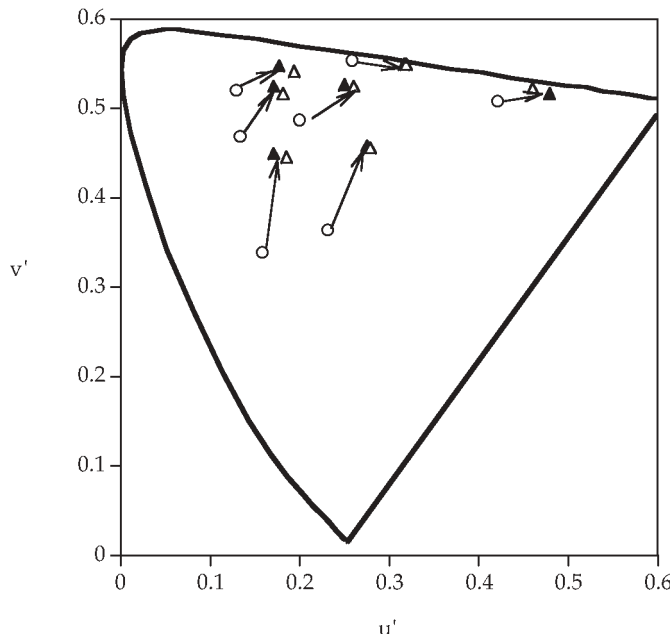


Figure 9.5 Prediction of some example corresponding-colors data using the Fairchild (1991b) model. Open triangles represent visual data and filled triangles represent model predictions

adaptation transform known as the Bradford transformation. The Bradford transformation is essentially a von Kries transformation with an additional exponential nonlinearity on the blue channel only and optimized cone responsivities. The nonlinearity on the blue channel introduced some practical issues with respect to inversion of the CIECAM97s model, so a new emphasis was placed on simple linear chromatic adaptation transforms (or CATs as they have come to be called) through optimization of the matrix transformation from *XYZ* to *RGB* values prior to the von Kries normalization.

Fairchild (2001) published a review of various linear CATs for consideration in a revised version of CIECAM97s ultimately to become CIECAM02 (see Chapter 16). A variety of techniques for deriving optimal matrix transformations were explored and each produced slightly different results with various advantages or disadvantages. The common result was that, with an optimized matrix transformation, a linear CAT could be derived that would perform as well as the nonlinear CAT incorporated in CIECAM97s for all available data sets. This encouraging result led to the ultimate derivation of CIECAM02 by CIE TC8-01 with a linear CAT.

The decision by TC8-01 to use a linear CAT was an easy one. The more difficult decision was which optimized matrix transformation to select. The candidate matrices were quite similar and all shared the characteristic that the responsivities they defined were more spectrally sharp (narrower, more

spectrally distinct, and including negative values) than cone responsivities. While the physiological plausibility of a simple von Kries transformation on such optimized responsivities is questionable, the models might well represent a more accurate simple black-box prediction of the output of the combined mechanisms of chromatic adaptation in the human visual system. The von Kries predictions obtained using sharpened responsivities tend to be more color constant than von Kries predictions obtained using cone responsivities. This prediction of improved color constancy likely mimics the enhancements produced by higher-level adaptation mechanisms.

Calabria and Fairchild (2001) performed a practical intercomparison of the various linear CATs that had been proposed. Their results indicated that images computed with the various optimized matrices were indistinguishable for any practical applications. The only linear CAT that produced significantly different results was that based on cone responsivities. Thus, the Calabria and Fairchild (2001) work confirmed that significant gains were made by using optimized transformation matrices as opposed to simple cone responsivities. This result was consistent with the tests completed by CIE TC8-01 on various corresponding colors data sets. Since the various optimized matrices performed identically within practical limits, TC8-01 then moved on to secondary criteria to select the transformation ultimately used in CIECAM02, known as CAT02.

The Breneman (1987) results showing incomplete chromatic adaptation inspired a series of experiments (Fairchild 1990) aimed at measuring the degree of chromatic adaptation to various forms of adapting stimuli. This work led to the development of yet another modification of the von Kries hypothesis that included the ability to predict the degree of adaptation based on the adapting stimulus itself (Fairchild 1991a,b). This model, like Nayatani's model, is designed to be fully compatible with CIE colorimetry; however, it is more rooted in the field of imaging science rather than in illumination engineering. It was designed to be a relatively simple model and to include discounting-the-illuminant and the Hunt effect, in addition to incomplete chromatic adaptation.

9.7 CAT02

As described in the preceding section, CIE TC8-01 (CIE 2004) selected a linear CAT based on a matrix optimized to a wide variety of corresponding-colors data while maintaining approximate compatibility with the nonlinear transformation in CIECAM97s. The chromatic adaptation transform thus specified is known as CAT02 and is presented in Equations 9.39 and 9.40.

$$\begin{vmatrix} X_2 \\ Y_2 \\ Z_2 \end{vmatrix} = \mathbf{M}_{\text{CAT02}}^{-1} \begin{vmatrix} R_{\text{adapt2}} & 0.0 & 0.0 \\ 0.0 & G_{\text{adapt2}} & 0.0 \\ 0.0 & 0.0 & B_{\text{adapt2}} \end{vmatrix} \begin{vmatrix} 1/R_{\text{adapt1}} & 0.0 & 0.0 \\ 0.0 & 1/G_{\text{adapt1}} & 0.0 \\ 0.0 & 0.0 & 1/B_{\text{adapt1}} \end{vmatrix} \mathbf{M}_{\text{CAT02}} \begin{vmatrix} X_1 \\ Y_1 \\ Z_1 \end{vmatrix} \quad (9.39)$$

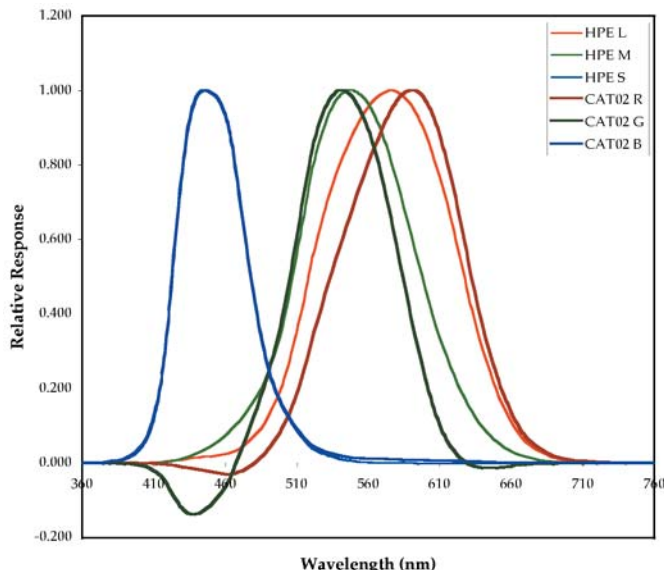


Figure 9.6 Comparison of the Hunt–Pointer–Estevez cone responsivities (thin lines, labeled HPE) with the ‘sharpened’ responsivities used in the CAT02 chromatic adaptation transform (thick lines, labeled CAT02). Note how the ‘sharpened’ responsivities are more spectrally distinct, narrower, and include some negative values. All responsivities have been normalized to set their maximum value to 1.0

$$\mathbf{M}_{\text{CAT02}} = \begin{vmatrix} 0.4002 & 0.7076 & -0.0808 \\ -0.2263 & 1.1653 & 0.0457 \\ 0.0 & 0.0 & 0.9182 \end{vmatrix} \quad (9.40)$$

The process follows the normal von Kries transformation with a conversion from CIE tristimulus values (XYZ) to sharpened cone responsivities (RGB) using the $\mathbf{M}_{\text{CAT02}}$ matrix transformation. The RGB values are then divided by the adapting RGB values for the first viewing condition and multiplied by the adapting RGB values for the second viewing condition prior to a linear transformation back to corresponding CIE tristimulus values. In Figure 9.6, the spectral responsivities represented by $\mathbf{M}_{\text{CAT02}}$ are contrasted with the Hunt–Pointer–Estevez cone responsivities used in many chromatic adaptation transformations and color appearance models.

It should also be noted that Equations 9.39 and 9.40 represent CAT02 in its simplest form under the assumption of complete chromatic adaptation. Simple enhancements to the transformation to allow for the prediction of incomplete chromatic adaptation and discounting the illuminant are presented in the full description of CIECAM02 in Chapter 16.

10

Color Appearance Models

The chromatic adaptation transforms discussed in Chapter 9 go a long way toward extending tristimulus colorimetry toward the prediction of color appearance. However, they are still limited in that they can only predict matches across disparate viewing conditions (i.e., corresponding colors). A chromatic adaptation transform alone cannot be used to describe the actual color appearance of stimuli. To do this, one must use the appearance parameters defined in Chapter 4 — the absolute color appearance attributes of brightness, colorfulness, and hue and the relative color appearance attributes of lightness, chroma, saturation, and, again, hue. These terms are used to describe the color appearance of stimuli. Chromatic adaptation transforms provide no measure of correlates to these perceptual attributes. This is the domain of color appearance models.

10.1 DEFINITION OF COLOR APPEARANCE MODELS

The world of color measurement is full of various descriptors of color such as tristimulus values, chromaticity coordinates, uniform chromaticity scales, uniform color spaces, and ‘just plain-old’ color spaces. Sometimes it is difficult to keep all the names and distinctions straight. So just what is it that sets a color appearance model apart from all of these other types of color specification? CIE Technical Committee 1-34, *Testing Color Appearance Models*, was given the task of evaluating the performance of various color appearance models and recommending a model for general use. Thus, one of the first tasks of this committee became the definition of just what constitutes a color appearance model in order to be included in the tests (Fairchild 1995a).

TC1-34 agreed on the following definition: a color appearance model is any model that includes predictors of at least the relative color appearance attributes of lightness, chroma, and hue. For a model to include reasonable predictors of these attributes, it must include at least some form of a chromatic adaptation transform. Models must be more complex to include predictors of brightness and colorfulness or to model other luminance-dependent effects such as the Stevens effect or the Hunt effect.

Given the above definition, some fairly simple uniform color spaces, such as the CIE 1976 $L^*a^*b^*$ color space (CIELAB) and the CIE 1976 $L^*u^*v^*$ color space (CIELUV), can be considered color appearance models. These color spaces include simple chromatic adaptation transforms and predictors of lightness, chroma, and hue. The general construction of a color appearance model and then a discussion of CIELAB as a specific example are presented in the following sections.

10.2 CONSTRUCTION OF COLOR APPEARANCE MODELS

Some general concepts that apply to the construction of all color appearance models are described in this section. All color appearance models for practical applications begin with the specification of the stimulus and viewing conditions in terms of CIE XYZ tristimulus values (along with certain absolute luminances for some models). The first process applied to these data is generally a linear transformation from XYZ tristimulus values to cone responses in order to more accurately model the physiological processes in the human visual system. The importance of beginning with CIE tristimulus values is a matter of practicality. There is a great deal of color measurement instrumentation that is available to quickly and accurately measure stimuli in terms of CIE tristimulus values. The CIE system is also a well-established, international standard for color specification and communication.

Occasionally, vision-science-based models of color vision and appearance are based upon cone responsivities that are not linear transformations of CIE color matching functions (e.g., Guth 1995). The small advantage in performance that such an approach provides is far outweighed by the inconvenience in practical applications.

Given tristimulus values for the stimulus, other data regarding the viewing environment must also be considered in order to predict color appearance. This is illustrated by all of the color appearance phenomena described in Chapters 6 and 7. As a minimum, the tristimulus values of the adapting stimulus (usually taken to be the light source) are also required. Additional data that might be utilized include the absolute luminance level, colorimetric data on the proximal field, background, and surround, and perhaps other spatial or temporal information.

Given some or all of the above data, the first step in a color appearance model is generally a chromatic adaptation transform such as those described in Chapter 9. The post-adaptation signals are then combined into higher-

level signals, usually modeled after the opponent theory of color vision and including threshold and/or compressive nonlinearities. These signals are then combined in various ways to produce predictors of the various appearance attributes. Data on the adapting stimulus, background, surround, etc. are incorporated into the model at the chromatic adaptation stage and later stages as necessary.

This general process can be witnessed within all of the color appearance models described in this book. However, each model has been derived with a different approach and various of the previously given aspects are stressed to a greater or lesser degree. A simple example of a color appearance model that follows most of the construction steps outlined above is CIELAB. The interpretation of the CIELAB color space as a color appearance model is described in the next section.

10.3 CIELAB

Those trained in traditional colorimetry usually have a negative reaction when they hear CIELAB described as a color appearance model. This is because the CIE (1986) went to great lengths to make sure that it was called a uniform color space and not an appearance space. CIELAB was developed as a color space to be used for the specification of color differences. In the early 1970s, there were as many as 20 different formulas being used to calculate color differences. To promote uniformity of practice pending the development of a better formula, the CIE recommended two color spaces, CIELAB and CIELUV, for use in 1976 (Robertson 1977, 1990). The Euclidean distance between two points in these spaces is taken to be a measure of their color difference (ΔE_{ab}^* or ΔE_{uv}^*). As an historical note, in 1994 the CIE recommended a single better formula for color difference measurement, based on the CIELAB space, known as ΔE_{94}^* (Berns 1993a, CIE 1995b). In the process of creating a color difference formula, the CIE happened to construct a color space with some predictors of color appearance attributes. Perhaps it is not surprising that the best way to describe the difference in color of two stimuli is to first describe the appearance of each. Thus, with appropriate care, CIELAB can be considered a color appearance model.

Calculating CIELAB Coordinates

To calculate CIELAB coordinates, one must begin with two sets of CIE XYZ tristimulus values, those of the stimulus, $X_nY_nZ_n$, and those of the reference white, $X_nY_nZ_n$. These data are utilized in a modified form of the von Kries chromatic adaptation transform by normalizing the stimulus tristimulus values by those of the white (i.e., X/X_n , Y/Y_n , and Z/Z_n). Note that the CIE tristimulus values are not first transformed to cone responses as would be necessary for a true von Kries adaptation model. These adapted signals are

then subject to a compressive nonlinearity represented by a cube root in the CIELAB equations. This nonlinearity is designed to model the compressive response typically found between physical energy measurements and perceptual responses (e.g., Stevens 1961). These signals are then combined into three response dimensions corresponding to the light–dark, red–green, and yellow–blue responses of the opponent theory of color vision. Finally, appropriate multiplicative constants are incorporated into the equations to provide the required uniform perceptual spacing and proper relationship between the three dimensions. The full CIELAB equations are given in Equations 10.1–10.4.

$$L^* = 116f(Y/Y_n) - 16 \quad (10.1)$$

$$a^* = 500[f(X/X_n) - f(Y/Y_n)] \quad (10.2)$$

$$b^* = 200[f(Y/Y_n) - f(Z/Z_n)] \quad (10.3)$$

$$f(\omega) = \begin{cases} (\omega)^{1/3} & \omega > 0.008856 \\ 7.787(\omega) + 16/116 & \omega \geq 0.008856 \end{cases} \quad (10.4)$$

The alternative forms for low tristimulus values were introduced by Pauli (1976) to overcome limitations in the original CIELAB equations that limited their application to values of X/X_n , Y/Y_n , and Z/Z_n greater than 0.01. Such low values are not often encountered in color materials, but sometimes are found in flare-free specifications of imaging systems. It is critical to use the full set of Equations 10.1–10.4 in cases for which low values might be encountered.

The L^* measure given in Equation 10.1 is a correlate to perceived lightness ranging from 0.0 for black to 100.0 for a diffuse white (L^* can sometimes exceed 100.0 for stimuli such as specular highlights in images). The a^* and b^* dimensions correlate approximately with red–green and yellow–blue chroma perceptions. They take on both negative and positive values. Both a^* and b^* have values of 0.0 for achromatic stimuli (i.e., white, gray, black). Their maximum values are limited by the physical properties of materials rather than the equations themselves.

The CIELAB L^* , a^* , and b^* dimensions are combined as Cartesian coordinates to form a three-dimensional color space as illustrated in Figure 10.1. This color space can also be represented in terms of cylindrical coordinates as shown in Figure 10.2. The cylindrical coordinate system provides predictors of chroma C_{ab}^* and hue h_{ab} (hue angle in degrees) as expressed in Equations 10.5 and 10.6.

$$C_{ab}^* = \sqrt{(a^{*2} + b^{*2})} \quad (10.5)$$

$$h_{ab} = \tan^{-1}(b^*/a^*) \quad (10.6)$$

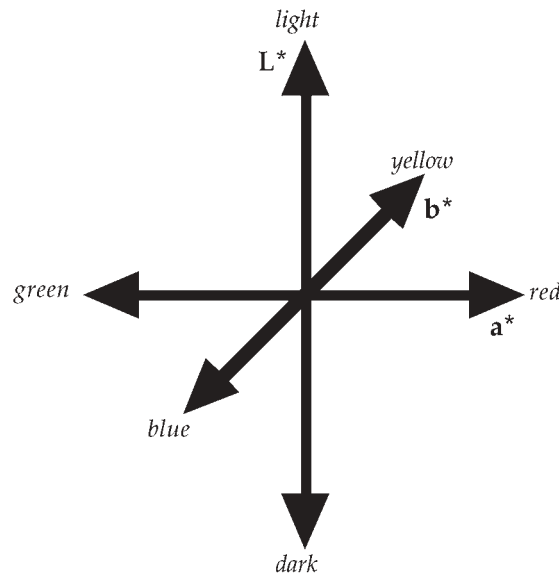


Figure 10.1 Cartesian representation of the CIELAB color space

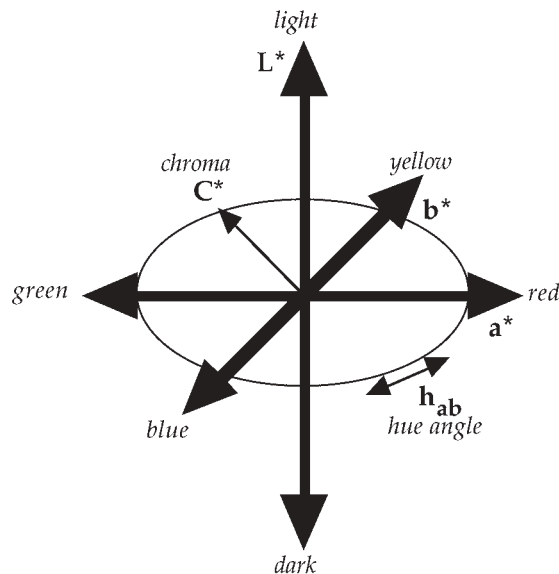


Figure 10.2 Cylindrical representation of the CIELAB color space

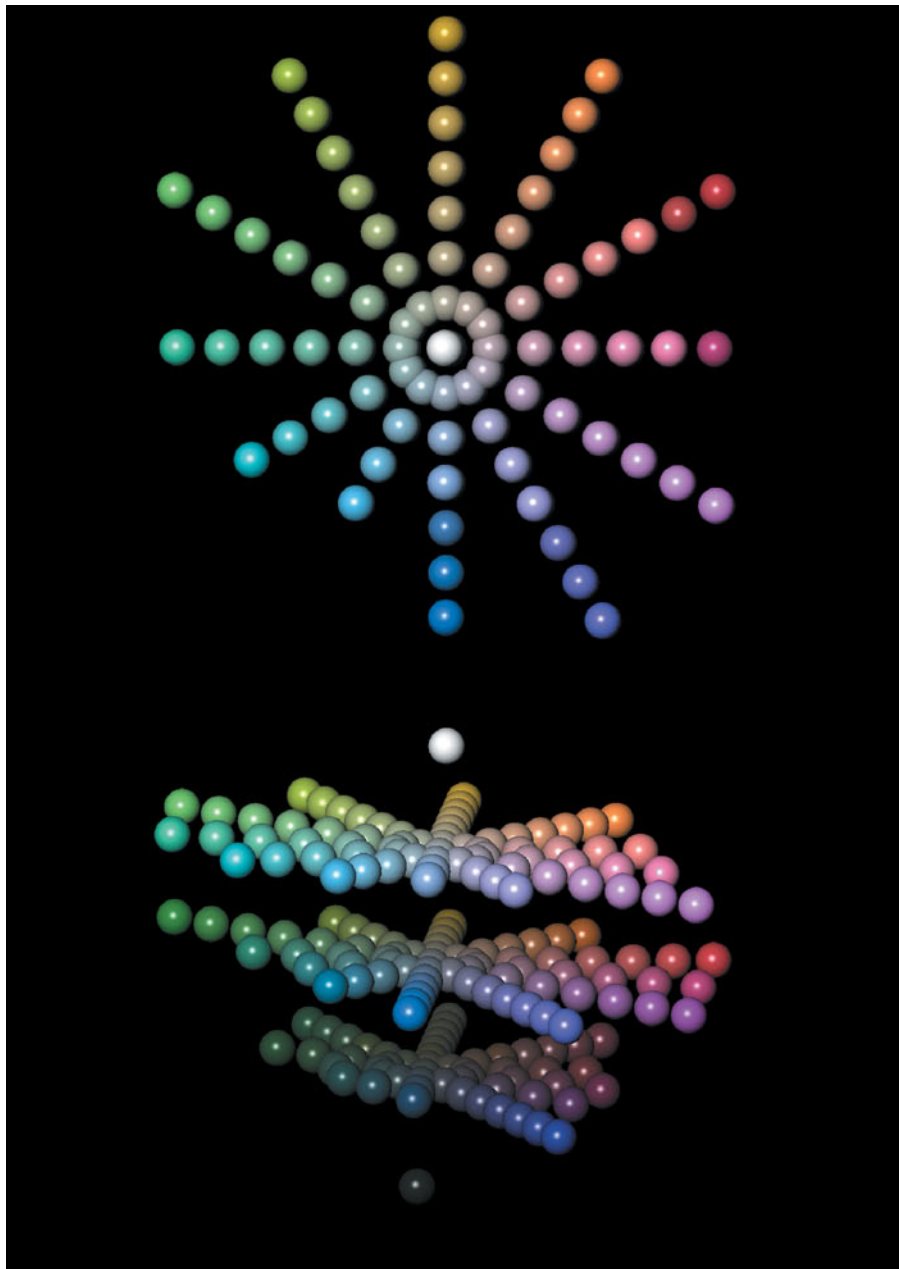


Figure 10.3 Two views of a three-dimensional computer graphics rendering of a sampling of the CIELAB color space along the lightness, chroma, and hue dimensions

Table 10.1 Example CIELAB calculations

Quantity	Case 1	Case 2	Case 3	Case 4
X	19.01	57.06	3.53	19.01
Y	20.00	43.06	6.56	20.00
Z	21.78	31.96	2.14	21.78
X_n	95.05	95.05	109.85	109.85
Y_n	100.00	100.00	100.00	100.00
Z_n	108.88	108.88	35.58	35.58
L^*	51.84	71.60	30.78	51.84
a^*	0.00	44.22	-42.69	-13.77
b^*	-0.01	18.11	2.30	-52.86
C_{ab}^*	0.01	47.79	42.75	54.62
h_{ab}	270.0	22.3	176.9	255.4

C^* has the same units as a^* and b^* . Achromatic stimuli have C^* values of 0.0 (i.e., no chroma). Hue angle, h_{ab} , is expressed in positive degrees starting from 0° at the positive a^* axis and progressing in a counter-clockwise direction. Figure 10.3 is a full-color three-dimensional representation of the CIELAB color space sampled along the lightness, chroma, and hue angle dimensions.

The CIELAB formula takes the XYZ tristimulus values of a stimulus and the reference white as input and produces correlates to lightness L^* , chroma, C_{ab}^* , and hue, h_{ab} as output. Thus CIELAB is a simple form of a color appearance model. Table 10.1 provides worked examples of CIELAB calculations.

While the CIELAB space provides a simple example of a color appearance model, there are some known limitations. The perceptual uniformity of the CIELAB space can be evaluated by examining plots of constant hue and chroma contours from the *Munsell Book of Color*. Such a plot is illustrated in Figure 10.4. Since the Munsell system is designed to be perceptually uniform in terms of hue and chroma, to the extent that it realizes this objective Figure 10.4 should ideally be a set of concentric circles representing the constant chroma contours with straight lines radiating from the center representing constant hue. As can be seen in Figure 10.4, the CIELAB space does a respectable job of representing the Munsell system uniformly. However, further examination of constant hue contours using a CRT system (capable of achieving higher chroma than generally available in the *Munsell Book of Color*) have illustrated discrepancies between observed and predicted results (e.g., Hung and Berns 1995). Figure 10.5 shows constant perceived hue lines from Hung and Berns (1995). It is clear that these lines are curved in the CIELAB space, particularly for red and blue hues.

A similar examination of the CIELAB lightness scale can be made by plotting Munsell value as a function of L^* as shown in Figure 10.6. Clearly, the L^* function predicts lightness, as defined by Munsell value, quite well. In fact,

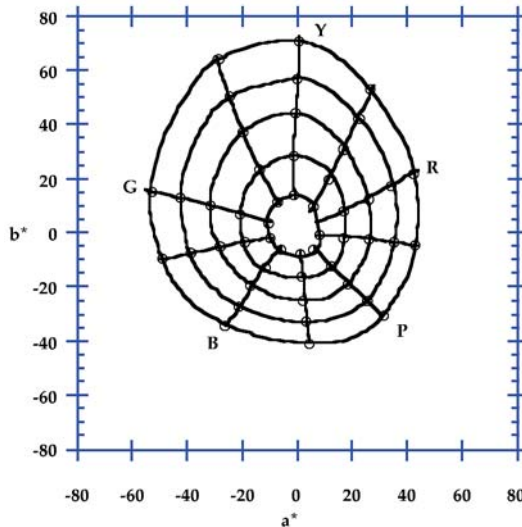


Figure 10.4 Contours of constant Munsell chroma and hue at value 5 plotted in the CIELAB a^*b^* plane

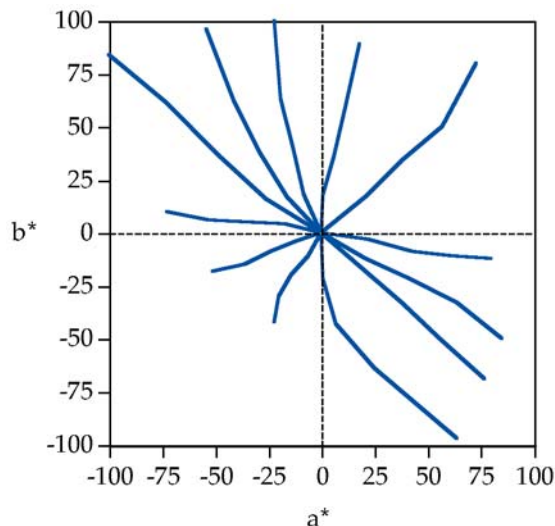


Figure 10.5 Contours of constant perceived hue from Hung and Berns (1995) plotted in the CIELAB a^*b^* plane

the L^* function predicts the original Munsell lightness scaling data better than the fifth-order polynomial used to define Munsell value (Fairchild 1995b). The result in Figure 10.6 is not surprising given the historical derivation of the L^* scale to be a close approximation to the Munsell value scale (Robertson 1990).

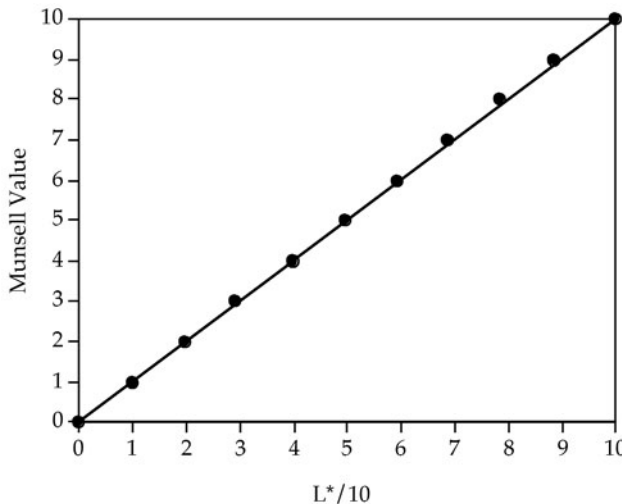


Figure 10.6 Munsell value plotted as a function of CIELAB L^* . The line represents a slope of 1.0 and is not fitted to the data

It is also worth noting that the perceptual unique hues (red, green, yellow and blue) do not align directly with the CIELAB a^*b^* axes. The unique hues under daylight illumination lie approximately at hue angles of 24° (red), 90° (yellow), 162° (green), and 246° (blue) (Fairchild 1996).

Other limitations of CIELAB are caused by the implementation of a von Kries-type chromatic adaptation transform using CIE XYZ tristimulus values rather than cone responsivities. This has been called a *wrong von Kries transform* (Terstiege 1972) as described in the next section.

Wrong von Kries Transform

Terstiege (1972) has referred to von Kries-type adaptation transforms applied to values other than cone responses (sometimes called fundamental tristimulus values) as *wrong von Kries transforms*. Thus, CIELAB incorporates a wrong von Kries transform through its normalization of CIE XYZ tristimulus values to those of the source. It is important to realize that the normalization of XYZ tristimulus values is not equivalent to the process of first transforming (linearly) to cone responses and then performing the normalization. This inequality is illustrated in Equations 10.7–10.11, which take a correct von Kries transformation in matrix form and convert it into an operation on CIE tristimulus values.

The wrong von Kries transformation incorporated in CIELAB can be expressed as a diagonal matrix transformation on CIE XYZ tristimulus values. A ‘right’ von Kries transformation is a diagonal matrix transformation of LMS cone responses as shown in Equation 10.7.

$$\begin{vmatrix} L_a \\ M_a \\ S_a \end{vmatrix} = \begin{vmatrix} k_l & 0 & 0 \\ 0 & k_M & 0 \\ 0 & 0 & k_S \end{vmatrix} \begin{vmatrix} L \\ M \\ S \end{vmatrix} \quad (10.7)$$

Since LMS cone responses can be expressed as linear transformations of CIE XYZ tristimulus values, Equation 10.8 can be derived from Equation 10.7 through a simple substitution and then Equation 10.9 follows through algebraic substitution.

$$\mathbf{M} \begin{vmatrix} X_a \\ Y_a \\ Z_a \end{vmatrix} = \begin{vmatrix} k_l & 0 & 0 \\ 0 & k_M & 0 \\ 0 & 0 & k_S \end{vmatrix} \mathbf{M} \begin{vmatrix} X \\ Y \\ Z \end{vmatrix} \quad (10.8)$$

$$\begin{vmatrix} X_a \\ Y_a \\ Z_a \end{vmatrix} = \mathbf{M}^{-1} \begin{vmatrix} k_l & 0 & 0 \\ 0 & k_M & 0 \\ 0 & 0 & k_S \end{vmatrix} \mathbf{M} \begin{vmatrix} X \\ Y \\ Z \end{vmatrix} \quad (10.9)$$

The nature of the matrix transformation \mathbf{M} is critical. \mathbf{M} is never a diagonal matrix. A typical \mathbf{M} matrix is given in Equation 10.10.

$$\mathbf{M} = \begin{vmatrix} 0.390 & 0.689 & -0.079 \\ -0.230 & 1.183 & 0.046 \\ 0 & 0 & 1.000 \end{vmatrix} \quad (10.10)$$

Evaluating Equation 10.9 using the \mathbf{M} matrix of Equation 10.10 results in Equation 10.11. Since the matrix transformation relating the tristimulus values of the stimulus before and after adaptation is not a diagonal matrix, the wrong von Kries transformation cannot be equal to a correct von Kries transformation applied on cone responses.

$$\begin{vmatrix} X_a \\ Y_a \\ Z_a \end{vmatrix} = \begin{vmatrix} 0.74k_l + 0.26k_M & 1.32k_l - 1.32k_M & -0.15k_l - 0.05k_m + 0.20k_S \\ 0.14k_l - 0.14k_M & 0.26k_l + 0.74k_M & -0.03k_l + 0.03k_S \\ 0 & 0 & k_S \end{vmatrix} \begin{vmatrix} X \\ Y \\ Z \end{vmatrix} \quad (10.11)$$

An interesting experimental example of the shortcoming of the wrong von Kries transformation embedded in the CIELAB equations has been described by Liu *et al.* (1995). They studied the perceived hue shift in the color of the gemstone tanzanite upon changes from daylight to incandescent illumination. Some rare examples of tanzanite appear blue under daylight and purple under incandescent light. However, the CIELAB equations predict that the change in hue for these gemstones would be from blue toward blue-green upon changing from daylight to incandescent. This prediction is in the opposite direction of the perceived hue change. If the same calculations are performed using a correct von Kries transformation acting on cone

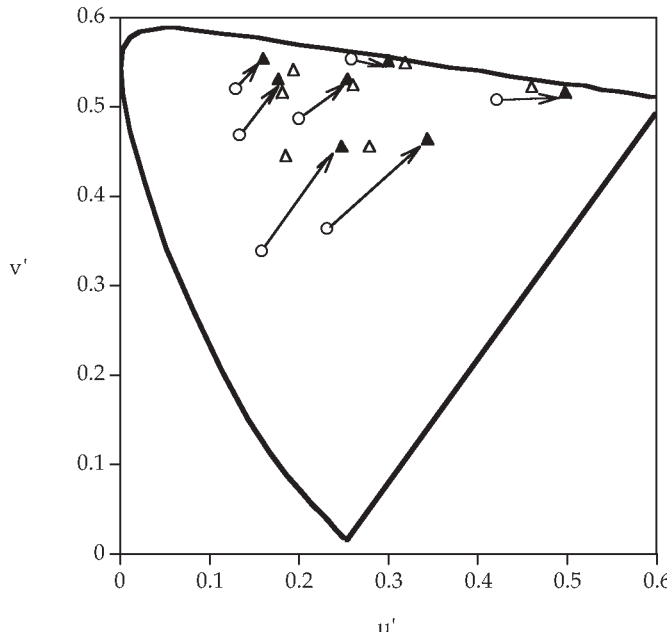


Figure 10.7 Prediction of some example corresponding colors data using the CIELAB model. Open triangles represent visual data and filled triangles represent model predictions

responsivities, the correct hue shift is predicted (Liu *et al.* 1995). Moroney (2003) explores the poor blue constancy of CIELAB in detail and expands on the above explanation.

The Breneman (1987) corresponding colors data that were used to compare chromatic adaptation models in Chapter 9 were also evaluated using the chromatic adaptation transform of the CIELAB equations. The predicted and observed results are illustrated using $u'v'$ chromaticity coordinates in Figure 10.7. The errors in the predictions are significantly larger than those found with a normal von Kries transformation (see Figure 9.2). The results indicate particularly large errors in the hue predictions for blue stimuli for this change in adaptation from daylight to incandescent. This is consistent with the errors observed by Liu *et al.* (1995) for tanzanite.

10.4 WHY NOT USE JUST CIELAB?

Given that CIELAB is a well-established, *de facto* international standard, color space that has been widely used for two decades and that it is capable of color appearance predictions, why are any other color appearance models necessary? As can be seen in Chapter 15, CIELAB performs quite well as a color appearance model in some applications. So why not just quit there and work with CIELAB?

The limitations of CIELAB discussed previously provide much of the answer to these questions. The modified von Kries adaptation transformation incorporated into the CIELAB equations is clearly less accurate than transformations that more closely follow known visual physiology. Also, there are limitations in CIELAB's ability to predict hue that prompt further work on appearance models.

There are also several aspects of color appearance that CIELAB is incapable of predicting. CIELAB incorporates no luminance-level dependency. Thus it is completely incapable of predicting luminance-dependent effects such as the Hunt effect and the Stevens effect. CIELAB also incorporates no background or surround dependency. Therefore it cannot be used to predict simultaneous contrast or the Bartleson-Breneman results showing a change in image contrast with surround relative luminance. CIELAB also has no mechanism for modeling cognitive effects, such as discounting the illuminant, that can become important in cross-media color reproduction applications. Lastly, CIELAB does not provide correlates for the absolute appearance attributes of brightness and colorfulness. As a reminder, it is useful to recall note 6 on the CIELAB space from CIE publication 15.2 (CIE 1986) which states:

These spaces are intended to apply to comparisons of differences between object colours of the same size and shape, viewed in identical white to middle-grey surroundings, by an observer photopically adapted to a field of chromaticity not too different from that of average daylight.

This long list of limitations seems to indicate that it should be possible to significantly improve upon CIELAB in the development of a color appearance model. Such models are described in the next few chapters. The CIELAB space should be kept in mind as a simple model that can be used as a benchmark to measure whether more sophisticated models are indeed improvements.

10.5 WHAT ABOUT CIELUV?

Since CIELAB can be considered a color appearance model, what about the other color space that the CIE recommended in 1976, CIELUV? CIELUV has many of the same properties as CIELAB (e.g., stimulus and source chromaticities as input and lightness, chroma, and hue predictors as output), so it might deserve equal attention.

CIELUV incorporates a different form of chromatic adaptation transform than CIELAB. It uses a subtractive shift in chromaticity coordinates (u' - u'_n , v' - v'_n) rather than a multiplicative normalization of tristimulus values (X/X_n , Y/Y_n , Z/Z_n). The subtractive adaptation transform incorporated in CIELUV is even farther from physiological reality than the wrong von Kries transform of CIELAB. This subtractive shift can result in predicted corresponding colors being shifted right out of the gamut of realizable colors. (This produces pre-

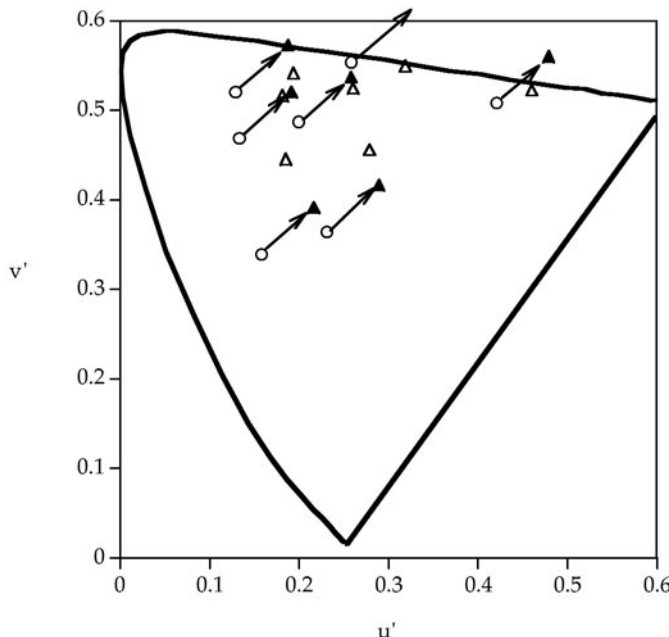


Figure 10.8 Prediction of some example corresponding colors data using the CIELUV model. Open triangles represent visual data and filled triangles represent model predictions

dicted tristimulus values less than zero, which cannot happen with the CIELAB transformation.) Even if this does not occur, the transform is likely to shift predicted colors outside the gamut of colors producible by any given device. In addition to this problem, the CIELUV adaptation transform is extremely inaccurate with respect to predicting visual data. This is illustrated nicely in Figure 10.8, which shows the CIELUV predictions of the Breneman (1987) corresponding colors data. Figure 10.8 illustrates how some colors are shifted outside the gamut of realizable colors (outside the spectrum locus on the $u'v'$ chromaticity diagram) and the inaccuracy of all the predictions.

The difficulties with the CIELUV adaptation transform are reason enough to eliminate it from serious consideration as an appearance model. However, additional evidence is provided by its poor performance for predicting color differences. The current CIE recommendation for color difference specification, CIE94 (CIE 1995b), is based on the CIELAB color space. So are the more recent CIE DE2000 (CIE 2001) color difference equations. While the DE2000 equations are more recent, their added complexity over the CIE94 specification is probably unwarranted in most applications. Alman *et al.* (1989) provide experimental evidence for the poor performance of CIELUV as a color difference equation. Additional comparisons between CIELUV and CIELAB have been made by Robertson (1990).

11

The Nayatani *et al.* Model

The next few chapters describe details of the most widely discussed and used color appearance models. This chapter discusses the color appearance model developed by Nayatani and his co-workers that has evolved as one of the more important early colorimetry-based models. This model, along with Hunt's model (described in Chapter 12), is a complete color appearance model capable of predicting the full array of color appearance parameters defined in Chapter 4 for a fairly wide range of viewing conditions.

11.1 OBJECTIVES AND APPROACH

The Nayatani *et al.* color appearance model evolved as a natural extension of their chromatic adaptation model described in Chapter 9 (Nayatani *et al.* 1981) in conjunction with the attributes of a color appearance model first outlined by Hunt (1982, 1985). The Nayatani *et al.* color appearance model was first described in Nayatani *et al.* (1986, 1987) and most recently revised and summarized in Nayatani *et al.* (1995). The latter version of the model is described in this chapter.

As with any color appearance model, it is important to note the context in which the Nayatani *et al.* model was formulated. The researchers who developed this model come from the field of illumination engineering, in which the critical application of color appearance models is the specification of the color rendering properties of light sources. This application provides significantly different challenges from those encountered in the field of image reproduction. Thus, those interested in image reproduction might find some aspects of the Nayatani *et al.* model inappropriate for their needs. The reverse is also true. Models derived strictly for imaging applications might not fulfill the requirements for illumination engineering applications.

Despite the different pedigrees of the various models, it is worthwhile to stretch them to applications for which they were not designed. The best possible result will be that they work well (indicating good generality) and the worst outcome is that something more is learned about the important differences in applications. Thus, while the Nayatani *et al.* model was not designed for imaging applications, it is certainly worthy of evaluation in any application that might require a color appearance model.

The model attempts to predict a wide range of color appearance phenomena including the Stevens effect, the Hunt effect, and the Nelson–Judd effect in addition to the effects of chromatic adaptation. It is designed to predict the color appearance of simple patches on uniform mid-to-light-gray backgrounds. It is not designed for complex stimuli or changes in background or surround. The model includes output values designed to correlate with all of the important color appearance attributes including brightness, lightness, colorfulness, chroma, and hue. The model's design for simple stimuli on uniform backgrounds highlights the distinction between it and models such as Hunt's, RLAB, and CIECAM02 that were designed with specific attributes for imaging applications. These apparent limitations of the model are not limitations at all for lighting and illumination color-rendering applications.

11.2 INPUT DATA

The input data for the model include the colorimetric and photometric specification of the stimulus, the adapting illuminant, and the luminance factor of the background. Specifically, the required data include the following:

- The luminance factor of the achromatic background is expressed as a percentage Y_o , limited to values equal to or greater than 18%.
- The color of the illumination x_o, y_o is expressed in terms of its chromaticity coordinates for the CIE 1931 standard colorimetric observer.
- The test stimulus is specified in terms of its chromaticity coordinates x, y and its luminance factor Y .
- The absolute luminance of the stimulus and adapting field is defined by the illuminance of the viewing field E_o expressed in lux.

In addition, two other parameters must also be specified to define the model's required input:

- The normalizing illuminance E_{or} which is expressed in lux and usually in the range of 1000–3000 lux.
- The noise term n used in the nonlinear chromatic adaptation model which is usually taken to be 1.

From these input data, a variety of intermediate and final output values are calculated according to the model. The equations necessary for

determining these values are presented in the following sections. A few preliminary calculations are required before proceeding with the main features of the model. The first is the calculation of the adapting luminance and the normalizing luminance in cd/m² according to Equations 11.1 and 11.2.

$$L_o = \frac{Y_o E_o}{100\pi} \quad (11.1)$$

$$L_{or} = \frac{Y_o E_{or}}{100\pi} \quad (11.2)$$

Equations 11.1 and 11.2 are valid given the assumption that the background is a Lambertian diffuser.

Second, in the Nayatani *et al.* model, the transformation from CIE tristimulus values to cone responsivities for the adapting field is expressed in terms of chromaticity coordinates rather than tristimulus values. This necessitates the calculation of the intermediate values of ξ (xi), η (eta), and ζ (zeta) as illustrated in Equations 11.3–11.5.

$$\xi = (0.48105x_o + 0.78841y_o - 0.08081)/y_o \quad (11.3)$$

$$\eta = (-0.27200x_o + 1.11962y_o + 0.04570)/y_o \quad (11.4)$$

$$\zeta = 0.91822(1 - x_o - y_o)/y_o \quad (11.5)$$

11.3 ADAPTATION MODEL

As with all color appearance models, the first stage of the Nayatani *et al.* color appearance model is a chromatic adaptation transformation. The adaptation model used is a refined form of the nonlinear model of chromatic adaptation described in Chapter 9 (Nayatani *et al.* 1981, CIE 1994). In the formulation of the color appearance model, the chromatic adaptation model is embedded in other equations. Rather than separate the two, the treatment in Nayatani *et al.* (1995) will be followed and the important features of the chromatic adaptation model that are embedded in other equations will be pointed out to clarify the formulation of the color appearance model.

First, the cone responses for the adapting field must be calculated in terms of the absolute luminance level. This relies on the chromaticity transform described in Equations 11.3–11.5, the illuminance level E_o , and the luminance factor of the adapting background Y_o as formulated in Equation 11.6.

$$\begin{vmatrix} R_o \\ G_o \\ B_o \end{vmatrix} = \frac{Y_o E_o}{100\pi} \begin{vmatrix} \xi \\ \eta \\ \zeta \end{vmatrix} \quad (11.6)$$

Given the adapting-level cone responses from Equation 11.6, the exponents of the nonlinear model of chromatic adaptation are calculated as described by Equations 11.7–11.9. Note that, in this formulation, the exponent for the short-wavelength sensitive cones (B in Nayatani's notation) differs from the exponents for the middle- and long-wavelength-sensitive cones (R and G in Nayatani's notation).

$$\beta_1(R_o) = \frac{6.469 + 6.362R_o^{0.4495}}{6.469 + R_o^{0.4495}} \quad (11.7)$$

$$\beta_1(G_o) = \frac{6.469 + 6.362G_o^{0.4495}}{6.469 + G_o^{0.4495}} \quad (11.8)$$

$$\beta_2(B_o) = \frac{8.414 + 8.091B_o^{0.5128}}{8.414 + B_o^{0.5128}} \times 0.7844 \quad (11.9)$$

An additional exponential factor that depends on the normalizing luminance must also be calculated using the same functional form as the exponents for the middle- and long-wavelength-sensitive cones as shown in Equation 11.10.

$$\beta_1(L_{or}) = \frac{6.469 + 6.362L_{or}^{0.4495}}{6.469 + L_{or}^{0.4495}} \quad (11.10)$$

The cone responses for the test stimulus are calculated from their tristimulus values using a more traditional linear transformation given in Equation 11.11.

$$\begin{vmatrix} R \\ G \\ B \end{vmatrix} = \begin{vmatrix} 0.40024 & 0.70760 & -0.08081 \\ -0.22630 & 1.16532 & 0.04570 \\ 0.0 & 0.0 & 0.91822 \end{vmatrix} \begin{vmatrix} X \\ Y \\ Z \end{vmatrix} \quad (11.11)$$

Finally, two scaling coefficients, $e(R)$ and $e(G)$, are calculated according to Equations 11.12 and 11.13.

$$e(R) = \begin{cases} 1.758 & R \geq 20\xi \\ 1.0 & R < 20\xi \end{cases} \quad (11.12)$$

$$e(G) = \begin{cases} 1.758 & G \geq 20\eta \\ 1.0 & G < 20\eta \end{cases} \quad (11.13)$$

The above calculations provide all the intermediate data necessary to implement the nonlinear chromatic adaptation model within the color appearance model. The precise use of these values is described within the appearance equations as they come into play.

11.4 OPPONENT COLOR DIMENSIONS

The cone responses are transformed directly into intermediate values representing classical opponent dimensions of visual response: an achromatic channel and two chromatic channels. These equations, used to model these opponent processes, also incorporate the nonlinear chromatic adaptation model.

First, the achromatic response Q is calculated using Equation 11.14.

$$Q = \frac{41.69}{\beta_1(L_{\text{or}})} \left[\frac{2}{3} \beta_1(R_o) e(R) \log \frac{R+n}{20\xi+n} + \frac{1}{3} \beta_1(G_o) e(G) \log \frac{G+n}{20\eta+n} \right] \quad (11.14)$$

At first, Equation 11.14 looks fairly complex, but its components can be readily teased apart and understood. First, the general structure of Equation 11.14 is such that the achromatic response is calculated as a weighted sum of the outputs of the long- and middle-wavelength cone responses (R and G) as is often postulated in color vision theory. The outputs are summed with relative weights of $2/3$ and $1/3$, which correspond to their relative population in the human retina. They are first normalized after addition of noise n , by the cone responses for the adapting stimulus represented by ξ and η according to a von Kries-type transformation. The value of n is typically taken to be 1.0 although it can vary. A logarithmic transform is then taken to model the compressive nonlinearity that is known to occur in the human visual system. Given the logarithmic transformation, the exponents (β terms) of the nonlinear chromatic adaptation model become multiplicative factors along with the scaling factors $e(R)$ and $e(G)$, as shown in Equation 11.14. All that remains is one more scaling factor 41.69, and the luminance-dependent, exponential adjustment, $\beta_1(L_{\text{or}})$, to complete the equation. Thus the achromatic response can be simply expressed as a weighted sum of the post-adaptation signals from the long- and middle-wavelength-sensitive cones.

Next, preliminary chromatic channel responses t (red-green) and p (yellow-blue), are calculated in a similar manner using Equations 11.15 and 11.16.

$$t = \beta_1(R_o) \log \frac{R+n}{20\xi+n} - \frac{12}{11} \beta_1(G_o) \log \frac{G+n}{20\eta+n} + \frac{1}{11} \beta_2(B_o) \log \frac{B+n}{20\xi+n} \quad (11.15)$$

$$p = \frac{1}{9} \beta_1(R_o) \log \frac{R+n}{20\xi+n} + \frac{1}{9} \beta_1(G_o) \log \frac{G+n}{20\eta+n} - \frac{2}{9} \beta_2(B_o) \log \frac{B+n}{20\xi+n} \quad (11.16)$$

The explanation of Equations 11.15 and 11.16 follows the same logic as that for the achromatic response, Equation 11.14. Beginning with the t response; it is a weighted combination of the post-adaptation signals from each of the three cone types. The combination is the difference between the long- and middle-wavelength-sensitive cones with a small input from the short-wavelength-sensitive cones that adds with the long-wavelength

response. This results in a red minus green response that also includes some reddish input from the short wavelength end of the spectrum that is often used to explain the violet (rather than blue) appearance of those wavelengths. It is also required for correct prediction of unique yellow. The *p* response is calculated in a similar manner by adding the long- and middle-wavelength-sensitive cone outputs to produce a yellow response and then subtracting the short-wavelength cone output to produce the opposing blue response. The weighting factors were those of the original Hunt model.

It is of interest to note that the *t* and *p* notation is derived from the terms tritanopic and protanopic response. A tritanope has only the red-green response *t* and a protanope has only the yellow-blue response *p*. The *Q*, *t*, and *p* responses are used in further equations to calculate correlates of brightness, lightness, saturation, colorfulness, and hue.

One aspect of the hue correlate, hue angle θ is calculated directly from *t* and *p* as shown in Equation 11.17.

$$\theta = \tan^{-1} \left(\frac{p}{t} \right) \quad (11.17)$$

Hue angle is calculated as a positive angle from 0° to 360° , beginning from the positive *t* axis, just as is done in the CIELAB color space (CIE 1986). The hue angle is required to calculate some of the other appearance correlates since a hue-dependent adjustment factor is required in some cases.

11.5 BRIGHTNESS

The brightness B_r of the test sample is calculated using Equation 11.18.

$$B_r = Q + \frac{50}{\beta_1(L_{or})} \left[\frac{2}{3} \beta_1(R_o) + \frac{1}{3} \beta_1(G_o) \right] \quad (11.18)$$

Q is the achromatic response, given by Equation 11.14, which is adjusted using the adaptation exponents in order to include the dependency upon absolute luminance level that is required for brightness, as opposed to lightness.

It is also necessary to calculate the brightness of an ideal white B_{rw} , according to Equation 11.19, derived by substituting Equation 11.14 evaluated for a perfect reflector into Equation 11.18.

$$B_{rw} = \frac{41.69}{\beta_1(L_{or})} \left[\frac{2}{3} \beta_1(R_o)(1.758) \log \frac{100\xi + n}{20\xi + n} + \frac{1}{3} \beta_1(G_o)(1.758) \log \frac{100\eta + n}{20\eta + n} \right] \\ + \frac{50}{\beta_1(L_{or})} \left[\frac{2}{3} \beta_1(R_o) + \frac{1}{3} \beta_1(G_o) \right] \quad (11.19)$$

11.6 LIGHTNESS

The achromatic lightness L_P^* of the test sample is calculated directly from the achromatic response Q by simply adding 50 as shown in Equation 11.20. This is the case since the achromatic response can take on both negative and positive values with a middle gray having $Q = 0.0$ while lightness is scaled from 0 for a black to 100 for a white.

$$L_P^* = Q + 50 \quad (11.20)$$

A second lightness correlate, known as normalized achromatic lightness L_N^* , is calculated according to the CIE definition that lightness is the brightness of the test sample relative to the brightness of a white as shown in Equation 11.21.

$$L_N^* = 100 \left(\frac{B_r}{B_{rw}} \right) \quad (11.21)$$

The differences between the two lightness correlates L_P^* and L_N^* are generally negligible. Neither of the lightness values correlate with the perceived lightness of chromatic object colors since the model does not include the Helmholtz–Kohlrausch effect (e.g., Fairchild and Pirrotta 1991, Nayatani *et al.* 1992). An additional model is necessary to include the Helmholtz–Kohlrausch effect, which is necessary for the comparison of the lightness or brightness of stimuli with differing hue and/or chroma.

11.7 HUE

Hue angle, θ , is calculated as shown previously in Equation 11.17, which is identical to the technique used in the CIELAB color space. More descriptive hue correlates can be obtained by determining the hue quadrature H and the hue composition H_C .

Hue quadrature H is a 400-step hue scale on which the unique hues take on values of 0 (red), 100 (yellow), 200 (green), and 300 (blue). The hue quadrature is computed via linear interpolation using the hue angle θ of the test sample, and the hue angles for the four unique hues, which are defined as 20.14° (red), 90.00° (yellow), 164.25° (green), and 231.00° (blue).

The hue composition H_C , describes perceived hue in terms of percentages of two of the unique hues from which the test hue is composed. For example, an orange color might be expressed as 50Y 50R, indicating that the hue is perceived to be halfway between unique red and unique yellow. Hue composition is computed by simply converting the hue quadrature into percent components between the unique hues falling on either side of the test color (again by a linear process). For example, a color stimulus with a hue angle

of 44.99° will have a hue quadrature of 32.98 and a hue composition of 33Y67R.

11.8 SATURATION

In the Nayatani *et al.* color appearance model, saturation is derived most directly and then the measures of colorfulness and chroma are derived from it. Saturation is expressed in terms of a red-green component, SRG, derived from the *t* response as shown in Equation 11.22 and a yellow-blue component SYB derived from the *p* response as shown in Equation 11.23.

$$S_{RG} = \frac{488.93}{\beta_1(L_{or})} E_s(\theta)t \quad (11.22)$$

$$S_{YB} = \frac{488.93}{\beta_1(L_{or})} E_s(\theta)p \quad (11.23)$$

The saturation predictors include a scaling factor 488.93 for convenience; the luminance-dependent *b* terms required to predict the Hunt effect; and a chromatic strength function, $E_s(\theta)$, that was introduced to correct the saturation scale as a function of hue angle (Nayatani 1995). It takes on the empirically derived form expressed in Equation 11.24.

$$\begin{aligned} E_s(\theta) = & 0.9394 - 0.2478 \sin \theta - 0.0743 \sin 2\theta + 0.0666 \sin 3\theta \\ & - 0.0186 \sin 4\theta - 0.0055 \cos \theta - 0.0521 \cos 2\theta \\ & - 0.0573 \cos 3\theta - 0.0061 \cos 4\theta \end{aligned} \quad (11.24)$$

Finally, an overall saturation correlate *S* is calculated using Equation 11.25. This is precisely the same functional form as the chroma calculation in CIELAB (Euclidean distance from the origin).

$$S = (S_{RG}^2 + S_{YB}^2)^{1/2} \quad (11.25)$$

11.9 CHROMA

Given the correlates for saturation described above, correlates of chroma can be easily derived by considering their definitions. As was illustrated in Chapter 4, saturation can be expressed as chroma divided by lightness. Thus chroma can be described as saturation multiplied by lightness. This is almost exactly the functional form for chroma in the Nayatani *et al.* model. The correlates for the red-green, yellow-blue, and overall chroma of the test sample are given in Equations 11.26–11.28.

$$C_{RG} = \left(\frac{L_P^*}{50} \right)^{0.7} S_{RG} \quad (11.26)$$

$$C_{YB} = \left(\frac{L_P^*}{50} \right)^{0.7} S_{YB} \quad (11.27)$$

$$C = \left(\frac{L_P^*}{50} \right)^{0.7} S \quad (11.28)$$

The only differences between the nominal definition of chroma and Equations 11.26–11.28 are the scaling factor of 50 and the slight nonlinearity introduced by the power function of lightness with an exponent of 0.7. This nonlinearity was introduced to better model constant chroma contours from the *Munsell Book of Color* (Nayatani *et al.* 1995).

11.10 COLORFULNESS

The predictors of colorfulness in the Nayatani *et al.* model can also be derived directly from the CIE definitions of the appearance attributes. Recall that chroma is defined as colorfulness of the sample relative to the brightness of a white object under similar illumination. Thus colorfulness is simply the chroma of the sample multiplied by the brightness of an ideal white as illustrated in Equations 11.29–11.31.

$$M_{RG} = C_{RG} \frac{B_{rw}}{100} \quad (11.29)$$

$$M_{YB} = C_{YB} \frac{B_{rw}}{100} \quad (11.30)$$

$$M = C \frac{B_{rw}}{100} \quad (11.31)$$

The normalizing value of 100 is derived as the brightness of an ideal white under illuminant D65 at the normalizing illuminance. It provides a convenient place to tie down the scale.

11.11 INVERSE MODEL

In many applications, and particularly image reproduction, it is necessary to use a color appearance model in both forward and reverse directions. Thus it

is important, or at least highly convenient, that the equations can be analytically inverted. Fortunately, the Nayatani *et al.* color appearance model can be inverted analytically. Nayatani *et al.* (1990a) published a paper that introduces the process for inverting the model for both brightness–colorfulness and lightness–chroma matches. While the model has changed slightly, the same general procedure can be followed.

In applying the model, it is often useful to consider its implementation as a simple step-by-step process. Thus the steps required to implement the model (and in reverse order to invert it) are given below.

1. Obtain physical data.
2. Calculate Q , t , and p .
3. Calculate θ , $E_s(\theta)$, H , and H_C .
4. Calculate B_r , B_{rw} , L_p^* , L_N^* , and S .
5. Calculate C .
6. Calculate M .

11.12 PHENOMENA PREDICTED

The Nayatani *et al.* color appearance model accounts for changes in color appearance due to chromatic adaptation and luminance level (Steven effect and Hunt effect). It also predicts the Helson–Judd effect. The model can be used for different background luminance factors (greater than 18%), but the model's authors caution against using it for comparisons between different luminance levels (Nayatani *et al.* 1990a). It cannot be used to predict the effects of changes in background color (simultaneous contrast) or surround relative luminance (e.g., Bartleson–Breneman equations.).

The Nayatani *et al.* color appearance model also does not incorporate mechanisms for predicting incomplete chromatic adaptation or cognitive discounting-the-illuminant. Nayatani (1997) has outlined a procedure to estimate the level of chromatic adaptation from experimental data. This is useful to allow the model to be used to predict the results of visual experiments in which chromatic adaptation is incomplete. However, this technique is of little value in practical applications in which a prediction of the level of chromatic adaptation must be made for a set of viewing conditions for which prior visual data are not available.

Example calculations using the Nayatani *et al.* color appearance model as described in this chapter are given for four samples in Table 11.1.

11.13 WHY NOT USE JUST THE NAYATANI *et al.* MODEL?

Given the extensive nature of the Nayatani *et al.* color appearance model and its inclusion of correlates for all of the important color appearance attributes, it is reasonable to wonder why the CIE hasn't simply adopted this

Table 11.1 Example Nayatani *et al.* color appearance model calculations

Quantity	Case 1	Case 2	Case 3	Case 4
X	19.01	57.06	3.53	19.01
Y	20.00	43.06	6.56	20.00
Z	21.78	31.96	2.14	21.78
X_n	95.05	95.05	109.85	109.85
Y_n	100.00	100.00	100.00	100.00
Z_n	108.88	108.88	35.58	35.58
E_o	5000	500	5000	500
E_{or}	1000	1000	1000	1000
B_r	62.6	67.3	37.5	44.2
L_P^*	50.0	73.0	24.5	49.4
L_N^*	50.0	75.9	29.7	49.4
θ	257.5	21.6	190.6	236.3
H	317.8	2.1	239.4	303.6
H_C	82B 18R	98R 2Y	61G 39B	96B 4R
S	0.0	37.1	81.3	40.2
C	0.0	48.3	49.3	39.9
M	0.0	42.9	62.1	35.8

model as a recommended color appearance model. There are several reasons this has not happened.

First it is worth reiterating the positive features of the Nayatani *et al.* model. It is a complete model in terms of output correlates. It is fairly straightforward (although the equations could be presented in a more simplified way) and it is analytically invertible.

However, there are some negative aspects of the model that prevent it from becoming the single best answer. It cannot account for changes in background, surround, or cognitive effects. Surround and cognitive factors are critical in image reproduction applications. It also does not predict adaptation level, which is also important in cross-media reproduction applications. It has been derived and tested mainly for simple patches, which might limit its usefulness in more complex viewing situations. The model also significantly over-predicts the Helson–Judd effect by predicting strong effects for illuminants that are not very chromatic (such as illuminant A). It is clear that the Helson–Judd effect does not occur under such conditions as was originally pointed out by Helson (1938) himself. Lastly, in various tests of color appearance models described in later chapters, the Nayatani *et al.* model has been generally shown to be not particularly accurate. The Nayatani *et al.* model also does not incorporate rod contributions to color appearance as can be found in the Hunt model.

Given all the above limitations, it is clear that this model cannot provide the ultimate answer for a single color appearance model. This does not

lessen its significance and contributions to the development of color appearance models. It is almost certain that some aspects of the Nayatani *et al.* model will find their way into whatever model is agreed upon for general use in the future as illustrated by the evolution of CIECAM97s and CIECAM02.

12

The Hunt Model

This chapter continues the review of some of the most widely discussed and used color appearance models with a description of the model developed by Robert William Gainer Hunt. This model is the most extensive, complete, and complex color appearance model that has been developed. Its roots can be traced to some of Hunt's early chromatic adaptation studies (Hunt 1952) up through its rigorous development in the 1980s and 1990s (Hunt 1982, 1985, 1987, 1991b, 1994, 1995).

The Hunt color appearance model is not simple, but it is designed to predict a wide range of visual phenomena and, as Hunt himself has stated, the human visual system is not simple either. While there are applications in which simpler models such as those described in later chapters are adequate, it is certainly of great value to have a complete model that can be adapted to a wider range of viewing conditions for more well defined or unusual circumstances. The Hunt model serves this purpose well and many of the other color appearance models discussed in this book can trace many of their features back to ideas that originally appeared in Hunt's model.

12.1 OBJECTIVES AND APPROACH

Hunt spent 36 years of his career in the Kodak Research Laboratories. Thus, the Hunt model has been developed in the context of the requirements for color image reproduction. This is a significantly different point of view than found in the field of illumination engineering from which the Nayatani *et al.* model discussed in Chapter 11 was developed. The imaging science influence on the Hunt model can be easily witnessed by examining its input parameters. For example, the surround relative luminance is an important factor that is not present in the Nayatani *et al.* model. Other examples can be found in parameters that are set to certain values for 'transparencies'

projected in a dark room' or 'television displays in a dim surround' or 'normal scenes.' Such capabilities clearly indicate that the model was intended to be applied to imaging situations. However, this is not the limit of the model's applicability. For example, it has also been extended for unrelated colors such as those found in traditional vision science experiments.

The Hunt model is designed to predict a wide range of visual phenomena including the appearance of related and unrelated colors in various backgrounds, surrounds, illumination colors, and luminance levels ranging from low scotopic to bleaching levels. In this sense it is a complete model of color appearance for static stimuli. Hunt's model, like most of the others described in this book, does not attempt to incorporate complex spatial or temporal characteristics of appearance.

To make reasonable predictions of appearance over such a wide range of conditions, the Hunt model requires more rigorous definition of the viewing field. Thus, Hunt (1991b) defined the components of the viewing field as described in Chapter 7. These components include the stimulus, the proximal field, the background, and the surround. The Hunt model is the only available model that treats each of these components of the viewing field separately.

While Hunt's model has been continuously evolving over the past two decades (see Hunt 1982, 1985, 1987, 1991b, and 1994 for major milestones), a comprehensive review of the model's current formulation can be found in Chapter 31 of the 5th Edition of Hunt's book, *The Reproduction of Colour* (Hunt 1995). The treatment that follows is adapted from that chapter. Those desiring more detail on Hunt's model should refer to Chapter 31 of Hunt's book.

12.2 INPUT DATA

The Hunt model requires an extensive list of input data. All colorimetric coordinates are typically calculated using the CIE 1931 standard colorimetric observer (2°). The chromaticity coordinates (x, y) of the illuminant and the adapting field are required. Typically, the adapting field is taken to be the integrated chromaticity of the scene, which is assumed to be identical to that of the illuminant (or source). Next, the chromaticities (x, y) and luminance factors Y of the background, proximal field, reference white, and test sample are required. If separate data are not available for the proximal field, it is generally assumed to be identical to the background. Also, the reference white is often taken to have the same chromaticities as the illuminant with a luminance factor of 100 if specific data are not available.

All of these data are relative colorimetric values. Absolute luminance levels are required to predict several luminance-dependent appearance phenomena. Thus the absolute luminance levels, in cd/m^2 , are required for the reference white and the adapting field. If the specific luminance of the

Table 12.1 Values of the chromatic and brightness surround induction factors

Situation	N_c	N_b
Small areas in uniform backgrounds and surrounds	1.0	300
Normal scenes	1.0	75
Television and CRT displays in dim surrounds	1.0	25
Large transparencies on light boxes	0.7	25
Projected transparencies in dark surrounds	0.7	10

adapting field is not available, it is taken to be 20% of the luminance of the reference white under the assumption that scenes integrate to a gray with a reflectance factor of 0.2. Additionally, scotopic luminance data are required in order to incorporate rod responses into the model (another feature unique to the Hunt model). Thus, the scotopic luminance of the adapting field in scotopic cd/m² is required. Since scotopic data are rarely available, the scotopic luminance of the illuminant L_{AS} can be approximated from its photopic luminance L_A and correlated color temperature T using Equation 12.1.

$$L_{AS} = 2.26L_A[(T/4000) - 0.4]^{1/3} \quad (12.1)$$

The scotopic luminance of the test stimulus relative to the scotopic luminance of the reference white is also required. Again, since such data are rarely available, an approximation is often used by substituting the photopic luminance of the sample relative to the reference white for the scotopic values.

Lastly, there are several input variables that are decided based on the viewing configuration. Two of these are the chromatic N_c and brightness N_b surround induction factors. Hunt (1995) suggests using values optimized for the particular viewing situation. Since this is often not possible, the nominal values listed in Table 12.1 are recommended.

The last two input parameters are the chromatic N_{cb} and brightness N_{bb} background induction factors. Again, Hunt recommends optimized values. Assuming these are not available, the background induction factors are calculated from the luminances of the reference white Y_W and background Y_b using Equations 12.2 and 12.3.

$$N_{cb} = 0.725(Y_W/Y_b)^{0.2} \quad (12.2)$$

$$N_{bb} = 0.725(Y_W/Y_b)^{0.2} \quad (12.3)$$

A final decision must be made regarding discounting-the-illuminant. Certain parameters in the model are assigned different values for situations in which discounting-the-illuminant occurs. Given all of the above data one can then continue with the calculations of the Hunt model parameters.

12.3 ADAPTATION MODEL

As with all of the models described in this book, the first step is a transformation from CIE tristimulus values to cone responses. In Hunt's model the cone responses are denoted $\rho\gamma\beta$ rather than *LMS*. The transformation used (referred to as the *Hunt–Pointer–Estevez transformation* also used in the Nayatani *et al.* and RLAB models) is given in Equation 12.4. For the Hunt model, this transformation is normalized such that the equal-energy illuminant has equal $\rho\gamma\beta$ values.

$$\begin{vmatrix} \rho \\ \gamma \\ \beta \end{vmatrix} = \begin{vmatrix} 0.38971 & 0.68898 & -0.07868 \\ -0.22981 & 1.18340 & 0.04641 \\ 0.0 & 0.0 & 1.0 \end{vmatrix} \begin{vmatrix} X \\ Y \\ Z \end{vmatrix} \quad (12.4)$$

The transformation from *XYZ* to $\rho\gamma\beta$ values must be completed for the reference white, background, proximal field, and test stimulus.

The chromatic adaptation model embedded in Hunt's color appearance model is a significantly modified form of the von Kries hypothesis. The adapted cone signals $\rho_a\gamma_a\beta_a$ are determined from the cone responses for the stimulus $\rho\gamma\beta$ and those for the reference white $\rho_w\gamma_w\beta_w$ using Equations 12.5–12.7.

$$\rho_a = B_\rho [f_n(F_L F_\rho \rho / \rho_w) + \rho_D] + 1 \quad (12.5)$$

$$\gamma_a = B_\gamma [f_n(F_L F_\gamma \gamma / \gamma_w) + \gamma_D] + 1 \quad (12.6)$$

$$\beta_a = B_\beta [f_n(F_L F_\beta \beta / \beta_w) + \beta_D] + 1 \quad (12.7)$$

The von Kries hypothesis can be recognized in Equations 12.5–12.7 by noting the ratios ρ/ρ_w , γ/γ_w , β/β_w at the heart of the equations. Clearly, there are many other parameters in Equations 12.5–12.7 that require definition and explanation; these are given below. First, $f_n()$ is a general hyperbolic function given in Equation 12.8 that is used to model the nonlinear behavior of various visual responses.

$$f_n[I] = 40[I^{0.73}/(I^{0.73} + 2)] \quad (12.8)$$

Figure 12.1 illustrates the form of Hunt's nonlinear function on log–log axes. In the central operating range, the function is linear and therefore equivalent to a simple power function (in this case with an exponent of about 1/2). However, this function has the advantage that it models threshold behavior at low levels (the gradual increase in slope) and saturation behavior at high levels (the decrease in slope back to zero). Such a nonlinearity is required to model the visual system over the large range in luminance levels that the Hunt model addresses.

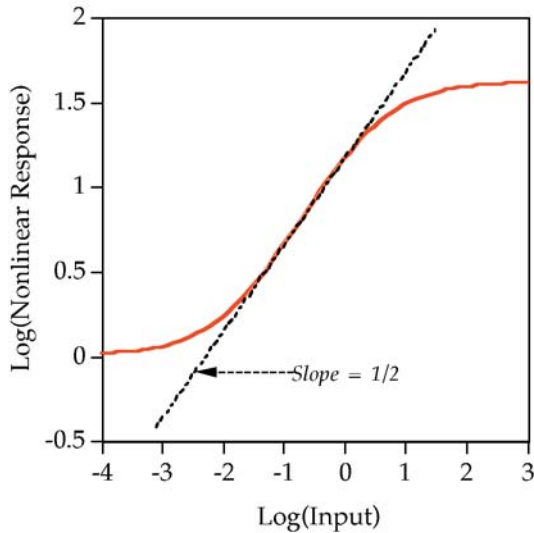


Figure 12.1 The nonlinear response function $f_n(0)$ of the Hunt color appearance model

F_L is a luminance-level adaptation factor incorporated into the adaptation model to predict the general behavior of light adaptation over a wide range of luminance levels. It also reintroduces the absolute luminance level prior to the nonlinearity, allowing appearance phenomena such as the Stevens effect and Hunt effect to be predicted. F_L is calculated using Equations 12.9 and 12.10.

$$F_L = 0.2k^4(5L_A) + 0.1(1 - k^4)^2(5L_A)^{1/3} \quad (12.9)$$

$$k = 1/(5L_A + 1) \quad (12.10)$$

F_ρ , F_γ and F_β are chromatic adaptation factors that are introduced to model the fact that chromatic adaptation is often incomplete. These factors are designed such that chromatic adaptation is always complete for the equal-energy illuminant (sometimes referred to as illuminant E). This means that the chromaticity of illuminant E always appears achromatic according to the model and thus F_ρ , F_γ and F_β are all equal to one. Such a prediction is supported by experimental results of Hurvich and Jameson (1951), Hunt and Winter (1975), and Fairchild (1991b). As F_ρ , F_γ and F_β depart from unity (in either direction depending on the adapting field color), chromatic adaptation is predicted to be less complete. The formulation of F_ρ , F_γ and F_β is given in Equations 12.11–12.16 and the behavior of these functions is illustrated in Figure 12.2 for F_ρ as an example.

$$F_\rho = (1 + L_A^{1/3} + h_\rho)/(1 + L_A^{1/3} + 1/h_\rho) \quad (12.11)$$

$$F_\gamma = (1 + L_A^{1/3} + h_\gamma) / (1 + L_A^{1/3} + 1/h_\gamma) \quad (12.12)$$

$$F_\beta = (1 + L_A^{1/3} + h_\beta) / (1 + L_A^{1/3} + 1/h_\beta) \quad (12.13)$$

$$h_p = 3\rho_w / (\rho_w + \gamma_w + \beta_w) \quad (12.14)$$

$$h_\gamma = 3\gamma_w / (\rho_w + \gamma_w + \beta_w) \quad (12.15)$$

$$h_\beta = 3\beta_w / (\rho_w + \gamma_w + \beta_w) \quad (12.16)$$

The parameters h_p , h_γ and h_β can be thought of as chromaticity coordinates scaled relative to illuminant E (since $\rho\gamma\beta$ themselves are normalized to illuminant E). They take on values of 1.0 for illuminant E and depart further from 1.0 as the reference white becomes more saturated. These parameters, taken together with the luminance level dependency L_A in Equations 12.11–12.13 produce values that depart from 1.0 by increasing amounts as the color of the reference white moves away from illuminant E (becoming more saturated) and the adapting luminance increases. The feature that chromatic adaptation becomes more complete with increasing adapting luminance is also consistent with the visual experiments cited above. This general behavior is illustrated in Figure 12.2 with a family of curves for various adapting luminance levels.

If discounting-the-illuminant occurs, then chromatic adaptation is taken to be complete and F_p , F_γ , and F_β are set equal to values of 1.0.

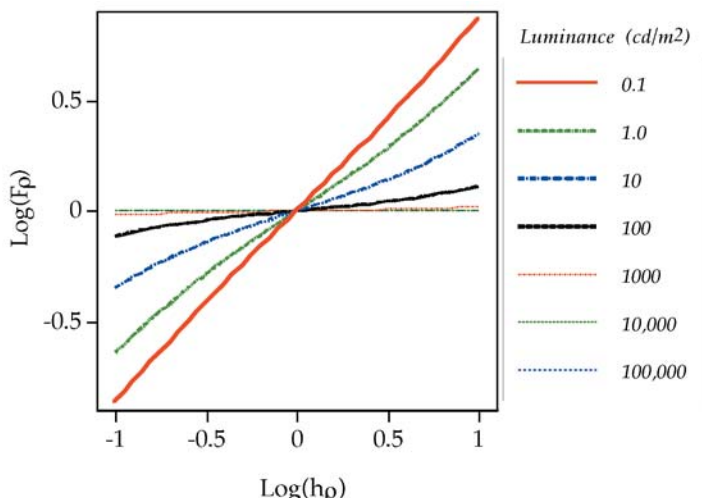


Figure 12.2 One of the chromatic adaptation factors F_p plotted as a function of the adapting chromaticity for a variety of adapting luminance levels. This function illustrates how adaptation becomes less complete (F_p departs from 1.0) as the purity of the adapting stimulus increases (h_p departs from 1.0) and the luminance level decreases

The parameters ρ_D , γ_D , and β_D are included to allow prediction of the Helson–Judd effect. This is accomplished by additive adjustments to the cone signals that are dependent upon the relationship between the luminance of the background Y_b , the reference white Y_W , and the test stimulus as given in Equations 12.17–12.19.

$$\rho_D = f_n[(Y_b/Y_W)F_L F_\gamma] - f_n[(Y_b/Y_W)F_L F_\rho] \quad (12.17)$$

$$\gamma_D = 0.0 \quad (12.18)$$

$$\beta_D = f_n[(Y_b/Y_W)F_L F_\gamma] - f_n[(Y_b/Y_W)F_L F_\beta] \quad (12.19)$$

The Helson–Judd effect does not occur in most typical viewing situations (Helson 1938). In such cases ρ_D , γ_D , and β_D should be set equal to 0.0. In cases for which discounting-the-illuminant occurs, there is no Helson–Judd effect and ρ_D , γ_D , and β_D are forced to 0.0 since F_ρ , F_γ , and F_β are set equal to 1.0. There are some situations in which it is desirable to have F_ρ , F_γ , and F_β take on their normal values while ρ_D , γ_D , and β_D are set to 0.0. These include the viewing of images projected in a darkened surround or viewed on CRT displays.

The last factors in the chromatic adaptation formulas (Equations 12.5–12.7) are the cone bleach factors B_ρ , B_γ , and B_β . Once again, these factors are only necessary to model visual responses over extremely large ranges in luminance level. They are formulated to model photopigment depletion (i.e., bleaching) that occurs at high luminance levels resulting in decreased photoreceptor output, as shown in Equations 12.20–12.22.

$$B_\rho = 10^7/[10^7 + 5L_A(\rho_W/100)] \quad (12.20)$$

$$B_\gamma = 10^7/[10^7 + 5L_A(\gamma_W/100)] \quad (12.21)$$

$$B_\beta = 10^7/[10^7 + 5L_A(\beta_W/100)] \quad (12.22)$$

The cone bleaching factors are essentially 1.0 for most normal luminance levels. As the adapting luminance L_A reaches extremely high levels, the bleaching factors begin to decrease, resulting in decreased adapted cone output. In the limit, the bleaching factors will approach zero as the adapting luminance approaches infinity. This would result in no cone output when the receptors are fully bleached (sometimes referred to as a *retinal burn*). Such adapting levels are truly dangerous to the observer and would cause permanent damage. However, the influence of the cone bleaching factors does begin to take effect at high luminance levels that are below the threshold for retinal damage such as outdoors on a sunny day. In such situations, one can observe the decreased range of visual response due to ‘too much light’ and a typical response is to put on sunglasses. These high luminance levels are not found in typical image reproduction applications (except, perhaps, in some original scenes).

The adaptation formulas (Equations 12.5–12.7) are completed with the addition of 1.0 designed to represent noise in the visual system.

If the proximal field and background differ from a gray, chromatic induction is modeled by adjusting the cone signals for the reference white used in the adaptation equations. This suggests that the state of adaptation is being influenced by the local color of the proximal field and background in addition to the color of the reference white. This type of modeling is completely consistent with observed visual phenomena. Hunt (1991b) has suggested one algorithm for calculating adjusted reference white signals ρ'_w , γ'_w , and β'_w from the cone responses for the background ρ_b , γ_b , and β_b , and proximal field ρ_p , γ_p , and β_p , given in Equations 12.23–12.28.

$$\rho'_w = \frac{\rho_w[(1-p)\rho_p + (1+p)/p_p]^{1/2}}{[(1+p)\rho_p + (1-p)/p_p]^{1/2}} \quad (12.23)$$

$$\gamma'_w = \frac{\gamma_w[(1-p)\gamma_p + (1+p)/p_\gamma]^{1/2}}{[(1+p)\gamma_p + (1-p)/p_\gamma]^{1/2}} \quad (12.24)$$

$$\beta'_w = \frac{\beta_w[(1-p)\beta_p + (1+p)/p_\beta]^{1/2}}{[(1+p)\beta_p + (1-p)/p_\beta]^{1/2}} \quad (12.25)$$

$$p_p = (\rho_p/\rho_b) \quad (12.26)$$

$$p_\gamma = (\gamma_p/\gamma_b) \quad (12.27)$$

$$p_\beta = (\beta_p/\beta_b) \quad (12.28)$$

Values of p in Equations 12.23–12.25 are taken to be between 0 and –1 when simultaneous contrast occurs and between 0 and +1 when assimilation occurs. In most practical applications, the background and proximal field are assumed to be achromatic and adjustments such as those given in Equations 12.23–12.25 are not used.

Now that the adapted cone signals ρ_a , γ_a , and β_a are available, it is possible to move onward to the opponent responses and color appearance correlates. The rod signals and their adaptation will be treated at the point they are incorporated in the achromatic response.

12.4 OPPONENT COLOR DIMENSIONS

Given the adapted cone signals ρ_a , γ_a , and β_a , opponent-type visual responses are calculated in a very simple manner as shown in Equations 12.29–12.32.

$$A_a = 2\rho_a + \gamma_a + (1/20)\beta_a - 3.05 + 1 \quad (12.29)$$

$$C_1 = \rho_a - \gamma_a \quad (12.30)$$

$$C_2 = \gamma_a - \beta_a \quad (12.31)$$

$$C_3 = \beta_a - \rho_a \quad (12.32)$$

The achromatic post-adaptation signal A_a is calculated by summing the cone responses with weights that represent their relative population in the retina. The subtraction of 3.05 and the addition of 1.0 represent removal of the earlier noise components followed by the addition of new noise. The three color difference signals C_1 , C_2 , and C_3 , represent all of the possible chromatic opponent signals that could be produced in the retina. These may or may not have direct physiological correlates, but they are convenient formulations and used to construct more traditional opponent responses as described below.

12.5 HUE

Hue angle in the Hunt color appearance model is calculated just as it is in other models once red-green and yellow-blue opponent dimensions are specified as appropriate combinations of the color difference signals described in Equations 12.30–12.32. Hue angle h_s is calculated using Equation 12.33.

$$h_s = \tan^{-1} \left[\frac{(1/2)(C_2 - C_3)/4.5}{C_1 - (C_2/11)} \right] \quad (12.33)$$

Given the hue angle h_s , a hue quadrature value H , is calculated by interpolation between specified hue angles for the unique hues with adjustment of an eccentricity factor e_s . The interpolating function is given by Equation 12.34.

$$H = H_1 + \frac{100[(h_s - h_1)/e_1]}{[(h_s - h_1)/e_1 + (h_2 - h_s)/e_2]} \quad (12.34)$$

H_1 is defined as 0, 100, 200, or 300 based on whether red, yellow, green, or blue, respectively, is the unique hue with the hue angle nearest to and less than that of the test sample. The values of h_1 and e_1 are taken from Table 12.2 as the values for the unique hue having the nearest lower value of h_s while h_2 and e_2 are taken as the values of the unique hue with the nearest higher value of h_s .

Hue composition H_C is calculated directly from the hue quadrature just as it was in the Nayatani *et al.* model described in Chapter 11. Hue composition is expressed as percentages of two unique hues that describe the composition of the test stimulus hue.

Finally, an eccentricity factor e_s must be calculated for the test stimulus to be used in further calculations of appearance correlates. This is accomplished

Table 12.2 Hue angles h_s and eccentricity factors e_s for the unique hues

Hue	h_s	e_s
Red	20.14	0.8
Yellow	90.00	0.7
Green	164.25	1.0
Blue	237.53	1.2

through linear interpolation using the hue angle h_s of the test stimulus and the data in Table 12.2.

12.6 SATURATION

As a step toward calculating a correlate of saturation, yellowness–blueness and redness–greenness responses must be calculated from the color difference signals according to Equations 12.34 and 12.35.

$$M_{YB} = 100[(1/2)(C_2 - C_3)/4.5][e_S(10/13)N_c N_{cb} F_t] \quad (12.34)$$

$$M_{RG} = 100[C_1 - (C_2/11)][e_S(10/13)N_c N_{cb}] \quad (12.35)$$

The constant values in Equations 12.34 and 12.35 are simply scaling factors. N_c and N_{cb} are the chromatic surround and background induction factors determined at the outset. F_t is a low-luminance tritanopia factor calculated using Equation 12.36.

$$F_t = L_A/(L_A + 0.1) \quad (12.36)$$

Low-luminance tritanopia is a phenomenon whereby observers with normal color vision become more and more tritanopic (yellow-blue deficient) as luminance decreases since the luminance threshold for short-wavelength-sensitive cones is higher than that for the other two cone types. As can be seen in Equation 12.36, F_t is essentially 1.0 for all typical luminance levels. It approaches zero as the adapting luminance L_A approaches zero, forcing the yellowness–blueness response to decrease at low luminance levels. This factor is also of little importance in most practical situations, but necessary to model appearance over an extremely wide range of luminance levels. For most applications, it is better to avoid this situation by viewing samples at sufficiently high luminance levels.

Given the yellowness–blueness and redness–greenness responses defined above, an overall chromatic response M is calculated as their quadrature sum as shown in Equation 12.37.

$$M = (M_{YB}^2 + M_{RG}^2)^{1/2} \quad (12.37)$$

Finally, saturation s is calculated from M and the adapted cone signals using Equation 12.38. This calculation follows the definition of saturation (colorfulness of stimulus relative to its own brightness) if one takes the overall chromatic response M to approximate colorfulness, and the sum of the adapted cone signals in the denominator of Equation 12.38 to approximate the stimulus brightness.

$$s = 50M/(\rho_a + \gamma_a + \beta_a) \quad (12.38)$$

12.7 BRIGHTNESS

Further development of the achromatic signals is required to derive correlates of brightness and lightness. Recall that the Hunt color appearance model is designed to function over the full range of luminance levels. In so doing, it must also incorporate the response of the rod photoreceptors, which are active at low luminance levels. The rod response is incorporated into the achromatic signal (which in turn impacts the predictors of chroma and colorfulness). The rod response after adaptation A_S is given by Equation 12.39. The subscript S is derived from the word scotopic, which is used to describe vision at the low luminance levels for which the rod response dominates.

$$A_S = 3.05B_S[f_n(F_{LS}S/S_W)] + 0.3 \quad (12.39)$$

The formulation of the adapted rod signal is analogous to the formulation of the adapted cone signals described previously (Equations 12.5–12.7). At its heart is a von Kries-type scaling of the scotopic response for the stimulus S , by that for the reference white S_W . F_{LS} is a scotopic luminance level adaptation factor given by Equations 12.40 and 12.41 that is similar to the cone luminance adaptation factor.

$$F_{LS} = 3800j^2(5L_{AS}/2.26) + 0.2(1 - j^2)^4(5L_{AS}/2.26)^{1/6} \quad (12.40)$$

$$j = 0.00001/[(5L_{AS}/2.26) + 0.00001] \quad (12.41)$$

The same nonlinear photoreceptor response function $f_n(j)$, is also used for the scotopic response (see Equation 12.8). The value 3.05 is simply a scaling factor and the noise level of 0.3 (rather than 1.0) is chosen since the rods are more sensitive than cones. Finally, a rod bleaching factor B_S is added to reduce the rod contribution to the overall color appearance as luminance level increases and the rods become less active. This factor is calculated using Equation 12.42. Examination of the rod bleaching factor in comparison with the cone bleaching factors given in Equations 12.20–12.22 shows that the rods will become saturated and their response will become significantly decreased at much lower luminance levels.

$$B_S = 0.5/\{1 + 0.3[(5L_{AS}/2.26)(S/S_W)]^{0.3}\} + 0.5/\{1 + 5[5L_{AS}/2.26]\} \quad (12.42)$$

Given the achromatic cone signal A_a (Equation 12.29), the adapted scotopic signal A_S (Equation 12.39), and the brightness background induction factor determined at the outset, an overall achromatic signal A is calculated using Equation 12.43.

$$A = N_{bb}[A_a - 1 + A_S - 0.3 + (1^2 + 0.3^2)^{1/2}] \quad (12.43)$$

All the constant values in Equation 12.43 represent removal of the earlier noise terms and then their reintroduction through quadrature summation.

The achromatic signal A is then combined with the overall chromatic signal M to calculate a correlate of brightness Q using Equation 12.44.

$$Q = \{7[A + (M/100)]\}^{0.6}N_1 - N_2 \quad (12.44)$$

The correlate of brightness Q depends on both the achromatic A and chromatic M responses in order to appropriately model the Helmholtz-Kohlrausch effect. Equation 12.44 also includes two terms N_1 and N_2 that account for the effects of surround on perceived brightness (e.g., Stevens effect and Bartleson-Breneman results discussed in Chapter 6). These terms are calculated from the achromatic signal for the reference white A_W and the brightness surround induction factor N_b (also determined at the outset), through Equations 12.45 and 12.46.

$$N_1 = (7A_W)^{0.5}/(5.33N_b^{0.13}) \quad (12.45)$$

$$N_2 = 7A_WN_b^{0.362}/200 \quad (12.46)$$

Note that since the achromatic signal for the reference white A_W is required, it is necessary to carry through all of the model calculations described above for the reference white in addition to the test stimulus. The brightness of the reference white Q_W , must also be calculated for use in later equations.

Another form of brightness, referred to as whiteness–blackness Q_{WB} , can be calculated in the Hunt model. This is a bipolar value similar to the Q value in the Nayatani *et al.* model that illustrates that black objects look darker and white objects look brighter as the adapting luminance level increases (another way to state the Stevens effect). Q_{WB} is calculated according to Equation 12.47 using the brightness of the background (which also must be calculated through the model).

$$Q_{WB} = 20(Q^{0.7} - Q_b^{0.7}) \quad (12.47)$$

12.8 LIGHTNESS

Given the brightness of the test stimulus Q and the brightness of the reference white Q_W the Hunt color appearance model correlate of lightness J is calculated as shown in Equation 12.48.

$$J = 100(Q/Q_W)^z \quad (12.48)$$

This formulation for lightness follows the CIE definition that lightness is the brightness of the test stimulus relative to the brightness of a white. This ratio is raised to a power z that models the influence of the background relative luminance on perceived lightness according to Equation 12.49. The exponent z increases as the background becomes lighter, indicating that dark test stimuli will appear relatively more dark on a light background than they would on a dark background. This follows the commonly observed phenomenon of simultaneous lightness contrast.

$$z = 1 + (Y_b/Y_W)^{1/2} \quad (12.49)$$

12.9 CHROMA

The Hunt color appearance model correlate of chroma C_{94} is determined from saturation s and the relative brightness (approximately lightness) following the general definitions given in Chapter 4 that indicate chroma can be represented as saturation multiplied by lightness. The precise formulation is given in Equation 12.50.

$$C_{94} = -2.44s^{0.69}(Q/Q_W)^{Y_b/Y_W}(1.64 - 0.29^{Y_b/Y_W}) \quad (12.50)$$

Equation 12.50 illustrates that chroma depends on the relative brightness of the stimulus Q/Q_W and on the relative luminance of the background Y_b/Y_W . The formulation for chroma given by Equation 12.50 was derived empirically based upon the results of a series of appearance scaling experiments (Hunt 1994, Hunt and Luo 1994).

12.10 COLORFULNESS

Given chroma, colorfulness can be determined by factoring in the brightness (or at least the luminance level). This is accomplished in the Hunt color appearance model by multiplying chroma C_{94} by the luminance level adaptation factor F_L (Equation 12.9) raised to a power of 0.15 as shown in Equation 12.51.

$$M_{94} = F_L^{0.15}C_{94} \quad (12.51)$$

Thus M_{94} is the colorfulness correlate for the Hunt color appearance model. It was also derived empirically through analysis of visual scaling results.

12.11 INVERSE MODEL

Unfortunately, because of its complexity, the complete Hunt color appearance model cannot be analytically inverted. It is an even more severe problem if one has only lightness, chroma, and hue correlates to start from, which is often the case. Many applications, particularly image reproduction, require a color appearance model to be used in both forward and reverse directions. Thus the lack of an analytical inverse introduces some difficulty in using the Hunt model for these applications. Hunt (1995) provides some suggestions for how to deal with this difficulty.

In all cases, it is easier to reverse the model if all the appearance correlates are available rather than just three. One alternative is to use the model without the scotopic response. This simplifies the inversion process since the introduction of the scotopic terms into higher-level equations is one feature that prevents analytical inversion. The predictions of the model are slightly changed when the scotopic response is ignored, but this difference might be negligible for many applications. Hunt (1995) suggests that this technique is appropriate for reference white luminances greater than 10 cd/m^2 . Most situations in which careful judgements of color reproduction are made are at luminance levels above 10 cd/m^2 .

Other techniques suggested by Hunt (1995) require successive approximation for some parts of the reverse model. In most applications, it is simpler to use successive approximation for the whole model, iterating until appropriate output tristimulus values are obtained that produce the appearance correlates that are available at the outset. This technique can be accomplished with a technique such as a Newton–Raphson optimization, and it can be applied when only lightness, chroma, and hue are available (in fact it is the only option). While a successive approximation technique can be very time consuming for large data sets, such as images, this drawback is overcome by using the forward and reverse models to build three-dimensional look-up tables, which are then used with an interpolation technique to convert image data. Then, the time-consuming model inversion process need only be performed once for each viewing condition in order to build the look-up table. This approach helps, but if users want to vary the viewing conditions, they must wait a long time for the look-up table to be recalculated before an image can be processed. The delay might be significant enough to render the full Hunt model impractical for some applications.

In applying the model, it is often useful to consider its implementation as a simple step-by-step process. Thus the steps required to implement the model (and in reverse, as possible, to invert it) are given below.

1. Obtain physical data and decide on other parameters.
2. Calculate cone excitations $\rho\gamma\beta$ for the various stimulus fields.
3. Calculate relative cone excitations.
4. Calculate the luminance-level adaptation factor F_L .
5. Calculate chromatic adaptation factors $F_\rho, F_\gamma, F_\beta$.
6. Calculate Helson–Judd effect parameters $\rho_D, \gamma_D, \beta_D$.
7. Calculate adapted cone signals $\rho_a, \gamma_a, \beta_a$.
8. Calculate achromatic A_a and color difference C_1, C_2, C_3 signals.
9. Calculate hue angle h_s .
10. Calculate hue quadrature H .
11. Calculate hue composition H_C .
12. Calculate eccentricity factor e_s .
13. Calculate low-luminance tritanopia factor F_t .
14. Calculate chromatic responses M and saturation s .
15. Calculate scotopic luminance adaptation factor F_{LS} .
16. Calculate scotopic response A_s .
17. Calculate complete achromatic response A .
18. Calculate brightness Q .
19. Calculate lightness J .
20. Calculate chroma C_{94} .
21. Calculate colorfulness M_{94} .
22. Calculate whiteness–blackness Q_{WB} .

The Hunt color appearance model is the most complex to implement of the traditional color appearance models described in this book. There are a couple of implementation techniques that can simplify program development and greatly improve computational speed. One is to go through the model and calculate all the parameters that are constant for a given set of viewing conditions first in a precalculation routine. This can be applied to all of the adaptation factors, correlates for the reference white, etc. Then, these precalculated data can be used for the remaining data calculations rather than recalculating the values for each stimulus (or pixel in an image). This can be particularly useful when transforming image data (or look-up tables) that might require the model calculations to be completed millions of times. Secondly, many of the equations, for example the achromatic response A (Equation 12.43), include operations on constants. The number of computations can be reduced by combining all of these constants into a single number first (some compilers will do this for you). For example, the $-1 - 0.3 + (1^2 + 0.3^2)^{1/2}$ can be converted into simply 1.044.

12.12 PHENOMENA PREDICTED

As stated previously, the Hunt color appearance model is the most extensive and complete color appearance model available. It has the following features:

Table 12.3 Example Hunt color appearance model calculations

Quantity	Case 1	Case 2	Case 3	Case 4
X	19.01	57.06	3.53	19.01
Y	20.00	43.06	6.56	20.00
Z	21.78	31.96	2.14	21.78
X _W	95.05	95.05	109.85	109.85
Y _W	100.00	100.00	100.00	100.00
Z _W	108.88	108.88	35.58	35.58
L _A	318.31	31.83	318.31	31.83
N _c	1.0	1.0	1.0	1.0
N _b	75	75	75	75
Discounting?	Yes	Yes	Yes	Yes
h _S	269.3	18.6	178.3	262.8
H	317.2	398.8	222.2	313.4
H _C	83B 17R	99R 1B	78G 22B	87B 13R
s	0.03	153.36	245.40	209.29
Q	31.92	31.22	18.90	22.15
J	42.12	66.76	19.56	40.27
C ₉₄	0.16	63.89	74.58	73.84
M ₉₄	0.16	58.28	76.33	67.35

- It is designed to predict the appearance of stimuli in a variety of backgrounds and surrounds at luminance levels ranging from the absolute threshold of human vision to cone bleaching.
- It can be used for related or unrelated stimuli (see Hunt 1991b for an explanation of how the model is applied to unrelated colors).
- It predicts a wide range of color appearance phenomena including the Bezold–Brücke hue shift, Abney effect, Helmholtz–Kohlrausch effect, Hunt effect, simultaneous contrast, Helson–Judd effect, Stevens effect, and Bartleson–Breneman observations.
- It predicts changes in color appearance due to light and chromatic adaptation and cognitive discounting-the-illuminant.
- It is unique in that it includes the contributions of rod photoreceptors.

While the list of appearance phenomena that the Hunt model addresses is extensive, this comes at the price of complexity (with no apologies required—the visual system is complex) that makes the model difficult to use in some applications.

Example calculations using the Hunt color appearance model as described in this chapter are given for four samples in Table 12.3. These results were calculated with the assumptions that the proximal field and background were both achromatic (same chromaticity as the source) with luminance factors of 20% and that the reference white also had the same chromaticity as the source with a luminance factor of 100%. Scotopic input was calculated

using the approximate equations described in this chapter. The Helson-Judd parameters were always set to 0.0.

12.13 WHY NOT USE JUST THE HUNT MODEL?

Given that the Hunt color appearance model seems to be able to do everything that anyone could ever want a color appearance model to do, why isn't it adopted as the single standard color appearance model for all applications? The main reason could be the very fact that it is so complete. In its completeness also lies its complexity. Its complexity makes application of the Hunt model to practical situations range from difficult to impossible. However, the complexity of the Hunt model also allows it to be extremely flexible. As will be seen in Chapter 15, the Hunt model is generally capable of making accurate predictions for a wide range of visual experiments. This is because the model is flexible enough to be adjusted to the required situations. Clearly, this flexibility and general accuracy are great features of the Hunt model. However, often it is not possible to know just how to apply the Hunt model (i.e., to decide on the appropriate parameter values) until after the visual data have been obtained. In other cases, the parameters actually need to be optimized, not just chosen, for the particular viewing situation. This is not a problem if the resources are available to derive the optimized parameters. However, when such resources are not available and the Hunt model must be used 'as is' with the recommended parameters, the model can perform extremely poorly (see Chapter 15). This is because the nominal parameters used for a given viewing condition are being used to make specific predictions of phenomena that may or may not be important in that situation. After the fact, adjustments can be made, but that might be too late. Thus, if it is not possible to optimize (or optimally choose) the implementation of the Hunt model, its precision might result in predictions that are worse than much simpler models for some applications.

Other negative aspects that counteract the positive features of the Hunt color appearance model are that it cannot be easily inverted and that it is computationally expensive, difficult to implement, and requires significant user knowledge to use consistently. The Hunt model also uses functions with additive offsets to predict contrast changes due to variation in surround relative luminance. These functions can result in predicted corresponding colors with negative tristimulus values for some changes in surround.

13

The RLAB Model

This chapter completes the discussion of some of the most widely used historical (pre-CIE models) color appearance models with a description of the RLAB model. While the Hunt and Nayatani *et al.* models discussed in the preceding chapters are designed to predict all of the perceptual attributes of color appearance for a wide range of viewing conditions, the RLAB model was designed with other considerations. RLAB was developed with the intent of producing a simple color appearance model capable of predicting the most significant appearance phenomena in practical applications. RLAB was developed with cross-media image reproduction as its target application and it has been effectively applied to such situations.

13.1 OBJECTIVES AND APPROACH

The RLAB color appearance model evolved from studies of chromatic adaptation (Fairchild 1990), chromatic adaptation modeling (Fairchild 1991a,b), fundamental CIE colorimetry (CIE 1986), and practical implications in cross-media image reproduction (Fairchild and Berns 1993, Fairchild 1994b). The starting point for RLAB is the CIELAB color space. While CIELAB can be used as an approximate color appearance model, it does have significant limitations. These include an inaccurate chromatic adaptation transform, no luminance-level dependency, no surround dependency, and no distinction for when discounting-the-illuminant occurs. While CIELAB has other limitations as a color appearance model, these are the most important for many practical applications. Thus, RLAB was designed to build on the positive aspects of CIELAB, and, by making additions, to address its limitations.

CIELAB provides good perceptual uniformity with respect to color appearance for average daylight illuminants. This is illustrated by the spacing of constant hue and chroma contours from the *Munsell Book of Color* shown in Figure 13.1. The contours plotted in Figure 13.1 are as good as, and in some

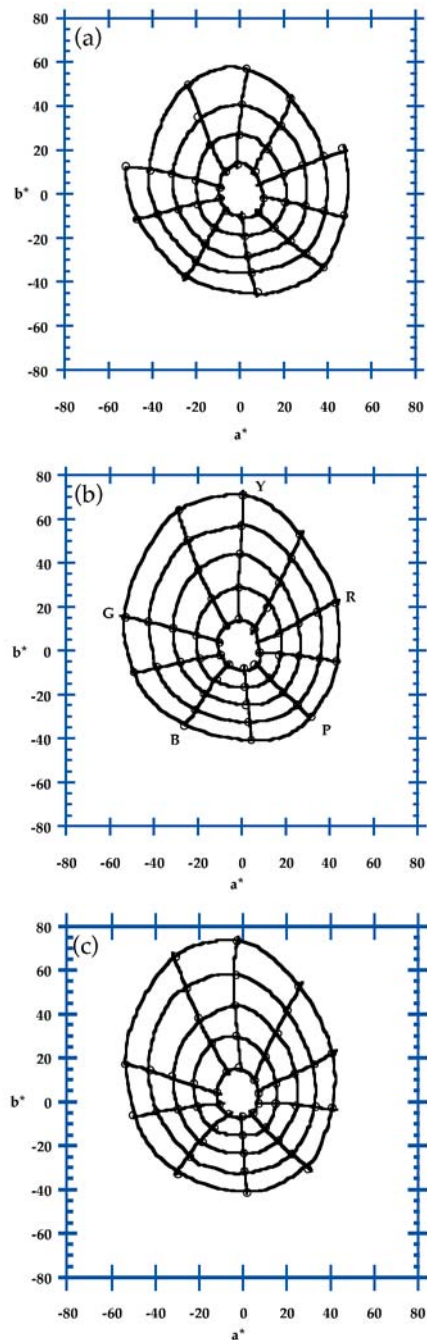


Figure 13.1 Contours of constant Munsell hue and chroma plotted in the CIELAB/RLAB color space at (a) value 3, (b) value 5, and (c) value 7

cases better, than those produced using any other color appearance model. However, due to CIELAB's 'wrong von Kries' chromatic adaptation transform, the good perceptual spacing of CIELAB quickly degrades as the illuminant moves away from average daylight. The concept of RLAB is to take advantage of the good spacing under daylight and familiarity of the CIELAB space while improving its applicability to non-daylight illuminants. This was accomplished by defining a reference set of viewing conditions (Illuminant D65, 318 cd/m², average surround, discounting the illuminant) for which the CIELAB space is used, and then using a more accurate chromatic adaptation transform (Fairchild 1991b, 1994b, 1996) to determine corresponding colors between the test viewing conditions and the reference viewing conditions. Thus, test tristimulus values are first transformed into corresponding colors under the reference viewing condition, and then a modified CIELAB space is used to describe appearance correlates.

In addition, the compressive nonlinearity (cube root) of the CIELAB space is adapted to become a function of the surround relative luminance. This allows the prediction of decreases in perceived image contrast as the surround becomes darker as suggested in the work of Bartleson (1975). The improved chromatic adaptation transform and the surround dependence enhance CIELAB in the two areas that are most critical in image reproduction.

RLAB was designed to include predictors of only relative color appearance attributes. Thus it can be used to calculate correlates of lightness, chroma, saturation, and hue, but it cannot be used to predict brightness or colorfulness. This limitation was imposed to keep the model as simple as possible and because the prediction of brightness and colorfulness have little importance in most image reproduction applications.

The fact that RLAB is based on the CIELAB space has benefit in addition to familiarity. Since the RLAB spacing is essentially identical to CIELAB spacing, color difference formulas such as CIELAB ΔE_{ab}^* (CIE 1986), CMC (Clarke *et al.* 1984), and CIE94 (CIE 1995b) can be used with results that are similar to those obtained when using CIELAB alone under average daylight illuminants.

A more detailed description of the RLAB model, as presented in this chapter, can be found in Fairchild (1996).

13.2 INPUT DATA

Input data for the RLAB model include the relative tristimulus values of the test stimulus (XYZ) and the white point ($X_nY_nZ_n$), the absolute luminance of a white object in the scene in cd/m², the relative luminance of the surround (dark, dim, average), and a decision on whether discounting-the-illuminant is taking place. The surround relative luminance is generally taken to be average for reflection prints, dim for CRT displays or televisions, and dark for projected transparencies under the assumption that these media are being

viewed in their typical environments. The surround is not directly tied to the medium. Thus it is certainly possible to have reflection prints viewed in a dark surround and projected transparencies viewed in an average surround. Discounting-the-illuminant is assumed to occur for object color stimuli such as prints and not to occur for emissive displays such as CRTs. Intermediate levels of discounting-the-illuminant are likely to occur in some situations such as the viewing of projected transparencies.

13.3 ADAPTATION MODEL

The following equations describe the chromatic adaptation model built into RLAB. It is based on the model of incomplete chromatic adaptation described by Fairchild (1991b) and later modified (Fairchild 1994b, 1996). This transformation is also discussed in Chapter 9. One begins with a conversion from CIE tristimulus values ($Y = 100$ for white) to fundamental tristimulus values as illustrated in Equations 13.1 and 13.2. All CIE tristimulus values are normally calculated using the CIE 1931 Standard Colorimetric Observer (2°). The transformation must also be completed for the tristimulus values of the adapting stimulus.

$$\begin{vmatrix} L \\ M \\ S \end{vmatrix} = \mathbf{M} \begin{vmatrix} X \\ Y \\ Z \end{vmatrix} \quad (13.1)$$

$$\mathbf{M} = \begin{vmatrix} 0.3897 & 0.6890 & -0.0787 \\ -0.2298 & 1.1834 & 0.0464 \\ 0.0 & 0.0 & 1.0000 \end{vmatrix} \quad (13.2)$$

The transformation to cone responses is the same as that used in the Hunt model. Matrix **M** is normalized such that the tristimulus values for the equal-energy illuminant ($X = Y = Z = 100$) produce equal cone responses ($L = M = S = 100$). The next step is calculation of the **A** matrix that is used to model the chromatic adaptation transformation.

$$\mathbf{A} = \begin{vmatrix} a_L & 0.0 & 0.0 \\ 0.0 & a_M & 0.0 \\ 0.0 & 0.0 & a_S \end{vmatrix} \quad (13.3)$$

The **A** matrix represents von Kries adaptation coefficients that are applied to the cone responses for the test stimulus (LMS). The von Kries-type coefficients are calculated using Equations 13.4–13.12.

$$a_L = \frac{p_L + D(1.0 - p_L)}{L_n} \quad (13.4)$$

$$a_M = \frac{p_M + D(1.0 - p_M)}{M_n} \quad (13.5)$$

$$a_S = \frac{p_S + D(1.0 - p_S)}{S_n} \quad (13.6)$$

The p terms describe the proportion of complete von Kries adaptation that is occurring. They are calculated using formulas that predict chromatic adaptation to be more complete as the luminance level increases and less complete as the color of the adapting stimulus departs from that of the equal energy illuminant. These terms are equivalent to the chromatic adaptation factors in the Hunt model and are calculated using the same equations given in Equations 13.7–13.12.

$$p_L = \frac{(1.0 + Y_n^{1/3} + \ell_E)}{(1.0 + Y_n^{1/3} + 1.0/\ell_E)} \quad (13.7)$$

$$p_M = \frac{(1.0 + Y_n^{1/3} + m_E)}{(1.0 + Y_n^{1/3} + 1.0/m_E)} \quad (13.8)$$

$$p_S = \frac{(1.0 + Y_n^{1/3} + s_E)}{(1.0 + Y_n^{1/3} + 1.0/s_E)} \quad (13.9)$$

$$\ell_E = \frac{3.0L_n}{L_n + M_n + S_n} \quad (13.10)$$

$$m_E = \frac{3.0M_n}{L_n + M_n + S_n} \quad (13.11)$$

$$s_E = \frac{3.0S_n}{L_n + M_n + S_n} \quad (13.12)$$

Y_n in Equations 13.7–13.9 is the absolute adapting luminance in cd/m^2 . The cone response terms with n subscripts (L_n, M_n, S_n) refer to values for the adapting stimulus derived from relative tristimulus values. The D factor in Equations 13.4–13.6 allows various proportions of cognitive discounting-the-illuminant. D should be set equal to 1.0 for hard-copy images, 0.0 for soft-copy displays, and an intermediate value for situations such as projected transparencies in completely darkened rooms. The exact value of the D factor can be used to account for the various levels of chromatic adaptation found in the infinite variety of practical viewing situations. The exact choice of intermediate values will depend upon the specific viewing conditions. Katoh (1994) has illustrated an example of intermediate adaptation in direct comparison between soft- and hard-copy displays and Fairchild

(1992a) has reported a case of intermediate discounting-the-illuminant for a soft-copy display. When no visual data are available and an intermediate value is necessary, a value of 0.5 should be chosen and refined with experience.

Note that if discounting-the-illuminant occurs and D is set equal to 1.0, then the adaptation coefficients described in Equations 13.4–13.6 reduce to the reciprocals of the adapting cone excitations exactly as would be implemented in a simple von Kries model.

After the \mathbf{A} matrix is calculated, the tristimulus values for a stimulus color are converted to corresponding tristimulus values under the reference viewing conditions using Equations 13.13 and 13.14.

$$\begin{vmatrix} X_{\text{ref}} \\ Y_{\text{ref}} \\ Z_{\text{ref}} \end{vmatrix} = \mathbf{RAM} \begin{vmatrix} X \\ Y \\ Z \end{vmatrix} \quad (13.13)$$

$$\mathbf{R} = \begin{vmatrix} 1.9569 & -1.1882 & 0.2313 \\ 0.3612 & 0.6388 & 0.0 \\ 0.0 & 0.0 & 1.0000 \end{vmatrix} \quad (13.14)$$

The \mathbf{R} matrix represents the inverse of the \mathbf{M} and \mathbf{A} matrices for the reference viewing conditions ($\mathbf{M}^{-1}\mathbf{A}^{-1}$) plus a normalization, discussed below, that are always constant and can therefore be precalculated. Thus Equation 13.13 represents a modified von Kries chromatic adaptation transform that converts test stimulus tristimulus values to corresponding colors under the RLAB reference viewing conditions (Illuminant D65, 318 cd/m², discounting-the-illuminant). The next step is to use these reference tristimulus values to calculate modified CIELAB appearance correlates as shown in the following sections.

13.4 OPPONENT COLOR DIMENSIONS

Opponent-type responses in RLAB are calculated using Equations 13.15–13.17.

$$L^R = 100(Y_{\text{ref}})^\sigma \quad (13.15)$$

$$a^R = 430[(X_{\text{ref}})^\sigma - (Y_{\text{ref}})^\sigma] \quad (13.16)$$

$$b^R = 170[(Y_{\text{ref}})^\sigma - (Z_{\text{ref}})^\sigma] \quad (13.17)$$

L^R represents an achromatic response analogous to CIELAB L^* . The red-green chromatic response is given by a^R (analogous to CIELAB a^*) and the yellow-blue chromatic response is given by b^R (analogous to CIELAB b^*).

Recall that, for the reference viewing conditions, the RLAB coordinates are nearly identical to CIELAB coordinates. They are not identical because Equations 13.15–13.17 have been simplified from the CIELAB equations for computational efficiency. The conditional compressive nonlinearities (i.e., different functions for low tristimulus values) of CIELAB have been replaced with simple power functions. This results in the exponents and the scaling factors being slightly different than the CIELAB equations. Fairchild (1996) provides more details on these differences. It is also worth noting that the divisions by the tristimulus values of the white point that are incorporated in the CIELAB equations are missing from Equations 13.15–13.17. This is because these normalizations are constant in the RLAB model and they have been built into the \mathbf{R} matrix given in Equation 13.14.

The exponents in Equations 13.15–13.17 vary, depending on the relative luminance of the surround. For an average surround $\sigma = 1/2.3$, for a dim surround $\sigma = 1/2.9$, and for a dark surround $\sigma = 1/3.5$. The ratios of these exponents are precisely in line with the contrast changes suggested by Bartleson (1975) and Hunt (1995) for image reproduction. More detail on the exponents can be found in Fairchild (1995b). As a nominal definition, a dark surround is considered essentially zero luminance, a dim surround is considered a relative luminance less than 20% of white in the image, and an average surround is considered a relative luminance equal to or greater than 20% of the image white. The precise nature and magnitude of the contrast changes required for various changes in image viewing conditions is still a topic of research and debate. Thus it is best to use these parameters with some flexibility. In some applications, it might be desired to use intermediate values for the exponents in order to model less severe changes in surround relative luminance. This requires no more than a substitution in the RLAB equations since they do not include the conditional functions that are found in the CIELAB equations. In addition, it might be desirable to use different exponents on the lightness L^R dimension than on the chromatic a^R and b^R dimensions. This can also be easily accommodated. The equations have been formulated as simple power functions to encourage the use of different exponents, which might be more appropriate than the nominal exponents for particular, practical viewing conditions.

Figure 13.2 illustrates the effect of changing the exponents. The left image (a) is a typical printed reproduction. The other two images (b and c) show the change in contrast necessary to reproduce the same appearance if the image were viewed in a dark surround. Note the increase in contrast required for viewing in a dark surround. In the middle image (b), the adjustment has been made on lightness contrast only. In the right image (c), the surround compensation has been applied to the chromatic dimensions, as well as to lightness. The right image (c) is similar to the reproduction that would be produced in a simple photographic system (since the contrast of all three film layers must be changed together) and is generally preferable. Note, however, that inter-image effects in real film could be used to compensate for some of the increase in saturation with contrast. The images in Figure 13.2

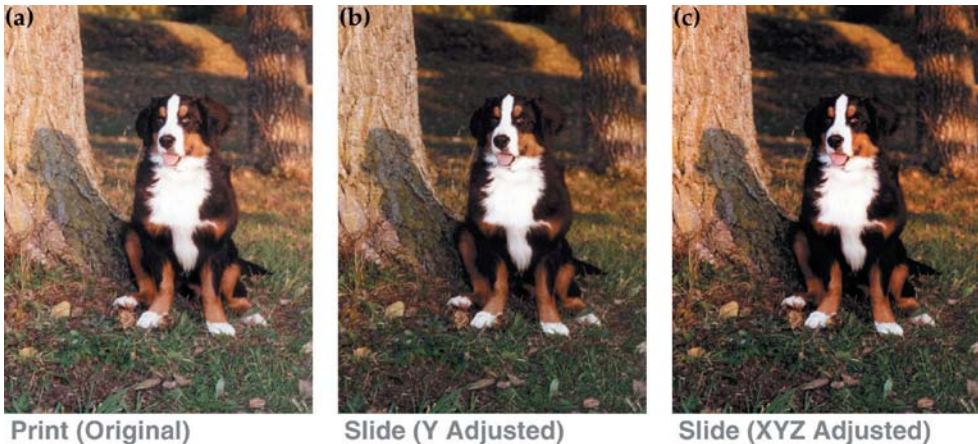


Figure 13.2 Images illustrating the change in image contrast necessary to account for appearance differences due to change in surround relative luminance. (a) Original print image. (b) Image for viewing in a dark surround, adjusted only in lightness contrast. (c) Image for viewing in a dark surround, adjusted in both lightness and chromatic contrast

should only be used to judge the relative impact of the adjustments since they are not being viewed in the appropriate viewing conditions.

13.5 LIGHTNESS

The RLAB correlate of lightness is L^R , given in Equation 13.15. No further calculations are required.

13.6 HUE

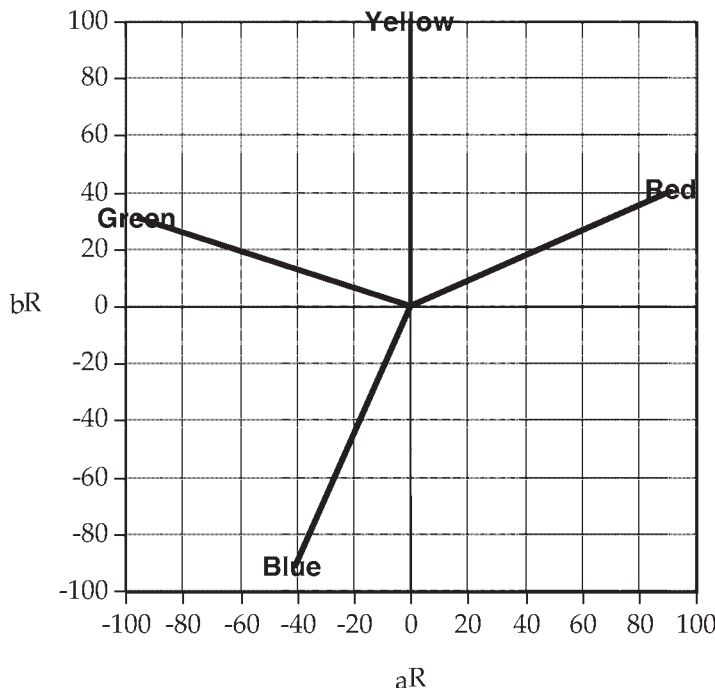
Hue angle h^R is calculated in the RLAB space using the same procedure as CIELAB. As in CIELAB, h^R is expressed in degrees, ranging from 0° to 360° measured from the positive a^R axis calculated according to Equation 13.18.

$$h^R = \tan^{-1}(b^R/a^R) \quad (13.18)$$

Hue composition can be determined in RLAB using a procedure similar to that of the Hunt model and Nayatani *et al.* model. This is useful when testing a color appearance model against magnitude estimation data and when it is desired to reproduce a named hue. Hue composition H^R can be calculated via linear interpolation of the values in Table 13.1. These were derived based on the notation of the Swedish Natural Color System (NCS) and are illus-

Table 13.1 Data for conversion from hue angle to hue composition

h^R	R	B	G	Y	H^R
24	100	0	0	0	R
90	0	0	0	100	Y
162	0	0	100	0	G
180	0	21.4	78.6	0	<i>B79G</i>
246	0	100	0	0	B
270	17.4	82.6	0	0	<i>R83B</i>
0	82.6	17.4	0	0	<i>R17B</i>
24	100	0	0	0	R

**Figure 13.3** Illustration of the hue angles of the perceptually unique hues in the RLAB color space

trated in Figure 13.3, which is a useful visualization of the loci of the unique hues since they do not correspond to the principal axes of the color space. The unique hue locations are the same as those in the CIELAB space under only the reference conditions. Example hue composition values are listed in Table 13.1 in italics.

13.7 CHROMA

RLAB chroma C^R is calculated in the same way as CIELAB chroma, as shown in Equation 13.19.

$$C^R = \sqrt{(a^R)^2 + (b^R)^2} \quad (13.19)$$

13.8 SATURATION

In some applications, such as the image color manipulation required for gamut mapping, it might be desirable to change colors along lines of constant saturation rather than constant chroma. Wolski, Allebach, and Bouman (1994) have proposed such a technique and Montag and Fairchild (1996, 1997) also describe such situations. *Saturation* is defined as colorfulness relative to brightness, *chroma* is defined as colorfulness relative to the brightness of a white, and *lightness* is defined as brightness relative to the brightness of a white. Therefore, saturation can be defined as chroma relative to lightness. Chroma C^R and lightness L^R are already defined in RLAB; thus saturation s^R is defined as shown in Equation 13.20.

$$s^R = C^R/L^R \quad (13.20)$$

It is of interest to note that a progression along a line of constant saturation is the series of colors that can be observed when an object is viewed in ever deepening shadows. This could be why transformations along lines of constant saturation, rather than chroma, are sometimes useful in gamut mapping applications.

13.9 INVERSE MODEL

Since the RLAB model was designed with image reproduction applications in mind, computational efficiency and simple inversion were considered of significant importance. Thus the RLAB model is very easy to invert and requires a minimum of calculations. A step-by-step procedure for implementing the RLAB model is given below.

Step 1. Obtain the colorimetric data for the test and adapting stimuli and the absolute luminance of the adapting stimulus. Decide on the discounting-the-illuminant factor and the exponent (based on surround relative luminance).

Step 2. Calculate the chromatic adaptation matrix **A**.

Step 3. Calculate the reference tristimulus values.

Step 4. Calculate the RLAB parameters L^R , a^R , and b^R .

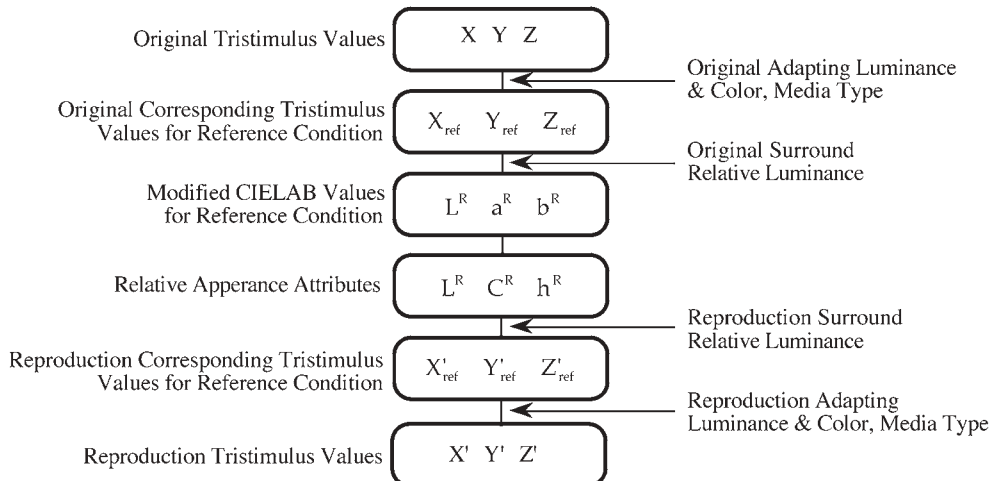


Figure 13.4 A flow chart of the application of the RLAB model to image reproduction applications

Step 5. Use a^R and b^R to calculate C^R and h^R .

Step 6. Use h^R to determine H^R .

Step 7. Calculate s^R using C^R and L^R .

In typical color reproduction applications, it is not enough to know the appearance of image elements; it is necessary to reproduce those appearances in a second set of viewing conditions as illustrated in Figure 13.4. To accomplish this, one must be able to calculate CIE tristimulus values, XYZ , from the appearance parameters $L^R a^R b^R$ and the definition of the new viewing conditions. These tristimulus values are then used, along with the imaging-device characterization, to determine device color signals such as RGB or CMYK. The following equations outline how to calculate CIE tristimulus values from RLAB $L^R a^R b^R$. If starting with $L^R C^R h^R$, one must first transform back to $L^R a^R b^R$ using the usual transformation from cylindrical to rectangular coordinates.

The reference tristimulus values are calculated from the RLAB parameters using Equations 13.21–13.23 with an exponent, σ , appropriate for the second viewing condition.

$$Y_{\text{ref}} = \left(\frac{L^R}{100} \right)^{1/\sigma} \quad (13.21)$$

$$X_{\text{ref}} = \left[\left(\frac{a^R}{430} \right) + (Y_{\text{ref}})^{\sigma} \right]^{1/\sigma} \quad (13.22)$$

$$Z_{\text{ref}} = \left[(Y_{\text{ref}})^{\sigma} - \left(\frac{b^R}{170} \right) \right]^{1/\sigma} \quad (13.23)$$

The reference tristimulus values are then transformed to tristimulus values for the second viewing condition using Equation 13.24 with an **A** matrix calculated for the second viewing conditions.

$$\begin{vmatrix} X \\ Y \\ Z \end{vmatrix} = (\mathbf{RAM})^{-1} \begin{vmatrix} X_{\text{ref}} \\ Y_{\text{ref}} \\ Z_{\text{ref}} \end{vmatrix} \quad (13.24)$$

13.10 PHENOMENA PREDICTED

The RLAB model provides correlates for relative color appearance attributes only (lightness, chroma, saturation, and hue). It cannot be used to predict brightness and colorfulness. This limitation is of little practical importance for image reproduction since there are few applications in which brightness and colorfulness are required. RLAB includes a chromatic adaptation transform with a parameter for discounting-the-illuminant, and predicts incomplete chromatic adaptation to certain stimuli (e.g., RLAB correctly predicts that a CRT display with a D50 white point will retain a yellowish appearance). It also includes variable exponents, σ , that modulate image contrast as a function of the surround relative luminance. These are the most important color appearance phenomena for cross-media image reproduction applications. If it is necessary to predict absolute appearance attributes (i.e., brightness and colorfulness) or more unusual appearance phenomena, then more extensive appearance models such as the Nayatani *et al.* and Hunt models described in preceding chapters should be considered.

Example calculations for the RLAB color appearance model are given in Table 13.2.

13.11 WHY NOT USE JUST THE RLAB MODEL?

The RLAB model is simple, straightforward, easily invertible, and has been found to be as accurate as, or better than, more complicated color appearance models for many practical applications. Given all of these features, why wouldn't RLAB be considered as a recommendation for a single, universal color appearance model?

RLAB's weaknesses are the same as its strengths. Since it is such a simple model, it is not exhaustive in its prediction of color appearance phenomena. It does not include correlates of brightness and colorfulness. It cannot be applied over a wide range of luminance levels. It does not predict some color

Table 13.2 Example RLAB color appearance model calculations

Quantity	Case 1	Case 2	Case 3	Case 4
X	19.01	57.06	3.53	19.01
Y	20.00	43.06	6.56	20.00
Z	21.78	31.96	2.14	21.78
X _n	95.05	95.05	109.85	109.85
Y _n	100.00	100.00	100.00	100.00
Z _n	108.88	108.88	35.58	35.58
Y _n (cd/m ²)	318.31	31.83	318.31	31.83
σ	0.43	0.43	0.43	0.43
D	1.0	1.0	1.0	1.0
L ^R	49.67	69.33	30.78	49.83
a ^R	0.00	46.33	-40.96	15.57
b ^R	-0.01	18.09	2.25	-52.61
h ^R	270.0	21.3	176.9	286.5
H ^R	R83B	R2B	B74G	R71B
C ^R	0.01	49.74	41.02	54.87
s ^R	0.00	0.72	1.33	1.10

appearance phenomena such as the Hunt effect, the Stevens effect (although these could be simulated by making s change with adapting luminance rather than surround relative luminance), and the Helson–Judd effect. In practical imaging applications, these limitations are of little consequence due to device gamut limitations. In other applications, where these phenomena might be important, a different color appearance model is required. In summary, RLAB performs well for the image reproduction applications for which it was designed, but is not comprehensive enough for all color appearance situations that might be encountered.

14

Other Models

The preceding chapters have reviewed four of the most widely used and general color appearance models representing the evolution toward the CIECAM models presented in the following chapters. These and other models are continually being modified and introduced. This chapter provides overviews of two more color appearance models — one that has been evolving for many years and a second that is relatively new. For various reasons discussed herein, these models are not as well suited for general application as those described in earlier chapters or the more refined CIECAM models. However, various aspects of their formulation are of interest both historically and for development of future models or applications. Thus they have been included to appropriately cover their potential impact on the field.

14.1 OVERVIEW

The formulation of color appearance models remains an area of active, ongoing research. That explains why this book can only provide an overview of the associated problems and several approaches to solving them. It is not possible to present a single model of color appearance that will solve all problems if followed in a ‘cookbook’ manner. This is the ‘Holy Grail’ for researchers in the field, but not likely to be achieved in short order. Chapters 10–13 presented some of the best historically available approaches to problems of color appearance specification and reproduction. Chapters 15 and 16 present more recent CIE color appearance models, CIECAM97s and CIECAM02. One of those models is likely to be the most appropriate solution for any given application. However, one model is not likely to be the best solution for all applications. Since the development of color appearance models is an ongoing endeavor, it is important to describe other models that have had, or are likely to have, significant impact on the field.

Two such models are described in this chapter:

1. The ATD model formulated by Guth (1995), which has a history of development dating back over 20 years (Guth 1994a).
2. A more recent model derived by Luo *et al.* (1996) known as LLAB.

A third model was under development by CIE Technical Committee 1-34 as an attempt to promote uniformity of practice in color appearance specification for industry when the first edition of this book was published. The then current status of this CIE color appearance model was described in an appendix. In the intervening years that model, CIECAM97s, was published and widely used and revised. It is discussed in Chapter 15. The results of further research on CIECAM97s (within CIE TC8-01) resulted in further improvements being adopted by the CIE in the CIECAM02 model, described in Chapter 16.

14.2 ATD MODEL

The ATD model, developed by Guth, is a different type of model from those described in earlier (and later) chapters. In fact, according to the CIE TC1-34 definition of what makes a color appearance model, it cannot be considered a color appearance model. This is because the model was developed with different aims. It is described as a model of color vision, or more appropriately the first few stages of color vision.

Guth (1994a,b) has given a good overview of the development and performance of the model. The model's history dates back as far as 1972. The ATD model was developed to predict a wide range of vision science data on phenomena such as chromatic discrimination, absolute thresholds, the Bezold-Brücke hue shift, the Abney effect, heterochromatic brightness matching, light adaptation, and chromatic adaptation. The ATD model is capable of making remarkable predictions of vision data for these phenomena. However, most such experiments have been performed using unrelated stimuli. Thus the model is designed for unrelated stimuli and only by somewhat arbitrary modification of the model can it be applied to related colors. This background explains why the model incorporates measures of color discrimination, brightness, saturation, and hue, but does not distinguish other important appearance attributes such as lightness, colorfulness, and chroma. This limits the model's applicability somewhat, but its general structure and chromatic adaptation transformation are certainly worthy of further study and attention.

The ATD model has been modified and used in practical imaging applications. Such applications have been described by Granger (1994, 1995). Granger took advantage of the opponent colors encoding of the ATD model to develop a space that is useful for describing color appearance and doing color manipulations in desktop publishing. However, Granger did not incorporate any chromatic adaptation transformation in his modified ATD model; thus the utility of the model is limited to a single illumination white point

unless a user is willing to make the erroneous assumption that printed color images represent color-constant stimuli.

Objectives and Approach

As stated above, the ATD model has a long history of development aimed at the prediction of various color vision data. Guth (1995) refers to it as a 'model for color perception and visual adaptation,' and that is certainly an appropriate description. Regarding what the model is intended for, Guth (1995) states that it 'should now be seriously considered by the vision community as a replacement for all models that are currently used to make predictions (or to establish standards) that concern human color perception.' This is an ambitious goal that clearly overlaps the objectives of some of the other models described in this book. As discussed below it is also an extreme overstatement of the capabilities of the model.

One of the latest revisions of the ATD model referred to as ATD95 is described in the following sections. The treatment in Guth (1995) has been followed. Earlier papers such as Guth (1991) should also be referred to in order to obtain a more global understanding of the model's derivation and capabilities. Interested readers are encouraged to look for more recent literature on modifications of the model.

The model begins with nonlinear cone responses followed by a nonlinear von Kries-type receptor gain control and two stages of opponent responses necessary for the prediction of various discrimination and appearance phenomena. Finally the model includes a neural compression of the opponent signals. The letters *A*, *T*, and *D* are abbreviations for achromatic, tritanopic, and deuteranopic mechanisms. The *A* system signals brightness, the *T* system redness–greenness, and the *D* system yellowness–blueness.

Input Data

The input data for the ATD model operating on unrelated colors are the $X'Y'Z'$ tristimulus values (Judd's modified tristimulus values, not CIE XYZ tristimulus values) expressed in absolute luminance units. The $X'Y'Z'$ tristimulus values are scaled such that Y' is set equal to Y (photopic luminance) expressed in trolands. Trolands are a measure of retinal illuminance that factors in the eye's pupil diameter. Since the pupil diameter is controlled by the scene luminance (to some degree), Guth (1995) suggests converting from luminance in cd/m^2 to retinal illuminance in trolands by raising the luminance to the power of 0.8 and multiplying by 18 as a reasonable approximation. Strictly, the ATD model is incompatible with CIE colorimetry since it is based on Judd-modified $X'Y'Z'$ tristimulus values rather than CIE XYZ tristimulus values. However, Guth (1995) states that 'it is probably true that XYZ s rather than $X'Y'Z$'s can be used in most situations.' For the remainder

of this chapter, it will be assumed that CIE XYZ tristimulus values are used.

For predictions involving related colors, the absolute tristimulus values expressed in trolands must also be available for the adapting stimulus, $X_0Y_0Z_0$. Guth (1995) is equivocal on how to obtain these values, so it will be assumed that they are the tristimulus values for a perfect white under illumination similar to the test stimulus.

No other input data are required, or used, in the ATD model. Thus it is clear that it cannot be used to account for background, surround, or cognitive effects.

Adaptation Model

As with all of the models presented in this book, the first step of the ATD model is a transformation from CIE (or Judd) tristimulus values to cone responses. However, a significant difference in the ATD model is that the cone responses are nonlinear and additive noise signals are incorporated at this stage. The transformations are given in Equations 14.1–14.3.

$$L = [0.66(0.2435X + 0.8524Y - 0.0516Z)]^{0.70} + 0.024 \quad (14.1)$$

$$M = [1.0(-0.3954X + 1.1642Y + 0.0837Z)]^{0.70} + 0.036 \quad (14.2)$$

$$S = [0.43(0.04Y + 0.6225Z)]^{0.70} + 0.31 \quad (14.3)$$

Chromatic adaptation is then modeled using a modified form of the von Kries transformation as illustrated in Equations 14.4–14.6.

$$L_g = L[\sigma/(\sigma + L_a)] \quad (14.4)$$

$$M_g = M[\sigma/(\sigma + M_a)] \quad (14.5)$$

$$S_g = S[\sigma/(\sigma + S_a)] \quad (14.6)$$

L_g , M_g , and S_g are the post-adaptation cone signals. The constant σ is varied to predict different types of data, but is nominally set equal to 300. The cone signals for the adapting light L_a , M_a , and S_a are determined from a weighted sum of the tristimulus values for the stimulus itself and for a perfect white (or other adapting stimulus), as shown in Equations 14.7–14.9, which are then transformed to cone signals using Equations 14.1–14.3.

$$X_a = k_1X + k_2X_0 \quad (14.7)$$

$$Y_a = k_1Y + k_2Y_0 \quad (14.8)$$

$$Z_a = k_1Z + k_2Z_0 \quad (14.9)$$

For unrelated colors, there is only self-adaptation and k_1 is set to 1.0 while k_2 is set to 0.0. For related colors such as typical colorimetric applications, k_1 is set to 0.0 and k_2 is set to a value between 15 and 50 (Guth 1995). In some cases, the observer might adapt to both the test stimulus and the white point to some degree, and some other combination of values, such as $k_1 = 1.0$ and $k_2 = 5.0$, would be used (Guth 1995). Guth (1995) makes no specific recommendation on how to calculate cone signals for the adapting light. It is left open for interpretation. However, it is worth noting that as the value of k_2 increases, the adaptation transform of Equations 14.4–14.6 becomes more and more like the nominal von Kries transformation. This is also true as s is decreased. Thus it is not difficult to make the ATD model perform almost the same as a simple von Kries model for color reproduction applications. It is therefore recommended that Guth's maximum value of k_2 equal to 50 be used with k_1 set to 0.0.

Opponent Color Dimensions

The adapted cone signals are then transformed into two sets of initial opponent signals. The first stage initial signals are denoted A_{1i} , T_{1i} , and D_{1i} and calculated according to Equations 14.10–14.12. The second stage initial signals, calculated using Equations 14.13–14.15 are denoted A_{2i} , T_{2i} , and D_{2i} .

$$A_{1i} = 3.57L_g + 2.64M_g \quad (14.10)$$

$$T_{1i} = 7.18L_g - 6.21M_g \quad (14.11)$$

$$D_{1i} = -0.70L_g + 0.085M_g + 1.00S_g \quad (14.12)$$

$$A_{2i} = 0.09A_{1i} \quad (14.13)$$

$$T_{2i} = 0.43T_{1i} + 0.76D_{1i} \quad (14.14)$$

$$D_{2i} = D_{1i} \quad (14.15)$$

The final ATD responses after compression are calculated for both the first and second stages according to Equations 14.16–14.21.

$$A_1 = A_{1i}/(200 + |A_{1i}|) \quad (14.16)$$

$$T_1 = T_{1i}/(200 + |T_{1i}|) \quad (14.17)$$

$$D_1 = D_{1i}/(200 + |D_{1i}|) \quad (14.18)$$

$$A_2 = A_{2i}/(200 + |A_{2i}|) \quad (14.19)$$

$$T_2 = T_{2i}/(200 + |T_{2i}|) \quad (14.20)$$

$$D_2 = D_{2i}/(200 + |D_{2i}|) \quad (14.21)$$

The first-stage opponent responses are used to model apparent brightness and discriminations (absolute and difference thresholds). Discriminations are modeled using Euclidean distance in the $A_1T_1D_1$ three-dimensional space with a visual threshold set to approximately 0.005 units. The second-stage mechanisms are used to model large color differences, hue, and saturation.

Perceptual Correlates

The ATD model incorporates measures to predict brightness, saturation, and hue. The brightness correlate is the quadrature summation of the A_1 , T_1 , and D_1 responses as illustrated in Equation 14.22.

$$A_1 = A_{1i}/(200 + |A_{1i}|) \quad (14.22)$$

Saturation is calculated as the quadrature sum of the second-stage chromatic responses T_2 and D_2 , divided by the achromatic response A_2 , as shown in Equation 14.23.

$$A_1 = A_{1i}/(200 + |A_{1i}|) \quad (14.23)$$

Guth (1995) incorrectly uses the terms saturation and chroma interchangeably. However, it is clear that the formulation of Equation 14.23 is a measure of saturation rather than chroma since it is measured relative to the achromatic response for the stimulus rather than that of a similarly illuminated white.

Guth (1995) indicates that hue is directly related to H as defined in Equation 14.24. However, the ratio in Equation 14.24 is equivocal (giving equal values for complementary hues, infinite values for some, and undefined values for others) and it is therefore necessary to add an inverse tangent function as is typical practice.

$$H = T_2/D_2 \quad (14.24)$$

There are no correlates of lightness, colorfulness, chroma, or hue composition in the ATD model.

Phenomena Predicted

The ATD model accounts for chromatic adaptation, heterochromatic brightness matching (Helmholtz–Kohlrausch effect), the Bezold–Brücke hue shift,

Table 14.1 Example ATD color vision model calculations

Quantity	Case 1	Case 2	Case 3	Case 4
X	19.01	57.06	3.53	19.01
Y	20.00	43.06	6.56	20.00
Z	21.78	31.96	2.14	21.78
X_0	95.05	95.05	109.85	109.85
Y_0	100.00	100.00	100.00	100.00
Z_0	108.88	108.88	35.58	35.58
$Y_0(\text{cd/m}^2)$	318.31	31.83	318.31	31.83
σ	300	300	300	300
k_1	0.0	0.0	0.0	0.0
k_2	50.0	50.0	50.0	50.0
A_1	0.1788	0.2031	0.1068	0.1460
T_1	0.0287	0.0680	-0.0110	0.0007
D_1	0.0108	0.0005	0.0044	0.0130
A_2	0.0192	0.0224	0.0106	0.0152
T_2	0.0205	0.0308	-0.0014	0.0102
D_2	0.0108	0.0005	0.0044	0.0130
B_r	0.1814	0.2142	0.1075	0.1466
C	1.206	1.371	0.436	1.091
H	1.91	63.96	-0.31	0.79

the Abney effect, and various color discrimination experiments. It includes correlates for brightness and saturation. A correlate for hue can also be easily calculated although hue composition has not been specifically defined. The model is also inadequately defined for related stimuli since it does not include correlates for lightness and chroma. There is no way to distinguish between brightness–colorfulness matching and lightness–chroma matching using the ATD model. It is unclear which type of matching is predicted by the adaptation transform, but it is likely to be more similar to brightness–colorfulness matching due to the way absolute units are used in the ATD model. The ATD model cannot be used (without modification) to predict background or surround effects or effects based on medium changes, such as discounting the illuminant. Examples of calculated values using the ATD model as described in this chapter are given in Table 14.1.

Why Not Use Just the ATD Model?

The ATD model provides a simple, elegant framework for the early stages of signal processing in the human color vision system. While the framework is clearly sound given the wide range of data the model can be used to predict, it is not well defined for particular applications. There are several aspects of

the model that require further definition or specification for practical application. Thus, the flexibility of the ATD model that allows it to predict a wide range of data also precludes it from being practically useful. The model can be applied to practical applications with some modification as has been done by Granger (1994, 1995). However, even this formulation is incomplete as a color appearance model since it neglects chromatic adaptation.

The ATD model has the advantages that it is fairly simply and generally easily invertible (for $k_1 = 0.0$). Its disadvantages include the lack of a strict definition of its implementation, inadequate treatment of related colors (necessary for most applications), and lack of cognitive factors. Strictly speaking, the ATD model is also not directly relatable to CIE tristimulus values. Since it does not incorporate distinct predictors for lightness and chroma, it actually cannot be considered a color appearance model. However, as a framework for visual processing and discrimination, it certainly warrants some attention.

14.3 LLAB MODEL

The LLAB model is a more recent entry into the field of color appearance models. It is similar in structure to the RLAB model described in Chapter 13. However, the LLAB model does incorporate a different range of effects than the RLAB model. The LLAB color appearance model was developed by Luo, Lo and Kuo (1996). However, prior to their publication, the LLAB model was revised by Luo and Morovic (1996) in a conference proceedings. The treatment in this chapter follows the revised model, but includes some comments on the original formulation presented in Luo, Lo, and Kuo (1996). LLAB is designed as a colorimetric model and is clearly an extension of CIE colorimetry (as opposed to a vision model). It was synthesized from the results of a series of experiments on color appearance and color difference scaling.

The LLAB model is designed to be a universal model for color matching, color appearance specification, and color difference measurement. It therefore incorporates features from previous work in both areas of study. Like RLAB, it is designed to be relatively simple and not inclusive of all visual phenomena. It is not as simple as the RLAB model. It does, however, predict some effects that RLAB cannot (the converse is also true).

Objectives and Approach

The LLAB model, as described by Luo *et al.* (1996), is derived from an extensive series of data derived by Luo and his co-workers on color appearance scaling and color discrimination. This work has resulted in tests of color appearance models and the development of color difference equations as summarized by Luo *et al.* (1996). The LLAB model is an attempt to synthesize this work into a single coherent model.

The formulation of the LLAB model is similar to RLAB in concept, but differs markedly in detail. It begins with a chromatic adaptation transform known as the BFD transform (developed at Bradford University and previously unpublished) from the test viewing conditions to defined reference conditions. Then, modified CIELAB coordinates are calculated under the reference conditions and appearance correlates are specified. The surround relative luminance is accounted for using variable exponents as in RLAB. The colorfulness scale is adjusted based on the nonlinear chroma functions incorporated into the CMC color difference equation (Clarke *et al.* 1984). LLAB also incorporates a factor for lightness contrast due to the relative luminance of the background. Hue angle is defined the same way as in CIELAB and hue composition is specified according to techniques similar to those used by Nayatani *et al.*, Hunt, and RLAB. Lastly, lightness and chroma weighting factors can be applied for the calculation of color differences in a manner identical to that used in the CMC and CIE94 color difference equations. Thus the full designation of the model is LLAB(l:c).

Input Data

The LLAB model requires the relative tristimulus values of the stimulus XYZ , the reference white $X_0Y_0Z_0$, the luminance (in cd/m^2) of the reference white L , and the luminance factor of the background Y_b . It also requires choices regarding the discounting-the-illuminant factor D , the surround induction factor F_S , the lightness induction factor F_L , and the chroma induction factor F_C . Values for specified viewing conditions are given in Table 14.2.

Adaptation Model

In the LLAB model, the BFD adaptation transform is used to calculate corresponding colors under a reference viewing condition. The BFD transform is a modified von Kries transform in which the short-wavelength-sensitive cone signals are subjected to an adaptation-dependent nonlinearity, while the

Table 14.2 Values of induction factors for the LLAB model

	D	F_S	F_L	F_C
Reflection samples and images in average surround				
Subtending $> 4^\circ$	1.0	3.0	0.0	1.00
Subtending $< 4^\circ$	1.0	3.0	1.0	1.00
Television and VDU displays in dim surround	0.7	3.5	1.0	1.00
Cut-sheet transparency in dim surround	1.0	5.0	1.0	1.10
35 mm projection transparency in dark surround	0.7	4.0	1.0	1.00

middle- and long-wavelength-sensitive cone signals are subject to a simple von Kries transform. The first step is a transform from CIE XYZ tristimulus values to normalized cone responses, denoted *RGB*, as shown in Equations 14.25 and 14.26.

$$\begin{vmatrix} R \\ G \\ B \end{vmatrix} = \mathbf{M} \begin{vmatrix} X/Y \\ Y/Y \\ Z/Y \end{vmatrix} \quad (14.25)$$

$$\mathbf{M} = \begin{vmatrix} 0.8951 & 0.2664 & -0.1614 \\ -0.7502 & 1.7135 & 0.0367 \\ 0.0389 & -0.0685 & 1.0296 \end{vmatrix} \quad (14.26)$$

It should be noted that the transform in Equations 14.25 and 14.26 is atypical in two ways. First, the CIE tristimulus values are always normalized to *Y* prior to the transform. This results in all stimuli with identical chromaticity coordinates having the same cone signals (a luminance normalization). This normalization is required to preserve achromatic scales through the nonlinear chromatic adaptation transform described below. Second, the transform itself does not represent plausible cone responses, but rather ‘spectrally sharpened’ cone responses with negative responsivity at some wavelengths. These responsivities tend to preserve saturation across changes in adaptation and impact predicted hue changes across adaptation. Despite the fact that the BFD transformation results in *RGB* signals that cannot be considered physiologically plausible cone responses, they will be referred to as cone responses for simplicity. The cone responses are then transformed to the corresponding cone responses for adaptation to the reference illuminant. The reference illuminant is defined to be CIE illuminant D65 using the 1931 standard colorimetric observer ($X_{0r} = 95.05$, $Y_{0r} = 100.0$, $Z_{0r} = 108.88$). The transformation is performed using Equations 14.27–14.30.

$$R_r = [D(R_{0r}/R_0) + 1 - D]R \quad (14.27)$$

$$G_r = [D(G_{0r}/G_0) + 1 - D]G \quad (14.28)$$

$$B_r = [D(B_{0r}/B_0^\beta) + 1 - D]B^\beta \quad (14.29)$$

$$\beta = (B_0/B_{0r})^{0.0834} \quad (14.30)$$

In the event that the *B* response is negative, Equations 14.29 is replaced with Equations 14.31 to avoid taking a root of a negative number.

$$B_r = -[D(B_{0r}/B_0^\beta) + 1 - D]|B|^\beta \quad (14.31)$$

The *D* factors in Equations 14.27–14.31 allow for discounting the illuminant. When discounting occurs, *D* = 1.0 and observers completely adapt to the

color of the light source. If there is no adaptation, $D = 0.0$ and observers are always adapted to the reference illuminant. For intermediate values of D , observers are adapted to chromaticities intermediate to the light source and the reference illuminant (with D specifying the proportional level of adaption to the source). This is different from the D value in RLAB, which allows for various levels of incomplete adaptation that depend on the color and luminance of the source. ($D = 0.0$ in RLAB does not mean no adaptation, rather it means incomplete adaptation to that particular source.)

The final step of the chromatic adaptation transformation is the conversion from the cone signals for the reference viewing condition to CIE tristimulus values $X_r Y_r Z_r$ using Equation 14.32.

$$\begin{vmatrix} X_r \\ Y_r \\ Z_r \end{vmatrix} = \mathbf{M}^{-1} \begin{vmatrix} R_r Y \\ G_r Y \\ B_r Y \end{vmatrix} \quad (14.32)$$

Opponent Color Dimensions

The corresponding tristimulus values under the reference illuminant (D65) are then transformed to preliminary opponent dimensions using modified CIELAB formulae as illustrated in Equations 14.33–14.36.

$$L_L = 116f(Y_r/100)^z - 16 \quad (14.33)$$

$$z = 1 + F_L(Y_b/100)^{1/2} \quad (14.34)$$

$$A = 500[f(X_r/95.05) - f(Y_r/100)] \quad (14.35)$$

$$B = 200[f(Y_r/100) - f(Z_r/108.88)] \quad (14.36)$$

The z exponent is incorporated to account for lightness contrast from the background. It is similar to the form used in the Hunt model. Since the L_L , A , and B dimensions follow the definitions of the CIELAB equations, the non-linearity is dependent on the relative tristimulus values as shown in Equations 14.37 and 14.38. For values of $\omega > 0.008856$, Equation 14.37 is used.

$$f(\omega) = (\omega)^{1/F_s} \quad (14.37)$$

For values of $\omega \leq 0.008856$, Equations 14.38 is used.

$$f(\omega) = [(0.008856^{1/F_s} - 16/116)/0.008856]\omega + 16/116 \quad (14.38)$$

The value of F_s depends on the surround relative luminance as specified in Table 14.2. This is the similar to the surround dependency incorporated in the RLAB model.

Perceptual Correlates

The LLAB model includes predictors for lightness, chroma, colorfulness, saturation, hue angle, and hue composition. The lightness predictor L_L is defined in Equation 14.33. The chroma predictor Ch_L , and colorfulness predictor C_L , are derived using a nonlinear function similar to that incorporated in the CMC color difference equation as a chroma weighting function. This incorporates the behavior of the CMC color difference equation into the LLAB color space as shown in Equations 14.39–14.43.

$$C = (A^2 + B^2)^{1/2} \quad (14.39)$$

$$Ch_L = 25 \ln(1 + 0.05C) \quad (14.40)$$

$$C_L = Ch_L S_M S_C F_C \quad (14.41)$$

$$S_C = 1.0 + 0.47 \log(L) - 0.057[\log(L)]^2 \quad (14.42)$$

$$S_M = 0.7 + 0.02L_L - 0.0002L_L^2 \quad (14.43)$$

F_C is the chroma induction factor defined in Table 14.2. SC provides the luminance dependency necessary to predict an increase in colorfulness with luminance. Thus C_L is truly a colorfulness predictor. S_M provides a similar lightness dependency.

Saturation is defined in LLAB as the ratio of chroma to lightness as shown in Equation 14.44.

$$S_L = Ch_L / L_L \quad (14.44)$$

LLAB hue angle h_L , is calculated in the usual way according to Equation 14.45.

$$h_L = \tan^{-1}(B/A) \quad (14.45)$$

Hue composition in NCS notation is calculated via linear interpolation between the hue angles for the unique hues, which are defined as 25° (red), 93° (yellow), 165° (green), and 254° (blue).

The final opponent signals are calculated using the colorfulness scale C_L , and the hue angle h_L , as shown in Equations 14.46 and 14.47.

$$A_L = C_L \cos(h_L) \quad (14.46)$$

$$B_L = C_L \sin(h_L) \quad (14.47)$$

There were no predictors of brightness, chroma, or saturation defined in the LLAB model as initially published by Luo, Lo and Kuo (1996). In the

revised version (Luo and Morovic 1996), the predictors of chroma and saturation were added.

Color Differences

The LLAB model incorporates the chroma weighting function from the CMC color difference equation. This chroma dependency is the most important factor that produces the improved performance of the CMC color difference equation over the simple CIELAB ΔE_{ab}^* equation. Thus LLAB($l:c$) color differences are defined by Equation 14.48.

$$\Delta E_L = [(\Delta L_L/l)^2 + \Delta A_L^2 + \Delta B_L^2]^{1/2} \quad (14.48)$$

The lightness weight l is defined to be 1.0, 1.5, and 0.67 for perceptibility, acceptability, and large color differences, respectively. The chroma weight c (not present in this formulation) is always set equal to 1.0.

Phenomena Predicted

The revised LLAB model accounts for chromatic adaptation, lightness induction, surround relative luminance, discounting-the-illuminant, and the Hunt effect. It cannot predict the Stevens effect, incomplete chromatic adaptation, or the Helmholtz–Kohlrausch effect. It also cannot predict the Helson–Judd effect.

LLAB includes predictors for lightness, chroma, saturation, colorfulness, and hue in its latest revision (Luo and Morovic 1996). This corrected the unnatural combination of appearance attributes (lightness, colorfulness, hue) in the original version (Luo, Lo, and Kuo 1996). The natural sets are lightness, chroma, and hue or brightness, colorfulness, and hue. The original LLAB formulation could not be used to calculate either brightness–colorfulness matches or lightness–chroma matches. It could be used to predict lightness–colorfulness matches, which probably have little practical utility. If corresponding colors are predicted at constant luminance, then the lightness–colorfulness matches become equivalent to lightness–chroma matches. Interestingly, the original LLAB formulation did not meet the CIE TC1-34 requirements of a color appearance model that it include predictors of at least lightness, chroma, and hue. These limitations were corrected in the Luo and Morovic (1996) formulation presented in this chapter.

Table 14.3 includes example calculations of LLAB appearance attributes for a few stimuli.

Table 14.3 Example LLAB color appearance model calculations

Quantity	Case 1	Case 2	Case 3	Case 4
X	19.01	57.06	3.53	19.01
Y	20.00	43.06	6.56	20.00
Z	21.78	31.96	2.14	21.78
X ₀	95.05	95.05	109.85	109.85
Y ₀	100.00	100.00	100.00	100.00
Z ₀	108.88	108.88	35.58	35.58
L (cd/m ²)	318.31	31.83	318.31	31.83
Y _b	20.0	20.0	20.0	20.0
F _S	3.0	3.0	3.0	3.0
F _L	1.0	1.0	1.0	1.0
F _C	1.0	1.0	1.0	1.0
L _L	37.37	61.26	16.25	39.82
Ch _L	0.01	30.51	30.43	29.34
C _L	0.02	56.55	53.83	54.59
s _L	0.00	0.50	1.87	0.74
h _L	229.5	22.3	173.8	271.9
H _L	72B 28G	98R 2B	90G 10B	86B 14R
A _L	-0.01	52.33	-53.51	1.76
B _L	-0.01	21.43	5.83	-54.56

Why Not Use Just the LLAB Model?

The LLAB model has the advantages that it is fairly simple, incorporates a potentially accurate adaptation model, includes surround effects, and has a reliable built-in measure of color differences. However, its original formulation could not be considered a complete appearance model since it had predictors for the unusual combination of lightness, colorfulness, and hue with no predictor of chroma. The revised formulation includes both chroma and saturation predictors. LLAB has a serious drawback in that it is not analytically invertible. LLAB is also not capable of predicting incomplete chromatic adaptation. The revised formulation does include the D factor that can be used to model cognitive effects that occur upon changes in media. Lastly, it was not tested with data independent of those from which it was derived (mainly since the CIE models were derived soon after LLAB's publication). It is possible that some of the parameters in the model have been too tightly fit to one collection of visual data and might not generalize well to other data. However, its good performance on the LUTCHI data from which it was derived suggests that it has potential to be quite useful for some applications.

The CIE Color Appearance Model (1997), CIECAM97s

Publication of the first edition of this book coincided with the creation and publication of the first CIE color appearance model, CIECAM97s. At that time it was clear there was a significant amount of interest in the establishment and use of a single, standardized, color appearance model, but it was uncertain how effective a single CIE model could be. The industrial demand for such a model led the CIE to step up its efforts to establish a model to be put into use, tested, and perhaps recommended as a standard later on. CIECAM97s represents such a model and also represents a significant accomplishment in the field of color appearance modeling. This chapter provides an overview of the development and formulation of CIECAM97s. It is not an extensive treatment, since an improved model, the subject of Chapter 16, has been developed by the CIE. As will be seen in this chapter, the CIE experiment of CIECAM97s was a great success and led to real progress in color appearance models.

15.1 HISTORICAL DEVELOPMENT, OBJECTIVES, AND APPROACH

In March of 1996 the CIE held an expert symposium on *Colour Standards for Image Technology* in Vienna (CIE 1996b). While the symposium covered many aspects of image technology for which the CIE could provide guidance or standards to assist industry, one of the most critical issues was the establishment of a color appearance model for general use. Industrial participants

in the symposium recognized the need to apply a color appearance model, but requested guidance from the CIE in establishing a single model that could be used throughout the industry to promote uniformity of practice and compatibility between various components in modern open imaging systems.

The push toward a single model was highlighted and summarized in a presentation by Hunt made at that symposium (CIE 1996b) entitled 'The Function, Evolution, and Future of Colour Appearance Models.' In that presentation, Hunt reviewed the current status and historical development of various models and presented 12 principles for consideration in establishing a single model. These principles are reproduced here verbatim (CIE 1996b).

1. *The model should be as comprehensive as possible, so that it can be used in a variety of applications; but at this stage, only static states of adaptation should be included, because of the great complexity of dynamic effects.*
2. *The model should cover a wide range of stimulus intensities, from very dark object colours to very bright self-luminous colour. This means that the dynamic response function must have a maximum, and cannot be a simple logarithmic or power function.*
3. *The model should cover a wide range of adapting intensities, from very low scotopic levels, such as occur in starlight, to very high photopic levels, such as occur in sunlight. This means that rod vision should be included in the model; but because many applications will be such that rod vision is negligible, the model should be usable in a mode that does not include rod vision.*
4. *The model should cover a wide range of viewing conditions, including backgrounds of different luminance factors, and dark, dim, and average surrounds. It is necessary to cover the different surrounds because of their widespread use in projected and self-luminous displays.*
5. *For ease of use, the spectral sensitivities of the cones should be a linear transformation of the CIE \bar{x} , \bar{y} , \bar{z} or \bar{x}_{10} , \bar{y}_{10} , \bar{z}_{10} functions, and the $V'(\lambda)$ function should be used for the spectral sensitivity of the rods. Because scotopic photometric data is often unknown, methods of providing approximate scotopic values should be provided.*
6. *The model should be able to provide for any degree of adaptation between complete and none, for cognitive factors, and for the Helson–Judd effect, as options.*
7. *The model should give predictions of hue (both as hue-angle, and as hue-quadrature), brightness, lightness, saturation, chroma, and colourfulness.*
8. *The model should be capable of being operated in a reverse mode.*
9. *The model should be no more complicated than is necessary to meet the above requirements.*
10. *Any simplified version of the model, intended for particular applications, should give the same predictions as the complete model for some specified set of conditions.*

11. *The model should give predictions of colour appearance that are not appreciably worse than those given by the model that is best in each application.*
12. *A version of the model should be available for application to unrelated colours (those seen in dark surrounds in isolation from other colours).*

The conclusion drawn at the symposium was that the CIE should immediately begin work on the formulation of such a model with the goal that it be completed prior to the AIC (International Colour Association) quadrennial meeting to be held in Kyoto in May, 1997. The CIE decided that TC1-34 was the most appropriate committee to complete this work and expanded its terms of reference at the 1996 meeting of CIE Division 1 in Gothenburg to include:

To recommend one colour appearance model. This model should give due consideration to the findings of other relevant Technical Committees.

TC1-34 immediately began work on the formulation of a CIE model (both simple and comprehensive versions). A technical report on the simple version, CIECAM97s, was published (CIE 1998). The comprehensive version was never formulated due to an apparent lack of interest and demand.

TC1-34 members R.W.G. Hunt and M.R. Luo agreed to develop the first set of equations for consideration of the committee. The working philosophy of TC1-34 was to essentially follow the 12 principles outlined by Hunt in the development of a comprehensive CIE model and a simplified version for practical applications. The general concept was to develop a comprehensive model (like the Hunt model) that can be applied to a wide range of color appearance phenomena and a simplified version (like the RLAB model) that is sufficient for applications such as device-independent color imaging with the additional constraint that the two versions of the model be compatible for some defined set of conditions.

In preparing these models, revised versions of the Hunt color appearance model were developed. These are referred to as the Bradford-Hunt 96S (simple) model and the Bradford-Hunt 96C (comprehensive) model. These models represented one intermediate step in the formulation of CIECAM97s and were included in the first edition of this book (Fairchild 1998a) courtesy of the authors (Hunt 1996). These models were not approved by TC1-34 as the CIE model; however, they served as the starting point for the committee and provide good illustrations of how the twelve principles above could be fulfilled. As expected these models underwent some significant revision prior to consideration of the full committee. R.W.G. Hunt and M.R. Luo provided two revised models for TC1-34 consideration prior to the Kyoto meeting. In addition M. Fairchild provided a third alternative and K. Richter provided a fourth. These four alternatives were considered at the May 1997 meeting of TC1-34 in Kyoto and an agreement was reached to adopt one of the Hunt and Luo alternatives as the simple form of the CIE Color Appearance Model

(1997), designated CIECAM97s. This model is presented in the following sections. The model was formally approved and published by the CIE (1998). A comprehensive version of the model that extends upon CIECAM97s, to be designated CIECAM97c, was never formulated. A significantly simpler alternative with similar performance over a limited range of viewing conditions was prepared by Fairchild, but not recommended by the committee since it was not as extensible to a comprehensive form as the model selected to become CIECAM97s. (In hindsight, this shouldn't have been a concern.) This model has been designated as the ZLAB color appearance model and is presented in Section 15.7 since it has proven useful in some simple image reproduction applications.

15.2 INPUT DATA

Some slight, but important, revisions were made to the Bradford–Hunt 96S model to derive the model agreed upon by TC1-34 to become the CIECAM97s model, i.e., the simple version of the CIE Color Appearance Model (1997). These include a reformulation of the surround compensation to use power functions in order to avoid predictions of corresponding colors with negative CIE tristimulus values and a clear definition of the adaptation level factor D . It is important to note that the formulation of CIECAM97s builds upon the work of many researchers in the field of color appearance. This was a key issue in TC1-34's establishment of this model as the best of what is currently available. Various aspects of the model can be traced to work of (in alphabetical order) Bartleson, Breneman, Fairchild, Estevez, Hunt, Lam, Luo, Nayatani, Rigg, Seim, and Valberg among others. Since a comprehensive model was never formulated, those interested in color appearance predictions for more extreme viewing conditions (such as high luminance levels when bleaching occurs or low luminance levels when the rods become active) or more esoteric appearance phenomena (such as the Helson–Judd effect) should explore use of the Hunt model described in Chapter 12.

The input data to the model are the luminance of the adapting field (normally taken to be 20% of the luminance of white in the adapting field) L_A , the tristimulus values of the sample in the source conditions, XYZ , the tristimulus values of the source white in the source conditions, $X_wY_wZ_w$, the relative luminance of the source background in the source conditions Y_b . Additionally, the constants c for the impact of surround, N_c a chromatic induction factor, F_{LL} a lightness contrast factor, and F a factor for degree of adaptation, must be selected according to the guidelines in Table 15.1.

15.3 ADAPTATION MODEL

An initial chromatic adaptation transform is used to go from the source viewing conditions to the equal-energy-illuminant reference viewing conditions

Table 15.1 Input parameters for the CIECAM97s model

Viewing condition	<i>c</i>	<i>N_c</i>	<i>F_{LL}</i>	<i>F</i>
Average surround, samples subtending > 4°	0.69	1.0	0.0	1.0
Average surround	0.69	1.0	1.0	1.0
Dim surround	0.59	1.1	1.0	0.9
Dark surround	0.525	0.8	1.0	0.9
Cut-sheet transparencies	0.41	0.8	1.0	0.9

(although tristimulus values need never be expressed in the reference conditions). First, tristimulus values for both the sample and white are normalized and transformed to spectrally sharpened cone responses using the transformation given in Equations 15.1 and 15.2.

$$\begin{bmatrix} R \\ G \\ B \end{bmatrix} = \mathbf{M}_B \begin{bmatrix} X/Y \\ Y/Y \\ Z/Y \end{bmatrix} \quad (15.1)$$

$$\mathbf{M}_B = \begin{bmatrix} 0.8951 & 0.2664 & -0.1614 \\ -0.7502 & 1.7135 & 0.0367 \\ 0.0389 & -0.0685 & 1.0296 \end{bmatrix} \quad (15.2)$$

The chromatic adaptation transform is a modified von Kries transformation (performed on a type of chromaticity coordinates) with an exponential nonlinearity added to the short-wavelength-sensitive channel as given in Equations 15.3–15.6. In addition, the variable *D* is used to specify the degree of adaptation. *D* is set to 1.0 for complete adaptation or discounting the illuminant. *D* is set to 0.0 for no adaptation. *D* takes on intermediate values for various degrees of incomplete chromatic adaptation. Equation 15.7 allows calculation of *D* for various luminance levels and surround conditions.

$$R_c = [D(1.0/R_w) + 1 - D]R \quad (15.3)$$

$$G_c = [D(1.0/G_w) + 1 - D]G \quad (15.4)$$

$$B_c = [D(1.0/B_w^p) + 1 - D] |B|^p \quad (15.5)$$

$$p = (B_w/1.0)^{0.0834} \quad (15.6)$$

$$D = F - F/[1 + 2(L_A^{1/4}) + (L_A^2/300)] \quad (15.7)$$

If *B* happens to be negative, then *B_c* is also set to be negative. Similar transformations are also made for the source white since they are required in later calculations. Various factors must be calculated prior to further

calculations as shown in Equations 15.8–15.12. These include a background induction factor n , the background and chromatic brightness induction factors N_{bb} and N_{cb} , and the base exponential nonlinearity z .

$$k = 1/(5L_A + 1) \quad (15.8)$$

$$F_L = 0.2k^4(5L_A) + 0.1(1 - k^4)^2(5L_A)^{1/3} \quad (15.9)$$

$$n = Y_b/Y_w \quad (15.10)$$

$$N_{\text{bb}} = N_{\text{cb}} = 0.725(1/n)^{0.2} \quad (15.11)$$

$$z = 1 + F_{\text{LL}}n^{1/2} \quad (15.12)$$

The post-adaptation signals for both the sample and the source white are then transformed from the sharpened cone responses to the Hunt–Pointer–Estevez cone responses as shown in Equations 15.13 and 15.14 prior to application of a nonlinear response compression.

$$\begin{bmatrix} R' \\ G' \\ B' \end{bmatrix} = \mathbf{M}_H \mathbf{M}_B^{-1} \begin{bmatrix} R_c Y \\ G_c Y \\ B_c Y \end{bmatrix} \quad (15.13)$$

$$\mathbf{M}_H = \begin{bmatrix} 0.38971 & 0.68898 & -0.07868 \\ -0.22981 & 1.18340 & 0.04641 \\ 0.00 & 0.00 & 1.00 \end{bmatrix} \quad (15.14)$$

The post-adaptation cone responses (for both the sample and the white) are then calculated using Equations 15.15–15.17.

$$R'_a = \frac{40(F_L R'/100)^{0.73}}{[(F_L R'/100)^{0.73} + 2]} + 1 \quad (15.15)$$

$$G'_a = \frac{40(F_L G'/100)^{0.73}}{[(F_L G'/100)^{0.73} + 2]} + 1 \quad (15.16)$$

$$B'_a = \frac{40(F_L B'/100)^{0.73}}{[(F_L B'/100)^{0.73} + 2]} + 1 \quad (15.17)$$

15.4 APPEARANCE CORRELATES

Preliminary red–green and yellow–blue opponent dimensions are calculated using Equations 15.18 and 15.19.

$$G_c = [D(1.0/G_w) + 1 - D]G \quad (15.18)$$

$$B_c = [D(1.0/B_w^p) + 1 - D]|B|^p \quad (15.19)$$

The hue angle h is then calculated from a' and b' using Equation 15.20.

$$h = \tan^{-1}(b/a) \quad (15.20)$$

Hue quadrature H and eccentricity factor e , are calculated from the following unique hue data in the usual way (linear interpolation):

Red: $h = 20.14$, $e = 0.8$, $H = 0$ or 400

Yellow: $h = 90.00$, $e = 0.7$, $H = 100$

Green: $h = 164.25$, $e = 1.0$, $H = 200$

Blue: $h = 237.53$, $e = 1.2$, $H = 300$

Equations 15.21 and 15.22 illustrate calculation of e and H for arbitrary hue angles where the quantities subscripted 1 and 2 refer to the unique hues with hue angles just below and just above the hue angle of interest.

$$e = e_1 + (e_2 - e_1)(h - h_1)/(h_2 - h_1) \quad (15.21)$$

$$H = H_1 + \frac{100(h - h_1)/e_1}{(h - h_1)/e_1 + (h_2 - h)/e_2} \quad (15.22)$$

The achromatic response is calculated as shown in Equation 15.23 for both the sample and the white.

$$A = [2R'_a + G'_a + (1/20)B'_a - 2.05]N_{bb} \quad (15.23)$$

Lightness J is calculated from the achromatic signals of the sample and white using Equation 15.24.

$$J = 100(A/A_w)^{cz} \quad (15.24)$$

Brightness Q is calculated from lightness and the achromatic for the white using Equation 15.25.

$$Q = (1.24/c)(J/100)^{0.67}(A_w + 3)^{0.9} \quad (15.25)$$

Finally, saturation s ; chroma C ; and colorfulness M ; are calculated using Equations 15.26–15.28, respectively.

$$s = \frac{50(a^2 + b^2)^{1/2}100e(10/13)N_c N_{cb}}{R'_a + G'_a + (21/20)B'_a} \quad (15.26)$$

$$C = 2.44s^{0.69}(J/100)^{0.67n}(1.64 - 0.29^n) \quad (15.27)$$

$$M = CF_L^{0.15} \quad (15.28)$$

15.5 INVERSE MODEL

The CIECAM97s Model can be nearly analytically inverted, but requires one approximation since the Y value on inversion is not easily computed (step 8). Beginning with lightness J , chroma C , and hue angle h , the process is as follows:

1. From J obtain A .
2. From h obtain e .
3. Calculate s using C and J .
4. Calculate a and b using s , h , and e .
5. Calculate R'_a , G'_a , and B'_a from A , a , and b .
6. Calculate R' , G' , and B' from R'_a , G'_a , and B'_a .
7. Calculate $R_c Y$, $G_c Y$, and $B_c Y$ from R' , G' , and B' .
8. Calculate Y from $R_c Y$, $G_c Y$, and $B_c Y$ using M_B^{-1} (approximation).
9. Calculate R_c , G_c , and B_c from $R_c Y$, $G_c Y$, and $B_c Y$ and Y .
10. Calculate R , G , and B from R_c , G_c , and B_c .
11. Calculate X , Y , and Z from R , G , B , and Y .

While CIECAM97s cannot be simply inverted in an analytical form, its inversion is far simpler and more accurate than some previous models. Thus CIECAM97s has been of far more practical utility. A detailed explanation of the inversion process can be found at <www.cis.rit.edu/Fairchild/CAM.html>.

15.6 PHENOMENA PREDICTED

Although CIECAM97s is a fairly simple model it is also quite complete in the variety of phenomena predicted. It includes correlates of all the important appearance dimensions (lightness, brightness, chroma, colorfulness, saturation, and hue) and it can predict a wide range of adaptation-, surround-, and luminance-dependent effects. It is not applicable to extremely high or low luminance levels, which are atypical of careful color judgements. Example calculations using the CIECAM97s color appearance model as described in this chapter are given for four samples in Table 15.2. A spreadsheet with these example calculations can be found at <www.cis.rit.edu/fairchild/CAM.html>.

Table 15.2 Example CIECAM97s calculations

Quantity	Case 1	Case 2	Case 3	Case 4
X	19.01	57.06	3.53	19.01
Y	20.00	43.06	6.56	20.00
Z	21.78	31.96	2.14	21.78
X _w	95.05	95.05	109.85	109.85
Y _w	100.00	100.00	100.00	100.00
Z _w	108.88	108.88	35.58	35.58
L _A	318.31	31.83	318.31	31.83
F	1.0	1.0	1.0	1.0
D	0.997	0.890	0.997	0.890
Y _b	20.0	20.0	20.0	20.0
N _c	1.0	1.0	1.0	1.0
F _{LL}	1.0	1.0	1.0	1.0
F _L	1.17	0.54	1.17	0.54
N _{bb} , N _{cb}	1.0	1.0	1.0	1.0
h	212.3	19.3	175.4	250.8
H	269.5	399.4	217.7	306.9
HC	70B 30G	99R 1B	82G 18B	93B 7R
J	42.44	65.27	21.04	39.88
Q	32.86	31.88	20.54	22.96
s	0.15	146.98	232.18	180.56
C	0.50	61.96	72.99	66.85
M	0.51	56.52	74.70	60.98

15.7 THE ZLAB COLOR APPEARANCE MODEL

A simple model was derived from the various models submitted to TC1-34 for consideration of the committee. Ultimately the committee determined that a more extensible model was required for recommendation as CIECAM97s. Thus, the simpler model was abandoned by the committee and has been rennotated by the author as the ZLAB color appearance model (Fairchild 1998b). It was derived from the CIECAM97s, LLAB, and RLAD models with significant input from the work of Luo and Hunt submitted to TC1-34. The ZLAB model was designed to perform nearly as well as the CIECAM97s model for a limited set of viewing conditions. These limitations include a restriction to intermediate values of adapting luminance since the hyperbolic non-linearity has been replaced with a square-root function that describes the hyperbolic function well for intermediate luminance levels. Additionally, the ZLAB model is limited to medium gray backgrounds in order to further simplify computation. Lastly, ZLAB is limited to the prediction of the relative appearance attributes of lightness, chroma, saturation, and hue. It cannot be used to predict colorfulness or brightness. This is due to the removal of most of the luminance dependencies resulting in significantly simplified

equations. The ZLAB model performs identically to CIECAM97s for most corresponding colors calculations since it utilizes the same chromatic adaptation transform. It also performs very nearly as well for the prediction of appearance scaling data. The ZLAB model has found some useful application in image reproduction where gamut mapping and lack of viewing conditions control are major limiting factors obviating the need for a more complex model.

Input Data

The input data to the model are the luminance of the adapting field, L_A (taken to be 0.2 times the luminance of a reference white), the tristimulus values of the sample in the source conditions, XYZ , the tristimulus values of the source white in the source conditions $X_wY_wZ_w$.

Chromatic Adaptation

As with CIECAM97s the Bradford chromatic adaptation transform is used to go from the source viewing conditions to corresponding colors under the reference (equal-energy illuminant) viewing conditions. First, all three sets of tristimulus values are normalized and transformed to sharpened cone responses using the Bradford transformation as given in Equations 15.29 and 15.30.

$$\begin{bmatrix} R \\ G \\ B \end{bmatrix} = \mathbf{M} \begin{bmatrix} X/Y \\ Y/Y \\ Z/Y \end{bmatrix} \quad (15.29)$$

$$\mathbf{M} = \begin{bmatrix} 0.8951 & 0.2664 & -0.1614 \\ -0.7502 & 1.7135 & 0.0367 \\ 0.0389 & -0.0685 & 1.0296 \end{bmatrix} \quad (15.30)$$

The chromatic-adaptation transform is a modified von Kries transformation (performed on a type of chromaticity coordinates) with an exponential nonlinearity added to the short-wavelength-sensitive channel as given in Equations 15.31–15.34. In addition, the variable D is used to specify the degree of adaptation. D is set to 1.0 for complete adaptation or discounting the illuminant. D is set to 0.0 for no adaptation. D is set to intermediate values for various degrees of incomplete chromatic adaptation. The D variable could be left as an empirical parameter, or calculated using Equation 15.35, as in CIECAM97s, with $F = 1.0$ for average surrounds and $F = 0.9$ for dim or dark surrounds. If Equation 15.35 is used, it is the only place absolute luminance is required in the ZLAB model.

$$R_c = [D(1.0/R_w) + 1 - D]R \quad (15.31)$$

$$G_c = [D(1.0/G_w) + 1 - D]G \quad (15.32)$$

$$B_c = [D(1.0/B_w^p) + 1 - D]|B|^p \quad (15.33)$$

$$p = (B_w/1.0)^{0.0834} \quad (15.34)$$

$$B_c = [D(1.0/B_w^p) + 1 - D]|B|^p \quad (15.35)$$

If B happens to be negative, then B_c is also set to be negative. R_c , G_c , and B_c represent the corresponding colors of the test stimulus under the reference condition (i.e., illuminant E). The final step in the adaptation transform is to convert from the sharpened cone responses back to CIE XYZ tristimulus values for the reference condition as illustrated in Equation 15.36.

$$\begin{bmatrix} X_c \\ Y_c \\ Z_c \end{bmatrix} = \mathbf{M}^{-1} \begin{bmatrix} R_c Y \\ G_c Y \\ B_c Y \end{bmatrix} \quad (15.36)$$

Apearance Correlates

Opponent responses are calculated using modified CIELAB-type equations with the power-function nonlinearity defined by the surround relative luminances. These were derived from a simplification of the CIECAM97s model by recalling that the hyperbolic nonlinear function in CIECAM97s can be approximated by a square-root function for intermediate luminances. Thus the opponent responses reduce to the forms given in Equations 15.37 and 15.38.

$$A = 500 \left[(X_c/100)^{\frac{1}{2\sigma}} - (Y_c/100)^{\frac{1}{2\sigma}} \right] \quad (15.37)$$

$$B = 200 \left[(Y_c/100)^{\frac{1}{2\sigma}} - (Z_c/100)^{\frac{1}{2\sigma}} \right] \quad (15.38)$$

The exponents are directly related to those used in CIECAM97s as illustrated in Table 15.3. The values of $1/\sigma$ (called c) in CIECAM97s are modified to $1/2\sigma$ in ZLAB in order to incorporate the square-root approximation to the hyperbolic nonlinearity of CIECAM97s.

Hue angle is calculated in the typical manner as illustrated in Equation 15.39.

$$h^z = \tan^{-1} \left(\frac{B}{A} \right) \quad (15.39)$$

Table 15.3 ZLAB surround parameters

Surround			
	Average	Dim	Dark
$1/\sigma$	0.69	0.59	0.525
$1/2\sigma$	0.345	0.295	0.2625

Hue composition is also determined in the usual way via linear interpolation between the defined angles for the unique hues. These are $h_r^z = 25^\circ$, $h_y^z = 93^\circ$, $h_g^z = 165^\circ$, and $h_b^z = 254^\circ$.

ZLAB is only specified for a background of medium (20%) luminance factor. Thus the z parameter in the CIECAM97s model takes on a constant value of 1.45 and lightness L^z is expressed as shown in Equation 15.40.

$$L^z = 100(Y_c/100)^{\frac{1.45}{2\sigma}} \quad (15.40)$$

Chroma C^z is given by Equation 15.41 as originally defined in the LLAB model to predict magnitude estimation data well. Saturation s^z is simply the ratio of chroma to lightness as illustrated in Equation 15.42.

$$C^z = 25 \log_e [1 + 0.05(A^2 + B^2)^{1/2}] \quad (15.41)$$

$$s^z = C^z/L^z \quad (15.42)$$

If rectangular coordinates are required for color space representations, they can easily be obtained from C^z and h^z using Equations 15.43 and 15.44.

$$a^z = C^z \cos(h^z) \quad (15.43)$$

$$b^z = C^z \sin(h^z) \quad (15.44)$$

Inverse Model

The ZLAB model is extremely simple to operate in the inverse direction. Starting with lightness, chroma, and hue angle the following steps are followed.

1. Calculate $(A^2 + B^2)^{1/2}$ from C^z .
2. Calculate A and B from $(A^2 + B^2)^{1/2}$ and h^z .
3. Calculate X_c , Y_c , and Z_c from L^z , A, and B.
4. Calculate R_c , G_c , and B_c from X_c , Y_c , and Z_c .

5. Calculate R , G , and B from R_c , G_c , and B_c .
6. Calculate X , Y , and Z from R , G , and B .

15.8 WHY NOT USE JUST CIECAM97S?

It was a truly unprecedented event that CIE TC1-34 was able to agree upon the derivation of the CIECAM97s model within a one-year time frame, as was its goal. As anticipated in the first edition of this book, the CIE approval procedures did not introduce any changes of significance to the model. It is important to note that CIECAM97s was considered an interim model with the expectation that it would be revised as more data and theoretical understanding became available. Industrial response to the CIECAM97s model was strong and it was quickly brought to bear on commercial applications, particularly in the imaging industry. Application of CIECAM97s, and further scientific research, quickly led to understanding of limitations in its formulation and performance as well as the creation of additional data for improvements. The great success of CIECAM97s was in the focus it provided to researchers and engineers in the field. With everyone focusing on a single model for testing and improvement, it became possible to make rapid, significant improvement. The fruits of that work are the recently published CIECAM02 color appearance model that is the topic of Chapter 16.

The existence of CIECAM97s is one reason to not use just CIECAM97s. CIECAM02 is a simpler formulation with better performance. Also, CIECAM97s might be too complex for some applications. In such cases, models like ZLAB, RLAB, or the combination of a chromatic adaptation transform with CIELAB might be adequate.

16

CIECAM02

CIECAM97s was a great success. If that's so, then why is there a CIECAM02 model? The answer is that the natural evolution or color appearance models was anticipated and encouraged with the publication of CIECAM97s. That is exactly why the year (97) is in the name. The success of CIECAM97s is that it allowed a variety of researchers and practitioners in color appearance to focus their efforts on a single model. This focus quickly led to suggested improvements in CIECAM97s that ultimately led to the formulation of a simpler and more effective model called CIECAM02. This chapter discusses the derivation and formulation of CIECAM02, the current CIE color appearance model, a model likely to remain the current CIE recommendation for some time.

16.1 OBJECTIVES AND APPROACH

As soon as CIECAM97s was published, the intense scrutiny it was subjected to resulted in suggestions for its improvement and in some cases for simple corrections to certain elements. With the creation of CIE Division 8, *Image Technology*, came the formation of its first technical committee. This was CIE TC8-01, *Colour Appearance Modeling for Colour Management Systems*, chaired by Nathan Moroney and charged with suggesting revisions to CIECAM97s and perhaps a new CIE model. The ultimate result of TC8-01's work to collect and test suggested revisions of CIECAM97s has been the formulation and publication of a revised color appearance model, CIECAM02 (CIE 2004, Moroney *et al.* 2002). Note that CIECAM02 has no 's' notation at the end of its name. This is because there is no intention to create a comprehensive version (especially since CIECAM97c was never created) and even if one were created, a 'c' could be added at the end of its name.

A number of potential improvements to CIECAM97s were suggested and these were compiled into a single publication on behalf of TC8-01 by Fairchild (2001). The adjustments considered and ultimately included in CIECAM02 in some form included:

- Linearization of the chromatic adaptation transform to simplify the model and facilitate analytical inversion (Finlayson and Drew 1999, Finlayson and Süsstrunk 2000, Li *et al.* 2000a,b)
- Correction of anomalous surround compensation (Moroney 2002, Li *et al.* 1999), Li *et al.* 2000a,b)
- Correction of the lightness scale for perfect black stimuli (Moroney 2002, Li *et al.* 1999, Li *et al.* 2000a,b)
- Correction of chroma scale expansion for color of low chroma (Wyble and Fairchild 2000, Newman and Pirrotta 2000)
- Inclusion of a continuously variable surround compensation (Fairchild 1995b, 1996)
- Improved response compression function to facilitate an improved saturation correlate (Hunt *et al.* 2003)

After significant consideration of all the suggested revisions, TC8-01 converged on a single set of new equations and formulated a revised model designated CIECAM02 (CIE 2004, Moroney *et al.* 2002). The year remains in the name as acknowledgement that much remains to be learned about color appearance psychophysics and modeling. Simply put, CIECAM02 is simpler in formulation, easier to invert, and performs as well as, if not better, than CIECAM97s for all available data sets. CIECAM02 should be considered for any applications that were previously served well by CIECAM97s. The following sections describe the formulation and use of CIECAM02.

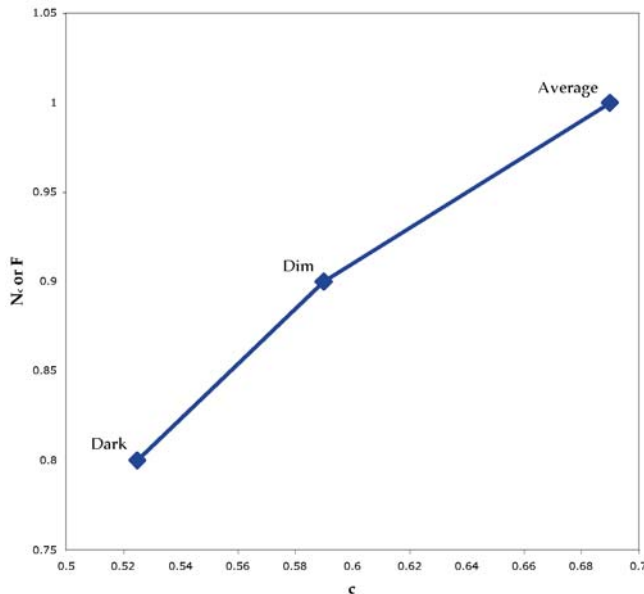
16.2 INPUT DATA

Input data for the CIECAM02 include the relative tristimulus values of the test stimulus (XYZ) and the white point ($X_wY_wZ_w$), the adapting luminance (often taken to be 20% of the luminance a white object in the scene) L_A , in cd/m^2 , the relative luminance of the surround (dark, dim, average), and a decision on whether discounting-the-illuminant is taking place. The surround relative luminance is generally taken to be average for reflection prints, dim for CRT displays or televisions, and dark for projected transparencies under the assumption that these media are being viewed in their typical environments. The surround is not directly tied to the medium. Thus it is certainly possible to have reflection prints viewed in a dark surround and projected transparencies viewed in an average surround. Discounting-the-illuminant is generally assumed to occur for object color stimuli such as prints and not to occur for emissive displays such as CRTs. When discounting the illuminant occurs, the D factor in the chromatic adaptation model is set to 1.0. Otherwise it is computed as described in Section 16.3.

Once the surround relative luminance is established, Table 16.1 is used to set the values of c an exponential nonlinearity, N_c the chromatic induction factor, and F the maximum degree of adaptation. In CIECAM02, intermediate values for these parameters are allowed. If intermediate values are

Table 16.1 Input parameters for the CIECAM02 model

Viewing condition	c	N_c	F
Average surround	0.69	1.0	1.0
Dim surround	0.59	0.9	0.9
Dark surround	0.525	0.8	0.8

**Figure 16.1** Linear relationship between surround parameters used for the computation of intermediate, continuously variable, surround settings in CIECAM02

desired, the proper procedure is to choose the intermediate value for c and then compute the corresponding intermediate values for N_c and F via linear interpolation as shown in the relationship plotted in Figure 16.1. These values have been corrected slightly from those in CIECAM97s and the number of conditions has been reduced to a more meaningful, and simpler, set.

16.3 ADAPTATION MODEL

One of the most important changes in CIECAM02 is the use of a linear, von Kries-type chromatic adaptation transform (as described in more detail in Chapter 9). This results in a simpler model with equivalent performance (Calabria and Fairchild 2001) and allows for a simple analytical inversion of CIECAM02 (another significant improvement over CIECAM97s). One begins with a conversion from CIE tristimulus values (scaled approximately

between 0 and 100, rather than 0 and 1.0) to RGB responses based on the optimized transform matrix $\mathbf{M}_{\text{CAT02}}$, as illustrated in Equations 16.1 and 16.2. All CIE tristimulus values are normally calculated using the CIE 1931 standard colorimetric observer (2°). The transformation must also be completed for the tristimulus values of the adapting stimulus.

$$\begin{vmatrix} R \\ G \\ B \end{vmatrix} = \mathbf{M}_{\text{CAT02}} \begin{vmatrix} X \\ Y \\ Z \end{vmatrix} \quad (16.1)$$

$$\mathbf{M}_{\text{CAT02}} = \begin{vmatrix} 0.7328 & 0.4296 & -0.1624 \\ -0.7036 & 1.6975 & 0.0061 \\ 0.0030 & 0.0136 & 0.9834 \end{vmatrix} \quad (16.2)$$

The transformation to cone responses is the same as that used in the Hunt model. Matrix $\mathbf{M}_{\text{CAT02}}$ is normalized such that the tristimulus values for the equal-energy illuminant ($X = Y = Z = 100$) produce equal cone responses ($L = M = S = 100$).

The D factor, for degree of adaptation, is computed as a function of the adapting luminance L_A , and surround F , according to Equation 16.3. If complete discounting-the-illuminant is assumed, then D is simply set to 1.0. Theoretically, D ranges from 1.0 for complete adaptation to 0.0 for no adaptation. As a practical limitation, it will rarely go below 0.6.

$$D = F \left[1 - \left(\frac{1}{3.6} \right) e^{\left(\frac{-(L_A + 42)}{92} \right)} \right] \quad (16.3)$$

Once D is established, the tristimulus responses for the stimulus color are converted to adapted tristimulus responses $R_C G_C B_C$, representing corresponding colors for an implied equal-energy illuminant reference condition using Equations 16.4–16.6. $R_W G_W B_W$ are the tristimulus responses for the adapting white.

$$R_C = [(100D/R_W) + (1 - D)]R \quad (16.4)$$

$$G_C = [(100D/G_W) + (1 - D)]G \quad (16.5)$$

$$B_C = [(100D/B_W) + (1 - D)]B \quad (16.6)$$

A Note on the CIECAM02 Chromatic Adaptation Transform

Equations 16.4–16.5 represent the most general form of the CIECAM02 chromatic adaptation transform as a simple von Kries transform to implicit equal-energy reference conditions with incomplete adaptation. This trans-

formation can be used consistently, independent of the remainder of the CIECAM02 model. It can also be applied regardless of the scaling of initial tristimulus values (0 to approximately 100 as normal in CIECAM02, or 0 to approximately 1.0 as sometimes used). It is recommended that Equations 16.4–16.6 be used in all applications of CIECAM02 to maximize generality and minimize confusion in the function of the adaptation transform. However, the CIE (2004) technical report on CIECAM02 provides slightly different default equations as given in Equations 16.4a–16.6a.

$$R_C = [(Y_W D / R_W) + (1 - D)] R \quad (16.4a)$$

$$G_C = [(Y_W D / G_W) + (1 - D)] G \quad (16.5a)$$

$$B_C = [(Y_W D / B_W) + (1 - D)] B \quad (16.6a)$$

Since Y_W , the Y tristimulus value of white, is normally 100, the two sets of equations are normally indistinguishable. However, there are times when Y_W values different from 100 are used, such as when one considers paper, rather than the perfect reflecting diffuser, to be white in a printing application. While it appears that the Y_W factor in Equations 16.4a–16.6a might account for the change in adopted white, it does not. Such normalization is already built into the equations with R_W , G_W , and B_W . The Y_W terms serves no meaningful purpose and is a remnant of an earlier model formulation (similar to that in CIECAM97s) that was not corrected prior to publication of the CIE technical report. There will be little effect of the difference in equations on final computed appearance correlates since the scaling of appearance relative to the white point is accomplished in later equations (such as that for lightness J) in CIECAM02. However, the transform in Equations 16.4a–16.6a cannot be used without the remainder of the CIECAM02 model. Doing so will produce inconsistent results (e.g., white from one viewing condition might not map to white in a second viewing condition). If the adaptation transform is to be used separately from the full CIECAM02 model, the form in Equations 16.4–16.6 must be used for consistent predictions. Also, it should be noted that the Y_W factor in Equations 16.4a–16.6a does not normalize the scaling of tristimulus values (it actually has the opposite effect) and values scaled from 0 to approximately 100 should be used as input to CIECAM02.

Remainder of CIECAM02 Adaptation Model

Next a number of viewing-condition-dependent components are computed as intermediate values required for further computations. These include a luminance-level adaptation factor F_L , and induction factors N_{bb} and N_{cb} , and the base exponential nonlinearity z that each depend on the background relative luminance Y_b . These factors are computed using Equations 16.7–16.11.

$$k = 1/(5L_A + 1) \quad (16.7)$$

$$F_L = 0.2k^4(5L_A) + 0.1(1 - k^4)^2(5L_A)^{1/3} \quad (16.8)$$

$$n = \frac{Y_b}{Y_w} \quad (16.9)$$

$$N_{bb} = N_{cb} = 0.725(1/n)^{0.2} \quad (16.10)$$

$$z = 1.48 + \sqrt{n} \quad (16.11)$$

In order to apply post-adaptation nonlinear compression, the adapted RGB responses must first be converted from the MCAT02 specification to Hunt–Pointer–Estevez fundamentals that more closely represent cone responsivities. This transformation is represented by Equations 16.12–16.14 and can be thought of as a conversion from the CAT02 RGB system back to CIE tristimulus values then to cone responsivities. The relative spectral responsivities of the CAT02 system and the Hunt–Pointer–Estevez fundamentals are illustrated in Figure 16.2.

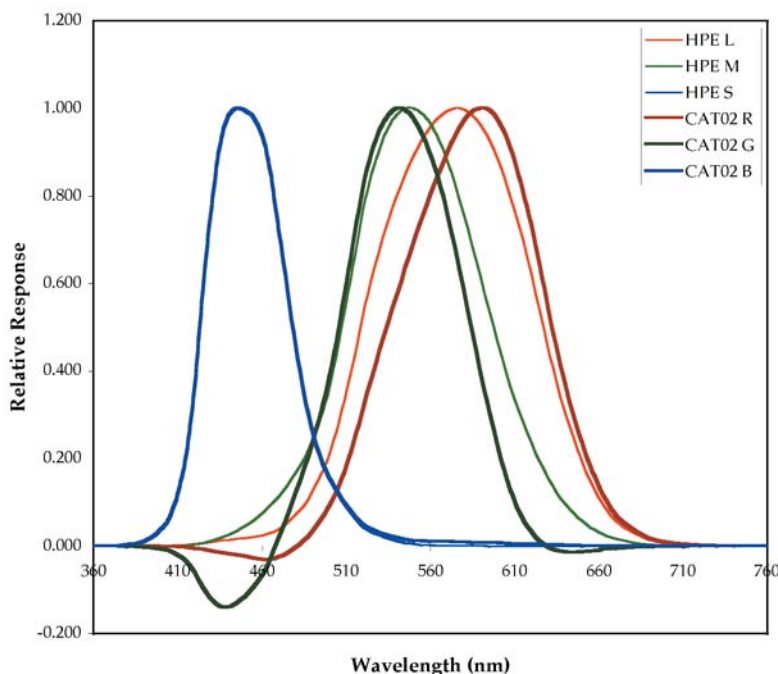


Figure 16.2 The relative spectral responsivities for the M_{CAT02} primaries and the Hunt–Pointer–Estevez cone fundamentals. Note that both are simple linear transformations of the CIE 2° color matching functions

$$\begin{vmatrix} R' \\ G' \\ B' \end{vmatrix} = \mathbf{M}_{\text{HPE}} \mathbf{M}_{\text{CAT02}}^{-1} \begin{vmatrix} R_C \\ G_C \\ B_C \end{vmatrix} \quad (16.12)$$

$$\mathbf{M}_{\text{HPE}} = \begin{vmatrix} 0.38971 & 0.68898 & -0.07868 \\ -0.22981 & 1.18340 & 0.04641 \\ 0.00000 & 0.00000 & 1.00000 \end{vmatrix} \quad (16.13)$$

$$\mathbf{M}_{\text{CAT02}}^{-1} = \begin{vmatrix} 1.096124 & -0.278869 & 0.182745 \\ 0.454369 & 0.473533 & 0.072098 \\ -0.009628 & -0.005698 & 1.015326 \end{vmatrix} \quad (16.14)$$

The post-adaptation nonlinearities are similar in form to those in CIECAM97s, but slightly modified to produce a simple power-function response over a larger dynamic range. This facilitates a simple definition of saturation later in the model. For much of the normal operating range of these functions, they are similar to simple square-root functions. These nonlinearities are given in Equations 16.15–16.17.

$$R'_a = \frac{400(F_L R'/100)^{0.42}}{27.13 + (F_L R'/100)^{0.42}} + 0.1 \quad (16.15)$$

$$G'_a = \frac{400(F_L G'/100)^{0.42}}{27.13 + (F_L G'/100)^{0.42}} + 0.1 \quad (16.16)$$

$$B'_a = \frac{400(F_L B'/100)^{0.42}}{27.13 + (F_L B'/100)^{0.42}} + 0.1 \quad (16.17)$$

These values are then used to create opponent color responses and formulate correlates of color appearance.

16.4 OPPONENT COLOR DIMENSIONS

Initial opponent-type responses in CIECAM02 are calculated using Equations 16.18 and 16.19.

$$a = R'_a - 12G'_a/11 + B'_a/11 \quad (16.18)$$

$$b = (1/9)(R'_a + G'_a - 2B'_a) \quad (16.19)$$

16.5 HUE

Hue angle h is calculated in CIECAM02 space using the same procedure as CIELAB. As in CIELAB, h is expressed in degrees ranging from 0° to 360° , measured from the positive a axis calculated according to Equation. 16.20.

Table 16.2 Data for conversion from hue angle to hue quadrature

	Red	Yellow	Green	Blue	Red
<i>i</i>	1	2	3	4	5
h_i	20.14	90.00	164.25	237.53	380.14
e_i	0.8	0.7	1.0	1.2	0.8
H_i	0	100	200	300	400

$$h = \tan^{-1}(b/a) \quad (16.20)$$

Next an eccentricity factor e_t is computed. This factor is similar to that in CIECAM97s, but has been formulated analytically as given in Equation 16.21.

$$e_t = 1/4 \left[\cos\left(h \frac{\pi}{180} + 2\right) + 3.8 \right] \quad (16.21)$$

Hue quadrature and hue composition can be determined through linear interpolation of the data given in Table 16.2 using Equation 16.22.

$$H = H_i + \frac{100(h - h_i)/e_i}{(h - h_i)/e_i + (h_{i+1} - h)/e_{i+1}} \quad (16.22)$$

16.6 LIGHTNESS

An initial achromatic response is computed by weighted summation of the nonlinear adapted cone responses modified with the brightness induction factor as illustrated in Equation 16.23. A similar quantity must also be computed for the white in order to facilitate computation of lightness and brightness.

$$A = [2R'_a + G'_a + (1/20)B'_a - 0.305]N_{bb} \quad (16.23)$$

Lightness J is then simply computed from the achromatic response, A , achromatic response for white A_W , the surround factor c , and the base exponent z , according to Equation 16.24.

$$J = 100(A/A_W)^{cz} \quad (16.24)$$

16.7 BRIGHTNESS

The CIECAM02 correlate to brightness Q is computed from lightness J , the achromatic response for white A_W , the surround factor c , and the luminance-level adaptation factor F_L , as shown in Equation 16.25.

$$Q = (4/c)\sqrt{J/100} (A_W + 4) F_L^{0.25} \quad (16.25)$$

16.8 CHROMA

A temporary quantity t , that is related to saturation and incorporates the chromatic induction factors for surround and background (N_c and N_{cb}) as well as the eccentricity adjustment e_t , is computed as the basis for chroma, colorfulness, and saturation correlates. The formula for t is given in Equation 16.26.

$$t = \frac{(50\,000/13)N_c N_{cb} e_t \sqrt{a^2 + b^2}}{R'_a + G'_a + (21/20)B'_a} \quad (16.26)$$

CIECAM02 chroma C , is then computed by multiplying a slightly nonlinear form of t by the square root of lightness J , with some adjustment for background n , as shown in Equation 16.27. This formulation, as with most of the model, is based on empirical fitting to various color appearance scaling data.

$$C = t^{0.9} \sqrt{J/100} (1.64 - 0.29^n)^{0.73} \quad (16.27)$$

16.9 COLORFULNESS

The colorfulness correlate in CIECAM02 is calculated by scaling the chroma predictor C , by the fourth root of the luminance-level adaptation factor F_L , as illustrated in Equation 16.28. This makes sense since colorfulness is related to chroma, but increases with adapting luminance while chroma is relatively constant across changes in luminance.

$$M = C F_L^{0.25} \quad (16.28)$$

16.10 SATURATION

Lastly, a simple and logically defined predictor of saturation s is defined in CIECAM02 as the square root of colorfulness relative to brightness in Equation 16.29. This is analogous to the CIE definition of saturation as the colorfulness of a stimulus relative to its brightness.

$$s = 100 \sqrt{M/Q} \quad (16.29)$$

16.11 CARTESIAN COORDINATES

Color spaces related to appearance models are normally specified in terms of cylindrical coordinates of lightness, chroma, and hue (JCh) or brightness,

colorfulness, and hue (Qm). However in some applications it is useful to have the equivalent Cartesian coordinates. While this computation is a simple coordinate transformation, it was never explicitly defined in CEICAM97s. Thus Cartesian coordinates for chroma, colorfulness, and saturation dimensions are defined in Equations 16.30–16.35.

$$a_C = C \cos(h) \quad (16.30)$$

$$b_C = C \sin(h) \quad (16.31)$$

$$a_M = M \cos(h) \quad (16.32)$$

$$b_M = M \sin(h) \quad (16.33)$$

$$a_s = s \cos(h) \quad (16.34)$$

$$b_s = s \sin(h) \quad (16.35)$$

16.12 INVERSE MODEL

Particularly for color reproduction applications, an inverse color appearance model is of practical importance. CIECAM02 is a significant improvement over CIECAM97s in terms of simplicity of inversion. This is largely due to the adoption of a simple linear chromatic adaptation transform. In addition, the CIE technical report on CIECAM02 includes a detailed explanation of the model inversion and worked examples (CIE 2004). A step-by-step procedure for implementing the CIECAM02 model in reverse is given below (starting from JCh).

- Step 1. Calculate t from C and J .
- Step 2. Calculate e_t from h .
- Step 3. Calculate A from A_w and J .
- Step 4. Calculate a and b from t , e_t , h , and A .
- Step 5. Calculate R'_a , G'_a , and B'_a from A , a and b .
- Step 6. Use the inverse nonlinearity to compute R' , G' , and B' .
- Step 7. Convert to R_C , G_C , and B_C , via linear transform.
- Step 8. Invert the chromatic adaptation transform to compute R , G , and B and then X , Y , and Z .

16.13 IMPLEMENTATION GUIDELINES

Another improved feature of the CIECAM02 technical report (CIE 2004) are more detailed guidelines for implementation of the model. Several worked examples are provided along with examples of parameter settings. This

Table 16.3 Example CIECAM02 parameter settings for typical applications

Example	Ambient lighting in lux (cd/m ²)	Scene or device white luminance	L_A (cd/m ²)	Adopted white point	Surround
Surface color evaluation in a light booth	1000 (318.3)	318.30	63.66	Light booth WP	Average
Viewing self-luminous display at home	38 (12)	80	16	Between display and ambient WPs	Dim
Viewing slides in dark room	0 (0)	150	30	Between projector WP and E	Dark
Viewing self-luminous display in office	500 (159.2)	80	16	Between display WP and office illumination	Average

information is valuable to those interested in implementing the model in forward and reverse directions rather than simply understanding the concepts of its formulation. Table 16.3 illustrates some of the example parameter settings included in the report. The surround is considered average when the luminance of the surround white is greater than 20% of the scene, or image, white and dim when the surround luminance is less than 20%. A dark surround setting is used when the surround has essentially no luminance.

16.14 PHENOMENA PREDICTED

CIECAM02 can predict all the phenomena that can be predicted by CIECAM97s. It includes correlates of all the typical appearance attributes (relative and absolute) and can be applied over a large range of luminance levels and states of chromatic adaptation. Like CIECAM97s, CIECAM02 is not applicable to situations in which there is significant rod contribution to vision or at extremely high luminances in which cone bleaching might occur. It is appropriate to think of CIECAM02 as a simpler and better version on CIECAM97s. Example calculations for CIECAM02 are given in Table 16.4.

16.15 WHY NOT USE JUST CIECAM02?

If one is looking for an internationally agreed upon color appearance model with a relatively simple formulation that performs as well as, if not better, than any similar model at present, then CIECAM02 is the answer. There is

Table 16.4 Example CIECAM02 calculations

Quantity	Case 1	Case 2	Case 3	Case 4
X	19.01	57.06	3.53	19.01
Y	20.00	43.06	6.56	20.00
Z	21.78	31.96	2.14	21.78
X _W	95.05	95.05	109.85	109.85
Y _W	100.00	100.00	100.00	100.00
Z _W	108.88	108.88	35.58	35.58
L _A	318.31	31.83	318.31	31.83
F	1.0	1.0	1.0	1.0
D	0.994	0.875	0.994	0.875
Y _b	20.0	20.0	20.0	20.0
N _c	1.0	1.0	1.0	1.0
F _L	1.17	0.54	1.17	0.54
N _{bb} ,N _{cb}	1.0	1.0	1.0	1.0
h	219.0	19.6	177.1	248.9
H	278.1	399.6	220.4	305.8
H _C	78B 22G	100R	80G 20B	94B 6R
J	41.73	65.96	21.79	42.53
Q	195.37	152.67	141.17	122.83
s	2.36	52.25	58.79	60.22
C	0.10	48.57	46.94	51.92
M	0.11	41.67	48.80	44.54
a _C	-0.08	45.77	-46.89	-18.69
b _C	-0.07	16.26	2.43	-48.44
a _M	-0.08	39.27	-48.74	-16.03
b _M	-0.07	13.95	2.43	-41.56
a _s	-1.83	49.23	-58.72	-21.67
b _s	-1.49	17.49	2.93	-56.18

no scientific reason to prefer CIECAM97s over CIECAM02 and CIECAM02 is simpler to implement and use in practical settings. In some situations, the detailed knowledge and control of viewing conditions required to best take advantage of CIECAM02 might not be available. In such situations, simpler models might well suffice. In general the logical progression of color appearance models is to begin by simply using CIELAB. If CIELAB is found to be inadequate for the application, then a combination of CIELAB with a better chromatic adaptation model (like the CAT02 linear chromatic adaptation transform) would be the next logical step. If additional flexibility was required, a slightly more complex model like RLAB, or RLAB with the adaptation transform replaced with the CAT02 transform, would be most appropriate. Then, if further sophistication is required, CIECAM02 would be the best choice. Lastly, if CIECAM02 is not adequate for the given situation (such as when rod contributions are to be predicted), then the Hunt model would be the most comprehensive choice.

16.16 OUTLOOK

CIECAM02 represents a significant advance in color appearance models over the six years between its publication and the initial formulation of CIECAM97s. Immediately upon the publication of CIECAM97s, limitations were noted, suggestions for improvements were made, and a new CIE committee was formed to suggest improvements. Currently, no similar situations are arising with respect to CIECAM02. It appears that the time between CIECAM02 and the next CIE color appearance model will be significantly longer than six years. One reason for this is that this type of model seems to be predicting the available visual data to within experimental uncertainty. Thus there is no room for significant improvement until more precise (and accurate) experimental data become available or until vastly larger volumes of data are produced to allow improved prediction of the mean response. The cost and difficulty of collecting such data as well as inherent inter-observer variability make it unlikely that significant improvements in the available data will be obtained in the foreseeable future.

Instead, many researchers in the field of color appearance are turning to more complex viewing situations and deriving models with new and different capabilities. Such capabilities include computational prediction of spatial and temporal effects. These types of models were only just being considered when the first edition of this book was published, but are becoming more of a practical reality as the second edition is being produced. The concepts of such models and one example are described in Chapter 20. Perhaps such models are the direction color appearance modeling will move in the future. Meanwhile, it is likely that CIECAM02 will see significant practical adoption and use. It will be interesting to see the degree to which it is considered a practical success.

17

Testing Color Appearance Models

Chapters 10–16 described several color appearance models with little reference to data on the visual phenomena they are intended to predict. In contemplating the existence of this variety of color appearance models, it is logical to wonder just how well they work. Quantitative tests of the models are certainly required (as with any scientific theory, they must be supported by data); unfortunately far more has been published on the formulation of the models than their actual performance. There are several reasons for this. The first is the paucity of reliable data measuring observers' perceptions of color appearance. The second is that the models themselves have evolved at a rate that outpaced researchers' abilities to evaluate their performance. Fortunately, both of these situations continue to change. This chapter reviews some of the experimental work to test color appearance models and collect additional color appearance data for future model testing. This remains an active area of research and it is to be expected that additional tests (and model revisions) will continue to be published.

17.1 OVERVIEW

One might expect that the derivation of color appearance models of the sophistication presented in Chapters 10–16 would require extensive data. This is true; however, the data used to derive the models come from a long history of vision experiments, each aimed at one particular aspect of color appearance. These include the experiments described in Chapter 6 on color appearance phenomena. The models were then formulated to simultaneously predict a wide variety of these phenomena. In so doing, quite sophisticated models can be derived with little or no data that test the wide variety of predictions. To truly test the models, visual data scaling the appearance

attributes of brightness, lightness, colorfulness, chroma, and hue are required. Alternately, visual evaluations of the performance can be made for existent models.

A variety of tests of color appearance models have been performed. Unfortunately, none of these tests is completely satisfactory and the question of which model is best cannot be unequivocally answered for all situations. The various tests that have been performed can be classified into four general groups as described in the following sections:

- Qualitative tests of various phenomena
- Prediction of corresponding colors data
- Magnitude estimation of appearance attributes
- Direct psychophysical comparison of the predictions of various models.

Each of these types of tests contributes to the evaluation of models in a unique way and none is adequate, on its own, to completely specify the best color appearance model. There are also organized activities within the CIE technical committee structure aimed at the evaluation of color appearance models. These activities draw upon evaluations in each of the four groups described above with the ultimate aim to recommend models and procedures for color appearance specification.

17.2 QUALITATIVE TESTS

There are a variety of model tests that can be considered qualitative for one reason or another. A test is qualitative if the results show general trends in the predictions rather than providing numerical comparisons of various models. Such tests include

- Calculations showing that a particular appearance phenomenon can be predicted (e.g., colorfulness increases with luminance)
- Prediction of trends from historical data
- Comparisons with color order systems
- Abridged visual experiments on model features.

Nayatani *et al.* (1988) published an early example of qualitative evaluation of their color appearance model. They looked at two sets of data. The first was the predicted color appearance of Munsell samples under CIE illuminant A and the second was the evaluation of results from a color rendering experiment of Mori and Fuchida (1982). Their predictions for the Munsell samples showed that their model predicted the Helson–Judd effect under illuminant A while a von Kries transformation would not. Nayatani *et al.* followed this up with a brief visual experiment in which three observers (including the authors) observed a small Helson–Judd effect for samples viewed under an incandescent lamp. They also examined some color discrimination

observations that correlated better with results from their model than predictions made using a von Kries transformation. They also showed that the Nayatani *et al.* color appearance model made reasonable predictions of the Mori and Fuchida corresponding colors data. However, they did not compare these results with other models.

As illustrated in the Nayatani *et al.* (1988) study cited above, color order systems are often used to evaluate the performance of appearance models. The systems used are those based on color appearance (Munsell and NCS) as described in Chapter 5. In many cases when formulating a model, its authors will plot contours of Munsell hue, value, and chroma in order to evaluate the perceptual uniformity of the model.

Alternatively, contours of constant NCS hue, whiteness–blackness, and chromaticness can be examined. The assumption is that the color order systems have been constructed with accurate appearance scales. Thus, for example, a model should be able to predict that samples with constant Munsell hue have the same predicted hue and make analogous predictions for Value (lightness) and chroma. Many authors have included plots of Munsell or NCS contours along with the formulation of their models. Examples include Nayatani *et al.* (1987, 1990b), Guth (1991), Hunt (1995), and Fairchild and Berns (1993). In fact, the latest revision of the Nayatani *et al.* (1995) model was formulated to correct discrepancies in plots of Munsell hue and chroma contours at various value levels. Seim and Valberg (1986) provide a more quantitative analysis of the Munsell system in the CIELAB color space and propose alternative equations similar to those found in the Hunt model. Wyble and Fairchild (2000) performed quantitative analyses of the Munsell system in various color appearance models that helped lead to some of the improvements in CIECAM02.

Nayatani *et al.* (1990b) published an interesting comparison of the Hunt and Nayatani *et al.* models. This included plots of Munsell contours in the color spaces of each model as well as flow charts comparing the computational procedure for each model. While this work is interesting, at this point it is largely historical since both models have been revised significantly since it was published. Plots of Munsell and NCS contours do provide some insight into the performance and properties of various color appearance models; however, none of the published results include a quantitative comparison between the color order systems and color appearance models. For example, constant hue contours should plot as straight radial lines and constant chroma contours as concentric, evenly spaced circles. It would be possible to derive measures of how close the models come to producing these results; see Wyble and Fairchild (2000) for an example. Perhaps this has not often been done because the results would not be terribly impressive. Another reason is that the perceptual uncertainty of the color order systems is not well defined, making it difficult to know how good the predictions should be. Examination of the published results suggests that the models perform about equally well in these qualitative comparisons. This conclusion is confirmed by a study of constant-hue contours completed by Hung and Berns

(1995) in which extensive visual evaluations were made. Quantitative analysis by Hung and Berns (1995) showed that the observed constant hue contours were not adequately predicted by any color appearance model and that no single model was clearly superior. Moroney (2000a) and others have shown that more recent color spaces such as IPT, CIECAM97s, and CIECAM02 perform better for constant-hue predictions.

Hunt (1991b) provides an excellent example of qualitative evaluation of his appearance model. For example, Hunt (1991b) shows how the model predicts cone and rod saturation, the Stevens effect, the Hunt effect, and the effect of surround relative luminance on image contrast, as well as other effects. One fascinating demonstration that Hunt (1991b) predicts is the appearance of objects in a filtered slide. In a classic demonstration (Hunt 1995), a cyan filter is superimposed over a yellow cushion in a slide, resulting in the cushion appearing green. However, if the same filter is placed over the entire slide, the cushion retains much of its yellow appearance due to chromatic adaptation. This effect is strongest for projected slides, but can be observed in printed images as well (Hunt 1995). The effect is also simulated in Figure 17.1 with the filter being added over the banana. Hunt (1991b) shows that his model is capable of predicting this effect. It is worth noting that simpler models, including CIELAB and RLAB, are also capable of predicting this effect (Fairchild and Berns 1993).

Perhaps the most useful result of qualitative analysis of color appearance models is a summary of the various effects that can be predicted by each model. Table 17.1 provides such a summary. While Table 17.1 is useful to gauge the capabilities of each model, it is important to remember that it

Table 17.1 Color appearance phenomena predicted by various color appearance models. Check marks indicate that the model is capable of directly making the prediction

	ATD	CIELAB	LLAB	RLAB	Nayatani	Hunt	CIECAM
Lightness		✓	✓	✓	✓	✓	✓
Brightness	✓				✓	✓	✓
Chroma		✓	✓	✓	✓	✓	✓
Saturation	✓		✓	✓	✓	✓	✓
Colorfulness			✓		✓	✓	✓
Hue angle	✓	✓	✓	✓	✓	✓	✓
Hue			✓	✓	✓	✓	✓
Helson-Judd effect					✓	✓	
Stevens effect					✓	✓	✓
Hunt effect	✓		✓	✓	✓	✓	✓
Helmholtz-Kohlrausch effect	✓				✓	✓	
Bartleson-Breneman results			✓	✓		✓	✓
Discounting-the-illuminant			✓	✓		✓	✓
Incomplete adaptation				✓		✓	✓
Color difference		✓	✓	✓		✓	?
Others	✓				✓	✓	

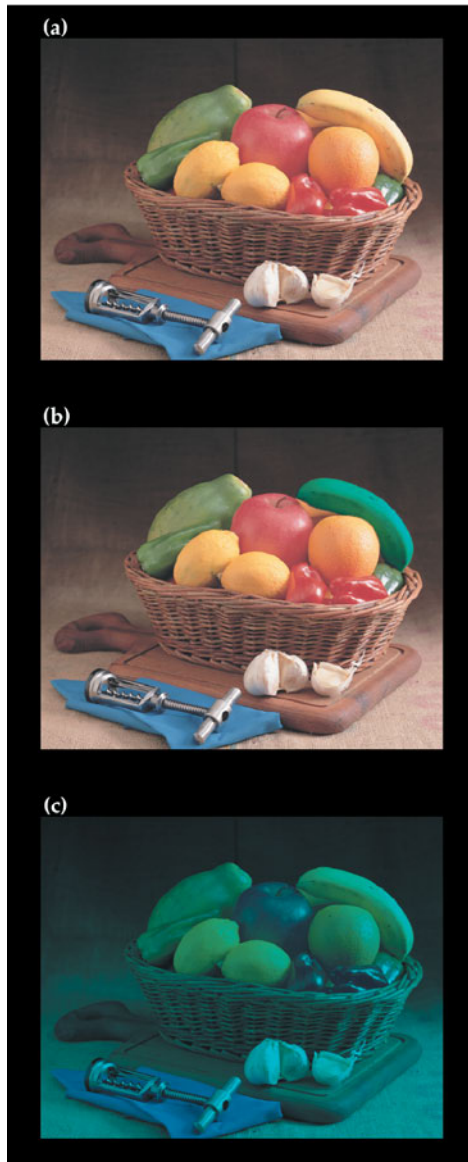


Figure 17.1 An illustration of chromatic adaptation. (a) Original image. (b) Simulation of a cyan filter placed over the yellow banana, resulting in the appearance of a green banana. (c) Simulation of the same cyan filter placed over the entire image. Note how the banana in (c) returns to a yellowish appearance despite being physically identical to the banana in (b). Original image part of the ISO SCID set

includes no information on how accurately each model can predict the various phenomena. This lack of information on accuracy is the most significant drawback of qualitative model tests and necessitates the additional tests described in the following sections.

17.3 CORRESPONDING COLORS DATA

Corresponding colors data were described in Chapter 8 with respect to the study of chromatic adaptation. In addition, corresponding colors data can be collected and analyzed for a wide range of color appearance phenomena in addition to simple chromatic adaptation. Corresponding colors are defined by two sets of tristimulus values specifying stimuli that match in color appearance for two disparate sets of viewing conditions. Recall that if the change in viewing conditions has an impact on color appearance, then the corresponding tristimulus values of the stimuli will be different in absolute value.

Corresponding colors data are used to test color appearance models by taking the tristimulus values for the first viewing condition and transforming them to the matching tristimulus values under the second viewing condition. The predicted corresponding colors can then be compared with visually observed corresponding colors to determine how well the model performs. The results are often analyzed in terms of RMS deviations between predicted and observed colors in either a uniform chromaticity space (e.g., $u'v'$) or a uniform color space, (e.g., CIELAB). Recall that Nayatani *et al.* (1990a) illustrated the important distinction between lightness–chroma and brightness–colorfulness matches. Complete color appearance models can be used to predict either type of match. The two types of matches will be different if there is a change in luminance level between the two viewing conditions in question.

One of the most extensive series of experiments measuring corresponding colors data for color appearance analysis was completed by the Color Science Association of Japan (CSAJ) and reported by Mori *et al.* (1991). Data from four experiments performed by CSAJ were summarized by Mori *et al.* (1991).

1. An experiment on chromatic adaptation from illuminant D65 to illuminant A simulators at an illuminance of 1000 lux. Judgements were made by 104 observers on 87 samples using a modified haploscopic matching technique.
2. An experiment that collected data consisting of measurements of the Hunt effect using five colored samples judged under illuminant D65 simulators at five different illuminance levels by 40 observers.
3. An experiment that collected data representing measurements of the Stevens effect using five neutral samples viewed under five different illuminance levels by 31 observers.
4. An experiment that examined the Helson–Judd effect for achromatic samples viewed under highly chromatic fluorescent light sources. These data represent one of the most extensive studies, with the largest numbers of observers, completed in the area of color appearance to date.

Unfortunately, Mori *et al.* (1991) reported only qualitative analyses of the experimental results. They showed plots of predicted and observed corresponding colors for the chromatic adaptation experiment and the Nayatani,

von Kries, and Hunt models. Mori *et al.* (1991) concluded that the Nayatani model made the best predictions. However, examination of their plots suggests that Hunt's model provides similar performance to it and the von Kries transform perhaps works better than both of them. They illustrated that the Nayatani *et al.* model could predict the Hunt effect data well, but they did not compare the results with predictions of the Hunt model. Similar analyses were performed for the Stevens effect and Helson–Judd effect data. The results showed a fairly small Stevens effect that was over-predicted by the Nayatani *et al.* model. The Helson–Judd effect, while observed in this experiment, was also over-predicted by the Nayatani *et al.* model. Further, quantitative analyses of these data have been carried out through CIE TC1-34 and are described later in the chapter.

Breneman (1987) collected a fairly extensive set of corresponding colors data for changes in chromatic adaptation and luminance level. These data were used to evaluate various chromatic adaptation transforms and color appearance models by Fairchild (1991a,b). The models were compared in terms of RMS deviations between observed and predicted results in the CIE 1976 $u'v'$ chromaticity diagram. The chromatic adaptation data were best predicted by the Hunt and RLAB models followed by the Nayatani and von Kries models. The CIELAB and CIELUV models performed the worst for these data. Breneman's data showed a small Hunt effect that was over-predicted by the Hunt and Nayatani *et al.* models and not predicted at all by the other models. The RMS deviations produced by of both sets of models are similar in magnitude, suggesting that making no prediction is as accurate as an over-prediction for these particular data.

Luo *et al.* (1991b) converted some of their magnitude scaling data (described in Section 17.4) to sets of corresponding colors for various changes in viewing conditions. They generated three sets of corresponding colors data for changes in chromatic adaptation from CIE illuminant D65 to D50, D65 to A, and D65 to white fluorescent, and then evaluated six different chromatic adaptation transforms using mean and RMS color differences in the CIELAB space. The results showed that the Bradford model, the basis of LLAB and CIECAM97s, performed best. The Hunt, Nayatani *et al.*, and CIELAB models performed similarly and almost as well. These were followed by the simple von Kries transformation and a transformation proposed by Bartleson. Additional results can be found in Kuo *et al.* (1995).

Braun and Fairchild (1997) performed an experiment in which observers were asked to adjust CRT-displayed images to match printed images viewed under a different white point. Matching images were obtained for five observers using two different images for white point changes from 3000 K to 6500 K and 9300 K to 6500 K. The data were analyzed by segmenting the images into meaningful object regions to avoid overly weighting large image areas. The corresponding colors were analyzed in terms of average and RMS CIELAB color differences. The results showed that RLAB, LLAB, and CIELAB best predicted the observed corresponding colors. The Hunt and Nayatani *et al.* models did not perform as well.

The above-mentioned studies illustrate the variety of corresponding colors experiments that have been completed. Unfortunately, a clear picture of relative model performance does not emerge from the analysis of these results. This is partly due to the fact that the models have changed, and new ones have emerged, since some of the results were published.

17.4 MAGNITUDE ESTIMATION EXPERIMENTS

Magnitude estimation experiments involve asking observers to directly assign numerical values to the magnitude of their perceptions. The utility of such experimental techniques was brought into focus by the classic study of Stevens (1961). Magnitude estimation experiments allow the rather direct measurement of the magnitudes of color appearance attributes such as lightness, chroma, and hue for various stimuli and viewing conditions. These data can then be used to evaluate various color appearance models and derive new models.

The most extensive series of experiments on the magnitude scaling of color appearance has been carried out through the Loughborough University of Technology Computer Human Interface (LUTCHI) Research Centre as published in a series of papers by Luo *et al.* (1991a,b, 1993a,b, 1995), the results of which have been summarized by Hunt and Luo (1994).

1. Luo *et al.* (1991a)

Six or seven observers were each asked to scale the lightness, colorfulness, and hue of between 61 and 105 stimuli presented in a series of 21 different viewing conditions. The viewing conditions varied in white point, medium, luminance level, and background. The results showed that the most significant influences on color appearance were background and white point. Other effects were not clearly present in the data. One reason for this is the intrinsically high uncertainty in magnitude estimation experiments. The uncertainty in the data was expressed in terms of coefficients of variation CV which can be thought of as percentage standard deviations. The overall CV values for intra-observer variability were about 13 for lightness, 18 for colorfulness, and 9 for hue. No color appearance models were evaluated in part I.

One problem with the LUTCHI studies is the rather unusual choice of appearance attributes that were scaled, lightness, colorfulness, and hue. The authors claim that colorfulness is more natural than chroma. However, chroma is the more appropriate attribute to scale with lightness. It is the attribute that observers normally associate with objects, and it does not require that the observers be taught its definition. At a single luminance level it is probably reasonable to assume that chroma and colorfulness are related by a simple scaling factor. However, there is no reason to believe that chroma and colorfulness are linearly related across changes in luminance.

2. Luo *et al.* (1991b)

The part one data were used to evaluate various color appearance and chromatic adaptation models. The models were analyzed by calculating CV values between the observed results and the model predictions. As an overall summary, the Hunt model performed best for lightness, followed by CIELAB and then Nayatani. For colorfulness, no model performed particularly well, but Hunt's model (and a version of Hunt's modified with respect to these data) performed slightly better than others. For hue, the Hunt model performed significantly better than the Nayatani *et al.* model. Other models were not tested for hue. These data were also used to formulate later versions of the Hunt model.

3. Luo *et al.* (1993a)

Additional data were collected to check previous results, extend the range of conditions, and include the scaling of brightness, and then used to test various models. Four observers took part in the scaling for collection of new data for a CIE illuminant D50 simulator at six different luminance levels. Analyses of the results showed that the Hunt model performed best overall. For lightness scaling, CIELAB performed nearly as well when the lowest luminance level was ignored. For colorfulness and hue scaling, the Hunt model performed substantially better than the Nayatani *et al.* model.

4. Luo *et al.* (1993b)

In this part they, extended their experimental technique to the evaluation of transmissive media including both projected transparencies and transparencies viewed on light boxes. Between five and eight observers took part in these experiments, scaling lightness, colorfulness, and hue for a total of 16 different sets of viewing conditions. They found that the Hunt model did not perform as well as in previous experiments and proposed some changes that have been incorporated in the latest version of the model. CIELAB performed very well for these data, in fact better than the unmodified Hunt model. The Nayatani *et al.* model performed worse than both CIELAB and the unmodified Hunt model. The Hunt model with modifications based on the experimental data performed best overall.

5. Luo *et al.* (1995)

The phenomenon of simultaneous contrast was specifically examined. Five or six observers scaled lightness, colorfulness, and hue of samples in systematically varied proximal fields presented on a CRT display. The results showed that all three dimensions of color appearance are influenced by induction (as expected). Evaluation of the Hunt model (the only model capable of directly accounting for simultaneous contrast) showed that it did not perform well and required further modification.

Hunt and Luo (1994) summarize the first four parts of the LUTCHI experiments and how the results were used to refine the Hunt color appearance model. Overall, they show that the Hunt model predicts the hue results with

CVs between 7 and 8 while the inter-observer variability CV is 8. For lightness, the model CVs range from 10 to 14 with the inter-observer variability of 13. For colorfulness, the model CVs are around 18 with inter-observer variability of 17. Thus they conclude that the Hunt model is capable of predicting the experimental results as well as the results from one observer would predict the mean. This is impressive, and certainly a good result, but it should be kept in mind that these data are not independent of the model formulation.

Many of the results of the LUTCHI experiments were also contributed to the efforts of CIE TC1-34 in order to allow the evaluation of more recent color appearance models and the formulation of CIECAM97s. The results of these analyses are described in Section 17.6. Unfortunately, the data themselves have been deemed proprietary by the research sponsors and were not been released for a number of years. Ultimately these data were made publicly available and used as one of the data sets for development of CIECAM02.

17.5 DIRECT MODEL TESTS

One way to overcome the limited precision of magnitude estimation experiments is to take advantage of more refined psychophysical techniques to evaluate model performance. One such technique involves paired comparison experiments in which observers view two stimuli at a time and simply choose which is better. The results are then analyzed using the law of comparative judgements to derive an interval scale and associated uncertainties. To evaluate color appearance models in this fashion, one must begin with an original stimulus (or image) in one set of viewing conditions and then calculate the corresponding stimulus (or image) for the second set of viewing conditions using each model to be tested. The observers then look at each possible pair of stimuli and choose which is a better reproduction of the original in its viewing condition. The interval scale results are then used to measure the relative performance of each model. The significant drawback of this approach is that the results cannot be used to derive new models and are limited to the models available and included at the time of the experiment. An extensive series of these experiments has been conducted at the Munsell Color Science Laboratory at Rochester Institute of Technology and summarized by Fairchild (1996). The results of these and other experiments are described below.

Fairchild and Berns (1993) described an early and simplified form of these experiments to confirm the utility of color appearance models in cross-media image reproduction applications. They examined the transformation from prints viewed under either illuminant A or D50 simulators to CRT displays with a D65 white point and various backgrounds using a simple successive binocular viewing technique. Six different images were used and 14 observers took part in the experiment. Comparisons were made between no model (CIE XYZ reproduction), CIELAB, and RLAB. The results indicated that observers

chose the RLAB reproduction as the best nearly 70% of the time, the CIELAB image about 30% of the time, and the XYZ image almost never. This result showed that a color appearance transformation was indeed required for these viewing conditions and that the RLAB model outperformed CIELAB.

Kim *et al.* (1993) examined the performance of eight color appearance transformations for printed images viewed under different viewing conditions. Original prints were viewed under a CIE illuminant A simulator and reproductions calculated using the various appearance transformations were viewed under CIE illuminant D65 simulators at three different luminance levels. A paired-comparison experiment was completed and an interval scale was derived using the law of comparative judgements. A successive-Ganzfeld haploscopic viewing technique (Fairchild, Pirrotta, and Kim 1994) was used with 30 observers. The results showed that the Hunt, RLAB, CIELAB, and von Kries models performed similarly to one another and significantly better than the other models. The Nayatani *et al.* model performed worse than each of the above models. Three models performed significantly worse and were not included in further experiments. These included CIELUV, LABHNU2, and a proprietary model. The Nayatani *et al.* model performed poorly due to its prediction of the Helson–Judd effect resulting in yellowish highlights and bluish shadows in the reproductions. The Helson–Judd effect cannot be observed for complex stimuli under these viewing conditions. CIELUV and the others performed poorly due to their intrinsically flawed chromatic adaptation transformations.

Pirrotta and Fairchild (1995) performed a similar experiment using simple stimuli on gray backgrounds rather than images. The first phase of this study was a computational comparison of the various models in order to find the stimuli and viewing conditions for which the models differed the most such that the visual experiments could concentrate on these differences. It is useful to examine a few of these results. Figure 17.2 shows the CIELAB coordinates of corresponding colors under CIE illuminant A at 1000 lux for neutral Munsell samples of values 3, 5, and 7 viewed under CIE illuminant D65 at either 1000 or 10 000 lux. The points labeled F illustrate the incomplete adaptation predicted by the Fairchild (1991b) model used in RLAB. The points labeled N show the prediction of the Helson–Judd and Stevens effects incorporated in the Nayatani *et al.* model. The points labeled H show the prediction of the Stevens effect for the condition with a luminance change according to the Hunt model. Figure 17.2 illustrates the extreme prediction of the Helson–Judd effect for illuminant A according to the Nayatani *et al.* model.

Figure 17.3 illustrates the wide range of corresponding color predictions for a 5PB 5/12 Munsell sample under the same viewing conditions. One should note the extreme differences in the predictions of the various models as the scales of the plots in Figure 15.3 encompass 50 CIELAB units. The Pirrotta and Fairchild (1995) visual experiment used a paired-comparison technique with 26 observers, 10 stimulus colors, and a change in viewing conditions from an illuminant A simulator at 76 cd/m^2 to an illuminant D65

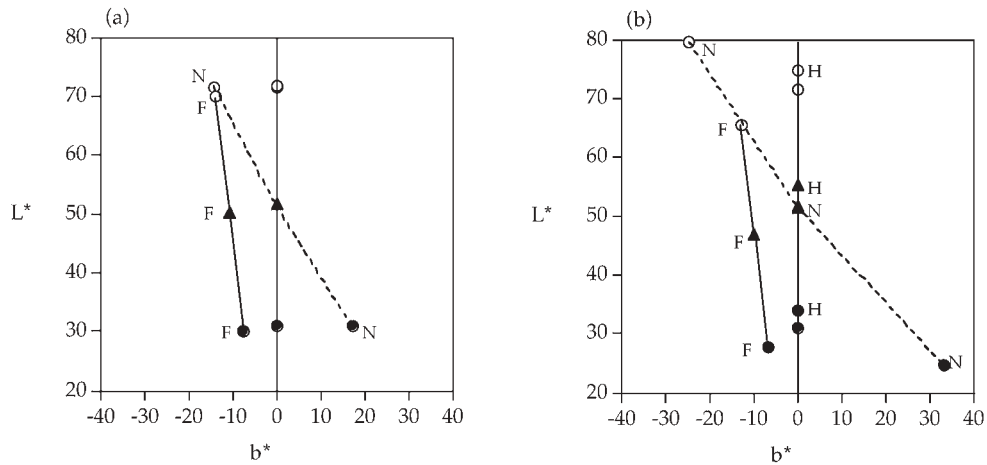


Figure 17.2 Illustration of differences between predictions of various appearance models represented in the CIELAB L^* - b^* plane. Neutrals at (a) 1000 lux and (b) 10 000 lux

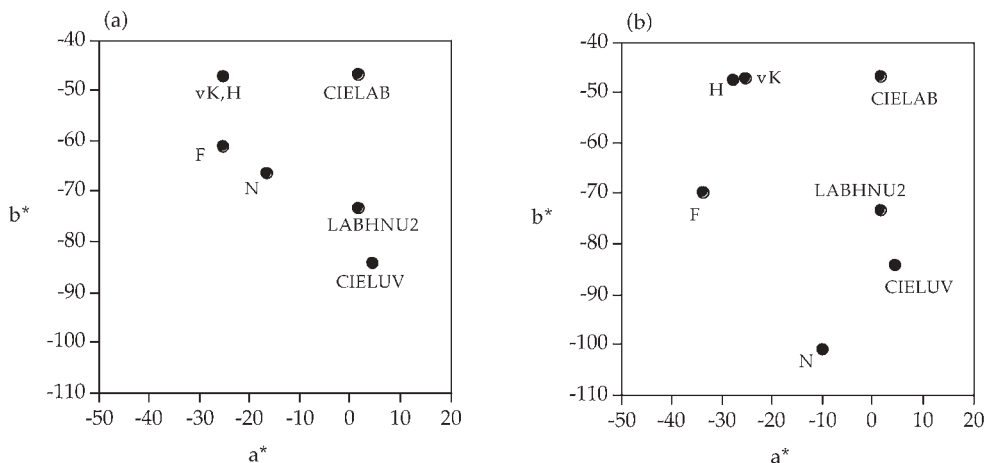


Figure 17.3 Illustration of differences between predictions of various appearance models represented in the CIELAB a^* - b^* plane. 5PB 5/12 at (a) 1000 lux and (b) 10 000 lux

simulator at 763 cd/m^2 . The results showed that the Hunt model performed best. Von Kries, CIELAB, and the Nayatani *et al.* model performed similarly to one another, but not as well as the Hunt model. CIELUV and the Fairchild (1991b) model performed significantly worse. These results led to the revision of the adaptation model incorporated in RLAB (Fairchild 1996).

Braun *et al.* (1996) investigated viewing techniques and the performance of color appearance models for changes in image medium and viewing

conditions. They examined the reproduction of printed images viewed under CIE illuminant D50 and A simulators on a CRT display with a CIE illuminant D65 white point. Fifteen observers took part in this experiment using five different viewing techniques. It was concluded that a successive binocular viewing technique with a 60 second adaptation period provided the most reliable results. Interestingly, a simultaneous binocular viewing technique, common in many practical situations, produced completely unreliable results. The experiment utilized five different pictorial images with a variety of content. The result showed significant differences in the performance of each model tested. The order of performance from best to worst was RLAB, CIELAB, von Kries, Hunt, and Nayatani *et al.*

Fairchild *et al.* (1996) performed a similar experiment on the reproduction of CRT displayed images as projected 35 mm slides. The CRT display was set up with both illuminant D65 and D93 white points at 60 cd/m² and viewed in dim surround. The projected image had a 3900 K white point at 109 cd/m² with a dark surround. Fifteen observers completed the experiment with three different pictorial images. The RLAB model performed best, followed by CIELAB and von Kries with similar performance and then the Hunt model. The Nayatani *et al.* model was not included in the final visual experiments since it produced clearly inferior images due to its prediction of the Helson-Judd effect and the limited number of images that could be included in the experiment.

Braun and Fairchild (1997) extended the experiments of Braun *et al.* (1996) to a wide variety of viewing conditions. Ten different sets of viewing conditions were investigated using between 14 and 24 observers. The viewing conditions varied in white point, luminance level, background, and surround. Overall, the RLAB model performed best. For changes in white point, CIELAB and a von Kries transformation also performed well. The Hunt and Nayatani *et al.* models did not perform as well as those three. Similar results were obtained for changes in luminance level. For changes in background, the Hunt model performed poorly, apparently because it over-predicted the effect for complex images. The models that did not account for changes in background performed better. This result was as expected since the background of an image does not coincide with what is normally considered the background of a stimulus (i.e., an image element). For changes in surround, RLAB performed worst with the Hunt model performing poorly as well. These were the only two models that accounted for the surround change and, while they were predicting the correct trend, both models over-predicted the effect for these viewing conditions.

Braun and Fairchild (1997) extended the corresponding colors experiment described in Section 15.3 by including the results of the image matching technique in a paired comparison experiment with other color appearance models. In this research, a paired comparison experiment was carried out that included model predictions as well as the matching images generated by the observers, and statistical linear transformations between white points derived from the match data. Five observers took part in the image matching

experiment and 32 were used in the paired-comparison experiment. The results showed that the RLAB model produced a matching image that was as good as the image produced by observers and the statistical models. The CIELAB, von Kries, and Hunt models did not perform as well as RLAB.

Lo *et al.* (1996) and Luo *et al.* (1996) presented the results of paired comparison experiments for the reproduction of printed images on CRT displays. They evaluated five different changes in white point at constant luminance using nine to 18 observers. The results show that the CIELUV model performs significantly worse than all of the other models tested. The other models performed similarly to one another, with the LLAB model performing slightly better for adaptation from illuminant A to illuminant D65.

There are other similar experiments that have been more recently completed or are underway in a variety of laboratories. The results of these ongoing experiments and those described above have been used by various CIE committees in the formulation, testing and revision of color appearance models. To date this type of research has validated the CIE models as consistently among the best, if not the best, for various applications.

17.6 CIE ACTIVITIES

It is certainly difficult to digest all the above results and come up with a single answer to the question of which color appearance model is best or which should be used in a particular application. There are too many experimental variables in addition to ongoing refinement of the models to draw conclusions from the literature alone. These are some of the reasons why there are a large number of published appearance models and no international consensus on a single model for various applications. The CIE is actively addressing these issues through the activities of three of its technical committees and reporterships, as described below.

TC1-34, Testing Colour-Appearance Models

CIE Technical Committee 1-34, Testing Colour Appearance Models, was established to evaluate the performance of various models for the prediction of color appearance of object colors. TC1-34 published guidelines for co-ordinated research on testing color appearance models (Fairchild 1995a) that outline its plan of work with the intention of motivating researchers to perform additional model tests. In addition, TC1-34 collected various sets of data and test results and completed additional tests. Those results were never published in a CIE technical report on the committee's progress due to disagreements within the committee on interpretation of the results. A summary of the additional C1-34 analyses on the CSAJ, LUTCHI, and RIT experiments discussed previously follows. Ultimately, CIE TC1-34 was assigned the task of formulating a CIE color appearance model. That task

was completed with the creation and publication of CIECAM97s (see Chapter 15 and CIE 1998).

The TC1-34 analyses of the CSAJ data included calculations of RMS deviations in CIELAB space for the chromatic adaptation, Stevens effect, and Hunt effect data. For the chromatic adaptation data, the Hunt, RLAB, and CIELAB models perform similarly to one another and better than the others. They are followed, in order of performance, by the Nayatani *et al.*, LABHNU, and CIELUV models. For the Stevens effect data, the Hunt model performs best, followed by RLAB, CIELAB, LABHNU, and CIELUV, which perform identically since they predict no effect. The Nayatani *et al.* model performs worst since it over-predicts the effect. For the Hunt effect data, the Hunt model performs best, the Nayatani *et al.* next, followed by the models that do not predict any effect (RLAB, CIELAB, LABHNU, and CIELUV).

Additional analyses of the LUTCHI data contributed to CIE TC1-34 show that the Hunt model performs best, followed by RLAB, CIELAB, and then finally the Nayatani *et al.* model. The TC1-34 summary of the RIT direct model tests shows differing results for images and simple stimuli. For images, the Hunt, CIELAB, and RLAB models perform similarly and best, followed by Nayatani *et al.* and LABHNU in a tie, and then by CIELUV with the worst performance. For simple stimuli, the Hunt model performed best, the CIELUV model worst, and the others performed similarly in between those two. An overall ranking of the TC1-34 analyses results in the following ordering of model performance: Hunt, RLAB, CIELAB, Nayatani *et al.*, LABHNU, and CIELUV. Analyses of the LLAB model for all of the data have not been completed, but it performs better than the Hunt model for the LUTCHI data and is likely to also do well on the other data.

CIE TC1-34 concluded that no one or two of the published color appearance models could be recommended for general use. There were a variety of reasons for this. One of the most significant was that the models were still evolving and more tests were required to make strong conclusions. To this end, TC1-34 turned formulating a CIE color appearance model that incorporated the best features of the published models while avoiding their various pitfalls. That model, CIECAM97s, was recommended by the CIE for general use to promote uniformity of practice and further evaluation to promote the future development of an even better model. Ultimately this work led to the formulation of CIECAM02. TC1-34 was disbanded successfully after the publication of CIECAM97s.

TC1-27, Specification of Colour Appearance for Reflective Media and Self-luminous Display Comparisons

CIE Technical Committee 1-27 was established to evaluate the performance of various color appearance models in CRT-to-print image reproduction. TC1-27 has also published a set of guidelines for coordinated research (Alessi 1994). The various experiments of Braun *et al.* and Lo *et al.* described in Section 15.5 represent contributions to the activities of TC1-27. Addi-

tional experiments are being carried out in three or four other laboratories that will be contributed to TC1-27. It is expected that TC1-27 will collect the various results, summarize them, and prepare a progress report within the next few years. This committee worked in conjunction with CIE TC1-34 with respect to the evaluation of CIECAM97s.

TC1-33, Color Rendering

As described in Chapter 18, the CIE procedure for calculating a color rendering index for light sources is based on an obsolete color space. CIE Technical Committee 1-33 was established to formulate a new procedure for calculating a color rendering index for light sources. There are two aspects to this problem. The first is the specification of a calculation procedure and the second is the selection of a color space in which to do the calculations. A color appearance model is necessary since color rendering indices must be compared for light sources of various colors. TC1-33 developed new procedures and published a closing report (CIE 1999), but did not arrive at a new recommendation.

TC1-52, Chromatic Adaptation Transform

TC1-52 was established to formulate a chromatic adaptation transform that could be used, independent of a given color appearance model. It collected and evaluated various data sets and transforms, but failed to come to a single recommendation since multiple models performed equivalently. The most logical choice, to simply use the chromatic adaptation transform in CIECAM02, could not be agreed upon by the committee. A final report of the TC1-52 analyses and results was published (CIE 2003).

R1-24 Color Appearance Models

Upon closure of TC1-34, CIE Division 1 assigned a reporter on color appearance models. The task of a reporter is to keep track of developments in a technical area and make recommendations to the CIE if it appears that a new TC should be formed. This reportership was recently concluded since all of the relevant CIE activity on color appearance models was taking place in TC8-01 and it was reaching conclusion by publishing a new model, CIECAM02.

TC8-01, Color Appearance Modeling for Color Management Applications

TC8-01 has been a very productive technical committee and ultimately created the latest CIE color appearance model, CIECAM02 (see Chapter 16 and

CIE 2004). The committee also performed a variety of model tests that are summarized in a number of papers including those by Fairchild (2001), Li *et al.* (2002), and Moroney (2002); it has recently completed its activities and closed successfully.

TC8-04, Adaptation Under Mixed Illumination Conditions

The work of TC8-04 examines techniques to estimate the state of chromatic adaptation when multiple illumination conditions exist (e.g., a self-luminous display in an office environment that has illumination of a different color than the display white point). A technical report will be forthcoming from this committee in 2004 or 2005 and should provide some practical guidance for appearance predictions in such situations.

TC8-08, Testing of Spatial Color Appearance Models

One future direction for color appearance models is more systematic and automatic modeling of the spatial properties of human vision. This is conceptually described in Chapter 20. TC8-08 was formed in 2003 to make recommendations on how to best psychophysically evaluate such models for applications such as the rendering of high-dynamic-range images.

R8-05 Image Appearance

Related to spatial appearance models is the new general class of models referred to as image appearance models (see Chapter 20). A reportership has been established in 2003 to monitor progress in this new field and make recommendations for the formation of a TC if progress warrants CIE consideration for recommending a single model. It is not expected that these models would reach the level of a CIE recommendation for many years. It is reasonable to say that the state of image appearance models in 2003 is similar to the state of color appearance models 20 years earlier.

R8-06, Results of CIECAM02

With the successful closure of TC8-01, a new reportership has been established to monitor the application and testing of CIECAM02 and make recommendations for the creation of a new TC should the published results indicate need to investigate further improvements in color appearance modeling. There are no immediate indications that revisions to CIECAM02 will come as quickly as those to CIECAM97s.

17.7 A PICTORIAL REVIEW OF COLOR APPEARANCE MODELS

No sets of equations or lists of RMS deviations or coefficients of variation can truly communicate the differences among the various color appearance models. To appreciate these differences it is useful to view images that have been calculated using the various models. Figures 17.4–17.6 illustrate the predictions of various historical models (Fairchild and Reniff 1996). While the models included are now somewhat out of date, the images still provide useful context in comparing the various formulations. These figures cannot be generally used to indicate which models are best. They should just be considered a display of the relative performance of the various models for these types of predictions. With such a consideration in mind, the viewing conditions for these figures are not critical (although a high-luminance, D65 simulator would be ideal). Figure 17.4 illustrates the images viewed under illuminant D65 that would be predicted as matches to an original image viewed under CIE illuminant A for 14 different color models. The models include CIE XYZ to illustrate the original image, CIELAB, CIELUV, LAB-HNU2 (Richter 1985), von Kries, spectrally sharpened von Kries (Drew and Finlyason 1994), ATD, Nayatani *et al.*, Hunt (discounting), Hunt (no discounting), Hunt (incomplete adaptation, no Helson–Judd effect), RLAB (discounting), RLAB (partial discounting), and RLAB (no discounting).

There are several features to note in this set of images:

- The XYZ image shows a rendering of the original illuminant A image data with no adaptation model.
- The hard-copy versions of RLAB and Hunt are very similar to the von Kries model in this situation. These produce what have been found to be generally the best results in experiments completed to date.
- The LLAB model produces more saturated reddish hues due to the characteristics of its ‘cone responses’ and a bluish hue shift due to its nonlinear adaptation model for the blue channel.
- CIELAB produces hue shifts (in comparison with von Kries *et al.*), particularly noticeable in the sky and grass colors, due to its ‘wrong von Kries’ adaptation model.
- Incomplete adaptation can be noted by the yellowness of the RLAB soft-copy image, along with the intermediate level of adaptation in the RLAB slide image.
- The Hunt soft-copy image includes the Helson–Judd effect (yellow highlights and blue shadows), which can be seen even more strongly in the Nayatani *et al.* image.
- The Hunt slide image is more similar to the RLAB soft-copy image.
- The ATD model also predicts incomplete levels of adaptation due to the nature of its formulation that treats stimuli in a more absolute, rather than relative, sense.
- The spectrally sharpened von Kries transform produces highly saturated reddish hues. This is to be expected from the ‘color-constancy-preserving’ nature of sharpened responsivities.



Figure 17.4 Comparison of the predictions of various appearance models for change in chromatic adaptation from Illuminant A to Illuminant D65. Original image data represents reproduction of tristimulus values with no adjustment for adaptation. Original images: Portland Head Light, Kodak Photo Sampler PhotoCD, © 1991, Eastman Kodak; Picnic, Courtesy Eastman Kodak; Macbeth ColorChecker® Color Rendition Chart

- The CIELUV and LABHNU2 models produce unusual hue shifts due to their subtractive adaptation models. In fact, they produce predictions outside the gamut of physically realizable colors if a D65-to-A transformation is performed rather than the A-to-D65 transformation illustrated.



Figure 17.5 Comparison of the predictions of various appearance models for change in luminance from illuminant D65 at 100 cd/m² to illuminant D65 at 10 000 cd/m². Original image data represents reproduction of tristimulus values with no adjustment for luminance and therefore the predictions of all models that do not account for luminance level changes. See Figure 17.4 caption for image credits

Figure 17.5 illustrates the changes predicted for changes in adapting luminance from 100 cd/m² to 10 000 cd/m² with a constant D65 white point. These predictions are presented for the models with luminance dependencies (ATD, LLAB, Nayatani *et al.*, Hunt, and RLAB) in addition to a single image representing all of the other models. The original image was ‘gammut compressed’ to allow all of the model predictions to remain within gamut. The RLAB model has very little luminance dependency and therefore produces an image very similar to the original. The Hunt and Nayatani *et al.* models produce images of lower contrast. This is to be expected according to the Hunt and Stevens effects. These low-contrast images would appear to be of higher contrast when viewed at a high luminance level. The Nayatani *et al.* model predicts a larger luminance-dependent effect than the Hunt model. The ATD model makes the opposite prediction. Since it is based on absolute rather than relative signals, the ATD model predicts that a brighter, higher-contrast image will be required at the higher luminance levels. This prediction is incorrect.



Figure 17.6 Comparison of the predictions of various appearance models for change in surround relative luminance from Illuminant D65 with an average surround to Illuminant D65 with a dark surround. Original image data represents reproduction of tristimulus values with no adjustment for surround and therefore the predictions of all models that do not account for surround changes. See Figure 17.4 caption for image credits

Figure 17.6 shows predictions for a change in surround from average to dark at a constant D65 white point for the surround-sensitive models (LLAB, Hunt, and RLAB) in addition to a single image representing all of the other models. All three models illustrate the increase in contrast required for image viewing in a dark surround. The LLAB and RLAB models have similar predictions, with the RLAB model predicting a bit stronger effect than the LLAB model. The Hunt model uses functions with additive offsets to predict the surround-dependent contrast changes. These offsets force some dark colors to have predicted corresponding colors with negative tristimulus values. Since this is physically impossible, pixels with such colors have been mapped to black. This illustrates one practical limitation of using the Hunt model for changes in surround.

18

Traditional Colorimetric Applications

Given all the effort put into the formulation, evaluation, and refinement of color appearance models, it is natural to wonder if they have practical application beyond the natural scientific curiosity that has driven much of the historical research on color appearance phenomena. In recent years, it has been the development of technology, and thus applications, that has really pushed the scientific investigation of color appearance and development of models. These applications can be divided into two general categories:

1. Image reproduction, which is the subject of Chapter 19.
2. The area of color measurement and specification, the subject of this chapter.

Colorimetry has steadily evolved over the past century. For many applications, simple tristimulus (XYZ) colorimetry or CIELAB-type color difference specifications are sufficient. However, there are some applications in the traditional fields of colorimetry that require further evolution. A few of these are discussed in this chapter.

18.1 COLOR RENDERING

Color rendering refers to the way in which various light sources influence, or ‘render,’ the color appearance of objects. For example, it is possible for two light sources to be of the same color while one is a natural daylight and the other is a fluorescent source made up of two narrow-band phosphors that

happen to add together to make the same white. While the color of the two sources will match, the appearances of objects illuminated by these two sources will differ tremendously. This phenomenon is obviously important in the engineering of artificial illumination and the choice of light sources for various installations. If illumination was specified strictly on its efficiency, or its efficacy, the appearance of objects in our environment would be quite disturbing. To aid in this application, the CIE has defined a color rendering index as a measure of the quality with which a light source renders the colors of objects.

Current Techniques and Recommendations

The current CIE recommended techniques for calculation of color rendering indices are described in CIE Publication 13.3 (CIE 1995a). Light sources are evaluated relative to reference illuminants, which are defined to be the CIE D-series of illuminants for correlated color temperatures greater than or equal to 5000 K and Planckian radiators for correlated color temperatures less than 5000 K. The reference illuminant is chosen such that it has the same correlated color temperature as the test source. Differences in color between the test source and reference illuminant are accounted for using a von Kries-type chromatic adaptation transform. The CIE technique defines a special color rendering index according to Equation 18.1.

$$R_i = 100 - \Delta E_i \quad (18.1)$$

The color difference calculation ΔE_i is based on the Euclidean distance between the color of the sample under the test and reference sources in the now obsolete CIE $U^*V^*W^*$ space. A general color rendering index R_a is defined as the average of the special color rendering indices for eight specified Munsell samples. Examples of general color rendering indices for various light sources are given in Table 18.1.

Table 18.1 Example values of color rendering indices

Source	R_a
Tungsten halogen	100
Illuminant D65	100
Xenon	93
Daylight fluorescent	92
Cool white fluorescent	58
Tri-band fluorescent	85
High pressure sodium	25
Mercury	45
Metal halide	80

Application of Color Appearance Models

The fundamental question in the specification of color rendering properties of light sources is the specification of the appearance of colored objects under different light sources. In some cases, it is necessary to compare the appearance of objects under sources of different colors. It might also be of interest to compare the rendering properties of sources at different luminance levels. To make comparisons of color appearance across changes in illumination color and luminance level, an accurate color appearance model is required. Thus, given appropriate standard references, one would be able to compare the quality of color rendering of a tungsten source with that of a daylight source and have meaningful results.

Future Directions

While there is certainly room for improved measures of color rendering based on an accurate color appearance model, the current status of color appearance models precludes a large change in the capabilities of an index. Currently, CIE Technical Committee 1-33, Colour Rendering, proposed some revised procedures for the specification of color rendering. The first step was to define a new procedure for calculation, independent of the color space used.

That procedure, using the CIELAB color space combined with an improved chromatic adaptation transform (originally the Nayatani *et al.* nonlinear transform was considered, but the CAT02 transform would be a better current solution), would be an improvement over the current color rendering index.

With the current type of color rendering index, in which sources are only compared with a standard illuminant of the same correlated color temperature, the color appearance model is not being used for a large change in chromatic adaptation. Thus it is doubtful whether any color appearance model would be significantly better than any other, including CIELAB, for this calculation. Only when a more sophisticated technique for specifying color rendering across large changes in light source color and/or luminance level is formulated will a more complicated color appearance model be required.

18.2 COLOR DIFFERENCES

The measurement of color differences has wide application in a variety of industries. Such measurements are required to set and maintain color tolerances for the production and sale of all colored materials. Ideally, one would be able to take a metric of color difference, such as CIELAB ΔE_{ab}^* , and consider it as a ratio scale of perceived color differences. This would require that

color differences of the same perceived magnitude have the same ΔE_{ab}^* for all areas of color space. Another requirement would be for the perceptions of color differences to scale linearly with measured ΔE_{ab}^* . A third desirable feature would be for ΔE_{ab}^* values measured under one illuminant to be perceptually equal to ΔE_{ab}^* values measured under any other illuminant such that color differences could be directly compared across different light sources. It has been well established that the CIELAB color space is not uniform for the measurement of color differences and does not meet any of the above requirements. In fact, this might not be possible in any Euclidean color space.

Current Techniques and Recommendations

The weaknesses of the simple CIELAB ΔE_{ab}^* formula have been addressed both within and outside CIE activities. For example, the CMC color difference formula is designed to address some of the nonuniformities in the CIELAB space in order to make color difference measurements in one region of color space equivalent to measurements in other regions of color space. CIE Technical Committee 1-29 investigated the CMC and other equations as possible refinements of the CIELAB ΔE_{ab}^* formula. They concluded that the CMC color difference equation was more complex than warranted by the available visual data, and they created a simplified formula known as CIE ΔE_{94}^* (CIE, 1995). The ΔE_{94}^* equations are specified in Equations 18.2–18.5.

$$\Delta E_{94}^* = \left[\left(\frac{\Delta L^*}{k_L S_L} \right)^2 + \left(\frac{\Delta C_{ab}^*}{k_C S_C} \right)^2 + \left(\frac{\Delta H_{ab}^*}{k_H S_H} \right)^2 \right]^{1/2} \quad (18.2)$$

$$S_L = 1 \quad (18.3)$$

$$S_C = 1 + 0.045 C_{ab}^* \quad (18.4)$$

$$S_H = 1 + 0.015 C_{ab}^* \quad (18.5)$$

C_{ab}^* in Equations 18.4 and 18.5 refers to the CIELAB chroma of the standard sample of the color difference pair or, alternatively, to the geometric mean of the two chroma values. Parametric factors, k_L , k_C , and k_H , are introduced to correct for variation in perceived color difference caused by certain experimental variables such as sample size, texture, separation, etc. Under reference conditions the parametric factors are all set to 1.0. Reference conditions are defined as follows:

Illuminant: CIE illuminant D65 simulator

Illuminance: 1000 lux

Observer: normal color vision

Viewing mode: object

Sample size: greater than 4° visual angle

Sample separation: minimal, direct edge contact

Color difference magnitude: 0–5 CIELAB units

Structure: visually homogeneous.

The reference conditions of the ΔE^*_9 equations illustrate the limitations of the CIELAB space for the specification of color appearance. These are the areas in which it might be possible for a color appearance model to make a contribution to the specification of color differences. More recently (CIE 2001) the CIE has recommended a substantially more complex, empirical color difference equation based upon the CIELAB color space, referred to as DE2000. The DE2000 equation could legitimately be considered to complex, with unreasonable implied precision, for the available perceptual data. Thus, the ΔE^*_9 equations, are often a more practical and reasonable choice.

Application of Color Appearance Models

In the area of color difference specification, color appearance models could be used to incorporate some of the parametric effects directly into the equation. For example, an accurate color appearance model could incorporate the effects of the background and luminance level on color difference perception. A color appearance model would also make it possible to directly compare color differences measured for different viewing conditions. This has applications in the calculation of indices of metamericism, as described below. Color appearance models would also make it possible to calculate color differences between a sample viewed in one condition and a second sample viewed in another different conditions. This could be useful for critical colors such as those on warning signs or corporate trademarks.

It is reasonable to expect that a color difference equation could be optimized in a color appearance space, like CIECAM02, with performance equal to, or better than, equations like ΔE^*_9 and DE2000. Recently, Li *et al.* (2003) have shown this to be the case.

Future Directions

Currently there is little activity aimed at incorporating color appearance models beyond CIELAB into practical color difference specification. Perhaps this is because of the effort already invested in fine-tuning CIELAB within various industries. Instead, research activity (which is not abundant) is aimed at further refining equations within CIELAB, such as DE2000 and ΔE^*_9 , and defining the influence of parametric effects such as gloss, texture, sample separation, sample size, etc. Also, the majority of effort in the formulation of color appearance models has been in the area of chromatic

adaptation transforms, and little attention has been paid to color difference specification within the color appearance spaces. The notable historical exception is the formulation of the LLAB space (Luo *et al.* 1996) in which color appearance and color difference were treated simultaneously and the recent efforts by Li *et al.* (2003) to derive similar equations in CIECAM02. Also, the RLAB space (Fairchild 1996) has been formulated to preserve the CIELAB spacing such that CIE color difference formulas such as ΔE_{94}^* could still be used.

Another interesting future direction for color difference specification is the incorporation of the spatial characteristics of human visual performance into the difference metric such that the relative sensitivity to color variations of various spatial frequencies is appropriately treated. Examples of this type of metric can be found in the work of Maximus *et al.* (1994), Zhang and Wandell (1996), and Johnson and Fairchild (2003a,b). Chapter 20 discusses future directions for these ideas.

18.3 INDICES OF METAMERISM

Metamerism, the fact that two stimuli can match in color while having disparate spectral power distributions, is both a great benefit and severe detriment to a variety of industries. Techniques to quantify the degree of metamerism for various stimuli are of significant value. There are two types of metamerism to be measured:

1. Illuminant metamerism
2. Observer metamerism

Measures of the degree of metamerism for specific stimuli are called indices of metamerism.

Illuminant metamerism is generally of most concern. It occurs when two objects match in color for one illuminant, but mismatch for a second illuminant. This happens when the spectral reflectance functions of the two stimuli differ, but those differences are unimportant with respect to the visual response functions (color matching functions) when integrated with the spectral power distribution of the first illuminant. When the illuminant is changed, these differences might become apparent to an observer. Illuminant metamerism is often a problem in industries that produce colored materials. If they produce two materials that are a metameric match to one another, they might mismatch under some practical viewing conditions. If the two materials are an identical match, meaning their spectral reflectance functions are identical, then they are not metameric and will match for any illuminant.

Observer metamerism is more difficult to quantify, but perhaps equally important. It is caused by the normal variations in the color responsivities of various observers. Observer metamerism is defined by two stimuli with

differing spectral power distributions that match for a given observer. When these stimuli are examined by a second observer, they might no longer match. Again, stimuli that are identical spectral matches will match for any observer. Thus, illuminant metamerism becomes apparent when the illuminant is changed and observer metamerism becomes apparent when the observer is changed.

Current Techniques and Recommendations

CIE Publication 15.2 (CIE 1986) describes a technique to calculate an index of metamerism for change in illuminant. Essentially the recommendation is to calculate a CIELAB ΔE_{ab}^* , or any other color difference metric, for the illuminant under which the two stimuli do not match. This could be any illuminant of interest as long as the two stimuli match under the illuminant of primary interest. There is no clear recommendation on how to calculate this index of metamerism when the two stimuli are not perfect matches under the primary illuminant. In such a case, technically, there is no metamerism, but simply a pair of stimuli with an unstable color difference. Techniques for overcoming this limitation have been discussed by Fairman (1987).

CIE Publication 80 (CIE 1989) describes a technique for calculation of an index of metamerism for change in observer. Essentially, the standard colorimetric observer is replaced with a standard deviate observer and the color difference between the two stimuli is calculated for this new observer. The concept is sound, but the data on which the standard deviate observer were based had been normalized resulting in an under-prediction of the degree of observer metamerism (Alfvin and Fairchild 1997). Nimeroff *et al.* (1961) described a technique whereby a complete standard observer system, including mean and covariance color matching functions, could be specified. This concept is similar to the idea of the CIE (1989) technique, but it has never been fully implemented due to a lack of data.

Application of Color Appearance Models

Color appearance models could be of some utility in the quantification of illuminant metamerism since it involves the comparison of stimuli across changes in illumination. Essentially the contribution to an index of illuminant metamerism would be the availability of a color difference metric that is consistent across a variety of illuminants. Also, an accurate color appearance model would allow the creation of a new type of metric for single stimuli. A single sample cannot be considered metameric since it does not match anything. However, it is common to talk of a single sample being metameric when its apparent color changes significantly with a change in illuminant. This is really a lack of color constancy. A good color appearance model would allow one to calculate a color difference metric between a sample under one

illuminant and the same sample under a second illuminant, thus allowing the creation of an index of color constancy. This could be useful for objects that are intended to look the same color under various illumination conditions, such as those containing safety colors.

There really is little use for a color appearance model in the specification of observer metamerism beyond the potential for a better color difference metric. The measurement of observer metamerism is an excellent example of a situation in which the problem needs to first be completely addressed at the level of basic colorimetry. In other words, the observer variability in tristimulus values must first be adequately specified before it is necessary to be concerned about the improvements that a color appearance model could make. This path should be taken as a model for all potential applications of color appearance models.

Future Directions

There is little activity aimed at the improvement of indices of metamerism. For illuminant metamerism, effort is concentrated on the improvement of color difference metrics. For observer metamerism, there seems to be little call for a better metric, despite the flaws in the current metric (which is not widely used). This situation could be because it is difficult enough to address problems of illuminant metamerism to cause the difficulties associated with observer metamerism to be considered of second order at this time.

18.4 A GENERAL SYSTEM OF COLORIMETRY?

Consideration of some of the problems of traditional colorimetry described in this chapter leads one to wonder whether it might be possible to create a general system of colorimetry that could be used to address all the problems of interest. Currently, colorimetry has taken a very evolutionary form of development moving from CIE XYZ tristimulus values to the CIELAB color space, to enhancements of CIELAB for measuring color difference and color appearance. This development is useful to ensure compatibility with industrial practices that are based on previous standard procedures. However, the level of complexity is getting to the point where there might be multiple color models, each more appropriate for a different application. CIELAB and CIELUV were recommended by the CIE in 1976 to limit the number of color difference formulae being used internationally to two, rather than the ever increasing number that were being used prior to that time. That recommendation was quite successful and has resulted in CIELAB becoming essentially the only color space in use (along with a few color difference equations based on it). Perhaps a similar state of affairs is currently developing in the area of color appearance models and recent recommendations from the CIE will bring about some order. However, it is still likely that systems for color

appearance and for color difference will be separate in practice. The LLAB model (Luo *et al.* 1996) represents one interesting attempt to bring colorimetry together with one general model. Li *et al.* (2003) have begun to carry this work forward with respect to CIECAM02. Perhaps this approach should be pursued.

An alternate approach is to start over from scratch, taking advantage of the progress in visual science and colorimetry over the last century, to create a new system of colorimetry that is superior for all steps in the process and can find a wide range of applications in science, technology, and industry. Color appearance models take a step in this direction by first transforming from CIE tristimulus values to cone responses and then building up color appearance correlates from there. There is also activity within the CIE (e.g., TC1-36, Fundamental Chromaticity Diagram with Physiologically Significant Axes) to develop a system of colorimetry based on more accurate cone responsivities that are not necessarily tied to a CIE Standard Colorimetric Observer. It is thought that such a system would find wide use in color vision research. Boynton (1996) has reviewed the history and status of such work. Perhaps some convergence between the two activities is needed to develop a better, general system of colorimetry that could be used by everyone. Unfortunately, this paragraph is just as true for the second edition of this book in 2004 as it was when written for the first edition in 1997!

Device-independent Color Imaging

A computer user takes a photograph, has it processed and printed, scans the print into the system, displays it on the monitor, and finally prints it on a digital printer. This user has completed at least three input–process–display cycles on this image. Despite spending large sums of money on various imaging hardware, it is extremely unlikely that the colors in the final print look anything like the original object or are even satisfactory. There are also intermediate images that might be compared with one another and the original object.

The system described above is an ‘open system’. This means that the user chose each of the components and put them together. Each of the imaging devices has its own intrinsic physical process for image input, processing, and/or display and they are not necessarily designed to function with each other. If each component functions in its native mode, then the results produced with an open system are nearly unpredictable. One reason for this is the open nature of the systems; there are too many possible combinations of devices to make them all work well with one another.

Allowing the devices to function in their own intrinsic color dimensions is what is known as *device-dependent color imaging*. The difficulty with device-dependent coordinates is that the RGB coordinates from a scanner might not mean the same thing as the RGB signals used to drive a monitor or printer. To solve these problems and produce reliable results with open systems, device-independent color imaging processes must be used. The concept of device-independent color imaging is to provide enough information along with the image color data such that the image data could, if necessary, be described in coordinates that are not necessarily related to any particular device. Transformations are then performed to represent those colors on any particular device.

The strong technological push for reliable device-independent color imaging over the last decade has stressed the scientific capabilities in the area of color appearance modeling since the various images are typically viewed in a wide variety of viewing conditions. While it has been recognized for some time that a color appearance model is necessary for successful device-independent color imaging, there has not been a simple solution to that problem available. The first 17 chapters of this book present some of the issues and problems that must be addressed while this chapter provides an overview of the basic concepts required to put the pieces together and build systems.

Device-independent color imaging has become the focus of many scientists and engineers over recent years. It is impossible to cover the scope of issues involved in a single chapter. Entire books dedicated to this topic have become available (Giorgianni and Madden 1997, Kang 1997, Sharma 2003). In recent years, color management systems have become more commonplace and many books aimed at advanced end-users have been published (e.g., Fraser *et al.* 2003, Stone 2003) Also, Hunt's text on color reproduction (Hunt 1995) provides much necessary insight into the fundamentals of traditional and digital color reproduction. Sharma and Trussel (1997) have published a review paper on the field of digital color imaging that includes hundreds of references. The treatment in this chapter is culled from a series of earlier works (Fairchild 1994a, 1995b, 1996).

19.1 THE PROBLEM

The application of basic colorimetry produces significant improvement in the construction of open color imaging systems by defining the relationships between device coordinates (e.g., RGB, CMYK) and the colors detected or produced by the imaging systems. However, it is important to recall that matching CIE tristimulus values across various imaging devices is only part of the story. If an image is reproduced such that it has CIE tristimulus values identical to the original, then it will match the original in appearance as long as the two are viewed under identical viewing conditions (matching those for which the tristimulus values were calculated). Since originals, reproductions, and intermediate images are rarely viewed under identical conditions, it becomes necessary to introduce color appearance models to the system in order to represent the appearance of the image at each stage of the process.

Issues in device-independent color imaging that color appearance models can be used to address include changes in white point, luminance level, surround, medium (viewing mode), etc. Since these parameters normally vary for different imaging modalities, the necessity for color appearance models is clear. The introduction of color appearance models allows the systems to be set up and used to preserve, or purposefully manipulate, the appearances of image elements in a controlled manner at each step. Thus, users can view an image on an LCD display, manipulate it as they choose, and then make

prints that accurately reproduce the appearance of the image on the LCD with the aid of color appearance models.

Of course, it is not always possible, or desirable, to exactly reproduce the appearance of an original image. Color appearance models can be useful in these situations as well. One problem is that different imaging devices are capable of producing different ranges of colors, known as their *color gamut*. A given stimulus on an LCD display produces a certain appearance. It might not be possible to produce a stimulus on a given printer that can replicate that appearance. In such cases, a color appearance model can be used to adjust the image in a perceptually meaningful way to produce the best possible result. In other cases, the viewing conditions might limit the gamut of a reproduction. For example, photographic prints of outdoor scenes are often viewed under artificial illumination at significantly lower luminance levels than the original scene. At the lower luminance level it is impossible to produce the range of luminance and chromatic contrast that is witnessed in the original scene. Thus it is common for consumer photographic prints to be produced with increased physical contrast to overcome this change in viewing conditions. Color appearance models can be used to predict such effects and guide the design of systems to address them.

Another advantage of color appearance models in device-independent color imaging is in the area of image editing. It is more intuitive for untrained users to manipulate the colors in images along perceptual dimensions such as lightness, hue, and chroma, rather than through device coordinates such as CMYK. A good color appearance model can improve the correlation between tools intended to manipulate these dimensions and the changes that users implement on their images.

19.2 LEVELS OF COLOR REPRODUCTION

Hunt (1970, 1995) has defined six different objectives for color reproduction:

1. Spectral Color Reproduction

Spectral color reproduction involves identical reproduction of the spectral reflectance curves of the original image or objects. Two techniques that are so impractical as to be of only historical interest, the Lippman and microdispersion methods (see Hunt 1995), managed to fulfill this difficult objective. Modern color reproduction techniques take advantage of metamerism by using RGB additive primaries or CMY subtractive primaries, thus eliminating the possibility of spectral reproduction except in cases in which the original is comprised of the same imaging materials. Recently developed, and currently developing, printing techniques that utilize six or more inks provide an opportunity for better approximations to spectral color reproduction that might be useful in applications such as mail-order catalogs or fine-art reproductions (in addition to expanding the output gamut).

2. Colorimetric Color Reproduction

Colorimetric color reproduction is defined via metameric matches between the original and the reproduction such that they both have the same CIE XYZ tristimulus values. This will result in the reproduction of color appearances in cases for which the original and reproduction of the same size are viewed under illuminants with the same relative spectral power distribution, luminance, and surround. Hunt, however, does not make equality of luminance level a requirement for colorimetric color reproduction.

3. Exact Color Reproduction

Exact color reproduction is defined as colorimetric color reproduction with the additional constraint that the luminance levels be equal for the original and the reproduction.

4. Equivalent Color Reproduction

Equivalent color reproduction is defined to acknowledge situations in which the color of illumination for the original and the reproduction differ. In such cases, precise reproduction of CIE tristimulus values would result in images that were clearly incorrect since nothing has been done to account for chromatic adaptation. Equivalent color reproduction thus requires the tristimulus values and the luminances of the reproduction to be adjusted such that they produce the same appearances as found in the original. This requires the differences between the original and the reproduction viewing conditions to be incorporated using some form of color appearance or chromatic adaptation model. When there are large changes in luminance level between the original and the reproduction, it might be impossible to produce appearance matches, especially if the objective is brightness-colorfulness matching rather than lightness-chroma matching.

5. Corresponding Color Reproduction

Corresponding color reproduction addresses the luminance issue by neglecting it to a degree. A corresponding color reproduction is one that is adjusted such that its tristimulus values are those required to produce appearance matches if the original and the reproduction were viewed at equal luminance levels. This eliminates the problems that arise when trying to reproduce brightly illuminated originals in dim viewing conditions and vice versa. It can be thought of as an approximation to lightness-chroma matching if one were willing to assume (incorrectly) that lightness and chroma are constant across changes in luminance level. Since lightness and

chroma are far more constant across luminance changes than brightness and colorfulness, this assumption might not be too bad, especially given practical gamut-mapping constraints.

6. Preferred Color Reproduction

Preferred color reproduction is defined as reproduction in which the colors depart from equality of appearance to those in the original in order to give a more pleasing result. This might be applicable in situations such as consumer photography in which consumers prefer to have prints that reproduce colors closer to their memory colors for objects such as skin tones, vegetation, sky, bodies of water, etc. However, as Hunt (1970) points out, 'the concepts of spectral, colorimetric, exact, equivalent, and corresponding color reproduction provide a framework which is a necessary preliminary to any discussion of deliberate distortions of colour reproduction.'

19.3 A REVISED SET OF OBJECTIVES

Hunt's objectives for color reproduction provide a good summary of the problems encountered in color reproduction and how they can be addressed using concepts of basic and advanced colorimetry. It is interesting to note that these objectives were originally published long before issues in device-independent color imaging were commonly discussed (Hunt 1970). A slight rearrangement and simplification of Hunt's objectives can be used to define five levels of color reproduction that provide a framework for modern color imaging systems.

1. Color Reproduction

Color reproduction refers to simple availability devices capable of producing color graphics and images. There is usually great excitement surrounding the initial commercial availability of color devices of any given type. While this might not seem like much of an accomplishment, it is worth remembering that personal computers with reasonable color capabilities have been available for less than 20 years. The plethora of high-quality input and output devices is very recent. When these technologies are first introduced, users are excited simply by the fact that they now have color available where previously it was not. However, this 'honeymoon period' quickly wears off and users begin to demand more from their color imaging devices — they want to have devices that produce and reproduce colors with some semblance of control and accuracy. This pushes open-systems technology toward the next levels of color reproduction.

2. Pleasing Color Reproduction

Pleasing color reproduction refers to efforts to adjust imaging devices and algorithms such that consumers find the resulting images acceptable. Such images might not be accurate reproductions and they are probably not the preferred reproductions, but they look pleasing and are found acceptable to most consumers of the images. This level of reproduction can often be achieved through trial and error without requiring any of the concepts of device-independent color imaging. The approach to obtaining pleasing color reproduction in open systems would be similar to the approaches historically taken in closed imaging systems to achieve similar goals or, in some cases, preferred color reproduction. Pleasing color reproduction can be a reasonable final goal for a color reproduction system in which observers have no knowledge of the original scene or image and, therefore, no expectations beyond desiring a pleasing image.

3. Colorimetric Color Reproduction

Colorimetric color reproduction includes calibration and characterization of imaging devices. This means that for a given device signal, the colorimetric coordinates of the image element produced (or scanned) are known with a reasonable degree of accuracy and precision. With colorimetric color reproduction, a user can put together a system in which an image is scanned, the data are converted to colorimetric coordinates (e.g., CIE XYZ), and then these coordinates are transformed into appropriate RGB signals to display on an LCD, or into CMYK signals for output to a printer. Of course, it is not necessary for the image data to actually be transformed through the device-independent color space. Instead, the full transform from one device, through the device-independent space, to the second device can be constructed and implemented for enhanced computational efficiency and minimization of quantization errors. Such a system allows the CIE tristimulus values of the original image to be accurately reproduced on any given output device. This is similar to Hunt's definition of *colorimetric* color reproduction. To achieve colorimetric color reproduction, devices and techniques for the colorimetric characterization and calibration of input and output devices must be readily available. A variety of such techniques and devices is available commercially, but the degree to which colorimetric color reproduction can actually be achieved by typical users is dubious. Unfortunately, the state of the art for most users is just color reproduction; colorimetric color reproduction has yet to be reliably achieved. Colorimetric color reproduction is useful only when the viewing conditions for the original and reproduced images are identical since this is the only time that tristimulus matches represent appearance matches. When the viewing conditions differ, as they usually do, one must move from colorimetric color reproduction to the next level.

4. Color Appearance Reproduction

Color appearance reproduction requires a color appearance model, information about the viewing conditions of the original and reproduced images, and accurate colorimetric calibration and characterization of all the devices. For color appearance reproduction, the tristimulus values of the original image are transformed to appearance correlates, such as lightness, chroma, and hue, using information about the viewing conditions such as white point, luminance, surround, etc. Information about the viewing conditions for the image to be reproduced is then used to transform these appearance correlates into the tristimulus values necessary to produce them on the output device. Color appearance reproduction is necessary to account for the wide range of media and viewing conditions found in different imaging devices. This is similar to Hunt's equivalent color reproduction applied to lightness-chroma matches. Color appearance reproduction has yet to become a commercial reality and perhaps it cannot for typical users. However, even when reasonable color appearance reproduction does become available, there will be cases when users will desire reproductions that are not accurate appearance matches to the originals. Such cases enter the domain of color preference reproduction.

5. Color Preference Reproduction

Color preference reproduction involves purposefully manipulating the colors in a reproduction such that the result is preferable to the users over an accurate appearance reproduction. The objective is to produce the best possible reproduction for a given medium and subject. This is similar to Hunt's definition of preferred color reproduction.

Note that to achieve each level of reproduction in open systems it is necessary to have first achieved the lower levels. To summarize, the five levels involve simply reproducing colors, reproducing pleasing colors, equality of tristimulus values, equality of appearance attributes, and manipulation of appearance attributes to 'improve' the result. In closed systems it is not necessary for technology to progress through each of the five levels. This is because the path of image data is defined and controlled throughout the whole process. For example, in color photography, the film sensitivities, dyes, processing procedures, and printing techniques are all well defined. Thus it is possible to design a photographic negative film to produce pleasing or preferred color reproduction without having the capability for colorimetric or color appearance reproduction since the processing and printing steps are well defined. A similar system exists in color television with standard camera sensitivities, signal processing, and output device setup. In open systems, an intractable number of combinations of input, processing, display, and output devices can be constructed and used together. The manufacturer of each subsystem cannot possibly anticipate all of the possible

combinations of devices that might be used with it. Thus the only feasible solution is to have each device in the system develop through the five levels described above such that colorimetric, or color appearance, data (or the information necessary for obtaining it) can be handed off from one device to the next in the process known as device-independent color imaging.

19.4 GENERAL SOLUTION

Figure 19.1 is a flow chart of the general process of device-independent color imaging. At the top of the diagram is the original image as represented by some input device. (Note that this ‘input’ could come from a display device such as a CRT.) The colorimetric characterization of the input device is then used to transform the device coordinates (e.g., *RGB*) to colorimetric coordinates such as CIE XYZ or CIELAB, which are referred to as device-independent color spaces since the colorimetric coordinates do not depend on any specific imaging device.

The second step is to apply a chromatic adaptation and/or color appearance model to the colorimetric data with additional information on the viewing conditions of the original image in order to transform the image data into dimensions that correlate with appearance such as lightness, hue, and chroma. These coordinates, that have accounted for the influences of the particular device and the viewing conditions, are referred to as *viewing-conditions-independent space*. At this point, the image is represented purely by its original appearance. This is the point where it is most appropriate to perform manipulations on the image colors. These manipulations might include gamut mapping, preference editing, tone reproduction adjustments, spatial scaling operations, certain forms of error diffusion, etc. At this point, the image is in its final form with respect to the appearances that are to be reproduced. Now the process must be reversed.

This highlights the utility of an analytically invertible color appearance model. The viewing conditions for the output image, along with the final image appearance data, are used in an inverted color appearance model to transform back from the viewing conditions independent space to a device-independent color space such as CIE XYZ tristimulus values. These values, together with the colorimetric characterization of the output device, are used to transform to the device coordinates (e.g., CMYK) necessary to produce the desired output image. The following sections provide some additional detail on each step of this process.

Note that the literal implementation of the processes of device-independent color imaging as described above requires substantial computational resources. For example, to avoid severe quantization errors, image processing is usually performed on floating-point image data with floating-point computational precision when working within the intermediate color appearance spaces. While this is acceptable for color imaging research, it is not practical in most commercial color imaging systems, particularly those that are

limited to 24-bits-per-pixel color data. In such cases, the processes described above are used to construct the systems and algorithms, while implementation is left to multidimensional interpolation within eight-bits-per-channel look-up tables (LUTs). It is interesting to note that the computer graphics industry, as opposed to the color imaging/publishing industry, typically works with floating-point, and higher-precision integer, image data. Perhaps the confluence of the two fields will solve some historical computational issues and limitations.

19.5 DEVICE CALIBRATION AND CHARACTERIZATION

Device calibration refers to setting the imaging device to a known state. This might represent a certain white point, gain, and offset for a CRT or certain relationships between density and drive signal for a printer. Calibration ensures that the device is producing consistent results, both from day to day and from device to device. However, device calibration can be completed with absolutely no information about the relationship between device coordinates and the colorimetric coordinates of the input or output image. Colorimetric characterization of the device is required to obtain this information. *Characterization* refers to the creation of a relationship between device coordinates and a device-independent color space — the first step in Figure 19.1.

Device calibration is usually an issue for the manufacturer, rather than the user, and the techniques depend heavily on the technology. Thus calibration will not be discussed further except to stress its importance. If consistent results are necessary from day to day or from device to device, then careful and frequent device calibration is necessary. There are tradeoffs that can be made between calibration and characterization. If careful calibration is not possible, then accuracy can be achieved through frequent characterization. If an extremely good calibration procedure is available, it might be possible to perform the colorimetric characterization just once, as long as the device is frequently calibrated.

Three Approaches to Device Characterization

There are three main approaches to device characterization:

1. Physical modeling
2. Empirical modeling
3. Exhaustive measurement.

Of course, there are also procedures that combine aspects of one or more of these techniques. In all cases, it is typical to use the characterization to build a three-dimensional look-up table (LUT) that is used in conjunction with an interpolation procedure to process the vast amounts of image data that are encountered.

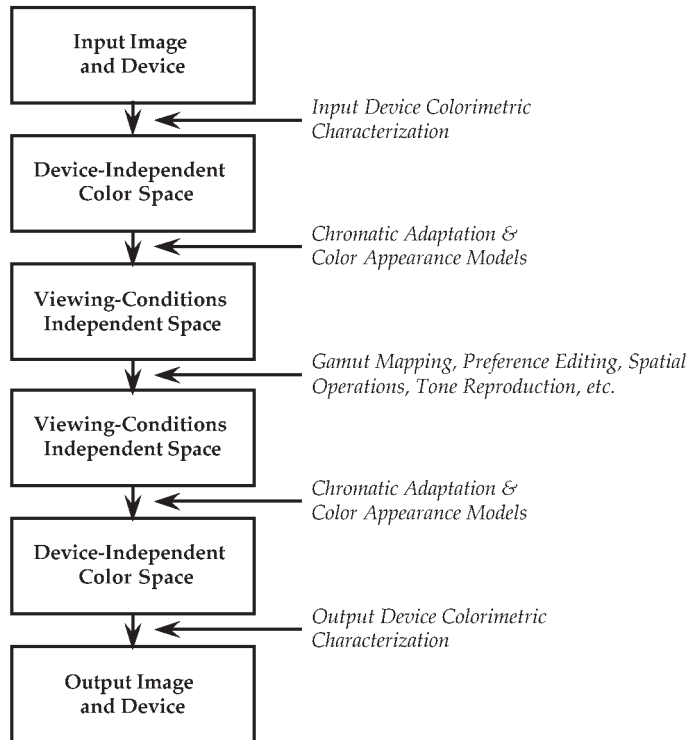


Figure 19.1 A flow chart of the conceptual process of device-independent color imaging

Physical Modeling

Physical modeling of imaging devices involves building mathematical models that relate the colorimetric coordinates of the input or output image elements to the signals used to drive an output device or the signals originating from an input device. Such models can be derived for all types of imaging devices with varying degrees of difficulty. A physical model for a scanner would involve a step to first linearize the signals with respect to luminance, or perhaps absorbance, and then a second step to transform the signals to CIE tristimulus values. Depending on the scanner design, knowledge of the physical properties of the material being scanned might be required. This could be avoided if the scanner were designed as a colorimeter rather than with arbitrary *RGB* responsivities.

A physical model for a CRT display involves a nonlinear transform to convert drive voltages to the corresponding *RGB* phosphor luminances, followed by a linear transformation to CIE *XYZ* tristimulus values. A physical model for a hard-copy output device requires a transformation from drive signals to

concentrations of dyes, pigments, or inks and then a color mixing model to predict spectral reflectances or transmittances that can then be used to calculate CIE XYZ tristimulus values. The advantage of physical device models is that they are robust, typically require few colorimetric measurements in order to characterize the device, and allow for easy recharacterization if some component of the imaging system is modified. The disadvantage is that the models are often quite complex to derive and can be complicated to implement. Physical models are often used for CRT display characterization.

Empirical Modeling

Empirical modeling of imaging devices involves collecting a fairly large set of data and then statistically fitting a relationship between device coordinates and colorimetric coordinates. Such models are often implemented to transform directly to CIELAB coordinates to avoid quantization difficulties in CIE XYZ tristimulus values.

Empirical models are often high-order multidimensional polynomials or, alternatively, neural network models of significant complexity. Empirical models require fewer measurements than look-up table techniques, but more than physical models. Empirical models are also often poorly behaved near the edge of the device gamut, producing very large systematic errors. Since empirical models have no relationship to the physics of the imaging devices, they must be recreated each time a change is made in any component of the system. Empirical models are often used for scanner characterization.

Exhaustive Measurement

The final class of characterization techniques involves exhaustive measurement of the output for a complete sampling of the device's gamut. (Signals for a large sampling of known input colors can be collected for scanner characterization.) Typically, something like a $9 \times 9 \times 9$ sampling of the device drive signals is output and colorimetrically measured. This results in a total of 729 measurements. Many more measurements might be used for devices with poor image-to-image or device-to-device repeatability. The array of colorimetric data must then be nonlinearly interpolated to populate a higher density (e.g., $33 \times 33 \times 33$) look-up table (LUT) that can be used to process image data via multidimensional interpolation. Disadvantages of such techniques include the large number of measurements that must be made, difficulties in interpolating the highly nonlinear data, the need to redo the entire process if any aspect of the device changes, and difficulty in creating the inverse solutions that are typically required. The advantage of exhaustive measurement techniques that make them popular is that they require no knowledge of the device physics. Exhaustive measurement and LUT interpolation techniques are often used for printer characterization.

Types of Colorimetric Measurements

Different types of colorimetric measurements are required for characterization of various imaging devices.

CRT or LCD display characterization requires spectroradiometric or colorimetric measurements of the phosphor chromaticities in order to derive the RGB-to-XYZ transformation and relative radiometric or photometric measurements to derive the nonlinear transfer functions for each channel. Berns (1996) reviews a practical procedure for the calibration and characterization of CRT displays. Berns *et al.* (1993a,b) provide further details on the measurement and characterization of CRT displays. Berns *et al.* (2003) also provide details on the measurements and techniques for LCD characterization.

Printers and other output devices require spectrophotometric measurements (spectral reflectance or transmittance) to characterize the device colorants or derive colorimetric coordinates for various illuminants or sources. Additional, densitometric measurements might be of value to characterize tone-transfer functions. Issues in the colorimetric characterization of binary and multilevel display devices have been discussed by a variety of authors including Jarvis *et al.* (1976), Engeldrum (1986), Gentile *et al.* (1990a), Rolleston and Balasubramanian (1993), Berns (1993b), and Haneishi *et al.* (1996).

Scanners and digital cameras require spectroradiometric evaluation of their channel spectral responsivities or empirical estimates of them. Spectroradiometric data on the illumination system is also required. Additionally, spectroradiometric linearity evaluation and characterization is required for the detector systems. Often, scanner data for well-characterized input targets are collected to derive relationships between scanner signals and colorimetric coordinates. The colorimetric calibration and characterization of input devices has been described by Hung (1991), Kang (1992), Engeldrum (1993), Rodriguez and Stockham (1993), and Berns and Shyu (1995).

Flare, Metamerism, and Fluorescence

There are three additional issues regarding colorimetric measurements that are often overlooked in device characterization, but require attention: flare, metamerism, and fluorescence.

Flare

Typically, the spectrophotometric or colorimetric measurements made to characterize a device are performed with specialized instrumentation and specially prepared samples. Such measurements are not made in the actual viewing situation for the device. Any real viewing situation includes flare. The spectral energy distribution and level of the flare must be measured and added to any real colorimetric characterization of an imaging device. Since

flare is an additive mixture of light with the image, it can be treated as a simple addition of the tristimulus values of the flare to the tristimulus values of the image data. This addition might result in the need to recalculate the image white point and renormalize data appropriately. In some cases, flare might be image dependent and require a more sophisticated treatment. Alternatively, measurements of image color must be made *in situ*, using a telespectroradiometer that will include the flare of the viewing environment in the measurement.

Metamerism

Metamerism causes difficulties in both input and output devices. For input devices, metamerism combined with non-colorimetric sensor responsivities can defeat all hope of obtaining reliable color reproduction. At the output end, it is necessary to characterize devices using spectral reflectance or transmittance functions integrated with the actually viewing spectral power distributions in order to derive colorimetric coordinates. This is necessary for reasonable accuracy, even when using standardized viewing sources. For example, the colors observed under a fluorescent D50 simulator can differ dramatically from those calculated using CIE illuminant D50.

Fluorescence

The colorimetry of fluorescent materials is a significant challenge since the energy emitted by the material is a function of the incident energy from the illuminating source. Since this is not the case for non-fluorescent materials, the light source used for spectrophotometric measurement has no impact on the colorimetric coordinates calculated for any particular illuminant. Fluorescent materials must be measured using illumination that closely simulates the illuminant to be used in colorimetric calculations in order to obtain reasonable accuracy. The best practical solution is to measure fluorescent materials in their final viewing conditions using a telespectroradiometer.

Fluorescence is an important issue in imaging applications since many substrates (i.e., most paper) and many inks and dyes are fluorescent. Grum and Bartleson (1980) provide an excellent overview of the colorimetry of fluorescent materials. Gonzalez and Fairchild (2000) examined the significance of fluorescence in the colorimetry of typical printing materials.

Multidimensional LUT Interpolation

No matter what approach is taken to characterize an imaging device, the end result is typically used to construct a multidimensional LUT for practical implementations. This is because it is necessary to complete the many layers of nonlinear transformations and color space conversions required with computational precision significantly greater than the eight bits per channel found in most imaging devices. Such computations take prohibitive

amounts of time on typical desktop imaging systems. Thus multidimensional LUT interpolation is implemented for the end-to-end transform for convenience and efficiency. The construction of multidimensional LUTs and their use through interpolation has been described by Hung (1993) and Kasson *et al.* (1993, 1995).

Multidimensional LUT interpolation is implemented in a variety of ways including proprietary software such as Adobe Photoshop® and other ‘color management’ software that use these techniques for color space transformations. Multidimensional LUTs are also implemented in the PostScript® Level 2 (Adobe Systems Incorporated, 1990) page-description language in the form of color rendering dictionaries. Another well-known open system that provides the framework for the implementation of multidimensional LUTs for device characterization is the ICC profile format (International Color Consortium, 1995; www.color.org) that serves as a cross-platform standard for a wide variety of system-level color management systems.

19.6 THE NEED FOR COLOR APPEARANCE MODELS

The process of device-independent color imaging described by Figure 19.1 illustrates the necessity of color appearance models. There are two main needs for these models—image editing and viewing-condition transformations. Image manipulations such as color preference reproduction and gamut mapping are best performed in the perceptually significant dimensions (e.g., lightness, chroma, and hue) of a color appearance model. Clearly the transformation of colorimetric coordinates from one set of viewing conditions (white point, luminance, surround, medium, etc.) to a second set of viewing conditions requires a color appearance model.

The only way to avoid the use of a color appearance model in device-independent color imaging is to specify a rather strong set of constraints. The original and the reproduction must be viewed in the same medium, under identical viewing conditions, with identical gamuts, and with the objective of colorimetric color reproduction. In such a constrained world, colorimetric and color appearance reproduction are identical. Clearly, the above constraints are far too severe for all but the most specialized applications. Thus the use of color appearance models in device-independent color imaging is unavoidable if high-quality, reliable results are to be obtained in open systems.

19.7 DEFINITION OF VIEWING CONDITIONS

One key unresolved issue in the implementation of color appearance models in device-independent color imaging is the definition and control of viewing conditions. Even a perfect color appearance model is of little utility if the actual viewing conditions are not the same as those used in the model calculations. (The metamerism problems between CIE illuminants and their physical simulators is one straightforward example of this difficulty.)

Part of the difficulty in controlling the viewing conditions is definition of the fields. Hunt (1991b) has done the most extensive job of defining the various components of the viewing field. However, even with Hunt's extended definitions, it is difficult to decide which portions of the field should be considered the proximal field, the background, and the surround when viewing complex image displays in typical viewing conditions. For example, is the background of an image the area immediately adjacent to the image borders or should it be considered to be the areas adjacent to individual elements within the image? The latter definition might be more appropriate; however, it requires substantially more complex image-wise computations that are often completely impractical. However the particular aspects of the viewing conditions are defined, it is important that the treatment is consistent across all image transformations to avoid the introduction of bias simply due to the use of color appearance models. As a practical definition, the background for images should be defined as the area immediately around the image border with the surround defined as the remainder of the viewing environment; this definition of background, however, is different from that used by Hunt as described in Chapter 7. The definition of proximal field is unnecessary in image reproduction since the spatial relationships of the various image elements is constant in the original and the reproduction. The proximal field becomes important when it is desired to reproduce the color appearance of an image element in a completely different context (e.g., logo colors, trademark colors).

Even with strict definitions of the various components of the viewing field, it is of paramount importance that the viewing conditions be carefully controlled for successful device-independent color imaging. If users are unwilling to control the viewing conditions carefully, they should expect nothing less than unpredictable color reproduction. Viewing condition parameters that must be carefully controlled for successful color appearance reproduction include:

- The spectral power distribution of the light source
- Luminance level
- Surround color and relative luminance
- Background color and relative luminance
- Image flare (if not already incorporated in the device characterization)
- Image size and viewing distance (i.e., solid angle)
- Viewing geometry.

Also, observers must make critical judgements of the various images only after sufficient time has passed to allow full adaptation to the respective viewing conditions.

Braun *et al.* (1996) illustrated the importance of controlling the viewing conditions for cross-media image comparisons. They concluded that the best technique for critical judgements was successive binocular viewing in which the observer viewed first one image display with both eyes and then switched to the other display, allowing approximately one minute to adapt to

the new viewing conditions. The arrangement was such that only one image display could be viewed at a time and the one-minute adaptation was required each time the observer changed from one display to the other. Unfortunately, the most common technique, simultaneous binocular viewing, in which the original and the reproduction (in a different medium and white point) are viewed simultaneously side-by-side produces unacceptable results. In such cases, the observer's state of chromatic adaptation cannot be reliably predicted since it depends on the relative amount of time spent viewing each image. In general, the best results will be obtained if a single, intermediate adaptation point is assumed. However, the result of such a choice will be a reproduction that matches the original when viewed side-by-side, but that looks quite strange when viewed by itself.

For example, if a CRT has a 9300 K white point and a reproduced print is viewed under a D50 simulator, the required print to produce a simultaneously viewed match will have an overall blue cast. When this print is viewed in isolation, still under a D50 simulator, it will appear unacceptably bluish and be considered a poor match. Katoh (1995) has investigated the problems with simultaneous viewing of images in different media. However, if a successive viewing technique with sufficient adaptation time is used, an excellent neutrally balanced 9300 K CRT image will be matched by a neutrally balanced print viewed under a D50 simulator. Thus both color appearance matching and high individual image quality can be obtained with appropriate viewing procedures.

Once the viewing conditions are appropriately defined and controlled, some computational advantage can be obtained through judicious precalculation procedures. Such procedures rely on parsing the implementation of the color appearance models into parts that need only be calculated once for each viewing condition and those that require calculation for each image element. The most efficient implementation procedure is then to precalculate the model parameters that are viewing-condition dependent and then use this array of data for the individual appearance model calculations performed on each pixel or element of a LUT. For example, when using RLAB for a change in white point and luminance with a constant surround, the change in viewing conditions can be precalculated down to a single 3×3 matrix transform that is applied to the CIE XYZ tristimulus values of the original in order to determine the tristimulus values of the reproduction. This is a significant computational simplification that makes it possible to allow users to interactively change the settings in a color appearance model such that they can choose the illuminant under which a given image will be viewed.

19.8 VIEWING-CONDITIONS-INDEPENDENT COLOR SPACE

Device-independent color spaces are well understood as representations of color based on CIE colorimetry that are not specified in terms of any particular imaging device. (Alternatively, a device-independent color space can

be defined as a transform from CIE coordinates to those of some standardized device (e.g., Anderson *et al.* 1996) The introduction of color appearance models to the process, as illustrated in Figure 19.1, creates the additional concept of a viewing-conditions-independent color space. The viewing-conditions-independent coordinates extend CIE colorimetry to specify the color appearance of image elements at a level that does not rely on outside constraints. Such a representation encodes the perceptual correlates (e.g., lightness, chroma, and hue) of the image elements. This representation facilitates editorial adjustments to the image colors necessary for color preference reproduction and gamut mapping.

It is also worth noting that the viewing conditions themselves might introduce ‘perceptual gamut limits.’ For example, the lightness, chroma, and hue of certain image elements viewed under a high luminance level cannot be reproduced in an image viewed at a low luminance level. In other words, certain color perceptions simply cannot be produced in certain viewing conditions.

The limitations of ‘perceptual gamut limits’ do not in any way reduce the utility of color appearance models. In fact, they can only be reliably defined using color appearance models. It is interesting to note that the concept of viewing-conditions-independent color space has a correlate in the field of cognitive science. Davidoff (1991) presents a model of object color representation that ultimately encodes color in terms of an output lexicon, the words we use to describe color appearance. Such a representation can be thought of as a high-level color appearance model in which colors are specified by name, as people do, rather than with the mathematically necessary reduction to scales of the five requisite color appearance attributes.

19.9 GAMUT MAPPING

It would be misleading to suggest that all the problems of device-independent color imaging would be solved by use of a reliable, accurate color appearance model. Even with a perfect color appearance model, the critical question of color gamut mapping would remain. The development of robust algorithms for automated gamut specification and color mappings for various devices and intents remains as perhaps the most important unresolved issue in cross-media color reproduction (Fairchild 1994a).

The gamut of a color imaging device is defined as the range of colors that can be produced by the device as specified in some appropriate three, or more, dimensional color space. (It is important to reiterate that color gamuts must be expressed in a three-dimensional color space, since two-dimensional representations such as those often plotted on chromaticity diagrams are misleading.) The most appropriate space for the specification of a device gamut is within the coordinates of a color appearance model since the impact of viewing conditions on the perceived color gamut can be properly represented. For example, only a complete color appearance model will show

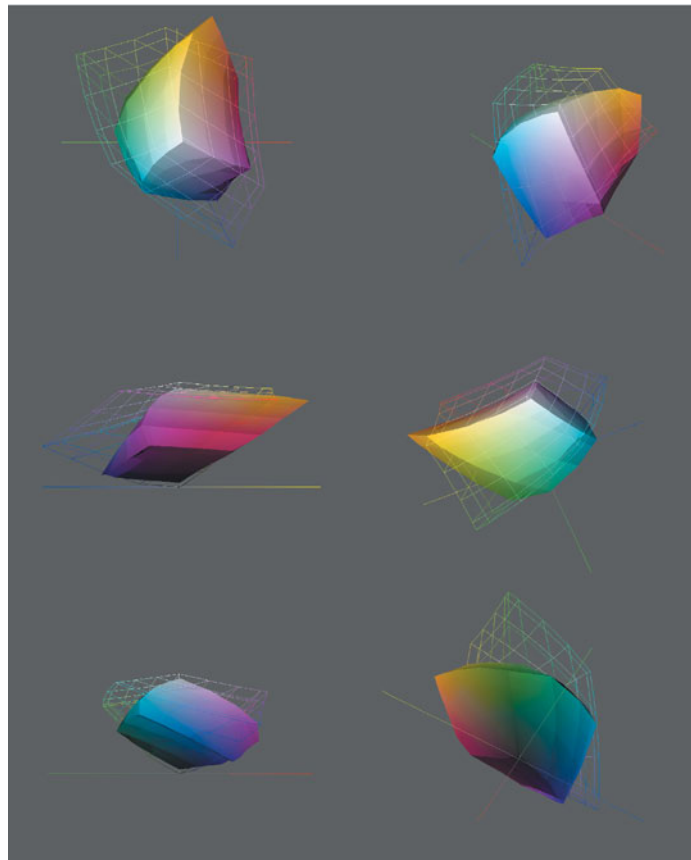


Figure 19.2 Several views of three-dimensional representations of device gamuts in the CIELAB color space. The solid model is the gamut of a typical dye-diffusion thermal-transfer printer and the wireframe model is the gamut of a typical CRT display

that the color gamut of a printer shrinks to zero volume as the luminance decreases! Generally, a device gamut should be represented by the lightness, chroma, and hue dimensions within the chosen appearance model. However, in some cases, it might be more appropriate to express the gamut in terms of brightness, colorfulness, and hue. Examples of such cases include projection systems or other displays susceptible to ambient flare in which the absolute luminance level has a significant impact on the perceived color image quality.

Figure 19.2 illustrates various views of three-dimensional models of two device gamuts. These gamuts are plotted in the CIELAB color space. The wireframe model represents the gamut of a typical monitor with SMPTE phosphors and a D50 white point. The solid model represents the color gamut of a typical dye-diffusion printer under CIE illuminant D50. Note that the gamut of the CRT display exceeds that of the printer for light colors,

while the gamut of the printer exceeds that of the CRT for some darker colors. This three-dimensional gamut representation should clear up some misconceptions about color gamuts. For example, Figure 19.2 illustrates the large extent to which color gamuts are not coincident and the fact that printer gamuts often extend outside the range of CRT gamuts. Typically, it is assumed that CRT gamuts are significantly larger than most printer gamuts. This is a result of examination of two-dimensional gamut boundaries in chromaticity diagrams while neglecting the third dimension of color space.

Gamut mapping is the process of adjusting the colors in an image such that it can be represented on a given device. For example, it might be desired to use a CRT display to reproduce a dark, saturated cyan that is present on a print. If the CRT cannot produce the desired color, the image element must be shifted to an appropriate color that is within the CRT gamut. The opposite problem might also arise in which a device is capable of producing more saturated colors than present in the original image. If the full gamut of the output device is not utilized, users might be displeased with the results since they know that the device is capable of producing a wider range of colors. Thus, image colors might also be adjusted to fill color gamuts as well. Therefore the problem of gamut mapping can be described as gamut *compression* in regions where the desired color falls outside the device gamut and gamut expansion in regions where the gamut of image colors does not fully utilize the device gamut. Proper gamut expansion requires full knowledge of the source image's gamut and computationally expensive image-dependent processing. Thus it might not be fully implemented within practical systems for some time. This is somewhat counter to the common perception that gamut mapping is only a problem of gamut compression. Color adjustments in the opposite direction represent an equally important, and perhaps more challenging, problem. Clearly, a color appearance model is the best place to specify gamuts and perform mapping transformations since the manipulations can be carried out on perceptually meaningful dimensions.

A variety of gamut mapping techniques have been suggested, but a generalized, automated algorithm that can be used for a variety of applications has yet to be developed. Perhaps some lessons can be learned from the field of color photography (Evans *et al.* 1953, Hunt 1995) in which optimum reproductions are thought to be those that preserve the hue of the original, map lightness to preserve its relative reproduction and the mean level, and map chroma such that the relationships between the relative chromas of various image elements are retained. Of course, such guidelines would be overruled by specific color preferences. Beginning with such approaches and considering other practical constraints, issues of color gamut mapping have been discussed by Stone *et al.* (1988), Gentile *et al.* (1990b), Hoshino and Berns (1993), Wolski *et al.* (1994), and Montag *et al.* (1996, 1997).

While a general solution to the gamut-mapping problem has not been derived, some fundamental concepts can be suggested. For pictorial images, a reasonable gamut-mapping solution can be obtained by first linearly scaling the lightnesses such that the white and black points match and the

middle gray ($L^* = 50$) is kept constant. Next, hue is preserved as chroma is clipped to the gamut boundary for compression or linearly scaled for expansion. An alternative approach is to clip the out-of-gamut colors to the gamut boundary at a minimum distance in a uniform color space while eliminating the constant-hue constraint. Such approaches are likely to be too simplistic and do not produce the optimum results (e.g., Wolski *et al.* 1994, Montag *et al.* 1996, 1997, Braun and Fairchild 1999a,b).

For other image types, such as business graphics, other gamut mapping strategies might be more appropriate. One such approach is to preserve the chroma of image elements while changing hue if necessary in order to retain the impact and intent of business graphic images. These differences highlight the importance of understanding the intent for an image when making a reproduction. Depending on the intended application for a given image, the optimum gamut-mapping strategy will vary. The difference between pictorial images and business graphics is readily apparent. However, even among pictorial images, different gamut-mapping strategies might be more appropriate for various applications. For example, the best strategy for a scientific or medical image will be different than that for a fine-art reproduction, which will in turn be different from that for a consumer snapshot.

19.10 COLOR PREFERENCES

Once the problems of color appearance and gamut mapping are solved, there will remain one last color operation, the mapping of colors to those that are preferred by observers for a given application. Thus accurate color reproduction might not be the ultimate goal, but rather a required step along the way. Color mapping for preference reproduction should be addressed simultaneously with gamut mapping since the two processes deliberately force inaccurate color reproduction and will certainly impact each other. Like gamut mapping, color preference mapping is intent-, or application-dependent. In some applications, such as scientific and medical imaging, accurate color reproduction might be an objective that cannot be compromised. In pictorial imaging, preferred reproduction of certain object colors (e.g., sky, skin, foliage) might be biased toward the idealized memory color of these objects. In abstract images, such as business graphics, preferred color reproduction might depend more upon the device capabilities or intended message than on the colors of the original image.

An additional factor in color preference reproduction is the cultural dependency of color preferences. It is well established in the color reproduction industry that preferred color reproduction systems sold into different cultures have different color capabilities and cannot be substituted between cultures without a loss in sales. While it seems certain that such cultural biases exist, they are not well documented (publicly) and their cause is not well understood. Many such effects have achieved the level of folklore and might only exist for historical reasons. For example, certain customers might have a strong preference for certain color reproduction capabilities

because they have grown accustomed to those properties and consider any change to be negative. Such biases are certainly cultural, but they are learned responses. This illustrates the point that most, if not all, cultural biases in color preference reproduction are learned in some way (this is the fundamental definition of culture). The topic of cultural biases is certainly an interesting one and worthy of additional research and exploration. Fernandez *et al.* (2002) failed to find any significant cultural biases in image preference in one recent study. They showed that individual variation in preferences were larger than any changes in the cultural averages. It would be particularly interesting to see if biases, if indeed they exist at all, could be traced historically to see if they change with advances in communication and interchange of image information.

The concept of cultural dependency in color preference reproduction sparks several interesting possibilities. However, there are also significant individual differences in color preference reproduction as well. In fact, while there might be significant differences in color preference between cultures, it is almost certainly true that the range of color preferences of individuals within any given culture exceeds the differences between the mean levels (confirmed by Fernandez *et al.* 2002). One need only attempt to produce a single ideal image for two observers to understand the magnitude of such differences in preference.

19.11 INVERSE PROCESS

Thus far, the process of moving image data into the middle of the flow chart in Figure 19.1 has been described. Once all of the processing at this level is complete, the image data is conceptually in an abstract space that represents the appearances to be reproduced on the output image. At this point, the entire process must be reversed to move from the viewing-conditions independent color space, to a traditional device-independent color space, to device coordinates, and then ultimately to the reproduced image. This process highlights the importance of working in both the forward and reverse directions in order to successfully create reproductions. Clearly, the entire process is facilitated by the use of analytically invertible color appearance models and device characterizations. The main advantage is that such models allow the user to manipulate a setting on the imaging device, or change the viewing conditions, and still be able to recreate the process and produce an image in a reasonable amount of time. If the models must be iteratively inverted or recreated through exhaustive measurements, it might be completely impractical for a user to adjust any settings in order to obtain a desired result.

19.12 EXAMPLE SYSTEM

The previous discussions provide an overview of the process of device-independent color imaging. It is useful to examine an illustrative example of

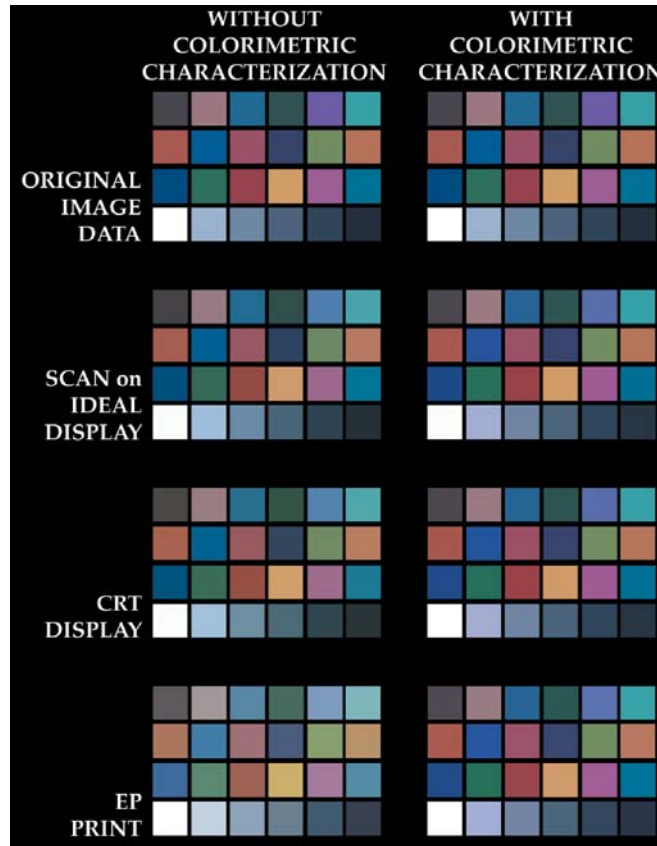


Figure 19.3 Examples of color reproduction accuracy in a typical desktop imaging system without and with colorimetric calibration and characterization

the results that can be obtained with such processes. The impact of various color appearance models in the chain was illustrated in Chapter 17 (Figures 17.4–17.6). Figure 19.3 illustrates the quality of color reproduction that can be obtained with high-quality device characterizations, as described in the previous sections, in comparison with the reproductions that would be obtained using the devices right out of the box with no additional calibration or characterization.

The example system consists of typical high-end image input, processing, display, and printing devices for the home-computer market. The images in Figure 19.3 are synthesized representations of the colors that are actually obtained at various steps in the process. While the images are synthesized representations of the results, the colors are accurate representations of the results obtained in a real system. The original image is taken to be a photographic print of a Macbeth ColorChecker® Chart (McCamy *et al.* 1976) as illustrated in the first row of Figure 19.3. The image is scanned using a 600

dpi flat-bed scanner with 10-bits-per-channel quantization. The second row of Figure 19.3 illustrates the accuracy of the scanned image as represented on a theoretically ideal display (i.e., the display introduces no additional error). The image on the left illustrates the result obtained with no colorimetric characterization (just gamma correction), while the image on the right illustrates the accuracy obtained with a characterization technique such as that outlined by Berns and Shyu (1995).

The next step involves display on a high-resolution CRT as illustrated in the third row of Figure 19.3. The left image illustrates the result of assuming the monitor and video driver are set up to the nominally defined system gamma (e.g., 1.8 for a Macintosh® system, 1.3–1.5 for a Silicon Graphics system, 2.2–2.5 for a Windows® system). It is assumed that any deviation from the nominal white point goes unnoticed due to chromatic adaptation. The image on the right illustrates the accuracy obtained with a specific characterization of the display systems using the techniques described by Berns (1996). Note that these images include both the scanner errors and the monitor errors as the full system is being constructed.

The final step is to print the image on a 600 dpi color laser printer. The image on the left illustrates the result obtained when using the default printer driver and PostScript® Printer Description (PPD) file. The image on the right illustrates the results obtained when a three-dimensional LUT is constructed using a measurement technique with a $9 \times 9 \times 9$ sampling of the gamut. Again, these final images illustrate errors that have been propagated through the entire imaging system. Clearly careful colorimetric characterization of the three devices making up this system can result in significantly improved results. Unfortunately, the current state of technology does not allow typical users to achieve this level of colorimetric accuracy. However, the potential does exist. The ICC implementation described in the next section provides a framework. What remains to be implemented is the production of devices that can be accurately calibrated and characterized in the factory (and remain stable) such that typical users will not have to be concerned about calibrating and characterizing the devices themselves.

19.13 ICC IMPLEMENTATION

The International Color Consortium (1995) has provided a framework for a more universally implemented system to implement the process of device-independent color imaging as illustrated in Figure 19.1 through their specification of the ICC Profile Format. The consortium consists of approximately 50 corporations and organizations involved in color reproduction software, hardware, computer systems, and operating systems. The profile format is a specification of a data structure that can be used to describe device characterizations (both models and LUTs), viewing conditions, and rendering intent. Such profiles can be used in conjunction with various imaging devices or connected with images to facilitate communication of the colorimetric his-

tory of image data. The profile format provides a structure for communication of the required data such that the profiles can be easily interchanged among different computers, operating systems, and/or software applications. While the ICC profile provides the data necessary to implement device-independent color imaging, it is up to the software and hardware developers to build software to utilize this information to complete the system. Such software is referred to as a *color management system* and is quickly becoming more and more integrated into operating systems. There is also a significant requirement for the development of profiles to accurately characterize various devices, appearance transformations, gamut-mapping transformations, and color preference mappings. The quality of a system based on ICC profiles will depend on the capabilities of the color management software and the quality of the profiles. With high-quality implementations, the ICC profile specification provides the framework and potential for excellent results.

The construction and implementation of the ICC profile format and color management systems and other compatible software is an evolving process. The current status and profile format documentation can be found at the ICC world-wide web site, www.color.org. The ICC documents also contain information on other ongoing international standardization activities relevant to device-independent color imaging applications.

Profile Connection Space

One important concept of the ICC specification is the profile connection space. It is often misunderstood because the exact definition and implementation of the profile connection space remains an issue of discussion and debate within ICC. The most recent ICC documentation should be referred to for an up-to-date discussion of this topic.

Essentially, the profile connection space is defined by a particular set of viewing condition parameters that are used to establish reference viewing conditions. The concept of the profile connection space is that a given input device profile will provide the information necessary to transform device coordinates to a device-independent color specification (CIE XYZ or CIELAB) of the image data that represents the appearances of the original image data in the viewing conditions of the profile connection space (or from CIE specifications in profile connection space to device coordinates for an output device profile). The technique for obtaining this transformation is not yet agreed upon. As an example, the original definition of the ICC profile connection space reference viewing conditions are as follows:

Reference reproduction medium: idealized print with $D_{\min} = 0.0$

Reference viewing environment: ANSI PH2.30 standard booth

Surround: normal

Illumination color: that of CIE illuminant D50

Illuminance: 2200 ± 470 lux

Colorimetry: ideal, flareless measurement

Observer: CIE 1931 standard colorimetric observer (implied)

Measurement geometry: unspecified

As an example of using ICC profiles with the profile connection space, imagine a system with a digital camera calibrated for D65 illumination, a CRT display with a 9300 K white point, and a printer with output viewed under D50 illumination. An input profile for the digital camera would have to provide the information necessary to first transform from the camera device coordinates, say *RGB*, to CIE tristimulus values for illuminant D65 using typical device calibration and characterization techniques. The tristimulus values for illuminant D65 and the viewing conditions of image capture would then need to be transformed to corresponding tristimulus values for the profile connection space (illuminant D50, etc.) using some color appearance model. All the information necessary to perform the transformation from device coordinates to corresponding tristimulus values in the profile connection space would have to be incorporated into the input device profile.

The CRT display would have an output device profile that would include the information necessary to transform from the profile connection space to corresponding tristimulus values for the CRT viewing conditions (9300 K white point, dim surround, etc.) and then through a device characterization to the *RGB* values required to display the desired colors. When implemented within a color management system, the two device profiles would be concatenated such that the *RGB* data from the camera is transformed directly to the *RGB* data for the display without ever existing in any of the several intermediate spaces or, indeed, even in the profile connection space.

Assuming the printer is set up and characterized for viewing conditions that match the profile connection space, the output device profile for the printer only needs to include information for the transform from illuminant D50 CIE coordinates to the device coordinates.

An interesting ‘feature’ of this process is that a device profile is required to provide the transformation from device coordinates to the profile connection space, even for situations in which a color appearance model would normally not be required. For example, if the camera is set up for D65 illumination and the monitor is set up with a D65 white point, then it makes no sense to first transform through the appearance models to get to the D50 profile connection space and then come back out to a D65 display. Since profiles are concatenated by color management systems, this is not a problem as long as a single color appearance model is agreed upon. The ICC is working toward this objective, but at the present time, there is no single recommended color appearance model for the construction of ICC profiles. Thus an input device profile builder might implement the Hunt model to get into the profile connection space, while an output device profile builder might implement the RLAB model to come out of the profile connection space. Since there are significant differences between the various appearance models, processed images might change dramatically in situations for which a color appearance model was not even required. The existence of CIE color

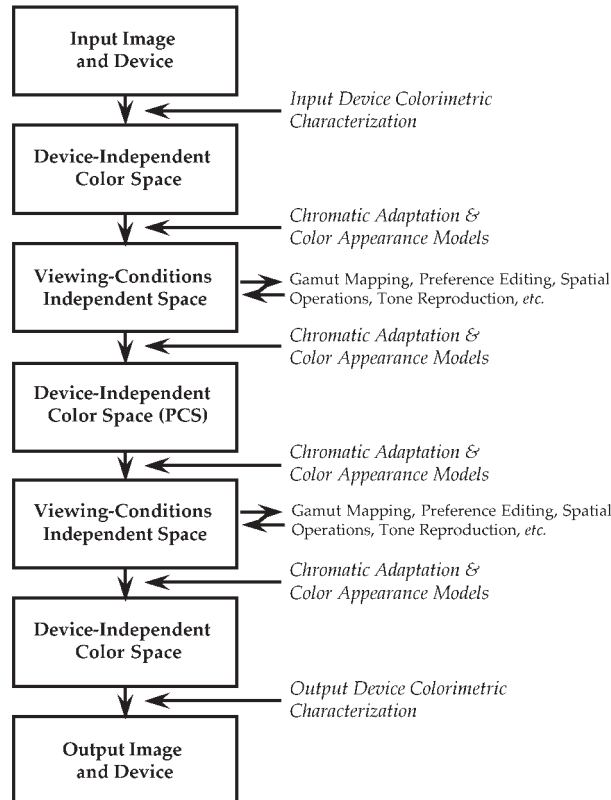


Figure 19.4 A revision of the flow chart in Figure 19.1 to accommodate the concept of a profile connection space as described by the ICC

appearance models might help remedy this situation. The latest ICC documentation should be examined to see how these and other issues are being addressed.

The concept of the profile connection space is completely compatible with the process described by Figure 19.1. The only addition required is a transformation out of the viewing-conditions-independent color space into a device-independent color space (CIE XYZ or CIELAB) for the viewing conditions of the profile connection space. At this point the conceptual interchange of data from one device to the other occurs. Finally, a transformation from the device-independent color space for the profile connection space viewing conditions to the viewing-conditions-independent color space is made prior to adjustments for the viewing conditions of the output. This process is illustrated in Figure 19.4. The concept of the information processing is not changed. The profile connection space can be thought of as a virtual imaging device. This means that the original flow chart of Figure 19.1 is still used, but either the input device (for output situations) or the output device (for input situations) becomes the profile connection space 'virtual device.'

20

Image Appearance Modeling and the Future

Color appearance modeling has made some significant advances in the six years between editions of this book. The general approach of the models presented in this book is to isolate color from other dimensions of visual performance as much as possible. It is possible, and perhaps likely, that such models have progressed about as far as they can and that further advances will require different types of models. Recently, Fairchild and Johnson (2002, 2003, 2004) have proposed a different sort of model referred to as an image appearance model. An image appearance model extends color appearance models to incorporate properties of spatial and temporal vision allowing prediction of appearance in complex stimuli and the measurement of image differences (the first step toward an image quality metric). This chapter reviews the concept of image appearance modeling and presents one such model, known as iCAM. The treatment is largely based on the Fairchild and Johnson (2004) review article. Finally, this chapter ends with some speculation on what might happen in the near future in the areas of color appearance modeling and image appearance modeling. For updates on the current status of various models and key references that appeared after publication of this book, refer to the associated website, <www.cis.rit.edu/fairchild/CAM.html>. For updates on iCAM and related source code, refer to <www.cis.rit.edu/mcs1/iCAM>.

20.1 FROM COLOR APPEARANCE TO IMAGE APPEARANCE

The history of image measurement helps set the context for the formulation and application of image appearance models, a somewhat natural evolution of color appearance, spatial vision, and temporal vision models when they are considered in a holistic sense, rather than as individual research fields. Early imaging systems were either not scientifically measured at all, or measured with systems designed to specify the variables of the imaging system itself. For example, densitometers were developed for measuring photographic materials with the intent of specifying the amounts of dye or silver produced in the film. In printing, similar measurements would be made for the inks as well as measures of the dot area coverage for halftone systems. In electronic systems like television, system measurements such as signal voltages were used to colorimetrically quantify the imaging system (Hunt 1995). Vision-based measurements of imaging systems for image-quality do have a long history as illustrated by the example of Schade's (1956) pioneering work. However, as imaging systems evolved in complexity and openness, the need for device-independent image measures became self-evident.

Image Colorimetry

Electronic imaging systems, specifically the development of color television, prompted the first application of device-independent color measurements of images. Wright (1981b), in fact, points out that color television could not have been invented without colorimetry. The CIE system was used very successfully in the design and standardization of color television systems (including recent digital television systems).

Application of CIE colorimetry to imaging systems became much more prevalent with the advent of digital imaging systems and the use of computer systems to generate and proof content ultimately destined for other media. The use of CIE colorimetry to specify images across the various devices promised to solve some of the new color reproduction problems created by open, digital systems. The flexibility of digital systems also made it possible and practical to perform colorimetric transformations on image data in attempts to match the colors across disparate devices and media.

Research on imaging device calibration and characterization has spanned the range from fundamental color measurement techniques to the specification of a variety of devices including CRT, LCD, and projection displays, scanners and digital cameras, and various film recording and print media. Some of the concepts and results of this research have been summarized by Berns (1997). Such capabilities are a fundamental requirement for research and development in color and image appearance. Research on device characterization and calibration provides a means to tackle more fundamental problems in device-independent color imaging. For example, conceptual research on design and implementation of device-independent color imaging

(Fairchild 1994a), gamut mapping algorithms to deal with the reproduction of desired colors that fall outside the range that can be obtained with a given imaging device (Braun and Fairchild 2000), and computer graphics rendering of high-quality spectral images that significantly improve the potential for accurate color in rendered scenes (Johnson and Fairchild 1999). This type of research built upon, and contributed to, research on the development and testing of color appearance models for cross-media image reproduction.

Color Difference Equations

Color difference research has culminated with the recently published CIEDE2000 color difference formula (Luo *et al.* 2001). At the heart of such color difference equations lies some form of uniform color space. The CIE initially recommended two such color spaces in 1976, CIELAB and CIELUV. Both spaces were initially described as interim color spaces, with the knowledge that they were far from complete. With a truly uniform color space, color differences can then be taken to be a simple measure of distance between two colors in the space, such as CIE ΔE_{ab}^* . The CIE recognized the nonuniformity of the CIELAB color space, and formulated more advanced color difference equations such as CIE DE94 and CIEDE2000. These more complicated equations are very capable of predicting perceived color differences of simple color patches.

Image Difference

The CIE color difference formulae were developed using simple color patches in controlled viewing conditions. There is no reason to believe that they are adequate for predicting color difference for spatially complex image stimuli. The S-CIELAB model (Zhang and Wandell 1996) was designed as a spatial pre-processor to the standard CIE color difference equations, to account for complex color stimuli such as halftone patterns. The spatial preprocessing uses separable convolution kernels to approximate the contrast sensitivity functions (CSF) of the human visual system. The CSF serves to remove information that is imperceptible to the visual system. For instance, when viewing halftone dots at a certain distance the dots tend to blur, and integrate into a single color. A pixel-by-pixel color difference calculation between a continuous image and a halftone image would result in very large errors, while the perceived difference might in fact be small. The spatial preprocessing would blur the halftone image so that it more closely resembles the continuous tone image.

S-CIELAB represents the first incarnation of an image difference model based upon the CIELAB color space and color difference equations. Recently this model has been refined and extended into a modular framework for image color difference calculations (Johnson and Fairchild 2001a, 2003a,b).

This framework, discussed in Section 20.3, refines the CSF equations from the S-CIELAB model, and adds modules for spatial frequency adaptation, spatial localization, and local and global contrast detection.

Color Appearance

Unfortunately, fundamental CIE colorimetry does not provide a complete solution for image specification. By their very nature, the images produced or captured by various digital systems are examined in widely disparate viewing conditions, from the original captured scene, to a computer display in a dim room, to printed media under a variety of light sources to projection displays in dark rooms. Thus color appearance models were developed to extend CIE colorimetry to the prediction of color appearance (not just color matches) across changes in media and viewing conditions (not just within a single condition). Color appearance modeling research applied to digital imaging systems was very active throughout the 1990s, culminating with the recommendation of the CIECAM97s model in 1997 (Chapter 15) and its revision, CIECAM02, in 2002 (Chapter 16). The development of these models was also enabled by visual experiments performed to test the performance of published color appearance models in realistic image reproduction situations (e.g., Braun and Fairchild 1997). Such research on color appearance modeling in imaging applications naturally highlighted the areas that are not adequately addressed for spatially complex image appearance and image quality problems.

Image Appearance and Image Quality

Color appearance models account for many changes in viewing conditions, but are mainly focused on changes in the color of the illumination (white point), the illumination level (luminance), and surround relative luminance. Such models do not directly incorporate any of the spatial or temporal properties of human vision and the perception of images. They essentially treat each pixel of an image (and each frame of a video) as completely independent stimuli.

Visual adaptation to scenes and images is not only spatially localized according to some low-pass characteristics, but also temporally localized in a similar manner. To predict the appearance of digital video sequences, particularly those of high dynamic range, the temporal properties of light and chromatic adaptation must be considered. To predict the quality (or image differences) of video sequences, temporal filtering to remove imperceptible high-frequency temporal modulations (imperceptible ‘flicker’) must be added to the spatial filtering that removes imperceptible spatial artifacts (e.g., noise or compression artifacts).

It is easy to illustrate that adaptation has a significant temporal low-pass characteristic. For example, if one suddenly turns on the lights in a darkened

room (as upon first awakening in the morning), the increased illumination level is at first dazzling to the visual system, essentially overexposing it. After a short period of time, the visual system adapts to the new, higher level of illumination and normal visual perception becomes possible. The same is true when going from high levels of illumination to low levels (imagine driving into a tunnel in the daytime). Fairchild and Reniff (1995) and Rinner and Gegenfurtner (2000) have made detailed measurements of the time-course of chromatic adaptation. These results suggest temporal integration functions that could be used in models of moving image appearance and also illustrate one of the mechanisms for spatially low-pass adaptation stimuli due to the influence of ever-present eye movements.

There has been significant research on video quality and video quality metrics, often aimed at the creation and optimization of encoding/compression/decoding algorithms such as MPEG2 and MPEG4. By analogy, the still-image visible differences predictor of Daly (1993) is quite applicable to the prediction of the visibility of artifacts introduced into still images by JPEG image compression. The Daly model was designed to predict the probability of detecting an artifact. Instead of focusing on threshold differences in quality, the focus in developing iCAM has been on the prediction of image quality scales (e.g., scales of sharpness, contrast, graininess) for images with changes well above threshold. Such suprathreshold image differences are a different domain of image quality research based on image appearance.

Likewise, a similar situation exists in the area of video quality metrics. Metrics have been published to examine the probability of detection of artifacts in video, but there appear to be no models of video image appearance designed for rendering video and predicting the magnitudes of perceived differences in video sequences. Two well-known video image quality models, the Sarnoff JND model and the NASA DVQ model, are briefly described below to contrast their capabilities with the objectives of the iCAM model.

The Sarnoff JND model is the basis of the *JNDmetrix* software package <www.jndmetrix.com> and related video quality hardware. The model is briefly described in a technical report published by Sarnoff (2001) and more fully disclosed in other publications (ATIS 2001). It is based on the multi-scale model of spatial vision published by Lubin (1993, 1995) with some extensions for color processing and temporal variation. The Lubin model is similar in nature to the Daly model in that it is designed to predict the probability of detection of artifacts in images. These are threshold changes in images, often referred to as just-noticeable differences, or JNDs. The Sarnoff JND model has no mechanisms of chromatic and luminance adaptation, as are included in the iCAM model. The input to the Sarnoff model must first be normalized (which can be considered a very rudimentary form of adaptation). The temporal aspects of the Sarnoff model are also not aimed at predicting the appearance of video sequences, but rather at predicting the detectability of temporal artifacts. As such, the model only uses two frames (four fields) in its temporal processing. Thus, while it is capable of predicting the perceptibility of relatively high-frequency temporal variation in the video

(flicker) it cannot predict the visibility of low frequency variations that would require an appearance-oriented, rather than JND-oriented, model. The Sarnoff model also is not designed for rendering video. This is not a criticism of the model formulation, but an illustration of how the objective of the Sarnoff JND model is significantly different from that of the iCAM model. While it is well accepted in the vision science literature that JND predictions are not linearly related to suprathreshold appearance differences, it is certainly possible to use a JND model to try to predict suprathreshold image differences and the Sarnoff JND model has been applied with some success to such data.

A similar model, the *DVQ* (Digital Video Quality) metric has been published by Watson (1998) and Watson *et al.* (2001) of NASA. The *DVQ* metric is similar in concept to the Sarnoff JND model, but significantly different in implementation. Its spatial decomposition is based on the coefficients of a discrete cosine transformation (DCT) making it amenable to hardware implementation and likely making it particularly good at detecting artifacts introduced by DCT-based video compression algorithms. It also has a more robust temporal filter that should be capable of predicting a wider array of temporal artifacts. Like the Sarnoff model, the *DVQ* metric is aimed at predicting the probability of detection of threshold image differences. The *DVQ* model also includes no explicit appearance processing through spatial or temporal adaptation, or correlates of appearance attributes and therefore also cannot be used for video rendering. Again, this is not a shortcoming, but rather a property of the design objectives for the *DVQ* model.

While color appearance modeling has been successful in facilitating device-independent color imaging and is incorporated into modern color management systems, there remains significant room for improvement and extension of capabilities. To address these issues with respect to spatial properties of vision and image perception and image quality, the concept of image appearance models has been recently introduced and implemented (Fairchild and Johnson 2002, Fairchild 2002a,b). These models combine attributes of color appearance models with attributes of spatial vision models that have been previously used for image quality metrics in an attempt to further extend the capabilities of color appearance models. Historically color appearance models largely ignored spatial vision (e.g., CIECAM97s, CIECAM02) while spatial vision models for image quality largely ignored color (Daly 1993, Lubin 1993). Some exceptions include the retinex model (Land 1986, 1964, Land and McCann 1971, McCann *et al.* 1976) and its various derivatives (Funt *et al.* 2000, Barnard and Funt 1997, Brainard and Wandell 1986). The spatial ATD model (Granger 1993) and the S-CIELAB model (Zhang and Wandell 1996) also address some of these issues to various extents. While the retinex model was never designed as a complete model of image appearance and quality, its spatially variable mechanisms of chromatic adaptation and color constancy serve some of the same purposes in image rendering and provide some of the critical groundwork for image appearance modeling.

The goal in developing an image appearance model has been to bring these research areas together to create a single model applicable to image appearance, image rendering, and image quality specifications and evaluations. One such model for still images, referred to as iCAM, is detailed in this chapter. This model was built upon previous research in uniform color spaces (Ebner and Fairchild 1998), the importance of image surround (Fairchild 1995b), algorithms for image difference and image quality measurement (Johnson and Fairchild 2003a, Fairchild 2002a,b), insights into observers eye movements while performing various visual imaging tasks and adaptation to natural scenes (Babcock *et al.* 2003, Webster and Mollon 1997), and an earlier model of spatial and color vision applied to color appearance problems and high-dynamic-range (HDR) imaging (Pattanaik *et al.* 1998).

Color and Image Appearance Models

A model capable of predicting perceived color difference between complex image stimuli is a useful tool, but has some limitations. Just as a color appearance model is necessary to fully describe the appearance of color stimuli, an image appearance model is necessary to describe spatially complex color stimuli. Color appearance models allow for the description of attributes such as lightness, brightness, colorfulness, chroma, and hue. Image appearance models extend upon this to also predict such attributes as sharpness, graininess, contrast, and resolution.

A uniform color space also lies at the heart of the of an image appearance model. The modular image difference framework allows for great flexibility in the choice of color spaces. Examples are the CIELAB color space, similar to S-CIELAB, the CIECAM02 color appearance model, or the IPT color space (Ebner and Fairchild 1998). Thus, the modular image difference framework can be implemented within the iCAM model as described in this chapter to create a full image appearance and image difference model. It could also be implemented in other color spaces if desired.

Models of image appearance can be used to formulate multi-dimensional models of image quality. For example it is possible to take weighted sums of various appearance attributes to determine a metric of overall image quality, as described by Keelan (2002) and Engledrum (2002). Essentially these models can augment or replace human observations to weight image attributes with overall appearances of quality. For instance a model of quality might involve weighted sums of tonal balance, contrast, and sharpness. A step towards this type of model is illustrated in the following sections.

20.2 THE ICAM FRAMEWORK

Figure 20.1 presents a flowchart of the general framework for the iCAM image appearance model as applied to still images. For input, the model

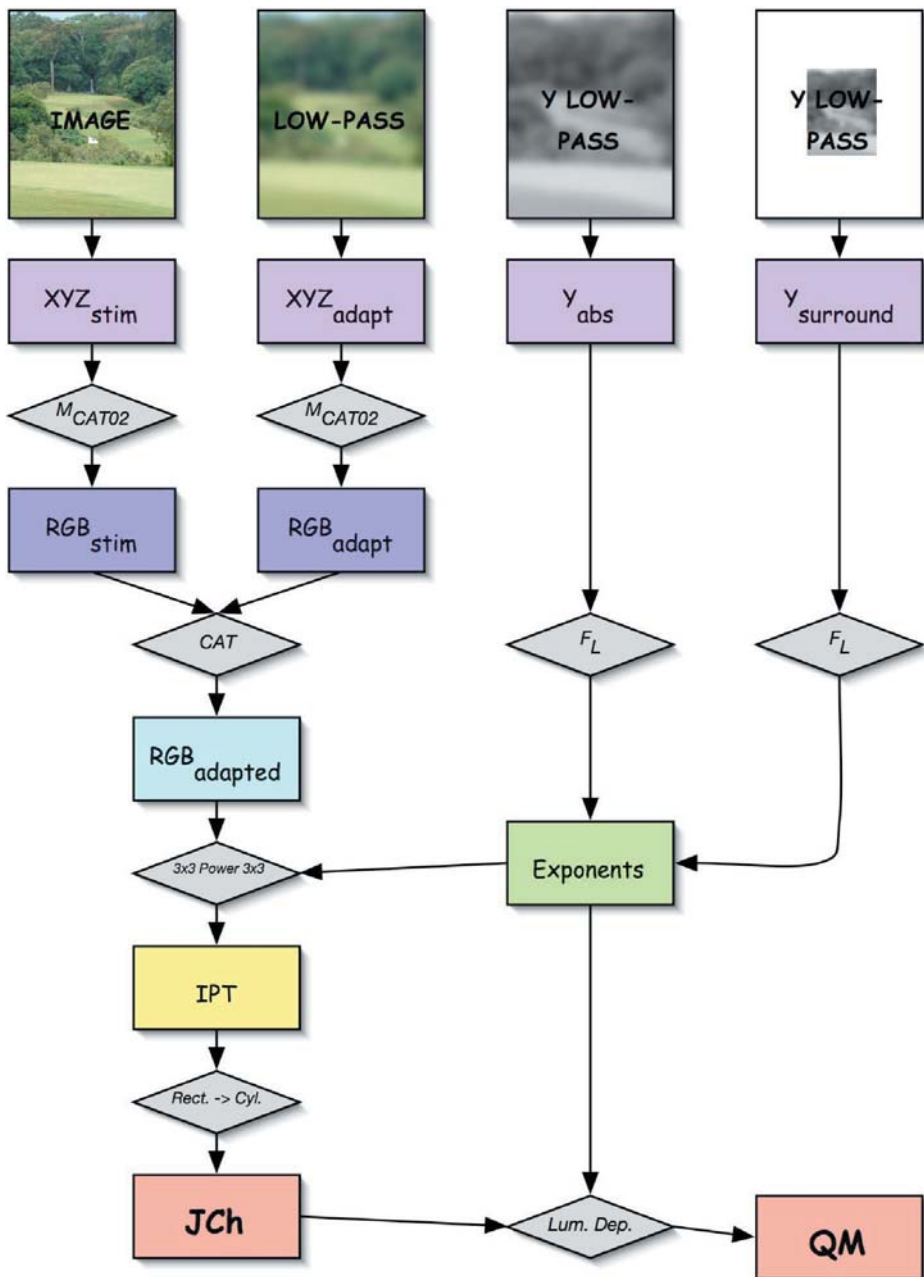


Figure 20.1 Flowchart of the iCAM image appearance model. Inputs to the model are CIE tristimulus values, XYZ , for the stimulus image or scene and a low-pass version used as an adapting stimulus and absolute luminance information for the low-pass image and surround. Adapted signals are computed using the linear chromatic adaptation transform from CIECAM02 and then converted into an opponent space IPT , using the luminance information to modulate a compressive nonlinearity. The rectangular IPT coordinates are then converted to cylindrical correlates of lightness J , chroma C , and hue h . The lightness and chroma correlates can then be scaled by a function of the absolute luminance information to provide correlates of brightness QM and colorfulness M . If desired, a saturation correlate can be computed as the ratio of chroma to lightness (or colorfulness to brightness)

requires colorimetrically characterized data for the image (or scene) and surround in absolute luminance units. The image is specified in terms of relative CIE XYZ tristimulus values. The adapting stimulus is a low-pass filtered version of the CIE XYZ image that is also tagged with absolute luminance information necessary to predict the degree of chromatic adaptation. The absolute luminances Y of the image data are also used as a second low-pass image to control various luminance-dependent aspects of the model intended to predict the Hunt effect (increase in perceived colorfulness with luminance) and the Stevens effect (increase in perceived image contrast with luminance). Lastly, a low-pass, luminance Y image of significantly greater spatial extent is used to control the prediction of image contrast that is well-established to be a function of the relative luminance of the surrounding conditions (Bartleson and Breneman equations). The specific low-pass filters used for the adapting images depend on viewing distance and application. Additionally, in some image rendering circumstances it might be desirable to have different low-pass adapting images for luminance and chromatic information to avoid desaturation of the rendered images due to local chromatic adaptation. This is one example of application dependence in image appearance modeling. Local chromatic adaptation might be appropriate for image-difference or image-quality measurements, but inappropriate for image-rendering situations.

The first stage of processing in iCAM is to account for chromatic adaptation. The chromatic adaptation transform embedded in CIECAM02 has been adopted in iCAM since it was well researched and established to have excellent performance with all available visual data. It is also a relatively simple chromatic adaptation model amenable to image-processing applications. The chromatic adaptation model, given in Equations 20.1–20.6, is a linear von Kries normalization of *RGB* image signals to the *RGB* adaptation signals derived from

$$\begin{vmatrix} R \\ G \\ B \end{vmatrix} = \mathbf{M}_{\text{CAT02}} \begin{vmatrix} X \\ Y \\ Z \end{vmatrix} \quad (20.1)$$

$$\mathbf{M}_{\text{CAT02}} = \begin{vmatrix} 0.7328 & 0.4296 & -0.1624 \\ -0.7036 & 1.6975 & 0.0061 \\ 0.0030 & 0.0136 & 0.9834 \end{vmatrix} \quad (20.2)$$

$$D = F \left[1 - \left(\frac{1}{3.6} \right) e^{\left(\frac{-L_A - 42}{92} \right)} \right] \quad (20.3)$$

$$R_C = \left[\left(100 \frac{D}{R_W} \right) + (1 - D) \right] R \quad (20.4)$$

$$G_C = \left[\left(100 \frac{D}{G_W} \right) + (1 - D) \right] G \quad (20.5)$$

$$B_C = \left[\left(100 \frac{D}{B_W} \right) + (1 - D) \right] B \quad (20.6)$$

the low-pass adaptation image at each pixel location ($R_W G_W B_W$). The *RGB* signals are computed using a linear transformation from *XYZ* to *RGB* derived by CIE TC8-01 in the formulation of CIECAM02. The von Kries normalization is further modulated with a degree-of-adaptation factor D that can vary from 0.0 for no adaptation to 1.0 for complete chromatic adaptation. Equation 20.3 is provided in the CIECAM02 formulation, and used in iCAM, for computation of D as a function of adapting luminance L_A , for various viewing conditions. Alternatively the D factor can be established manually. The chromatic adaptation model is used to compute corresponding colors for CIE Illuminant D65 that are then used in the later stages of the iCAM model. This is accomplished by taking the adapted signals for the viewing condition, $R_C G_C B_C$, and then inverting Equations 20.1–20.6 for an illuminant D65 adapting white point and with $D = 1.0$. It should be noted that, while the adaptation transformation is identical to that in CIECAM02, the iCAM model is already significantly different since it uses spatially modulated image data as input rather than single color stimuli and adaptation points. One example of this is the modulation of the absolute luminance image and surround luminance image using the F_L function from CIECAM02 given in Equation 20.7. This function, slowly varying with luminance, has been

$$F_L = 0.2 \left(\frac{1}{(5L_A + 1)} \right)^4 (5L_A) + 0.1 \left(1 - \left(\frac{1}{(5L_A + 1)} \right)^4 \right)^2 (5L_A)^{1/3} \quad (20.7)$$

established to predict a variety of luminance-dependent appearance effects in CIECAM02 and earlier models. Since the function has been established and understood, it was also adopted for the early stages of iCAM. However, the manner in which the F_L factor is used in CIECAM02 and iCAM are quite different.

The next stage of the model is to convert from *RGB* signals (roughly analogous to cone signals in the human visual system) to opponent-color signals (light–dark, red–green, and yellow–blue; analogous to higher-level encoding in the human visual system) that are necessary for constructing a uniform perceptual color space and correlates of various appearance attributes. In choosing this transformation, simplicity, accuracy, and applicability to image processing were the main considerations. The color space chosen was the *IPT* space previously published by Ebner and Fairchild (1998). The *IPT* space was derived specifically for image processing applications to have a relatively simple formulation and specifically to have a hue angle component

with good prediction of constant perceived hue (important in gamut-mapping applications). More recent work on perceived hue has validated the applicability of the *IPT* space. The transformation from *RGB* to the *IPT* opponent space is far simpler than the transformations used in CIECAM02. The process, expressed in Equations 20.8–20.12, involves a linear transformation to a different cone-response space, application of power-function nonlinearities, and then a final linear transformation to the *IPT* opponent space (*I* light–dark; *P* red–green, *T* yellow–blue).

$$\begin{bmatrix} L \\ M \\ S \end{bmatrix} = \begin{bmatrix} 0.4002 & 0.7075 & -0.0807 \\ -0.2280 & 1.1500 & 0.0612 \\ 0.0 & 0.0 & 0.9184 \end{bmatrix} \begin{bmatrix} X_{D65} \\ Y_{D65} \\ Z_{D65} \end{bmatrix} \quad (20.8)$$

$$\begin{aligned} L' &= L^{0.43}; & L &\geq 0 \\ L' &= -|L|^{0.43}; & L &\leq 0 \end{aligned} \quad (20.9)$$

$$\begin{aligned} M' &= M^{0.43}; & M &\geq 0 \\ M' &= -|M|^{0.43}; & M &\leq 0 \end{aligned} \quad (20.10)$$

$$\begin{aligned} S' &= S^{0.43}; & S &\geq 0 \\ S' &= -|S|^{0.43}; & S &\leq 0 \end{aligned} \quad (20.11)$$

$$\begin{bmatrix} I \\ P \\ T \end{bmatrix} = \begin{bmatrix} 0.4000 & 0.4000 & 0.2000 \\ 4.4550 & -4.8510 & 0.3960 \\ 0.8056 & 0.3572 & -1.1628 \end{bmatrix} \begin{bmatrix} L' \\ M' \\ S' \end{bmatrix} \quad (20.12)$$

The power-function nonlinearities in the *IPT* transformation are a critical aspect of the iCAM model. First, they are necessary to predict response compression that is prevalent in most human sensory systems. This response compression helps to convert from signals that are linear in physical metrics (e.g., luminance) to signals that are linear in perceptual dimensions (e.g., lightness). The CIECAM02 model uses a hyperbolic nonlinearity for this purpose. The behavior of which is that of a power function over the practical ranges of luminance levels encountered. Secondly, and a key component of iCAM, the exponents are modulated according to the luminance of the image (low-pass filtered) and the surround. This is essentially accomplished by multiplying the base exponent in the *IPT* formulation by the image-wise computed F_L factors with appropriate normalization. These modulations of the *IPT* exponents allow the iCAM model to be used for predictions of the Hunt, Stevens, and Bartleson/Breneman effects mentioned previously. They also happen to enable the tone mapping of high-dynamic-range images into low-dynamic-range display systems in a visually meaningful way (see example in Figure 20.7).

For image-difference and image-quality predictions, it is also necessary to apply spatial filtering to the image data to eliminate any image variations at

spatial frequencies too high to be perceived. For example, the dots in a printed halftone image are not visible if the viewing distance is sufficiently large. This computation is dependent on viewing distance and based on filters derived from human contrast sensitivity functions. Since the human contrast sensitivity functions vary for luminance (band-pass with sensitivity to high frequencies) and chromatic (low-pass) information, it is appropriate to apply these filters in an opponent space. Thus in image quality applications of iCAM, spatial filters are applied in the *IPT* space. Since it is appropriate to apply spatial filters in a linear signal space, they are applied in a linear version of *IPT* prior to conversion into the non-linear version of *IPT* for appearance predictions. Johnson and Fairchild (2001a, 2003a,b) have recently discussed some of the important considerations for this type of filtering in image-difference applications and specified the filters used, based on available visual data. Since the spatial filtering effectively blurs the image data, it is not desirable for image rendering applications in which observers might view the images more closely than the specified viewing distance. Example contrast sensitivity functions, derived from fits to experimental data, used to define spatial filters for image difference computations are given in Equation 20.13 for the luminance *I*, channel and Equation 20.14 for the chromatic *P* and *T* channels (Johnson and Fairchild 2001a).

$$\text{CSF}_{\text{lum}}(f) = a \cdot f^c \cdot e^{-b \cdot f} \quad (20.13)$$

$$\text{CSF}_{\text{chrom}}(f) = a_1 \cdot e^{-b_1 \cdot f c_1} + a_2 \cdot e^{-b_2 \cdot f c_2} \quad (20.14)$$

The parameters *a*, *b*, and *c* in Equation 20.13 are set to 75, 0.2, and 0.8 respectively for the luminance CSF, applied to the *I* channel. In Equations 20.13 and 20.14, spatial frequency *f* is defined in terms of cycles per degree of visual angle (cpd). For the red-green chromatic CSF, applied to the *P* dimension, the parameters (*a*₁, *b*₁, *c*₁, *a*₂, *b*₂, *c*₂) in Equation 20.14 are set to (109.14, -0.00038, 3.424, 93.60, -0.00367, 2.168). For the blue-yellow chromatic CSF, applied to the *T* dimension, they are set to (7.033, 0.000004, 4.258, 40.69, -0.10391, 1.6487).

It is only appropriate to apply these spatial filters when the goal is to compute perceived image differences (and ultimately image quality). This is an important distinction between spatially localized adaptation (good for rendering and image quality metrics) and spatial filtering (good for image quality metrics, bad for rendering). In image quality applications, the spatial filtering is typically broken down into multiple channels for various spatial frequencies and orientations. For example, Daly (1993), Lubin (1993), and Pattanaik *et al.* (1998) describe such models. More recent results suggest that, while such multi-scale and multi-orientation filtering might be critical for some threshold metrics, it is often not necessary for data derived from complex images and for supra-threshold predictions of perceived image differences (Johnson and Fairchild 2001a, 2003a, Watson and Ramirez 2000).

Thus, to preserve the simplicity and ease of use of the iCAM model, single-scale spatial filtering with isotropic filters was typically adopted.

Once the *IPT* coordinates are computed for the image data, a simple coordinate transformation from rectangular to cylindrical coordinates is applied to obtain image-wise predictors of lightness J , chroma C , and hue angle h as shown in Equations 20.15–20.17. Differences in these dimensions can be used to compute image difference statistics and those used to derive image quality metrics. The overall Euclidean difference in *IPT* is referred to as ΔIm (Equation 20.20), for image difference, to distinguish it from a traditional color difference metric ΔE that includes no spatial filtering. In some instances, correlates of the absolute appearance attributes of brightness Q and colorfulness M are required. These are obtained by scaling the relative attributes of lightness and chroma with the appropriate function of F_L derived from the image-wise luminance map as shown in Equations 20.18 and 20.19.

$$J = I \quad (20.15)$$

$$C = \sqrt{P^2 + T^2} \quad (20.16)$$

$$h = \tan^{-1} \left(\frac{P}{T} \right) \quad (20.17)$$

$$Q = \sqrt[4]{F_L} J \quad (20.18)$$

$$M = \sqrt[4]{F_L} C \quad (20.19)$$

$$\Delta Im = \sqrt{\Delta I^2 + \Delta P^2 + \Delta T^2} \quad (20.20)$$

For image rendering applications it is necessary to take the computed appearance correlates JCh and then render them to the viewing conditions of a given display. The display viewing conditions set the parameters for the inversion of the *IPT* model and the chromatic adaptation transform (all for an assumed spatially uniform display adaptation typical of low-dynamic-range output media). This inversion allows the appearance of original scenes or images from disparate viewing conditions to be rendered for the observer viewing a given display. One important application of such rendering is the display of high-dynamic-range (HDR) image data on typical displays.

20.3 A MODULAR IMAGE-DIFFERENCE MODEL

A framework for a color image difference metric has recently been described by Johnson and Fairchild (2001b). That modular image difference metric is incorporated into the iCAM appearance model to address both image appearance and differences/quality within a single model. The image difference

framework was designed to be modular in nature, to allow for flexibility and adaptation. The framework itself is based upon the S-CIELAB spatial extension to the CIELAB color space. S-CIELAB merges traditional color difference equations with spatial properties of the human visual system. This was accomplished as a spatial filtering pre-processing, before a pixel-by-pixel color difference calculation.

The modular framework further extends this idea by adding several processing steps, in addition to the spatial filtering. These processing steps are contained in independent modules, so they can be tested and refined. Several modules have been defined (Johnson and Fairchild 2003a) and include spatial filtering, adaptation, and localization, as well as local and global contrast detection. Figure 20.2 shows a general flowchart with several distinct modules. These modules and their origins are described briefly below.

Spatial Filtering

The behavior of the human visual system in regards to spatially complex stimuli has been well studied over the years dating back to the seminal work of Campbell and Robson (1968) and Mullen (1985). Summaries of current knowledge and techniques for quantifying spatial vision can be found in several books (e.g., DeValois and DeValois 1988, Kelly 1994, Wandell 1995). The contrast sensitivity function describes this behavior in relation to spatial frequency. Essentially the CSF is described in a post-retinal opponent color space, with a band-pass nature for the luminance channel and low-pass nature for the chrominance channels. S-CIELAB uses separable convolution kernels to approximate the CSF, and modulate image details that are imperceptible. More complicated contrast sensitivity functions that include both modulation and frequency enhancement were discussed in detail by Johnson and Fairchild (2001a). Other models with similar features include the previously mentioned Lubin (1993), Daly (1993), MOM,(Pattanaik *et al.* 1998) S-CIELAB,(Zhang and Wandell 1996) and spatial ATD (Granger 1993) models. Other relevant discussions and models can be found in the work of Li *et al.* (1998), Taylor *et al.* (1997, 1998), and Brill's (1997) extension of the Lubin/Sarnoff model.

Spatial Frequency Adaptation

The contrast sensitivity function in this framework serves to modulate spatial frequencies that are not perceptible, and enhance certain frequencies that are most perceptible. Generally CSFs are measured using simple grating stimuli with care taken to avoid spatial frequency adaptation. Spatial frequency adaptation essentially decreases sensitivity to certain frequencies based upon information present in the visual field. An early and classic description of spatial frequency adaptation was published by Blakemore and

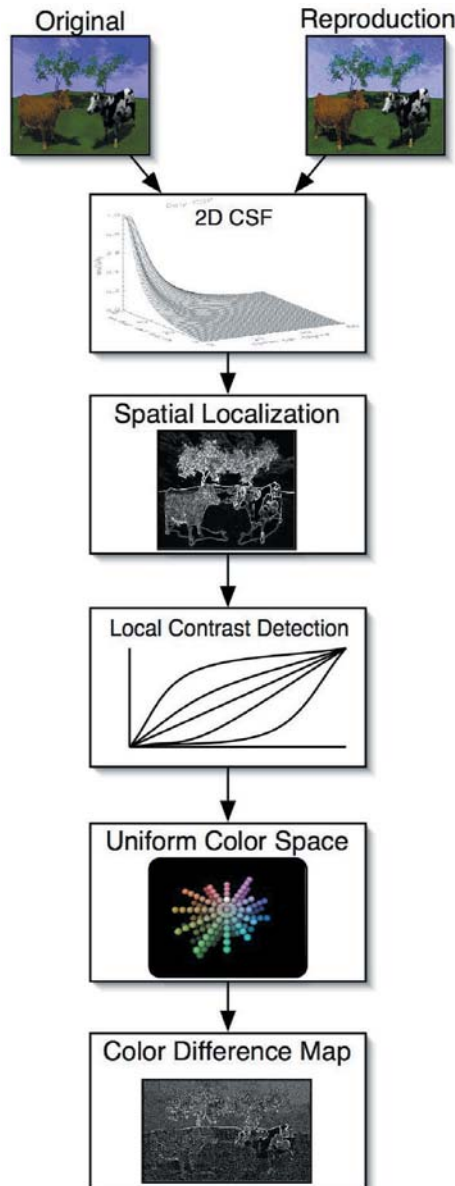


Figure 20.2 Flowchart of a modular image-difference metric

Campbell (1969). It should be noted that a multi-scale, or multi-channel, spatial vision model is not required to predict spatial frequency adaptation. Instead, all that is required is that the CSF functions be allowed to change shape as a function of adaptation (clearly indicating the existence of multi-scale mechanisms).

Since spatial frequency adaptation cannot be avoided in real world viewing conditions, several models of spatial frequency adaptation have been described for practical applications (Johnson and Fairchild 2001b). These models alter the nature of the CSF based upon either assumptions of the viewing conditions, or based upon the information contained in the images themselves.

Spatial Localization

The band-pass and low-pass contrast sensitivity serve to modulate high-frequency information, including high-frequency edges. The human visual system is generally acknowledged to be very adept at detecting edges. To accommodate this behavior, a module of spatial localization has been developed. This module can be as simple as an image processing edge-enhancing kernel, although that kernel must change as a function of viewing distance. Alternatively, the CSF can be modified to boost certain high-frequency information. The formulation and utility of edge-detection algorithms in vision applications has been well described by Marr (1982).

Local Contrast Detection

This module serves to detect local and global contrast changes between images. The utility of such processing in real visual systems has been described by Tolhurst and Heeger (1997). The current implementation is based upon the nonlinear mask based local contrast enhancement described by Moroney (2000b). Essentially a low-pass image mask is used to generate a series of tone-reproduction curves. These curves are based upon the global contrast of the image, as well as the relationship between a single pixel and its local neighborhood.

Color Difference Map

The output of the modular framework is a map of color differences ΔIm corresponding to the perceived magnitude of error at each pixel location. This map can be very useful for determining specific causes of error, or for detecting systematic errors in a color imaging system. Often it is useful to reduce the error map into a more manageable dataset. This can be accomplished using image statistics, so long as care is taken. Such statistics can be image mean, maximum median, or standard deviation. Different statistics might be more valuable than others depending on the application, as perhaps the mean error better describes overall difference, while the max might better describe threshold differences.

20.4 IMAGE APPEARANCE AND RENDERING APPLICATIONS

Figure 20.3 illustrates implementation of the iCAM framework required to complete an image rendering process necessary for HDR image tone mapping. The components essential in this process are the inversion of the *IPT* model for a single set of spatially constant viewing conditions (the display) and the establishment of spatial filters for the adapting stimuli used for local luminance adaptation and modulation of the *IPT* exponential non-linearity. While the derivation of optimal model settings for HDR image rendering is still underway, quite satisfactory results have been obtained using the settings outlined in Figure 20.3. Details of this algorithm were published by Johnson and Fairchild (2003c).

The iCAM model has been successfully applied to prediction of a variety of color appearance phenomena such as chromatic adaptation (corresponding colors), color appearance scales, constant hue perceptions, simultaneous contrast, crispening, spreading, and image rendering. (Fairchild and Johnson 2002).

Since iCAM uses the same chromatic adaptation transform as CIECAM02, it performs identically for situations in which only a change in state of chromatic adaptation is present (i.e., change in white point only). CIE TC8-01 has worked very hard to arrive at this adaptation transform and it is clear

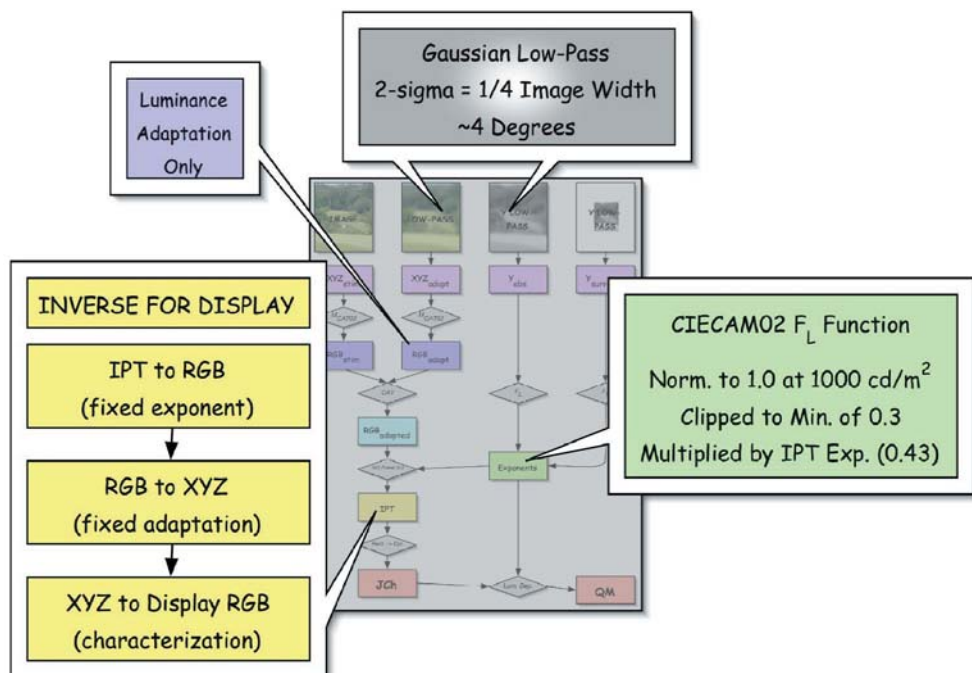


Figure 20.3 Implementation of iCAM for tone mapping of HDR images

that no other model currently exists with better performance (although there are several with equivalent performance). Thus the chromatic adaptation performance of iCAM is as good as possible at this juncture.

The appearance scales of iCAM are identical to the *IPT* scales for the reference viewing conditions. The *IPT* space has the best available performance for constant hue contours and thus this feature is retained in iCAM. This feature makes accurate implementation of gamut-mapping algorithms far easier in iCAM than in other appearance spaces. In addition, the predictions of lightness and chroma in iCAM are very good and comparable to the best color appearance models in typical viewing conditions. The brightness and colorfulness scales will also perform as well as any other model for typical conditions. In more extreme viewing conditions, the performance of iCAM and other models will begin to deviate. It is in these conditions that the potential strengths of iCAM will become evident. Further visual data must be collected to evaluate the model's relative performance in such situations.

The color difference performance of iCAM will be similar to that of CIELAB since the space is very similar under the reference viewing conditions. Thus, color difference computations will be similar to those already commonly used and the space can be easily extended to have a more accurate difference equation following the successful format of the CIE94 equations. (Following the CIEDE2000 equations in iCAM is not recommended since they are extremely complex and fitted to particular discrepancies of the CIELAB space such as poor constant-hue contours.)

Simultaneous contrast (or induction) causes a stimulus to shift in appearance away from the color of the background in terms of opponent dimensions. Figure 20.4 illustrates a stimulus that exhibits simultaneous contrast in lightness (the gray square is physically identical on all three backgrounds) and its prediction by iCAM as represented by the iCAM lightness predictor. This prediction is facilitated by the local adaptation features of iCAM.

Crispening is the phenomenon whereby the color differences between two stimuli are perceptually larger when viewed on a background that is similar to the stimuli. Figure 20.5 illustrates a stimulus that exhibits chroma crispening and its prediction by the iCAM chroma predictor. This prediction is also facilitated by the local adaptation features of iCAM.

Spreading is a spatial color appearance phenomenon in which the apparent hue of spatially complex image areas appears to fill various spatially coherent regions. Figure 20.6 provides an example of spreading in which the red hue of the annular region spreads significantly from the lines to the full annulus. The iCAM prediction of spreading is illustrated through reproduction of the hue prediction. The prediction of spreading in iCAM is facilitated by spatial filtering of the stimulus image.

One of the most interesting and promising applications of iCAM is to the rendering of high-dynamic-range (HDR) images to low-dynamic-range display systems. HDR image data are quickly becoming more prevalent. Historically HDR images were obtained through computer graphics simulations computed with global illumination algorithms (e.g., ray tracing or

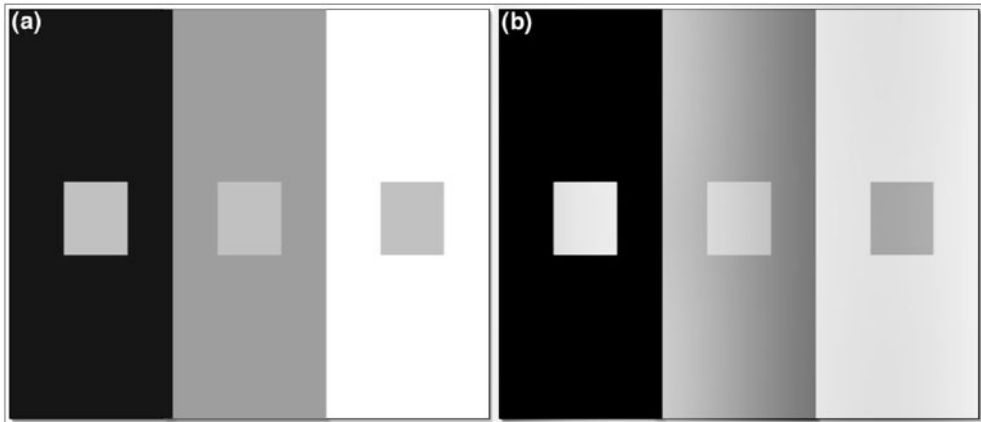


Figure 20.4 (a) Original stimulus and (b) iCAM lightness J image, illustrating the prediction of simultaneous contrast

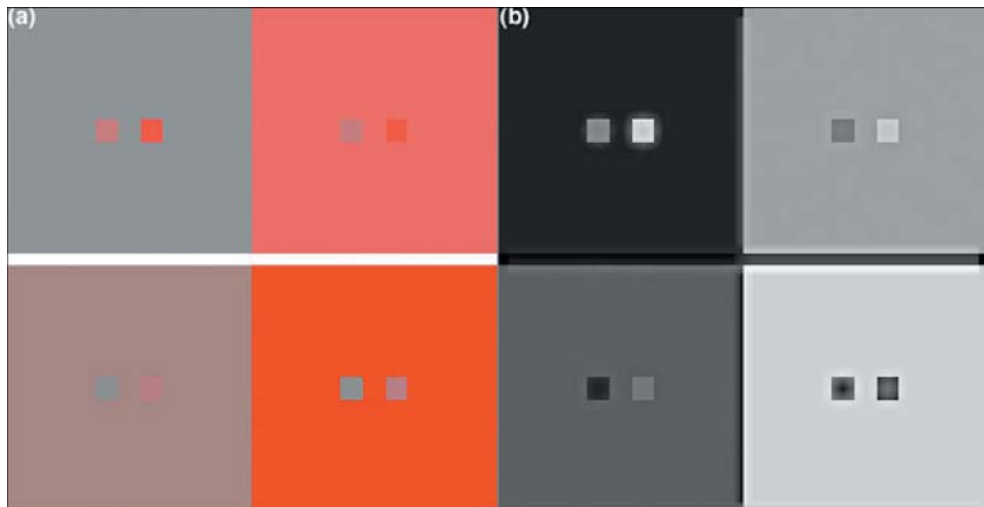


Figure 20.5 (a) Original stimulus and (b) iCAM chroma C image, illustrating the prediction of chroma crispening. Original image from <www.hpl.hp.com/personal/Nathan_Moroney/>

radiosity algorithms) or through the calibration and registration of images obtained through multiple exposures. Real scenes, especially those with visible light sources, often have luminance ranges of up to six orders of magnitude. More recently, industrial digital imaging systems have become commercially available that can more easily capture HDR image data. It is also apparent that consumer digital cameras will soon be capable of capturing greater

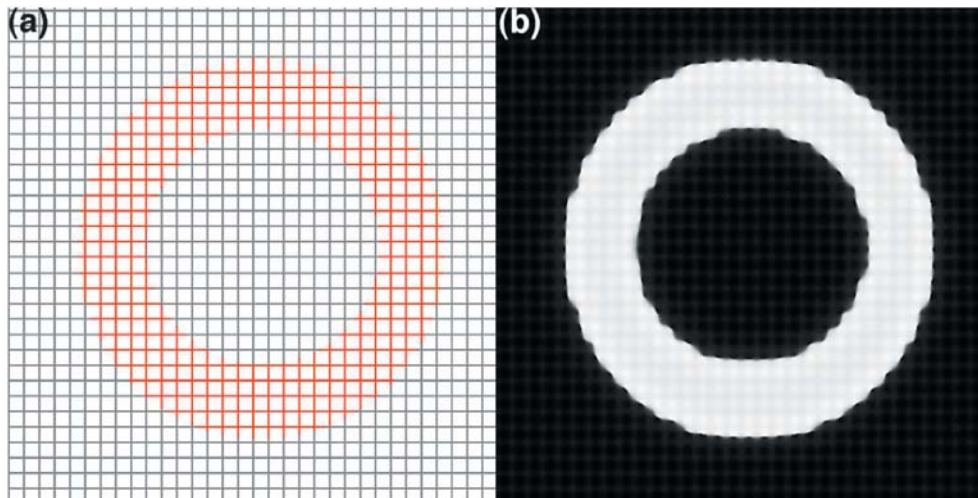


Figure 20.6 (a) Original stimulus and (b) iCAM hue h image, illustrating the prediction of spreading

dynamic ranges. Unfortunately display and use of such data are difficult and will remain so since even the highest-quality displays are generally limited in dynamic range to about two orders of magnitude. One approach is to interactively view the image and select areas of interest to be viewed optimally within the display dynamic range. This is only applicable to computer displays and not appropriate for pictorial imaging and printed output. Another limitation is the need for capability to work with greater than 24-bit (and often floating-point) image data. It is desirable to render HDR pictorial images onto a display that can be viewed directly (no interactive manipulation) by the observer and appear similar to what the observer would perceive if the original scene was viewed. For printed images, it is not just desirable, but necessary. Pattanaik *et al.* (1998) review several such HDR rendering algorithms and it is worth noting that several papers were presented on the topic at SIGGRAPH 2002 (Fattal *et al.* 2002, Durand and Dorsey 2002, Reinhard *et al.* 2002), illustrating continued interest in the topic.

Since iCAM includes spatially localized adaptation and spatially localized contrast control, it can be applied to the problem of HDR image rendering. Since the encoding in our visual system is of a rather low dynamic range, this is essentially a replication of the image appearance processing that goes on in the human observer and is being modeled by iCAM. Figure 20.7 illustrates application of the iCAM model to HDR images obtained fromDebevec <www.debevec.org>. The images in the left column of Figure 20.7 are linear renderings of the original HDR data normalized to the maximum presented simply to illustrate how the range of the original data exceeds a typical 24-bit (8 bits per RGB channel) image display. For example, the memorial image

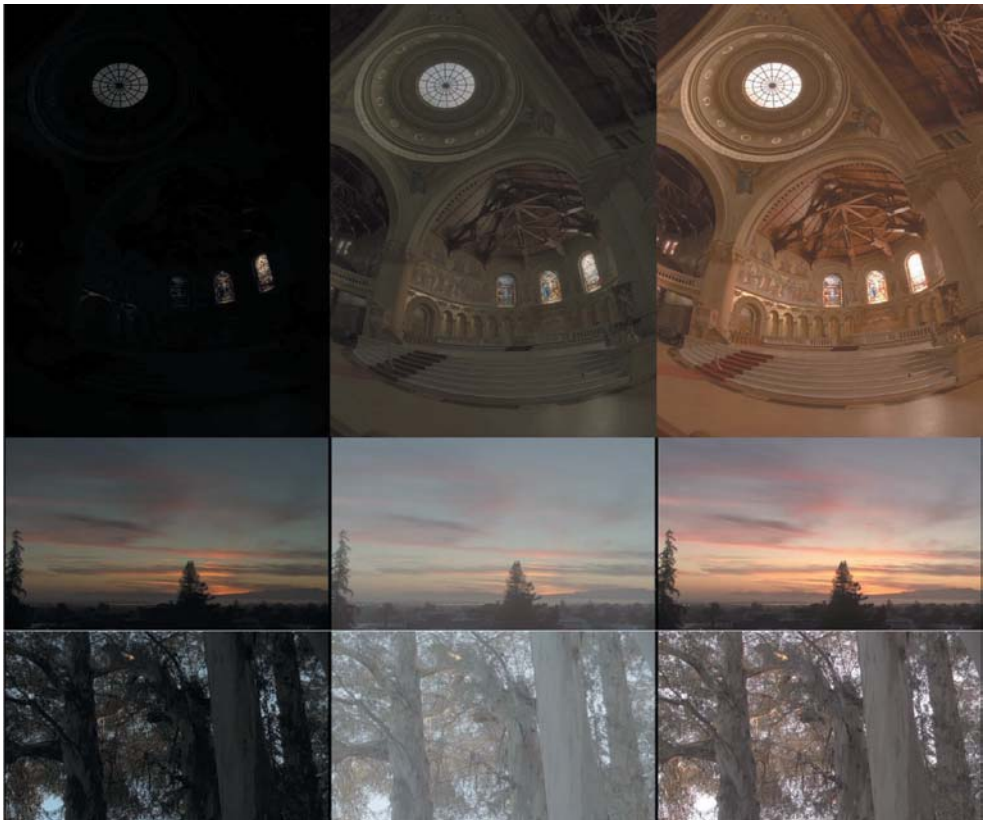


Figure 20.7 Three HDR images from <www.debevec.org>. The leftmost column illustrates linear rendering of the image data, the middle column illustrates manually optimized power-function transformations, and the rightmost column represents the automated output of the iCAM model implemented for HDR rendering (see Figure 20.3)

data (top row) have a dynamic range covering about six orders of magnitude since the sun was behind one of the stained-glass windows. The middle column of images represents a typical image-processing solution to rendering the data. One might consider a logarithmic transformation of the data, but that would do little to change the rendering in the first column. Instead the middle column was generated interactively by finding the optimum power-function transformation (also sometimes referred to as gamma correction; note that the linear images in the first column are already gamma corrected). For these images, transformations with exponents, or gammas, of approximately 1/6 (as opposed to 1/1.8 to 1/2.2 for typical displays) were required to make the image data in the shadow areas visible. While these power-function transformations do make more of the image data visible, they

required user interaction, tend to wash out the images in a way not consistent with the visual impression of the scenes, and introduce potentially severe quantization artifacts in shadow regions. The rightmost column of images shows the output of the iCAM model with spatially localized adaptation and contrast control (as shown in Figure 20.3). These images both render the dynamic range of the scene to make shadow areas visible and retain the colorfulness of the scene. The resulting iCAM images are quite acceptable as reproductions of the HDR scenes (equivalent to the result of dodging and burning historically done in photographic printing). It is also noteworthy that the iCAM-rendered images were all computed with an automated algorithm (Johnson and Fairchild 2003c) mimicking human perception with no user interaction.

20.5 IMAGE DIFFERENCE AND QUALITY APPLICATIONS

A slightly different implementation of iCAM is required for image quality applications in order to produce image maps representing the magnitude of perceived differences between a pair of images. In these applications, viewing-distance-dependent spatial filtering is applied in a linear *IPT* space and then differences are computed in the normal nonlinear *IPT* space. Euclidean summations of these differences can be used as an overall image difference map and then various summary statistics can be used to predict different attributes of image difference and quality. This process is outlined in Figure 20.8 and detailed in Johnson and Fairchild (2003a).

Image quality metrics can be derived from image difference metrics that are based on normal color difference formulas applied to properly spatially filtered images. This approach has been used to successfully predict various types of image quality data (Johnson and Fairchild 2001b). Figure 20.9 illustrates the prediction of perceived sharpness (Johnson and Fairchild 2000) and contrast (Calabria and Fairchild 2002) differences in images through a single summary statistic (mean image difference). This performance is equivalent to, or better than, that obtained using other color spaces optimized for the task (Johnson and Fairchild 2001b).

The contrast results in Figure 20.9(a) were obtained by asking observers to scale perceived image contrast for a collection of images of various content subjected to a variety of transformations (Fairchild and Johnson 2003). The resulting interval scale (average data) is plotted as perceived contrast in Figure 20.9(a) and the model prediction of image difference from the original (arbitrarily selected) is compared with it. Ideally the data would follow a V-shape with two line segments of equal absolute slope on either side of the origin. The perceived contrast data are well predicted by the iCAM image difference.

The perceived sharpness results in Figure 20.9(b) were obtained in a similar manner using a significantly larger number of image manipulations and content (Johnson and Fairchild 2000). Observers were simply asked to scale

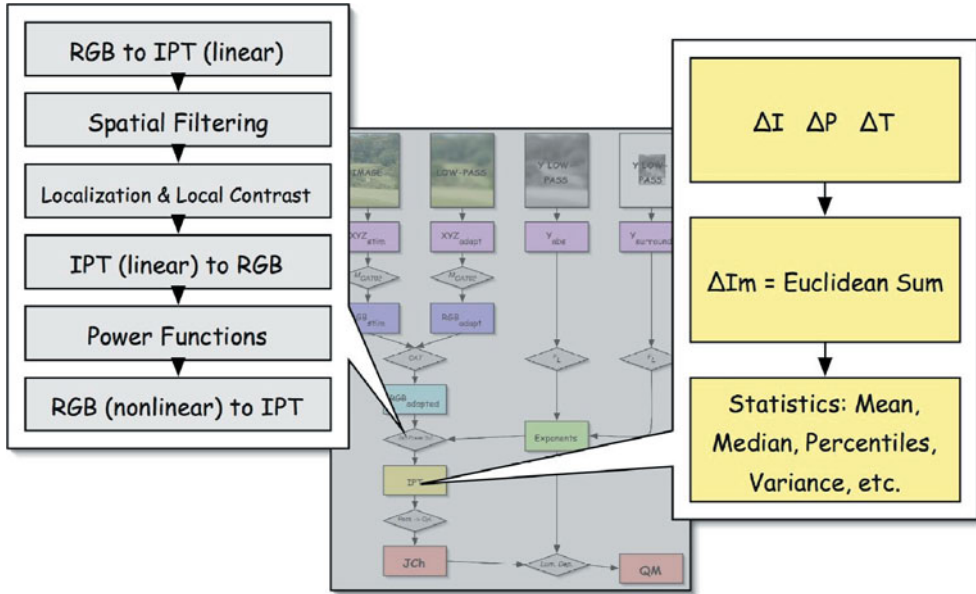


Figure 20.8 Implementation of iCAM for image difference and image quality metrics

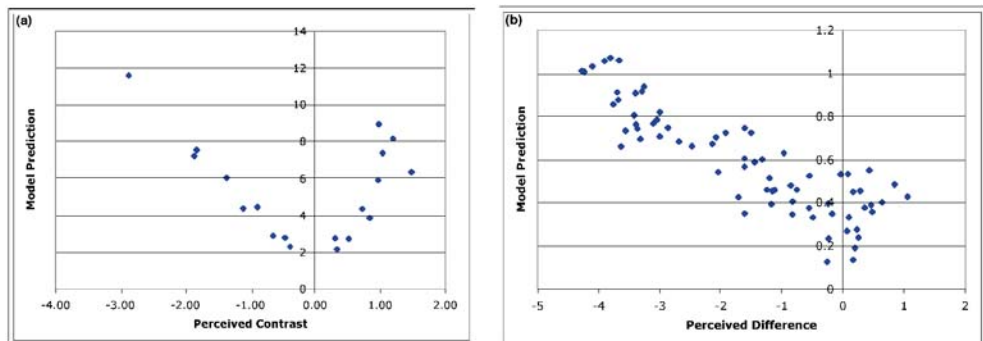


Figure 20.9 iCAM image differences as a function of (a) perceived image contrast and (b) perceived image sharpness for a variety of image transformations. (Note: desired predictions are a V-shaped data distributions since the perceptual differences are signed and the calculated differences are unsigned)

perceived sharpness and the results were converted to an interval scale, again with the original image as an arbitrary zero point. There is greater variability in these data, but it can be seen in Figure 20.9(b) that the results are again well predicted by a fairly simple mean image difference metric.

More details, source code, and ongoing improvements regarding iCAM can be found at www.cis.rit.edu/mcsl/iCAM.

20.6 FUTURE DIRECTIONS

The formulation, testing, and application of color appearance models has matured significantly in the years between the two editions of this book. While color appearance modeling remains an area of ongoing research, the types of models developed in the future might well follow the general concepts of image appearance modeling outlined in this chapter. Traditional color appearance models, such as CIECAM02, are somewhat mature and significant advances will likely require different types of models. This section speculates on what might happen in the near future by commenting on the same areas that were discussed in the final chapter of the first edition.

One Color Appearance Model?

Will there ever be a single color appearance model that is universally accepted and used for all applications? Absolutely not! The problem is too complex to be solved for all imaginable applications by a single model. Even the specification of color differences continues to be performed with two color spaces, CIELAB and CIELUV. While CIELAB is clearly preferable for such applications, a single color difference equation within the CIELAB space has yet to be widely accepted. There is no reason to expect the specification of a color appearance model to be any different.

The CIE activities in formulating CIECAM97s and CIECAM02 have been successful and have promoted uniformity of practice in industry and provide a significant step toward the establishment of a single, dominant technique for color appearance specification. Assuming these CIE activities continue to be well received, the use of color appearance models should become simpler and more uniform. However, there is no question that, for specific applications, other models will continue to be used and developed. Perhaps the use of color appearance models will reach a status similar to today's specification of color differences or color order systems in which a small number of techniques are dominant, with a wider variety of techniques still being used in some specific applications.

Other Color Appearance Models

This book has concentrated on the Hunt, Nayatani *et al.*, CIELAB, RLAB and CIE models as the key available color appearance models. These models cover the range of those that are likely to be considered for various applications in the foreseeable future. The probability of other similar color appearance models being published in the near future is low. Instead it is more likely that those involved in the above models will continue to contribute cooperatively to the development and comparative testing of the CIE model. New models will be new types of models such as iCAM.

Ongoing Research to Test Models

Given the recent increase in interest in color appearance models and their application to practical problems, the amount of research dedicated to the evaluation of model performance has also grown. This research is being carried out by a variety of scientists in industry and academia through individual programs, product development, and the activities of various CIE Technical Committees described in Chapter 17.

Of interest in the coming years will be an evaluation of the success of color appearance models in real applications, such as device-independent color imaging through the ICC profile framework. The results of these 'real world' tests will set a practical standard for color appearance modeling. It is entirely possible that a very simple level of modeling, such as a von Kries transform, will suffice if the control and specification of viewing conditions and the accuracy of device characterizations are not first improved. These are necessary prerequisites to the application of color appearance models.

An analog for the future development of color appearance models can be found in the specification of the color matching functions of the CIE 1931 Standard Colorimetric Observer. These functions were established over 70 years ago and have been successfully used in industry since that time. However, research on the measurement of more accurate color matching functions and the variability in those functions has continued since that time and is still ongoing. Such research has uncovered systematic errors in the CIE functions that are critical for some applications. In such applications, alternative color matching functions are often used. However, none of the discrepancies found through this research to date has been significant enough to warrant the abandonment of the 1931 recommendation that is firmly, and successfully, entrenched in a variety of industries. Perhaps a similar path will be followed in the area of color appearance models. If CIECAM02 finds wide acceptance and application, research on it and the other models presented in this book will continue. If an improvement that is truly significant for practical applications is found, it will be quickly adopted. However, this might not happen until well after the other fundamental issues (e.g., characterization accuracy, viewing condition control) are adequately addressed.

Ongoing Model Development

The first edition of this book stated:

An interesting direction that is likely to be pursued in the future is the incorporation of spatial and temporal effects into color appearance models. Some of the issues to be addressed have been discussed by Wandell (1993), Poirson and Wandell (1993, 1996), and Bäuml and Wandell (1996).

It is clear that this is coming to pass as described in the preceding sections of this chapter. Research along these lines will continue, with models being further refined, for the foreseeable future.

The first edition also speculated on the use of neural networks.

Another approach that is being investigated for the prediction of color appearance phenomena is the use of neural network models. Courtney et al. (1995a,b) presented interesting examples of such an approach.

This approach has seemed to fall out of favor in color appearance modeling.

What To Do Now

Given the current status of color appearance specification, it is perfectly reasonable to ask the question: 'What should I do now?' Some recommendations can be made based on the status of the models and tests as described in this book. The first point to remember is that a color appearance model should only be used if absolutely necessary. If the viewing conditions can be arranged to eliminate the need for an appearance transform, that is the best course of action. If a complete color appearance model is required, the Hunt model is probably the best choice. If that level of complexity is not required, CIECAM02 might be a good choice. It is even possible that CIELAB might be adequate as a color appearance model in some applications. The best recommendation is to work up this chain from the simplest solution to the higher levels of complexity until the problem is solved. It is also worth noting that models should not be 'mixed-and-matched' due to the significant differences between them. A single model should be used throughout a given system or process. The following listing summarizes this recommendation in order of increasing complexity and it should be noted that increasingly careful control of the viewing conditions is also required.

1. If possible, it is preferable to equate the viewing conditions such that simple tristimulus matches are also appearance matches.
2. If a white point change is necessary, CIELAB can be used as a reasonable first-order approximation of an appearance model.
3. If CIELAB is found to be inadequate, it can be enhanced by using a von Kries chromatic adaptation transform (on cone responses) to a reference viewing condition. An even better choice of adaptation transform would be a von Kries transform based on the CIECAM02 $\mathbf{M}_{\text{CAT02}}$ matrix.
4. If a more flexible adaptation model is required (e.g., hard-copy to soft-copy changes) and/or there are surround changes, then the RLAB model can be used without too much added complexity. Again, the adaptation transform in RLAB could be improved by substituting the CIECAM02 adaptation transform.

5. If control of the viewing conditions and stimulus warrant a complete color appearance model, or if predictions of brightness and colorfulness are required, then the CIECAM02 model should be used.
6. Lastly, if a full range of appearance phenomena and wide range of viewing conditions (e.g., very high or low luminances, rod responses) must be addressed, then the Hunt model should be used.

References

- I. Abramov, J. Gordon, and H. Chan, Color appearance across the retina: effects of a white surround, *J. Opt. Soc. Am. A* **9**, 195–202 (1992).
- E.H. Adelson, Perceptual organization and the perception of brightness, *Science* **2**, 2042–2044 (1993).
- Adobe Systems Incorporated, *PostScript® Language Reference Manual*, 2nd. Ed., Addison-Wesley, Reading, Mass. (1990).
- J. Albers, *Interaction of Color*, Yale University Press, New Haven, (1963).
- P.J. Alessi, CIE guidelines for coordinated research on evaluation of colour appearance models for reflection print and self-luminous display comparisons, *Color Res. Appl.* **19**, 48–58 (1994).
- R.L. Alfvin and M.D. Fairchild, Observer variability in metameric color matches using color reproduction media, *Color Res. Appl.* **22**, 174–188 (1997).
- D.H. Alman, R.S. Berns, G.D. Snyder, and W.A. Larson, Performance testing of color-difference metrics using a color tolerance dataset, *Color Res. Appl.* **14**, 139–151 (1989).
- M. Anderson, S. Chandrasekar, R. Motta, and M. Stokes, Proposal for a standard color space for the internet — sRGB, *IS&T/SID 4th Color Imaging Conference*, Scottsdale, 238–246 (1996).
- ANSI PH2.30-1989, *American National Standard for Graphic Arts and Photography — Color Prints, Transparencies, and Photomechanical Reproductions — Viewing Conditions*, American National Standards Institute, New York, (1989).
- L.E. Arend and A. Reeves, Simultaneous color constancy, *J. Opt. Soc. Am. A* **3**, 1743–1751 (1986).
- L.E. Arend and R. Goldstein, Simultaneous constancy, lightness and brightness, *J. Opt. Soc. Am. A* **4**, 2281–2285 (1987).
- L.E. Arend and R. Goldstein, Lightness and brightness over spatial illumination gradients, *J. Opt. Soc. Am. A* **7**, 1929–1936 (1990).
- L.E. Arend, A. Reeves, J. Schirillo, and R. Goldstein, Simultaneous color constancy: papers with diverse Munsell values, *J. Opt. Soc. Am. A* **8**, 661–672 (1991).
- L.E. Arend, How much does illuminant color affect unattributed colors?, *J. Opt. Soc. Am. A* **10**, 2134–2147 (1993).
- ASTM, *Standard Terminology of Appearance*, E284-95a (1995).
- ASTM, *Standard Guide for Designing and Conducting Visual Experiments*, E1808-96 (1996).
- ATIS, Objective perceptual video quality measurement using a JND-based full reference technique, *Alliance for Telecommunications Industry Solutions Technical Report T1.TR.PP.75-2001*, (2001).
- M. Ayama, T. Nakatsue, and P.K. Kaiser, Constant hue loci of unique and binary balanced hues at 10, 100, and 1000 td, *J. Opt. Soc. Am. A* **4**, 1136–1144 (1987).
- J.S. Babcock, J.B. Pelz and M.D. Fairchild, Eye tracking observers during color image evaluation tasks, *SPIE/IS&T Electronic Imaging Conference*, SPIE Vol. **5007**, Santa Clara, 218–230 (2003).

- W.G.K. Backhaus, R. Kliegl, and J.S. Werner, Eds., *Color Vision: Perspectives from Different Disciplines*, Walter de Gruyter, Berlin, (1998).
- H.B. Barlow and J.D. Mollon, *The Senses*, Cambridge University Press, Cambridge, (1982).
- K. Barnard and B. Funt, Analysis and improvement of multi-scale retinex, *Proceedings of the 5th IS&T/SID Color Imaging Conference*, Scottsdale, 221–226 (1997).
- C.J. Bartleson, Memory colors of familiar objects, *J. Opt. Soc. Am.*, **50**, 73–77 (1960).
- C.J. Bartleson and E.J. Breneman, Brightness perception in complex fields, *J. Opt. Soc. Am.*, **57**, 953–957 (1967).
- C.J. Bartleson, Optimum image tone reproduction, *J. SMPTE* **84**, 613–618 (1975).
- C.J. Bartleson, Brown, *Color Res. Appl.* **1**, 181–191 (1976).
- C.J. Bartleson, A review of chromatic adaptation, *AIC Proceedings, Color 77*, 63–96 (1978).
- C.J. Bartleson and F. Grum, *Optical Radiation Measurements Vol 5: Visual Measurements*, Academic, Orlando (1984).
- K.-H. Bäuml and B.A. Wandell, Color appearance of mixture gratings, *Vision Res.* **36**, 2894–2864 (1996).
- K.H. Bäuml, Simultaneous color constancy: how surface color perception varies with the illuminant, *Vision Res.* **39**, 1531–1550 (1999).
- A. Berger-Schunn, *Practical Color Measurement*, Wiley, New York (1994).
- R.S. Berns, The mathematical development of CIE TC1-29 proposed color difference equation: CIELCH, *AIC Proceedings, Color 93*, C19-1 (1993a).
- R.S. Berns, Spectral modeling of a dye diffusion thermal transfer printer, *J. Electronic Imaging* **2**, 359–370 (1993b).
- R.S. Berns, R.J. Motta, and M.E. Gorzynski, CRT colorimetry, part I: Theory and practice, *Color Res. Appl.* **18**, 299–314 (1993a).
- R.S. Berns, M.E. Gorzynski, and R.J. Motta, CRT colorimetry, part II: Metrology, *Color Res. Appl.* **18**, 315–325 (1993b).
- R.S. Berns and M.J. Shyu, Colorimetric characterization of a desktop drum scanner using a spectral model, *J. Electronic Imaging* **4**, 360–372 (1995).
- R.S. Berns, Methods for characterizing CRT displays, *Displays* **16**, 173–182 (1996).
- R.S. Berns, A generic approach to color modeling, *Color Res. Appl.* **22**, 318–325 (1997).
- R.S. Berns, *Billmeyer and Saltzman's Principles of Color Technology*, 3rd. Ed., John Wiley & Sons, New York (2000).
- R.S. Berns, S.R. Fernandez, and L. Taplin, Estimating black-level emissions of computer-controlled displays, *Color Res. Appl.* **28**, 379–383 (2003).
- K.T. Blackwell and G. Buchsbaum, The effect of spatial and chromatic parameters on chromatic induction, *Color Res. Appl.* **13**, 166–173 (1988a).
- K.T. Blackwell and G. Buchsbaum, Quantitative studies in color constancy, *J. Opt. Soc. Am. A* **5**, 1772–1780 (1988b).
- C. Blakemore and F.W. Campbell, On the existence of neurons in the human visual system selectively sensitive to the orientation and size of retinal images, *J. of Physiology* **203**, 237–260 (1969).
- B. Blakeslee and M.E. McCourt, A multiscale spatial filtering account of the White effect, simultaneous brightness contrast and grating induction, *Vision Res.* **39**, 4361–4377 (1999).
- R.M. Boynton, *Human Color Vision*, Optical Society of America, Washington, (1979).
- R.M. Boynton, History and current status of a physiologically based system of photometry and colorimetry, *J. Opt. Soc. Am. A* **13**, 1609–1621 (1996).

- D.H. Brainard and B.A. Wandell, Analysis of the retinex theory of color vision, *J. Opt. Soc. Am. A* **3**, 1651–1661 (1986).
- D.H. Brainard and B.A. Wandell, Asymmetric color matching: how color appearance depends on the illuminant, *J. Opt. Soc. Am. A* **9**, 1433–1448 (1992).
- G.J. Braun and M.D. Fairchild, Image lightness rescaling using sigmoidal contrast enhancement functions, *J. of Electronic Imaging* **8**, 380–393 (1999a).
- G.J. Braun and M.D. Fairchild, General-purpose gamut-mapping algorithms: Evaluation of contrast-preserving rescaling functions for color gamut mapping, *IS&T/SID 7th Color Imaging Conference*, Scottsdale, 167–192 (1999b).
- G.J. Braun and M.D. Fairchild, General-purpose gamut-mapping algorithms: Evaluation of contrast-preserving rescaling functions for color gamut mapping, *J. Im. Sci. and Tech.* **44**, 343–350 (2000).
- K.M. Braun and M.D. Fairchild, Evaluation of five color-appearance transforms across changes in viewing conditions and media, *IS&T/SID 3rd Color Imaging Conference*, Scottsdale, 93–96 (1995).
- K.M. Braun, M.D. Fairchild, and P.J. Alessi, Viewing environments for cross-media image comparisons, *Color Res. Appl.* **21**, 6–17 (1996).
- K.M. Braun and M.D. Fairchild, Testing five color appearance models for changes in viewing conditions, *Color Res. Appl.* **21**, 165–174 (1997).
- K.M. Braun and M.D. Fairchild, Psychophysical generation of matching images for cross-media color reproduction, *J. Soc. Info. Disp.* **8**, 33–44 (2000).
- E.J. Breneman, Corresponding chromaticities for different states of adaptation to complex visual fields, *J. Opt. Soc. Am. A* **4**, 1115–1129 (1987).
- P. Bressan, Revisitation of the luminance conditions for the occurrence of the achromatic neon color spreading illusion, *Perception & Psychophysics* **54**, 55–64 (1993).
- H. Brettel, F. Vienot, and J.D. Mollon, Computerized simulation of color appearance for dichromats, *J. Opt. Soc. Am. A* **14**, 2647–2655 (1997).
- M.H. Brill and G. West, Chromatic adaptation and color constancy: A possible dichotomy, *Color Res. Appl.* **11**, 196–227 (1986).
- M.H. Brill, Color management: New roles for color transforms, *IS&T/SID 5th Color Imaging Conference*, Scottsdale, 78–82 (1997).
- A.J. Calabria and M.D. Fairchild, Herding CATs: A comparison of linear chromatic-adaptation transforms for CIECAM97s, *IS&T/SID 9th Color Imaging Conference*, Scottsdale, 174–178 (2001).
- A.J. Calabria and M.D. Fairchild, Compare and contrast: Perceived contrast of color images, *Proc. of IS&T/SID 10th Color Imaging Conference*, 17–22 (2002).
- F.W. Campbell and J.G. Robson, Application of Fourier analysis to the visibility of gratings, *J. of Physiology* **197**, 551–566 (1968).
- M.E. Chevreul, *The Principles of Harmony and Contrast of Colors*, (1839). (Reprinted, Van Nostrand Reinhold, New York, 1967).
- E.-J. Chichilnisky and B.A. Wandell, Photoreceptor sensitivity changes explain color appearance shifts induced by large uniform backgrounds in dichoptic matching, *Vision Res.* **35**, 239–254 (1995).
- CIE, *Colorimetry*, CIE Publ. No. 15.2, Vienna (1986).
- CIE, *International Lighting Vocabulary*, CIE Publ. No. 17.4, Vienna (1987).
- CIE, *Special Metamerism Index: Change in Observer*, CIE Publ. No. 80, Vienna (1989).
- CIE, *CIE 1988 2° Spectral Luminous Efficiency Function for Scotopic Vision*, CIE Publ. No. 86, Vienna (1990).
- CIE, *A Method of Predicting Corresponding Colours under Different Chromatic and Illuminance Adaptations*, CIE Tech. Rep. 109, Vienna (1994).

- CIE, *Method of Measuring and Specifying Colour Rendering Properties of Light Sources*, CIE Publ. No. 13.3, Vienna (1995a).
- CIE, *Industrial Colour-Difference Evaluation*, CIE Tech. Rep. 116, Vienna (1995b).
- CIE, *Report to CIE Division 1 from TC1-31 Colour Notations and Colour-Order Systems*, (1996a).
- CIE, *CIE Expert Symposium '96 Color Standards for Image Technology*, CIE Pub. x010, Vienna (1996b).
- CIE, *The CIE 1997 Interim Colour Appearance Model (Simple Version)*, CIECAM97s, CIE Pub. 131 (1998).
- CIE, *CIE Collection/Colour Rendering (TC1-33 Closing Remarks)*, CIE Pub. 135/2 rendering (1999).
- CIE, *Improvement to Industrial Colour difference Evaluation*, CIE Pub 142 (2001).
- CIE, CIE TC1-52 Technical Report, *A Review of Chromatic Adaptation Transforms* (2003).
- CIE, CIE TC8-01 Technical Report, *A Colour Appearance Model for Color Management Systems: CIECAM02*, CIE Pub. 159 (2004).
- F.J.J. Clarke, R. McDonald, and B. Rigg, Modification to the JPC 79 colour-difference formula, *J. Soc. Dyers Colourists* **100**, 128–132 (1984).
- J.B. Cohen, *Visual Color and Color Mixture: The Fundamental Color Space*, University of Illinois Press, Urbana (2001).
- F.W. Cornelissen and E. Brenner, On the role and nature of adaptation in chromatic induction, *Channels in the Visual Nervous System: Neurophysiology, Psychophysics and Models*, B. Blum, Ed., Freund Publishing, London, 109–123 (1991).
- F.W. Cornelissen and E. Brenner, Simultaneous colour constancy revisited: An analysis of viewing strategies, *Vision Res.* **35**, 2431–2448 (1995).
- S.M. Courtney, L.H. Finkel, and G. Buchsbaum, A multistage neural network for color constancy and color induction, *IEEE Trans. on Neural Networks* **6**, 972–985 (1995a).
- S.M. Courtney, L.H. Finkel, and G. Buchsbaum, Network simulations of retinal and cortical contributions to color constancy, *Vision Res.* **35**, 413–434 (1995b).
- B.J. Craven and D.H. Foster, An operational approach to color constancy, *Vision Res.* **32**, 1359–1366 (1992).
- S. Daly, The Visible Differences Predictor: An algorithm for the assessment of image fidelity, in *Digital Images and Human Vision*, A. Watson, Ed., MIT, Cambridge, 179–206 (1993).
- J. Davidoff, *Cognition Through Color*, MIT Press, Cambridge, (1991).
- P.B. Delahunt and D.H. Brainard, Control of chromatic adaptation: Signals from separate cone classes interact, *Vision Res.* **40**, 2885–2903 (2000).
- G. Derefeldt, Colour appearance systems, Chapter 13 in *The Perception of Colour*, P. Gouras, Ed., CRC Press, Boca Raton, 218–261 (1991).
- R.L. DeValois, C.J. Smith, S.T. Kitai, and S.J. Karoly, Responses of single cells in different layers of the primate lateral geniculate nucleus to monochromatic light, *Science* **127**, 238–239 (1958).
- R.L. DeValois and K.K. DeValois, *Spatial Vision*, Oxford University Press, Oxford (1988).
- P. De Weerd, R. Desimone, and L.G. Ungerleider, Perceptual filling-in: a parametric study, *Vision Res.* **38**, 2721–2734 (1998).
- M.S. Drew and G.D. Finlayson, Device-independent color via spectral sharpening, *IS&T/SID 2nd Color Imaging Conference*, Scottsdale, 121–126 (1994).
- F. Durand and J. Dorsey, Fast bilateral filtering for the display of high-dynamic-range images, *Proceedings of SIGGRAPH 2002*, San Antonio, 257–266 (2002).

- M. D'Zmura and P. Lennie, Mechanisms of color constancy, *J. Opt. Soc. Am. A* **3**, 1662–1672 (1986).
- F. Ebner, and M.D. Fairchild, Development and testing of a color space (IPT) with improved hue uniformity, *IS&T/SID 6th Color Imaging Conference*, Scottsdale, 8–13 (1998).
- P.G. Engeldrum, Four color reproduction theory for dot formed imaging systems, *J. Imag. Tech.* **12**, 126–131 (1986).
- P.G. Engeldrum, Color scanner colorimetric design requirements, *Proc. SPIE* **1909**, 75–83 (1993).
- P.G. Engeldrum, A framework for image quality models, *J. Imag. Sci. Tech.* **39**, 312–318 (1995).
- P.G. Engeldrum, *Psychometric Scaling: A Toolkit for Imaging Systems Development*, Imcotech Press, Winchester (2000).
- P.G. Engledrum, Extending image quality models, *Proc IS&T PICS Conference*, 65–69 (2002).
- R.M. Evans, Visual processes and color photography, *J. Opt. Soc. Am.* **33**, 579–614 (1943).
- R.M. Evans, *An Introduction to Color*, John Wiley & Sons, New York, (1948).
- R.M. Evans, W.T. Hanson, and W.L. Brewer, *Principles of Color Photography*, John Wiley & Sons, New York, (1953).
- M.D. Fairchild, *Chromatic Adaptation and Color Appearance*, Ph.D. Dissertation, University of Rochester (1990).
- M.D. Fairchild, A model of incomplete chromatic adaptation, *Proceedings of the 22nd Session of the CIE (Melbourne)* 33–34 (1991a).
- M.D. Fairchild, Formulation and testing of an incomplete-chromatic-adaptation model, *Color Res. Appl.* **16**, 243–250 (1991b).
- M.D. Fairchild and E. Pirrotta, Predicting the lightness of chromatic object colors using CIELAB, *Color Res. Appl.* **16**, 385–393 (1991).
- M.D. Fairchild, Chromatic adaptation and color constancy, in *Advances in Color Vision Technical Digest*, Vol. 4 of the OSA Technical Digest Series (Optical Society of America, Washington, D.C.), 112–114 (1992a).
- M.D. Fairchild, Chromatic adaptation to image displays, *TAGA* **2**, 803–824 (1992b).
- M.D. Fairchild and P. Lennie, Chromatic adaptation to natural and artificial illuminants, *Vision Res.* **32**, 2077–2085 (1992).
- M.D. Fairchild, Chromatic adaptation in hard-copy/soft-copy comparisons, *Color Hard Copy and Graphic Arts II, Proc. SPIE* **1912**, 47–61 (1993a).
- M.D. Fairchild, Color Forum: The CIE 1931 Standard Colorimetric Observer: Mandatory retirement at age 65?, *Color Res. Appl.* **18**, 129–134 (1993b).
- M.D. Fairchild and R.S. Berns, Image color appearance specification through extension of CIELAB, *Color Res. Appl.* **18**, 178–190 (1993).
- M.D. Fairchild, E. Pirrotta, and T.G. Kim, Successive-Ganzfeld haploscopic viewing technique for color-appearance research, *Color Res. Appl.* **19**, 214–221 (1994).
- M.D. Fairchild, Some hidden requirements for device-independent color imaging, *SID International Symposium*, San Jose, 865–868 (1994a).
- M.D. Fairchild, Visual evaluation and evolution of the RLAB color space, *IS&T/SID 2nd Color Imaging Conference*, Scottsdale, 9–13 (1994b).
- M.D. Fairchild, Testing colour-appearance models: Guidelines for coordinated research, *Color Res. Appl.* **20**, 262–267 (1995a).
- M.D. Fairchild, Considering the surround in device-independent color imaging, *Color Res. Appl.* **20** 352–363 (1995b).

- M.D. Fairchild and R.L. Alfvín, Precision of color matches and accuracy of color matching functions in cross-media color reproduction, *IS&T/SID 3rd Color Imaging Conference*, Scottsdale, 18–21 (1995).
- M.D. Fairchild and L. Reniff, Time-course of chromatic adaptation for color-appearance judgements, *J. Opt. Soc. Am. A* **12**, 824–833 (1995).
- M.D. Fairchild, R.S. Berns, and A.A. Lester, Accurate color reproduction of CRT-displayed images as projected 35 mm slides, *J. Elec. Imaging* **5**, 87–96 (1996).
- M.D. Fairchild, Refinement of the RLAB color space, *Color Res. Appl.* **21**, 338–346 (1996).
- M.D. Fairchild and L. Reniff, A pictorial review of color appearance models, *IS&T/SID 4th Color Imaging Conference*, Scottsdale, 97–100 (1996).
- M.D. Fairchild, *Color Appearance Models*, Addison Wesley, Reading (1998a).
- M.D. Fairchild, The ZLAB color appearance model for practical image reproduction applications, *Proceedings of the CIE Expert Symposium '97 on Colour Standards for Image Technology, CIE Pub. x014*, 89–94 (1998b).
- M.D. Fairchild, A revision of CIECAM97s for practical applications, *Color Res. Appl.* **26**, 418–427 (2001).
- M.D. Fairchild, Image quality measurement and modeling for digital photography, *International Congress on Imaging Science '02*, Tokyo, 318–319 (2002a).
- M.D. Fairchild, Modeling color appearance, spatial vision, and image quality, *Color Image Science: Exploiting Digital Media*, Wiley, New York, 357–370 (2002b).
- M.D. Fairchild and G.M. Johnson, Meet iCAM: A next-generation color appearance model, *IS&T/SID 10th Color Imaging Conference*, Scottsdale, 33–38 (2002).
- M.D. Fairchild and G.M. Johnson, Image appearance modeling, *Proc. SPIE/IS&T Electronic Imaging Conference*, SPIE Vol. **5007**, Santa Clara, 149–160 (2003).
- M.D. Fairchild and G.M. Johnson, The iCAM framework for image appearance, image differences, and image quality, *J. of Electronic Imaging* **13**, 126–138 (2004).
- H.S. Fairman, Metameric correction using parameric decomposition, *Color Res. Appl.* **12**, 261–265 (1987).
- R. Fattal, D. Lischinski, and M. Werman, Gradient domain high dynamic range compression, *Proceedings of SIGGRAPH 2002*, San Antonio, 249–256 (2002).
- G. Fechner, *Elements of Psychophysics Vol I*, (Translated by H.E. Adler), Holt, Rinehart, and Winston, New York (1966).
- S. Fernandez and M.D. Fairchild, Observer preferences and cultural differences in color reproduction of scenic images, *IS&T/SID 10th Color Imaging Conference*, Scottsdale, 66–72 (2002).
- G.D. Finlayson, M.S. Drew, and B.V. Funt, Spectral sharpening: Sensor transformations for improved color constancy, *J. Opt. Soc. Am. A* **11**, 1553–1563 (1994a).
- G.D. Finlayson, M.S. Drew, and B.V. Funt, Color constancy: Generalized diagonal transforms suffice, *J. Opt. Soc. Am. A* **11**, 3011–3019 (1994b).
- G.D. Finlayson and M.S. Drew, Positive Bradford curves through sharpening, *IS&T/SID 7th Color Imaging Conference*, Scottsdale, 227–232 (1999).
- G.D. Finlayson and S. Süsstrunk, Performance of a chromatic adaptation transform based on spectral sharpening, *IS&T/SID 8th Color Imaging Conference*, Scottsdale, 49–55 (2000).
- D.J. Finney, *Probit Analysis*, 3rd Ed., Cambridge University Press, Cambridge, UK (1971).
- J.D. Foley, A. van Dam, S.K. Feiner, and J.F. Hughes, *Computer Graphics: Principles and Practice*, 2nd Ed., Addison-Wesley, Reading, Mass., (1990).

- D.H. Foster and S.M.C. Nascimento, Relational colour constancy from invariant cone-excitation ratios, *Proc. R. Soc. Lond. B* **257**, 115–121 (1994).
- B. Fraser, C. Murphy and F. Bunting, *Real World Color Management*, Peachpit Press, Berkeley (2003).
- K. Fuld, J.S. Werner, and B.R. Wooten, The possible elemental nature of brown, *Vision Res.* **23**, 631–637 (1983).
- B. Funt, F. Ciurea, and J.J. McCann, Retinex in Matlab, *Proc. of IS&T/SID 8th Color Imaging Conference*, 112–121 (2000).
- K.R. Gegenfurtner and L.T. Sharpe, *Color Vision: From Genes to Perception*, Cambridge University Press, Cambridge (1999).
- R.S. Gentile, E. Walowitz, and J.P. Allebach, Quantization multilevel halftoning of color images for near-original image quality, *J. Opt. Soc. Am. A* **7**, 1019–1026 (1990a).
- R.S. Gentile, E. Walowitz, and J.P. Allebach, A comparison of techniques for color gamut mismatch compensation, *J. Imaging Tech.* **16**, 176–181 (1990b).
- G.A. Gescheider, *Psychophysics: Method, Theory, and Application*, 2nd. Ed., Lawrence Erlbaum Associates, Hillsdale (1985).
- A.L. Gilchrist, When does perceived lightness depend on perceived spatial arrangement?, *Perception & Psychophysics* **28**, 527–538 (1980).
- E. Giorgianni and T. Madden, *Digital Color Management: Encoding Solutions*, Addison-Wesley, Reading, Mass., (1997).
- S. Gonzalez and M.D. Fairchild, Evaluation of bispectral spectrophotometry for accurate colorimetry of printing materials, *IS&T/SID 8th Color Imaging Conference*, Scottsdale, 39–43 (2000).
- E.M. Granger, Uniform color space as a function of spatial frequency, *SPIE/IS&T Electronic Imaging Conference*, SPIE Vol. **1913**, San Jose, 449–457 (1993).
- E.M. Granger, ATD, appearance equivalence, and desktop publishing, *SPIE Vol. 2170*. 163–168 (1994).
- E.M. Granger, Gamut mapping for hard copy using the ATD color space, *SPIE Vol. 2414*. 27–35 (1995).
- F. Grum and C.J. Bartleson, *Optical Radiation Measurements Vol. 2, Color Measurement*, Academic Press, New York (1980).
- J. Guild, The colorimetric properties of the spectrum, *Phil. Trans. Roy. Soc. A* **230**, 149–187 (1931).
- S.L. Guth, Model for color vision and light adaptation, *J. Opt. Soc. Am. A* **8**, 976–993 (1991).
- S.L. Guth, ATD model for color vision I: Background, *SPIE Vol. 2170*. 149–152 (1994a).
- S.L. Guth, ATD model for color vision II: Applications, *SPIE Vol. 2170*. 153–168 (1994b).
- S.L. Guth, Further applications of the ATD model for color vision, *SPIE Vol. 2414*. 12–26 (1995).
- J.C. Handley, Comparative analysis of Bradley-Terry and Thurstone-Mosteller paired comparison models for image quality assessment, *IS&T PICS Conference Proceedings*, Montreal, 108–112 (2001).
- H. Haneishi, T. Suzuki, N. Shimoyama, and Y. Miyake, Color digital halftoning taking colorimetric color reproduction into account, *J. Elec. Imaging* **5**, 97–106 (1996).
- A. Hard and L. Sivik, NCS — Natural Color System: A Swedish standard for color notation, *Color Res. Appl.* **6**, 129–138 (1981).

- M.M. Hayhoe, N.I. Benimoff, and D.C. Hood, The time-course of multiplicative and subtractive adaptation processes, *Vision Res.* **27**, 1981–1996 (1987).
- M.M. Hayhoe, and M.V. Smith, The role of spatial filtering in sensitivity regulation, *Vision Res.* **29**, 457–469 (1989).
- H. v. Helmholtz, *Handbuch der physiologischen Optick*, 1st Ed. Voss, Hamburg (1866).
- H. Helson, Fundamental problems in color vision. I. The principle governing changes in hue, saturation, and lightness of non-selective samples in chromatic illumination, *J. Exp. Psych.* **23**, 439–477 (1938).
- H. Helson, D.B. Judd, and M.H. Warren, Object color changes from daylight to incandescent filament illumination, *Illum. Eng.* **47**, 221–233 (1952).
- E. Hering, *Outlines of a theory of the light sense*, Harvard Univ. Press, Cambridge (1920). (trans. by L.M. Hurvich and D. Jameson, 1964.).
- T. Hoshino and R.S. Berns, Color gamut mapping techniques for color hard copy images, *Proc. SPIE*, **1909**, 152–165 (1993).
- P.-C. Hung, Colorimetric calibration for scanners and media, *Proc. SPIE* **1448**, 164–174 (1991).
- P.-C. Hung, Colorimetric calibration in electronic imaging devices using a look-up-table model and interpolations, *J. Electronic Imaging* **2**, 53–61 (1993).
- P.-C. Hung and R.S. Berns, Determination of constant hue loci for a CRT gamut and their predictions using color appearance spaces, *Color Res. Appl.* **20**, 285–295 (1995).
- D.M. Hunt, S.D. Kanwaljit, J.K. Bowmaker, and J.D. Mollon, The chemistry of John Dalton's color blindness, *Science* **267**, 984–988 (1995).
- D.M. Hunt, K.S. Dulai, J.A. Cowing, C. Julliot, J.D. Mollon, J.K. Bowmaker, W.-H. Li, D. Hewett-Emmett, Molecular evolution of trichromacy in primates, *Vision Res.* **38**, 3299–3306 (1998).
- R.W.G. Hunt, The effects of daylight and tungsten light-adaptation on color perception, *J. Opt. Soc. Am.* **40**, 362–371 (1950).
- R.W.G. Hunt, Light and dark adaptation and the perception of color, *J. Opt. Soc. Am.* **42**, 190–199 (1952).
- R.W.G. Hunt, Objectives in colour reproduction, *J. Phot. Sci.* **18**, 205–215 (1970).
- R.W.G. Hunt, I.T. Pitt, and L.M. Winter, The preferred reproduction of blue sky, green grass and caucasian skin in colour photography, *J. Phot. Sci.* **22**, 144–150 (1974).
- R.W.G. Hunt and L.M. Winter, Colour adaptation in picture-viewing situations, *J. Phot. Sci.* **23**, 112–115 (1975).
- R.W.G. Hunt, Sky-blue pink, *Color Res. Appl.* **1**, 11–16 (1976).
- R.W.G. Hunt, The specification of colour appearance. I. Concepts and terms, *Color Res. Appl.* **2**, 55–68 (1977).
- R.W.G. Hunt, Colour terminology, *Color Res. Appl.* **3**, 79–87 (1978).
- R.W.G. Hunt, A model of colour vision for predicting colour appearance, *Color Res. Appl.* **7**, 95–112 (1982).
- R.W.G. Hunt and M.R. Pointer, A colour-appearance transform for the CIE 1931 standard colorimetric observer, *Color Res. Appl.* **10**, 165–179 (1985).
- R.W.G. Hunt, A model of colour vision for predicting colour appearance in various viewing conditions, *Color Res. Appl.* **12**, 297–314 (1987).
- R.W.G. Hunt, Hue shifts in unrelated and related colours, *Color Res. Appl.* **14**, 235–239 (1989).
- R.W.G. Hunt, *Measuring Colour*, 2nd Ed., Ellis Horwood, New York, (1991a).

- R.W.G. Hunt, Revised colour-appearance model for related and unrelated colours, *Color Res. Appl.* **16**, 146–165 (1991b).
- R.W.G. Hunt, Standard sources to represent daylight, *Color Res. Appl.* **17**, 293–294 (1992).
- R.W.G. Hunt, An improved predictor of colourfulness in a model of colour vision, *Color Res. Appl.* **19**, 23–26 (1994).
- R.W.G. Hunt and M.R. Luo, Evaluation of a model of colour vision by magnitude scalings: Discussion of collected results, *Color Res. Appl.* **19**, 27–33 (1994).
- R.W.G. Hunt, *The Reproduction of Colour*, 5th Ed., Fountain Press, England, (1995).
- R.W.G. Hunt, Personal Communication, October 14, (1996).
- R.W.G. Hunt, Measuring Color, 3rd Ed., Fountain Press, England (1998).
- R.W.G. Hunt, C.J. Li, and M.R. Luo, Dynamic cone response function for models of colour appearance, *Color Res. Appl.* **28**, 82–88 (2003).
- R.S. Hunter and R.W. Harold, *The Measurement of Appearance*, 2nd Ed., Wiley, New York (1987).
- L.M. Hurvich and D. Jameson, A psychophysical study of white. III. Adaptation as a variant, *J. Opt. Soc. Am.* **41**, 787–801 (1951).
- L.M. Hurvich, *Color Vision*, Sinauer Associates, Sunderland, Mass., (1981).
- T. Indow, Multidimensional studies of Munsell color solid, *Psych. Rev.* **95**, 456–470 (1988).
- International Color Consortium, *ICC Profile Format Specification*, Version 3.3 (1996). (<http://www.color.org>)
- D. Jameson and L.M. Hurvich, Some quantitative aspects of an opponent-colors theory: I. Chromatic responses and spectral saturation, *J. Opt. Soc. Am.* **45**, 546–552 (1955).
- D. Jameson and L.M. Hurvich, Essay concerning color constancy, *Ann. Rev. Psychol.* **40**, 1–22 (1989).
- J.F. Jarvis, C.N. Judice, and W.H. Ninke, A survey of techniques for the display of continuous tone images on bilevel displays, *Comp. Graphics Image Proc.* **5**, 13–40 (1976).
- E.W. Jin and S.K. Shevell, Color memory and color constancy, *J. Opt. Soc. Am. A* **13**, 1981–1991 (1996).
- D.J. Jobson, Z. Rahman, and G.A. Woodell, A multi-scale retinex for bridging the gap between color images and the human observation of scenes, *IEEE Trans. Im. Proc.* **6**, 956–976 (1997).
- G.M. Johnson and M.D. Fairchild, Full-spectral color calculations in realistic image synthesis, *IEEE Computer Graphics & Applications* **19:4**, 47–53 (1999).
- G.M. Johnson and M.D. Fairchild, Sharpness rules, *Proc of IS&T/SID 8th Color Imaging Conference*, 24–30 (2000).
- G.M. Johnson and M.D. Fairchild, On contrast sensitivity in an image difference model, *Proc. of IS&T PICS Conference*, 18–23 (2001a).
- G.M. Johnson and M.D. Fairchild, Darwinism of color image difference models, *Proc. of IS&T/SID 9th Color Imaging Conference*, 108–112 (2001b).
- G.M. Johnson and M.D. Fairchild, Measuring images: Differences, quality, and appearance, *SPIE/IS&T Electronic Imaging Conference*, SPIE Vol. **5007**, Santa Clara, 51–60 (2003a).
- G.M. Johnson and M.D. Fairchild, A top down description of S-CIELAB and CIEDE2000, *Color Res. Appl.* **28**, 425–435 (2003b).
- G.M. Johnson and M.D. Fairchild, Rendering HDR images, *IS&T/SID 11th Color Imaging Conference*, Scottsdale, 36–41 (2003c).

- D.B. Judd, Hue, saturation, and lightness of surface colors with chromatic illumination, *J. Opt. Soc. Am.* **30**, 2–32 (1940).
- D.B. Judd, Appraisal of Land's work on two-primary color projections, *J. Opt. Soc. Am.* **50**, 254–268 (1960).
- P.K. Kaiser and R.M. Boynton, *Human Color Vision*, 2nd Ed., Optical Society of America, Washington, (1996).
- H. Kang, Color scanner calibration, *J. Imaging Sci. Tech.* **36**, 162–170 (1992).
- H. Kang, *Color Technology for Electronic Imaging Devices*, SPIE, Bellingham, Wash. (1997).
- J.M. Kasson, W. Plouffe, and S.I. Nin, A tetrahedral interpolation technique for color space conversion, *Proc. SPIE* **1909**, 127–138 (1993).
- J.M. Kasson, S.I. Nin, W. Plouffe, and J.L. Hafner, Performing color space conversions with three-dimensional linear interpolation, *J. Elec. Imaging* **4**, 226–250 (1995).
- N. Katoh, Practical method for appearance match between soft copy and hard copy, in *Device-Independent Color Imaging*, SPIE Vol. 2170, 170–181 (1994).
- N. Katoh, Appearance match between soft copy and hard copy under mixed chromatic adaptation, *IS&T/SID 3rd Color Imaging Conference*, Scottsdale 22–25 (1995).
- D. Katz, *The World of Colour*, Trubner & Co., London (1935).
- B.W. Keelan, *Handbook of Image Quality: Characterization and Prediction*, Marcel Dekker, New York, NY (2002).
- D.H. Kelly, Ed., *Visual Science and Engineering: Models and Applications*, Marcel Dekker, New York (1994).
- T.G. Kim, R.S. Berns, and M.D. Fairchild, Comparing appearance models using pictorial images, *IS&T/SID 1st Color Imaging Conference*, Scottsdale, Ariz. 72–77 (1993).
- J.J. Koenderink and W.A. Richards, Why is snow so bright?, *J. Opt. Soc. Am. A* **9**, 643–648 (1992).
- J.M. Kraft and J.S. Werner, Spectral efficiency across the life span: flicker photometry and brightness matching, *J. Opt. Soc. Am. A* **11**, 1213–1221 (1994).
- J.B. Kruskal and M. Wish, *Multidimensional Scaling*, Sage Publications, Thousand Oaks, CA, (1978).
- R.G. Kuehni, *Color Space and Its Divisions: Color Order from Antiquity to the Present*, John Wiley & Sons, Hoboken (2003).
- W.-G. Kuo, M.R. Luo, and H.E. Bez, Various chromatic-adaptation transformations tested using new colour appearance data in textiles, *Color Res. Appl.* **20**, 313–327 (1995).
- I. Kuriki and K. Uchikawa, Limitations of surface-color and apparent-color constancy, *J. Opt. Soc. Am. A* **13**, 1622–1636 (1996).
- E.H. Land, Color vision and the natural image part II, *Proc. Nat. Acad. Sci.*, **45**, 636–644 (1959).
- E.H. Land, The retinex, *American Scientist* **52**, 247–264 (1964).
- E.H. Land and J.J. McCann, Lightness and the retinex theory, *J. Opt. Soc. Am.* **61**, 1–11 (1971).
- E.H. Land, The retinex theory of color vision, *Scientific American* **237**, 108–128 (1977).
- E.H. Land, Recent advances in retinex theory, *Vision Res.* **26**, 7–21 (1986).
- P. Lennie and M. D'Zmura, Mechanisms of color vision, *CRC Critical Reviews in Neurobiology* **3**, 333–400 (1988).

- B. Li, G.W. Meyer, and R.V. Klassen, A comparison of two image quality models, *SPIE/IS&T Electronic Imaging Conference*, SPIE Vol. 3299, San Jose, 98–109 (1998).
- C.J. Li, M.R. Luo and R.W.G. Hunt, The CAM97s2 model, *IS&T/SID 7th Color Imaging Conference*, Scottsdale 262–263 (1999).
- C.J. Li, M.R. Luo and R.W.G. Hunt, A revision of the CIECAM97s model, *Color Res. Appl.* **25** 260–266 (2000a).
- C.J. Li, M.R. Luo and B. Rigg, Simplification of the CMCCAT97, *IS&T/SID 8th Color Imaging Conference*, Scottsdale 56–60 (2000b).
- C.J. Li, M.R. Luo, R.W.G. Hunt, N. Moroney, M.D. Fairchild and T. Newman The performance of CIECAM02, *IS&T/SID 10th Color Imaging Conference*, Scottsdale 28–32 (2002).
- C.J. Li, M.R. Luo and G. Cui, Colour-differences evaluation using colour appearance models, *IS&T/SID 11th Color Imaging Conference*, Scottsdale 127–131 (2003).
- Y. Liu, J. Shigley, E. Fritsch, and S. Hemphill, Abnormal hue-angle change of the gemstone tanzanite between CIE illuminants D65 nad A in CIELAB color space, *Color Res. Appl.* **20**, 245–250 (1995).
- M.-C. Lo, M.R. Luo, and P.A. Rhodes, Evaluating colour models' performance between monitor and print images, *Color Res. Appl.* **21**, 277–291 (1996).
- A. Logvinenko and G. Menshikova, Trade-off between achromatic colour and perceived illumination as revealed by the use of pseudoscopic inversion of apparent depth, *Perception* **23**, 1007–1023 (1994).
- A.D. Logvinenko, On derivation of spectral sensitivities of the human cones from trichromatic colour matching functions, *Vision Res.* **38**, 3207–3211 (1998).
- R.B. Lotto and D. Purves, The empirical basis of color perception, *Consciousness and Cognition* **11**, 609–629 (2002).
- J. Lubin, The use of psychophysical data and models in the analysis of display system performance, in *Digital Images and Human Vision*, A. Watson, Ed., MIT, Cambridge, 163–178 (1993).
- J. Lubin, A visual discrimination model for imaging system design and evaluation, in *Vision Models for target Detection and Recognition*, E. Peli, Ed., World Scientific, Singapore, 245–283 (1995).
- M.R. Luo, A.A. Clarke, P.A. Rhodes, A. Schappo, S.A.R. Scrivner, and C.J. Tait, Quantifying colour appearance. Part I. LUTCHI colour appearance data, *Color Res. Appl.* **16**, 166–180 (1991a).
- M.R. Luo, A.A. Clarke, P.A. Rhodes, A. Schappo, S.A.R. Scrivner, and C.J. Tait, Quantifying colour appearance. Part II. Testing colour models performance using LUTCHI color appearance data, *Color Res. Appl.* **16**, 181–197 (1991b).
- M.R. Luo, X.W. Gao, P.A. Rhodes, H.J. Xin, A.A. Clarke, and S.A.R. Scrivner, Quantifying colour appearance. Part III. Supplementary LUTCHI color appearance data, *Color Res. Appl.* **18**, 98–113 (1993a).
- M.R. Luo, X.W. Gao, P.A. Rhodes, H.J. Xin, A.A. Clarke, and S.A.R. Scrivner, Quantifying colour appearance. Part IV. Transmissive media, *Color Res. Appl.* **18**, 191–209 (1993b).
- M.R. Luo, X.W. Gao, and S.A.R. Scrivner, Quantifying colour appearance. Part V. Simultaneous contrast, *Color Res. Appl.* **20**, 18–28 (1995).
- M.R. Luo, M.-C. Lo, and W.-G. Kuo, The LLAB(*l:c*) colour model, *Color Res. Appl.* **21**, 412–429 (1996).
- M.R. Luo and J. Morovic, Two unsolved issues in colour management — colour appearance and gamut mapping, *5th International Conference on High Technology*, Chiba, Japan, 136–147 (1996).

- M.R. Luo, G. Cui, and B. Rigg, The development of the CIE 2000 Colour Difference Formula, *Color Res. Appl.* **26**, 340–350 (2001).
- D.L. MacAdam, Chromatic adaptation, *J. Opt. Soc. Am.* **46**, 500–513 (1956).
- D.L. MacAdam, A nonlinear hypothesis for chromatic adaptation, *Vis. Res.* **1**, 9–41 (1961).
- D.L. MacAdam, Uniform color scales, *J. Opt. Soc. Am.* **64**, 1691–1702 (1974).
- D.L. MacAdam, Colorimetric data for samples of the OSA uniform color scales, *J. Opt. Soc. Am.* **68**, 121–130 (1978).
- D.L. MacAdam, Ed., *Selected Papers on Colorimetry — Fundamentals*, SPIE Milestone Series, Vol. MS 77, SPIE, Bellingham, Wash. (1993).
- L.T. Maloney and B.A. Wandell, Color constancy: A method for recovering surface spectral reflectance, *J. Opt. Soc. Am. A* **3**, 29–33 (1986).
- D. Marr, *Vision*, Freeman, New York (1982).
- R. Mausfeld and R. Niederée, An inquiry into relational concepts of colour, based on incremental principles of colour coding for minimal relational stimuli, *Perception* **22**, 427–462 (1993).
- B. Maximus, A. De Metere, and J.P. Poels, Influence of thickness variations in LCDs on color uniformity, *SID 94 Digest*, 341–344 (1994).
- J.C. Maxwell, On the theory of three primary colors, *Proc. Roy. Inst.*, **3**, 370–375 (1858–62).
- C.S. McCamy, H. Marcus, and J.G. Davidson, A color rendition chart, *J. App. Phot. Eng.* **11**, 95–99 (1976).
- J.J. McCann, S. McKee, and T. Taylor, Quantitative studies in retinex theory: A comparison between theoretical predictions and observer responses to 'Color Mondrian' experiments, *Vision Res.* **16**, 445–458 (1976).
- J. McCann, Color Sensations in Complex Images, *IS&T/SID 1st Color Imaging Conference*, Scottsdale, 16–23 (1993).
- E.D. Montag and M.D. Fairchild, Simulated color gamut mapping using simple rendered images, *Proc. SPIE* **2658**, 316–325 (1996).
- E.D. Montag and M.D. Fairchild, Evaluation of gamut mapping techniques using simple rendered images and artificial gamut boundaries, *IEEE Transactions on Image Processing* **6**, 977–989 (1997).
- E.D. Montag, Louis Leon Thurstone in Monte Carlo: Creating error bars for the method of paired comparison, *Proceedings of the SPIE/IS&T Electronic Imaging Conference*, in press (2004).
- L. Mori and T. Fuchida, Subjective evaluation of uniform color spaces used for color-rendering specification, *Color Res. Appl.* **7**, 285–293 (1982).
- L. Mori, H. Sobagaki, H. Komatsubara, and K. Ikeda, Field trials on CIE chromatic adaptation formula, *Proceedings of the CIE 22nd Session*, Melbourne, 55–58 (1991).
- N. Moroney, Assessing hue constancy using gradients, *Proceedings of the SPIE/IS&T Electronic Imaging Conference* **3963**, 294–300 (2000a).
- N. Moroney, Local color correction using non-linear masking, *Proc. of IS&T/SID 8th Color Imaging Conference*, 108–111 (2000b).
- N. Moroney, M.D. Fairchild, R.W.G. Hunt, C.J. Li, M.R. Luo, and T. Newman, The CIECAM02 color appearance model, *IS&T/SID 10th Color Imaging Conference*, Scottsdale, 23–27 (2002).
- N. Moroney, A hypothesis regarding the poor blue constancy of CIELAB, *Color Res. App.* **28**, 371–378 (2003).
- K.T. Mullen, The contrast sensitivity of human color vision to red-green and blue-yellow chromatic gratings, *J. of Physiology* **359**, 381–400 (1985).

- M. Murphy, *Golf in the Kingdom*, Viking, New York (1972).
- Y. Nayatani, K. Takahama, and H. Sobagaki, Estimation of adaptation effects by use of a theoretical nonlinear model, *Proceedings of the 19th CIE Session*, Kyoto, 1979, CIE Publ. No. 5, 490–494 (1980).
- Y. Nayatani, K. Takahama, and H. Sobagaki, Formulation of a nonlinear model of chromatic adaptation, *Color Res. Appl.* **6**, 161–171 (1981).
- Y. Nayatani, K. Takahama, H. Sobagaki, and J. Hiroto, On exponents of a nonlinear model of chromatic adaptation, *Color Res. Appl.* **7**, 34–45 (1982).
- Y. Nayatani, K. Takahama, and H. Sobagaki, Prediction of color appearance under various adapting conditions, *Color Res. Appl.* **11**, 62–71 (1986).
- Y. Nayatani, K. Hashimoto, K. Takahama, and H. Sobagaki, A nonlinear color-appearance model using Estévez–Hunt–Pointer primaries, *Color Res. Appl.* **12**, 231–242 (1987).
- Y. Nayatani, K. Takahama, and H. Sobagaki, Field trials on color appearance of chromatic colors under various light sources, *Color Res. Appl.* **13**, 307–317 (1988).
- Y. Nayatani, K. Takahama, H. Sobagaki, and K. Hashimoto, Color-appearance model and chromatic adaptation transform, *Color Res. Appl.* **15**, 210–221 (1990a).
- Y. Nayatani, T. Mori, K. Hashimoto, K. Takahama, and H. Sobagaki, Comparison of color-appearance models, *Color Res. Appl.* **15**, 272–284 (1990b).
- Y. Nayatani, Y. Gomi, M. Kamei, H. Sobagaki, and K. Hashimoto, Perceived lightness of chromatic object colors including highly saturated colors, *Color Res. Appl.* **17**, 127–141 (1992).
- Y. Nayatani, Revision of chroma and hue scales of a nonlinear color-appearance model, *Color Res. Appl.* **20**, 143–155 (1995).
- Y. Nayatani, H. Sobagaki, K. Hashimoto, and T. Yano, Lightness dependency of Chroma scales of a nonlinear color-appearance model and its latest formulation, *Color Res. Appl.* **20**, 156–167 (1995).
- Y. Nayatani, A simple estimation method for effective adaptation coefficient, *Color Res. Appl.* **22**, 259–274 (1997).
- S.M. Newhall, Preliminary report of the O.S.A. subcommittee on the spacing of the Munsell colors, *J. Opt. Soc. Am.* **30**, 617–645 (1940).
- T. Newman and E. Pirrotta, The darker side of colour appearance models and gamut mapping, *Proceedings of Colour Image Science 2000*, Derby 215–223 (2000).
- D. Nickerson, History of the Munsell Color System and its scientific application, *J. Opt. Soc. Am.* **30**, 575–586 (1940).
- D. Nickerson, History of the Munsell Color System, Company, and Foundation, I., *Color Res. Appl.* **1**, 7–10 (1976a).
- D. Nickerson, History of the Munsell Color System and its scientific application, *Color Res. Appl.* **1**, 69–77 (1976b).
- D. Nickerson, History of the Munsell Color System, *Color Res. Appl.* **1**, 121–130 (1976c).
- T.H. Nilsson and T.M. Nelson, Delayed monochromatic hue matches indicate characteristics of visual memory, *J. Exp. Psych.: Human Perception and Performance* **7**, 141–150 (1981).
- I. Nimeroff, J.R. Rosenblatt, and M.C. Dannemiller, Variability of spectral tristimulus values, *J. Res. NBS* **65**, 475–483 (1961).
- OSA, Psychological concepts: Perceptual and affective aspects of color, Chapter 5 in *The Science of Color*, Optical Society of America, Washington, 145–171 (1963).
- S.E. Palmer, *Vision Science: Photons to Phenomenology*, MIT Press, Cambridge (1999).

- S.N. Pattanaik, J.A. Ferwerda, M.D. Fairchild, and D.P. Greenberg, A multiscale model of adaptation and spatial vision for image display, *Proceedings of SIGGRAPH 98*, 287–298 (1998).
- H. Pauli, Proposed extnsion of the CIE recommendation on Uniform color spaces, color difference equations, and metric color terms, *J. Opt. Soc. Am.* **36**, 866–867 (1976).
- E. Pirrotta and M.D. Fairchild, Directly testing chromatic-adaptation models using object colors, *Proceedings of the 23rd Session of the CIE (New Delhi)* Vol. 1, 77–78 (1995).
- A.B. Poirson and B.A. Wandell, Appearance of colored patterns: Pattern-color separability, *J. Opt. Soc. Am. A* **10**, 2458–2470 (1993).
- A.B. Poirson and B.A. Wandell, Pattern-color separable pathways predict sensitivity to simple colored patterns, *Vision Res.* **36**, 515–526 (1996).
- J. Pokorny, V.C. Smith, and M. Lutze, Aging of the human lens, *Appl. Opt.* **26**, 1437–1440 (1987).
- D.M. Purdy, Spectral hue as a function of intensity, *Am. J. Psych.* **43**, 541–559 (1931).
- D. Purves, R.B. Lotto, and S. Nundy, Why we see what we do, *American Scientist* **90**, 236–243 (2002).
- E. Reinhard, M. Stark, P. Shirley, and J. Ferwerda, Gradient domain high dynamic range compression, *Proceedings of SIGGRAPH 2002*, San Antonio, 267–276 (2002).
- K. Richter, Cube-root color spaces and chromatic adaptation, *Color Res. Appl.* **5**, 7–11 (1980).
- K. Richter, *Farbempfindungsmerkmal Elementarbunton und Buntheitsabstände als Funktion von Farbart und Leuchtdichte von In- und Umfeld*, Bundesanstalt für Materialprüfung (BAM) Forschungsbericht 115, Berlin, (1985).
- M. Richter and K. Witt, The story of the DIN color system, *Color Res. Appl.* **11**, 138–145 (1986).
- O. Rinner and K.R. Gegenfurtner, Time course of chromatic adaptation for color appearance discrimination, *Vision Res.* **40**, 1813–1826 (2000).
- A.R. Robertson, A new determination of lines of constant hue, *AIC Color* 69, Stockholm, 395–402 (1970).
- A.R. Robertson, The CIE 1976 color-difference formulae, *Color Res. Appl.* **2**, 7–11 (1977).
- A.R. Robertson, Historical development of CIE recommended color difference equations, *Color Res. Appl.* **15**, 167–170 (1990).
- A.R. Robertson, Figure 6–2 Presented at the 1996 ISCC Annual Meeting, Orlando, Fla. (1996).
- M.A. Rodriguez and T. G. Stockham, ‘Producing colorimetric data from densitometric scans,’ *Proc. SPIE* **1913**, 413–418 (1993).
- R. Rolleston and R. Balasubramanian, ‘Accuracy of various types of Neugebauer Model,’ *Proceedings IS&T/SID Color Imaging Conference*, Scottsdale, Ariz., 32–37 (1993).
- Sarnoff Corporation, *JND: A human vision system model for objective picture quality measurement*, Sarnoff Technical Report from www.jndmetrix.com, (2001).
- O.H. Schade, Optical and photoelectric analog of the eye, *J. Opt. Soc. Am.* **46**, 721–739 (1956).
- B.E. Schefrin and J.S. Werner, Age-related changes in the color appearance of broad-band surfaces, *Color Res. Appl.* **18**, 380–389 (1993).

- J. Schirillo, A. Reeves, and L. Arend, Perceived lightness, but not brightness, of achromatic surfaces depends on perceived depth information, *Perception & Psychophysics* **48**, 82–90 (1990).
- J. Schirillo and S.K. Shevell, Lightness and brightness judgments of coplanar retinally noncontiguous surfaces, *J. Opt. Soc. Am. A* **10**, 2442–2452 (1993).
- J. Schirillo and L. Arend, Illumination changes at a depth edge can reduce lightness constancy, *Perception & Psychophysics* **57**, 225–230 (1995).
- J. Schirillo and S.K. Shevell, Brightness contrast from inhomogeneous surrounds, *Vision Res.* **36**, 1783–1796 (1996).
- T. Seim and A. Valberg, Towards a uniform colorspace: A better formula to describe the Munsell and OSA Color Scales, *Color Res. Appl.* **11**, 11–24 (1986).
- C.C. Semmelroth, Prediction of lightness and brightness on different backgrounds, *J. Opt. Soc. Am.* **60**, 1685–1689 (1970).
- G. Sharma and H.J. Trussel, Digital color imaging, *IEEE Trans. Im. Proc.* **6**, 901–932 (1997).
- G. Sharma, Ed., *Digital Color Imaging Handbook*, CRC Press, Boca Raton (2003).
- S.K. Shevell, The dual role of chromatic backgrounds in color perception, *Vision Res.* **18**, 1649–1661 (1978).
- S.K. Shevell, Color and brightness: Contrast and context, *IS&T/SID 1st Color Imaging Conference*, Scottsdale, 11–15 (1993).
- J.M. Speigle and D.H. Brainard, Is color constancy task independent?, *IS&T/SID 4th Color Imaging Conference*, Scottsdale, 167–172 (1996).
- L. Spillman and J.S. Werner, *Visual Perception: The Neurophysiological Foundations*, Academic Press, San Diego, (1990).
- R. Stanziola, The Colorcurve System®, *Color Res. Appl.* **17**, 263–272 (1992).
- S.S. Stevens, To honor Fechner and repeal his law, *Science* **133**, 80–86 (1961).
- J.C. Stevens and S.S. Stevens, Brightness functions: Effects of adaptation, *J. Opt. Soc. Am.* **53**, 375–385 (1963).
- W.S. Stiles and J.M. Burch, N.P.L. colour-matching investigation: Final report (1958), *Optica Acta* **6**, 1–26 (1959).
- A. Stockman, L.T. Sharpe, and C. Fach, The spectral sensitivity of the human short-wavelength sensitive cones derived from threshold and color matches, *Vision Res.* **39**, 2901–2927 (1999).
- A. Stockman and L.T. Sharpe, The spectral sensitivities of the middle- and long-wavelength-sensitive cones derived from measurements in observers of known genotype, *Vision Res.* **40**, 1711–1737 (2000).
- M. Stokes, M. Fairchild, and R.S. Berns, Precision requirements for digital color reproduction, *ACM Trans. Graphics* **11**, 406–422 (1992).
- M.C. Stone, W.B. Cowan, and J.C. Beatty, Color gamut mapping and the printing of digital images, *ACM Trans. Graphics* **7**, 249–292 (1988).
- M.C. Stone, *A Field Guide to Digital Color*, A.K. Peters, Natick (2003).
- G. Svaetichin, Spectral response curves from single cones, *Acta Physiologica Scandinavica* **39** (Suppl. 134), 17–46 (1956).
- K. Takahama, H. Sobagaki, and Y. Nayatani, Analysis of chromatic adaptation effect by a linkage model, *J. Opt. Soc. Am.* **67**, 651–656 (1977).
- K. Takahama, H. Sobagaki, and Y. Nayatani, Formulation of a nonlinear model of chromatic adaptation for a light-gray background, *Color Res. Appl.* **9**, 106–115 (1984).
- R. Taya, W.H. Ehrenstein, and C.R. Cavonius, Varying the strength of the Munker-White effect by stereoscopic viewing, *Perception* **24**, 685–694 (1995).

- C.C. Taylor, Z. Pizlo, J.P. Allebach, and C.A. Bouman, Image quality assessment with a Gabor pyramid model of the human visual system, *IS&T/SPIE Electronic Imaging Conference*, SPIE Vol. **3016**, San Jose, 58–69 (1997).
- C.C. Taylor, Z. Pizlo, and J.P. Allebach, Perceptually relevant image fidelity, *IS&T/SPIE Electronic Imaging Conference*, SPIE Vol. **3299**, San Jose, 110–118 (1998).
- H. Terstiege, Chromatic adaptation: A state-of-the-art report, *J. Col. & Appear.* **1**, 19–23 (1972).
- L.L. Thurstone, A law of comparative judgment, *Psych. Review* **34**, 273–286, (1927).
- L.L. Thurstone, *The Measurement of Values*, University of Chicago Press, Chicago (1959).
- D.J. Tolhurst and D.J. Heeger, Comparison of contrast-normalization and threshold models of the responses of simple cells in cat striate cortex, *Visual Neuroscience* **14**, 293–309 (1997).
- W.S. Torgerson, A law of categorial judgment, in *Consumer Behavior*, L.H. Clark, Ed., New York University Press, New York, 92–93 (1954).
- W.S. Torgerson, *Theory and Methods of Scaling*, Wiley, New York (1958).
- A. Valberg and B. Lange-Malecki, ‘Colour constancy’ in Mondrian patterns: A partial cancellation of physical chromaticity shifts by simultaneous contrast, *Vision Res.* **30**, 371–380 (1990).
- J. von Kries, Chromatic adaptation, *Festschrift der Albrecht-Ludwig-Universität*, (Fribourg) (1902) [Translation: D.L. MacAdam, *Sources of Color Science*, MIT Press, Cambridge, (1970)].
- J. Walraven, Discounting the background — the missing link in the explanation of chromatic induction, *Vision Res.* **16**, 289–295 (1976).
- B.A. Wandell, Color appearance: The effects of illumination and spatial pattern, *Proc. Natl. Acad. Sci. USA* **90**, 9778–9784 (1993).
- B.A. Wandell, *Foundations of Vision*, Sinauer, Sunderland, Mass., (1995).
- A.B. Watson, Toward a perceptual video quality metric, *Human Vision and Electronic Imaging III*, SPIE Vol. 3299, 139–147 (1998).
- A.B. Watson and C.V. Ramirez, A standard observer for spatial vision, *Investigative Ophthalmology and Visual Science* **41**, S713 (2000).
- A.B. Watson, J. Hu, and J.F. McGowan, DVQ: A digital video quality metric based on human vision, *J. of Electronic Imaging* **10**, 20–29 (2001).
- M.A. Webster and J.D. Mollon, The influence of contrast adaptation on color appearance, *Vision Res.* **34**, 1993–2020 (1994).
- M.A. Webster and J.D. Mollon, Adaptation and the color statistics of natural images, *Vision Res.* **37**, 3283–3298 (1997).
- J.S. Werner and B.E. Schefrin, Loci of achromatic points throughout the life span, *J. Opt. Soc. Am. A* **10**, 1509–1516 (1993).
- D.R. Williams, N. Sekiguchi, W. Haake, D. Brainard, and O. Packer, The cost of trichromacy for spatial vision, in *From Pigments to Perception* (A. Valberg and B.B. Lee, Eds.), Plenum Press, New York 11–22 (1991).
- M. Wolski, J.P. Allebach, and C.A. Bouman, Gamut mapping: Squeezing the most out of your color system, *IS&T/SID 2nd Color Imaging Conference*, Scottsdale, 89–92 (1994).
- W.D. Wright, A re-determination of the trichromatic coefficients of the spectral colours, *Trans. Opt. Soc.* **30**, 141–161 (1928–29).
- W.D. Wright, Why and how chromatic adaptation has been studied, *Color Res. Appl.* **6**, 147–152 (1981a).

- W.D. Wright, 50 years of the 1931 CIE standard observer for colorimetry, *AIC Color 81*, Paper A3 (1981b).
- D.R. Wyble and M.D. Fairchild, Prediction of Munsell appearance scales using various color appearance models, *Color Res. Appl.* **25**, 132–144 (2000).
- G. Wyszecki, Current developments in colorimetry, *AIC Color 73*, 21–51 (1973).
- G. Wyszecki and W.S. Stiles, *Color Science: Concepts and Methods, Quantitative Data and Formulae*, Wiley, New York, (1982).
- G. Wyszecki, Color appearance, Chapter 9 in *Handbook of Perception and Human Performance*, Wiley, New York, (1986).
- X. Zhang and B.A. Wandell, A spatial extension of CIELAB for digital color image reproduction, *SID 96 Digest*, (1996).

Index

- Abney effect, 117–119
absorptance, 60
achromatic color, defined, 84
adaptation
 chromatic. See chromatic adaptation
 and chromatic induction, 113, 124
 dark, 22–23, 34, 148, 151–152, 159
 light, 22–23, 148–149, 152
 mechanisms of, 21
 motion, 155–156
 spatial frequency, 155
additive mixtures, 95, 103
additivity, Grassmann's law of, 70
adjustment, method of, 43
advanced colorimetry, 34
afterimages, 149, 155
Albers, Josef, 113
amacrine cells, of retina, 4
aqueous humor, 3
art, color-order systems in, 95, 102, 106
ASTM Standard Guide for Designing and
 Conducting Visual Experiments, 35
asymmetric matching, 43, 46, 160
ATD color appearance model
 adaptation model for, 220, 224
 brightness equation in, 210, 218–220
 chroma equation in, 220
 data for, 208, 210, 216
 example of, 279, 281
 hue equation in, 216–217, 221
 limitations of, 197
 objectives and approach of, 196
 opponent-color dimensions in, 200
 perceptual correlates in, 201
 predictions of, 201, 205
 saturation equation in, 201–202
axons, defined, 5
- background, defined, 137
Bartleson–Breneman equations, 126, 130
basic colorimetry, 51
Bezold–Brücke hue shift, 116, 118–119
bidirectional reflectance distribution
 functions (BRDF), 63
bidirectional transmittance distributions
 functions, 63
black-body radiator, 58
blackness, NCS value, 95
blind spot, 6, 10–12
Bradford–Hunt 96c color appearance model,
 208
Bradford–Hunt 96s color appearance model,
 208
brain
 visual area 1 of, 13, 15
 and visual signal processing, 12, 15
brightness, 86
 chromaticity and, 117–119
 –colorfulness reproduction, 92
 in color appearance, 85
 defined, 79
 luminance and, 100
cameras, digital, 319
category scaling, 47–48
characterization
 approaches to, 238
 defined, 243–244, 248, 250
 goals of, 54
chroma, 87, 92
 in color appearance, 85
 defined, 84–85, 87–88, 90
 equation for, 90
 Munsell, 85
chromatic adaptation, 19, 21, 23–25
cognitive mechanisms of, 127
defined, 120
example of, 112, 114, 118, 120, 128
high-level, 149, 154
mechanics of, 124
models of, 148–149, 152–154, 157, 159,
 162, 164–165
photoreceptors in, 148, 151, 153, 157
physiology of, 149, 154
receptor gain control in, 151, 153
sensory mechanisms of, 157, 159–160
subtractive mechanisms of, 149, 153
time course of, 159
treatises on, 158
chromatic adaptation models, 146–149,
 152–153, 157–160, 162–165
 applications of, 164–165
CAT02 transform, 183–184, 191–195
 concerns of, 166
 equations for, 162–163
Fairchild's model, 183, 190–191

- MacAdam's model, 166, 172
 Nayatani's model, 172–174, 177–178, 181
 retinex theory, 171–172
 treatises on, 158
 von Kries model, 151, 157, 165
- chromatic adaptation transforms, 163–164
 chromatic color, defined, 84
 chromatic contrast, 34, 28f
 contrast sensitivity functions for, 33–34, 27f
 chromatic induction, 113, 124
 chromaticity and brightness, 119
 diagrams of, 77–78
 chromaticness, NCS value, 100–102
 CIE illuminants, 56, 58–59
 characteristics of, 63, 66, 130
 CIE 1931 Standard Colorimetric Observer, 73, 76, 61t, 74t, 307
 CIE 1964 Supplementary Standard Colorimetric Observer, 77, 82
 CIE 1976 Uniform Chromaticity Scales, 78–79
 CIECAM02 color appearance model, 238–239
 adaptation model in, 241, 246, 251
 brightness, 239–240
 Cartesian coordinates, 246–247
 chroma, 243–244
 colorfulness, 239, 243–244, 246
 hue, 239, 243
 input data, 240–241, 246
 inverse model, 243
 implementation guidelines, 245
 lightness, 239, 243
 objectives, 240, 245
 opponent dimensions, 248
 phenomena predicted, 243
 saturation, 239
 CIECAM97s color appearance model, 238
 appearance correlates in, 246
 chromatic adaptation in, 239, 241, 243, 245–248, 250–251
 data for, 239–240
 historical background for, 239, 241, 244, 246, 248
 invertibility, 259–260
 CIELAB color space, xv, 81
 color differences in, 78, 80–81
 coordinates of, 161
 described, 154, 159–160, 162–163
 example of, 229
 lightness scale of, 161
 limitations of, 170
 mapping of, 164, 179
 recommended usage of, 300, 303, 306
 testing of, 264
 uniformity of, 185, 189
 utility of, 305
 wrong von Kries transforms in, 191–192, 194
 CIELAB ΔE_{ab}^* , 80–81
 CIELUV color space, 81, 194–195
 example of, 279, 281
 testing of, 264
 CIE94 color difference model, 81
 CMC color difference equation, 81
 CMYK, device coordinates, 315
 color(s)
 adaptation to, 19
 characteristics of, 63, 66
 constancy of, 24, 132–133, 164–165
 corresponding, 159–162, 164, 162f–163f, 255, 261–262
 defined, 47, 159
 memory, 24, 130, 132
 related, 84, 146, 162, 164
 triangle of, 54–55, 66, 82, 55f
 tristimulus values and, 70–71
 unrelated, 88–89, 120, 130
 color appearance
 cognitive aspects of, 132
 spatial influences on, 112, 125, 128
 color appearance models, applications of, 238
 ATD, 239
 Bradford–Hunt models, 246
 CIECAM02, 238–239
 CIECAM97s, 238–239
 CIELAB, 184–186, 189, 191–195
 CIELUV, 184, 194–195
 color attributes and, 84–85, 89, 91
 construction of, 184–185
 corresponding-colors data and, 255, 261–262
 current cutting edge, 300
 defined, 183, 189
 developments for the future, 299, 306
 and device independent color imaging, 309–310, 312–313, 315, 321–322, 324, 330–331
 direct-model testing of, 264
 Hunt's, 196–197, 201, 203, 205–206
 LLAB, 239, 245–246, 249–251
 magnitude-estimation experiments and, 263
 Nayatani's, 196–199, 202–207
 pictorial review of, 253
 psychophysics and, 53, 66
 qualitative testing of, 264
 research on, 299
 RLAB, 225, 227–228, 230–232, 234–237
 testing of, 94, 165, 264
 utility of, 90
 variety of, 301, 304–305
 visual system and, 35, 46, 52
 ZLAB, 255, 260–263

- color appearance phenomena, 108
 color appearance reproduction, 255, 261
 color constancy, 24, 132–133
 computational, 164–165
 color differences specifications, 64
 color differences measurement, 245
 application of color appearance models to, 254
 future directions for, 253
 recommendations for, 260
 techniques of, 246
 color gamut, 261
 color measurement, 285
 based on ICC Profile Format, xiv
 color matching, 70–73, 76–77, 74t
 color matching functions, 70–72, 76–77
 average, 71, 81
 color naming systems, 109
 types of, 97, 104, 106–107
 color order systems, 94–96, 103, 106–109
 applications of, 94–95, 97–98, 102–103, 106–109
 in art and design, 105, 107
 in communication, 107
 in education, 107–108
 in evaluation of color appearance models, 104
 and imaging systems, 98, 108, 110
 limitations of, 102, 107–108
 in visual experiments, 106
 color preference reproduction, 287
 color preferences, 314, 324, 327–328, 331
 color rendering, 279, 293–295
 application of color appearance models to, 278–281, 283–287, 289–295
 CIE technical committee on, 279, 291–293
 future directions for, 294
 indices for, 293
 recommendations for, 293–294
 techniques of, 285, 287, 289, 294
 color reproduction
 defined, 273–274
 enhancing accuracy of, 282
 levels of, 275
 color spaces(s)
 CIE, xiii, 78–79
 color differences in, 78, 80–81
 viewing-conditions-independent, 283
 color temperature, 56–58
 color vision
 deficiencies of, 31
 historic theories of, 17
 spatial properties of, 27, 28f
 temporal properties of, 26
 color vision deficiencies, 17–18, 30–33
 gender and, 31
 screening for, 33
 colorcurve system, 102–103, 106
 colorfulness, 87–93
 in color appearance, 85
 defined, 84
 varying directly with luminance, 113, 121, 124
 colorimetric color reproduction, 274
 colorimetry
 absolute, 58, 60, 75
 advanced, 53–54, 82
 basic, xviii, 53–56, 66–67, 82
 defined, 54
 future directions in, 263
 normalized, 75
 origin of, 66
 relative, 75
 colour standards for image technology, 240
 Commission Internationale de l'Eclairage (CIE), xiii
 activities of, 279, 291–292, 294
 See also CIE entries
 communication, color-order systems in, 107
 computational color constancy, 164–165
 cone monochromatism, 31, 33t
 incidence of, 33t
 cone responses
 transformation of tristimulus values to, 191
 cones, 4, 6, 8–11, 13–15, 21, 23, 27, 30, 34
 distinguished from rods, 30
 function of, 8–11
 relative abundance of, 29
 role in light and dark adaptation, 151
 spectral responsivities of, 66–67, 71, 76
 types of, 6, 8–9, 16–19, 21, 24, 27, 30–31, 33
 constant stimuli, method of, 30
 contrast
 varying directly with luminance, 116–117
 varying directly with surround, 125
 contrast sensitivity functions (CSFs), 26–27, 27f, 28f
 and eye movements, 29–30
 spatial, 26–27, 29, 34, 15f, 27f, 28f
 temporal, 26–27, 29, 28f
 cool white fluorescent lamp, and color rendering, 293–295
 cornea
 described, 1
 function of, 1
 correlated color temperature (CCT), 56, 58–59
 corresponding color reproduction, 283
 corresponding colors, 159–160, 164, 163f
 color appearance models and, 252
 Cowan equation, 119–120
 crispening, 113–115, 115f
 CRT display, 139
 characterization of, 295
 cubo-octahedron, 104

- Dalton, John, 31
dark adaptation, 19, 22–23, 34, 148–149, 151–152, 152f
curve of, 10, 21, 21f
daylight fluorescent lamp, and color rendering, 293–295
definitions, importance about being enormously careful about, 65
design, color-order systems in, 106
deuteranomaly, 31, 33t
incidence of, 33t
deutanopia, 30, 33t
incidence of, 33t
Deutsches Institut für Normung. See DIN
device calibration, 316
device characterization
approaches to, 316
defined, 310–312, 314, 322
goals of, 313
device-independent color imaging
color appearance models and, 309–310, 321
defined, 310
device calibration and characterization in, 316, 332
example system for, 328–329
gamut mapping and, 315, 321, 324, 326–327
general solution to, 315–316
as goal, 313, 327
ICC implementation of, 330
inverse process, 328
process of, 315, 321, 326, 328, 330, 317f
viewing conditions and, 309–311, 313–315, 320–324, 328–333
diffuse/normal viewing geometry, 64
digital cameras, characterization of, 319
DIN color system, 99
discounting the illuminant, 24, 34, 127
education, color-order systems in, 107
empirical modeling, 318
equivalent color reproduction, 311, 314
exact color reproduction, 311
eye
anatomy of, 1
optics of, 1, 3, 4
- Fairchild, M., 238
Fairchild's chromatic adaptation model, 177
equations of, 168
predictions by, 179
Farnsworth–Munsell 100-hue test, 33
Fechner's law, 38–39, 39f
filling-in, 12, 12f
film mode of appearance, 144
flare, 319–320, 322, 325
- fluorescence, 65
in output devices, 312–314, 319–320
fluorescent lamp, and color rendering, 293–295
forced-choice method, 44–45
45/normal viewing geometry, 63–64
fovea, 5, 8, 10–11, 29–30, 34
frequency-of-seeing curve, 44, 49
- gamut, 324
color, 308
defined, 324
limits to, 324
gamut mapping, 324
defined, 324
techniques for, 326, 330
ganglion cells, 5–7, 11–14
gender, and color vision deficiencies, 30–33, 33t
graphical rating, 47
Grassmann's laws, 70–71, 73
Guth's chromatic adaptation model, 175
equations of, 168
predictions by, 170, 173, 175
- haploscopic matching, 46, 160–161
hard-copy output, 159
Helmholtz–Kohlrausch effect, 107
Helson–Judd effect, 122–125, 124f
herding CATs, 179
Hering opponent-colors theory, 17–18
high pressure sodium lamp, and color rendering, 293–295
horizontal cells, of retina, 6
hue
in color appearance, 85
defined, 54
Munsell, 95–99, 101–104, 106–107, 97f
NCS value, 101
of nonselective samples, 122, 124, 124f
varying directly with colorimetric purity, 117, 121
varying directly with luminance, 116–117, 119, 117f, 119f, 121f
human visual response, quantification of, 66
Hunt–Pointer–Estevez transformation, 211
Hunt, R.W.G., 208, 246, 248, 250
Hunt color appearance model
adaptation model for, 196–200
advantages of, 318
brightness equations in, 201
chroma equation in, 203
colorfulness equation in, 204
data for, 192
example of, 259–260
hue equations in, 223, 223t
inversion of, 221
lightness equations in, 220

- Hunt color appearance model (*continued*)
 limitations of, 225, 237
 objectives and approach of, 196
 opponent-color dimensions in, 200
 predictions of, 209, 221, 224
 saturation equations in, 211
 testing of, 264
- Hunt effect, 108
- iCAM image appearance model, 340–341
 framework, 340, 346–347, 349–350
 future, 357–359
 image appearance and rendering, 350
 image difference and quality, 355
- ICC profile format, xiv
- illuminant A, 56, 58, 57f
- illuminant C, 58, 57f
- illuminant D50, 59f
 spectral power of, 59f
- illuminant D65, 56, 58, 81, 59f
 and color rendering, 229–301, 300t
 spectral power of, 56, 58, 59f
- illuminant F2, 59, 60f
 spectral power of, 59, 60f
- illuminant F8, 58–59, 60f
 spectral power of, 59, 60f
- illuminant F11, 58–59, 60f
 spectral power of, 58–59, 60f
- illuminant metamerism, 304–306
- illuminant mode of appearance, 143
- illuminants
 CIE, 53, 56, 58–59, 64, 67, 69–70, 72–73,
 76–82, 57f, 59f–60f, 61t, 69f, 68t
 discounting, 24, 34, 127
- illumination, standard, 63–64
- illumination mode of appearance, 144
- image appearance models, 335, 339–340
- image quality, 337–340, 345–346, 355, 356f
- image rendering, 339–340, 342, 345–347
- imaging systems, color-order systems in, 108
- indices of metamerism, 303–304, 306
 application of color appearance models to,
 301, 303, 305
 future directions for, 301, 303–304, 306
 recommendations for, 306
 techniques of, 300, 302, 304–305
- interaction of color, 113
- International Colour Association (AIC) 1997
 meeting, 254
- international lighting vocabulary, 84
- interval scale, defined, 41
- invertibility, 328
- iris, described, 4
- irradiance, 56
- Ishihara's Tests for Colour-Blindness, 33
- just-noticeable difference (JND), 38, 42
 experiments testing, 42–43, 45–46, 50–52
- L cones, 10
 relative abundance of, 13, 19, 29
 spectral responsivities of, 8, 13, 19, 9f
- LABHNU2 model, example of, 296
- Land two-color projection, 130
- lateral geniculate nucleus (LGN), 13
- lens
 described, 1, 6, 13, 17, 24, 34
 function of, 1, 3–5, 8–9
- light adaptation, 113, 146
 curve of, 19, 21f
 role of rods and cones in, 151
- light source
 defined, 54
 types of, 59, 75
- lightness, 78–81
 –chroma reproduction, 92, 92f–93f
 in color appearance, 85
 defined, 79
 equation for, 81
- limits, method of, 43
- linkage chromatic-adaptation model, 152,
 162–164, 163f
- LLAB color appearance model
 adaptation model for, 241, 246, 251
 chroma equation in, 239, 244
 color differences in, 243, 246, 250–251
 colorfulness equation in, 249
 data for, 239–240
 example of, 279, 260t
 hue equations in, 243
 lightness equation in, 243
 limitations of, 250
 objectives and approach of, 240, 245
 opponent-color dimensions in, 242, 248
 perceptual correlates in, 243, 249
 predictions of, 239
 saturation equation in, 239
 testing of, 264, 260t
- lookup tables (LUTs), 321, 330
 multidimensional, 320–321
- Lovibond Tintometer, 95
- luminance, 26, 67, 69, 73, 78
 and brightness, 107
 contrast sensitivity functions for, 26,
 27f–28f
 varying directly with colorfulness, 107
 varying directly with contrast, 113
 varying directly with hue, 111
- Luo, M.R., 254
- LUTCHI study, 285–287, 291
- M cones, 10, 15
 relative abundance of, 10–11, 42
 spectral responsivities of, 6, 8–9, 13, 19,
 23, 9f
- MacAdam's chromatic adaptation model,
 172

- Macbeth Color Checker Chart, 108
macula, 5–6, 34
magnitude estimation, 47–49
matching techniques, 45
Maxwell's color process, 130
McCollough effect, 155
measurement
 colorimetric, 311–321, 330, 332, 329f
 exhaustive, 316, 318, 328
memory color, 24, 34, 130, 132
memory matching, 46, 161
mercury lamp, and color rendering, 300t
mesopic vision, 8
metal halide lamp, and color rendering, 300t
metamerism, 67
 indices of, 303–304, 306
 in input and output devices, 312–313, 320
metameric, defined, 70
method of adjustment, 43
method of constant stimuli, 43–44
method of limits, 43
modeling
 empirical, 316, 318
 physical, 316–317
modular image difference model, 340
modulation transfer functions, 26
monochromatism, 31, 33t
 incidence of, 33t
Mori experiment, 123
motion adaptation, 155–156
multidimensional scaling (MDS), 48–49, 51f
Munsell Book of Color, 85
Munsell value scale, 85
- Natural Color System (NCS), 95, 99
 chromaticness in, 100–102, 101f
 hue in, 104
- Nayatani's chromatic-adaptation model as
 basis for color appearance model, 199
 equations of, 173
 forebears of, 173
 predictions by, 162, 164
- Nayatani's color appearance model
 adaptation model for, 205
 brightness equations in, 204
 chroma equations in, 204
 data for, 197
 example of, 279, 281
 hue equations in, 216–217, 222–223
 inversion of, 221
 lightness equations in, 220, 222
 limitations of, 225
 objectives and approach of, 208
 opponent-color dimensions in, 215–216
 predictions of, 209, 221, 224
 saturation equations in, 217–218, 220,
 222
 testing of, 264
- nominal scale, defined, 40–41
normal/diffuse viewing geometry, 64
normal/45 viewing geometry, 64
normalization constant, in colorimetry, 67,
 75–77
normalized colorimetry, 67, 75
- objects, recognition of, 24
oblique effect, 29
observer metamerism, 304–306
off-center ganglion cells, 15
on-center ganglion cells, 15
one-dimensional scaling, 46, 49
opponent-colors theory
 Hering's, 17–18
 modern, 17–19
opsin, 13
optic nerve, 4–6, 11, 13
optical illusions, 128
Optical Society of America Uniform Color
 Scales (OSA UCS), 103
ordinal scale, defined, 40–41, 47, 49
Ostwald system, 95, 103, 105–106
output lexicon, defined, 324
- paired comparison experiment, 48–49
Pantone Process Color Formula Guide, 95,
 109
- partition scaling, 47–48
pass-fail method, 44
perceptual threshold, 37
perfect reflecting diffuser (PRD), 65, 75
photometry, 67, 69, 73, 75
photopic luminous efficiency function, 72
photopic vision, 8–9
photoreceptors, 4–8, 11, 13, 15, 21, 34
 energy responses of, 10–11, 13, 15–16, 18,
 25, 27, 31
 gain control of, 149, 153
 see also cones; rods
- physical modeling, 316–317
- pigmented epithelium, 4–5
- Planckian radiator, 58
- pleasing color reproduction, 313
- PostScript Process Color Guide, 110
- power law, 39–40
- preferred color reproduction, 312–314, 327
- presbyopia, 3
- printers, characterization of, 319
- probit analysis, 45
- profile connection space, 331–332
- proportionality, Grassmann's law of, 73
- protanomaly, 31
 incidence of, 33t
- protanopia, 30
 incidence of, 33t
- proximal field, defined, 137
- pseudoisochromatic plates, 33

- psychometric function, 44–45
 psychophysics
 defined, 40–44, 47
 experimental concepts of, 41
 experimental design in, 35, 42
 history of, 37, 51
 relation to color appearance modeling, 36, 43, 46, 50–52
 pupil, in adaptation to light and dark, 149
 Purkinje shift, 10, 69
- radiance, 56–57, 65, 67, 75
 equation of, 58
 radiator, black-body, 58
 rank order experiment, 47
 ratio estimation, 47–48
 ratio scale, defined, 41
 receptive fields, 14–16, 26, 14f–15f
 receptor gain control, 149
 reflectance, 60, 63–65
 distribution functions of, 63
 related color, 86–89, 91
 defined, 84, 85, 87, 89, 92
 relative spectral power distribution, 56, 58–59, 75, 57f, 59f–60f, 61t
 response compression, 154, 154f
 retina
 described, 6, 13, 17, 24, 34
 light perception in, 6
 light processing in, 5, 15–16
 structure of, 5–6
 retinal, 11, 13
 retinex theory, 171–172
 RGB, device coordinates, 308
 rhodopsin, 9, 13
 Richter, K., 254
 RLAB color appearance model
 adaptation model for, 228
 chroma equation in, 234
 data for, 227, 234, 233t
 example of, 279, 281
 hue equation in, 232
 inversion of, 234
 lightness equation in, 231–232, 234, 232f
 limitations of, 225, 237
 objectives and approach of, 225
 opponent-color dimensions in, 230
 predictions of, 227, 236
 saturation equations in, 234, 236
 testing of, 264
 usefulness of, 359
 rod monochromatism, 31, 33t
 incidence of, 33t
 rods, 4, 6, 8–11, 13, 21, 34
 distinguished from cones, 30
 function of, 1, 3, 5, 12–13, 17, 26, 34
 luminous efficiency function for, 67, 69–70, 72, 69f
- relative abundance of, 10–11
 role in light and dark adaptation, 148
- S cones, 9–10, 27
 relative abundance of, 10–11, 34
 spectral responsivities of, 8–9, 13, 19
 saturation, 88–91
 defined, 89, 92
 equation for, 90
 scales
 types of, 59, 75
 uses of, 95, 106
 scaling
 multidimensional, 38, 40, 42, 44
 one-dimensional, 46–47, 49
 scanners, characterization of, 316
 scotopic luminous efficiency function, 68t
 scotopic vision, 8–9
 simultaneous binocular viewing, 323
 simultaneous contrast, 112–116, 124, 130, 132, 112f
 complexity of, 114f
 example of, 112, 114, 118, 120, 112f, 115f, 128, 131f
 and shape, 112, 130, 128f
 vs. spreading, 113, 115–116, 116f
 sodium lamp, and color rendering, 293–295
 soft-copy display, 159
 spatial CSFs, 27, 29
 spatial frequency adaptation, 155
 spatial perception, and chromatic perception, 134
 Specification of Colour Appearance for Reflective Media and Self-Luminous Display Comparisons (CIE technical committee), 292
 spectral color reproduction, 310
 spectral luminous efficiency, 67, 69
 spectral power distribution, 54–59, 67, 70–71, 73, 75, 59f
 spectrophotometry, 60
 CIE standards for, 65
 spectroradiometry, 56
 spreading, 113, 115–116, 116f
 vs. simultaneous contrast, 112–113, 115–116, 124, 130, 132, 112f, 114f, 116f, 128f
 stage theory, 19
 staircase procedures, 45
 Stevens effect, 121–122, 125, 123f
 Stevens power law, 38–40
 stimulus
 characteristics of, 130
 defined, 120, 132
 subtractive mixtures, 95
 successive binocular viewing, 322
 surface mode of appearance, 144

- surround
contrast and, 113, 116, 124, 130, 132, 116f
defined, 120, 132
- tapetum, 5
- TC1-27, Specification of Color Appearance for Reflective Media and Self-Luminous Display Comparisons, 292
- TC1-33, Color Rendering, 293
- TC1-34, Testing Colour Appearance Models, 291
model preparation by, 254
- temporal CSFs, 29
10 ∞ observer, 76
- testing color appearance models, 183
- Testing Colour Appearance Models
(CIE technical committee), 291
model preparation by, 254
- threshold experiments, 36, 42
types of, 38, 40, 42–44
- Thurstone's law, 48
- tintometer, 95
- transmittance, 60, 63, 71, 75, 63f
distribution functions of, 63
- tri-band fluorescent lamp, and color rendering, 293–295
- trichromatic theory, 17, 19
- tristimulus values, 54, 70–73, 75–77, 79, 73f
measurement of, 134
transformation to cone responses, 167–169, 172–173, 175
XYZ, xiii–xiv, 72–73, 76
- tritanomaly, 31
incidence of, 33t
- tritanopia, 30
incidence of, 33t
- Troland, defined, 240
- Trumatch Colorfinder, 109
- tungsten halogen, lamp, and color rendering, 293–295
- two-color projections, 130
2° color-matching functions, 76
- unrelated color, 88–89
defined, 89, 143
- viewing
anomalies of, 141–145
modes of, 134, 141, 143–144, 144t
- viewing conditions, definition of, 303–304
- viewing-conditions-independent space, 301
- viewing field
colorimetric specifications of, 138
components of, 134–135, 138, 141, 136f
configuration of, 135–136, 138
- viewing geometries, 63–64
- vision
experiments on, 35–38, 42–43, 45–47, 50–52
human, 55–56, 66, 55f
- visual area 13, 16
- visual experiments, 106
types of, 38, 40, 42–44
- visual threshold, 37
- vitreous humor, 3, 32
- volume mode of appearance, 144
- von Kries chromatic-adaptation model
equations of, 178–179
history of, 166
predictions by, 178–179, 181
testing of, 264
- Ware equation, 119–120
- Weber, E.H., 37
- Weber's law, 37–38
- whiteness, NCS value, 99–104, 106, 108, 101f
- wrong von Kries transforms, 191–192, 194, 180f
- xenon lamp, and color rendering, 293–295
- XYZ tristimulus values, xiii, 73
- yes-no method, 44
- ZLAB color appearance model, 255, 260
appearance correlates in, 257, 262
chromatic adaptation in, 255–256, 261, 264
data for, 264
invertibility of, 263
similarities of CIECAM97s, 252, 254–255, 259–264